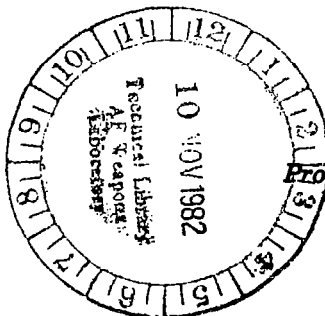


Atmospheric Effects and Potential Climatic Impact of the 1980 Eruptions of Mount St. Helens



TECH LIBRARY KAFB, NM

LOAN COPY: RETURN TO
AFWL TECHNICAL LIBRARY
KIRTLAND AFB, N.M.



*Proceedings of a symposium
held at Washington, D.C.
November 18-19, 1980*

NASA



NASA Conference Publication 2240

Atmospheric Effects and Potential Climatic Impact of the 1980 Eruptions of Mount St. Helens

*Edited by
Adarsh Deepak
Institute for Atmospheric Optics and
Remote Sensing
Hampton, Virginia*

Proceedings of a symposium
sponsored by the National Aeronautics
and Space Administration and
held at Washington, D.C.
November 18-19, 1980

NASA
National Aeronautics
and Space Administration
**Scientific and Technical
Information Branch**

1982

PREFACE

This volume presents the technical proceedings of the Symposium on Mount St. Helens: Its Atmospheric Effects and Potential Climatic Impact, held in Washington, DC, 18-19 November 1980. The symposium was sponsored by NASA Headquarters, Office of Space and Terrestrial Applications, on behalf of the U.S. National Climate Program, and was organized by the Institute for Atmospheric Optics and Remote Sensing (IFAORS). The purpose of the symposium was to present invited papers, both review and tutorial, on atmospheric and climatic aspects of the 1980 eruptions of Mount St. Helens. James P. Friend, Drexel University, was the symposium technical chairman, and Adarsh Deepak, IFAORS, was the symposium organizing chairman.

To ensure that the major disciplines involved were properly represented, a scientific program committee was organized which was composed of the following scientists: Adarsh Deepak, IFAORS; E. F. Danielsen, NASA Ames Research Center; J. J. DeLuisi, NOAA Environmental Research Laboratory; J. P. Friend, Drexel University; M. P. McCormick, NASA Langley Research Center; R. E. Newell, MIT; J. B. Pollack, NASA Ames Research Center; R. A. Schiffer, NASA Headquarters; W. A. Sprigg, National Climate Program Office; N. Sundararaman, FAA Headquarters; and W. E. Wilson, EPA Environmental Sciences Research Laboratory. The symposium program was divided into six paper presentation sessions and one summary session. Thirty-six papers covering various atmospheric and climatic aspects of the eruptions were presented in the sessions under the guidance of the following session chairman:

R. A. Schiffer	Nature and Impact of Volcanic Eruptions
R. J. Charlson	In Situ Measurements of Effluents
M. P. McCormick	Remote Sensing Measurements
E. F. Danielsen	Transport and Dispersion of Volcanic Effluents
J. P. Friend	Chemistry of Volcanic Effluents
R. E. Newell	Weather and Potential Climate Impact
J. P. Friend	Summary

The current state of knowledge, as well as the results of the latest investigations in specific areas of research, was discussed. Over 120 scientists from universities, nonprofit organizations, research laboratories, and government agencies in the United States, Canada, England, Italy, France, and Belgium participated in the symposium. Of the thirty-six papers presented at the symposium, complete texts of twenty-six are included in this volume. In addition, two papers submitted after the symposium for the proceedings are included.

The symposium was followed by a two-day workshop in which a group of experts assessed and summarized the state of knowledge of the various atmospheric and climatic aspects of the 1980 eruptions of Mount St. Helens, and recommended research areas in which further efforts are needed. The workshop report, edited by Reginald E. Newell and Adarsh Deepak, has been published as NASA SP-458.

The editor wishes to acknowledge the enthusiastic support and cooperation of the authors, members of the scientific program committee, session chairman, and participants for making this a successful and stimulating symposium. It is a pleasure to acknowledge the staff of IFAORS and Spectrum Press for organizing the symposium and preparing this manuscript for publication. Thanks are due the other members of the organizing committee, R. A. Schiffer, M. P. McCormick, and J. P. Friend, whose active assistance in the various aspects of the symposium assured its success. Additional support provided by M. P. McCormick, Aerosol Research Branch, NASA Langley Research Center, to enhance the scope and quality of the symposium is gratefully acknowledged.

It is, perhaps, the first time that such a compilation of authoritative papers on the atmospheric and potential climatic aspects of a volcanic eruption has been published. It is hoped that this symposium proceedings and the workshop report will serve as reference volumes for several years to come.

Adarsh Deepak



CONTENTS

PREFACE.....	iii
PARTICIPANTS.....	ix

SESSION 1. NATURE AND IMPACT OF VOLCANIC ERUPTIONS

Chairman: R. Schiffer

1. THE MAY 18, 1980, ERUPTION OF MOUNT ST. HELENS: THE NATURE OF THE ERUPTION, WITH AN ATMOSPHERIC PERSPECTIVE.....	1
W. I. Rose, Jr., and M. F. Hoffman	
2. VOLCANOES AND CLIMATE.....	15
Owen B. Toon	
3. IMPACT OF MOUNT ST. HELENS ERUPTION ON ECOSYSTEMS.....	37
J. C. Engibous, L. K. Bustad, R. A. Kennedy, G. O. Klock, E. C. Klostermeyer, and R. P. Preston	
4. IMPACT OF MOUNT ST. HELENS ERUPTION ON HYDROLOGY AND WATER QUALITY.....	43
J. E. Bonelli, H. E. Taylor, and J. M. Klein	

SESSION 2. IN SITU MEASUREMENTS OF EFFLUENTS

Chairman: R. J. Charlson

5. PRECURSOR GASES OF AEROSOLS IN THE MOUNT ST. HELENS ERUPTION PLUMES AT STRATOSPHERIC ALTITUDES.....	47
E. C. Y. Inn, J. F. Vedder, E. P. Condon, and D. O'Hara	
6. TIME VARIATIONS OF AEROSOLS IN THE STRATOSPHERE FOLLOWING MOUNT ST. HELENS ERUPTIONS.....	55
Neil H. Farlow, Kenneth G. Snetsinger, Verne R. Oberbeck, Guy V. Ferry, George Polkowski, and Dennis M. Hayes	
7. DUSTSONDE MEASUREMENTS OF THE MOUNT ST. HELENS VOLCANIC DUST CLOUD OVER WYOMING.....	65
J. M. Rosen and D. J. Hofmann	
8. PHYSICAL AND CHEMICAL CHARACTERISTICS OF MOUNT ST. HELENS AIRBORNE DEBRIS.....	83
W. A. Sedlacek, G. H. Heiken, E. J. Mroz, E. S. Gladney, D. R. Perrin, R. Leifer, I. Fisenne, L. Hinchliffe, and R. L. Chuan	

SESSION 3. REMOTE SENSING MEASUREMENTS

Chairman: M. P. McCormick

9. SAGE MEASUREMENTS OF MOUNT ST. HELENS VOLCANIC AEROSOLS.....	109
G. S. Kent	
10. MEASUREMENTS OF STRATOSPHERIC AEROSOL OVER MAUNA LOA, HAWAII, AND BOULDER, COLORADO.....	117
John J. DeLuisi, Bernard G. Mendonca, and Kirby J. Hanson	
11. GROUND-BASED AND AIRBORNE MEASUREMENTS OF MOUNT ST. HELENS STRATOSPHERIC EFFLUENTS.....	125
M. P. McCormick	

SESSION 4. TRANSPORT AND DISPERSION OF VOLCANIC EFFLUENTS

Chairman: E. Danielsen

12. DISTRIBUTION OF MOUNT ST. HELENS DUST INFERRED FROM SATELLITES AND METEOROLOGICAL DATA.....131
James D. Laver
13. MOUNT ST. HELENS PLUME DISPERSION BASED ON TRAJECTORY ANALYSES.....141
Edwin F. Danielsen

SESSION 5. CHEMISTRY OF VOLCANIC EFFLUENTS

Chairman: J. Friend

14. A COMPARISON OF CONSTITUENTS OF MOUNT ST. HELENS ERUPTION CLOUDS WITH THOSE OF SOME OTHER VOLCANOS.....155
Richard D. Cadle and Leroy Heidt
15. SIMULATION STUDIES OF THE PHYSICAL AND CHEMICAL PROCESSES OCCURRING IN THE STRATOSPHERIC CLOUDS OF THE MOUNT ST. HELENS ERUPTIONS OF MAY AND JUNE 1980.....161
R. P. Turco, O. B. Toon, R. C. Whitten, R. G. Keese, and P. Hamill

SESSION 6. WEATHER AND POTENTIAL CLIMATE IMPACT

Chairman: R. Newell

16. THE CLIMATIC EFFECT OF EXPLOSIVE VOLCANIC ACTIVITY: ANALYSIS OF THE HISTORICAL DATA.....191
R. A. Bryson and B. M. Goodman
17. PROBLEMS IN THE CLIMATOLOGY OF THE 1980 MOUNT ST. HELENS ERUPTIONS....203
Howard J. Critchfield

CONTRIBUTED PAPERS

18. THE MECHANISMS OF FINE PARTICLES GENERATION AND ELECTRIFICATION DURING MOUNT ST. HELENS VOLCANIC ERUPTION.....211
Roger J. Cheng
19. MEASUREMENTS OF SO₂ IN THE MOUNT ST. HELENS DEBRIS.....219
J. B. Kerr, W. F. J. Evans, and C. L. Mateer
20. ASH LOADING AND INSOLATION AT HANFORD, WASHINGTON, DURING AND AFTER THE ERUPTION OF MOUNT ST. HELENS.....225
N. S. Laulainen
21. MOUNT ST. HELENS DUST VEIL OBSERVED AT BOULDER, COLORADO, BY OPTICAL TECHNIQUES.....241
Gordon Lerfald
22. AIRCRAFT SAMPLING OF THE SULFATE LAYER NEAR THE TROPOPAUSE FOLLOWING THE ERUPTION OF MOUNT ST. HELENS.....251
Erwin A. Lezberg, Dumas A. Otterson, William K. Roberts, and Leonidas C. Papathakos
23. AN INCURSION OF DUST IN THE SOUTHWESTERN UNITED STATES FROM APRIL 1980 ERUPTIONS OF MOUNT ST. HELENS.....261
L. A. Mathews, G. R. Roquemore, P. St. Amand, and J. P. Gibson
24. MOUNT ST. HELENS RELATED AEROSOL PROPERTIES FROM SOLAR EXTINCTION MEASUREMENTS.....269
J. J. Michalsky, E. W. Kleckner, and G. M. Stokes

25. DEPOSITION AND DOSE FROM THE MAY 18, 1980 ERUPTION OF MOUNT ST. HELENS.....	275
Kendall R. Peterson	
26. AMBIENT AIRBORNE SOLIDS CONCENTRATIONS INCLUDING VOLCANIC ASH AT HANFORD, WASHINGTON, SAMPLING SITES SUBSEQUENT TO THE MOUNT ST. HELENS ERUPTION.....	283
G. A. Sehmel	
27. THE FORMULATION OF LAMB'S DUST VEIL INDEX.....	293
P. M. Kelly and C. B. Sear	
28. FORWARD AND BACK SCATTERING OF SOLAR RADIATION BY THE STRATOSPHERIC LIMB AFTER MOUNT ST. HELENS ERUPTION.....	299
M. Ackerman and C. Lippens	

PARTICIPANTS

Charles Acquista, Department of Physics of Atmospheric Sciences, Drexel University, Philadelphia, PA 19081
Alan R. Bandy, Chemistry Department, Drexel University, Philadelphia, PA 10104
Ernest Bauer, Institute for Defense Analysis, 400 Army-Navy Drive, Arlington, VA 22202
Erik Berall, Yale University, 193 Mansfield Street, New Haven, CT 06511
Kenneth H. Bergman, National Science Foundation, Room 644, 1800 G Street, NW, Washington, DC 20550
Joe Bonelli, USGS, Water Resources Survey, 5293 Ward Road, Arvada, CO 80002
Reid A. Bryson, University of Wisconsin, 1225 W. Dayton Street, Madison, WI 53706
Richard Cadle, 4415 Chippewa Drive, Boulder, CO 80303
M. Carbonnelle, Commissariat A. L. Energie Atomique, DPR/SPT BP NO2, 91190 Gif Sur Yvette, France
Richard A. Carrigan, National Science Foundation, Washington, DC 20550
R. Roland Chan, NASA Headquarters, Washington, DC 20546
S. Chandra, NASA-Goddard Space Flight Center, Code 964, Greenbelt, MD 20771
R. J. Charlson, University of Washington, FC-05, Seattle, WA 98195
Roger J. Cheng, Atmospheric Sciences Research Center, State University of New York, Albany, NY 12222
Howard J. Critchfield, Office of the State Climatologist, Western Washington University, Bellingham, WA 98225
Ed Danielsen, NASA-Ames Research Center, Mail Stop 234-3, Moffett Field, CA 94035
Adarsh Deepak, Institute for Atmospheric Optics and Remote Sensing, 17 Research Drive, Hampton, VA 23666
John DeLuisi, NOAA-ERL-ARL-GMCC, 325 Broadway R 329, Boulder, CO 80303
F. dePercin, Hqs. Department of the Army, HQDA (DAEN-RDM), Washington, DC 20314
Carl Dinerman, NWSC Crane, Code 9042, Crane, IN 47522
Richard Dirks, National Science Foundation, Washington, DC 20550
Currie S. Downie, National Science Foundation, 2212 Wakefield Street, Alexandria, VA 22308
I. J. Eberstein, NASA-Goddard Space Flight Center, Code 964, Greenbelt, MD 20550
Walter Egan, Grumman Aerospace Corporation, Bethpage, NY 11714
J. C. Engibous, Washington State University, Pullman, WA 99164
Neil H. Farlow, NASA-Ames Research Center, Moffett Field, CA 94035
Giorgio Fiocco, Universita, Istituto di Fisica, Roma, Italy
Rex J. Fleming, NOAA, 6010 Executive Boulevard, Rockville, MD 20852
R. S. Fraser, NASA-Goddard Space Flight Center, Greenbelt, MD 20771
James P. Friend, Department of Chemistry, Drexel University, Philadelphia, PA 19104
Marvin A. Geller, NASA-Goddard Space Flight Center, Code 964, Greenbelt, MD 20771
Rochelle Ginsburg, IBM, Department E-23, Bldg. 5, IBM Corporation, Endicott, NY 13760
T. E. Graedel, Bell Laboratories, Room 1D-349, Murray Hill, NJ 07974
Arnold Gruber, NOAA-NESS, WWB, Room 706, Washington, DC 20233
J. E. Hansen, NASA-GISS, 2880 Broadway, New York, NY 10025
David M. Harris, U.S. Geological Society, 959 National Center, Reston, VA 22092
Bruce P. Hayden, University of Virginia, Clark Hall, Charlottesville, VA 22903
Grant Heiken, Los Alamos Scientific Lab., MS 575, P. O. Box 1663, Los Alamos, NM 87545
L. E. Hinchliffe, U.S. DOE/Env. Meas. Lab., 376 Hudson Street, New York, NY 10014
Henry G. Horak, P. O. Box 1663, MS 436, Los Alamos, NM 87545
Edward C. Y. Inn, NASA-Ames Research Center, MS 245-5, Moffett Field, CA 94035
Charles Jackman, NASA-Goddard Space Flight Center, Mail Code 964, Greenbelt, MD 20771
Edward O. Jess, VA Air Pollution Control Board, 9th Street State Office Building, Richmond, VA 23219
Joan M. Jordan, National Science Foundation, Room 644, 1800 G Street NW, Washington, DC 20008
P. M. Kelly, Climatic Research Unit, University of East Anglia, Norwich NR4 7TJ, United Kingdom
G. S. Kent, Institute for Atmospheric Optics and Remote Sensing, 17 Research Drive, Hampton, VA 23666
J. B. Kerr, Atmospheric Environment Service, 4905 Dufferin Street, Downsview, Ontario, Canada M3H 5T4

James W. Kerr, Box 4073, Falls Church, VA 22044
Richard A. Kerr, Science-Research News Section, 1515 Massachusetts Avenue, NW, Washington, DC 20005
Tom Kitterman, Meteorology Department, Lyndon State College, Lyndonville, VT 05819
H. A. Knapp, Institute for Defense Analysis, 400 Army-Navy Drive, Arlington, VA 22202
Delores J. Knipp, U.S. Air Force, ASD/WE, Wright Patterson AFB, OH 45433
Mark Kritz, Department of Chemistry, Drexel University, Philadelphia, PA 19106
Arthur Krueger, Climate Center/NWS/NOAA, World Weather Building, Washington, DC 20233
Michael J. Kurylo, NBS Room A253, Bldg. 222, Washington, DC 20234
G. Lambert, Centres des Faibles Radioactivities, CFR-CNRS, Domaine du CNRS, 91190 Gif Sur Yvette, France
N. S. Laulainen, Battelle Pacific NW, P.O. Box 999, Richland, WA 99352
James D. Laver, National Weather Service, NMC, World Weather Building, Room 201, Washington, DC 20233
Alan Lazrus, NCAR, P.O. Box 3000, Boulder, CO 80307
Robert Leifer, US Department of Energy, Environmental Measurements Laboratory, 376 Hudson Street, New York, NY 10014
G. M. Lerfald, NOAA/ERL, Boulder, CO 80303
Leon Leventhal, LFE Environmental Analysis Labs, 2030 Wright Avenue, Richmond, CA 94804
Erwin A. Lezberg, NASA-Lewis Research Center, 21000 Brookpark Road, Cleveland, OH 44135
Lester Machta, NOAA, Washington, DC
Gene Maier, NASA-Goddard Space Flight Center, Code 963, Greenbelt, MD 20071
Peter J. Maroulis, Drexel University, Chemistry Department, Philadelphia, PA 19104
Larry Mathews, Naval Weapons Center, Research Department, Code 382, China Lake, CA 93555
Michael Matson, NOAA/NESS, World Weather Building, Room 711, Washington, DC 20233
Lindsay McClelland, Smithsonian Institute, Washington, DC 20560
E. Richard McCormick, NASA Headquarters, Code E, Washington, DC 20546
M. P. McCormick, NASA-Langley Research Center, MS 234, Hampton, VA 23665
L. R. McMaster, NASA-Langley Research Center, MS 234, Hampton, VA 23665
J. J. Michalsky, Battelle Northwest Labs, Battelle Observatory, Richland, WA 99352
Herb Mitchell, R & D Associates, Suite 500, 1401 Wilson Boulevard, Arlington, VA 22209
Murray Mitchell, NOAA/EDIS/DX6, Room 615, Gramax Building, 8060 Thirteenth Street, Silver Spring, MD 20910
Boyce M. Morrison, Jr., National Bureau of Standards, A 145, 222, Washington, DC 20234
Jarvis Moyers, University of Arizona, Chemistry Department, Tucson, AZ 85721
Eugene J. Mroz, Los Alamos Scientific Lab, Box 1663, CNC-7, MS-514, Los Alamos, NM 87545
David Murcay, University of Denver, Department of Physics and Astronomy, University Park, Denver, CO 80210
Vance A. Myers, Consulting Meteorologist, 9900 Mosby Road, Fairfax, VA 22032
R. E. Newell, MIT/Department of Meteorology, 45-1520, Cambridge, MA 02139
Brand Nieman, Office of Research & Development/EPA, M/S RD643-B, Washington, DC 20460
Harry Otten, Penn State University, 130 Kennedy Street, State College, PA 16801
Tom Owens, NASA-Langley Research Center, Hampton, VA 23665
William A. Page, NASA-Ames Research Center, MS 245-5, Moffett Field, CA 94035
Frank Don Palluconi, NSA-JPL, 5472 Mersea Court, Burke, VA 22015
Kendall Peterson, Lawrence Livermore National Laboratory, Mail Code L-262, P.O. Box 808, Livermore, CA 94550
James B. Pollack, NASA-Ames Research Center, MS 245-3, Code SST, Moffett Field, CA 94035
Cyril Ponnampereuma, Laboratory of Chemical Evolution, University of Maryland, College Park, MD 20742
R. A. Rasmussen, Oregon Graduate Center for Study & Research, 19600 NW Walker Road, Beaverton, OR 97005
Alan Robock, University of Maryland, Department of Meteorology, College Park, MD 20740
Patricia Rogers, University of California, Irvine, Irvine, CA 92633

William I. Rose, Michigan Tech. University, Department of Geology, Houghton, MI 49931
James Rosen, University of Wyoming, Department of Physics & Astronomy, P.O. Box 3095, University Station, Laramie, WY 82071
Eric Rosenthal, Assoc. Director of Public Relations, Drexel University, 118 N 34th Street, Philadelphia, PA 19104
Lothar H. Ruhnke, Naval Research Laboratory, Washington, DC 20375
C. A. Russell, Bell Telephone Labs/Room 4B625, Crawfords Corner Road, Holmdel, NJ 07733
A. Sarna-Wojcicki, U.S. Geological Survey, 345 Middlefield Road, Menlo Park CA 94025
R. A. Schiffer, NASA-Headquarters, Code EBT-8, Washington, DC 20546
W. A. Sedlacek, Los Alamos Scientific Laboratory, MS 514, P.O. Box 1663, Los Alamos, NM 87545
George A. Sehmel, Pacific Northwest Laboratory, P.O. Box 999, Richland, WA 99352
Stephen Self, Arizona State University, Geology Department, Tempe, AZ 85281
William Shen, NOAA-NESS, Room 706, World Weather Building, Washington, DC 20233
Tom Simkin, Smithsonian Institute, NHB-Stop 119, Washington, DC 20560
J. Smagorinsky, US Department of Commerce/NOAA, Princeton University, P.O. Box 308, Princeton, NJ 08549
George I. Smith, Geological Survey, 345 Middlefield Road, Menlo Park, CA 94025
William A. Sprigg, Department of Commerce/NOAA, National Climate Program Office, 6010 Executive Boulevard, Rockville, MD 20852
Scott J. Staggs, NOAA, Room 711, World Weather Building, Washington, DC 20233
R. A. Stokes, Battelle NW Labs, Battelle Observatory, Richland, WA 99352
R. Stolarski, NASA-Goddard Space Flight Center, Greenbelt, MD 20771
Dick Storey, NASA-Langley Research Center, Hampton, VA 23665
Larry L. Stowe, NOAA/NESS, World Weather Building, Washington, DC 20233
N. Sundararaman, FAA/HAPP, Washington, DC
T. J. Swissler, Systems & Applied Sciences Corporation, 17 Research Drive, Hampton, VA 23666
N. D. Sze, Atmospheric & Environmental Research, Inc., 872 Massachusetts Avenue, Cambridge, MA 02139
B. Taylor, Atmospheric Environment Service, 4905 Dufferin Street, Downsview, Ontario, Canada N3H 5T4
Lonnie Thompson, Ohio State University-IPS, 125 S. Oval Mall, Columbus, OH 43210
Owen B. Toon, NASA-Ames Research Center, MS 245-3, Moffett Field, CA 94035
Arnold L. Torres, NASA-Wallops Flight Center, Wallops Island, VA 23337
Richard Turco, R & D Associates, P.O. Box 9695, Marina del Rey, CA 90291
Guido Visconti, Istituto di Fisica, Universita, p.zza Annunziata 1, 67100 L'Aquila, Italy
R. T. Watson, NASA Headquarters, Code EBT-8, Washington, DC 22302
Dave Woods, NASA-Langley Research Center, Hampton, VA 23665
M. F. Wu, Institute for Atmospheric Optics and Remote Sensing, 17 Research Drive, Hampton, VA 23666
G. K. Yue, Institute for Atmospheric Optics and Remote Sensing, 17 Research Drive, Hampton, VA 23666
R. Zander, University of Liege, Institute of Astrophysics, Liege, Belgium

THE MAY 18, 1980, ERUPTION OF MOUNT ST. HELENS: THE NATURE OF THE ERUPTION, WITH AN ATMOSPHERIC PERSPECTIVE

W. I. Rose, Jr. and M. F. Hoffman
Michigan Technological University, Houghton, Michigan

Mount St. Helens erupted somewhat less than 0.5 km^3 of magma (dense rock equivalent) on May 18, 1980. Many characteristics of the eruption are important for scientists interested in the atmospheric impact to consider. The May 18 event was unusually violent. As much as 35% of the volume of the airfall material fell outside of the 2.5 mm isopach, which encloses about $88,000 \text{ km}^2$. This extraordinary dispersive power was transmitted by an eruption column which reached heights of more than 20 km. There was a lateral blast (or surge) of unusually large dimensions associated with the onset of the eruption. The magma is dacitic in composition and had a low (< 500 ppm) sulfur content. Distal ashes contain much nonmagmatic (lithic) material, but smaller ($< 50 \mu\text{m}$) particles are mostly finely divided magmatic dacite. The grain size distributions of the ash are multimodal, frequently with peaks at 90, 25, and $10 \mu\text{m}$. The finer populations fell out faster than their terminal velocities as simple particles would suggest. It is inferred that large proportions of the fine ash fell out as composite particles. This condition greatly reduces the atmospheric burden of silicate particles. Some of the unusual aspects (violence, intense surges, multimodal grain size distributions, lithic content of the ashes) of the eruption may be due to its phreatomagmatic character. The hydrothermal system above the magma may have infiltrated the magma body at the onset of the eruption. An "overprint" of the geochemistry of this hydrothermal system on the geochemistry of the magmatic gas system is likely. One important feature is that reduced gas species may be much more abundant than in many eruptions. Another is that fine ash may form aggregates more readily. The later eruptions of Mount St. Helens have been mainly magmatic in character and lack many of the characteristics of the May 18 event.

I. INTRODUCTION

The purpose of this short paper is to put the Mount St. Helens activity of 1980 in a broad volcanological context. This will probably help atmospheric scientists to best interpret the abundance of data about this event, and its significance to volcano-atmosphere interactions. The impact of explosive (Plinian and Vulcanian) eruptions (ref. 1) on the atmosphere has been judged by some to be more important than the impact of more passive activity (lava flows, strombolian activity). How representative is the St. Helens eruption? In what ways is it unusual?.

II. OBSERVATIONAL DATA ON THE MAY 18 ERUPTION

Descriptions of the events which took place during the May 18 eruption are aided by excellent photographic records of the first few minutes (see ref. 2). Apparently the chain of events began with a large earthquake (magnitude 5.1). The north slope of the St. Helens cone which had been growing for 2 months at a rate of 1.5 m/day, detached itself and began to slide away. Ultimately the more than 2 km^3 of Mount St. Helens' cone, that was removed formed a 15 km-long hummocky debris flow in the North Fork of the Toutle River. Phreatic eruptions, similar to those which had taken place beginning on 27 March, then began from the summit crater. Within seconds, however, the character of the eruption changed dramatically. A strong lateral blast (pyroclastic surge) developed from the cone directed mainly to the north. This pyroclastic surge moved more than 20 km to the north of the cone and devastated about 700 km^2 of forest land. The surge deposit contained mainly material from the old Mount St. Helens cone, but also contained dacite rock which represented new magma. Dramatic testimony to the directed violence of this blast has

been cited by many. It is one of the most dramatic historic examples of pyroclastic surge. After the surge a huge Plinian eruption column rose to a height of more than 20 km. The ashes erupted in this Plinian phase were preserved partly as hot pyroclastic flows, restricted to the northern slopes of Mount St. Helens itself, and partly as an extensive ashfall deposit which is found to the east of the volcano. (See refs. 3 and 4.)

The Plinian eruption of 18 May 1980 lasted about 9 hours (0840-1740). Radar data demonstrate that the column height during this period was consistently greater than 13 km (Table I). There were four periods of increased ash loading of the atmosphere during the eruption as shown by the radar (see ref. 5). These periods occurred beginning at 0845, 1030, 1330 and 1600. The first ash pulse was the highest and moved eastward most rapidly (150 km/hr).

III. ASH PRODUCED IN THE PLINIAN ERUPTION

Since this ash material has the most direct effect on the atmospheric data, discussion of the other deposits are omitted in this paper. An excellent isopach map of the ash blanket of the May 18 eruption was compiled by Sarna-Wojcicki et al. (refs. 3 and 4). This map shows a secondary maximum in ash thicknesses far downwind in eastern Washington. This is an unusual, but not unknown feature of isopach maps. (See refs. 6 and 7.) It probably results from the combination of (1) high eruption column, (2) fine grain size of the ash, (3) high upper level winds, and (4) the influence of particle aggregation which is discussed below. Before the < 100 μm ash could fall from 5 to 20 km of height in the atmosphere, it drifted several hundred km downwind. Radar data, times of ashfall, and direct observations strongly support this interpretation of the secondary maximum.

It is a complex problem to calculate the volume of an ash blanket (see refs. 6 and 8). The greatest uncertainty for violent eruptions lies in estimating the amounts of far-flung ashes. Because of the heights of the eruption column at Mount St. Helens and the high winds, there is uncertainty in volume in spite of the excellent isopach map. The volume estimate of the ash blanket begins with determination of the area within isopachs (Table II). These data can then be integrated as shown in figure 1. Such an integration gives a rationale for estimating the volume of ash not represented in the measured isopach regions (see refs. 8 and 9). Results of these integrations are given in Table III. A volume of about 1.3 km³ is indicated which would correct to less than 0.5 km³ of dense rock. These estimates are larger than those of Sarna-Wojcicki et al. (0.82 km³) who did not consider ashes outside of the 2.5 mm isopach. (See refs. 3, 4, and 10.) A large proportion of the volume of airfall material (about 35%) fell outside of the 2.5 mm isopach which encloses 88,000 km². This means that the estimates of the total volume of airfall (1.3 km³) are uncertain and possibly too large, because the largest volume increments are farthest from the volcano, where isopach control is poorest. Fortunately, the density of the far-flung ashes is low, and minimizes the volume uncertainty for dense rock equivalents. The fact that the Mount St. Helens ash blanket was carried eastward across North America allows a rare opportunity to study distal ashes, those most relevant to atmospheric studies. Some results of these studies of the distal ashes are presented and are based on sampling of ashes as they fell at a series of sites from near the volcano to as far away as Bloomfield, Colorado.

To gain information on the size distribution of the ash we followed the following procedure: Samples were sieved down to 25 μm (5.50 or 500 mesh) by hand to minimize abrasion. Where the sample was split to facilitate sieving in the finer mesh sizes, both halves of the split were weighed and the results from the sieved split adjusted accordingly. The less than 25 μm fraction was examined with a Coulter Counter. See ref. 11 for method and application to grain size studies.

Grain size analyses of distal ashes (figure 2) show the fine-grained character of the material and multimodal size distributions. Many samples of ash have trimodal distributions with peaks at about 90, 25, and 10 μm . The bulk compositions of the ash (Table IV) range from andesite to dacite. The bulk composition of larger particles in distal ashes are andesitic. The smaller (< 50 μm) particles have a dacitic bulk composition. Ashes have finer grains and have less of the andesitic component with distance. The morphology of the coarser andesitic component contrasts sharply with the finer dacitic material (figure 3). The andesitic component is dominated by angular fragments of minerals (figure 4), the dacitic component is mainly vesicular shards of dacitic glass (figures 5,6).

The andesitic component of the ash is interpreted to be remnants of the Mount St. Helens cone, fragmented by the phreatic component of the eruption. There is also a component of phenocrysts from the

dacite magmas. The dacite component probably represents the new magma, which may be partly phreatomagmatic in origin. The multimodal grain size distribution and the generally finer grain size of the ashes are characteristics shared by the 1979 Soufriere eruption in St. Vincent.¹ This was also a phreatomagmatic eruption.

Chemical analyses of whole rock and size splits of selected ashes are shown in Table IV. Such data, together with SEM work, allow a thorough interpretation of these ashes. In ashes deposited relatively near the volcano, the 40 size splits of the ash were composed almost entirely of andesitic fragments (see Richland sample, Table IV). More distant samples with less of the coarser materials also have less of the andesitic admixture by a mixing calculation. From Richland to Spokane to Missoula the andesitic component decreases from 67% to 15% to less than 3%.

The dacitic component of the ash is dominant in all the finer size splits of distal ash, regardless of transport distance. By comparing the bulk compositions of these finer splits with the composition of large pumice blocks deposited near the volcano, the amounts of atmospheric fractionation of crystals can be estimated. This factor does not seem to vary much in the ashes studied. Missoula ashes have been enriched in the glass component by a factor of 17% (from 64% glass to 82%). Most of this enrichment is caused by plagioclase which is 26% of pumice blocks (and the magma) but only 11% of the Missoula ash (Table V). Any of the distal ash samples can be interpreted by a combination of size separation bulk chemical analysis, SEM examination, and mixing calculations.

From the work of Hooper et al. (ref. 12) it is known that the proportion of the andesitic component in Pullman-Moscow ash was larger in early ashes and decreased to very low levels after a few hours of ashfall.

Table VI shows terminal velocities calculated for ash particles of the three size populations. These values are maxima because they assume spherical particles with a specific gravity of 2.0. If appropriate geometries are assumed, the terminal velocities would decrease by 20 to 50%. (See ref. 13). The times required for 90 μm ashes to fall distances of 5 to 20 km are similar to the times observed for fallout at Pullman according to Hooper et al. (ref. 12). The times are far shorter than would be required for the 30- and 10- μm particles; yet these particles are dominant in the ash. This result strongly suggests that they fell as composite particles. Composite particles have been recorded in direct eruption cloud sampling by Rose et al. (ref. 14). It is believed that this accumulation process explains the peculiar multimodal grain size distribution of the ashes, because only the smaller particles are affected. Thus the sorting of ash particles in the deposit immediately before is excellent and consists of a simple population of 100 μm particles and aggregates of all the smaller particles. Clarification of the aggregation mechanism is important because it is crucial in producing the ash fallout observed.

Figure 7 shows ashes which fell at Bloomfield, Colorado on 19 May 1980 at 1130 hr local time. This material is well sorted equidimensional particles of about 30 to 50 μm size. Crystal fragments make up a significant portion of this ash and are more abundant than in the closer samples studied. Noticeable contamination of the sample with local dust occurred. It is suggested that these ashes represent particles which escaped early aggregation. Their fallout times (26 hrs.) are appropriate for their size if they fell as simple particles.

Conclusions about the distal ashes may be summarized thusly: (1) The total volume is less than about 1.3 km^3 and the total dense rock equivalent is $< 0.5 \text{ km}^3$. (2) Somewhere between 0 and 50% of the ashes is angular andesitic material which represents the old rock of the cone. The average amount of this material decreased both with distance and time. The grain size of this material is coarser than the rest of the ash. The average amount of andesitic component for the entire ash blanket is in the range of 15 to 25%. (3) The finer grain size particles are dominantly vesicular dacite. They probably represent the newly erupted Mount St. Helens magma. They are enriched in glass and depleted in crystals in comparison with the large pumice blocks. This effect is due probably to atmospheric fractionation. (4) The grain size distributions of the ashes are multimodal at 90, 25, and 10 μm , and the terminal velocities of the finer particles are too slow for them to have fallen out as simple particles. It is inferred that they fell as composite particles of about 90 μm .

¹Personal communication, H. Sigurdson, 1980.

IV. AGGREGATION MECHANISM OF FINE ASH PARTICLES

It has been shown that very large proportions (up to 80%) of the ash fell out long before it would be expected to do so as simple particles. It is clearly important to the volcano-climate considerations to decide the reason for this extensive removal. This is true because it is necessary to decide whether the mechanism is likely to operate in most eruption clouds or whether it is restricted to this particular case.

Zimon's (ref. 15) compilation on the adhesion of glass particles shows (1) finer particles adhere more readily than coarser ones, (2) humidity increases adhesive forces substantially by allowing capillary forces to develop, (3) sphericity is inversely related to adhesive force, (4) particle coulomb forces may produce adhesion if particles are charged preliminarily, (5) coulomb forces are reduced by humidity. Experiments to demonstrate the adhesion of ashes have not been made, but such work is important to do. Besides the humidity and coulomb forces described, ice crystal formation may also be a factor in accumulation.² Zimon's work shows that adhesion is often enhanced between different kinds of particles. Electrification of particles may also be an important factor in increasing accumulation.

It is important to determine whether the aggregation of fine ash particles is a typical feature of airfall ash. Considerable grain size information is available on airfall ashes. (See refs. 16 to 18.) Most of these data suggest simple unimodal grain size distributions with good sorting ($\sigma \cong 1.0$). There is no noticeable tendency for finer grained ashes to be more poorly sorted. One weakness of all these data, however, is that they give little information on grain sizes smaller than $30 \mu\text{m}$ ($< 5\phi$). Limited data on the size distribution of erupted particles smaller than $30 \mu\text{m}$ (refs. 14 and 19) suggest that fine particle size distributions are often multimodal. Aggregate particles are also observed. (See ref. 14, Plate 8, p. 685.) In these examples, however, the fine particle peaks make up no more than a shoulder on the grain size distribution. (See ref. 19, fig. 2.) In the Mount St. Helens ashes there is a clear trimodal distribution in many samples (fig. 2). This result may imply that the aggregation process was particularly effective in the Mount St. Helens eruption cloud. Table VII is a list of the ash samples cited in this paper.

V. SULFUR GASES IN THE ERUPTION

Glass inclusions inside phenocrysts in the 1980 Mount St. Helens magmas have been analyzed by Melson et al. (See ref. 20.) His data suggest that the Mount St. Helens magma had a very low sulfur content (< 500 ppm) compared with other eruptions. For example, Fuego, 1974 had a magmatic sulfur content of as much as 2800 ppm sulfur. (See ref. 21.)

It is not straightforward to infer the atmospheric loading of sulfur from the magmatic concentration and the mass of magma erupted because intrusive magma may contribute volatiles to the eruption but remain below the surface and because erupted material may retain and scavenge volatiles from the atmosphere. Nonetheless, it is anticipated that the sulfur loading of the atmosphere is less for the Mount St. Helens eruption than is the case for other recent eruptions of similar size.

Ashes falling out of the eruption cloud scavenged considerable concentrations of sulfate, equivalent to 100 to 1000 ppm sulfur on the ashes studied in this report.

VI. MAGNITUDE OF THE ERUPTION

The dense rock equivalent volume for the eruption of Mount St. Helens is under 0.5 km^3 . It consists of components of airfall, pyroclastic flows, surge and debris flow materials. The volume of the amphitheatre on the north side of the cone is considerably larger than the magma volume.

²Cheng, R. J.: The Mechanisms of Fine Particle Generation and Electrification During Mount St. Helens Volcanic Eruption. Paper 18 presented in this symposium, 1980.

If the magma volume is considered, the eruption is not unusually large. The number of eruptions of this volume or larger is approximately 30 since 1900. The height of the eruption column reached levels of more than 20 km. A large proportion of the ash volume fell very far from the volcano. Both of these facts attest to the unusual dispersive power of the eruption. Eruptions which disperse material so dramatically occur only about every 10 to 20 years worldwide.

VII. AN UNCERTAINTY: THE PHREATOMAGMATIC COMPONENT

One major uncertainty about the Mount St. Helens eruption is the extent of the phreatomagmatic component in the eruption. Several observations support a substantial phreatomagmatic component; these observations are:

- (1) The overall fine grain size of the ash, which is similar to phreatoplinian eruption (see ref. 22.);
- (2) The occurrence of phreatic activity during March-May, 1980, which demonstrated the existence of a hydrothermal system;
- (3) The abundance of finely divided lithic material in the airfall deposits;
- (4) The great dispersive power of the eruptions;
- (5) The long repose period and high rainfall of the Cascades which would tend to saturate the cone;
- (6) The existence of accretionary lapilli (concentric wet ash aggregates) in some of the ejecta;
- (7) The presence of prismatically fractioned, dense, glassy dacite in the surge (blast) deposits.

If the phreatomagmatic component of the eruption is significant, then the eruption might be expected to be unusual in its contribution of reduced gases, H_2O and possibly H_2SO_4 . These contributions might not be typical of every Plinian eruption. Ash removal of fine phreatoplinian ashes may be unusually efficient because of the increased abundance of H_2O . Although geologists disagree about the extent of the phreatomagmatic component, most agree that its influence was greatest in the earliest parts of the eruption (the surge) and declined thereafter. The post-May 18 activity is nearly completely magmatic and lacks many of the characteristics of the May 18 eruption.

VIII. CONCLUDING REMARKS

Every volcanic eruption offers some unique opportunities for insight into the volcanic processes. The Mount St. Helens eruption was unusual in allowing for detailed studies of distal ashfall, because fallout occurred on land. Fallout times for tephra and their grain sizes strongly suggest that a substantial amount of ash in many downwind areas fell as composite particles. This accumulation of fine particles into aggregates greatly minimized the atmospheric impact of fine silicate particles. The sulfur content of the Mount St. Helens magma is much lower than that for other recent eruptions, such as the 1974 Fuego event. The magnitude of the eruption is similar to that of about 30 worldwide eruptions since 1900. The dispersive power is unusually large, manifested by the high Plinian column and wide dispersion of ash. One uncertainty about the eruption is the extent of the phreatomagmatic component, which could affect the amounts and kinds of volatiles added to the atmosphere, the fragmentation of the ash, and the aggregation of the fine particles.

REFERENCES

1. Cadle, R. D., Lazrus, A. L., Huebert, B. J., Heidt, L. E., Rose, W. I., Jr., Woods, D. C., Chuan, R. L., Stoiber, R. E., Smith, D. B., and Zielinski, R. A.: Atmospheric Implications of Studies of Central American Volcanic Eruption Clouds, *J. Geophys. Res.*, vol. 84, 1979, pp. 6961-6968.
2. Christiansen, R. L.: Eruption of Mount St. Helens: Volcanology, *Nature*, vol. 285, 1980, pp. 531-533.
3. Sarna-Wojcicki, A. M., and Waitt, R. B.: Areal Distribution, Thickness and Composition of Volcanic Ash Erupted From Mount St. Helens on May 18, 1980, *Geol. Soc. Amer. Abst. with Prog.*, vol. 12, 1980, p. 515.
4. Sarna-Wojcicki, A. M., Shipley, S., Waitt, R. B., Dzurisin, D., Hays, W. H., Davis, J. O., Wood, S. H., and Baderidge, T.: Areal Distribution, Thickness and Volume of Downwind Ash from the May 18, 1980 Eruption of Mount St. Helens. U.S. Geol. Surv. Openfile Report 80-1078, 1980.

5. Rose, W. I., Jr., and Harris, D. M.: Radar Observations of Ash Clouds From the May 18, 1980 Mount St. Helens Eruption. Trans. A.G.U., vol. 61, 1980, p. 1136.
6. Walker, C. P. L.: The Taupo Pumice: Product of the Most Powerful Known (Ultraplinian) Eruption? J. Volcanol. Geoth. Res., vol. 8, pp. 69-94.
7. Larsson, W.: Vulkanische Asche vom Ausbruch des Chilenischen Vulkans Quizapu (1932) in Argentina gesammelt. Ein studie uber aolische Differentiation. Bull. Geol. Inst. Upsala, vol. 26, 1936, pp. 27-52.
8. Rose, W. I., Jr., Bonis, S., Stoiber, R. E., Keller, M., and Bickford, T.: Studies of Volcanic Ash From Two Recent Central American eruptions. Bull. Volcanol., vol. 37, pp. 338-364.
9. Drexler, J. W., Rose, W. I., Jr., Sparks, R. S. J., and Ledbetter, M. T.: The Los Chocoyos Ash, Guatemala: A Major Stratigraphic Marker in Middle America and in Three Ocean Basins. Quat. Res., vol. 13, 1980, pp. 327-345.
10. Sarna-Wojcicki, A. M., Shipley, S., Waitt, R. B., Jr., Dzurisin, D., and Wood, S. H.: Areal Distribution Thickness Mass Volume and Grain Size of Airfall Ash From the Six Major Eruptions of 1980. U.S. Geol. Survey Prof. Paper 1250, 1981.
11. Huang, T. C., Watkins, N. D., and Shaw, O. M.: Atmospherically-Transported Volcanic Glass in Deep Sea Sediments: Development of a Separation and Counting Technique. Deep Sea Research, vol. 22, 1975, pp. 185-196.
12. Hooper, R. R., Herrick, E. W., Laskowski, E. R., and Knowles, C. R.: Composition of the Mount St. Helens Ashfall in the Moscow-Pullman Area on 18 May 1980. Science, vol. 209, 1980, pp. 1125-1126.
13. Wilson, L., and Huang, T. C.: The Influence of Shape on the Atmospheric Settling Velocity of Volcanic Ash Particles, Earth Planet. Sci. Lett., vol. 44, 1979, pp. 311-324.
14. Rose, W. I., Jr., Chuan, R. L., Cadle, R. D., and Woods, D. C.: Small Particles in Volcanic Eruption Clouds. Amer. J. Sci., vol. 280, 1980, pp. 671-698.
15. Zimon, A. D.: Adhesion of Dust and Powder, Plenum Press (New York), 1969.
16. Walker, G. P. L.: Grain Size Characteristics of Pyroclastic Deposits. J. Geol., vol. 79, 1971, pp. 696-714.
17. Sheridan, M. F.: Particle Size Characteristics of Pyroclastic Tuffs. J. Geophys. Res., vol. 76, 1971, pp. 5627-5634.
18. Buller, A. T., and McManus, J.: Distinction Among Pyroclastic Deposits From Their Grain Size-Frequency Distributions. J. Geol., vol. 81, 1973, pp. 97-106.
19. Murrow, P. J., Rose, W. I., Jr., and Self, S.: Determination of the Total Grain Size Distribution in a Vulcanian Eruption Column and Its Implications to Stratospheric Aerosol Perturbation. Geophys. Res. Lett., vol. 7, 1980, pp. 893-896.
20. Melson, W. G., Hopson, C. A., and Kienle, C. F.: Petrology of Tephra From the 1980 Eruption of Mount St. Helens. Geol. Soc. Amer. Abst. with Prog., vol. 12, 1980, p. 482.
21. Rose, W. I., Jr., Anderson, A. T., Jr., Bonis, S. B., and Woodruff, L. G.: October 1974 Basaltic Tephra from Fuego Volcano, Guatemala: Description and History of the Magma Body, J. Volcanology Geoth. Res., vol. 4, 1978, pp. 3-53.
22. Self, S., and Sparks, R. S. J.: Characteristics of Widespread Pyroclastic Deposits Formed by the Interaction of Silicic Magma and Water. Bull. Volc., vol. 41, 1978, pp. 196-212.
23. Inman, D. L.: Methods of Describing the Size Distribution of Sediments, J. Sed. Petrol., vol. 22, 1953, pp. 125-145.
24. Harris, D. H., Rose, W. I., Jr., Roe, R., and Thompson, M. R.: Radar Observation of Ash Eruption at Mount St. Helens Volcano, Washington, Professional Paper 1250, U.S. Geological Survey, 1981.
25. Lapple, C. E.: Characteristics of Particles and Particle Dispersoids. Stanford Res. Inst. Jour., vol. 5, 1961, p. 94.

TABLE I: RADAR ESTIMATES OF HEIGHT OF TOP OF MAY 18 CLOUD. (From ref. 24.)

Local Time	Height, km
0845	< 20
0915	14
0938	14
1100	15
1158	17
1255	13
1330	15
1500	15
1605	16
1705	19
1900	7
2100	5
2230	5
0200 + 1	4

TABLE II: MOUNT ST. HELENS MAY 18 AIRFALL BLANKET: AREAS ENCLOSED BY ASH ISOPACHS. (From refs. 3, 4, and 10.)

Isopach, cm	Area, km ²
8	34
7	217
6	450
4	2,280
3	7,611
2	13,159
1	32,850
0.5	52,500
0.25	88,000
0.1	132,000
0.05	182,000

TABLE III: ST. HELENS' MAY 18 ASH BLANKET, RESULTS OF VOLUME INTEGRATION OF CURVES PLOTTED IN FIGURE 1. (Method from ref. 8.)

Isopach, cm	Volume Outside, km ³
7	1.26
6	1.25
5	1.24
4	1.23
3	1.20
2	1.10
1	0.31
0.5	0.61
0.25	0.45
0.1	0.30
0.05	0.22
0.005	0.08
0.0005	0.03

TABLE IV: X-RAY FLUORESCENCE ANALYSIS OF SELECTED BULK ASH SAMPLES AND VARIOUS SIZE SPLITS REPRESENTING GRAIN SIZE PEAKS (FIGURE 2). BELOW ARE THE ESTIMATED PROPORTIONS (BY MIXING CALCULATIONS) OF ANDESITIC AND DACITIC POPULATIONS.

	Richland (6)				Spokane			Missoula (17)		
	Bulk	40	5.50	Pan	Bulk	40	Pan	Bulk	5.50	Pan
SiO ₂	58.5	54.4	60.3	62.1	64.3	57.1	66.3	67.8	66.5	67.0
Al ₂ O ₃	18.3	18.0	17.4	17.4	17.2	18.5	16.8	16.1	16.3	16.1
Fe ₂ O ₃ *	5.8	7.9	4.5	5.1	3.9	6.6	3.3	4.5	4.5	4.6
MgO	2.6	3.3	2.4	2.7	1.8	2.5	1.8	1.5	1.3	1.6
CaO	5.4	6.1	4.8	4.3	3.6	5.6	3.0	4.1	4.5	4.0
Na ₂ O	4.6	4.3	4.2	4.6	4.8	4.6	4.9	4.6	4.4	5.5
K ₂ O	1.3	0.97	1.4	1.7	1.7	1.1	1.0	1.7	1.6	1.8
P ₂ O ₅	0.16	0.17	0.17	0.18	0.12	0.15	0.11	0.13	0.13	0.13
TiO ₂	<u>0.83</u>	<u>1.11</u>	<u>0.66</u>	<u>0.65</u>	<u>0.59</u>	<u>0.97</u>	<u>0.49</u>	<u>0.64</u>	<u>0.65</u>	<u>0.63</u>
	97.4	96.2	95.9	98.7	98.1	97.1	98.7	101.0	99.9	100.9
PROPORTIONS**										
Andesite	67	100	42	40	16	80	0	0	0	0
Dacite	33	0	57	60	84	20	100	100	100	100

*Total Fe as Fe₂O₃

**Calculated by mixtures of glass enriched dacite and andesite, verified approximately by SEM estimates. Values are relatively indicative and semiquantitative.

TABLE V: MOUNT ST. HELENS ASHES, MAY 18. [Data from personal communication from C. Meyer, July 1980, and unpublished chemical analysis (1980) by K. C. Wzynyak, S. S. Hughes, and E. M. Taylor and from Table IV.]

	Microprobe Glass	Bulk Pumice	Bulk Missoula	
SiO ₂	71.5	64.1	67.8	
Al ₂ O ₃	15.0	18.0	16.1	
Fe ₂ O ₃ *	2.5	4.6	4.5	
MgO	0.5	2.0	1.5	
CaO	2.3	4.8	4.1	
Na ₂ O	4.7	4.7	4.6	
K ₂ O	2.0	1.45	1.7	
P ₂ O ₅	—	—	0.13	
TiO ₂	<u>0.37</u>	<u>0.65</u>	<u>0.64</u>	
	99.00	99.90	101.00	
PROPORTIONS**				Δ
Glass	100	64.0	82.0	17.0
Plag	0	26.0	11.0	— 15.0
Hbd + Px	0	10.0	8.0	— 2.0
Magn	0	2.2	1.7	— 0.5

*Total Fe as Fe₂O₃.

**Mixing calculations using glass and mineral calculations.

TABLE VI: ESTIMATED TERMINAL VELOCITIES OF ASH PARTICLES OF VARIOUS DIAMETERS. [Data based on table of Lapple (ref. 25) and assumed spheres with a bulk density of 2.0 g/cc (Stokes-Cunningham factor, included) falling in air. Shape influence factors will decrease terminal velocities for the 90 μm ashes by factors of up to 5, based on Wilson and Huang (ref. 13).]

Diameter, μm	Terminal Velocity cm/sec	Time to Fall 5-20 km, hrs
90	40	3 - 10
25	3	45 - 190
10	0.6	230 - 900

TABLE VII: LIST OF SAMPLES CITED IN THIS REPORT. [Collected by J. W. Drexler, I. M. Lange, L. Zinser, and E. Rexius, personal communication, June 1980.]

No.	Site	Local Time of Fall
1	9 mi NW of Mount St. Helens (Toutle R.)	18 May 1100-1200
3	Spokane, pale, upper layer	18 May after 1800
4	W. Richland	18 May 1130-1700
5	Richland	18 May 1300-1400
6	Richland	18 May 1300-1400
17	Missoula	18 May 2200-0400 + 1
18	Bloomfield, Colorado	19 May 1130

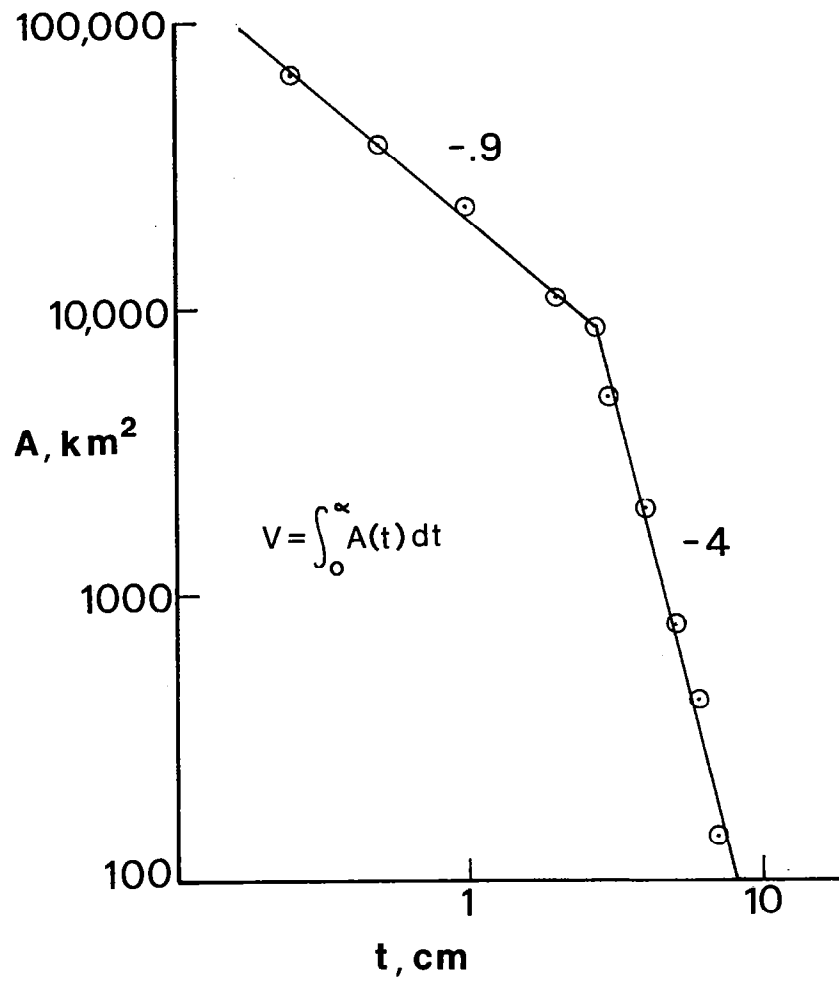


Figure 1. Variation of log area with log thickness for the 18 May 1980 ash blanket of Mount St. Helens. Data from Table II. Integration of this area under this curve from various thicknesses to zero thickness gives the data of Table III. (See also refs. 8 and 9.)

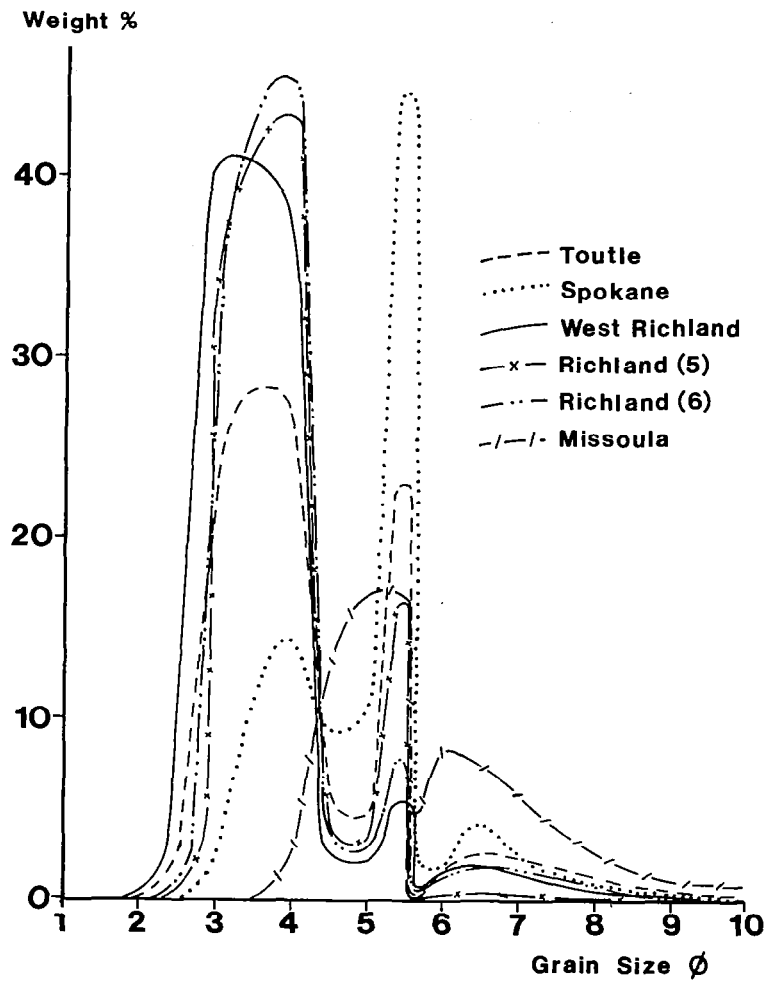


Figure 2. Grain size distribution of selected tephra samples from the May 18 ash blanket of Mount St. Helens. (Data given in ϕ units ($\phi = -\log$; base 2) of size in cm; ref. 23.)

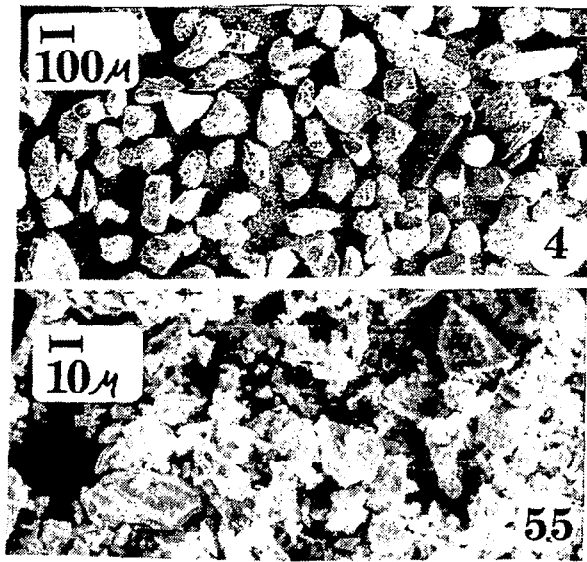


Figure 3. Scanning electron micrograph showing the contrasting morphology of the 40 ($\sim 100 \mu\text{m}$) and 5.50 splits of ash which fell at Spokane. The larger size split contains many lithic and crystal fragments. (See figure 4.) Shards of glass dominate the smaller size fraction.

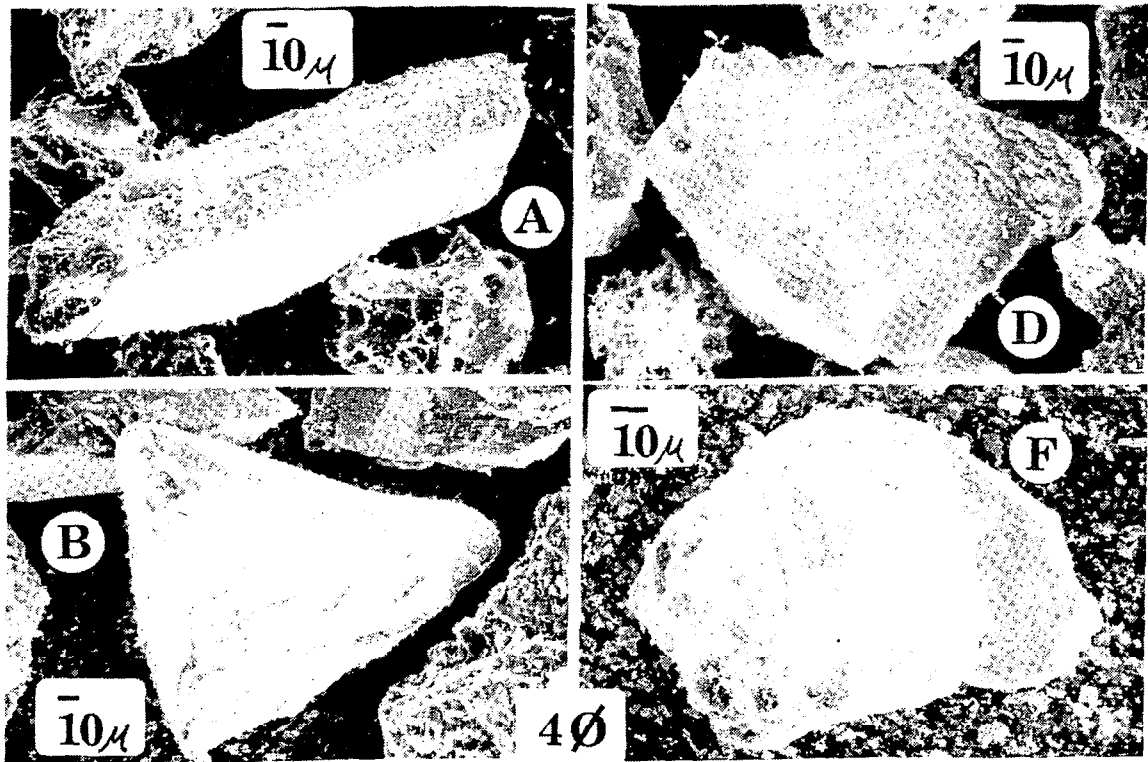


Figure 4. Individual particles of the 40 split of Spokane ash, identified by energy dispersive x-ray analysis. A is a hornblende crystal with a glass jacket. It is probably pyrogenic, and shows that crystals from the magma are also found in the 40 material. B and D are fragmented plagioclase crystals. F is a titaniferous magnetite grain. Many vesicular glass particles occur in this size split also.

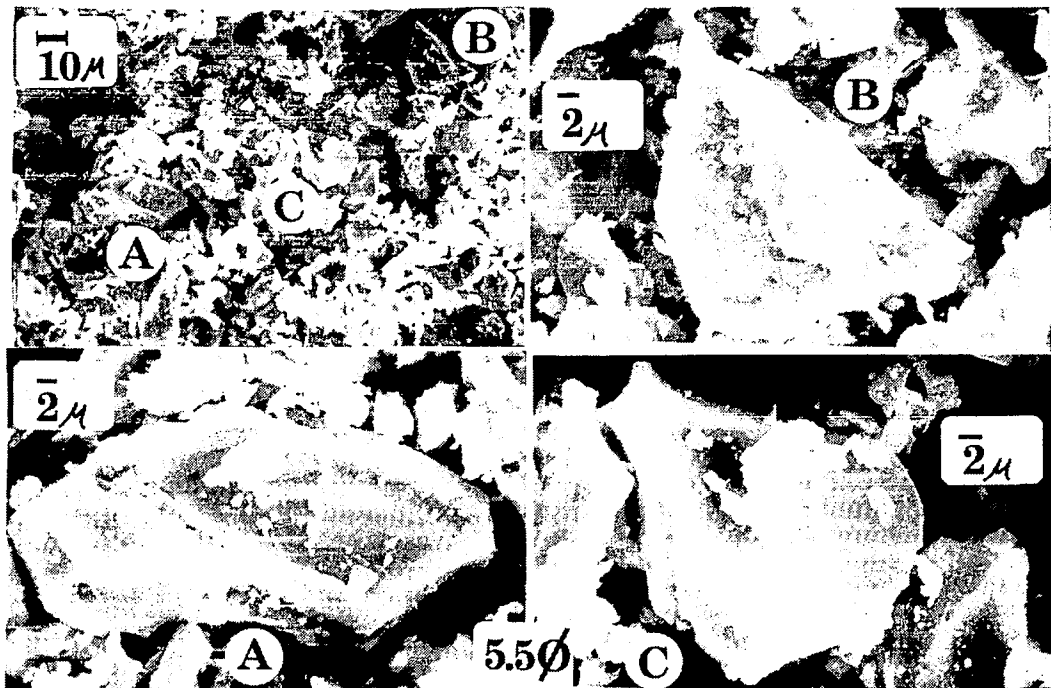


Figure 5. SEM images of the 5.50 split of Spokane ash. This material is chiefly shards of glass. A and C are glasses with compositions of 70% SiO₂, 5% K₂O. B is a composite grain, with the left side glass and the right side titaniferous magnetite. The bulk composition of this size split reflects glass enrichment.

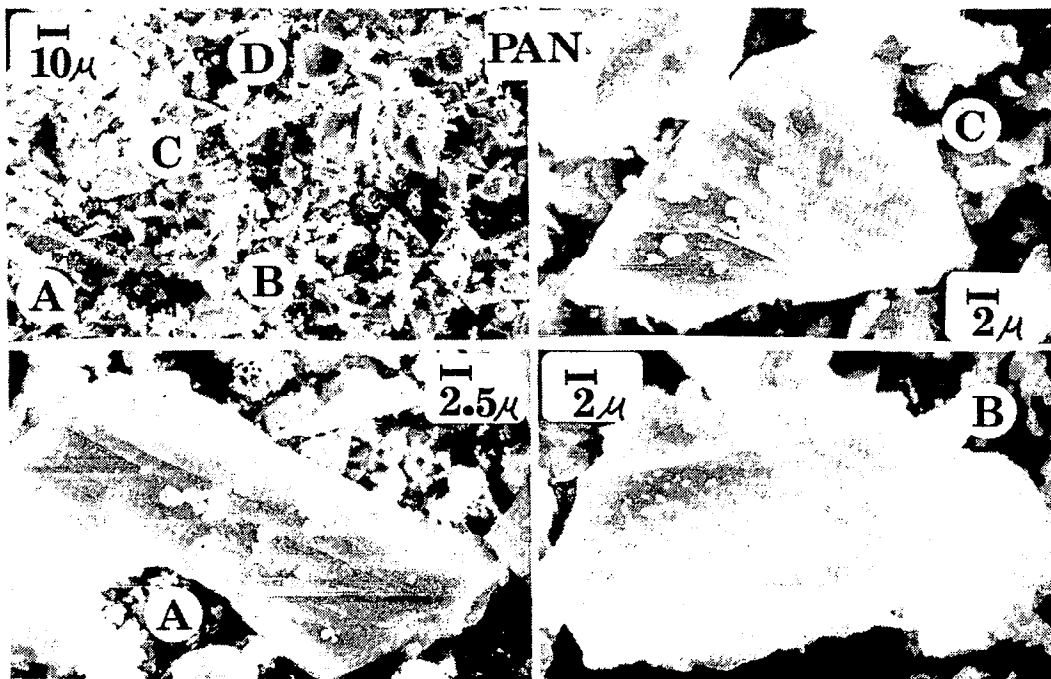


Figure 6. SEM images of the finest size split, finer than 5.50. A, B, C, and D are all glass shards with similar compositions.

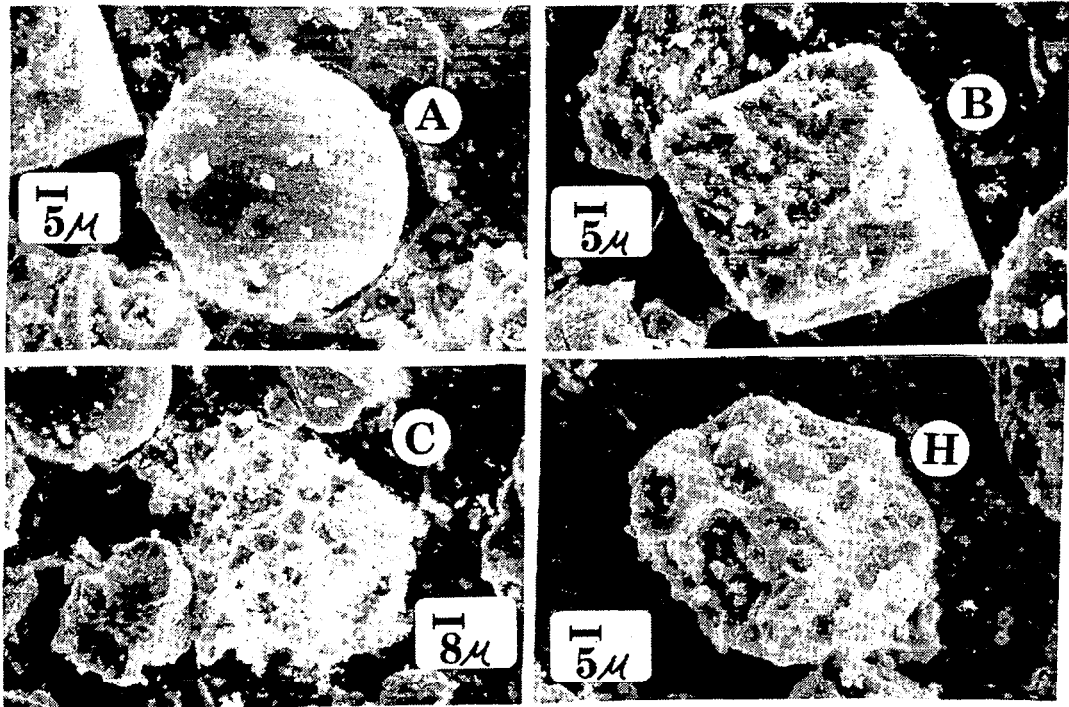


Figure 7. SEM imagery of ash particles which fell at Bloomfield, Colorado. This ash was rather well sorted with mostly 30 μm particles. A is a silicate particle, with less K and more Ti than St. Helens glass. It is fly ash contaminant. B is a plagioclase fragment and C and H are suspected to be vesicular Mount St. Helens glass.

VOLCANOES AND CLIMATE

Owen B. Toon

Space Science Division, NASA-Ames Research Center, Moffett Field, CA

The evidence that volcanic eruptions affect climate is reviewed. Single explosive volcanic eruptions cool the surface by about 0.3°C and warm the stratosphere by several degrees. Although these changes are of small magnitude, there have been several years in which these hemispheric average temperature changes were accompanied by severely abnormal weather. An example is 1816, the "year without summer" which followed the 1815 eruption of Tambora. Volcanic eruptions often occur in sequence. There is little evidence that sequences of volcanic eruptions cause ice ages. However, the period from 1500 to 1912 was one with many eruptions. Not a single large eruption which affected the Northern Hemisphere has occurred since 1912. The "Little Ice Age" which occurred between 1500 and 1900 and the warming which occurred between 1900 and 1940 correlate better with the record of volcanic activity than with any other possible cause of climatic change such as solar luminosity variations. In addition to statistical correlations between volcanoes and climate, a good theoretical understanding exists. The magnitude of the climatic changes anticipated following volcanic explosions agrees well with the observations. Volcanoes affect climate because volcanic particles in the atmosphere upset the balance between solar energy absorbed by the Earth and infrared energy emitted by the Earth. These interactions can be observed. The most important ejecta from volcanoes is not volcanic ash but sulfur dioxide which converts into sulfuric acid droplets in the stratosphere. For an eruption with its explosive magnitude, Mount St. Helens injected surprisingly little sulfur into the stratosphere. The amount of sulfuric acid formed is much smaller than that observed following significant eruptions and is too small to create major climatic shifts. However, the Mount St. Helens eruption has provided an opportunity to measure many properties of volcanic debris not previously measured and has therefore been of significant value in improving our knowledge of the relations between volcanic activity and climate.

I. INTRODUCTION

Benjamin Franklin may have been the first scientist to suggest that volcanic explosions might affect the weather. In May 1784 he wrote (1),

During several of the summer months of the year 1783, when the effects of the sun's rays to heat the Earth in these northern regions should have been the greatest, there existed a constant fog over all Europe, and great part of North America. This fog was a permanent nature; it was dry, and the rays of the sun seemed to have little effect toward dissipating it, as they easily do a moist fog arising from the water. They were, indeed, rendered so faint in passing through it that, when collected in the focus of a burning glass, they would scarce kindle brown paper. Of course, their summer effect in heating the earth was exceedingly diminished.

Hence, the surface was early frozen.

Hence, the first snows remained on it unmelted, and received continual additions.

Hence, perhaps the winter of 1783-1784 was more severe than any that happened for many years.

The cause of this universal fog is not yet ascertained. Whether it was adventitious to this earth, and merely a smoke proceeding from the consumption, by fire, of some of those great burning balls, or globes, which we happen to meet with in our course round the sun, and which are sometimes seen to kindle and be destroyed in passing our atmosphere, and whose smoke might be attracted and retained by our earth or whether it was the vast quantity of smoke, long continuing to issue during the

summer from Hecla, in Iceland, and that other volcano which arose out of the sea near the island, which smoke might be spread by various winds over the northern part of the world, is yet uncertain.

It seems, however, worthy the inquiry, whether other hard winters, recorded in history, were preceded by similar permanent and widely-extended summer fogs. Because, if found to be so, men might, from such fogs, conjecture the probability of a succeeding hard winter, and of the damage to be expected by the breaking up of frozen rivers in the spring and take such measures as are possible, and practicable, to secure themselves and effects from the mischiefs that attend the last.

Franklin noted that the “dry fog” from the volcanic eruption (or passing comet) preceded the bad winter of 1783—a statistical connection between volcanic eruptions and climate. More importantly he advanced a hypothesis to explain how the volcanic “fog” affected the weather. Franklin thought that the fog prevented sunlight from reaching the surface—which he was able to qualitatively demonstrate with his magnifying glass. He reasoned that with less sunlight available the surface should cool off.

Since Franklin’s observations many other scientists have studied the relation between volcanic explosions and weather. Most of these studies have consisted of statistical correlations between bad weather and single eruptions or between climatic anomalies and series of volcanic explosions. These studies do show that during many years with abnormal weather, such as 1783, there were volcanic perturbances. In addition, the major climatic shifts of the past 500 years occurred in parallel with variations in the level of volcanic activity. On the other hand, there is no evidence that volcanic explosions preceded and initiated the ice ages. Many years of abnormal weather—such as 1976 to 1978 when there were droughts in the Western United States and heavy snows in the Eastern United States—occurred without evidence of any major volcanic explosions. Volcanic eruptions are not responsible for all climate change nor all years of bad weather, but they may cause some of them.

These statistical studies have been augmented by theoretical calculations of the effects of volcanic eruptions on climate, and by measurements of the properties of volcanic debris. Some ways in which volcanoes affect the weather are understood. Benjamin Franklin’s basic idea has been made quantitative and the magnitude of the weather and climate changes observed has been found to be consistent with the theory. Of all the potential causes of climate change, volcanic eruptions are the best understood and best documented. This understanding, and the fact that a volcanic eruption establishes a unique time marker to identify when a perturbation occurs, makes volcanic explosions attractive to test the ability of models to calculate climate changes correctly.

In the following section, first a description in greater detail of the statistical evidence is made for a relation between volcanic explosions and climate changes. Then the mechanisms, by which the explosions affect climate, the observed properties of volcanic debris, and the theoretical models of the link between volcanic eruptions and climate are reviewed. Finally, the eruption of Mount St. Helens and its climatic implications are discussed.

II. STATISTICAL RELATIONS BETWEEN VOLCANIC EXPLOSIONS AND CLIMATIC CHANGES

A. Changes Observed After Single Eruptions

Mount Agung, the sacred mountain of the Indonesian island of Bali, erupted in March of 1963, killing over 1500 people and creating what National Geographic called a “Disaster in Paradise” (2). This eruption is the only large one to have occurred anywhere in the world since 1912. The debris from the eruption and its direct effect on the atmosphere were mainly restricted to the Southern Hemisphere. As discussed in greater detail by Newell¹, stratospheric temperatures increased after the eruption of Mount Agung and tropical surface temperatures decreased.

¹Reginald E. Newell, personal communication.

Figure 1 presents stratospheric temperatures during the period of the Agung eruption from radiosonde flights at a range of latitudes (3). The temperature of the stratosphere undergoes a quasi-biennial oscillation with an amplitude of about 1°C . In the Northern Hemisphere, the oscillation showed no marked change at the time of the Agung eruption (noted by an arrow). Very close to the equator, the stratospheric temperature increased following the Agung eruption, but the quasi-biennial oscillation had been steadily increasing in amplitude for several years so the increased temperature could have been part of that trend. However, in the Southern Hemisphere, where the quasi-biennial oscillation had rather constant amplitude, stratospheric temperatures did increase dramatically after the Mount Agung eruption. These trends are consistent with the observed spread of the dust. Very little dust entered the Northern Hemisphere, whereas heavy concentrations of volcanic dust were found in the Southern Hemisphere (4). As will be shown the magnitude of the warming observed after the Mount Agung eruption is consistent with theoretical calculations. The warming is mainly due to the absorption of terrestrial infrared energy by the volcanic aerosols, and a smaller contribution due to absorption of sunlight by the volcanic aerosols in the stratosphere.

Changes in tropospheric temperatures during the period of the Agung eruption were discussed by Angell and Korshover (5). Figure 2 presents the departures of the yearly mean temperature from the long term mean at the surface and between 800 and 300 mbar, for the Northern Hemisphere extratropics (30°N to 90°N), the tropics (30°N to 30°S), and the Southern Hemisphere extratropics (30°S to 90°S). In the troposphere and at the surface a cooling occurred worldwide after the eruption of Mount Agung. Although the temperature decreases at the surfaces are larger than the standard deviations of the data and are correlated between the three latitude regions, the temperature changes are not unusual in magnitude. It is interesting to note that the largest temperature decrease at the surface (0.6°C) following the Agung eruption occurred in the Northern Hemisphere and therefore could not have been caused directly by the volcanic dust. The atmospheric cooling was greatest (0.7°C) in the Southern Hemisphere extratropics.

The Mount Agung eruption is the only one for which stratospheric temperatures were observed. However, surface temperature records and indirect measures of surface temperature are available for several centuries. Several studies have been made to determine whether a surface cooling, such as observed after the Agung eruption, occurred after all eruptions. Numerous scientists beginning with Humphreys (1) found that a surface cooling does generally occur after large eruptions. Lamb (6) felt the cooling was so diagnostic that he used it to develop his dust veil index to rate the magnitudes of eruptions. For example, he ascribes a hemispheric cooling of 0.4°C to the eruption of Agung, 0.3°C to the 1912 eruption of Katmai, 0.6°C to the sequence of eruptions occurring from 1902 to 1904, and 0.5°C to the 1883 eruption of Krakatoa. Bray, Mass and Schneider, and Miles and Gildersleeves have made statistical studies of the temperature changes observed after the largest eruptions since 1811 (7-9). An example from Mass and Schneider (8) is shown in figure 3. They found an average temperature decrease of 0.3°C in the year after the eruption and 0.1°C or more 2 years after the eruption. In only a few cases did the temperatures increase after a major eruption. All the studies concluded that there was only about a 1 percent change in temperature, that the cooling after the eruptions was accidental, and that it was not the result of the eruption.

The climate changes which occurred after the individual eruptions may seem to be small, but these hemispheric temperature changes are often accompanied by much larger local variations. For example, Arakawa et al. (10) found that bad harvests in Japan prior to 1912 occurred frequently after large eruptions because of cool summers and early frosts. Lamb (11) states that all the years of very early fall frosts, as recorded by frost-damaged rings of trees in the Swiss Alps and in California, were years following the major volcanic eruptions.

Perhaps the most famous example of a volcanic eruption which had a profound effect on weather is that of Tambora. The Tambora eruption of 1815 killed about 50,000 people in Indonesia in the most violent eruption of recorded history. The following year became known as "The year without summer" or "Eighteen hundred and froze to death." Summer temperatures were 1 to 2.5°C cooler than normal throughout New England and Western Europe (12). The general cooling however, was accompanied in New England by snow during June, a frost in mid-July and then an early fall frost beginning in late August (13,14). The frost killed crops in New England, the price of corn shot upward and the winter of 1816 was one of great hardship. Many people moved to warmer regions of the United States after 1816 and added to the general migration from New England during the early 1800's. It was likewise cold in Britain, France, and Germany during 1816. Europe was just beginning its recovery from the Napoleonic wars; the battle of

Waterloo was fought during 1815. The bad weather led to crop failure, famines, and riots. The price of wheat in France was higher during 1817 than at any other time during the period from 1801 to 1912.

The bad weather of 1816 was not only of great importance to the people of that era, but it still has an impact on us today. Mary Shelley went on a summer vacation to Lake Geneva during 1816 with her poet friend Lord Byron and her soon-to-be husband Percy Shelley. The rainy, chilly summer prevented them from going outdoors and to relieve the boredom they began to tell ghost stories. A ghost story writing contest developed and Mary wrote Frankenstein. So out of the rain and cold a monster and a thousand monster movies were begun.

B. Changes Observed During Epochs of Volcanic Activity

Numerous scientists, noting that single volcanic eruptions have been followed by cooler weather during the year or two after the eruption, have attempted to correlate periods of intense volcanic activity with epochs of cold weather. For many years volcanoes were considered a prime candidate for initiating ice ages. However, this idea has not stood the test of time. On the other hand, there is good evidence that suggests that the climatic shifts of the last few hundred years have occurred in parallel with variations in the level of volcanic activity.

The volcanic theory of ice ages has suffered a decline in popularity for two reasons. First, the ice age record has greatly improved. It is now clear that there have been a large number of glacial advances during the previous few million years, and that these glacial advances have been highly periodic. The period of the ice ages corresponds well with the period of changes in the Earth's orbit (15), but there is no evidence that volcanic activity is highly periodic. Second there is a detailed record of volcanic activity during the previous glacial advance which shows that there was no increase in volcanic activity at the beginning of the glacial advance.

The record of volcanic activity during the last few million years comes partly from sea cores and partly from ice cores. Kennett and Thunell (16) counted the number of volcanic ash layers as a function of time in sea cores and presented evidence that the level of explosive volcanic activity had increased dramatically during the Quarternary when the glacial advances occurred (figure 4). However, these data are not sufficient to determine whether the volcanic activity caused the ice advance. It is even possible that the large changes in the mass of ice on the continents might have caused a variation in the level of volcanic activity.

During the Wisconsin glacial cycle which took place over the past 100,000 years, a record of climate and a record of volcanic activity were preserved in the Greenland and Antarctic polar caps. Ice cores from both poles showed no enhancements of particles during the early stages of the Wisconsin cycle and indicated that an epoch of volcanic activity did not trigger the ice age (Figure 5). Although there is a large increase in particle concentrations in the Greenland core when oxygen isotope ratios show the glacial maximum had been reached, the particles are not of volcanic origin but rather are windblown dust probably created by the ice sheets (17). In Antarctic ice (Figure 5) the ice sheets do record a remarkable amount of explosive volcanic activity over a 15,000 year period at the maximum of the Wisconsin ice age (18). Volcanoes may have affected the weather at the maximum of the ice age, but there is currently no evidence that they initiated the Wisconsin ice age.

The record of volcanic activity during the previous several hundred years has been statistically compared with the record of climate by a large number of workers. The meaning of these comparisons depends in part upon the reliability of the climate record and the reliability of the record of volcanic activity.

The record of volcanic activity comes from a variety of sources. Lamb (6), in his classic paper, attempted to identify all the major volcanic eruptions since 1500 from geologic records, direct observations of the explosions, or indirect observations of atmospheric phenomena. He then rated the importance of the eruption according to his dust veil index using the amount of material ejected by the volcano, the temperature decrease observed following the eruption or, after 1880, the decrease in transmission of sunlight observed following the volcanic eruption. Only the latter criteria is a direct measure of the magnitude of the eruption. Clearly, this method of rating volcanic activity is somewhat subjective. Mount St. Helens provides an example of an eruption which, if it had taken place before 1880, could have been improperly assessed by Lamb's

index. Mount Agung likewise has great uncertainty in its proper dust veil index being rated between 200 and 800 by various workers.

An alternate method of determining the level of volcanic activity is to search polar ice cores for changing levels of volcanic debris, mainly sulfates. Some difficulties with the polar core record are that to be detected the volcanic sulfate must exceed the background level of natural sulfate in the atmosphere, and that local volcanic activity may be weighted above more remote activity. Hammer (19) shows that the two techniques of assessing the volcanic record since 1770 do differ in detail. Both records, however, show that very few explosive volcanic eruptions have occurred since 1912, but prior to 1912 there were very many eruptions of significant magnitude. In addition, Lamb (6) finds that the most heavily perturbed periods since 1500 were from about 1750 to 1850 and from about 1880 to 1900. It would be useful to extend the polar core data to the period before 1770.

The climate record prior to 1900 is also not well known. Three types of climate records have been compared with the volcanic record, as well as with the record of solar activity which has also long been suspected of being linked to climate changes.

First, Lamb (6) and Bray (20) show that the maximum level of volcanic activity, as measured by the dust veil index, coincided with the maximum extent of sea ice near Iceland and the maximum number of glacial advances in the Northern Hemisphere (Figure 6) (21). These maxima occurred around 1800. Presumably, sea ice and glaciers are good integrators of shifts in climate over periods of many years.

Second, Lamb (6), Schneider and Mass (22) and Robock (23) among many others going back at least to the beginning of this century have tried to correlate the record of volcanic activity with short-response time-climate records extending back to about 1600. Lamb, as well as Schneider and Mass, primarily refer to high Northern latitude temperature records, especially those from England, and find that a cool period in the early 1800's and the warming at the beginning of the twentieth century correlate well with the volcanic record. However, both authors feel that the coldest period occurred during the middle of the 17th century which corresponds to the Maunder minimum in sunspots. Robock (23), on the other hand, studied a new temperature curve that is supposed to represent the entire Northern Hemisphere back to 1600. This newer curve does not show the 17th century to have been abnormally cool and therefore shows no correlation with the Maunder minimum. Indeed these hemispheric data suggest the early 1800's were the coldest period of the Little Ice Age. Robock (23) concludes that volcanic activity correlates well with the temperature records of the past 400 years, whereas solar activity does not.

One final comparison between volcanic activity and climate has been based upon the warming trend between the late 1800's and the mid-1900's which correlates well with the decline in volcanic activity. The importance of this correlation is that both the temperature record and the record of volcanic activity are well known during this period. Nearly all the investigators cited above agree that the correlation is very good. One major point of argument has been the time lag between the volcanic activity and the climate variation. The volcanic activity ceased around 1912 but temperatures did not reach their maxima until about 1940. This period seemed too long a delay to Miles and Gildersleeves (9) but seemed quite reasonable to Robock (24). An additional often mentioned problem is that the Northern Hemisphere cooling which occurred after 1940 does not correlate with an increase in volcanic activity; thus, at least the most recent portion of the climate record has not been controlled by volcanoes.

Statistical studies of the relations between climate and volcanic activity do show that large volcanic eruptions have an effect on the hemispheric mean temperature in the year following eruption. Furthermore, the level of volcanic activity correlated better than any other factor with the envelope of climate variability during the previous 500 years. An important point, that is often overlooked however, is that the link between volcanoes and climate is not just statistical. Unlike other potential causes of climate variability, such as solar luminosity fluctuations, the effects of volcanoes on climate can be quantified because their effects on the Earth's radiation balance can be measured.

III. THEORETICAL RELATIONSHIPS BETWEEN VOLCANIC EXPLOSIONS AND CLIMATE

The Earth's climate is controlled by a balance between solar energy which is absorbed by the atmosphere and surface, and infrared energy which is radiated back to space by the Earth's surface and atmosphere. This balance can be upset by the particles which large volcanic explosions inject into the atmosphere.



Unusual optical phenomena, often reported for a year or two following large eruptions, provide direct visual evidence that volcanic particles affect sunlight. These phenomena include a bright colored ring around the Sun and Moon, called the Bishop's ring after the Rev. Bishop who first reported it following the Krakatoa eruption. Sometime after an eruption the sun and moon appear to be blue or green, and this effect gives rise to the phrase "once in a blue moon." In addition, the sky color may shift from its normal deep blue to milky white. The most vivid signs that particles affect sunlight are the brilliant twilight colors which follow even minor explosive eruptions. Such colors were seen after the eruption of Volcan de Fuego in 1974 as well as following the eruption of Mount St. Helens. There were so many eruptions in the first decades of the 19th century that the twilight may normally have been quite colorful. It has been suggested that the English romantic painter J.M.W. Turner recorded these volcanic twilights in his landscape scenes which became famous for their colorful skies. The explanations of these colored rings and tinted skies are to be found in simple applications of the theory of light scattering and the theory of gaseous absorption in the atmosphere (25).

Probably the most significant optical observation after an eruption is the decrease in the strength of the direct solar beam, which Franklin first measured indirectly with his magnifying glass. Figure 7 presents a compilation of measurements of the perturbed optical depth of volcanic explosions. The optical depth is the logarithm of the transmission of light through the atmosphere. These measurements show that single eruptions are able to reduce the strength of the direct solar beam over large areas of the Earth by 25 percent for a month or two and by 10 percent for periods of a year or more. The visible optical depth of aerosols in the Earth's lower atmosphere is about 0.125; thus volcanic eruptions can more than double the total aerosol optical depth of the atmosphere (26).

In order to theoretically determine the net effect of the volcanic particles on the radiation budget, several aerosol properties must be known as discussed in detail by Toon and Pollack (26,27). First, the quantity of aerosol needs to be known. This could be determined by measuring the aerosol concentration from an airplane or the optical depth from a ground station but it is best done from satellites such as SAGE and SAM. The advantage of satellites is that global coverage is obtained, and contamination of the measurements by tropospheric aerosols is easily avoided. Second, the wavelength dependence of the aerosol opacity is needed to determine the relative effects of the aerosols on visible and infrared light. This effect is now best determined by measuring the aerosol size distribution and using Mie theory to calculate the dependence of the opacity on wavelength. Direct measurements could be made far into the infrared with current instruments which would provide an interesting check upon the calculations. Third, the angular scattering properties of the aerosols need to be determined in order to quantify the amount of sunlight forward scattered. Presently, the scattering phase function can only be calculated by using measured aerosol size distributions, but it will soon be possible to measure it by using aircraft-borne nephelometers. Finally, it is necessary to determine the optical constants of the aerosols in order to calculate the opacity and phase function as well as to determine the amount of light absorbed by the aerosols. The optical constants can be determined indirectly by finding the optical constants of the chemicals which compose the aerosols. This approach works well for infrared wavelengths, but the visible absorption may be dominated by minor impurities. Direct laboratory measurements using collected aerosols are needed in order to accurately determine the visible absorption. Measurements made after the Mount St. Helens eruption have greatly added to our knowledge of all these properties. Prior to the eruption of Mount St. Helens, the information was restricted to the quantity of aerosols and a crude knowledge of their composition.

Explosive volcanic eruptions inject large quantities of volcanic ash and gas into the stratosphere where the material may remain for a few years. The material slowly falls into the troposphere where it is removed by rainfall in a short time. Figure 7 provides a good measure of the typical period during which a significant quantity of dust remains in the stratosphere.

Large eruptions may inject several cubic kilometers of volcanic ash into the atmosphere, most of which quickly falls to the ground (6). From observations of the optical depth of volcanic debris once the debris has spread over a large area of the Earth (Figure 7) the total volume of volcanic material in the stratosphere can be fairly accurately determined. The volume after large eruptions, such as those of Agung, Katmai, and Krakatoa, range from 0.008 to 0.03 km³ (25). Since these volumes are only 0.1 percent to 1 percent of the total ejected volume, it might be imagined that most of the volcanic debris was composed of ash. However,

this does not seem to be the case. Rather most of the debris is apparently composed of a sulfate, probably sulfuric acid.

The evidence for the importance of sulfates is circumstantial. After the modest eruption of Volcan de Fuego in 1974, the aerosols were found to have a volatility similar to the normal stratospheric acid droplets (28). Gandrud and Lazrus (29,30) measured a large increase in sulfate after the Fuego eruption that was sufficient to account for the increased aerosol mass. After the powerful eruption of Mount Agung in 1963, Castleman et al. (31) found a large decrease in sulfates in the Southern Hemisphere stratosphere. At 40°S latitude, the mass of sulfate at an altitude of about 18 km reached a maximum of about 30 ppbm roughly 6 months after the eruption (Figure 8). The equivalent hemispheric sulfate volume is very close to the 0.01 km³ of aerosol estimated from the optical depth. Moreover figure 8 shows that the change in optical depth closely paralleled the change in sulfate mass at the same latitude. Collections of stratospheric debris following the Agung eruption were made by Mossop (32). Although he could not quantify the ratio of silicate to sulfate, he felt that sulfate was clearly dominant one year after the eruption. From Mossop's silicate data an approximate silicate mass can be obtained. As figure 8 shows, the silicate mass is much less than the sulfate mass a few months after the eruption.

The Mount St. Helens eruption is the first one for which the silicate to sulfate ratio has been determined and the first one for which the gas phase and particulate sulfur have both been measured. Hobbs et al. (33) measured the SO₂ content of the tropospheric volcanic plume on May 18th and found only modest quantities. Inn et al. (34) and Gandrud and Lazrus (30) measured SO₂ and sulfate in the stratosphere. The mixing ratio of the total of gas phase and particulate sulfur even in the dense plume was only an order of magnitude larger than that found for the whole stratosphere after the Agung eruption. Within a few days, as the plume dispersed slightly, the mass mixing ratio was comparable with Castleman et al.'s (31) measurements after the Agung eruption. The Mount St. Helens eruption seems to have injected a surprisingly small quantity of sulfur into the stratosphere. Hence, the geologic aspects of the eruption, particularly the sulfur content of the magma, may have played the most significant role in determining the impact of the Mount St. Helens eruption on climate.

The silicate to sulfate ratio has been reported so far only for the first few days after the Mount St. Helens eruption (35). Four days after the eruption the mass of ash and sulfate were comparable, but the sulfate mass was rapidly increasing due to chemical conversion of gas phase sulfur and the silicate mass was rapidly decreasing as the large rock particles fell out of the stratosphere. The evolution of silicate and sulfate provide important tests for stratosphere aerosol models which may allow the models to "scale" the Mount St. Helens eruption up and project the behavior of an eruption ejecting large quantities of sulfur.

Sulfate probably dominates over silicate by mass in the volcanic dust veil, but even a small amount of silicate could control the absorption of sunlight if the silicate is moderately absorbing. The visible single scattering albedo following the Mount St. Helens eruption was found to be 0.98 or greater by Ogren et al. (36). This value is consistent with the values expected by Toon and Pollack (26) for either volcanic glasses or mixtures of volcanic glasses with sulfuric acid. Other investigators have suggested that volcanic ash would be much more highly absorbant.

The size distribution of volcanic aerosols is required to calculate both the opacity as a function of wavelength and the angular scattering pattern. Several size distributions have been measured following the Mount St. Helens eruption, but have not yet been studied for their radiative properties. However, it is known that volcanic aerosols are strongly forward scattering so that much of the light missing from the direct solar beam still reaches the ground as diffuse skylight (figure 9). Since volcanic particles are large enough to scatter visible colors fairly efficiently, the sky appears milky white rather than blue after large eruptions. Dyer and Hicks (37) present observations of the direct, diffuse, and the total skylight in Australia after the Mount Agung eruption. Although the direct solar beam was reduced by nearly 25 percent, the diffuse skylight doubled so that the total sunlight reaching the surface was only slightly diminished (figure 9). No measurements have been made of the effects of volcanic aerosols on infrared energy, but theoretical studies by Pollack et al. (38, 39), among others have shown that the aerosols are large enough to perturb the infrared energy significantly. Indeed Pollack et al. (38,39) found that particles larger than 0.5 m could actually have such a large effect on the infrared that they could warm the surface instead of cooling it (figure 10). Since the particles initially injected by volcanoes may be larger than 0.5 m, the evolution of the size distribution, as the large particles fall out, is of great significance to the overall climatic effect.

Numerous theoretical studies have been conducted on the effects of volcanic aerosols on climate. Humphreys (1) argued that the volcanic particles were so small that they would backscatter to space half the solar radiation they intercepted, and they would not affect infrared radiation. He then deduced that a cooling of 6° to 7°C would occur after a large eruption. Humphrey's basic assumptions about backscattering being large and the effects on infrared light being small were wrong. In fact most of the light is forward scattered, and the effects of the particles on infrared light nearly compensate those on visible light. Pollack et al. (38-40) discuss the sensitivity of the calculations to many of the assumed parameters such as single scattering albedo and particle size. Figure 10 shows some of their calculations. Large silicate particles may warm the surface. Small sulfuric acid particles may lead to a cooling which linearly increased with optical depth. An optical depth of 0.02 to 0.03 is needed to cause a barely observable change in temperature.

Hansen et al. (41) calculated the time evolution of the stratospheric and tropical tropospheric temperatures following the eruption of Mount Agung. Figure 11 shows that their calculated temperatures agree favorably with the observed ones. In their model, as well as in earlier calculations (Pollack et al., 38,39) it was found that the absorption of infrared energy by the volcanic particles was the major factor in warming the stratosphere. The troposphere cooled because the volcanic particles reflected a small amount of sunlight back to space that would otherwise have reached the surface. Hansen et al. (41) as well as Pollack et al. (38,39) assumed the volcanic particles were largely sulfuric acid and had a size distribution that is identical to nonvolcanic size distributions (26). The Mount St. Helens eruption may provide the first opportunity to check these two important assumptions.

Pollack et al. (39) calculated the warming to be expected between the late 1800's and the middle of the 1900's due to the decline in volcanic activity which was illustrated in figure 7. The calculation was done by using the decade average optical depths to crudely represent the response time of the Earth-atmosphere system. As shown by figure 12, the increase in temperature due to the decline in volcanic activity is sufficient to match the observations. As discussed earlier, several workers have noted the statistical parallel between the volcanic activity and temperature record. These calculations show that the magnitude is also correct. Of course, further work must be done before it can be concluded that the decrease in volcanic activity was the actual cause of the warming trend between 1900 and 1940. It is interesting to note in figure 12 that the increasing level of CO₂ in the atmosphere should become a significant factor in the Earth's climate sometime during the next few decades.

IV. CONCLUDING REMARKS

A significant amount of evidence shows that single volcanic eruptions, which inject large quantities of sulfur dioxide into the stratosphere, are responsible for increasing stratospheric temperatures by several degrees and for cooling tropospheric temperatures by several tenths of a degree for a year or two following the eruption. On several occasions these small average temperature changes have been accompanied by severe local weather changes. Volcanic eruptions tend to occur in groups. The variations of volcanic activity during the previous 500 years have occurred in parallel with changes in climate. Although there are many possible causes of climate changes, including solar luminosity changes, volcanic activity is the best qualified agent of climate change, and shows the greatest correlation with the climate record.

The theory of the relation between volcanoes and climate is moderately well developed. The magnitude of calculated climate changes agrees well with observed changes. However, there are several uncertain parameters in the theory, most notably the volcanic particle size distribution and the visible single scattering albedo of the particles. New measurements of these properties after the Mount St. Helens eruption should significantly improve the theoretical models. The May 18 Mount St. Helens eruption was violently explosive. It injected an amount of ash into the lower atmosphere which was comparable with that of other eruptions which did create measurable changes in climate. However, the volcanic particles which affect climate are sulfates rather than silicates. The Mount St. Helens eruption seems to have been deficient in sulfur dioxide and therefore has not produced as large a number of particles as might have been anticipated. Figure 7 and Figure 10 show that major volcanic eruptions, with measurable effects on climate, usually have optical depths of several tenths. As discussed by the remote-sensing papers in this symposium, the eruption of Mount St. Helens produced an optical depth of several hundredths. Hence, because of its low sulfur emissions, Mount St. Helens probably will not produce a measurable shift in temperature and should be

rated with minor eruptions such as that of Volcan de Fuego. Nevertheless, measurements of the stratosphere particulates have greatly advanced the knowledge of volcanic debris and will help to resolve many of the outstanding problems in the theory of the connection between volcanic eruptions and climate.

REFERENCES

1. Humphreys, W.J., Physics of the Air, McGraw-Hill Co., 1940.
2. Booth, W.P., Matthews, S.W., and Sisson, R.F., Disaster in Paradise, Nat. Geo., Vol. 124, 1963, pp. 436-458.
3. McInturff, R.M., Miller, A.J., Angell, J.K., and Korshover, J., Possible Effects on the Stratosphere of the 1963 Mount Agung Volcanic Eruption, J. Atmos. Sci., Vol. 28, 1971, pp. 1304-1307.
4. Dyer, A.J., and Hicks, B.B., Global Spread of Volcanic Dust From the Bali Eruption of 1963, Quart. J. Meteor. Soc., Vol. 94, 1968, pp. 545-554.
5. Angell, J.K., and Korshover, K., Estimate of the Global Change in Temperature, Surface to 100 mb, Between 1958 and 1975, Mon. Wea. Rev., Vol. 105, 1977, pp. 375-385.
6. Lamb, H.H., Volcanic Dust in the Atmosphere With A Chronology and Assessment of its Meteorological Significance. Phil Trans. Roy. Soc. Lond., Vol. A266, 1970, pp. 425-533.
7. Bray, J.R., Vegetational Distribution, Tree Growth, and Crop Success in Relation to Recent Climatic Changes, Adv. Ecology Res., Vol. 7, 1971, p. 177.
8. Mass, C., and Schneider, S.H., Statistical Evidence on the Influence of Sunspots and Volcanic Dust on Long-Term Temperature Records, J. Atmos. Sci., Vol. 34, 1977, pp. 1995-2004.
9. Miles, M.K. and Gildersleeves, P.B., Volcanic Dust and Changes in Northern Hemisphere Temperature, Nature, Vol. 271, 1978, pp. 735-736.
10. Arakawa, A., Fujita, T., Ito, H., Masuda, Y., Matsumoto, S., Murakami, T., Ozawa, T., Suzuki, T., Takeuchi, M., and Tomatsu, K., Climatic Abnormalities as Related to the Explosions of Volcano and Hydrogen Bomb, Geophys. Mag. Tokyo, Vol. 26, 1955, pp. 231-255.
11. Lamb, H.H., Climate Present, Past and Future, Climatic History and the Future, Vol 2, Methuen, London, 1977.
12. Landsberg, H.E., and Albert, J.M., The Summer of 1816 and Volcanism, Weatherwise, Vol. 27, 1974, pp. 63-66.
13. Hoyt, J.B., The Cold Summer of 1816. Assoc. Am. Geog., Vol. 48, 1958, pp. 118-131.
14. Stommel, H., and Stommel, E., The Year Without Summer, Sci. Amer., Vol. 240, 1979, pp. 176-186.
15. Imbrie, J., and Imbrie, J.Z.Z., Modeling the Climatic Response to Orbital Variations, Science, Vol. 207, 1980, pp. 943-953.
16. Kennett, J.P., and Thunell, R.C., On Explosive Cenozoic Volcanism and Climatic Implications, Science, Vol. 196, 1977, pp. 1231-1234.
17. Thompson, L.G., Microparticles, Ice Sheets and Climate, Instr. of Polar Studies, Rep. 64 RF3416-A1, Ohio State Univ., 1977.
18. Gow, A.J., and Williamson, T., Volcanic Ash in the Antarctic Ice Sheet and its Possible Climatic Implications. Earth Planet. Sci. Lett., Vol. 13, 1971, pp. 210-218.
19. Hammer, C.U., Past Volcanism Revealed by Greenland Ice Sheet Impurities, Nature, Vol. 270, 1977, pp. 482-486.
20. Bray, J.R., Glacial Advance Relative to Volcanic Activity Since 1500 A.D. Nature, Vol. 248, 1974, pp. 42-43.
21. Koch, L., The East Greenland Ice, Medd. on Gronland, Vol. 130, 1945.
22. Schneider, S.H., and Mass, C., Volcanic Dust, Sunspots, and Temperature Trends, Science, Vol. 190, 1975, pp. 741-746.
23. Robock, A., The "Little Ice Age": Northern Hemisphere Average Observations and Model Calculations, Science, Vol. 206, 1979, pp. 1402-1404.
24. Robock, A., Internally and Externally Caused Changes. J. Atmos. Sci., Vol. 35, 1978, pp. 1111-1122.
25. Deirmandjian, D., On Volcanic and Other Particulate Turbidity Anomalies. Advan. Geophys. Vol. 16, 1973, pp. 267-296.
26. Toon, O.B., and Pollack, J.B., A Global Average Model of Atmospheric Aerosols for Radiative Transfer Calculations. J. Appl. Meteor., Vol. 15, 1976, pp. 225-246.

27. Toon, O.B., and Pollack, J.B., Atmospheric Aerosols and Climate, Amer. Sci., Vol. 68, 1980, pp. 268-278.
28. Hofmann, D.J., and Rosen, J.M. Balloon Observations of the Time Development of the Stratospheric Aerosol Event of 1974-1975, J. Geophys. Sci., Vol. 82, 1977, pp. 1435-1440.
29. Gandrud, B.W. and Lazrus, A.L., Long and Short Term Variability of the Stratospheric Sulfate Aerosol at High Latitudes. Geophys. Res. Lett., Vol. 8, 1981, pp. 21-22.
30. Gandrud, B.W. and Lazrus, A.L., Filter Measurements of Stratospheric Sulfate and Chloride in the Eruption Plume of Mount St. Helens, Science, Vol. 211, 1981, pp. 826-827.
31. Castleman, A.W. Jr., Munkelivitz, H.R., and Manowitz, B., Isotopic Studies of the Sulfur Component of the Stratospheric Aerosol Layer. Tellus, Vol. 26, 1974, pp.222-233.
32. Mossop, S.C., Volcanic Dust Collected at an Altitude of 20 km, Nature, Vol. 203, 1964, pp. 824-827.
33. Hobbs, P.V., Radke, L.F., Eltgroth, M.W., and Hegg, D.A., Airborne Studies of the Emissions From the Volcanic Eruptions of Mount St. Helens, Science, Vol. 211, 1981, pp. 816-818.
34. Inn, E.C.Y., Vedder, J.F., Condon, E.P., and O'Hara, D., Gaseous Constituents in the Plume of Mount St. Helen's Eruptions, Science, Vol. 211, 1981, pp. 821-823.
35. Vossler, T., Anderson, D.L., Aras, N.K., Phelan, J.M., and Zoller, W.H., Trace Element Composition of the Mount St. Helens Plume Stratospheric Samples from the May 18th Eruption, Science, Vol. 211, 1981, pp. 827-830.
36. Ogren, J.A., Charlson, R.J., Radke, L.F., and Domonkos, S.K., Measurements of Absorption of Visible Radiation by Aerosols in the Mount St. Helens Volcanic Plume, Science, 211, 1981, pp. 834-836.
37. Dyer, A.J., and Hicks, B.B., Stratospheric Transport of Volcanic Dust Inferred From Solar Radiation Measurements, Nature, Vol. 208, 1965, pp. 131-133.
38. Pollack, J.B., Toon, O.B., Sagan, C., Summers, A., Baldwin B., and VanCamp, W., Stratospheric Aerosols and Climatic Changes, A Theoretical Assessment, J. Geophys. Res., Vol. 81, 1976, pp. 1071-1083.
39. Baldwin, B., Pollack, J.B., Summers, A., Toon, O.B., Sagan, C., and VanCamp, W., Stratospheric Aerosols and Climatic Changes, Nature, Vol. 263, 1976, pp. 551-555.
40. Pollack, J.B., Toon O.B., and Wiedman, D., Radiative Properties of the Background Stratospheric Aerosols and Implications for Perturbed Conditions, Geophys. Res. Lett., Vol. 8, 1980, pp. 26-28.
41. Hansen, J.E., Wang, W., and Lacis, A.A., Mount Agung Eruption Provides Test of a Global Climatic Perturbation, Science, Vol. 199, 1978, pp. 1065-1068.

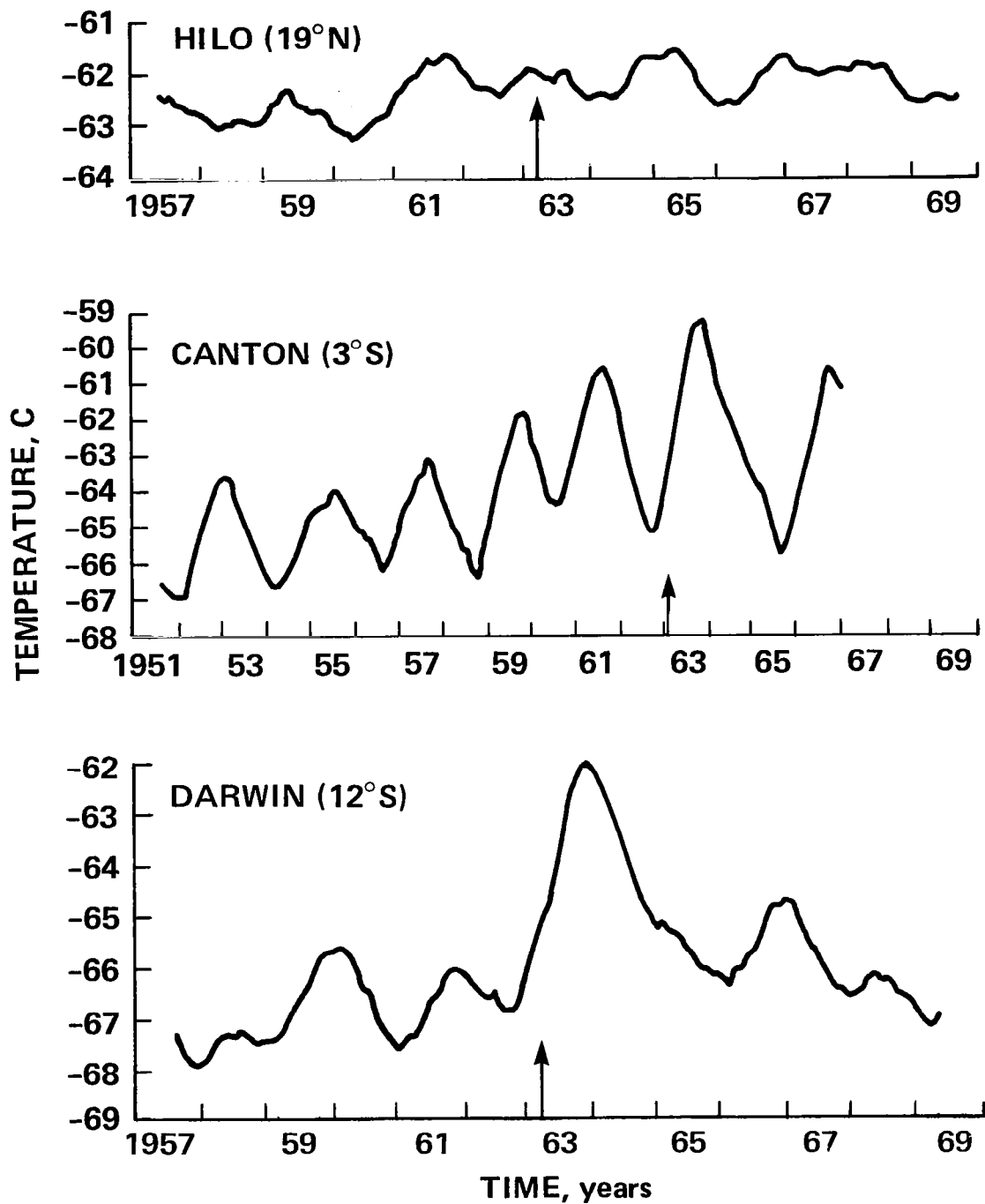


Figure 1. The temperature of the stratosphere at an altitude of about 20 km during the period of the Mount Agung eruption (3). Notice that only in the Southern Hemisphere can an unambiguous temperature increase be observed. The dust from Mount Agung was mainly restricted to the Southern Hemisphere. The arrow denotes the time of the Mount Agung eruption.

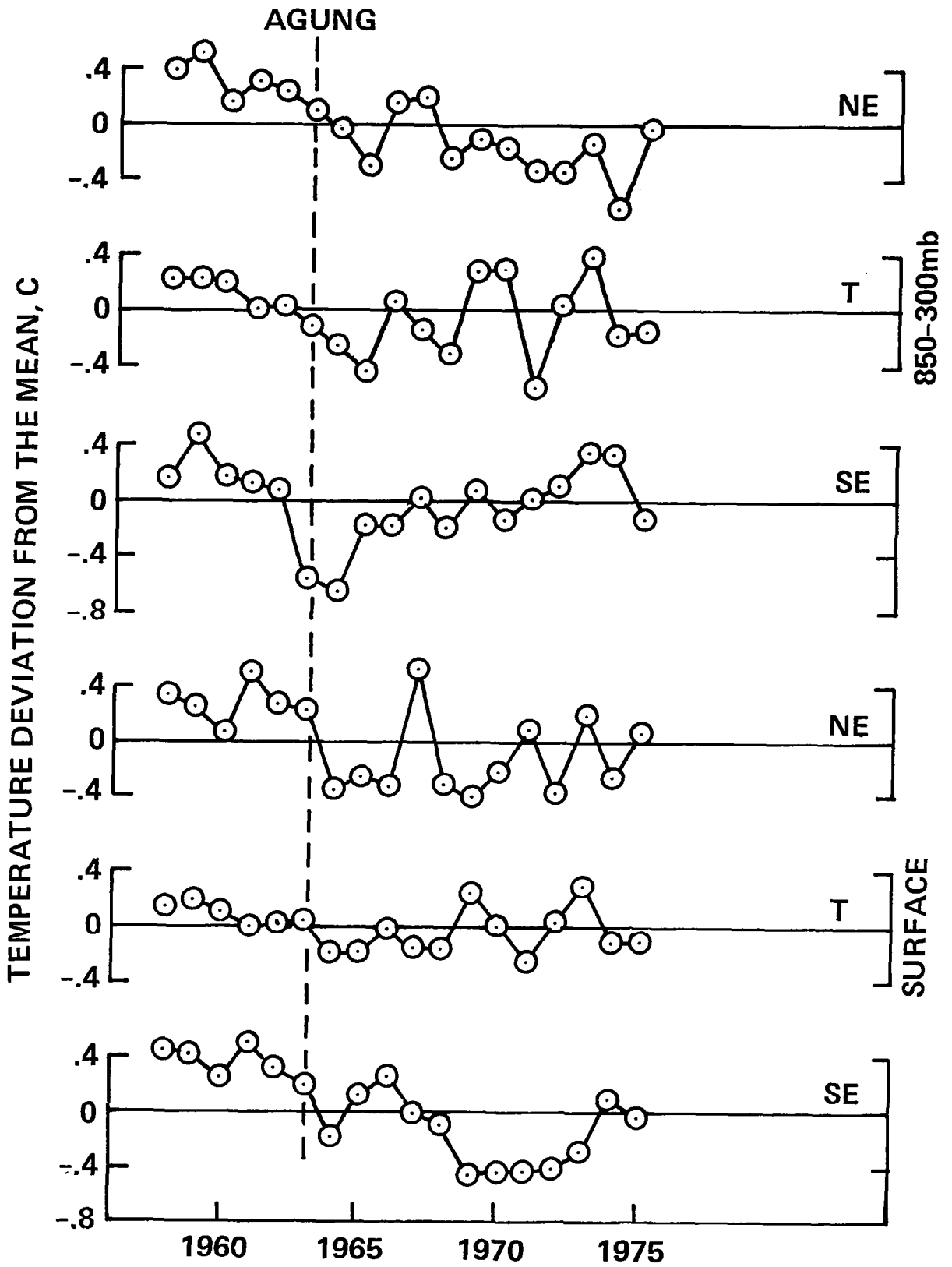


Figure 2. Time variation of the yearly temperature in the north extratropics (NE), tropics (T), and south extratropics (SE) at two heights during the period of the Mount Agung eruption. The dashed line denotes the year of the Mount Agung eruption. From Angell and Korshover (5).

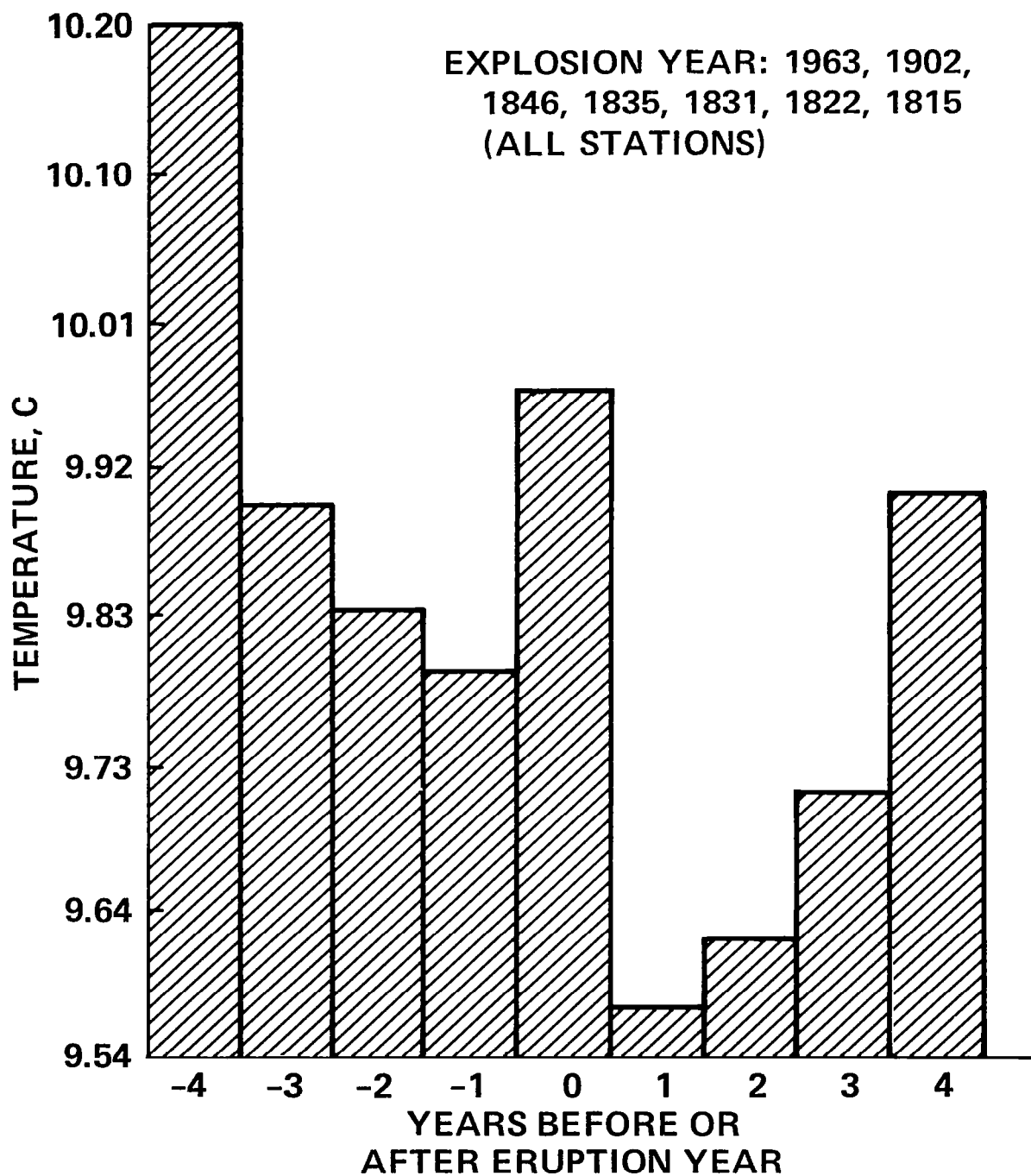


Figure 3. Mean temperature at a large number of stations during the years before and after several large eruptions. A statistically significant decrease of about 0.3°C occurs during the year following an eruption. From Mass and Schneider (8).

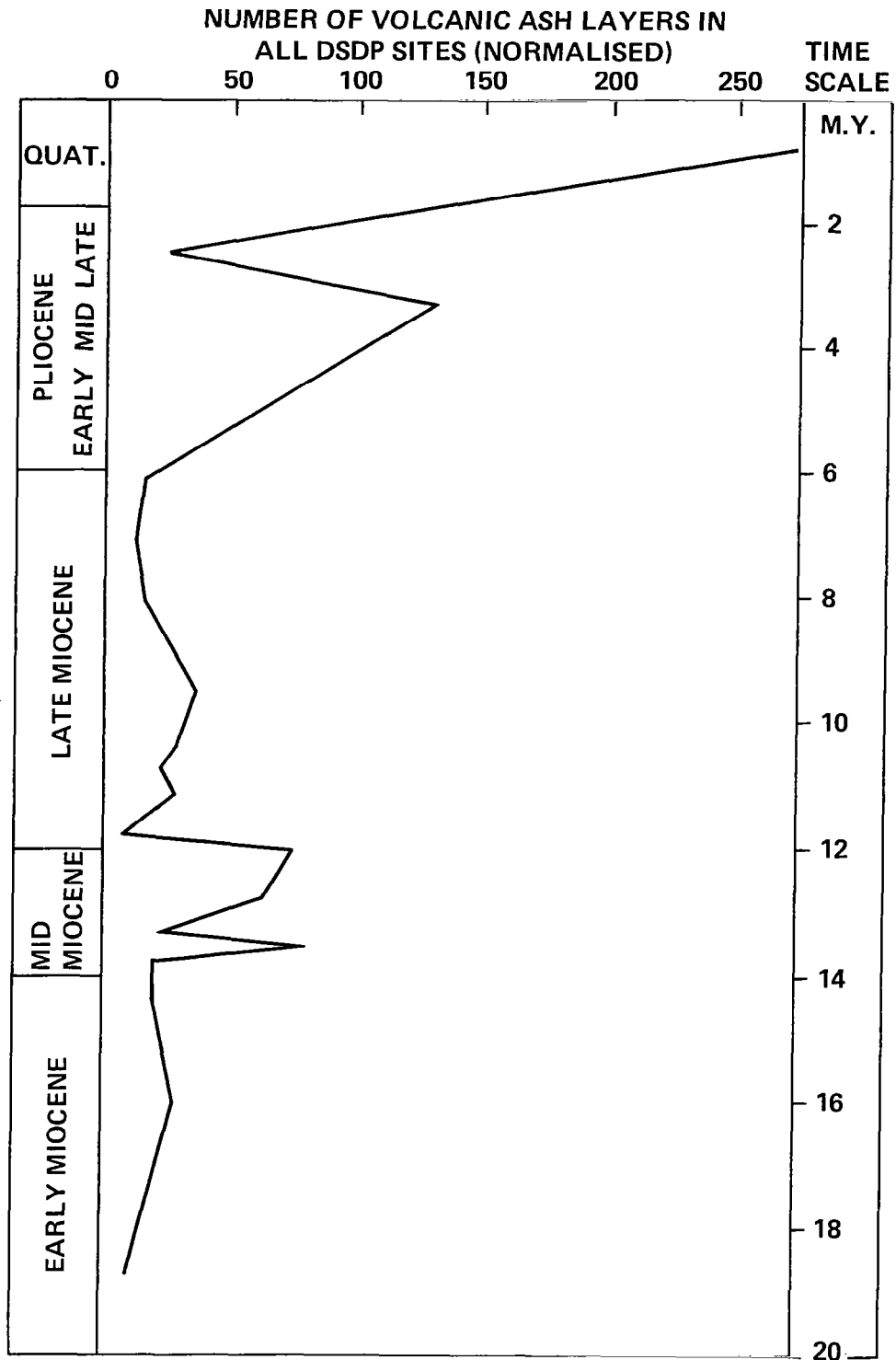


Figure 4. The record of explosive volcanic activity during the past 20 million years. During the ice ages the level of volcanic activity has increased. From Kennett and Thunell (16).

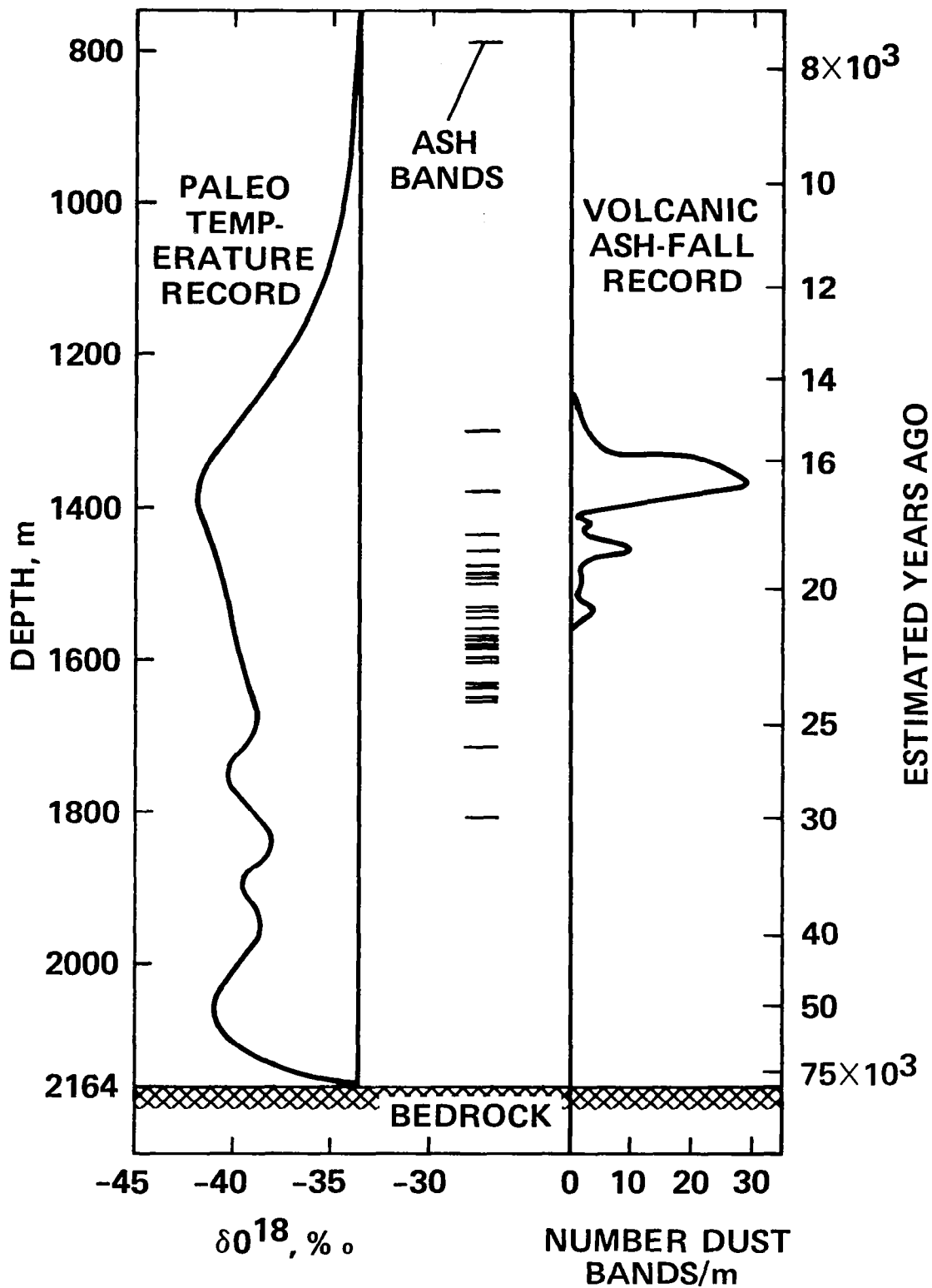


Figure 5. The record of explosive volcanic activity during the past 75,000 years as recorded in Antarctic ice (18). Note that many eruptions occurred at the maximum of the ice age 15,000 years ago, but none are recorded at the beginning of the ice age.

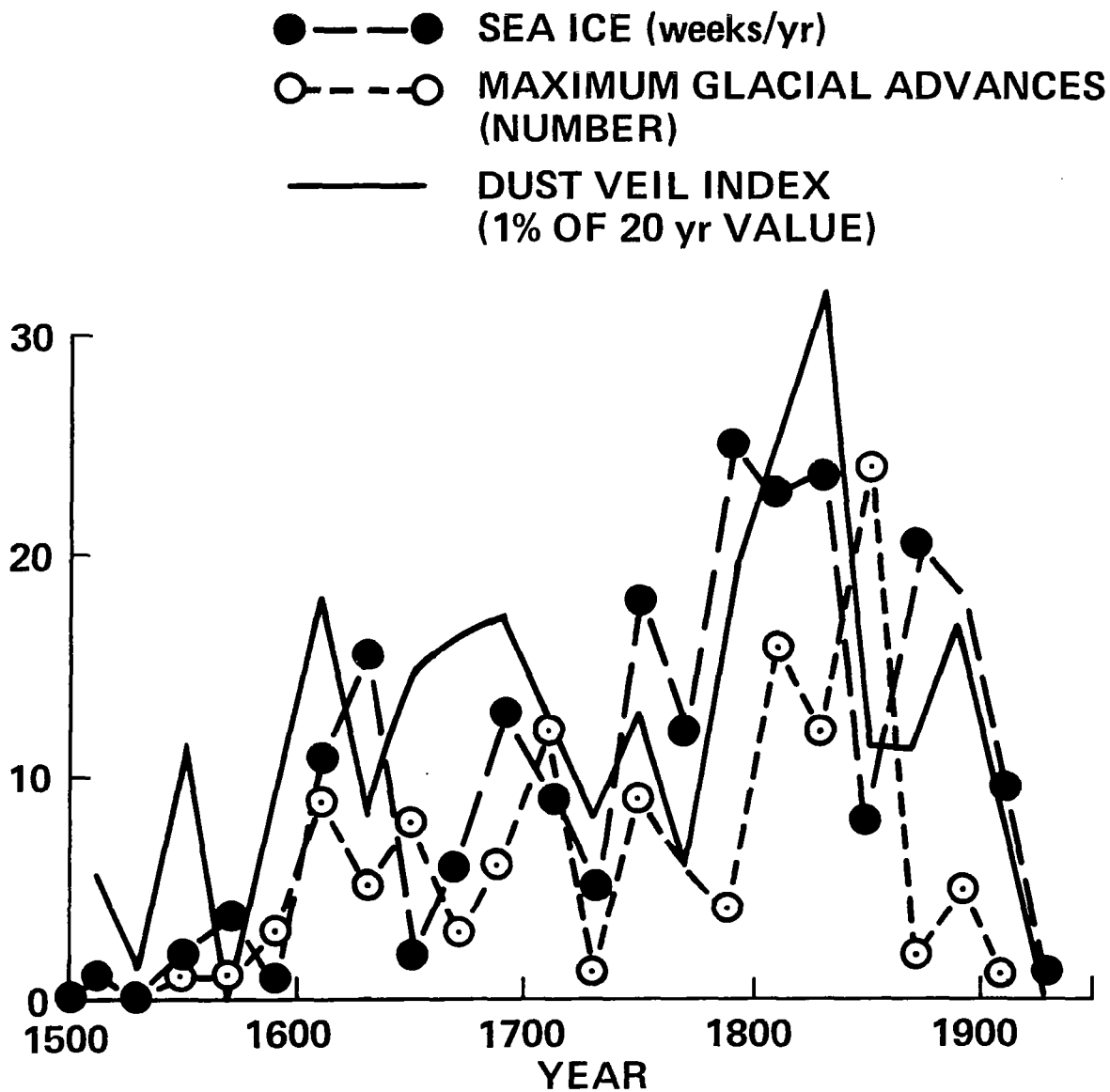


Figure 6. A record of volcanic activity during the past 500 years is compared with two climatic indicators. The volcanic activity is measured by Lamb's (6) dust veil index. The figure uses 20 year summations which must be multiplied by 100 to obtain the actual values in Lamb's tables. The number of weeks per year of Icelandic sea ice averaged over 20 year intervals is from Koch (21). Bray (7) compiled the number of maximum glacial advances at 20 year intervals. Note that the record of volcanic activity and ice extent compare favorably in detail. Each period of enhanced volcanic activity corresponds to a period of ice advance and the overall magnitude of the cycles match. These data suggest that the coldest portion of the Little Ice Age was during the early 1800's.

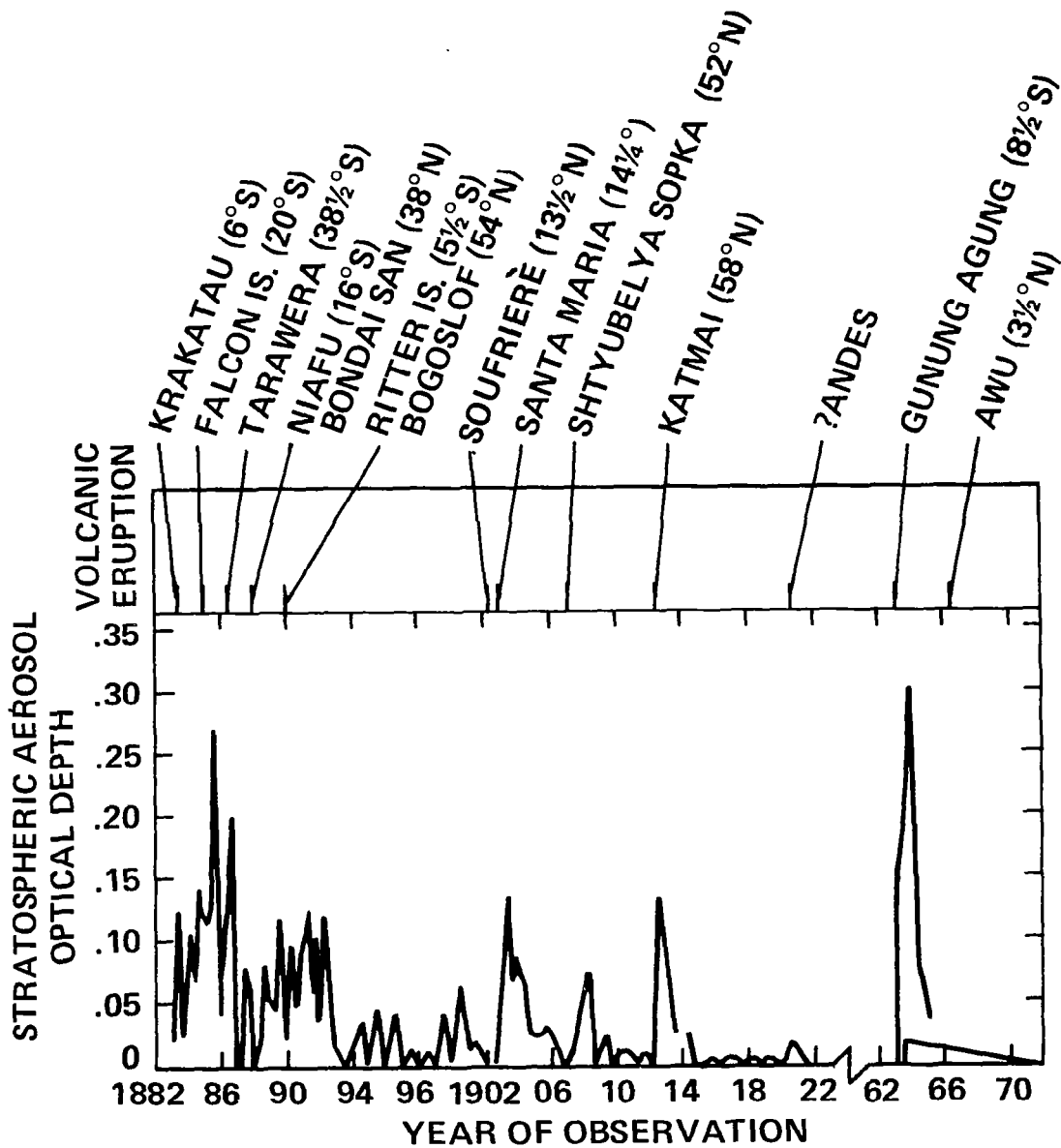


Figure 7. Volcanic optical depths and notable volcanic eruptions since 1880 were recorded. Note that a single eruption may yield an optical depth in excess of 0.1 for a year or two after the eruption. Volcanic activity ceased after 1912. The eruption of Mount Agung is the only large eruption to have occurred since 1912. Although large optical depths occurred in the Southern Hemisphere following the Agung eruptions, only small optical depths occurred in the Northern Hemisphere as shown by the double curve after 1963. The error bar in 1912 indicates a 1 day maximum and a one month maximum observed at Mount Wilson, California whereas the curve is an average over all the available stations in the Northern Hemisphere. From Pollack et al. (38).

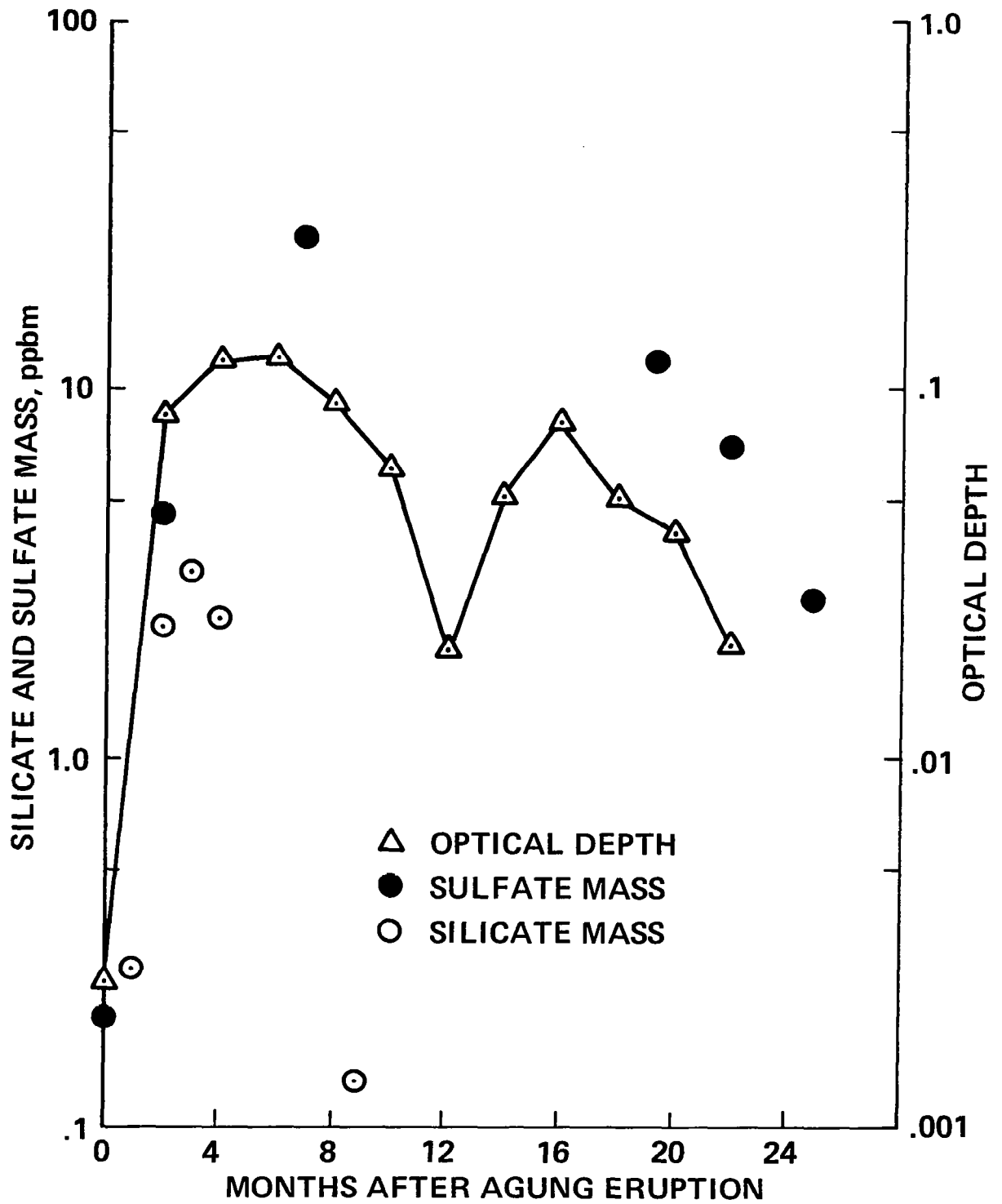


Figure 8. The optical depth over Australia during 1963 (37) is compared with the sulfate mass (31) and the silicate mass (32) measured above Australia near 20 km altitude. Note that the sulfate mass greatly exceeds the silicate mass and follows the trend of the optical depth fairly closely.

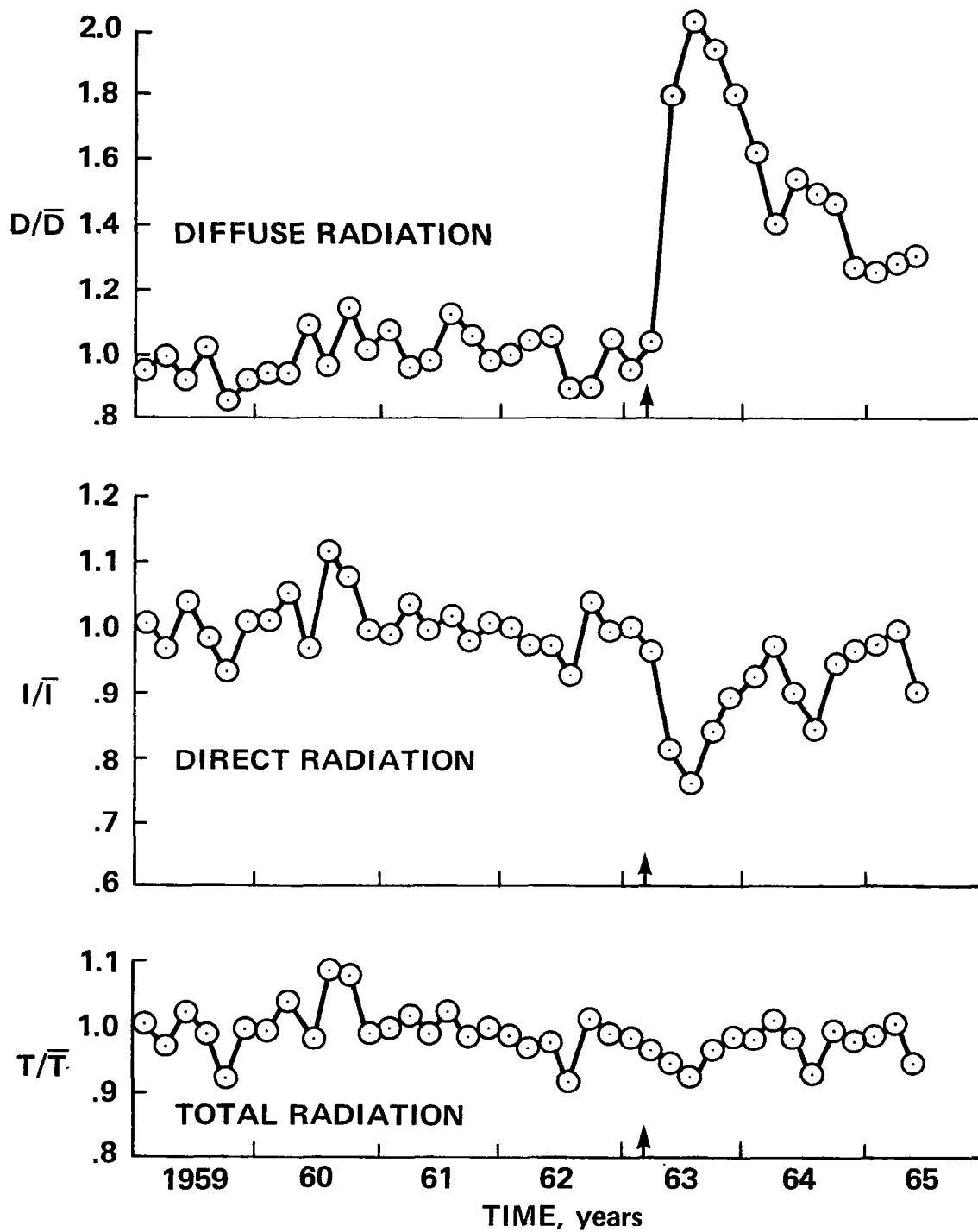


Figure 9. Deviations from the mean of the diffuse, direct, and total solar radiation in Australia during the period of the Agung eruption (marked by arrow). Note that the large decrease in direct radiation is compensated by an increase in diffuse radiation so that the change in total radiation is very small. Reproduced by permission from Dyer and Hicks (37), copyright 1965 Macmillan Journals Limited.

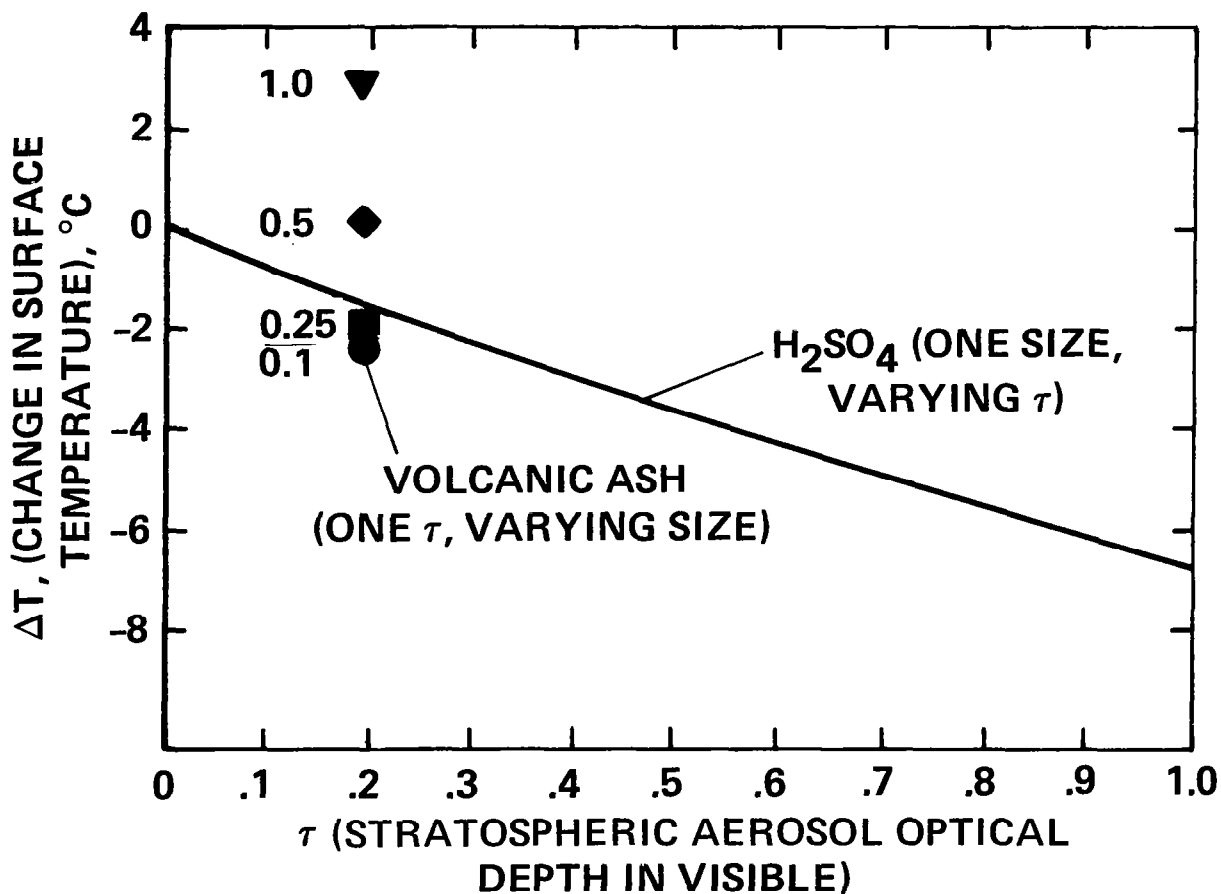


Figure 10. Dependence of surface temperature on stratospheric aerosol optical depth, size, and composition from Pollack et al. (38, 39). Note that silicate particles larger than $0.5 \mu\text{m}$ tend to warm the surface while small particles cool the surface. For fixed particle size, the cooling is nearly linear in optical depth. An optical depth of 0.1 produces a significant cooling for sulfuric acid particles.

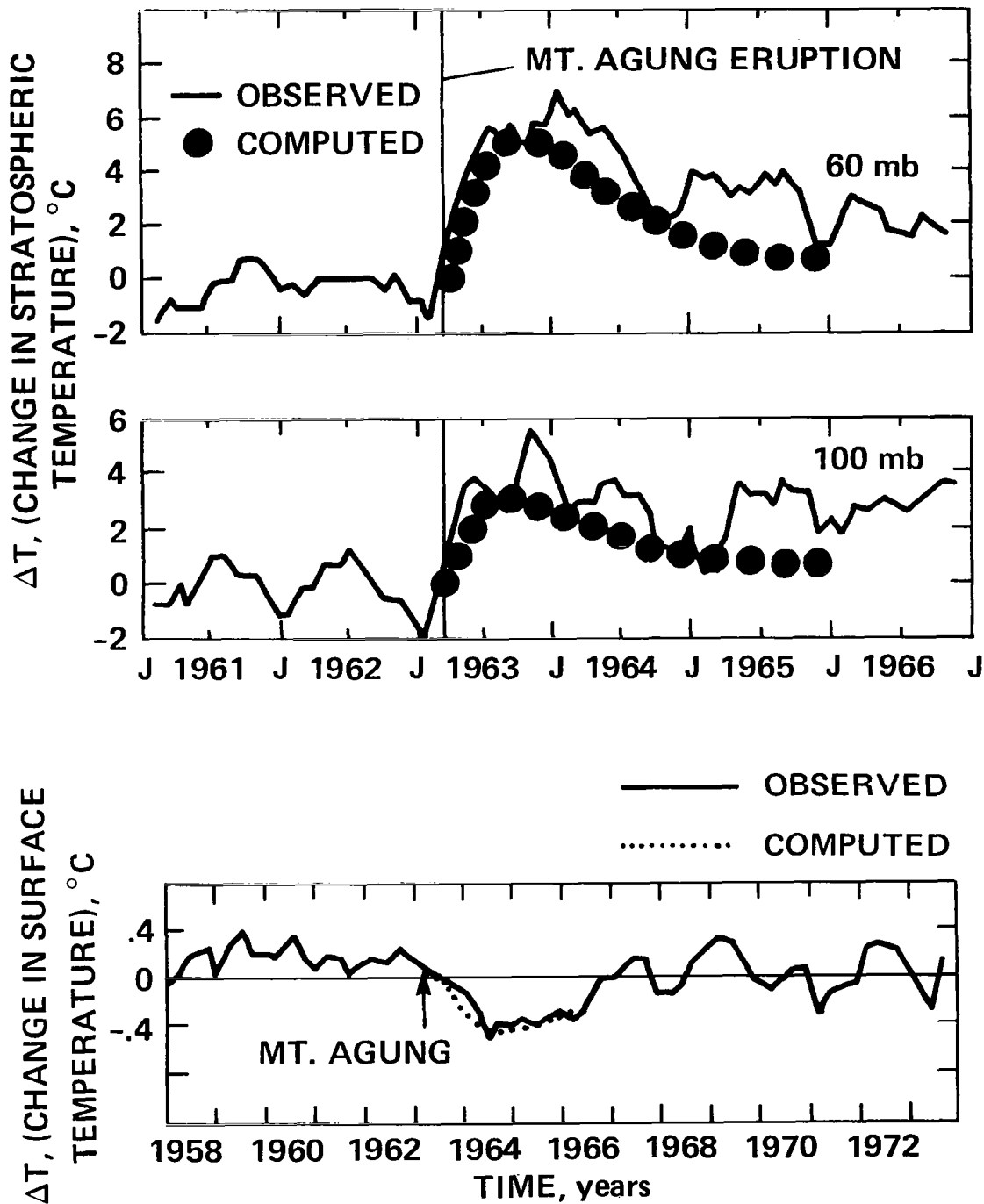


Figure 11. Calculated temperature changes after the Mount Agung eruption are compared with observed ones. From Hansen et al. (41). The stratosphere temperatures increased (a) because the aerosols absorbed terrestrial thermal radiation. The tropospheric temperatures (b) declined because the particles scattered sunlight back to space that would otherwise have reached the surface.

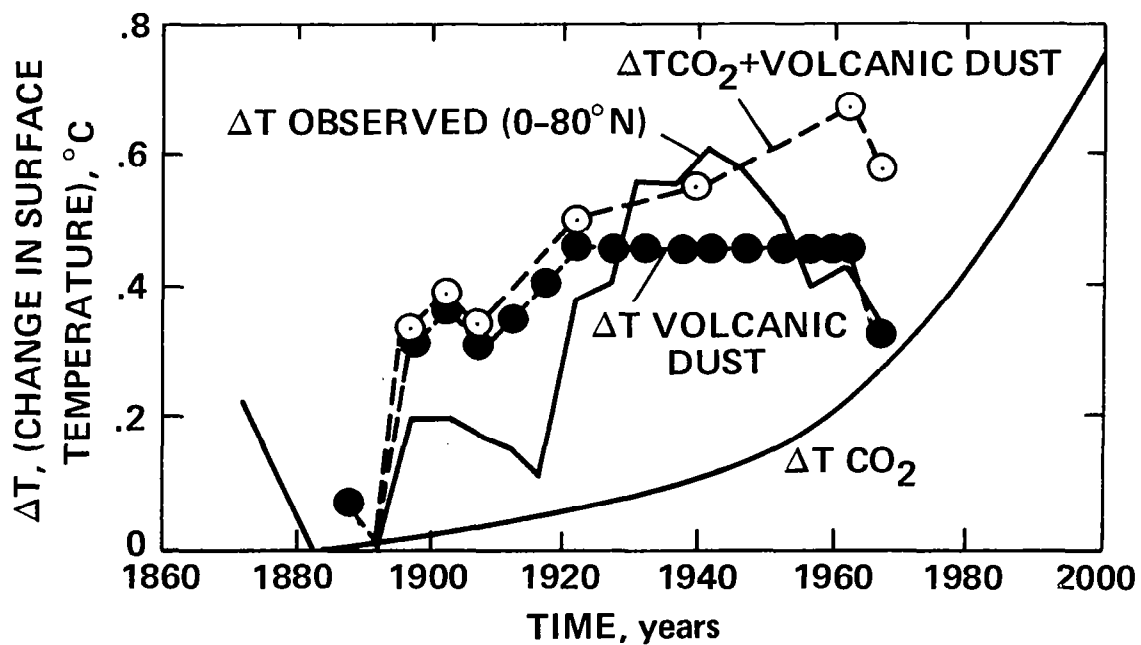


Figure 12. Temperature changes were calculated during the twentieth century by using the decade average of the optical depths (see figure 7). The changes agree well with those observed up to 1940 and are much larger than the changes to be expected due to CO₂ during the first half of the century. A significant warming due to CO₂ is expected at the end of the twentieth century (38,39).

IMPACT OF MOUNT ST. HELENS ERUPTION ON ECOSYSTEMS

J. C. Engibous, L. K. Bustad, R. A. Kennedy, G. O. Klock, E. C. Klostermeyer, and R. P. Preston
Washington State University, Pullman, WA

Initial and long-term effects of the ash deposition on the soils and agricultural crops in eastern Washington are best related to the amounts deposited, which ranged from a trace to about 15 centimeters. Chemically, the ash contains significant amounts (+ 400 ppm) of sulfur in forms available to crops, and modest amounts of certain other plant nutrients, except for copper, which is up to 50 percent above soil levels. Cadmium levels are substantially higher than those found in soils (6 compared with 0.5 ppm). One of the first effects of the ash deposit on plants was obviously the physical one of reducing light penetration into the leaves. As little as 1 mm of ash reduced light availability to the apple leaf by 90 percent or more and virtually stopped photosynthesis. Perhaps one of the most important effects of the ash on apple tree physiology was on the CO₂ compensation point, the balance point between photosynthesis and respiration. The CO₂ compensation point of leaves which received ash was 25 to 50 percent higher than leaves which were washed free of the ash residue. A shift in the compensation point as well as the observed decrease in the photosynthetic rate may be significantly affecting the growth of apple trees and other crops. It is believed that the effects of the ash on soils and crops are related to the physical damage from higher deposition rates, with some chemical burn of foliage. Some difficulties were encountered in harvesting crops in 1980. The impact of the May 18, 1980, volcanic eruption on forest ecosystems ranges from complete destruction to the light dusting of foliage. Major impacts were generally within 30 km and are defined with respect to extent and type of physical damage to the forest ecosystems. Two additional zones of impact are identified in the areas 30 to 600 km north and east of the volcano. These zones are differentiated by the dominant type of materials, whether lithic or pumice, deposited on the forest ecosystems. Ecologic impacts on the forest ecosystems are greatest in the physically damaged area less than approximately 30 km from the volcano crater. Insects were more severely affected by the ash fallout than many other organisms because of their small size and susceptibility to desiccation. If an insect managed to find an ash free surface it could not clean enough of the ash from its body to prevent the desiccant effects and soon died. When the wax layer of an insect's exoskeleton is removed, the insect loses water rapidly and dies when the water loss exceeds 30 percent. Houseflies lost 40 percent of their body water and had nearly 100 percent mortality in 8 hours. Other insects tested showed somewhat smaller losses. Insects such as grain beetles are adapted to a dry and dusty environment and lost only 3 percent of their weight and were still alive after 24 hours. Surviving insects will, in time, reproduce to their usual population levels so the adverse effect of the ash on insects will not be noticed by the average individual. Short term toxicity studies in rats showed them to be very tolerant to ingested volcanic ash. The ash administered was equivalent to 5 lbs (2270 g) of ash consumed by a 1,000 lb (454 kg) cow or 20 tablespoons (300 g) consumed by a person. A water solution was also administered orally, and no acute toxic effects were produced. Initially, with heavy dust concentrations, it was found that animals were reluctant to drink water that was standing in the open. When given fresh water, they immediately began drinking. Controlled research confirmed immediate observations following the ash fallout that food animals and horses were not affected by the ash. Where ash fall was heavy, coupled with short pastures, sheep resorted to the consumption of poisonous plants (hemlock) and subsequent deaths were noted. Chicks, dairy cows, calves, and lambs fed rations containing up to 30 percent volcanic ash (chicks) exhibited normal growth and production. Dairy cows fed up to 2.6 lbs of volcanic ash daily in their ration showed no ill effects and produced normally.

I. INTRODUCTION

The May 18, 1980, major pyroclastic eruption of Mount St. Helens made a significant deposition of tephra on the southern Cascade Range of Washington. It was estimated that more than 1 km³ of tephra from the eruption was distributed in a plume across large areas of Washington and neighboring states (1). Initial and long-term effects of the ash deposition on the soils and agricultural crops in Eastern Washington are best related to the amounts deposited, which ranged from a trace to about 15 cm. In most areas, the ash was promptly compacted by rains to about one-third the initial depth.

II. IMPACT ON SOILS

Chemically, the ash contains significant amounts (+ 400 ppm) of sulfur in forms available to crops, and modest amounts of certain other plant nutrients, except for copper, which is up to 50 percent above soil levels. Cadmium levels are substantially higher than found in soils (6 compared with 0.5 ppm). Except for sulfur, plant nutrient elements are mostly unavailable and are unlikely to contribute significantly to crop production through weathering processes.

From the soil standpoint, the most significant results of the ash fall are physical and impact water and temperature relationships in several ways. Prior to incorporation, the ash serves to reduce soil permeability to air and water vapor compared with most soils (2). It also retarded evaporation of water from soil and served to keep soils cooler during the 1980 growing season. Major concerns in the future are increased wind erosion from range lands and water erosion resulting from reduced infiltration under the winter precipitation regime which prevails in the Pacific Northwest.

III. IMPACT ON CROPS

One of the first effects of the ash deposit on plants was obviously the physical one of reducing light penetration into the leaves. As little as 1 mm of ash reduced light availability to the leaf by 90 percent or more and virtually stopped photosynthesis.¹ Even light dustings of ash (< 0.1 mm) had sizeable effects on the irradiance striking the leaf surface, but smaller, not statistically significant, effects on photosynthesis.

Perhaps one of the most important effects of the ash on physiology is on the CO₂ compensation point, the balance point between photosynthesis and respiration. The CO₂ compensation point of apple tree leaves which received ash is 25 to 50 percent higher than leaves which are washed free of the ash residue. Plant species with hairy (pubescent) leaf surfaces retain ash much more tenaciously than plants with smooth (glabrous) leaves; thus effects were more noticeable on apple leaves than on cherry leaves, for example.

In the short term, the commercial crop most severely damaged was alfalfa hay, with an economic loss to farmers in Eastern Washington estimated at \$35 million. From the standpoint of longer term effects of the ash fall on crops, much research is needed on photosynthesis and other plant processes as influenced by rate of ash application and length of time exposed. The excellent growing conditions that prevailed in 1979 and 1980 led to record yields of many crops, and makes it difficult, if not impossible, to assess the net effect of the May 18th explosion.

IV. IMPACT ON INSECTS

Insects were more severely affected by the ash fallout than many other organisms because of their small size and susceptibility to desiccation. Smaller insects were completely buried. If an insect managed to find an ash-free surface, it could not clean enough of the ash from its body to prevent the desiccant effects and soon died. The ash appeared to cling more readily to the insect integument than the ordinary dust an insect may encounter.

¹Kennedy, R. A., Unpublished data, Washington State Univ., 1980.

This condition was especially true of hairy insects like bees. Scanning electron microscope pictures show the ash to remain on the body surface under the hairs even after the bees were able to groom their bodies. For many years, entomologists have used silica aerogel and similar mineral dusts for cockroach control. These kill insects by abrading and absorbing the waxy layer from the insect's integument. An insect's exoskeleton is a multilayered structure well designed to prevent water loss. When the wax layer is removed, the insect loses water rapidly and dies when the water loss exceeds 30 percent. Early studies² at Washington State University showed that houseflies lost 40 percent of their body water and had nearly 100 percent mortality in 8 hours. Other insects tested showed somewhat smaller losses. Insects such as grain beetles are adapted to a dry and dusty environment and lost only 3 percent of their weight and were still alive after 24 hours.

Silica aerogels and volcanic ash have been tested as agricultural insecticides but were relatively ineffective at rates of about 100 pounds per acre. However, it is safe to conclude that at rates of 8 tons or more per acre, Mount St. Helens ash is a very effective physical control for most insects.

Many insects that were protected from the direct fallout were killed when they began normal activities on the morning of May 19. A thriving population of *Osmia* bees for fruit pollination had returned to their nests on Sunday when the sky began to darken and escaped the fallout since their nests were under shelter. They left their nests in the bright sunlight to seek nectar and pollen. They evidently soon became coated with ash from the flowers; not a single bee returned and dead bees were found on the ground. A similar fate came to other pollinators including honeybees and many other social and solitary bees. Since many flowers depend on a single species of bee for pollination, seed set on many wild plants such as bald-headed waterleaf was reduced.

Ants were also killed as they dug out of their nests but the colonies seem to have recovered. Insects that were protected in plant parts or were in protected immature stages of their life cycle escaped the effects. When rains settled the ash and reduced its dusty character emerging insects were less affected. Some insect pests such as grasshoppers were just hatching or were in early life stages and very susceptible. Washington faced a severe grasshopper outbreak but the ash fallout followed by cool wet weather eliminated the threat and no grasshopper control programs were carried out. Lady beetles were killed and this condition may have contributed to the unusually large aphid populations experienced this summer. Lady beetle populations continue to be low but large populations of syrphid flies, another aphid predator, have developed in their place.

Relatively little baseline data were available on insect populations immediately before the eruption and it will be difficult to document the effect of the ash on insect populations and to separate the effects from those of the unseasonably cool weather. Studies are being made on yellow jackets, larch casebearers and their parasites, alfalfa and wheat insects, and certain pollinators. The more mobile species will re-invade the ash fall areas from surrounding land. As the physical effects lessen due to rain and weathering, the surviving insects should in time reproduce to their usual population levels so the adverse effect of the ash on insects will not be noticed by the average individual. Many ecological changes will be difficult to document, but entomologists will likely note the apparent scarcity of some species and abundance of others and have cause to wonder if it is due to the eruption of Mount St. Helens.

V. IMPACT ON ANIMALS

Washington State University ewes, exposed to both the fallout and consumption of the ash in the pasture forage, have remained healthy and have shown no abnormal signs during or following the fallout. Feedlot cattle not under cover were exposed to the fallout; mixed rations were being prepared daily and therefore these cattle consumed ash in the feed only on the day of fallout. No abnormal signs were noted in these cattle; the watering devices for these cattle are outside and when these were cleaned of ash contamination, most

²Brown, John, Unpublished data, Washington State University, 1980.

of the cattle drank water; thus perhaps a reluctance to drink the ash-contaminated water was evident. These cattle are being slaughtered periodically and no abnormal signs have been noted during post-mortem examinations.

Based on mineral analysis on the ash, our animal scientists believe that if as much as 10 percent ash is consumed in the diet of farm livestock, none of the elements should present any toxic problems.

Day old chicks were placed on diets containing either 10, 20, or 30 percent ash and were compared with chicks fed the same diet without ash or chicks fed diets containing 10, 20, or 30 percent sand. After 5 weeks on these dietary regimes, the average weight of these birds is 1399, 1379, 1272, 1550 (controls), 1506, 1438, and 1313 grams, respectively. These growth rates are very good; there appears to be a 6 percent reduction in growth rate for each 10 percent volcanic ash in the diet compared with a 4 percent reduction for each 10 percent sand in the diet. Mortality has been low and is not related to the dietary treatments.

Four dairy calves, 3 to 4 months of age, were fed diets containing either 10 percent ash or a control diet (two calves on each diet). They were fed for 17 to 28 days when they were sacrificed for gross, histological, and tissue mineral determinations. These calves grew normally and did not exhibit any abnormal symptoms; no accumulation of ash in any segment of the gastrointestinal tract was noted. Tissue analyses are underway.

Two lactating dairy cows have been fed increasing levels of ash over a 5 week period. The ash was mixed with silage prior to feeding. Levels of ash in the ration dry matter have been increased from 0 to 6.3 percent at weekly intervals. Milk production has remained at expected levels over the 5 week period. These cows will be slaughtered at the end of the ash feeding period for postmortem and histological examination.

Feed availability and acceptability when contaminated with volcanic ash remain as the major questions for the livestock industry. This is especially true for alfalfa hay produced in the major ash fall area. The degree of volcanic ash contamination can be estimated by an ash analysis. Samples of contaminated alfalfa hay have ranged from 3 to 59 percent volcanic ash. Research is presently underway to determine whether alfalfa hay contaminated with 8 percent volcanic ash is acceptable to lactating dairy cows and if this degree of contamination affects milk production of these cows compared with that of cows fed uncontaminated alfalfa hay of comparable quality. Because the volcanic ash is inert in terms of energy and protein value, livestock and dairy producers have been advised to have an ash analysis made on alfalfa hay before purchase and a discount rate has been suggested based on the ash content of the hay.

College of Veterinary Medicine, Washington State University, gave special attention to the respiratory system of animals that had heavy dust exposure and were subsequently slaughtered. Initial examinations include gross and microscopic observations of the upper and lower respiratory tract, lung lavage with total and differential cell counts, particulate counts in alveolar macrophages, viability of alveolar macrophages, and an examination of alveolar macrophage fibroblast interaction. Material was stored for later determination of dry weight silica content if money is allocated to accomplish this research.

No pets or livestock were submitted for health problems directly related to the exposure to volcanic dust. Field investigations which included our own herds and flocks which had been in the dust continuously revealed no acute problems. Several avian species were affected since, being insectivorous, they had starved to death.

Extensive experimental evidence has shown general correlation between the ability of mineral dusts to cause lung fibrosis and their cytotoxicity to macrophages in vitro. Much public concern was expressed after reports that all the glass (amorphous, noncrystalline material) in the dust, because of its sharpness, would "tear the lung." The macrophages of the lung do not respect the shape of the material or its sharpness—rather, the material's surface properties are important. Macrophage studies were performed by Battelle-Richland, the Lovelace Foundation, and also by scientists in our College of Veterinary Medicine. Some chronically ill sheep were found to contain alveolar macrophages containing large amounts of dust. These cells were still viable and were performing the normal task of eliminating the dust; thus it is suggested that the dust is not toxic to the macrophages. This observation was confirmed by in vitro studies at Battelle and Lovelace in which the cytotoxicity of the various ash samples did not differ significantly from control values.

Short-term toxicity studies in rats showed them to be very tolerant to ingested volcanic ash. The ash administered was equivalent to 5 pounds of ash consumed by a 1,000 lb. cow or 20 tablespoons consumed by a person. A water solution was also administered orally, and no acute toxic effects were produced. Initially, with heavy dust concentrations, it was found that animals were reluctant to drink water that was standing in the open. We advised giving them fresh water and they immediately began drinking.

On the basis of the chemical and mineral compositions of the ash samples from this locale, preliminary biological experiments and clinical observations, it was reasoned that the short term hazard from the ash was minimal to people and animals. It is strongly recommended that long-term follow-up studies be conducted on animals and people inhabiting the same locale and experiencing high ash exposure over an extended period of time. Prolonged exposure to high levels of even nuisance dust can result in pulmonary disease, and the conditions after Mount St. Helens eruption provide a unique opportunity to determine the long-term effects with tools and techniques never available before.

VI. IMPACT ON FORESTS

Although the recent deposition of tephra on the landscape is of major significance to the nearby forest ecosystems, the estimated 10-kiloton blast of the eruption had a much greater impact as it caused major physical damage to the adjacent forest. Hot pyroclastic flows and cold mud flows also destroyed forest on the slopes of the volcano.

Because of the nature of the volcanic eruption and the ensuing tephra deposition, the effects on the forest ecosystems can be divided into five zones that reflect the degrees of impact. These five zones include (a) the "ground zero" area, (b) the area of heavy physical damage, (c) the periphery area, (d) the area where deposition is predominantly "lithic" ash, and (e) the eastern-most zone predominantly affected by pumiceous ash.

Within the "ground zero" area, nearly all evidence of pre-eruption forests was destroyed over nearly 2,500 hectares by the physical blast of the erupting mountain, hot pyroclastic flows, and cold mud flows. The pyroclastic flow damages are on the north and eastern slopes of the volcano; the mud flows, on the southern slopes. The previous forests destroyed were predominantly within the subalpine *Tsuga mertensianna* zone and upper elevation of the *Abies amabilis* zone described by Franklin and Dyrness (3). Because of the severity of the destruction, re-establishment of these former forest ecosystems will be extremely slow, even if there are no further major eruptions in the current series. The general characteristics of the residual forest soils as well as the tephra within the soil are very difficult to describe because of significant landform redistribution and extreme surface disturbance.

Within the area of heavy physical damage, the most noticeable feature is the extensive "blowdown" of former forest within the *Abies amabilis* zone. Trees up to 2 m in diameter lie in a general pattern reflecting the force field generated by the volcano eruption. This area is a fan shape extending northeast from the volcano approximately 7 to 20 km from the blast center. On the outer portions of the fan less damage occurs in the blast-protected areas. Total area involved is nearly 40,000 hectares. The area is well covered with a deposition of volcanic ash with maximum ash deposition near 25 to 30 cm. Significant depositions of tephra from previous eruptions of Mount St. Helens are also found within this zone. At a research sample collection location on Mount Margaret 13 km north of the crater, ash depth was measured at 25 cm. The lower one-half of the tephra was dark-colored, coarse lithic blast material whereas the upper one-half was light colored and finer-textured pumiceous ash. The extreme differences in texture between the two tephra deposition materials and the consequent soil water behavior characteristics will contribute to serious surface erosion on the steeper slopes. Summer rainfall has already caused surface erosion in this zone. Although some seed germination problems may be encountered on the tephra surface, regeneration of conifers within this zone is expected to be very rapid. In some areas the younger trees were protected by snow and unaffected during the May 18 eruption. Thus, the forest should re-establish rather quickly in this zone.

The area 20 to 30 km from the crater or periphery zone lying beyond the heavily damaged zone is highly variable, ranging from extensive blowdown and standing desiccated trees to relatively unaffected forest. Ash depths decrease to near 10 cm at the outer perimeter and should have relatively little direct effect on forest regeneration. The *Abies amabilis* forests within this zone that were desiccated by the hot gases emitted by the volcano pose some interesting forest management problems. Insect and disease activity are the

most pressing concerns. The best opportunities for salvage logging activity lie within this zone. However, there are major differences of opinion on how much soil disturbance should be permitted during salvage logging both here and in the heavily damaged zone. Leaving the fallen trees in place will provide barriers to protect the landscape from serious surface erosion. However, surface disturbance by some forms of salvage logging will enhance infiltration from heavy rainfall and melting snow and possibly reduce the probability of serious erosion. Thus, specific site judgment must be used in directing salvage operations.

In both the heavy damaged and periphery zones, the deposition of tephra on the forest floor is expected to have a significant impact on organic matter decomposition and forest nutrient cycling. Accelerated decomposition along with decreased evapotranspiration demand could lead to the leaching of important plant nutrients. Of most concern is the potential loss of nitrogen. The dark organic color observed in the Clearwater River drainage in late July 1980 indicates that this process is already influencing stream water quality.

Beyond the periphery zone of direct blast damage lies the region predominantly affected by the heavy deposition of predominantly dark-colored, coarse-textured lithic material. Because of the abundance of coniferous species and environmental diversity within this zone, a complex array of forest types was affected by the tephra deposition. However, there appears to be little negative impact on the forest vegetation with the exception of the unknown effects of ash-covered foliage. Depths of the deposition material within the zone reaching from 30 to 180 km from the volcano range between 1 and 5 cm. The long-term effects of the ash on the forest ecosystem activities are relatively unknown. Erosion can be expected on the exposed slopes and decomposition of the forest floor may be accelerated. This could also be considered a beneficial effect to the current forest as it may increase the availability of plant nutrients within the forest nutrient cycling process.

Beyond approximately 180 km, the dominant characteristic of ash changes from the dark-colored lithic material to the light-colored pumice of predominantly glass material. This material can generally be observed on the forest floor up to 600 km from the volcano. Hooper et al. (4) pointed out "the dark ash in bulk appears to represent silicic andesite, with abundant plagioclase both as phenocrysts and as ground mass, and may be derived from a part of the old volcanic cone dispersed in the first explosion. The pale ash in bulk has the composition of rhyodacite and may represent new magma." Besides color and textural differences between the two materials, the dark material's bulk densities range generally from 1.4 to 1.7 g/cm³, whereas the lighter material is generally from 1.1 to 1.3 g/cm³. The water-holding capacity of the light-colored material is markedly higher than that of the dark lithic material. The major deposition of this light-colored material was on agriculture and range lands, less than 1 cm being observed on forest lands, most noticeably in northern Idaho and western Montana. Because of the very small amounts of ash deposition in forest ecosystems within this zone, no major ecologic impacts are expected.

The impact of Mount St. Helens, May 18, 1980, volcanic eruption on forest ecosystems ranges from complete destruction to the light dusting of foliage. Major impacts were generally within 30 km of the volcano. Three zones of impact within 30 km are defined with respect to extent and type of physical damage to the areas 30 to 600 km north and east of the volcano. These zones are differentiated by the dominant type of materials, whether lithic or pumice, deposited on the forest ecosystems. Ecologic impacts on the forest ecosystems are greatest in the physically damaged area less than approximately 30 km from the volcano crater.

REFERENCES

1. Fruchter, Jonathan S., et al.: Mount St. Helens ash from the 18 May 1980 eruption: Chemical, Physical, Mineralogical, and Biological Properties. *Science*, vol. 209, 1980, pp. 1116-1125.
2. Cook, R. J., Barron, J. C., Papendick, R. I., and Williams, G. J., III.: Impact on Agriculture of the Mount St. Helens Eruptions. *Science*, vol. 211, 1981, pp. 16-22.
3. Franklin, Jerry F., and Dyrness, C. T.: Natural Vegetation of Oregon and Washington. USDA Forest Serv. Gen. Tech. Rept. PNW-8, 1973, 417 pp.
4. Hooper, P. R., Herrick, J. W., Laskowski, E. R., and Knowles, C. R.: Composition of the Mount St. Helens Ashfall in the Moscow-Pullman Area on 18 May 1980. *Science*, vol. 209, 1980, pp. 1125-1126.

IMPACT OF MOUNT ST. HELENS ERUPTION ON HYDROLOGY AND WATER QUALITY

J.E. Bonelli, H.E. Taylor, and J.M. Klein
U.S. Geological Survey, Water Resources Survey, Arvada, CO

The 1980 eruptions of Mount St. Helens in southeast Washington resulted in a pronounced effect on the surface and ground water resources of the state. In response to the volcanic activity, the U.S. Geological Survey intensified statewide surface and ground water sampling programs to determine the nature and magnitude of the volcanic-induced variations. Streams to the east of Mount St. Helens received the major ash fallout. Chemical effects were best noted in smaller streams sampled 60 to 70 miles northeast of Mount St. Helens. The chemical variations observed were pronounced but short lived. Sulfate and chloride increases in anionic composition were prevalent immediately following the eruption; however, the original bicarbonate predominance was again attained within several days. Suspended iron and aluminum concentrations were similarly elevated during the period of greatest ash deposition (highest turbidity); however, the dissolved concentrations remained relatively constant. Depressions of pH were minor and short lived. Streams draining to the south, tributaries to the Columbia river, showed little observable changes in water chemistry. Streams draining to the west (Toutle river and its tributaries) were compositionally affected by the various volcanic activities. Chloride and sulfate anion percentages exceeded the bicarbonate percentage up to one month following the eruption period. Streams and lakes sampled in the immediate vicinity of Mount St. Helens, in addition to trace metals, contained organic compounds derived from decomposing wood buried in the debris deposits. This organic material may constitute a significant source of organic compounds to surface and ground water for some time to come. This latter possibility is being studied in detail.

I. INTRODUCTION

The 1980 eruptions of Mount St. Helens in southwest Washington state resulted in pronounced hydrologic and water quality effects in areas affected by the blast, debris avalanche, mudflows, and ash. These effects are considered briefly here in two categories: those effects in the immediate vicinity of the volcano (blast, debris, and mudflows), and those effects associated with the volcanic ash deposition in watersheds downwind (east) from the volcano.

II. DISCUSSION

The surface and ground water hydrology of the Toutle and lower Cowlitz River valleys (Fig. 1) of southwestern Washington was dramatically altered by the mud, debris, and pyroclastic material mobilized by the May 18th eruption. Existing drainage areas, streams, and lakes were inundated with volcanic materials, and substantial flooding and sedimentation occurred in several areas up to 60 km from the volcano. In addition to widespread physical damage to the natural hydrologic system, municipal water supplies, sewage treatment facilities, septic systems, and water wells were adversely affected by sedimentation and flooding. Because of alteration of the existing terrain, continued flooding potential exists from newly formed lakes. This flooding potential is exacerbated by the inability of the scorched terrain in the blast zone to retain runoff from precipitation.

The major changes in the water chemistry of surface waters draining from areas affected by the volcanic effluents included increases in turbidity and in the concentrations of sulfate, chloride, total nitrogen, total organic nitrogen, iron, manganese, and aluminum.

In the ash-affected basins east of Mount St. Helens, the observed water quality changes were generally short lived and had a tendency to decrease in magnitude with distance from the volcano. The North Fork Ahtanum Creek near Tampico, Washington, is used in Figure 2 to illustrate the degree and duration of the compositional variations in water quality. Increases in sulfate and chloride were the major changes and were short lived. Few significant cation changes were observed. The hydrologic and water quality effects observed further east, and into north central Idaho and western Montana, were similar in character but smaller in magnitude. Isolated incidents of minor flooding occurred in eastern Washington because of temporary drainage obstructions by volcanic ash, but for the most part, hydrologic effects appear to be small.

Figure 3 shows the chemical changes seen in the Toutle River near Castle Rock, Washington, and indicates a greater persistence and variability of change due to continuing influx and leaching of sediments in the devastated headwater areas. In addition, the total concentrations of iron, manganese, and aluminum increased greatly over pre-eruption levels. There appeared to be no persistence of dissolved inorganic trace constituents that would constitute any known hazard to human health. However, a large amount of organic material (trees, plants, soil) trapped in the hot, wet volcanic debris is decomposing rapidly to form a variety of organic degradation products and gas (methane, carbon dioxide, and hydrogen sulfide). The persistence of these organic compounds and their role in the sustenance of various life forms in the water is being studied by the U.S. Geological Survey and other scientific organizations.

The 1980 volcanic activity of Mount St. Helens, including effects on soils, agriculture, surface and ground water resources, and precipitation chemistry, may have important long-term consequences. The U.S. Geological Survey is also conducting research in these and other areas as a part of a continuing research program in volcanology. A selected list of Survey publications and reports on these subjects is provided in the Bibliography.

BIBLIOGRAPHY

- Cummins, John: Mudflows resulting from the May 18, 1980 eruption of Mount St. Helens, Washington, Geological Survey Circular 850-B, 1981.
- Dion, N. D., and S. S. Embrey: Effects of Mount St. Helens eruption on selected lakes in Washington, Geological Survey Circular 850-B, 1981.
- Fuste, Luisa: Effects of the Mount St. Helens eruption on the benthic fauna of the Toutle River, Muddy River, and Pine Creek drainage basins, Washington. Geological Survey Circular 850-H, 1981.
- Klein, J. M.: Some effects of the May 18 eruption of Mt. St. Helens on river water quality, U.S. Geological Survey Professional Paper 1250, 1981.
- Lombard, R. L., M. B. Miles, L. M. Nelson, D. L. Kresch, and P. J. Carpenter: Mount St. Helens eruption of May 18, 1980—Impact on flooding in lower Cowlitz and lower Toutle Rivers, Washington, as of June 19, 1980. Geological Survey Circular 850-C, 1981.
- Pereira, W. E., C. E. Rostad, and H. E. Taylor: Mount St. Helens, Washington, 1980 volcanic eruption: Characterization of organic compounds in ash samples, *Geophys. Res. Lett.*, vol. 7(11), 1980, pp. 953.
- Pereira, W. E., C. E. Rostad, H. E. Taylor and J. M. Klein: Characterization of organic contaminants in environmental samples associated with Mt. St. Helens, 1980 volcanic eruption, *Environ. Sci. Technol.* (in press).
- Taylor, H. E. and F. E. Lichte: Chemical composition of Mt. St. Helens volcanic ash, *Geophys. Res. Lett.*, vol. 7(11), 1980, pp. 949.

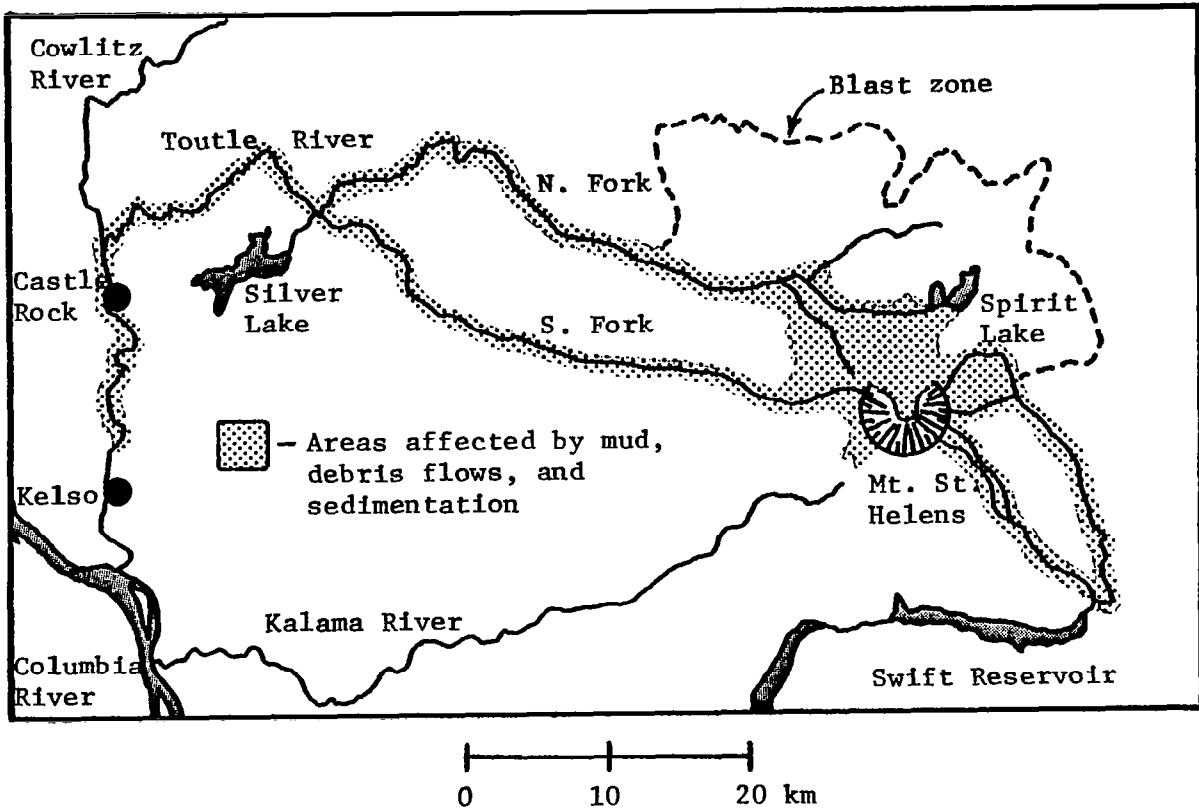


Figure 1. Mount St. Helens area of southwest Washington state.

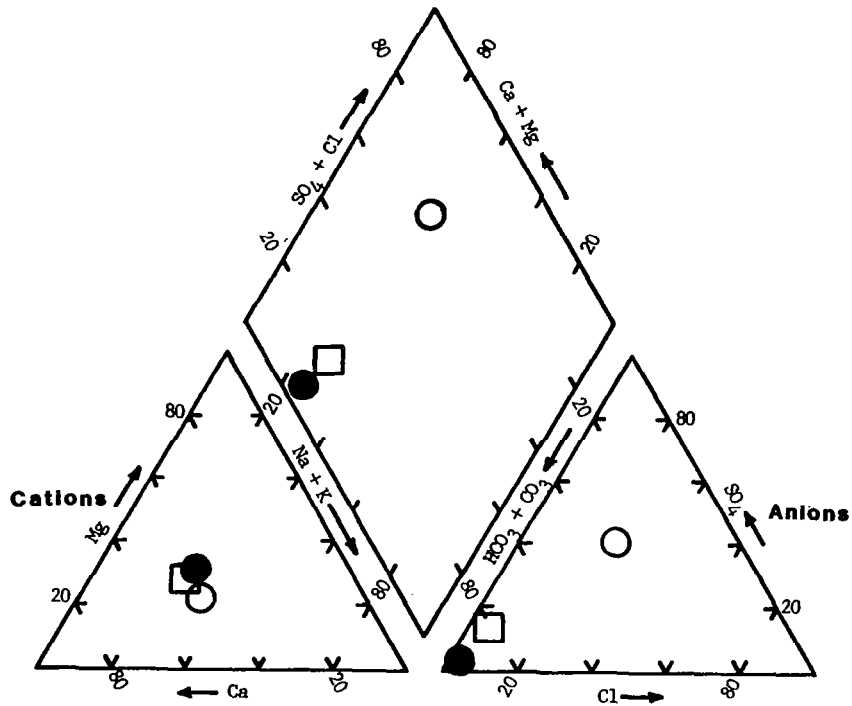


Figure 2. Ionic composition of North Fork Ahtanum Creek near Tampico, Washington (100 km east of Mount St. Helens), expressed as percentage of total major cations and anions found. ● pre-May 18, 1980 eruption; ○ May 18, 1980; □ June 24, 1980.

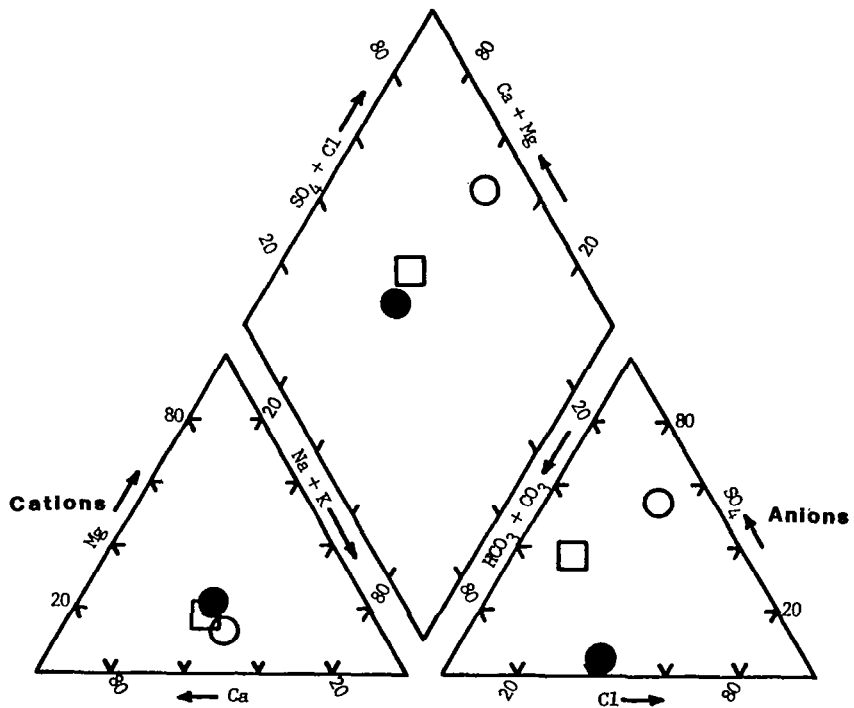


Figure 3. Ionic composition of Toutle River near Castle Rock, Washington, expressed as percentage of total major cations and anions found. ● pre-May 18, 1980 eruption; ○ May 20, 1980; □ June 24, 1980.

PRECURSOR GASES OF AEROSOLS IN THE MOUNT ST. HELENS ERUPTION PLUMES AT STRATOSPHERIC ALTITUDES

E. C. Y. Inn, J. F. Vedder, and E. P. Condon
NASA Ames Research Center, Moffett Field, CA

D. O'Hara
LFE Corporation, Richmond, CA

During the period from May 19 to June 17, 1980, nineteen stratospheric samples from the eruption plumes of Mount St. Helens were collected in five flight experiments. The plume samples were collected at various altitudes from 13.1 to 20.7 km by using the Ames cryogenic sampling system on board the NASA U-2 aircraft following the eruptions of May 18, May 25, and June 13, 1980. The enriched, cryogenically collected samples were analyzed by chromatography. The concentrations of aerosol precursor gases (OCS, SO₂, and CS₂), CH₃Cl, N₂O, CF₂Cl₂, and CFCl₃ were measured by gas chromatography. Large enhancement of the mixing ratio of SO₂ and moderate enhancement of CS₂ and OCS were found in the plume samples compared with similar measurement under pre-volcanic conditions. A fast decay rate of the SO₂ mixing ratio in the plume was observed. Measurement of Cl⁻, SO₂⁼, and NO₃⁻ by ion chromatography were also carried out on water solutions prepared from the plume samples. The results obtained with this technique imply large mixing ratios of HCl, (NO + NO₂ + HNO₃), and SO₂, in which these constituents are the respective sources of the anions. Measurement of the ²²²Rn concentration in the plume of the May 18 eruption will be reported. Other stratospheric constituents in the plume samples, such as H₂O, CO₂, CH₄, and CO, have also been observed.

I. INTRODUCTION

In studies of the formation and distribution of stratospheric sulfate aerosols, there is considerable interest in the impact of injection of large amounts of precursor gases into the stratosphere as a result of explosive volcanic eruptions. To understand the subsequent perturbations of the aerosol distribution induced by these eruptions, quantitative documentation of the time history of the changes in the physical and chemical nature of the injected material is required. In particular, information on the distribution in space and time of precursor gases, namely, the stable sulfur constituents, in the eruption plumes will serve to set constraints in theoretical models which are developed to describe the important photochemical processes in the formation and distribution of sulfate aerosols.

The explosive eruptions of Mount St. Helens during May and June 1980 in which substantial material was injected into the stratosphere provided us with a unique opportunity to conduct in situ sampling experiments. The first flight was about 24 hours after the first major eruption. Measurements of the concentration and distribution of precursor constituents in the eruption plumes in these sampling experiments are presented in this report.

II. EXPERIMENTAL DATA

Samples of gases in the eruption plumes were collected by using the Ames cryogenic sampling system on board the NASA U-2 aircraft (1). Briefly, the cryogenic collector consisted of a 1.9-cm OD x 1-meter-long glass tubing shaped in the form of a helical coil and immersed in liquid nitrogen. In these experiments all condensable constituents are trapped from about 200 STP liters of air in a flow-through configuration. The samples thus acquired are enriched about 1000-fold.

The techniques used for the analysis of the various constituents are as follows:

- Gas chromatograph-flame photometric detector: OCS, SO₂, CS₂
- Gas chromatograph-electron capture detector: N₂O, CF₂Cl₂, CFCl₃
- Gas chromatograph-photoionization detector: CH₃Cl
- Gas chromatograph-flame ionization detector: CH₄, CO
- Ion chromatograph-conductivity detector: Cl⁻, SO₄⁼, NO₃⁻
- Manometry: CO₂
- Radioactivity: ²²²Rn

The results and discussion presented in this report are focused mainly on the precursor gases OCS, SO₂ and the anions Cl⁻, SO₄⁼, and NO₃⁻.

Five sampling flight experiments were carried out in the eruption plumes of Mount St. Helens as follows: May 19 and 22 following the May 18 eruption, May 28 following the May 25 eruption, and June 14 and 17 following the June 13 eruption. A total of 19 cryogenically collected samples were acquired from these flight experiments.

III. PRE-VOLCANIC DATA

To assess the impact of volcanic emissions of precursor gases injected into the stratosphere, comparisons should be made of the concentration and distribution of these gases with those for nonvolcanic conditions. Fortunately, during 1978 and 1979 pre-volcanic measurements were made during flight experiments in California, Alaska, and Texas at altitudes from 15 to 31 km. These pre-volcanic data may be considered to characterize nonvolcanic conditions in the stratosphere. Figure 1 summarizes the pre-volcanic data (2).¹

IV. ENTRAINMENT

During the violent eruptions of Mount St. Helens, tropospheric air is entrained by the rapidly rising plume, which penetrates the tropopause; and the plume material is thus injected into the stratosphere. It is expected that relatively stable trace constituents of the tropospheric air may be transported into the stratosphere by this process. The trace constituents N₂O, CF₂Cl₂, and CFCl₃ whose vertical profiles in the stratosphere have been reported by a number of investigators are considered. These profiles are compared with the plume measurements (May 19) of the May 18 eruption. Figure 2 displays the trajectories of the plumes of this eruption.² The results are:

		<u>N₂O</u>	<u>CF₂Cl₂</u>	<u>CFCl₃</u>
<u>Stratosphere at 14 km</u>				
Troposphere	Plume	0.76	0.69	0.77
<u>Stratosphere at 14 km</u>				
Troposphere	Nonvolcanic	0.85	0.65	0.83

where the nonvolcanic ratios are calculated from data reported by Goldan et al. (3) of measurements made in Wyoming at a latitude comparable with the plume measurements. The rather good agreement between the two sets of ratios is surprising. This result implies either only small amounts of tropospheric air is entrained in the rising plume, or rapid diffusion and mixing occur after injection into the stratosphere within 24 hours after the eruption.

¹Model profiles were supplied by Turco et al., personal communication, 1980.

²Danielsen, private communication, 1980.

On the other hand, the results of the ^{222}Rn measurement for the 16.5 km sample of the May 19 flight experiment imply strong entrainment of tropospheric air. Thus, the measured radioactivity due to ^{222}Rn in the plume was 0.13 disintegrations per minute/L (STP), whereas for tropospheric air (over the Pacific Ocean) Moore et al. (4) report 0.0016 to 0.073 and for stratospheric air just above the tropopause 0.00028 to 0.00087. These results suggest that the mixing ratio of ^{222}Rn in the plume at stratospheric altitudes is very similar to that in tropospheric air. This similarity in concentration may well be the result of transport of tropospheric air into the stratosphere by entrainment in the rapidly rising eruption plume. Occluded ^{222}Rn released during the eruption will also contribute to the observed radioactivity in the stratospheric sample.

V. PRECURSOR GAS

Significant enhancement of the precursor gas concentrations in the plume of the May 18 eruption was observed and compared with nonvolcanic conditions. However, very little, if any, enhancement was evident in the plumes of the later eruptions. Measurements were made in two different plumes originating from this eruption as shown in figure 2. The May 19 flight experiment sampled the plume at 14, 15.2, and 16.5 km (100 mb trajectory). These flights were well below those of the May 22 experiment at 18.6 to 20.7 km (70 mb trajectory). The results of these two flight experiments are given in table I.

Comparison of the data in figure 1 with the results in table I shows that SO_2 is the dominant precursor gas in the plume, where its mixing ratio at 14.0 km is more than 2000 times greater than for pre-volcanic conditions. The SO_2 concentrations of the higher altitude plume (May 22 flight experiment) appeared to have decayed to almost pre-volcanic conditions. Plume measurements of SO_2 on May 26, 1980, have also been reported over Scandinavia at 11.3 km, just above the tropopause, with a peak concentration of 0.515 ppbv.³ Comparing this result with the 14.0 km result of 111 ppbv gives an exponential decay time constant of SO_2 concentration in the plume of about 1.3 days. This time is considerably faster than the conversion rate of SO_2 to H_2SO_4 of about one year in the stratosphere (5). Of course, diffusion and mixing need to be considered in accounting for the apparent time dependence of the SO_2 concentration in the plume.

Although OCS is the dominant precursor gas for nonvolcanic conditions, it is noted from Table I that SO_2 is the dominant constituent in the plume. There is only a modest enhancement of OCS in the higher altitude plume samples of May 22. The plume mixing ratio of OCS is only about 2 to 3 times greater than the nonvolcanic concentrations at those altitudes. It may be speculated that entrainment of tropospheric air may contribute to the observed enhancement. These results suggest that OCS in the plume may play only a minor role in the perturbations of the sulfur cycle following volcanic eruptions.

In the plume measurements of the May 19 flight experiment CS_2 has been observed, and the results are shown in table I. The pre-volcanic conditions suggested an upper limit of about 1 pptv at 15.2 km (2). Comparison of this result with the plume measurements indicates a modest enhancement of CS_2 . These results suggest entrainment of tropospheric air may contribute to the modest CS_2 enhancement, in view of recent measurements of CS_2 in the free troposphere to be about 30 pptv (6). Another, as yet unidentified, signal, similar in size to that for CS_2 has also been observed. The signal is well separated from the CS_2 signal and appears at a slightly longer retention time. It is likely that the signal is due to the presence of an unknown sulfur compound in the sample and efforts are now underway to identify it during postcalibration experiments.

The dominance of the SO_2 in the plume over that of OCS and CS_2 , which are compounds of sulfur in reduced form compared with that of SO_2 , is understandable on the basis of the chemical conditions in the rising gases. During the eruptive phase, the gases are heated to a high temperature, which gives rise to oxidizing conditions by the presence of O, OH, O_2 , and NO_2 in the plume. These conditions are therefore very favorable for the rapid oxidation of OCS and CS_2 to form SO_2 .

³Meixner et al., 1980, private communication.

The plume measurements included in table I for CH_3Cl , which revealed moderate enhancement of the mixing ratio, about 3 to 7 times the recently reported mixing ratios by Penkett et al. (7). Entrainment of tropospheric air cannot explain this enhancement and it appears that the enhanced CH_3Cl originates in the volcanic emission. Since the source of tropospheric CH_3Cl is that dissolved in the ocean, the source of the enhanced CH_3Cl in the plume may be the result of sea water seeping into the hot magma during the eruptive phase, vaporizing and thus releasing the dissolved CH_3Cl . Chemically produced CH_3Cl from CH_4 and gaseous chlorides reacting in the hot plume may also contribute to the observed enhanced concentration.

Evidence of enhanced amounts of water vapor have been observed in the plume of the 20.1 to 20.7 km sample (Table I). It was noted that a small amount of water was condensed on the walls of the analysis sample bottle. From an estimate of the amount of condensed water, it was calculated that its presence can be explained only by assuming a mixing ratio of water in the plume of about 30 to 160 ppmv. A similar finding was reported by the frost-point hygrometer experiment on the aircraft in the same sampling flight. The presence of this high concentration of water in the plume may have important consequences in the kinetics of the oxidation of SO_2 and conversion into H_2SO_4 .

The results of the precursor gas measurements in the plumes of the May 25 and June 13 eruptions will not be presented or discussed in this report, except for the following comments. The data obtained in these experiments yielded mixing ratios very similar to those for nonvolcanic conditions; that is, little or no enhancement was observed. This result, perhaps, is consistent with the observation that these eruptions were less intense than that of May 18.

VI. OTHER GASEOUS CONSTITUENTS IN THE ERUPTION PLUMES

Water solutions were prepared of the soluble constituents of some of the cryogenically collected plume samples and the anions of the dissolved samples were analyzed by ion chromatography. The results of these analyses are shown in Table II. In preparing these solutions, no attempt was made to exclude O_2 (air). Therefore, any sulfite (derived from SO_2) or nitrite (derived from NO_2) ions will be readily converted to $\text{SO}_4^{=}$ and NO_3^- , respectively, in the solution prior to analysis. Separate tests made by intentionally adding an oxidizing agent (H_2O_2) confirmed this.

In Table II the SO_2 mixing ratios (in parenthesis) have been included along with the $\text{SO}_4^{=}$ results. The latter are all larger than the corresponding SO_2 concentrations. Any H_2SO_4 in the plume, in the form of vapor or aerosol, that may be trapped in the cryogenic collector, would, in addition to SO_2 , contribute to the measured $\text{SO}_4^{=}$. Enhanced sulfate aerosol concentrations were found by other investigators during these flight experiments. The $\text{SO}_4^{=}$ results are qualitatively consistent with those of SO_2 and confirm the presence of enhanced amounts of the precursor gas in the eruption plume.

The presence of NO , NO_2 , and HNO_3 in solution contribute to the NO_3^- signal in the ion chromatographic measurements. In the NO_3^- plume measurements HNO_3 and NO_2 are probably the major contributors to the signal. The very high mixing ratio of 222 ppbv of NO_3^- for the 15.2 km plume sample of the May 19 flight experiment indicates the gaseous constituents responsible for NO_3^- originated in the volcanic emission.

The Cl^- results listed in Table II represent the total signal obtained in the ion chromatographic measurement. The shape of the observed signal, however, shows evidence of perturbation of the Cl^- signal by some other anion, possibly an organic anion, such as formate or acetate. No evidence of this perturbing signal is present in blank measurements. Since formaldehyde and formic acid are oxidation products of CH_4 in the atmosphere, it is likely that the perturbing signal is due to the formate ion. By comparison of the shape of a pure Cl^- with that of the perturbed signal, the Cl^- contribution is estimated to be about 1 to 10 percent of the total perturbed signal. Of course, the Cl^- originates mainly from HCl . Accordingly, the estimate of HCl in the 14.0 km sample is about 10 to 50 ppbv. This gives a ratio of $(\text{HCl})/(\text{SO}_2)$ of about 0.1 to 0.5. The eruption plume measurements of Fuego and Guatemalan volcanoes yielded similar ratios, as reported by Lazrus et al. (8).

ACKNOWLEDGMENTS

The authors thank Charles Smith of the Lawrence Livermore Laboratory for carrying out the ^{222}Rn analysis. They also would like to extend their appreciation and thanks to the Dionex Corporation for use of their ion chromatograph equipment and to their personnel, Greg Crook, Elizabeth Cathers, and Valerie Smith, for their help and expertise in the analysis of our plume samples. The dedicated technical assistance by Bernard Langedyk, Larry Robello, and Steve Monfort is gratefully acknowledged.

REFERENCES

1. Inn, E.C.Y., Vedder, J.F., Tyson, B.J., and O'Hara, D.: COS in the stratosphere. Geophys. Res. Lett., vol 6, 1979, pp. 191-193.
2. Inn, E.C.Y., Vedder, J.F., and O'Hara, D.: Measurement of stratospheric sulfur constituents. Geophys. Res. Lett., vol. 8, 1980, pp. 5-8.
3. Goldan, P.D., Kuster, W.C., Albritton, D.L., and Schmeltekopf, A.L.: Stratospheric CFCl_3 , CF_2Cl_2 , and N_2O height profile measurements at several latitudes. J. Geophys. Res., vol. 85, 1980, pp. 413-423.
4. Moore, Howard E., Poet, Stewart E., and Martell, Edward A.: Vertical profiles of ^{222}Rn and its long-lived daughters over the Eastern Pacific. Environ. Sci. Technol., vol. 11, 1977, pp. 1207-1210.
5. Cadle, Richard D.: Some effects of emission of explosive volcanoes on the stratosphere. J. Geophys. Res., vol. 85, 1980, pp. 4495-4498.
6. Maroulis, Peter J. and Bandy, Alan R.: Measurements of atmospheric concentrations of CS_2 in the Eastern United States. Geophys. Res. Lett., vol. 7, 1980, pp. 681-684.
7. Penkett, S. A., Derwent, R. G., Fabian, P., Borchers, R., and Schmidt, U., Methyl chloride in the stratosphere, Nature, vol. 283, 1980, pp. 58-60.
8. Lazrus, A.L., Cadle, R.D., Gandrud, B.W., Greenberg, J.P., Huebert, B.J., and Rose, W.I., Jr.: Sulfur and halogen chemistry of the stratosphere and of volcanic eruption plumes. J. Geophys. Res., vol. 85, 1979, pp. 7869-7875.

TABLE I. MIXING RATIOS^a (ppbv) OF GAS CONSTITUENTS IN MOUNT ST. HELENS PLUMES OF THE MAY 18, 1980 ERUPTION

Date Time (UT)	Coordinates °N/°W	Altitude km	OCS	SO ₂	CS ₂	CH ₂ Cl
5/19/80						
1606	44.4/108.6	14.0	0.87 ± 0.11	111 ± 1024	0.055 ± 0.028	2.89 ± 0.38
1539	45.2/111.0	15.2	0.47 ± 0.04	10.4 ± 1.0	0.0028 ± 0.0014	1.96 ± 0.28
1508	45.8/1114.0	16.5	0.067 ± 0.009	1.78 ± 0.39		0.280 ± 0.036
5/22/80						
1838	46.1/113.3	18.6-20.1	0.38 ± 0.11	0.091 ± 0.011	1.33 ± 0.17	
1938	47.0/113.5	20.1-20.7	1.20 ± 0.36	0.082 ± 0.037		5.0 ± 1.2
2009	46.3/114.0	20.1	0.91 ± 0.36	4.20 ± 0.55		3.19 ± 0.41
1938	47.3/112.6	20.7	0.022 ± 0.004	0.083 ± 0.011		0.183 ± 0.024

^aError limits are root-mean-square estimates of all known sources of uncertainty.

TABLE II. MIXING RATIOS^a (ppbv) OF ANIONS FROM WATER-SOLUBLE GAS CONSTITUENTS IN MOUNT ST. HELENS PLUMES

Date Time (UT)	Coordinates °N/°W	Altitude km	Cl ⁻	SO ₄ ⁼ (b)	NO ₃ ⁻
5/19/80 (Plume of May 18 eruption)					
1606	44.4/108.6	14.0	1000 ± 100	174 ± 17 (111)	6.2 ± 0.06
1539	45.2/111.0	15.2	42 ± 4 (10.4)		222 ± 22
5/28/80					
0235 ^c	48.5/125.4	18.3	467 ± 47	2.7 ± 0.27 (0.32)	6.1 ± 0.06
6/14/80					
2039 ^d	45.8/113.1	18.9	900 ± 90	5.7 ± 0.6 (2.26)	4.8 ± 5
6/17/80 (Plume of June 13 eruption)					
2204	42.4/114.3	18.9	671 ± 100	4.0 ± 0.6 (0.038)	3.5 ± 0.05

^aError limits are root-mean-square estimates of all known sources of uncertainty.

^bSO₂ mixing ratio in parenthesis in this column.

^cThis sample collected outside of plume.

^dThis sample collected presumably in plume of May 18 eruption.

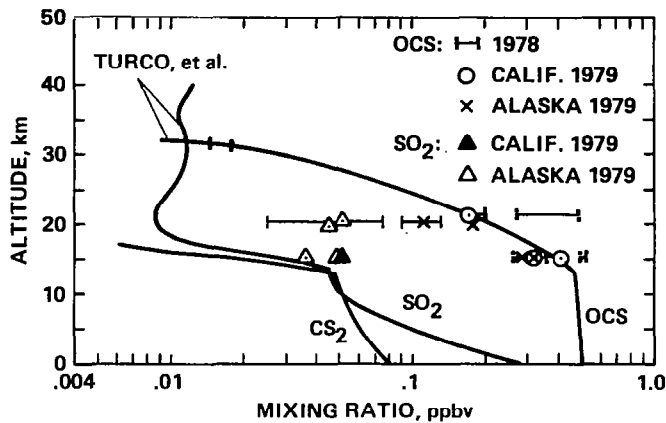


Figure 1. Pre-volcanic data of precursor gases from Inn et al. (2). Estimated upper limit mixing ratio of CS₂ at 15.2 km not plotted.

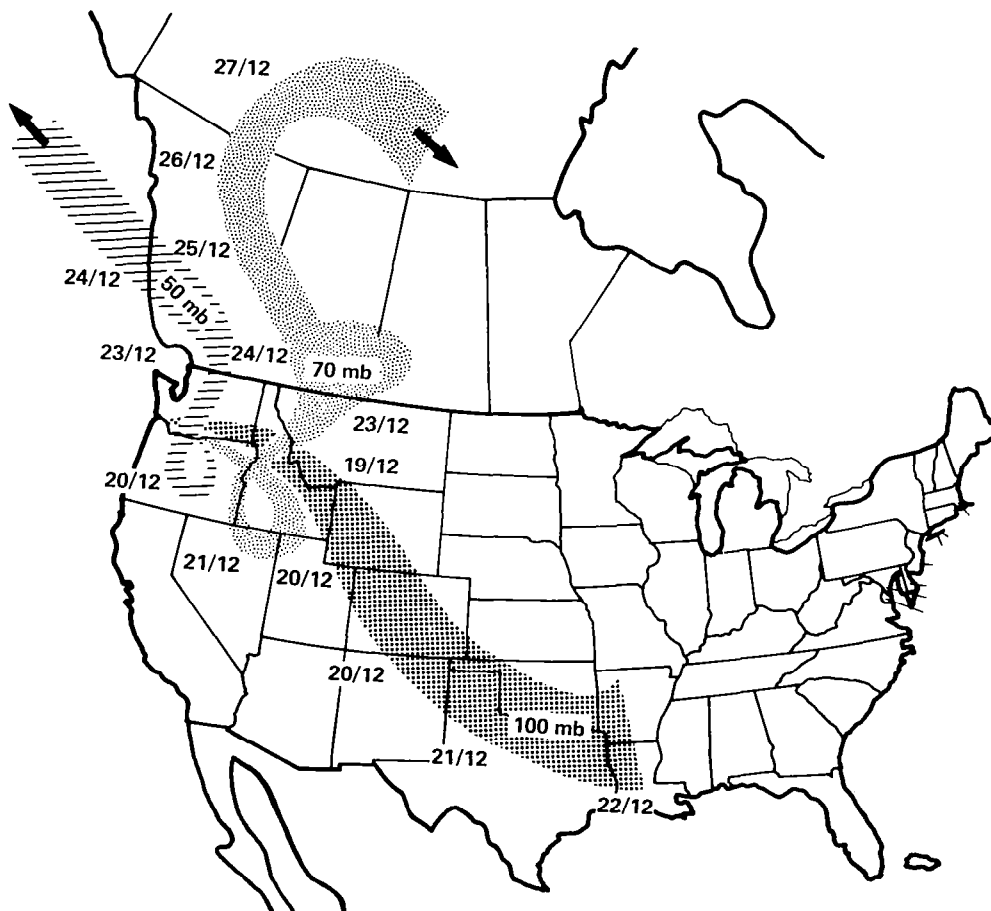


Figure 2. May 18, 1980 Mount St. Helens eruption plume trajectories. May date/universal time indicated for each trajectory. The May 19 and 22 experiments carried out in the 100 and 70 mb trajectory plumes, respectively.

TIME VARIATIONS OF AEROSOLS IN THE STRATOSPHERE FOLLOWING MOUNT ST. HELENS ERUPTIONS

Neil H. Farlow, Kenneth G. Snetsinger, Verne R. Oberbeck, and Guy V. Ferry
NASA Ames Research Center, Moffett Field, CA

George Polkowski and Dennis M. Hayes
LFE Corporation, Richmond, CA

Samples of stratospheric aerosols collected with U-2 aircraft for several months following the first three major eruptions of Mount St. Helens have been analyzed for ash and liquid acid content. Ash grain sizes and compositions vary depending on collection altitude, location within the drifting cloud, and days following their injection. Differing volume percentages of major ash components such as glass, plagioclase, hornblende, and pyroxene emphasize the inhomogeneity of the clouds. Size distributions of ash particles vary with altitude. Generally small particles are depleted more rapidly at low altitudes (12 km) than at higher altitudes (17-18 km). Although samples collected 1 day after the first eruption of May 18, 1980, were dry, flow marks on the aircraft indicated parts of the cloud contained heavy acid concentrations. Indeed, all other samples obtained within 1 to 4 days after later eruptions (May 25 and June 12, 1980) were covered with copious amounts of liquid acid. Proportions of liquid to ash varied considerably depending on sampling location and cloud age. Because the acid-coated ash globules were large, they rapidly fell from the stratosphere until, by late June 1980, only a residue of acid droplets remained. Size distributions and concentrations of these droplets have varied considerably over the past few months.

I. INTRODUCTION

Samples have been obtained of ash and acid aerosols in the stratosphere for 6 months following the spring and summer, 1980, eruptions of Mount St. Helens. The wire impactor system described by Ferry and Lem (1) and Farlow et al. (2) was used to collect these aerosols from high-flying U-2 aircraft. In this method particles impacted on fine wires of palladium and gold deployed from the instrument into the airstream. One of the gold wires coated with high viscosity silicone oil served to capture dry ash grains that might not stick to the bare wires. Collections were made at widely separated locations from Fairbanks, Alaska, to the Canal Zone, Panama. Although the most continuous records were obtained over California, some insight into the latitudinal dispersion of these aerosols was sought with short missions to the more remote regions.

The collections were examined to observe changes with time of ash and acid particle concentrations, compositions, and particle sizes to enable a better assessment of the effect of Mount St. Helens eruption on the upper atmosphere. The results were presented in two sections: first, descriptions of the characteristics of ash particles injected into the stratosphere, and, second, time variations of the acid aerosols.

II. RESULTS

A. Characteristics of Ash Particles

Table I presents general information about the stratospheric ash collections. Ash grains obtained 1 day after the eruption of May 18, 1980, were completely dry, whereas all ash collected later was covered with acid. The presence of this acid on most flights enabled the efficient capture of ash grains on the bare wires, while the silicone oil trapped dry ash on the initial flight.

The dry ash samples obtained May 19, 1980, over Montana at 14 and 17 km are composed of angular grains ranging in size from around 0.1 μm to as large as 30 μm , with median size around 0.3 μm (equivalent sphere diameters). A relative size distribution for the 14 km specimen is shown in figure 1(a). Because of the difficulty of completely removing the grains from the viscous silicone oil in which they were imbedded, the concentration of particles could not be accurately determined. Therefore, the relative size distribution obtained was normalized to a sample collected 3 days later (May 22) so it could be compared with a distribution of known concentration. In this comparison the general shapes of the curves and the particle size modes are similar. Mineral compositions of these dry particles are somewhat like those of the other samples collected later, in that glass and plagioclase are major components; however, the samples are otherwise quite different. Table I details the mineralogical features of all the collections. Mineralogy is derived from elemental analyses of individual ash grains by nondispersive x-ray methods in the scanning electron microscope. Mineralogical results from the 17 km sample over Montana on May 19 are also given in Table I, but no size distribution was obtained.

Although the first samples of ash were very dry, flow marks in dust on the aircraft wings suggested there were zones within the cloud containing large amounts of liquid, presumably acid, associated with the ash. The second flight to Montana on May 22, 4 days after the initial eruption, provided such an ash sample flooded with acid. Collecting wires were completely coated on the flight-facing side with coalesced acid drops encasing ash grains. Because the acid had converted to $(\text{NH}_4)_2\text{SO}_4$ in the laboratory environment (see Ref. 3 for experimental confirmation of such acid conversion), the ash grains could not be resolved in the scanning electron microscope until the sulfate crystals were removed. This removal was accomplished by heating the collecting surface in an oven at 250°C for 1-1/2 to 2 hours. Subsequent visual examination and x-ray analyses for sulfur showed that volatile sulfates had been removed; thus the ash grains were left intact and could be easily measured. This technique was used for all later samples where the presence of sulfate interfered with the ash grain analysis. Figure 1(b) presents the ash particle size distribution for this collection. Maximum sizes in this sample did not exceed about 3 μm equivalent sphere diameters.

Calculations of the log-normal functions that best fit the truncated size-frequency distributions were made and are drawn as solid curves on the data sets in figure 1. The general log-normal equation is:

$$\frac{dN/dr}{V} = \frac{N}{\sqrt{(2\pi)\sigma_1}V} \frac{1}{r} \exp \frac{-(\ln r - \ln r_1)^2}{2\sigma_1^2}$$

Parameter values for this equation are shown in figure 1, where N is the total number of particles, V is sample volume in cm^3 , r is particle radius, r_1 is median particle size and σ_1 is related to the standard deviation of the size frequency distribution. Although particles smaller than those observed, if collected, would give different log-normal fits, it is believed that those fits would be very similar to the present one because concentrations of such particles are very low. Error bars shown in figure 1(b) and later are 95 percent confidence intervals for the population as inferred from the samples. Again, nondispersive x-ray analysis provided elemental compositions from which mineralogy was derived for the May 22 sample. (See Table I.) In this group of particles, as in all other groups analyzed, there were no significant variations of compositions with particle size.

The stratospheric portion of the May 18 eruption cloud drifted eastward and circled the earth in about 16 days.¹ Its arrival was detected over California on June 3, when the collector, flown at 12 km, was again flooded with acid drops and ash grains. These grains were less than 3 μm in diameter. Although unusually large acid drops were also collected at 15 km on the same flight, and normal-background small acid drops at 18 km, no ash grains were found above the 12-km layer. The ash grain size distribution and mineralogy were derived by the same methods already described. Figure 1(c) and Table I show the particle size distributions with 95 percent confidence intervals, the log-normal fit parameter values, and the mineralogy.

¹Danielsen, E. (1980), Personal communication.

The second major eruption of Mount St. Helens occurred on May 25, 1980. Two samples of ash flooded with acid were obtained 2 days and 4 days after the eruption. (See Table I.) The first collection was obtained off the British Columbia coast and the second over California. By using the procedures outlined the size distributions and mineralogy shown in figures 1(d) and 1(e) and Table 1 for May 27 and May 29 were obtained. Again the ash grain sizes were less than $3\ \mu\text{m}$ diameter. Comparison of figure 1(d) with 1(b) suggests the size distributions at high altitudes for the first two eruptions are similar, as are the low altitude ones [figs. 1(c) and 1(e)], but high altitude distributions do not compare favorably with low altitude ones; nor, for that matter, do any of the mineral groups compare well with each other.

Finally it was possible to collect a sample of the third explosion of St. Helens on June 13 off the coast of Washington, the day following the volcano's eruption. This time the collecting surfaces were not flooded, although a dense collection of very large acid drops were obtained. Ash grains ($< 3\ \mu\text{m}$ diameter) were scattered about the surfaces and were stuck to the bare wires by a coating of acid around the individual grains. The analysis of the 12 km sample, by these methods, resulted in the data shown in figure 1(f) and Table I. The size distribution seen here is somewhat similar (mode radius near $0.6\ \mu\text{m}$) to the other low-altitude samples [figs. 1(c) and 1(e)].

An examination of the size distribution in figure 1 reveals that high-altitude specimens generally have particle size modes around $0.3\ \mu\text{m}$ radius, whereas low-altitude samples have modes at about $0.6\ \mu\text{m}$. Even though the distributions are similar at the large particle end, there is a marked decrease in the small particle component at low altitudes. Note, however, that the sizes of the ash grains do not represent the maximum sizes of the acid-ash globules. In all but the initial May 19 collection, the ash was flooded with acid; thus, for these few samples actual combined globule sizes were very large but could not be determined nor could the acid quantity be estimated.

The log-normal curves fit the experimental data closely at high altitudes [figs. 1(b) and 1(d)] and at one of the lower altitudes [fig. 1(f)]. They are well within the 95 percent confidence interval error bars that have been determined for each size group and are confirmed by the χ^2 test of fit. Such a good fit for volcanic ash is perhaps not surprising since, according to the theory of breakage (4), mechanical grinding (as must occur in the explosive breakup of volcanic material) produces a distribution of particles that closely fits the log-normal function. If this premise is accepted, then the two high-altitude samples [May 22 and 27, figs. 1(b) and 1(d)] and one of the low-altitude collections [June 13, fig. 1(f)] might be considered to be the most representative of the injected ash for their respective eruptions and altitudes. The other two low-altitude samples [May 29, fig. 1(e) and June 3, fig. 1(c)] do not closely fit log-normal functions and may have been perturbed by external events like size fractionation from fallout or meteorological effects.

By using the ash particle size distribution of figure 1, calculations were made of the mass and number of ash particles per unit volume of air sampled for each collection. (See fig. 2.) The volume of each grain was equated to that of an equivalent radius sphere ($\rho = 2.5\ \text{g cm}^{-3}$). In the comparisons in figure 2 it can be seen where the dominance of a few large particles in the sparse June 3 collection yields a very large mass compared with that of a more populous collection (May 22) containing many smaller grains. A possible trend is seen of decreasing particle concentration and mass with time after the second eruption (May 27, 2 days later compared with May 29, 4 days later). But such is not apparent for the first-eruption samples of May 22, 4 days later, compared with June 3, 16 days later. Inhomogeneity of different cloud portions is evident in these results.

Regarding mineralogy of the stratospheric ash, samples from different parts of the cloud produced by a given eruption are not similar, nor are data from different eruptions comparable. This condition is considered to be due to the inhomogeneity of the source rocks on Mount St. Helens. Note, however, that the glass-to-plagioclase ratio in the May 19 samples of the first eruption are somewhat alike; so are the glass/plagioclase ratios of the second-eruption samples. This result might suggest at least a rough consistency in source rock for these events. But whether the resemblances are fortuitous is not known. Some first eruption ash samples collected at ground level have been briefly examined. A coarse sample from Yakima had about equal amounts of plagioclase and glass, with less than 15 volume percent of other phases being present. Very fine-grained ash from Pullman was about 90 percent glass, the rest mostly plagioclase. Thus even the fine-grained ground sample is not like the stratospheric first-eruption collections. This further reflects the inhomogeneity of the ash produced.

Additional evidence for inhomogeneity of the ash cloud is found by comparing the two May 19 first-eruption samples (Table I). These were taken over the same location at nearly the same time, but at different altitudes, and are notably different mineralogically.

Because the 16-day sample from the first eruption is nearly all glass, it might be assumed that mineral fragments have somewhat been sorted out. But it is not likely that the later sample represents the same ash that was collected on the 19th or 22nd of May. Conceivably, a 16-day sample from another altitude or locality might contain more fine-grained minerals.

Maximum stratospheric perturbations from the eruptions of Agung (1963) and Fuego (1974) were observed in mid-northern latitudes about 3 months afterwards (5), although initial effects were seen much sooner. This time lapse occurred partly because of the slow conversion of injected sulfur gases to sulfuric acid drops. Stratospheric aerosol models (e.g., see Ref. 6), therefore, were designed principally to show the long-term effects of this slow gas conversion. The injection of large globules of ash and liquid by the St. Helens eruptions may cause different effects. Because the acid-coated ash particles were large, they have fallen quickly from the stratosphere and have left behind only smaller acid droplets and whatever sulfur gases were unreacted. In the next section the variations of the acid aerosol concentrations with time and location are explained to see whether gas-to-acid particle conversions can be detected.

B. Time Variations of Acid Aerosols

The eruption clouds from Mount St. Helens directly affected the lower stratosphere (12 km) over California in late May by flooding collectors with heavy amounts of acid and ash. (See figure 3.) High altitudes were, at first, unaffected. After the initial surges through June 3 of volcanic ash clouds, a buildup of acid aerosols devoid of obvious ash grains occurred first at low altitudes (12 km), followed by enhancements at 15 km, and heavy but transient, concentrations at 18 km. By late June the high altitude aerosols had dissipated to perhaps a small increase above pre-eruption averages. Aerosol concentrations at 12 to 15 km peaked in late June and then also subsided to near pre-eruption values by mid-July. Although the size distribution studies have not yet been completed, the acid droplets collected during the peak periods are characterized by small particles, enhancements suggestive of young aerosol particle growth observed by V. Oberbeck.² Clearly, over California the influence of the initial Mount St. Helens eruptions is now negligible.

Stratospheric samples at other locations were obtained during short excursions of the U-2 aircraft. Figure 4 shows the results obtained at latitudes extending from Alaska to Panama. Above Fairbanks, Alaska, in late July large increases of acid were observed at low altitudes (12 km) compared with those observed a year earlier. Only slight increases, if any, were seen at high altitudes. Unfortunately, the aerosol concentrations before and after this short sampling period are not known.

In the vicinity of Mount St. Helens and east to the Idaho-Wyoming-Montana region, special U-2 expeditions were conducted to penetrate visible volcanic clouds in the stratosphere. These clouds were characterized by distinct layering so that samples collected short distances from each other were very different. For example, of two specimens collected on May 19 (both mostly ash), only the high altitude one contained a small background of acid droplets (fig. 4); and on May 22, although one collection was completely flooded with acid and ash, the other consisted only of background acid aerosol. Similarly, the May 27 samples and, not so dramatically, the June 13 group also showed this variable behavior. By July 23, however, the sharp layering had diffused so that the adjacent altitudes were more uniformly enhanced with acid drops. Further north, by July 25, over Canada and Fairbanks, Alaska, only background concentrations were seen at 18 km. Finally, as the U-2 went to and returned from Panama, a slightly enhanced acid aerosol was observed in the 18 to 20 km zone over Florida, showing a rather consistent, thin droplet population.

In Panama (fig. 4) over a 3 week period in late August and September, most acid drop populations were approximately the same as we had measured there 1-1/2 years earlier. At the end of the sampling period, however, on September 21, a final collection between 18 and 20 km showed a strong increase over the earlier few weeks average particle concentrations. Cause of this sudden increase can only be guessed because further sampling there ended as the U-2 returned to California.

²Oberbeck, V. (1980), Personal Communication.

III. CONCLUDING REMARKS

Initial injections of volcanic debris into the stratosphere from Mount St. Helens eruptions in May and June, 1980, were highly layered and inhomogeneous. Although some parts of the first eruption cloud were devoid of liquid, other parts were heavily acidified as shown by flow streaks in dust on U-2 aircraft. Aerosol collections made 4 days after the first major eruption, and within 1 or more days after the next two eruptions, were flooded with liquid acid and ash. Although the concentrations of ash particles in the stratosphere were small, the large grains contributed to a major intrusion of mineral mass. But the diameters of the combined acid-ash globules were so large that within a month these particles had fallen from the region and had left behind only an enhanced acid aerosol layer. If these acid aerosols were formed by sulfur gas-to-particle conversions in the 12 to 18 km zone, as the presence of increased small "growth" particles suggests, then peak concentrations due to this were reached over California in mid and late June. Diffusion and dilution then reduced the populations to near pre-eruption values in this latitude region by late October, 1980. Enhanced acid aerosol populations were detected over Fairbanks, Alaska, in late July during a 1 week U-2 mission, but a similar excursion to Panama in September failed to show increased stratospheric aerosols there except perhaps, on the last day of the mission in late September.

These studies show that even though massive amounts of volcanic debris were introduced into the stratosphere by three major eruptions of Mount St. Helens 6 months ago, most of this material is now gone and has left behind only a slightly enhanced layer of acid droplets.

ACKNOWLEDGMENTS

The authors thank Harry Shade and Memorex Corporation for help in analyzing some of the volcano samples with their scanning electron microscope, and Jozef Erlichman, LFE Corporation, for his analysis of some ash grain compositions. We also thank J. H. Ferry, Yakima, Washington, for the St. Helens ash he sent us, and W. A. Page, NASA Ames Research Center, for the ash from Pullman, Washington.

REFERENCES

1. Ferry, G. V., and Lem, H. Y.: Aerosols in the Stratosphere, In Proceedings of the Second International Conference on the Environmental Impact of Aerospace Operations in the High Atmosphere, Am. Meteorol. Soc. (Boston, MA) 1974.
2. Farlow, N. H., Ferry, G. V., Lem, H. Y. and Hayes, D. M.: Latitudinal Variations of Stratospheric Aerosols, J. Geophys. Res., Vol. 84, 1979, pp. 733-743.
3. Hayes, D. M., Snetsinger, K. G., Oberbeck, V. R., and Farlow, N. H.: Reactivity of Stratospheric Aerosols to Small Amounts of Ammonia in the Laboratory Environments, Geophys. Res. Lett., 1980.
4. Aitchison, J. and Brown, J. A. C.: The Log-Normal Distribution, Cambridge Press, (Cambridge, England), 1976.
5. Hofmann, D. J., and Rosen, J. M.: Balloon Observation of the Time Development of the Stratospheric Aerosol Event of 1974-1975, J. Geophys. Res., Vol. 82, 1977, pp. 1435-1440.
6. Turco, R. P., Hamill, P., Toon, O. B., Whitten, R. C., and Kiang, C. S.: A One-Dimensional Model Describing Aerosol Formation and Evolution in the Stratosphere. I. Physical Processes and Mathematical Analogs, J. Atmos. Sci., Vol. 36, 1979, pp. 699-71.

TABLE I. CHARACTERISTICS OF MOUNT ST. HELENS ASH IN THE STRATOSPHERE

Date collected	Eruption sampled	Days after eruption	Altitude, km	Mineralogy (volume percent)				
				Glass	Plagioclase	Hornblende	Pyroxene	Other
5/19/80	1	1	14	65	32	2.3	0.1	Sulfides, biotite, chromite
5/19/80 ^a	1	1	17	37	16	21	13	SiO ₂ ^b
5/22/80	1	4	18	60	13	5.0	22	c
5/27/80	2	2	17	80	20	c	c	c
5/29/80	2	4	12	64	18	4.6	c	SiO ₂ , ^b sulfides, ilmenite
6/3/80	1	16	12	100	d	d	c	c
6/13/80	3	1	12	83	10	2	5	c

^aNot included in size distribution data, figure 1.

^bCristobalite?

^cNot found.

^dQuestionably present.

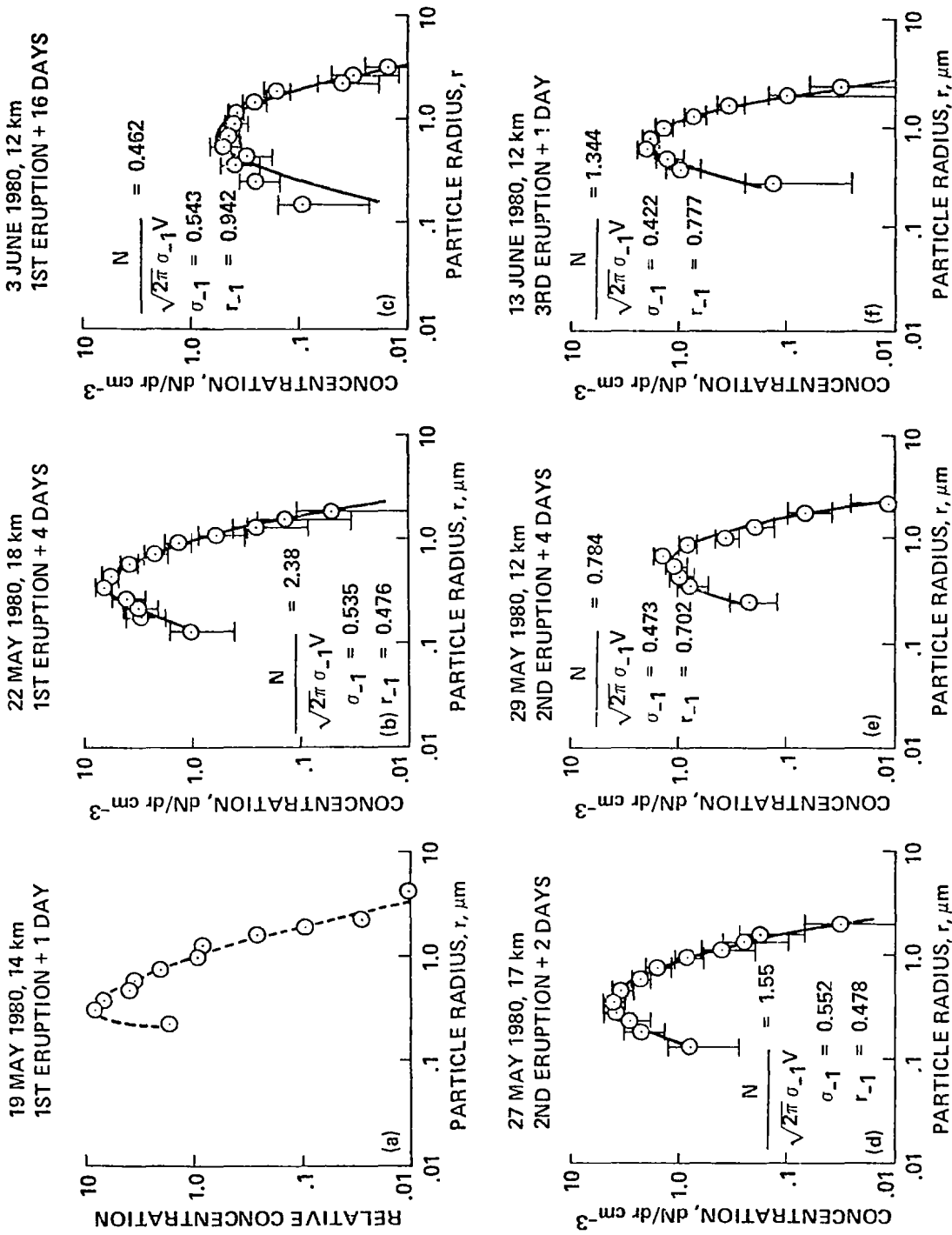


Figure 1. Ash grain particle size distributions in the stratosphere for three St. Helens eruptions. Solid curves are best fitting log-normal functions using the stated parameter values. Error bars are 95 percent confidence intervals for the population as inferred from the samples.

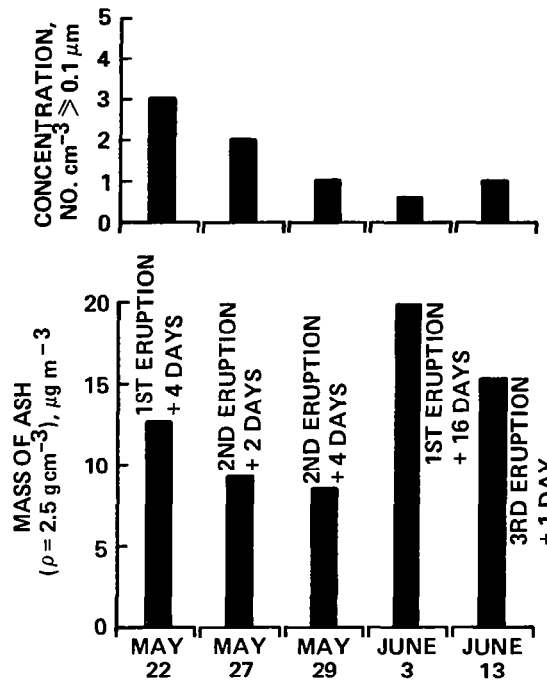


Figure 2. Concentration and mass of ash in the stratosphere after Mount St. Helens eruptions, 1980.

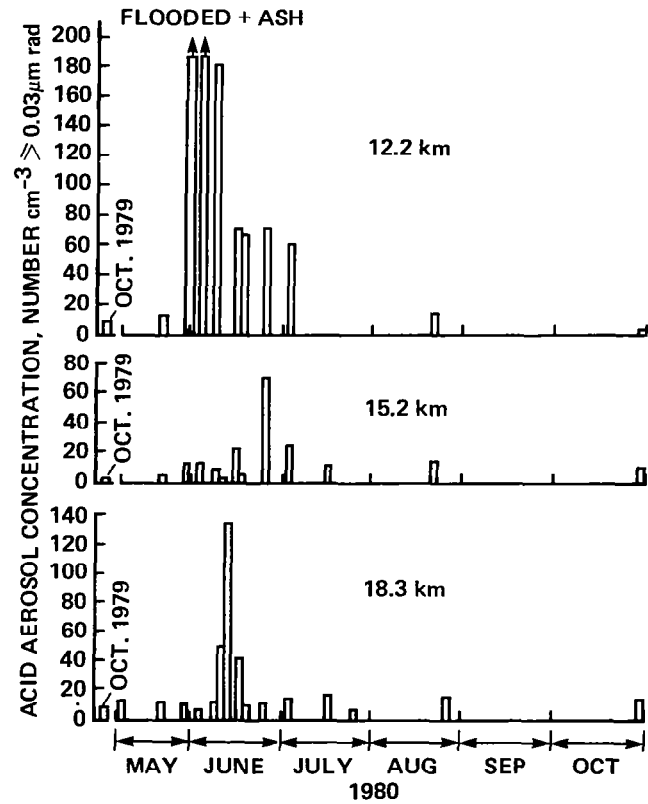


Figure 3. Time history of acid aerosol concentrations in the stratosphere above California after Mount St. Helens eruption, 1980.

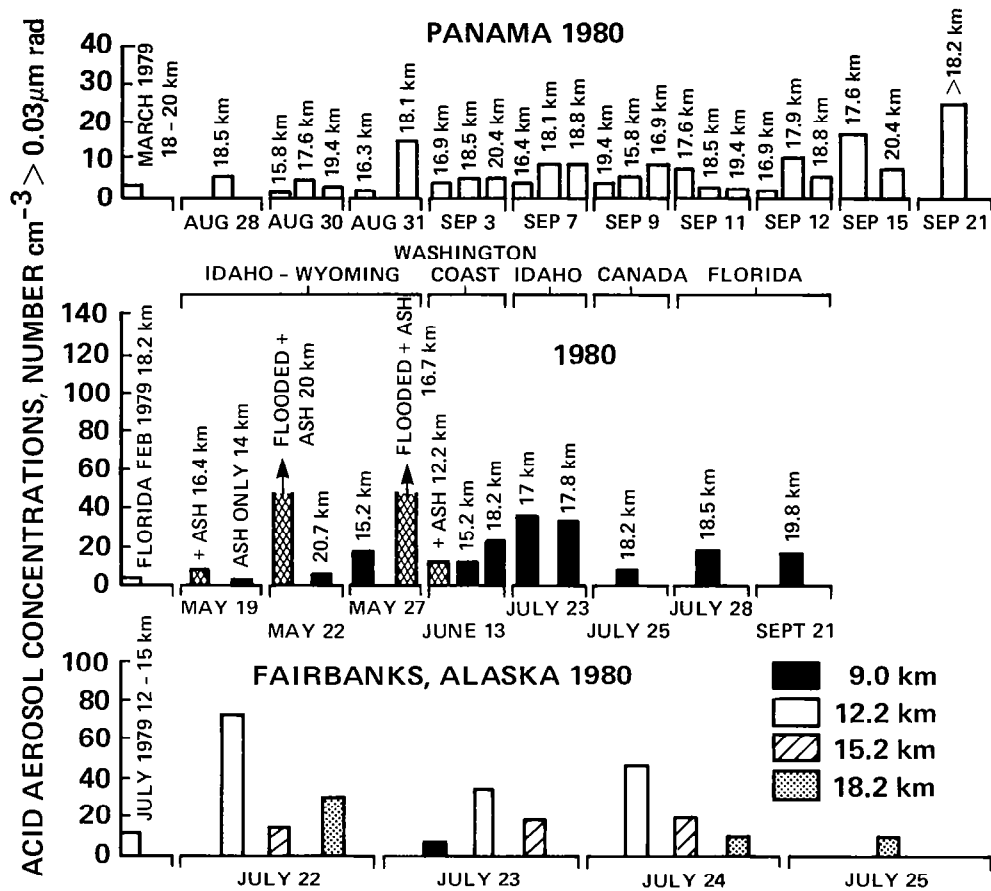


Figure 4. Time history of acid aerosol concentrations in the stratosphere above Panama, Florida, Northwest United States, and Alaska after Mount St. Helens eruptions, 1980.



DUSTSONDE MEASUREMENTS OF THE MOUNT ST. HELENS VOLCANIC DUST CLOUD OVER WYOMING¹

J. M. Rosen and D. J. Hofmann

University of Wyoming, Department of Physics and Astronomy, Laramie, Wyoming

Numerous balloon soundings of the aerosol (diameters ≥ 0.3 and $0.5 \mu\text{m}$) and condensation nuclei (CN) concentrations were made over Laramie, Wyoming following the eruption of Mount St. Helens in May of 1980. On several occasions the volatility of the particles was tested. In addition, special instrumentation was used to observe the evolution of particle size after the eruption. The results show that the particles in the initial cloud were relatively large and nonvolatile. In a relatively short time, however, the aerosol began showing a dominant volatile component. Although there were probably no CN in the original cloud due to the expected very short coagulation life time, high concentrations of unusually small CN particles were observed about a month after the eruption. By the end of September the CN profiles and associated particle size were practically back to normal. At present the aerosol particles (dia. $\geq 0.3 \mu\text{m}$) show about a three times larger concentration than before the eruption, most of the new material being in a layer centered around 19 km. The net effect of the more recent series of eruptions during the last half of October 1980 seems to be negligible.

I. INTRODUCTION

In the first 5 months following the May 18, 1980 eruption of Mount St. Helens, the University of Wyoming atmospheric physics group entered into a period of intensive balloon soundings with a goal of defining the initial character and distribution of the original eruption cloud as well as monitoring the subsequent short-term disturbances. Most of the soundings were made with dustsondes in which the vertical profile of the aerosol concentration with particle diameters greater than or equal to 0.3 (Channel I) and $0.5 \mu\text{m}$ (Channel II) was measured. In many soundings multiple instruments were flown and allowed for the simultaneous determination of other parameters such as volatility, condensation nuclei (CN) concentration, and CN size. In addition, wind and temperature information was routinely acquired from each sounding. Additional information concerning the nature of the instrumentation can be found elsewhere (1).

II. THE INITIAL ERUPTION CLOUD PASS

In the week following the eruption, six soundings were made, the first one occurring on May 19. The results of this initial sounding are illustrated in figure 1 and show the presence of a very pronounced layer of relatively large particles at about 13 km which at that time was slightly above the jet stream core. Other than this feature, the aerosol profile was essentially identical to pre-eruption measurements. Later on the same day, a volatility test of the aerosol was made by flying a double dustsonde with the intake on one heated to 150°C and the intake on the other kept at ambient temperature. Past experience has shown that if a volatile aerosol such as H_2SO_4 is present, a very much lower counting rate will be observed in the detector with the heated intake. The normal stratospheric aerosol has been shown to be volatile at 150°C (2). The results of

¹ This work was supported in part by the National Science Foundation, the National Aeronautics and Space Administration, the National Oceanic and Atmospheric Administration and the Office of Naval Research.

this volatility sounding are presented in figure 2 and show that in the volcanic layers themselves, the particles are nonvolatile whereas in the undisturbed regions, the usual volatile aerosol is observed. It is now believed that the nonvolatile material was ash particles similar in nature to the fallout associated with the main eruption.

A composite of soundings illustrating the passage of the eruption cloud over Laramie during the first week is shown in figure 3. As might be expected, the first part of the cloud to arrive was near the wind maximum. The layers moved upward with the passage of time; the effect due to the later arrival of the higher altitude portions of the original cloud.

Figure 3 also shows that on May 26 no disturbed stratospheric aerosol conditions were observed; thus, the approximate completion of the first passage was significant. It should be noted, however, that a few unusual layers were observed near the tropopause which were very probably associated with a relatively small eruption of Mount St. Helens which occurred the day before.

During the first week of soundings, no layers were observed above about 18 km. The wind data indicated that any part of the original eruption cloud above this altitude would probably be caught in the easterly stratospheric winds (just beginning at this time of year) and would therefore not be expected to pass over Laramie for some time. As will be discussed later, this part of the cloud finally did appear over Wyoming.

III. OVERVIEW OF DEVELOPMENTS IN THE FIRST FIVE MONTHS

Following the first week's effort, soundings were made at approximately weekly intervals. The results of these soundings, indicating the position and development of the layers, are shown in figure 4. To better organize a discussion of this figure, four general layers have been identified: the jet stream layer (12.5 to 15 km), the main layer and its predecessors (15 to 19 km), the transition layer (19 to 20 km), and the retrograde layer (above 20 km).

A. The Jet Stream Layer

This layer was observed on the very first sounding after the eruption (see fig. 1). It completed its initial global circuit on about June 3 when it was seen for the second time over Laramie. The observations strongly suggest that it was again seen over Laramie on June 20 after completing its second traversal. In all these cases, it appeared at or near the maximum in the wind profile. Figure 4 suggests that parts of this layer were observed on many occasions throughout the summer. However, the smaller eruptions occurring after the initial explosion on May 18 may also have been responsible for some of the material in the jet stream region. The low-altitude layers observed in the soundings on May 26 and October 22 are possible examples.

As indicated earlier, the particles in the jet stream layer were relatively large and nonvolatile on the initial pass. However, a test on June 27 showed that the aerosol in the general region of the jet stream was significantly volatile. Unfortunately, there was no well-defined jet stream layer present for this volatility test or the subsequent one on July 15. On the second and third passes, the layer displayed a much steeper size distribution and indicated the presence of relatively more small particles, although the overall concentration was diminished by a considerable factor. As will later be illustrated, the concentration in the jet stream had essentially returned to normal by at least the end of September 1980.

B. The Main Layer

A highly layered structure that turned out to be the predecessor of the now broad main layer appeared briefly over Laramie during the first week after the eruption (see fig. 3). Size distribution data indicated that there was considerable internal structure in these first layers, parts of them having an unusual amount of small particles and other parts had relatively larger particles similar to those observed in the initial jet stream layer. Unfortunately, there are no volatility tests available to assess the initial character of this layer.

The predecessors of the main layer disappeared at the end of the first week and did not reappear again until the sounding of July 10. The results of a volatility test conducted on July 15, as illustrated in figure 5, show that the main layer particles were mostly volatile at that time. The size distribution, as reflected in the aerosol count ratio profile also shown in figure 5, was still quite variable in the main layer region with some regions of relatively large particles and some of relatively small particles. The first condensation nuclei (CN) sounding conducted after the eruption was made on June 20 and showed surprisingly high CN concentrations up to 20 km. The general profile was very similar to that illustrated in figure 6 for the July 2 sounding.

It was also discovered that the unusual concentration of CN in the lower stratosphere was made up of particles much smaller than normal. This result was achieved by utilizing a diffusion battery technique to obtain the effective diffusion radius of the particles. In the actual flight configuration, two CN counters were used. One regular detector determined the ambient concentration while the other detector with the diffusion battery determined the percent transmission of the particles through the diffusion battery. In this way continuous information could be obtained. A well-known relationship between the measured percent transmission and the effective particle size (3) was then applied to obtain the size information as illustrated in figure 6.

Another size determination of the CN was made on August 27 and these results are illustrated in figure 7 along with a typical pre-eruption profile. Apparently, by August 27 the CN size and concentration was almost back to normal. A comparison of figures 6 and 7 shows the region in the lower stratosphere (13 to 19 km) where the unusually small CN were observed.

C. The Reversal Layer

The reversal layer occurred in a region where the summer winds changed from westerly to easterly, which for the purposes of this discussion is about 19 to 20 km. In this altitude interval the winds were generally very light and poorly defined in direction. The part of the original cloud caught in this reversal layer was first observed over Laramie in the sounding on June 2 and was moving toward the west. How it came to be over Laramie at this particular time is still unexplained. It was moving too slowly to have completed one global circuit.

The size distribution information indicated a more normal situation for this layer with the absence of the predominantly large particles as observed in the original jet stream layer. The results of a volatility test conducted on this layer (see fig. 8) show that the particles at this time were mostly volatile. After heating, however, the particles were predominantly large in this layer (as indicated by the small value of the aerosol count ratio in fig. 8) and this result suggests the presence of some of the original large solid ash particles.

CN layers were also found in this region and, as previously discussed, the particles first observed were of an unusually small size (see figs. 6 and 7). By the end of July the layers occurring in the transition region seemed to have gradually smoothed out and merged with the top side of the main layer even though they were moving in the opposite direction.

D. The Retrograde Layer

Since the wind reversal occurs at about 19 or 20 km, any material ejected to greater heights by the May 18 eruption would not be expected to pass over Laramie until it made a complete global circuit. This part of the cloud was first observed over Wyoming at about 24 km on July 10 moving toward the west and was reportedly detected by lidar over Europe about 10 days earlier (4). Figure 4 suggests that a second pass of this layer may have been observed over Wyoming in the August 27 sounding.

The particle profiles (including CN) associated with the first observation of the retrograde layer are shown in figure 9. A very distinct sharp layer is present which occurs at slightly higher altitudes in the

smaller particle profiles. This separation could perhaps be explained by differential gravitational sedimentation. As seen in figure 4, this layer separation feature (small particles on top—large particles on the bottom) was a frequently observed phenomenon.

The size distribution information obtained for the retrograde layer indicated that there were some very large particles as in the case of the initial jet stream layer. At first, it was thought that these were the original solid ash particles, but a volatility test on July 15 indicated that the large particles were mostly volatile (see fig. 5). The presence of the large particles is indicated by the low values of the aerosol count ratio at about 22.5 km in the same figure. This low count ratio feature persisted in the soundings for several months.

IV. PRESENT STATUS

A sounding typical of the present aerosol profile is shown in figure 10 along with a pre-eruption profile for comparison. It should be mentioned that just before the May 18 eruption, the stratospheric aerosol layer was in a disturbed state probably because of minor volcanic eruptions (5) and it is necessary to go back to November 1, 1979 to obtain a typical background sounding. Figure 10 shows that by September 23 the individual layers had smoothed out and had merged into a single layer centered around 17.5 km with a concentration about three times higher than that in the undisturbed background layer. The aerosol count ratio profile shows the last traces of the retrograde layer in which the values of the count ratio are unusually and persistently low.

Figure 7 indicated that by August 27 the CN profile and effective size were already approximately back to pre-eruption values; thus, the CN seemed to be disturbed for only a few months after the eruption. This condition may explain the inability to detect any change in the CN after the eruption of Fuego in 1974 when the first CN sounding was made about 5 months after an increase in aerosol was observed (6).

A comparison of figures 2 and 5 shows that there has been a two- or three-fold general increase in the nonvolatile aerosol between 16 and 24 km since the May 18 eruption. This material is perhaps a portion of the original ash cloud but has been diluted to a relatively low concentration by dispersion and possible differential sedimentation.

Figure 11 shows how the Mount St. Helens eruption has affected the stratospheric aerosol background and how it compares with that of Fuego in 1974. Apparently, the influence of the recent eruption on the equilibrium stratospheric aerosol layer was smaller by about a factor of two (mixing ratio of about 20 mg^{-1} as compared with about 40 mg^{-1} 5 months after the Fuego eruption). Figure 12 is an expanded version of figure 11 for the first few months following the eruption and shows the relatively fast decay of several identifiable layers. These net decay curves are a result of the dispersion of the initial cloud into relatively clean regions with possibly an additional build-up of nonvolatile material. Thus, a simple dispersion model, conservation of particles being assumed, may not be applicable in trying to explain the results of figure 12.

V. CONCLUDING REMARKS

It is perhaps worthwhile at this point to summarize a few of the major observations of this work:

1. The original ash cloud seen in the 12.5 to 15 km jet stream region was made up of relatively large non-volatile particles.
2. The aerosol above 16 km had a large volatile component shortly after the eruption, and from our data alone the possibility of direct injection of volatile particles into some parts of the stratosphere cannot be excluded.
3. Very small as well as very large volatile particles were observed in the first few months after the eruption in an altitude range which is now part of the main layer.
4. The layered structure disappeared in about 4 to 5 months after the eruption and a broad main layer centered at about 17.5 km emerged.

5. The stratospheric CN concentration and size, as observed one month after the eruption, was found to be in a highly disturbed state (high concentration of unusually small particles). However, by 3 months after the eruption the CN concentration and size had almost returned to pre-eruption values.

6. Some of the original nonvolatile ash particles are probably still present in the stratosphere but at low concentration when compared with the volatile particles.

7. A comparison of pre- and post-eruption profiles indicates a total stratospheric aerosol loading increase of about a factor of 3. This material is essentially all volatile.

8. Mount St. Helens increased the equilibrium stratospheric aerosol layer at northern midaltitudes by about one half that of the eruption of Fuego in 1974.

Further discoveries and deductions could undoubtedly be made if other observers' results were also taken into account. This will probably be done at a later date when the information has been satisfactorily documented.

REFERENCES

1. Hofmann, D. J., Rosen, J. M., and Pepin, T. J.; Stratospheric aerosol measurements I: Time variations at northern mid-latitudes. *J. Atmos. Sci.*, vol. 32, 1975, pp. 1446-1456.
2. Rosen, J. M.; The boiling point of stratospheric aerosols. *J. Appl. Meteorol.*, vol. 10, 1971, pp. 1044-1046.
3. Mercer, T. and Greene, T. D.; Interpretation of diffusion battery data. *Aerosol Sci.*, vol. 5, 1974, pp. 251-255.
4. Reiter, R., Jager, H., Carnuth, W., and Funk, W.; Lidar observations of the Mount St. Helens eruption clouds over Mid Europe, May to July 1980. *Geophys. Res. Letters*, vol. 7, 1980, pp. 1099-1101.
5. Rosen, J. M. and Hofmann, D. J.; A stratospheric aerosol increase. *Geophys. Res. Lett.*, vol. 7, 1980, pp. 669-672.
6. Rosen, J. M. and Hofmann, D. J.; Balloon borne measurements of condensation nuclei. *J. Appl. Meteorol.*, vol. 16, 1977, pp. 56-62.

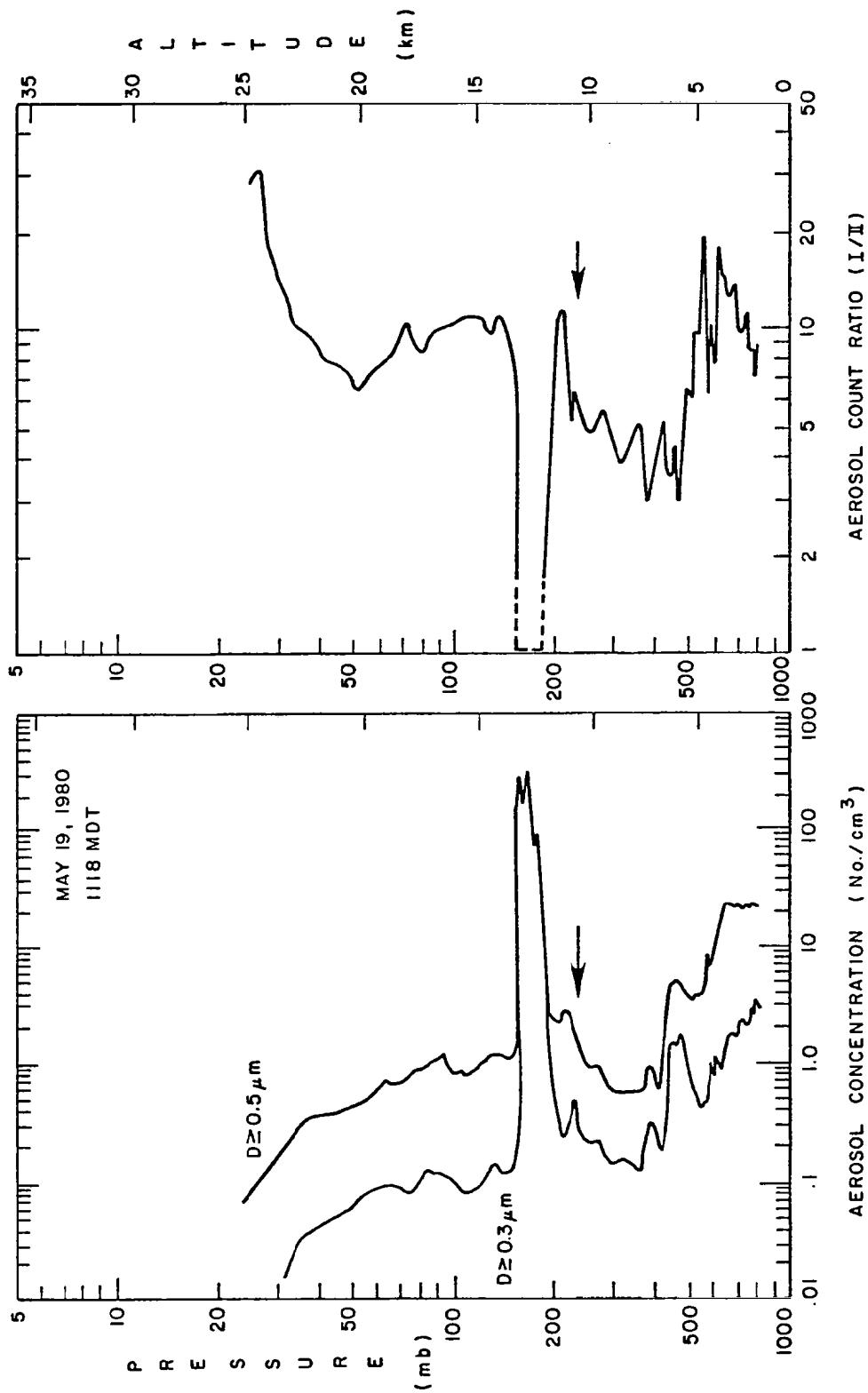


Figure 1. The first aerosol profile obtained after the eruption on May 18. The two curves refer to the cumulative concentration of the two different size particles measured in channels I and II. The aerosol count ratio is the concentration ratio between Channel I and II. The arrow marks the tropopause height.

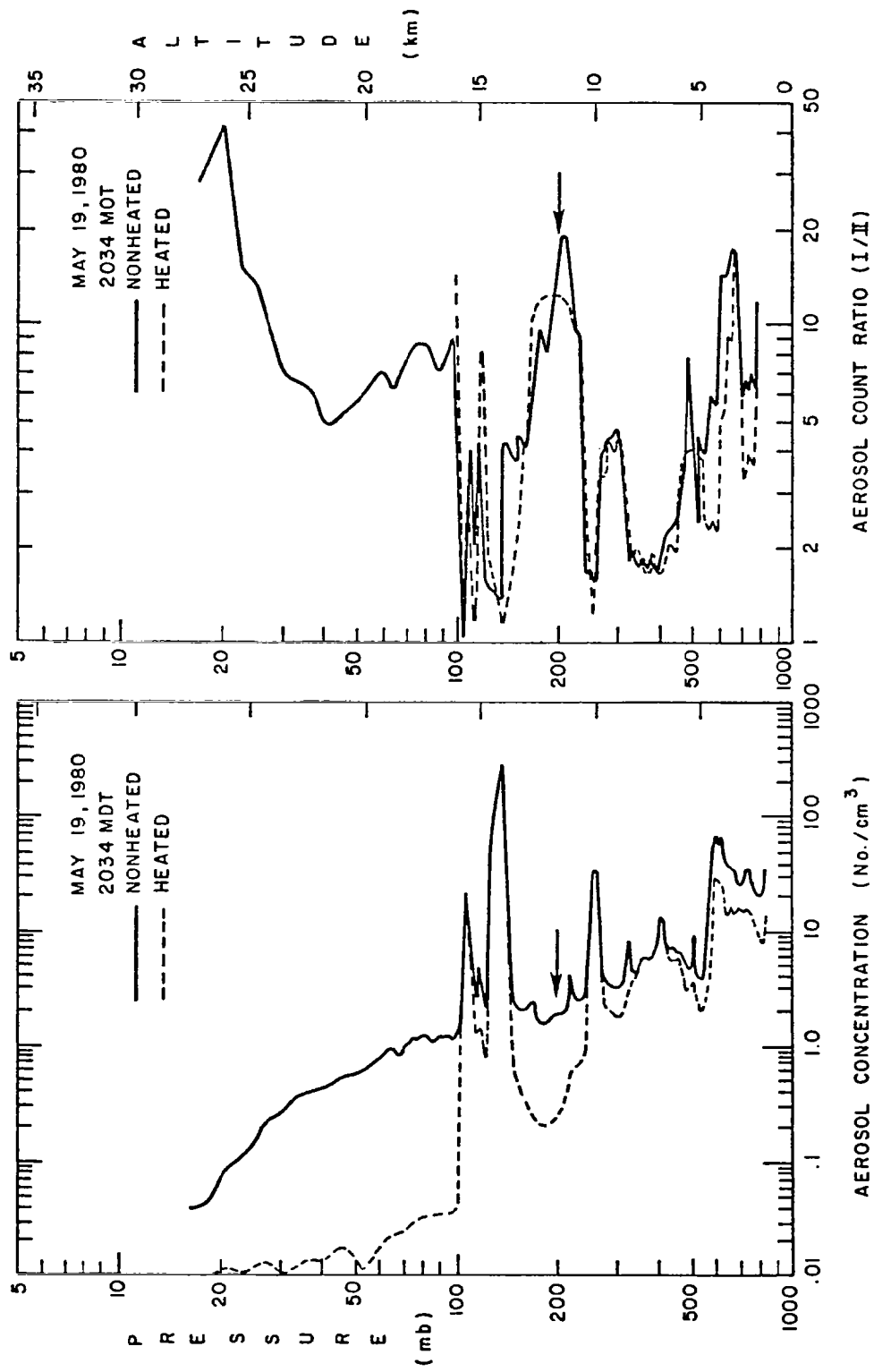


Figure 2. The result of a volatility test conducted a day after the eruption.

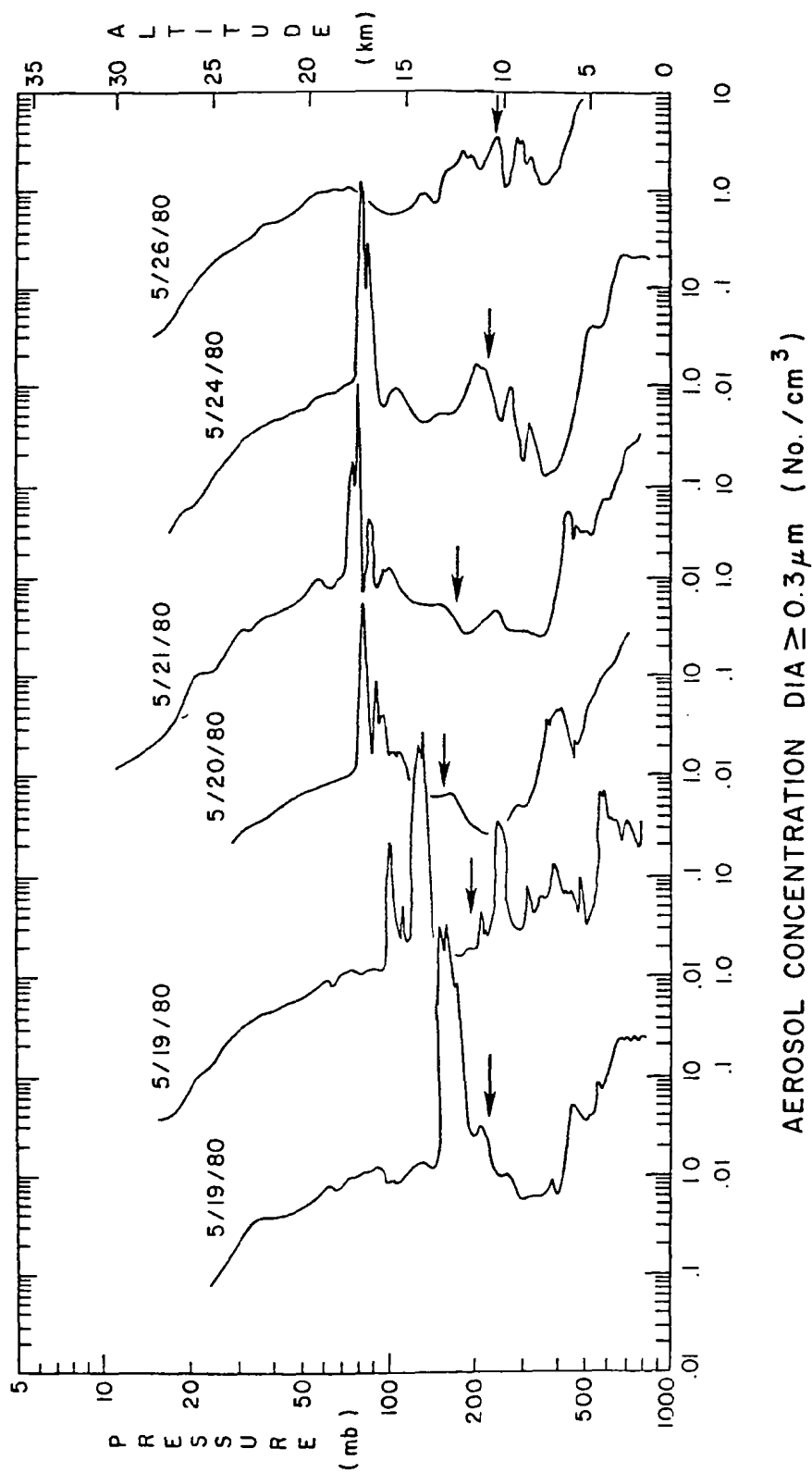


Figure 3. A composite of the first week's soundings.

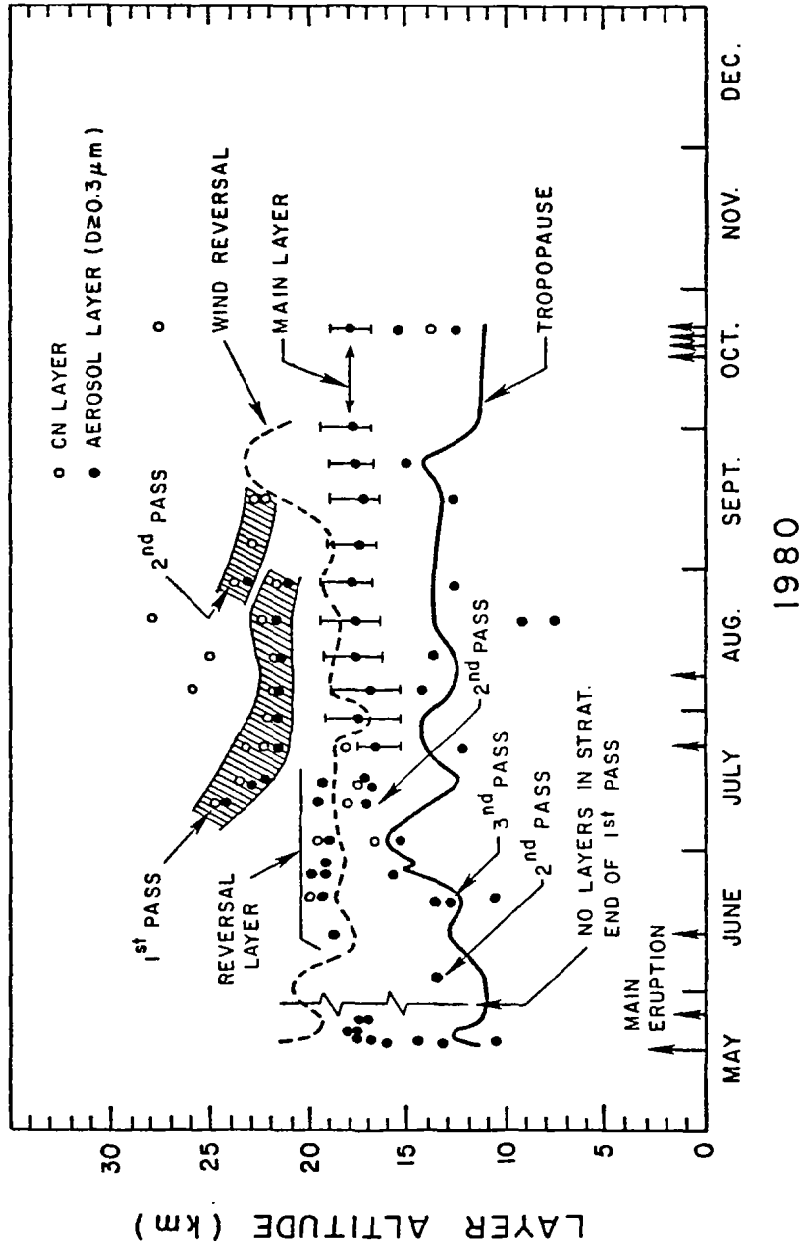


Figure 4. The development of the layered structure over Laramie during the first 5 months after the eruption. The vertical arrows represent eruption dates.

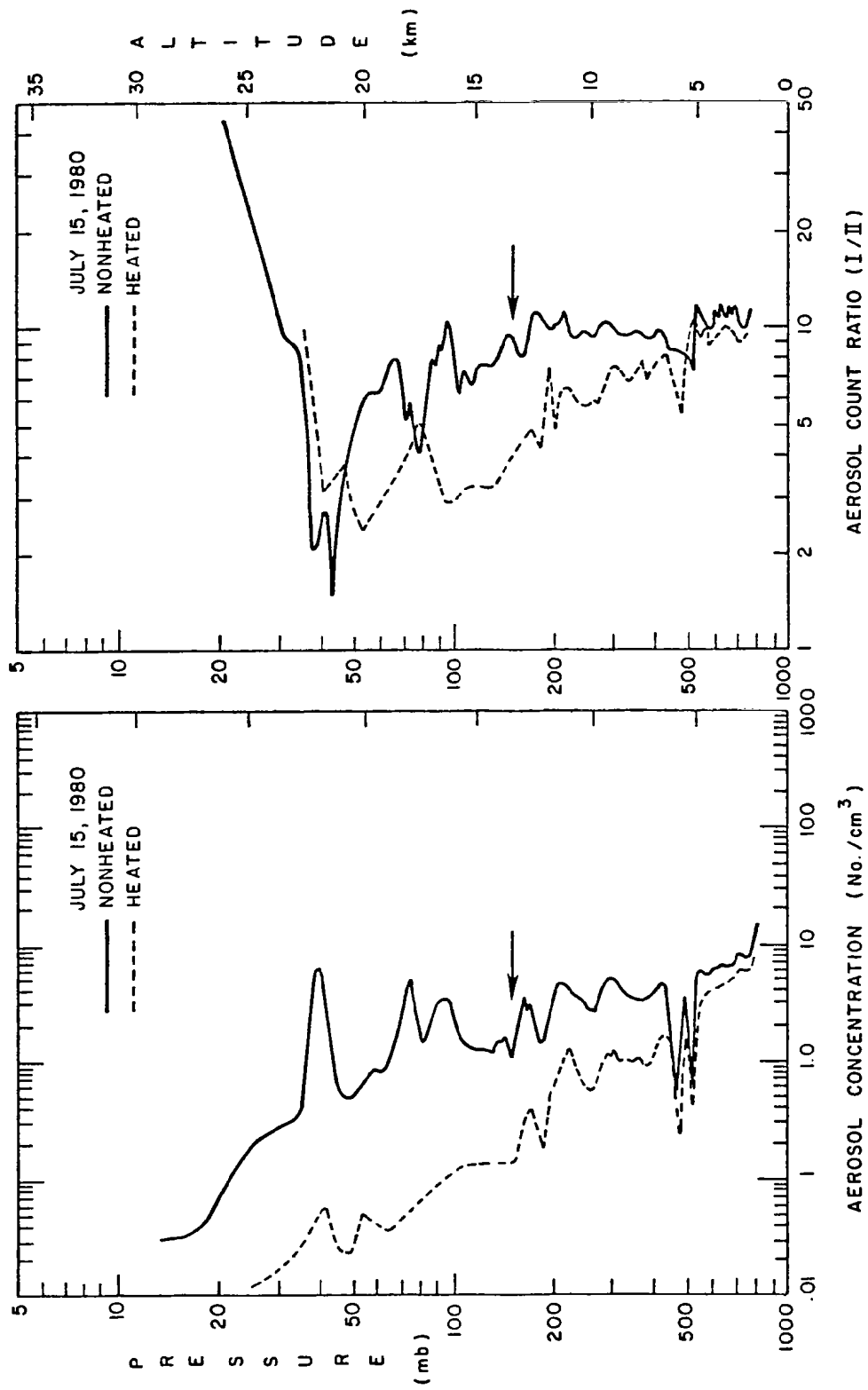


Figure 5. Results of a volatility test made on July 15, 1980.

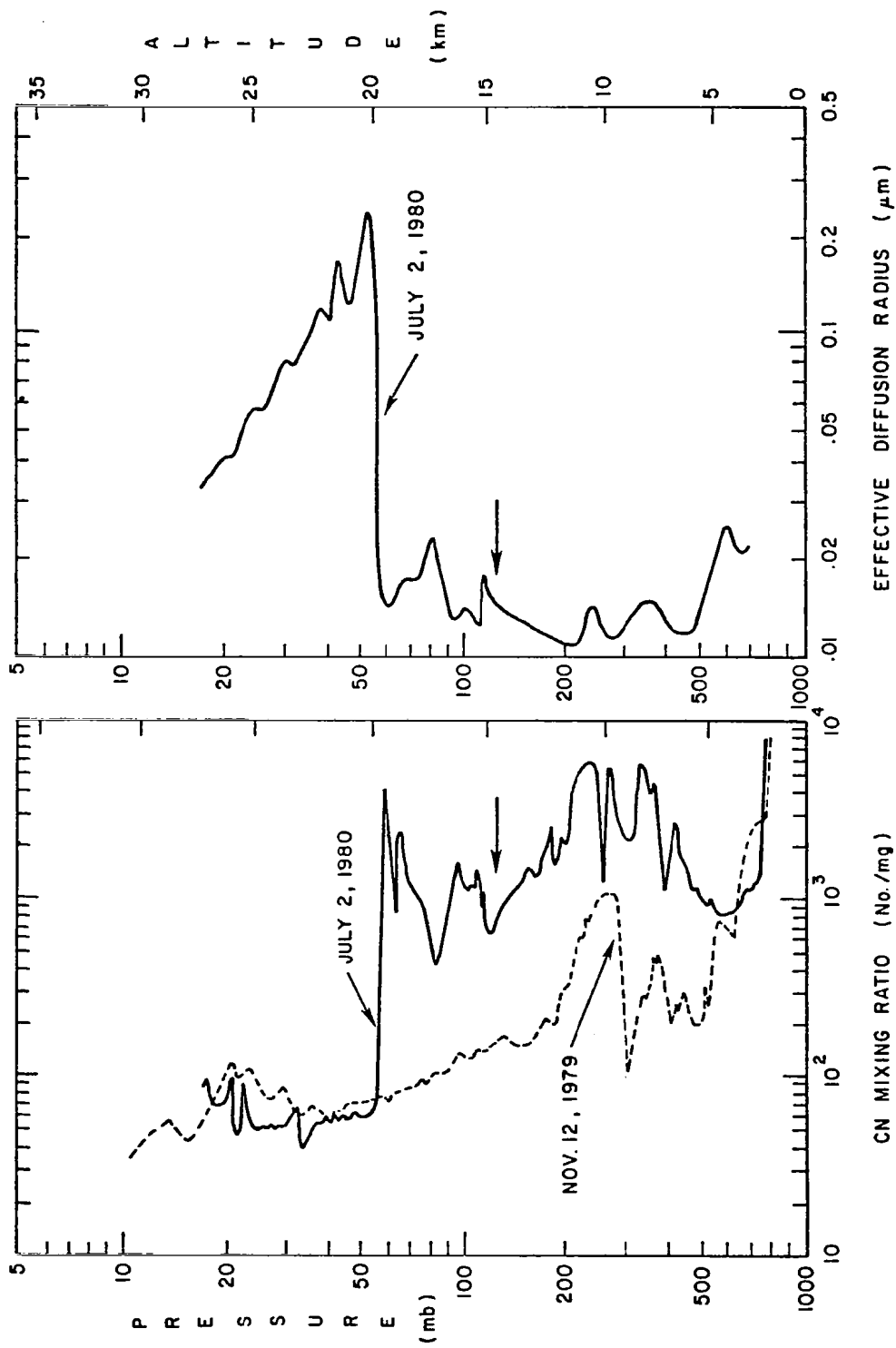


Figure 6. An early CN sounding compared with a pre-eruption profile.

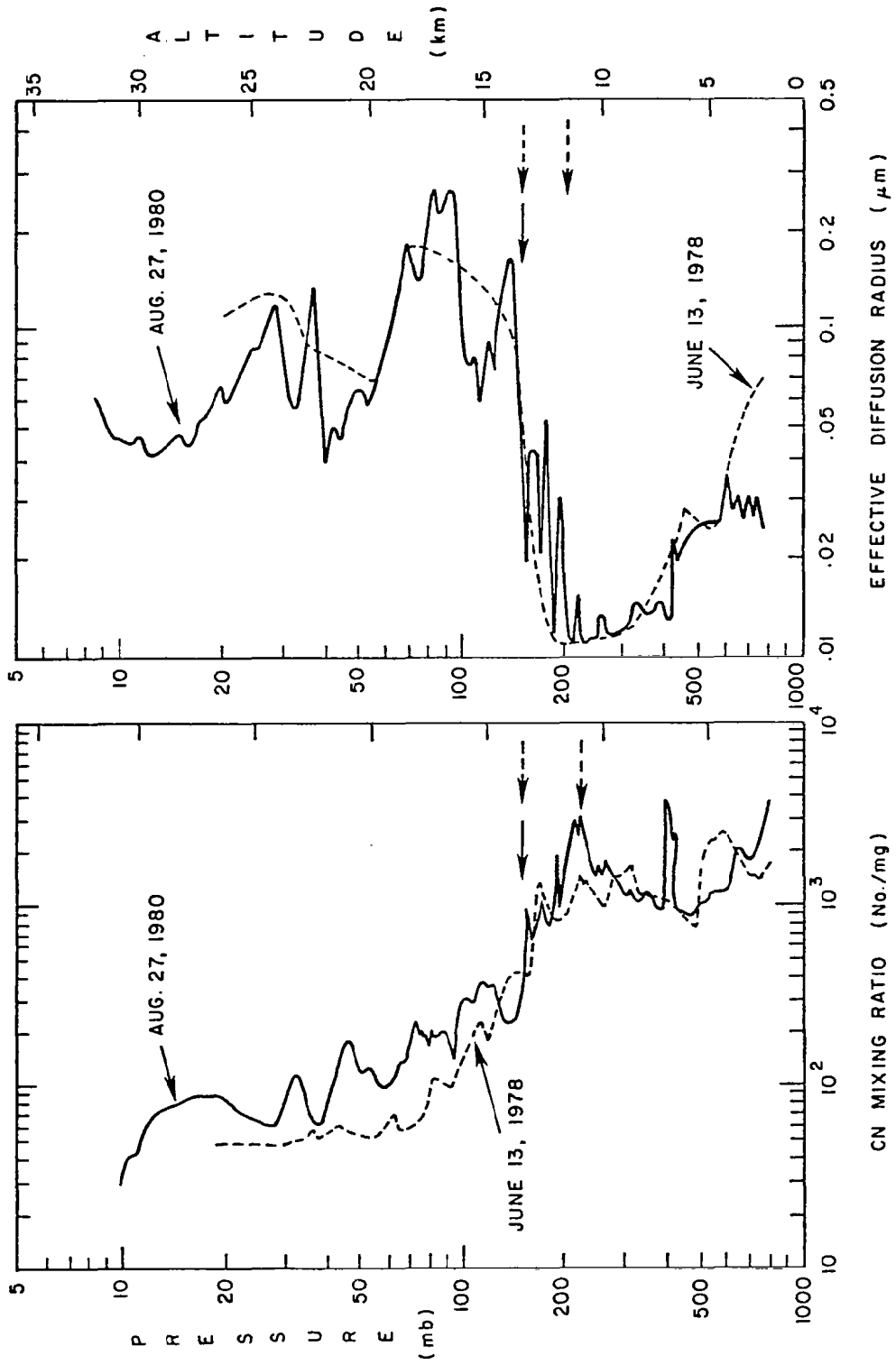


Figure 7. A later CN sounding compared with a pre-eruption profile.

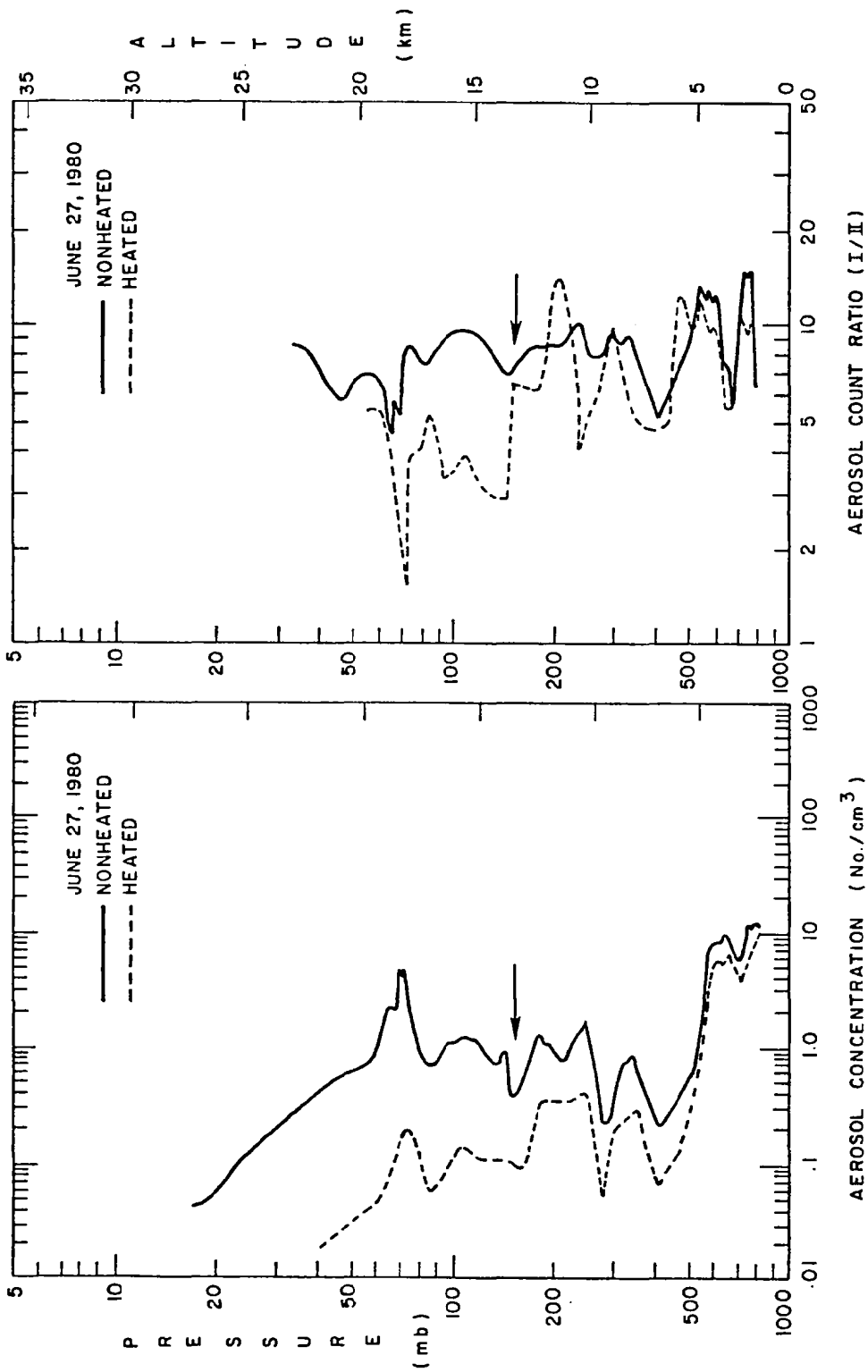


Figure 8. Results of a volatility test conducted on June 27, 1980.

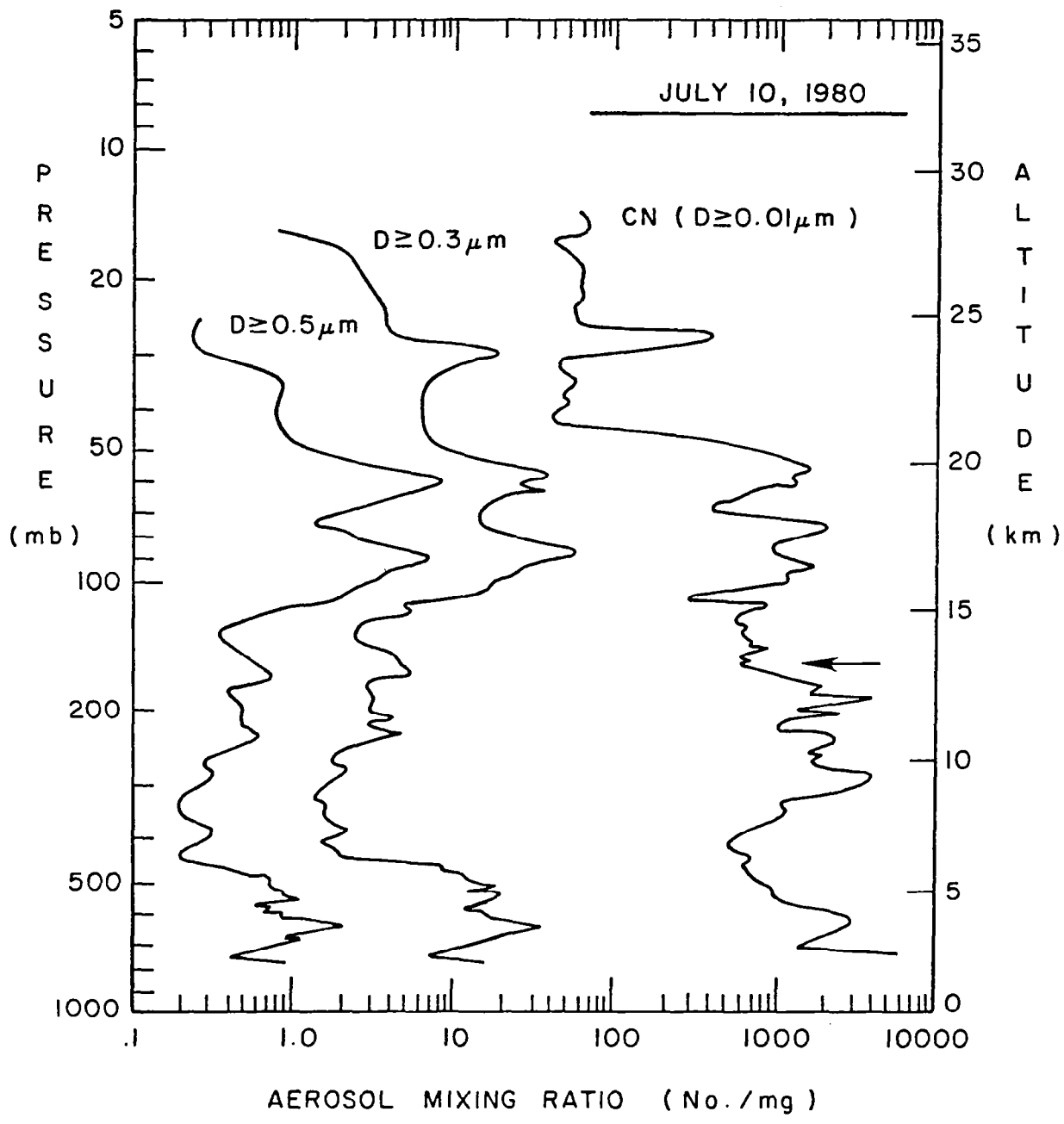


Figure 9. The results of a simultaneous dustsonde and CN flight showing the first arrival of a layer at 24 km.

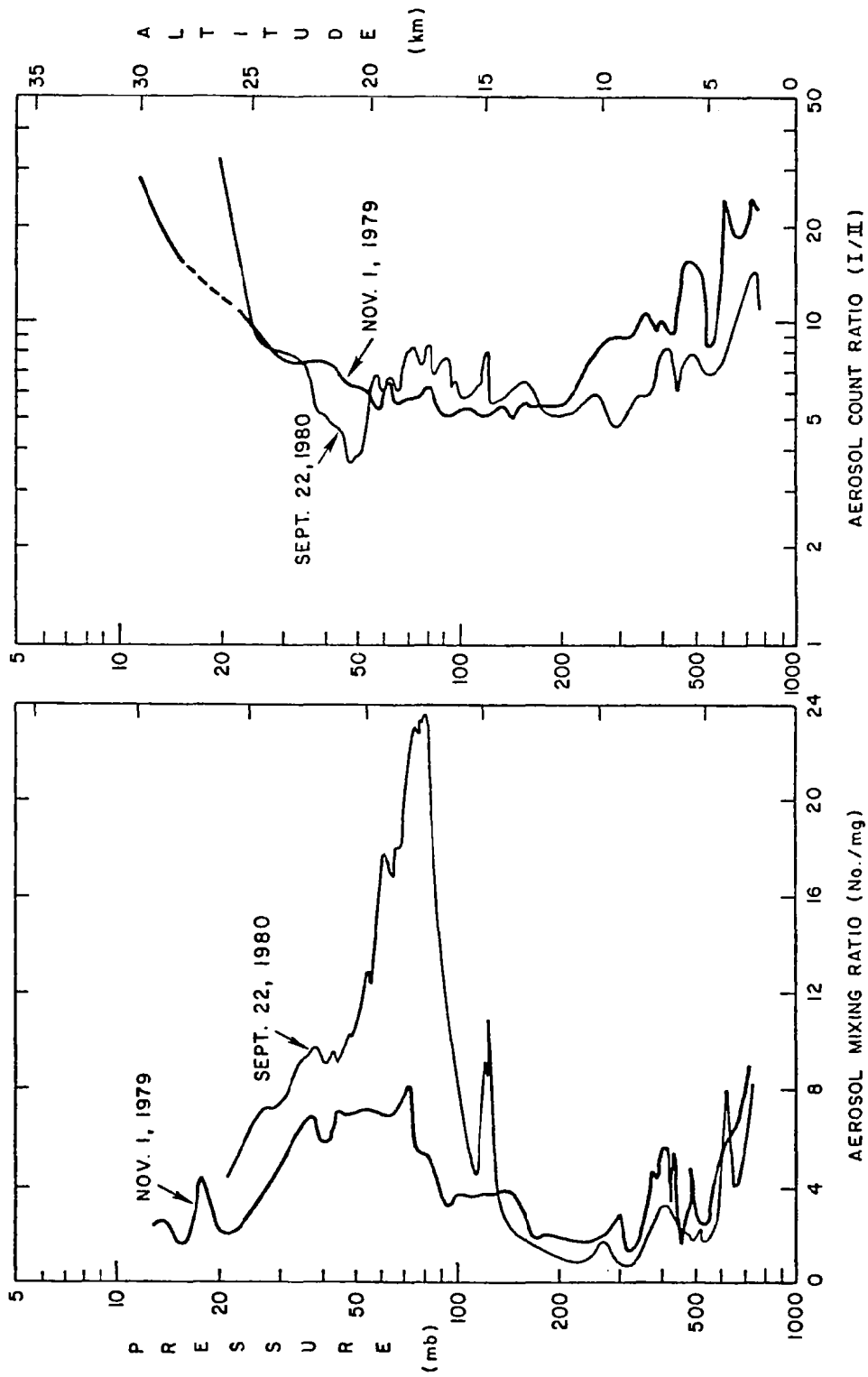


Figure 10. A comparison of present and pre-eruption profiles.

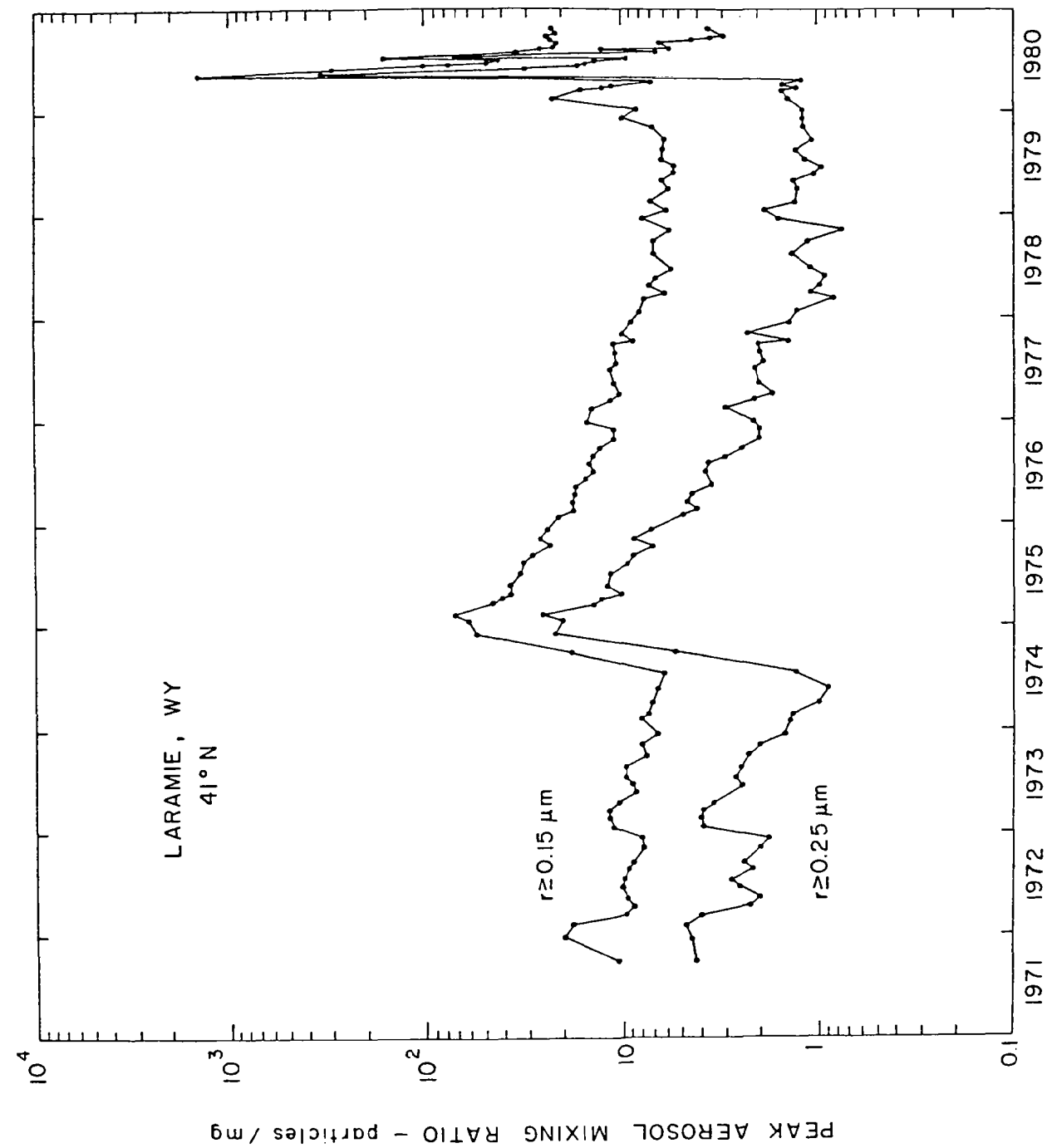


Figure 11. The maximum mixing ratio in the stratospheric aerosol layer as a function of time for the two sizes measured.

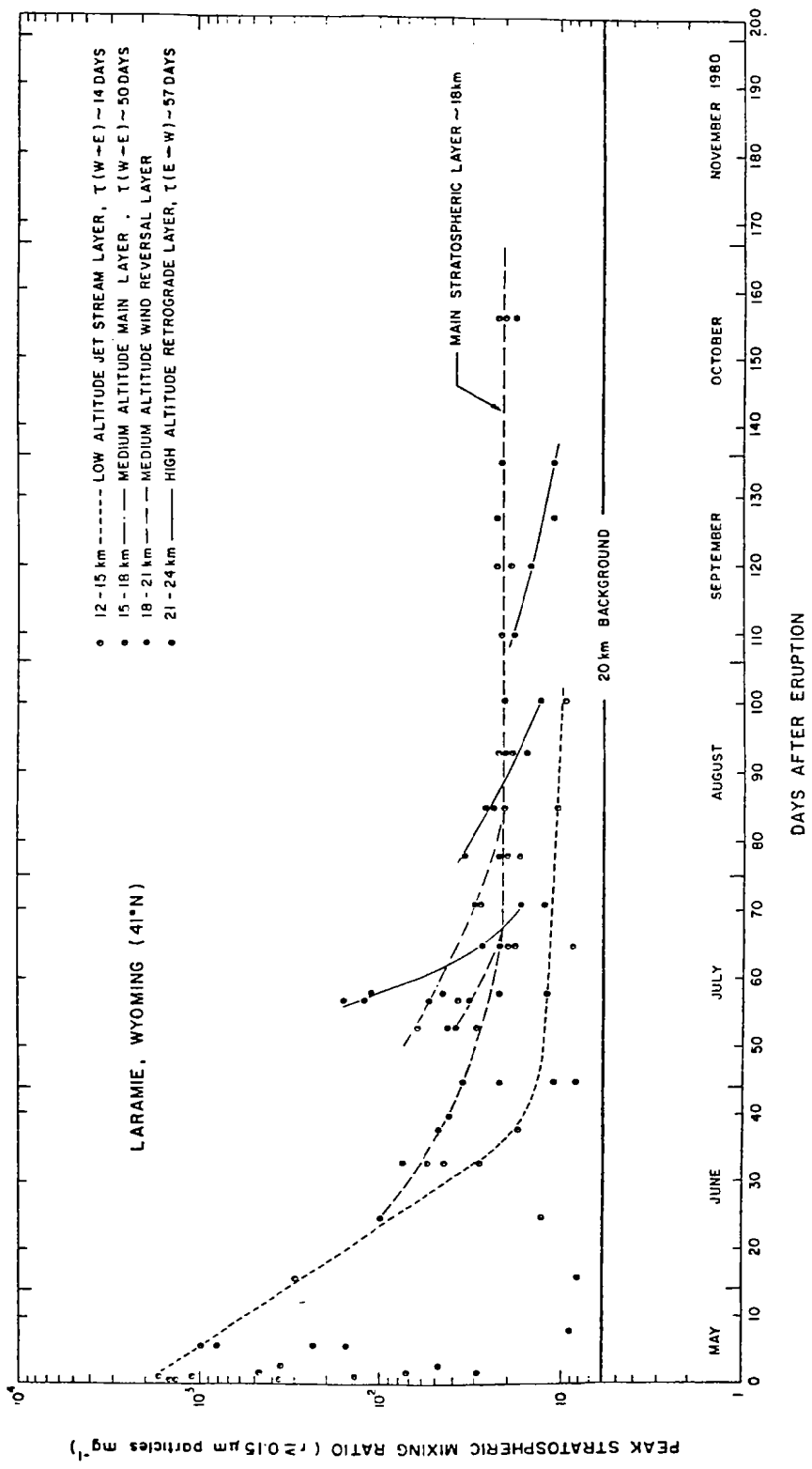


Figure 12. The mixing ratio of stratospheric aerosol layers during the first 5 months following the May 18 eruption. The lines show the decay of identifiable layers.



PHYSICAL AND CHEMICAL CHARACTERISTICS OF
MOUNT ST. HELENS AIRBORNE DEBRIS

W. A. Sedlacek, G. H. Heiken, E. J. Mroz, E. S. Gladney, and D. R. Perrin
Los Alamos National Laboratory, Los Alamos, NM¹

R. Leifer, I. Fisenne, L. Hinchliffe
USDOE, Environmental Measurements Laboratory, New York, NY

R. L. Chuan
Altadena, CA

Tephra and aerosols from the May 18, 1980 eruption of Mount St. Helens, Washington were sampled in the lower stratosphere with a WB-57F aircraft. The main body of the plume was intercepted over western Kansas on May 20, 48 hours after the eruption, at an altitude of 15.2 km. Concentrations on filter samples were 26 ng of SO_4^- /g of air and 579 ng of ash/g of air. Angular glass pyroclasts ranged in size from 0.5 to 10 μm , with a mean grain size of 2 μm . Samples collected at altitudes of 16.7 and 12.5 km had only traces of SO_4^- and ash.

A second flight was flown, 72 hours after the eruption, on May 21. From north Texas to central Wyoming, at an altitude of 15.2 km, < 0.5 to 38 ng of ash/g of air and 1.0 to 2.2 ng of SO_4^- /g of air were sampled. At an altitude of 18.3 km, from central Wyoming to NW New Mexico, the plume density and character were variable as described here:

Flight path (at 18.3 km)	Concentration (ng/g of air)	
	SO_4^-	Ash
N. W. Colorado	32.8	87.3
S. W. Colorado	0.6	11.6
N. W. New Mexico	36.1	29.6

Glassy pyroclasts similar to those sampled on the first flight ranged in diameter from 0.5 to 4 μm .

Trace element analysis revealed some volatile element enrichment, but far less than previously observed in the plume from the St. Augustine Volcano, 1976. Values of $^{210}\text{Po}/^{210}\text{Pb}$ were 0.7 to 1.32 and are comparable to the secular equilibrium value of 1.0 and far less than the ratios previously reported by Lambert.²

As previously reported for Soufriere of St. Vincent, this plume also was fractionated with altitude between ash and sulfate aerosol. Horizontal fractionation at a given altitude was also observed as different portions of the extended eruption were sampled. (See preceding table.) Rapid conversion to sulfate in the first two or three days is apparent.

Follow-up observation of the northern hemisphere SO_4^- aerosol burden in late July and early August 1980 revealed an increase by a factor of 2.5 above April 1980 measurements. Concentrations observed during April 1980 were increased by a factor of two above April 1979 (the lowest concentrations seen in the past three years). The April 1979 to April 1980 increase is attributed primarily to the November 1979 Sierra

¹Operated for the U. S. Department of Energy by the University of California.

²Lambert, personal communication, 1979.

Negra eruption with a slight stratospheric contribution from Soufriere of St. Vincent. The April 1980 to July 1980 increase in stratospheric SO_4^- (an additional factor of three above the April 1979 ambient, added to the Sierra Negra contribution) is attributed primarily to Mount St. Helens. The Mount St. Helens July 22 eruption was measured over the North central U.S. during the July sampling. Another distinct SO_4^- plume at 19.5 km observed over Alaska on August 10 and 11 apparently came from an unreported stratospheric injection from Gareloi Volcano on August 8, 1980.

Quartz crystal microbalance-cascade impactor measurements and filter sampling on the July-August 1980 flights revealed almost no residual ash in the stratosphere. The SO_4^- aerosol sizes centered between 0.6 and 0.3 μm aerodynamic diameter.

I. INTRODUCTION

For nearly 20 years WB-57F aircraft have been used to monitor radioactive species in the lower stratosphere over the western hemisphere. During the last decade, the same type of filters used to assay lower stratospheric concentrations of radioactive aerosols have also been analyzed for sulfate. Prior to June 1974, these sampling missions spanned four altitudes between 12.2 km and 19.2 km from 51°S to 75°N latitude four times a year. Since June, 1974, samples have been collected only three times each year (April, July, and October) from the equator to 75°N.

When Mount St. Helens erupted on May 18, 1980, with injection of a considerable mass of material into the upper troposphere and lower stratosphere, two flights were "borrowed" from the scheduled July 1980 airstream mission to obtain early time data. These chemical and physical data on the nature of the material injected provide a basis for understanding the subsequent rise and decay of lower stratospheric aerosol concentrations.

II. SAMPLING AND ANALYSIS

A sequential sampling system using cellulose fiber IPC-1478 filters collected aerosol for subsequent analysis. On some flights cascade impactors were used to measure size-dependent properties of the aerosol. The filter samples were assayed for radioactive and soluble species. After leaching for soluble ammonium, total nitrogen and sulfate analysis by autoanalyzer colorimetry, the filter residues were ashed at 400°C to destroy the cellulose and provide a measurement of the insoluble, nonvolatile volcanic ash. Portions of the filter were assayed for trace elements by neutron activation analysis (NAA). Additional portions were examined with scanning electron microscopy (SEM) and associated energy dispersive X-ray fluorescence to determine particle morphology, size, and mineral and glass phase distributions. Cascade impactor samples were also assayed by NAA and SEM to determine size dependence of elemental and morphological parameters. One of the cascade impactor samplers employs a series of quartz crystal microbalances (QCM) as the collecting surface for each stage and provides a direct measure of the distribution of mass against aerodynamic particle size. Whole air samples were taken for measurement of trace gases. Radon, carbon dioxide, and halocarbons were measured. Samples were collected on May 20 and 21, 1980 (about 48 and 72 hours after the May 18 eruption) as shown in figures 1 and 2 and on the regular thrice yearly project "Airstream" flights illustrated in figure 3.

III. RESULTS AND DISCUSSION

A. Mount St. Helens Atmospheric Plume Downwind 2000 to 3000 km from the Eruption of May 18, 1980

Concentrations of sulfate and insoluble-nonvolatile ash on the May 20 and 21 flights for each filter are indicated in Table I. Silicate ash particles ranged in size from 0.5 μm to 10 μm , with median sizes of 1.0 μm to 2.0 μm (Table I), as measured by SEM examination of the ash particles on the filters (prior to leaching for sulfate analysis). All the ash particles examined were angular glass pyroclasts (fig. 4); no mineral phases were observed in the high altitude samples. There appears to be a lower ash-particle size limit of about 0.5

μm (long axis). The apparent process by which the ash particles found at high altitude are formed is the fragmentation of thin glassy vesicle (bubble) walls. The very thin vesicle walls are indicative of high gas content in the erupted magma.

Examination of the sulfate and ash data given in Table I, together with the sampling locations given in figures 1 and 2 shows considerable vertical and lateral fractionation between these two classes of debris. The sulfate, which has gaseous precursors (SO_2 , COS, etc.) in the eruption cloud, tends to be enhanced at higher altitudes, similar to the trend of sulfate to ash ratios (1/15 to 6/1) observed for the April 17, 1979 eruption of Soufriere of St. Vincent ($13^\circ 20' \text{N}$, $61^\circ 11' \text{W}$). Horizontal differences in the cloud may be associated with temporal changes in the ejecta during the rather extended May 18 eruption. This is apparent in samples 12 to 15 at 18.29 km.

Neutron activation analysis data for the May 20 and 21, 1980 flights are listed in Table II. The results for each element are presented as percent of total ash collected on the filter expressed as the most usual oxide for each element. The total ash mass used as the basis for each sample includes the weighted residual ash on the filter (after the water soluble material has been leached out and the filter cellulose has been destroyed by heating to 400°C) plus the mass of sodium, potassium, calcium and magnesium measured in the leach solution by flame ionization atomic absorption. Mass not accounted for includes other soluble elements not measured by atomic absorption (AA) and insoluble material that is volatile at 400°C . Based on known chemical solubilities and volatilities, and comparison of these NAA data with independent elemental analyses of ash fall samples, it can reasonably be assumed that the "unaccounted for" mass is insignificant as regards computation of percent elemental composition. Although silica was not determined, it can be assumed to be essentially equal to the difference between 100 percent and the sum of the measured elemental contents.

Comparison of the arsenic concentration for sample 5 (Table II) with earth crustal abundance (5 ppm As) and preliminary data from two Mount St. Helens ash fall samples (average of 1.4 ppb As) shows much lower enrichment in plume samples than previously measured by Zoller³ at St. Augustine volcano. Similarly, the $^{210}\text{Po}/^{210}\text{Pb}$ ratios given in Table I are all near the secular equilibrium value of 1.0 and do not show great enhancement in the more volatile polonium of factors from 10 to 40 as reported by Lambert (1), for some volcanos. The Mount St. Helens Po/Pb results are similar to those which were found for the April 17, 1980 eruption of Soufriere of St. Vincent (2). However, sufficient data have not yet been compiled to understand what the volatile trace elements will tell us about the nature of the Mount St. Helens eruption.

In considering the elemental composition of the samples listed in Table II, one should bear in mind that samples 1 and 2 were collected below the tropopause and may contain some material which is not of Mount St. Helens origin. The analysis for sample 14 seems very unusual, since no aluminum was found and the iron content is very high. Based on sampling locations (see fig. 2), sample 15 should represent the early part of the rather extended May 18 eruption and sample 13, a later part. The unusual relationships of Al, Fe, Cl, Mn, and soluble Na and Ca compared with total Na and Ca contents found in samples 13, 14 and 15 may be due to changes in the character of the ash during the eruption.

Four-stage cascade impactor samples at 18.29 km on the May 21, 1980 flight were examined with the SEM and compared with pre-Mount St. Helens eruption samples. Two types of particles were apparent: (1) particles which were solid, nonvolatile in the SEM and whose measured dimensions exceeded the theoretical 50 percent cutoff aerodynamic diameter of the preceding stage; (2) particles which were volatile in the SEM but left countable impressions on the collecting substrate. Particle number concentrations for each stage are listed in Table III.

To understand the physical and chemical data from the samples collected on May 20 and 21, 1980, one would like to know the part of the eruption cloud that was being sampled. This requires linking the sampling data to cloud trajectories derived from soundings of atmospheric air movements. Two sets of trajectories have been put forward. Those computed by Dr. Ed Danielsen of National Aeronautics and Space Administration (NASA) Ames Research Center are shown in figure 5. Another set computed by Drs. Gus Telegodas and Roland Draxler of the National Oceanic and Atmospheric Administration (NOAA) Air Resources Laboratory are shown in figure 6. The 100-mb (16-km) NOAA trajectory is essentially the same

³Zoller, private communications, 1980.

as the NASA 100-mb trajectory shown in figure 5. The NOAA 200-mb (12-km) trajectory is slightly further north over Kansas and Missouri and is considerably faster than the 100-mb pathway. It seems evident that the May 20, 1980, intercept of high ash concentrations at 15.24 km over western Kansas (see fig. 1 and Table I, sample 5) was in a zone of wind shear between the 100-mb and 200-mb levels.

However, the 18.29-km sampling of May 21, 1980, does not match the NASA trajectories of figure 5 at 70 mb (18 km). One possibility is that the 100-mb material leaving the vicinity of Mount St. Helens (fig. 5) is "lofted" as it crosses the Rocky Mountains and is the debris which was sampled at 18.29 km on May 21. This phenomenon has been seen before in Aitken nuclei data (3). Of importance in this discussion is which U-2 aircraft sampling data from May 19 at positions closer to the eruption site should be compared with the WB-57 samples of May 21, U-2 data from 70 mb or U-2 data from 100 mb, when addressing questions of changes in the debris clouds physical and elemental composition during transport.

B. Comparison of Mount St. Helens Plume With Other Volcanic Plumes

In addition to the special sampling flights flown, routine sampling for the radioactive inventory of the upper atmosphere is done each spring, summer, and fall as part of Project Airstream. Sulfate data from the last two years of this sampling is listed in Tables IV-IX. A careful examination of seasonal changes in these data reveals that the upper atmosphere was relatively clean with regard to sulfate from late 1978 through late 1979. Excluding common data points between data sets where one or both concentrations were less than the detection limit of about 0.4 ppbm (parts per billion by mass), and averaging ratios of all other common data points between sets produced the relative changes in stratospheric sulfate concentration listed in Table X. The excluded values are primarily from data points at or below the tropopause. These ratios should be regarded as only suggestive (or confirmatory of other data) rather than definitive.

It appears that in July 1979 and October 1979, there was some small effect from Soufriere of St. Vincent (see Table XI of recent volcanoes with known stratospheric injection). The factor of two increase in SO_4^- from April 1979 to April 1980 can probably be attributed primarily to Sierra Negra, Galapagos Island ($0^\circ 50' \text{S}$, $91^\circ 10' \text{W}$). By July-August 1980, Mount St. Helens ($46^\circ 12' \text{N}$, $122^\circ 11' \text{W}$) appears to have increased the average SO_4^- concentration by a factor of 2.5 relative to the April 1980 level (three times the April 1979 ambient).

The July-August sampling (Table IX) also has revealed a stratospheric injection of fresh debris from a previously unnoticed explosive volcanic eruption. Samples collected at 19.2 km altitude from 150°W , 56°N to 62°N also had insoluble-nonvolatile ash associated with them and sulfate levels are enhanced considerably above the dispersed sulfate from the Mount St. Helens eruptions. The considerably raised sulfate on two filters together with detectable amounts of ash (the stratospheric ash from Mount St. Helens which was found on May 20 and 21 was no longer detectable by August by using our technique) indicate that the sampling track has probably crossed a fresh volcanic plume. The QCM impactor also showed about a factor of two increase in aerosol mass concentration at the same time. These samples were collected on August 10 and by considering Table XI, two possible volcanoes could have contributed, either the August 7 eruption of Mount St. Helens or the eruption of Mount Gareloi located in the Aleutian Islands ($51^\circ 45' \text{N}$, $178^\circ 4'$). Because of its isolation and cloud cover, the Gareloi eruption is all but unreported; however, on August 9, 1980 a Northwest Orient Airline pilot reported a plume up to 10.5 km (4). By using the 70-mb analysis data presented in figures 7 to 10, augmented by a few NOAA-6 polar orbiting satellite images, it is believed that the Gareloi volcano is the most likely candidate responsible for this stratospheric injection. The upper altitude meteorological data are very sparse in this area, but the satellite image does show a plume-like feature which could be from Gareloi Volcano on August 8 and another on August 9, at considerable height above the clouds, moving in the direction shown on figure 8. The progression, day-by-day, of plume trajectories of the Mount St. Helens August 7 eruption debris shown in figures 7 to 10 could not have produced the elevated sulfate concentrations sampled south of Anchorage, Alaska, during the Airstream flight. The step-by-step movement of a Gareloi plume indicated in figures 8 to 10 could have transported sulfate to the sampling site at the right time. The enhanced sulfate shown at 19.2 km altitude at 50°N which was collected on August 11, 1980, may be a part of the Gareloi plume carried further south by the upper level winds after splitting over the ocean or may be Mount St. Helens debris from the eruption of 7 August that has not cleared the area.

Some of the July-August 1980 flights also collected data with the ten-stage QCM cascade impactor. Other than the fresh debris found on July 24 from the July 22 Mount St. Helens eruption, the only material observed was sulfuric acid aerosol. On July 24 a bimodal aerosol distribution was observed. Sulfuric acid droplets had a mean size of $0.07 \mu\text{m}$ (aerodynamic diameter) and silicate ash had a mean size of $1.5 \mu\text{m}$ (aerodynamic diameter).

C. Sulfur Gas to Aerosol Conversion

Combining the July 22 eruption (July 24 sampling QCM data) with similar data from U-2 flights to sample the May 18 and 25 eruptions as shown in figure 11 suggests that (a) either some sulfuric acid is directly injected into the atmosphere or (b) sulfur gases are rapidly converted to SO_4^- . This is consistent with the observations reported for the Soufriere of St. Vincent eruption in 1979 (2). Since gas phase conversion of COS, CS_2 , and SO_2 by reaction with O_3 would take considerably longer than the few days evidenced here, the following thoughts are proposed for consideration. In a volcanic atmospheric injection, there are many fresh reactive surface sites available for catalyzing chemical reactions on the small ash fragments. There is also a considerable amount of water vapor present in the eruption cloud which upon exposure to ultraviolet light in the stratosphere will produce a considerably enhanced hydroxyl radical concentration. The localized concentrations of all the involved species, SO_2 , COS, CS_2 , OH, and ash are greatly enhanced in the eruption cloud. Early time local temperatures are higher in the eruption cloud due to radiative heating from hot ash particles. The technique of exposing an air mixture of SO_2 and H_2O to UV light in the laboratory to generate very small aerosols (presumably by formation of OH to react with SO_2) for testing and calibration of Aitken nuclei counters has been used by some experimenters.⁴ By considering these facts collectively, one should find that a mechanism for conversion of reduced sulfur gases to sulfate aerosol in a few days by surface-catalysed or free-radical reactions is very possible.

IV. CONCLUSIONS

1. The eruption plume from Mount St. Helens was fractionated vertically, the larger silicate ash particles being dominant at lower altitudes and smaller, sulfate particles more abundant at higher altitudes.
2. Horizontal fractionation of the eruption plume occurred because of temporal variations in the volcanic ejecta during the rather extended eruption.
3. Most of the larger silicate ash particles had settled out of the stratosphere by late July and left the smaller sulfate aerosol in the stratosphere.
4. The stratospheric sulfate aerosol concentration was increased by a factor of two from April 1979 to April 1980 predominately because of the November 1979 eruption of Sierra Negra, Galapagos Islands.
5. The stratospheric sulfate aerosol concentration was increased by a factor of 2.5 from April 1980 to late July 1980 because of the Mount St. Helens eruptions.
6. An unobserved explosive phase of the volcanic eruption of the Gareloi Volcano, Alaska, may have injected debris into the stratosphere in early August 1980.
7. The sulfur gases present in volcanic eruption clouds convert to sulfate aerosols within a few days instead of several months as would be predicted by an ozone oxidation mechanism.
8. Based on the stratospheric sampling history, in conjunction with an analysis of known explosive volcanic eruptions, it appears that the principal contributor to the aerosol layer of the lower stratosphere is injection of volcanic material.

⁴J. B. Haberl, private communication, 1980.

ACKNOWLEDGMENTS

We wish to express our thanks to the NASA Johnson Space Center pilots, scientific equipment operators, and ground support personnel who made possible the measurements of these data. NASA Johnson Space Center operates the WB-57F used for these flights for the U.S. Department of Energy Office of Health and Environment. Meteorological assistance by Dr. Sumner Barr of Los Alamos and from Gus Telegodas, Roland Draxler, Art Krueger, and Carl Erickson from NOAA greatly aided both the direction of the sampling flights and subsequent interpretation of data. Interactive communications with Dr. M. P. McCormick, Dr. Ed Danielsen, Bill Page, and Ervin Lezberg at other NASA research centers greatly enhanced this research effort.

REFERENCES

1. G. Lambert, A. Guisson, J. Sanak and B. Ardouin. Modification of the Atmospheric Polonium 210 to Lead 210 Ratio by Volcanic Emission. J. Geophys. Res. Vol. 84, 1980, pp. 6980-6986.
2. W. A. Sedlacek, G. Heiken, W. Zoller, M. Germani, D. Cronn and W. Nutmagul. Eruption Plume of Soufriere of St. Vincent, B.W.I. April 17, 1979. Science, 1981.
3. J. Podzimek, W. A. Sedlacek, and J. B. Haberl. Aitken Nuclei Measurements in the Lower Stratosphere. Tellus Vol. 29, 1977, pp. 116-127.
4. Scientific Event Alert Network Bulletin. Smithsonian Institution. Vol. 5, Aug. 31, 1980, pp. 7-8.

TABLE I
ANALYSIS FOR MAY 20 AND 21 FLIGHTS

Sample # (see figs. 1,2)	Altitude		Location	SO ₄ ⁼		Ash*		Median Size µm diam.	²¹⁰ Po ²¹⁰ Pb	Radon pCi/m ³ STP
	km	mb		Conc** ppbm	Conc** ppbm	Size Range µm diam.	Conc** ppbm			
May 20, 1980										
1	9.45	288	South Central Kansas	2.7	37.9	0.5-2.5	-	1.5	.50±0.1	8.75±.1
2	9.45	288	Central Kansas	1.5	5.6	0.5-3.0	-	1.5	.41±0.1	
3	12.50	179	Central Kansas	0.7	-	-	-	-	.47±0.1	.30±.01
4	12.50	179	Southwest Kansas	0.8	-	-	-	-	-	
5	15.24	117	West Kansas	25.9	578.6	0.5-10.0	-	2.0	.62±0.1	1.11±.1
6	15.24	117	West Kansas, Southwest Neb.	1.3	-	-	-	-	1.32±0.4	
7	16.77	91	SW Neb.-W Cent. Colorado	1.1	-	-	-	-	.70±0.1	.04±.02
8	16.77	91	W Cent. Colorado-SW Kansas	1.2	-	-	-	-	.44±0.1	
May 21, 1980										
9	15.24	117	North Texas-Central Colorado	1.6	-	0.5-4.0	-	1.5	.56±0.1	.61±.09
10	15.24	117	North Central Colorado	1.0	-	0.4-4.0	-	1.5	.68±0.2	.37±.09
11	15.24	117	South Central Wyoming	2.2	33.3	0.5-3.0	-	1.5	.72±0.1	
12	18.29	72	Cent. Wyo.-South Cent. Wyo.	5.0	38.0	0.5-3.0	-	1.0	.60±0.5	.54±.09
13	18.29	72	S Cent. Wyo.-W Cent. Colo.	32.8	87.3	0.5-5.0	-	1.0	1.04±0.2	
14	18.29	72	W Cent. Colo.-NW New Mexico	0.6	11.6	0.5-3.0	-	1.0	.15±0.09	.47±.09
15	18.29	72	NW N.M.-Central N.M.	36.1	29.6	0.5-3.0	-	1.0	-	

*Nonvolatile at 400°C insoluble in H₂O.

**Error limit estimated to be ±25%.

TABLE II
ELEMENTAL ANALYSIS DATA FOR FILTERS THAT COLLECTED SUFFICIENT ASH
FOR NAA AND AA ANALYSIS ON MAY 20 AND 21, 1980 FLIGHTS.

Element	Sample						
	1	2	5	11	13	14	15
Al ₂ O ₃	11.2%	29.7%	16.1%	17.1%	6.61%	%	11.7%
Fe ₂ O ₃	5.68	10.7	5.07	11.8	4.85	22.4	15.6
Na ₂ O (**)	4.01 (0.23)	7.61 (0.57)	6.30 (0.14)	7.39 (4.38)	2.71 (0.84)	2.96 (2.91)	6.13 (1.98)
CaO (**)	1.85 (0.47)	5.58 (1.46)	3.06 (0.035)	6.33 (1.86)	2.22 (1.27)	2.19 (6.58)	2.50 (2.68)
K ₂ O (**)	1.55 (0.049)	2.51 (0.088)	4.80 (0.075)	0.69 (0.085)	.69 (0.12)	(0.76)	(0.31)
BaO	0.362	1.36	0.059				0.052
Cl	0.088	1.23	0.170	0.90	0.37	2.93	0.42
MnO	0.058	0.158	0.069	0.085	0.084	3.09	0.28
CuO ₂	0.019	0.502	0.023	0.044	0.89	0.53	0.073
V ₂ O ₅	0.0064	0.021	0.0058	0.015	0.0015		0.0081
Co ₂ O ₃	0.0060		0.0020	0.030	0.0085		
Ce ₂ O ₃	0.0064	0.034	0.0065			0.26	.010
As ₂ O ₃			0.00065				
SeO ₂	0.00073		0.00039	0.0014	0.019		
La ₂ O ₃		0.017	0.0030				
Sm ₂ O ₃		0.00072	0.00049		0.0091		
Sc ₂ O ₃	0.0011		0.0015	0.0025	.00048		
Cr ₂ O ₃				0.034			
Eu ₂ O ₃			0.00015				
ThO ₂	0.00075	0.00029	0.00068		0.00053	0.0016	0.0021
MgO (**)	(0.13)	(0.42)	(0.069)	(0.26)	(0.21)	(0.69)	(0.66)
Total	24.97%	59.84%	35.74%	44.08%	18.66%	40.20%	38.02%
Ash							
ng/m ³ STP*	46,300	6,800	707,700	40,700	106,800	14,200	36,100
Soluble	412	177	2,283	2,871	2,659	1,746	2,157
Total	46,712	6,977	709,983	43,571	109,459	15,946	38,257
% Soluble	0.88	2.5	0.32	6.6	2.4	10.9	5.6
Altitude	9.45 km	9.45 km	15.24 km	15.24 km	18.3 km	18.3 km	18.3 km
Date Sampled	5/20	5/20	5/20	5/21	5/21	5/21	5/21

*Nonvolatile at 400°C and nonsoluble in H₂O by Neutron Activation Analysis.

**H₂O Soluble (Na₂O, CaO, K₂O, MgO) by Atomic Absorption.

TABLE III

FOUR STAGE IMPACTOR: SAMPLES COLLECTED AT 18.29 km on May 21, 1980

Stage	Aerodynamic diameter 50% cutoff	Pre-eruption		Post eruption	
1	0.13 μm	0	per cm^3	solid	3 per cm^3
				volatile	0
2	0.11	solid	0.3	solid	50
		volatile	10	volatile	20,000
3	0.07	solid	0.5	solid	50
		volatile	3	volatile	1
4	0.05		0	solid	25
				volatile	0

Table IV
October 1978 SO_4^- ppm

North Latitude	Altitude					
	12.20 km	13.72 km	15.24 km	16.77 km	18.29 km	19.21 km
0°-3°						
3°-6°				0.22		
6°-10°				0.43		0.60
10°-13°		0.06		0.25		0.61
13°-16°		0.06		0.20		0.57
16°-19°		0.08		0.17		0.50
19°-22°		0.05				0.45
22°-25°		0.05	0.08	0.38		0.46
25°-28°		0.08	0.21	0.29	0.61	0.86
28°-30°	0.17	0.12	0.23	0.68	0.60	1.23
30°-33°			0.12	0.26		0.73
33°-36°			0.22	0.51		0.56
37°-39°			0.20	0.53		0.62
39°-42°			0.17	0.82		
42°-45°			0.41	0.29		0.50
45°-48°			0.59	0.43		
48°-51°			0.33	0.54		0.78
51°-54°				0.71		
54°-58°				0.75		
58°-62°	0.27	0.33	0.67			0.59
62°-65°			0.74	0.80		0.46
65°-68°	0.35		0.80	0.77		0.47
68°-71°	0.36		0.76	0.78		0.52
71°-75°	0.40		0.68	0.81	0.40	

All values estimated to have 25% error limits.

Table v

April 1979 SO_4^- ppbm

North Latitude	Altitude					
	12.20	13.72 km	15.24 km	16.77 km	18.29 km	19.21 km
0°-3°			0.23	0.22	0.76	0.86
3°-6°			0.18	0.25	0.82	0.90
6°-10°	0.16	0.16	0.21	0.27	0.48	
10°-13°			0.24	0.36		
13°-16°			0.21	0.41		
16°-19°			0.25	0.42		0.49
19°-22°			0.29	0.37		0.59
22°-25°			0.27	0.34	0.58	0.48
25°-28°			0.28	0.37	0.47	0.74
28°-30°	0.17	0.27				
30°-33°		0.28	0.37	0.35		0.66
33°-36°		0.26	0.34	0.43		0.58
37°-39°		0.31	0.36			
39°-42°		0.34	0.39			
42°-45°		0.40	0.40			
45°-48°		0.40				
48°-51°			0.40	0.63		
51°-54°		0.43		0.55		
54°-58°		0.38		0.51		
58°-62°	0.49	0.43		0.64		
62°-65°	0.40					
65°-68°	0.55					
68°-71°	0.50			0.68		
71°-75°	0.48			0.74		

All values estimated to have 25% error limits.

Table VI
July 1979 SO_4^- ppbm

North Latitude	Altitude					
	12.20 km	13.72 km	15.24 km	16.77 km	18.29 km	19.21 km
0°-3°						
3°-6°						
6°-10°						
10°-13°						
13°-16°						
16°-19°			0.19			
19°-22°			0.21		0.50	
22°-25°		0.17			0.71	
25°-28°		0.12	0.16		0.05	
28°-30°	0.19	0.09				
30°-33°		0.12	0.16	0.41		
33°-36°		0.08	0.15	0.29		0.94
37°-39°		0.16	0.29	0.37		
39°-42°		0.18	0.22	0.51		
42°-45°		0.29	0.29			0.66
45°-48°		0.30	0.32	1.03		0.65
48°-51°		0.23		0.82		
51°-54°				0.86		
54°-58°		0.19		0.93		
58°-62°	0.31	0.45		0.92		0.68
62°-65°			0.58			
65°-68°	0.44		0.55			0.89
68°-71°	1.00		0.58	0.26		
71°-75°	0.49					

All values estimated to have 25% error limits.

Table VII

October-November 1979 SO_4^- ppm

North Latitude	Altitude					
	12.20 km	13.72 km	15.24 km	16.77 km	18.29 km	19.21 km
0°-3°			0.14	0.20	0.43	0.65
3°-6°			0.13	0.19	0.27	0.63
6°-10°		0.29	0.08	0.15	0.37	0.57
10°-13°			0.06			0.74
13°-16			0.08			0.74
16°-19°			0.10			0.66
19°-22°			0.07			0.82
22°-25°			0.09		0.52	0.68
25°-28°			0.10		0.64	1.01
28°-30°	0.10	0.11	0.16	0.35		1.00
30°-33°		0.08	0.37			
33°-36°		0.07	0.44	0.46		
37°-39°		0.06	0.12	0.48		
39°-42°		0.17	0.14	0.76		
42°-45°		0.22	0.33	0.59		
45°-48°		0.24	0.40			
48°-51°		0.35	0.28			
51°-54°		0.37				
54°-58°		0.50				
58°-62°						
62°-65°	0.27					
65°-68°	0.30					
68°-71°	0.26					
71°-75°	0.29					

All values estimated to have 25% error limits.

Table VIII
April 1980 SO_4^- ppm

North Latitude	Altitude					
	12.20 km	13.72 km	15.24 km	16.77 km	18.29 km	19.21 km
0°-3°			0.23	0.42	0.49	0.93
3°-6°			0.25	0.30	0.35	1.12
6°-10°		0.13	0.25	0.21	0.19	1.19
10°-13°		0.18	0.38	0.38		1.24
13°-16°		0.18	0.19	0.22		1.94
16°-19°		0.25	0.23	0.30		1.25
19°-22°		0.37	0.23	0.46		1.17
22°-25°		0.37	0.18	0.65		1.26
25°-28°		0.29	0.44	0.64		1.76
28°-30°	0.95	0.32	0.71	0.99	1.60	1.56
30°-33°		0.17	0.63	1.28		1.26
33°-36°		0.19	0.87	1.09		1.47
37°-39°		0.30	0.68	0.78		1.51
39°-42°		0.59	0.82	1.28		
42°-45°		0.63	1.11	1.18		
45°-48°		0.60	1.67	1.27		
48°-51°		1.07	1.04	1.02		0.66
51°-54°		0.58		1.28		
54°-58°		0.77		1.08		
58°-62°		0.69	1.03			1.16
62°-65°	0.81		0.81	1.20		0.83
65°-68°	0.80		0.83	1.40		0.96
68°-71°	0.92		0.74	1.10		0.99
71°-75°	0.99		0.89	1.15	0.91	

All values estimated to have 25% error limits.

Table IX

July-August 1980 SO_4^- ppbm

North Latitude	Altitude					
	12.20 km	13.72 km	15.24 km	16.77 km	18.29 km	19.21 km
0°-3°				0.33	1.09	
3°-6°				0.32	1.02	
6°-10°			0.22	1.09	1.25	1.53
10°-13°			0.14	0.79		1.52
13°-16°			0.29	1.17		1.66
16°-19°			0.26	1.74		1.79
19°-22°			0.38			1.76
22°-25°			0.83			2.16
25°-28°			0.61			1.45
28°-30°		0.12	1.52			
30°-33°		0.17	1.35	2.45		2.41
33°-36°		0.16	0.98	3.35		2.94 (1.7)*
37°-39°		0.14	0.97	3.60		3.04
39°-42°		0.21	2.22	2.82		
42°-45°		0.54	2.81	2.96		4.15
45°-48°			3.15	2.99		4.41
48°-51°			3.24	2.96		1.46
51°-54°			3.10	3.31		1.78
54°-58°			3.34	3.74		2.61 (6.9)*
58°-62°						8.83 (3.8)*
62°-65°			3.07	2.31		2.50
65°-68°			3.34	3.26		
68°-71°			2.70	1.87		
71°-75°			3.31	2.73	2.21	

*(nonvolatile - insoluble ash)

All values estimated to have 25% error limits.

TABLE X
RELATIVE CHANGES IN STRATOSPHERIC SULFATE INVENTORY

<u>Airstream Cycles Ratioed</u>	<u>Average Ratio</u>
April 1979 / October 1978	0.98
July 1979 / April 1979	1.50*
October-November 1979 / April 1979	1.24
April 1980 / April 1979	2.17
July-August 1980 / April 1979	4.82
July-August 1980 / July 1979	5.06
July-August 1980 / April 1980	2.57

*(very few common data points)

TABLE XI
KNOWN VOLCANIC ERUPTIONS WHICH ENTERED THE STRATOSPHERE DURING 1979-1980

		<u>Reported Altitude</u>
Soufriere of St. Vincent (13.33°N - 61.18°W)	13, 14 April 1979	
	17 April 1979	18.7 km base
Sierra Negra (0.83°S - 91.17°W)	13 November 1979	>14 km
Mt. St. Helens (46.20°N - 122.18°W)	18 May 1980	>20 km
	25 May 1980	>12 km
	12 June 1980	
	22 July 1980	16 km base
	7 August 1980	>13.5 km
Gareloi (51.80°N - 178.80°W)	8 August 1980	>10.5 km
Hekla (63.98°N - 19.70°W)	17 August 1980	≈15 km

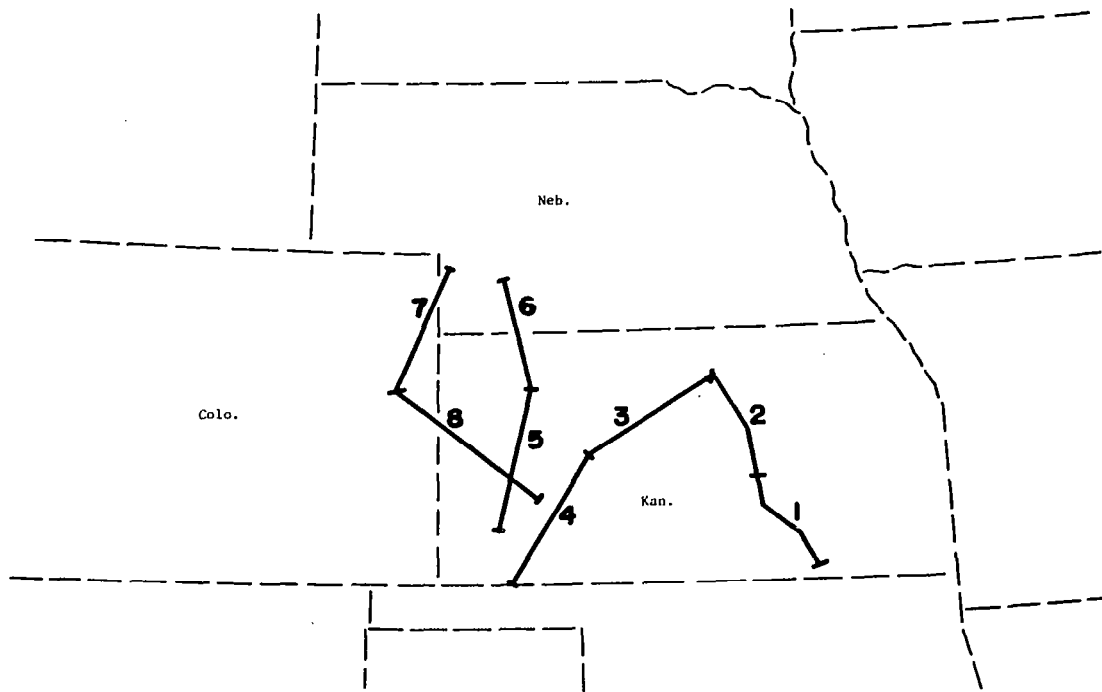


Figure 1. Flight path for sampling of plume from Mount St. Helens on May 20, 1980. (Sample numbers refer to tabulated data.)

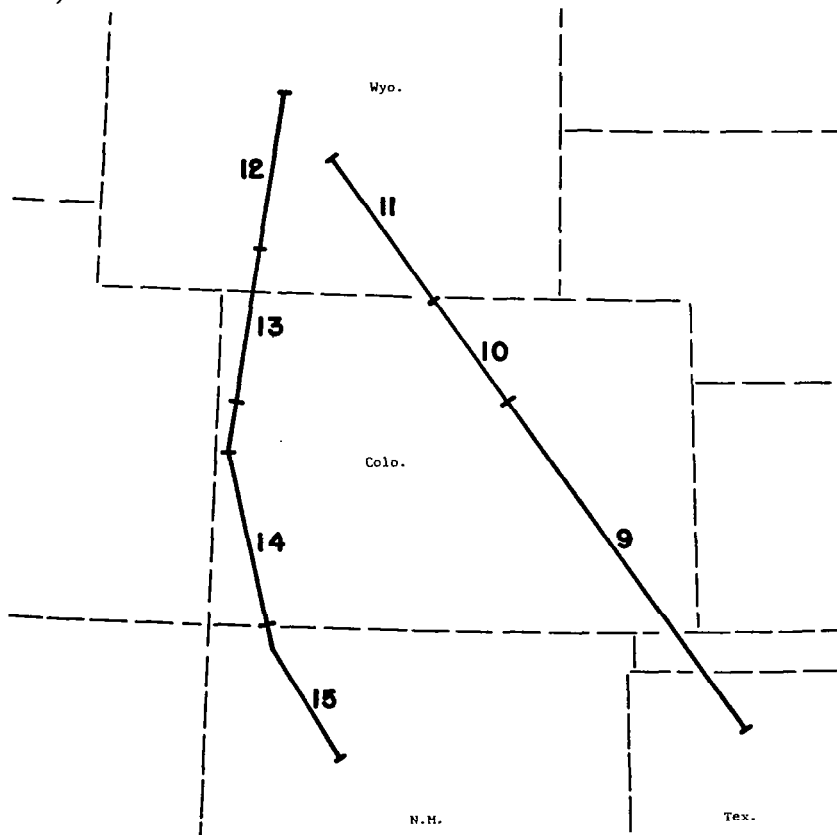


Figure 2. Flight path for sampling of plume from Mount St. Helens on May 21, 1980. (Sample numbers refer to tabulated data.)

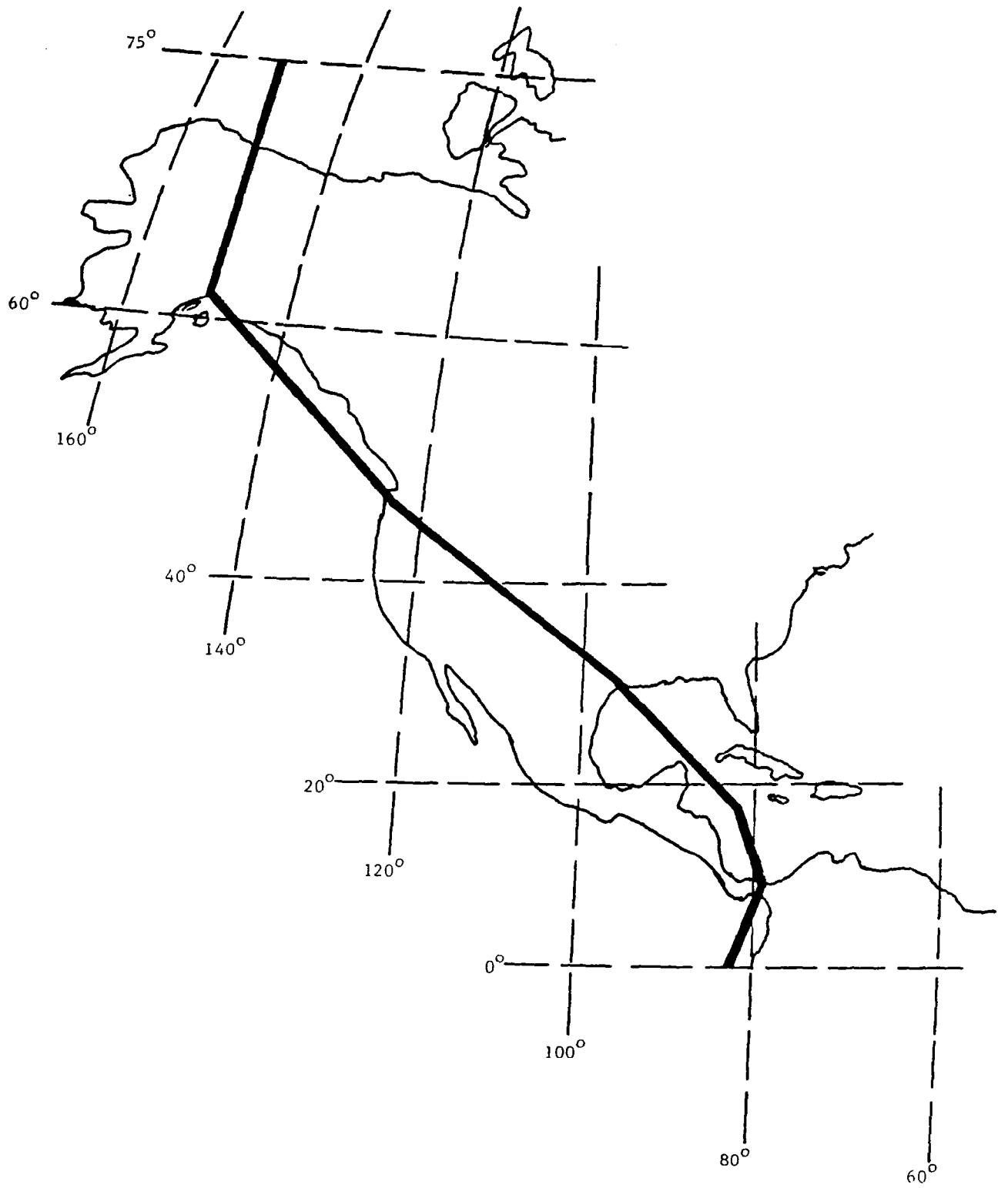


Figure 3. Sampling route for Project Airstream.



(a)



(b)

Figure 4. Typical scanning electron micrographs of pyroclasts collected on May 20 and 21. (a) Angular shard, showing curved surface of broken vesicle walls. Analysis indicates it is a silica-rich glass, similar to the rhyolitic glass component of ash fall samples. (b) Angular, blocky rhyolitic glass pyroclasts on a filter fiber.

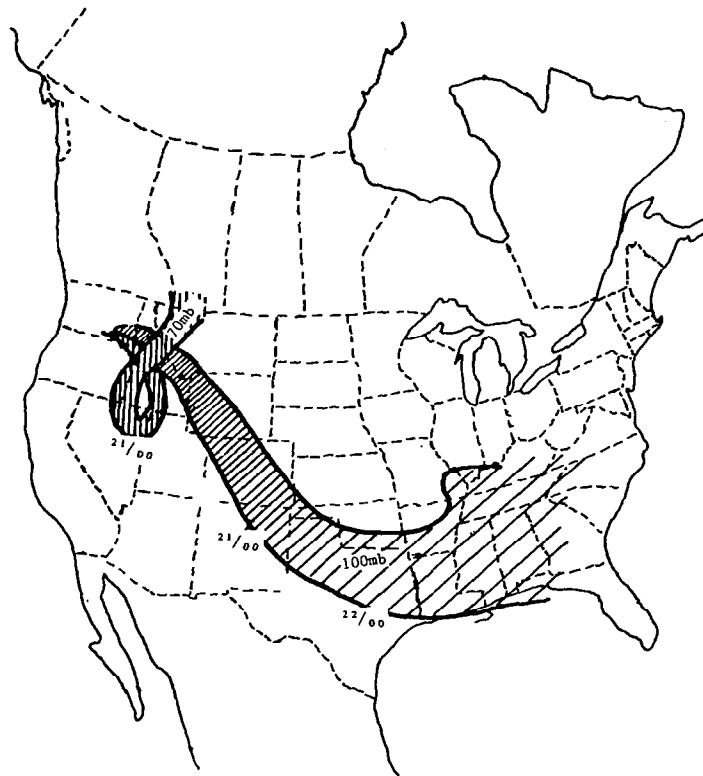


Figure 5. Upper air trajectories for the May 18, 1980, Mount St. Helens eruption debris calculated by NASA-Ames Research Center. (Leading-edge arrival times indicated as day/GMT time.)

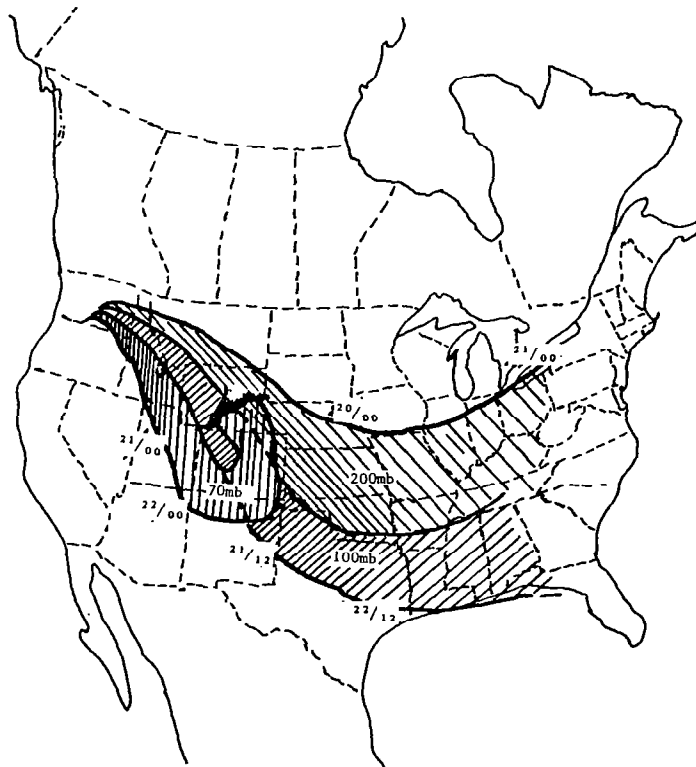


Figure 6. Upper air trajectories for the May 18, 1980 Mount St. Helens eruption debris calculated by NOAA/Air Resources Lab. (Leading-edge arrival times indicated as day/GMT time.)

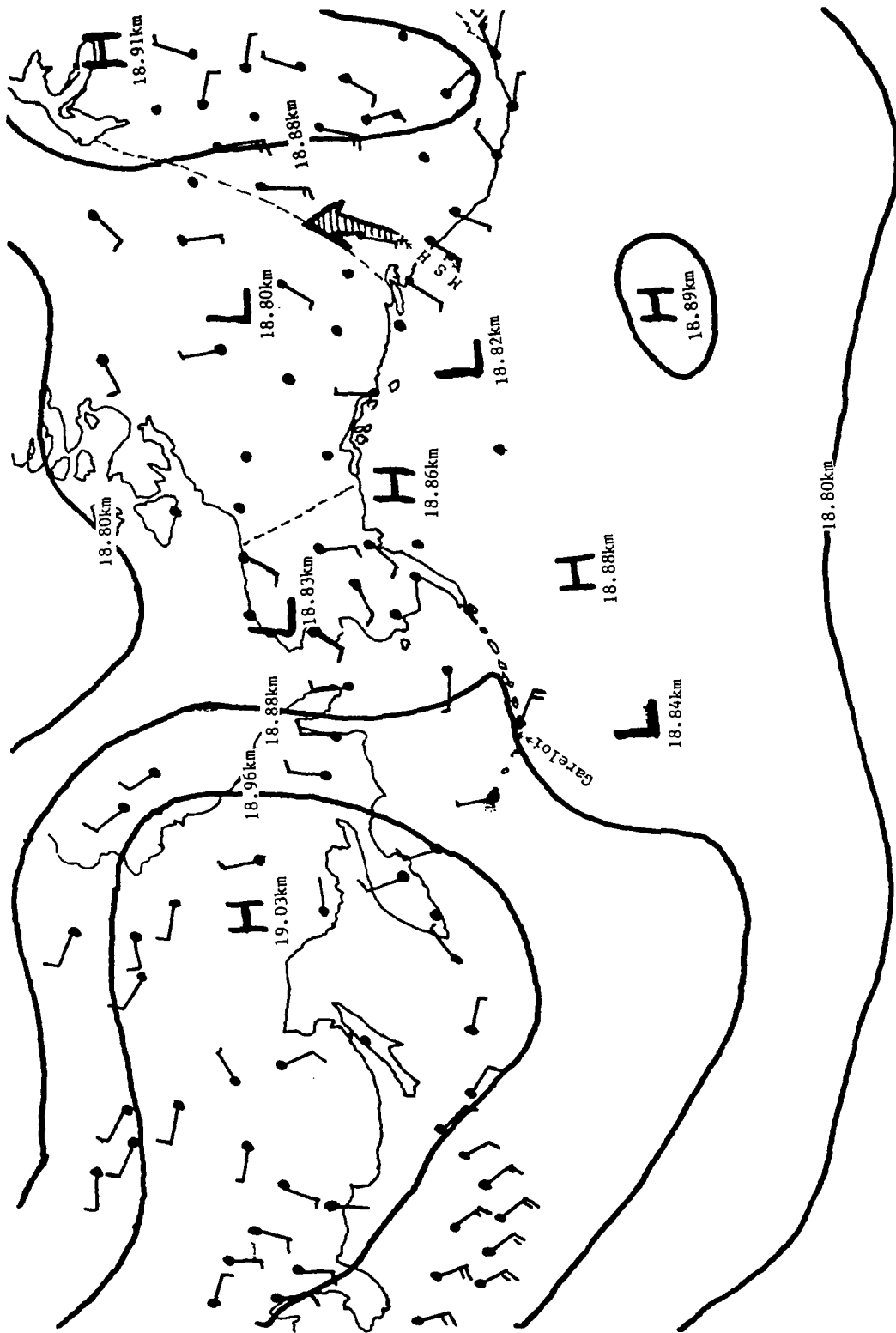


Figure 7. Meteorological analysis wind and height chart for 70 mb at 1200Z on August 7, 1980. (Hatched arrow indicates transport of Mount St. Helens eruption debris.)

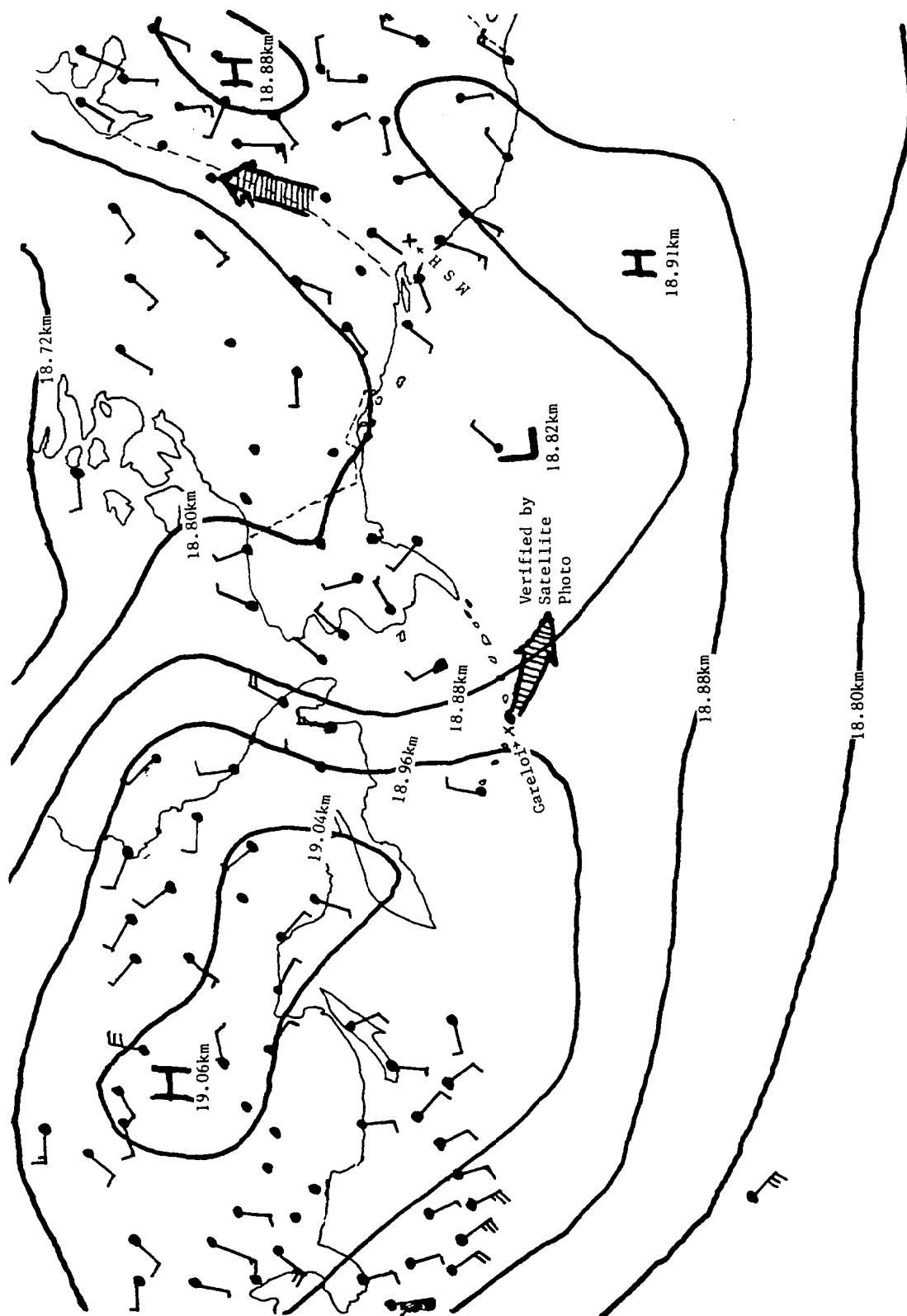


Figure 8. Meteorological analysis wind and height chart for 70 mb at 1200Z on August 8, 1980. (Hatched arrows indicate transport of Mount St. Helens and Gareloi debris.)

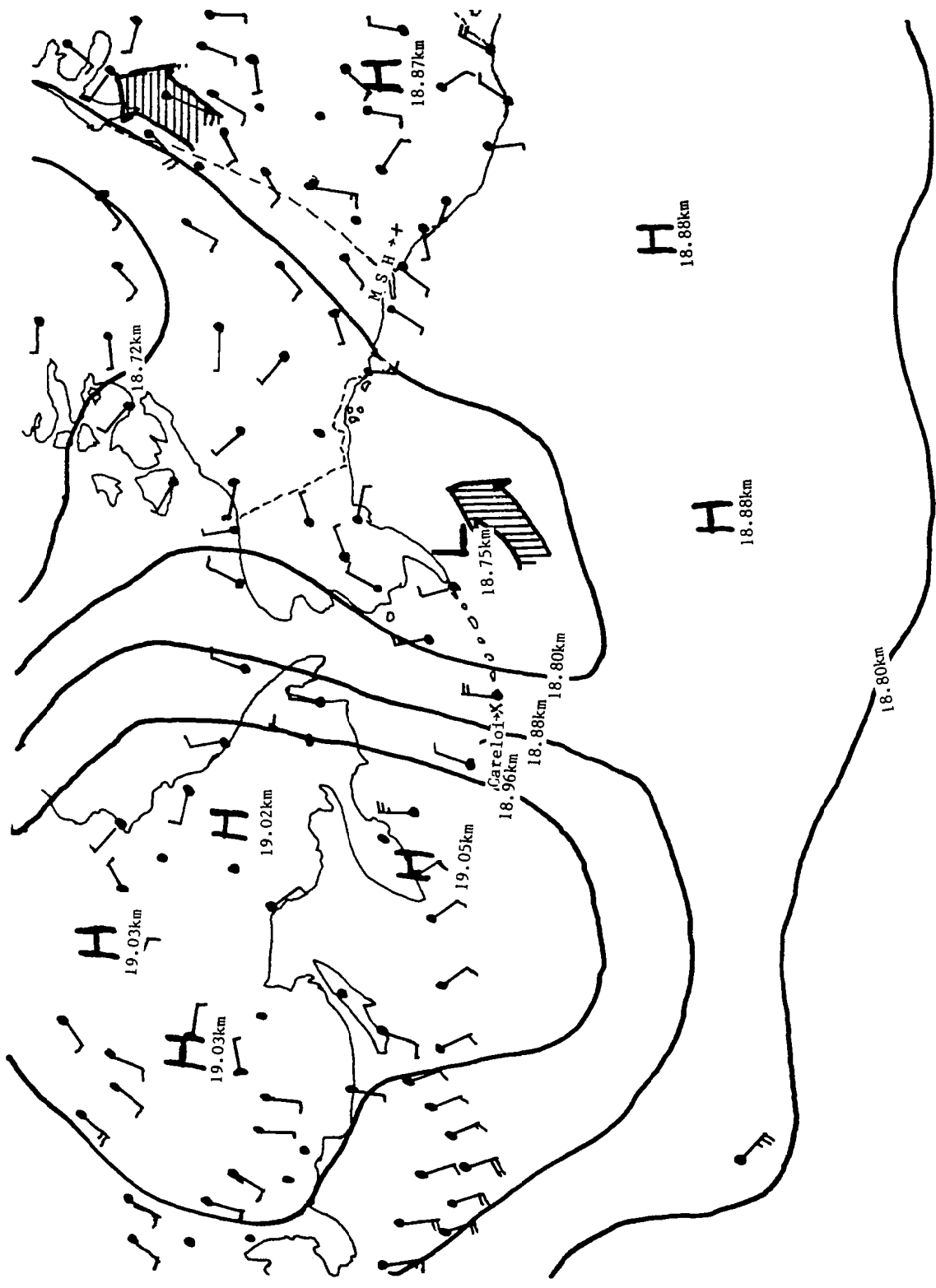


Figure 9. Meteorological analysis wind and height chart for 70 mb at 1200Z on August 9, 1980. (Hatched arrows indicate transport of Mount St. Helens and Gareloi debris.)

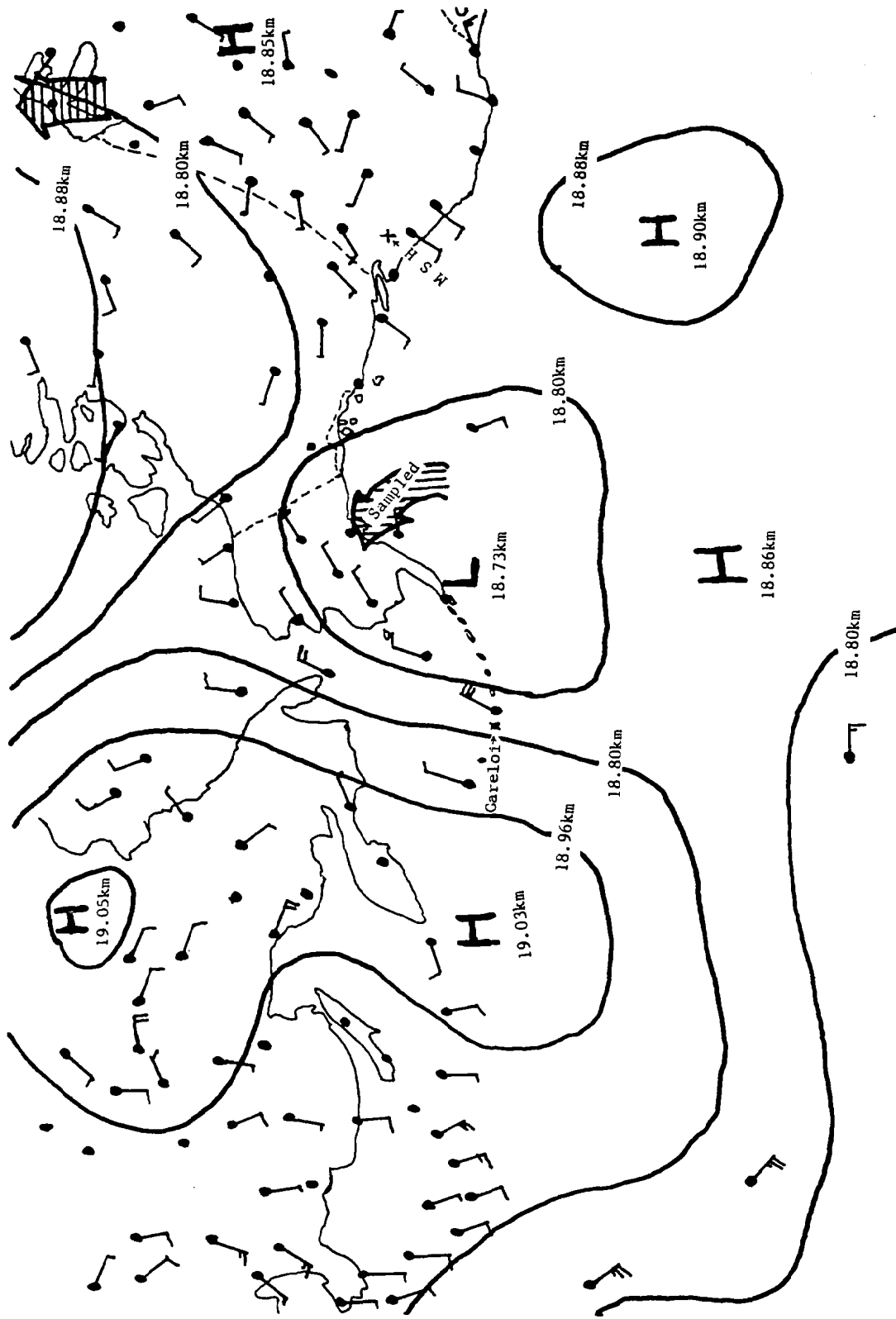


Figure 10. Meteorological analysis wind and height chart for 70 mb at 1200Z on August 10, 1980. (Hatched arrows indicate transport of Mount St. Helens and Gareloi debris.)

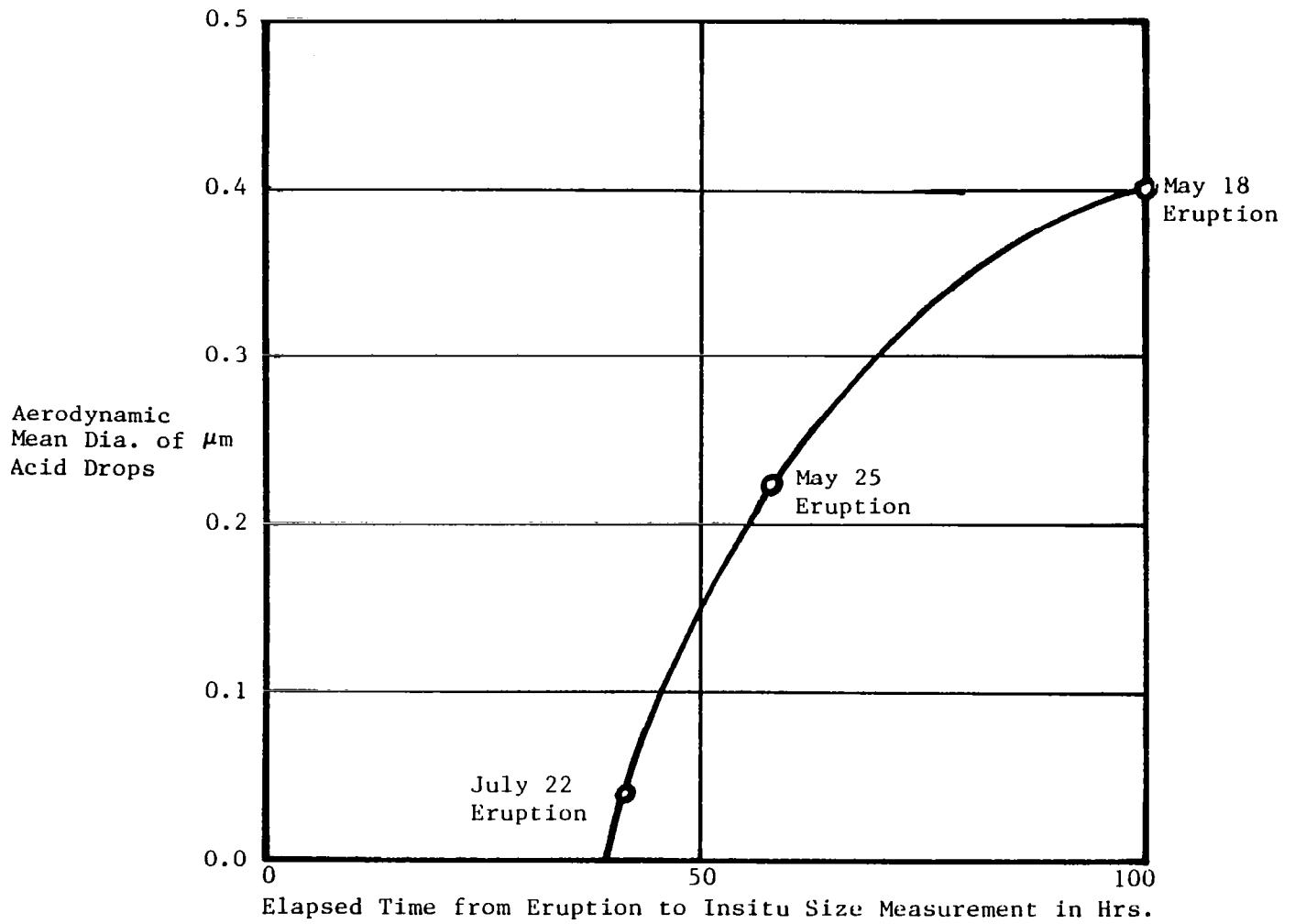


Figure 11. Sulfuric acid aerosol growth in the stratospheric plume from Mount St. Helens volcanic eruptions.

SAGE MEASUREMENTS OF MOUNT ST. HELENS VOLCANIC AEROSOLS

G.S. Kent

Institute for Atmospheric Optics and Remote Sensing, Hampton, VA

The SAGE satellite system has been used to make measurements on the optical extinction produced by stratospheric aerosols from the Mount St. Helens eruption. Two periods of observation have been analyzed so far. In the first period (May 21-31, 1980), SAGE moved southward from latitude 60°N, and crossed the United States approximately one week after the May 18th eruption. Enhancements in stratospheric extinction were confined to latitudes between about 55°N and 25°N and longitudes between 10°W and 140°W. Individual layers were observed up to altitudes of 23 km. The geographical location of these layers corresponded closely to that expected on the basis of high-altitude meteorological data. During June and much of July, SAGE was, by reason of its geographical position and other orbital characteristics, unable to make further measurements on the northern hemisphere. Between July 19th and August 12th a second southward pass over the northern hemisphere occurred and further observations were made. The volcanic aerosol in the stratosphere was now found to be widely distributed over the hemisphere, the maximum concentrations being north of 50°N. The aerosol showed considerable inhomogeneity and had reached as far south as 15°N but little, if any, had crossed the equator into the southern hemisphere. Individual layers at different heights were still distinguishable. The total stratospheric aerosol loading on this occasion appeared to be greater than in May and corresponded to an increase in global stratospheric mass of between 50 and 100 percent.

I. INTRODUCTION

NASA has launched two satellite systems, SAM II (Oct. 24, '78) and SAGE (Feb. 18, '79) designed specifically to measure stratospheric aerosol and gas concentrations (McCormick et al., 1979). The SAGE satellite system has an approximate geographic coverage of latitudes between 70°N and 70°S and has been well situated to observe enhanced stratospheric extinction produced by the Mount St. Helens eruption.

SAGE has four spectral channels; one channel is designed principally for aerosol measurement and is used to measure solar intensity profiles during each sunrise and sunset as the satellite orbits the earth. Since the orbital period is about 90 minutes, approximately 30 measurements (15 sunrises and 15 sunsets) can be made each day. During 1980, because of power supply problems, measurements were confined to sunsets only. The position on the earth's surface of the point of tangency of the sun's rays depends on the date and the orbital parameters and moves in a regular manner from the most northerly point to the most southerly, a cycle taking approximately two months. Measurements made on successive orbits are separated by about 24° in longitude and about 0.2° to 0.3° in latitude. After the St. Helens' eruption, SAGE was conveniently located to make measurements over the northern hemisphere in May 1980, and again in August 1980. Additional data, as yet unexamined, was obtained in September and October.

II. DISCUSSION

The transmission data from SAGE is inverted to give a profile of extinction as a function of altitude for each event. The vertical resolution is about 1 km and the extinction values (at 1.0 μm) have a root-means square error of about $5 \times 10^{-6} \text{ km}^{-1}$. This value corresponds to an accuracy of about 5 percent near the peak of the pre-eruption Mount St. Helens' aerosol layer. The extinction profiles may be integrated to give

optical depth above a given altitude in the stratosphere. The profiles are normally terminated at the lower end by tropospheric clouds. Typical extinction profiles corresponding to an undisturbed stratosphere and to a region of the stratosphere strongly affected by the Mount St. Helens eruption of May 18 are shown in figure 1. It can be seen in this example that the normal background extinction has a peak value of about 10^{-4} km^{-1} . The volcanic enhancement shown here has a peak value of greater than 10^{-3} and, during the period immediately after the eruption, values as high as 10^{-2} were observed.

On May 20th SAGE was making measurements over northern Canada and on May 25 over the latitude of Mount St. Helens. Significant stratospheric enhancements were seen on approximately 20 occasions during this period and ranged in latitude from 55°N to 25°N and in longitude from 20°W to 160°W . The results of a preliminary analysis of these measurements are shown in the map in figure 2 as a contour diagram of the optical depth above a model tropopause. As detailed meteorological data were not available for the period of observation, a tropopause model based on the same season in 1979 has been used. In order to avoid contamination of the data by a cloud near the tropopause itself, integration was commenced two kilometers above the tropopause. Only data for the region of the earth between the dashed lines (23°N to 58°N) have been studied so far. The more lightly shaded areas of the figure represent the typical background optical depth observed before the eruption. It can be seen at this time that the region of volcanically enhanced stratospheric aerosol covered a relatively small fraction of the earth's surface. Considerable vertical shearing of the materials had occurred, the highest layers at heights of 20 to 23 km being observed off the coast of Washington state. The lowest material, below 16 km, had swept across the United States and out over the Atlantic Ocean. This shearing and movement is consistent with the main features of the stratospheric wind system. Thin vertical layers, with thicknesses of 1 to 2 km, were observed as well as thick layers extending downwards into the troposphere.

The second set of SAGE observations was made in July and August and the corresponding contour diagram of optical depth is shown in figure 3. (SAGE was unfortunately in full sunlight between July 4 and July 20 and no data were obtainable during its northward sweep over the northern hemisphere.) As in figure 2, the more lightly shaded areas of the diagram (optical depth of $0.1 \text{ } \bar{\text{O}} \text{ } 2.0 \times 10^{-3}$) are representative of the background aerosol before the eruption. Inhomogeneities, of continental size, are still present in the data but the aerosol has spread over much of the northern hemisphere. The highest concentrations were to the north of the 50°N latitude and the material had spread as far south as 15°N but did not appear to have crossed the equator. Vertical shearing was still very evident in the data. Movement of the upper layers (above 20 km) corresponded well to that expected from analysis of high-altitude air movements. Values for the optical depth were, in general, lower than the extreme values observed in May but still varied from 1.0×10^{-3} to greater than 5.0×10^{-3} . The mean optical depth for the northern hemisphere in August was greater than the corresponding figure for May.

Both the August and May data have been used to estimate the mass of aerosol injected into the stratosphere by the volcano. This calculation involves certain assumptions concerning the amount of background aerosol present at the time of the eruption and the nature of the volcanic aerosol. The background aerosol has been estimated from earlier SAGE data and it has been assumed that the new aerosol is a sulphuric acid/water/ammonium sulphate mixture in the proportions 9:3:4 (Russell et al., 1980). This assumption may not be completely valid for the May data, when an appreciable nonvolatile aerosol component was probably present, but is thought to be a reasonable model for the aerosol in August. The particle size distribution has been modelled on pre-eruption distributions since dustsonde measurements of particle size after the May 18th eruption indicated a return to normal values by the latter part of July (Rosen and Hofmann, 1980). Estimated mass loading values are shown in Table I, where it can be seen that the northern hemisphere mass loading had more than doubled in August 1980. The much lower figure for May is subject to greater inaccuracies than the August value because of poorer sampling and the

possibility of having missed one or more localized concentrations. The possibility of having missed a significant fraction of the aerosol is considered to be small and the two figures for mass loading are believed to be significantly different. The most plausible reason for the mass increase between May and August is thought to be gas-to-particle conversion during the intervening period.

III. CONCLUDING REMARKS

SAGE is continuing to make global measurements of stratospheric extinction. As further data sets become available for analysis, it is anticipated that it will be possible to follow the aerosol movement and to make further estimates of mass loading. It should then be possible to not only follow the global movement of the aerosol but also to map its growth and subsequent decay.

ACKNOWLEDGMENTS

The author wishes to thank Dr. M.P. McCormick and his group at NASA LaRC for much helpful assistance and discussion. The author also wishes to thank the SAGE science team for releasing the preliminary data on which this work was based.

REFERENCES

1. McCormick, M.P.; Hamill, P.; Pepin, T.J.; Chu, W.P.; Swissler, T.J.; and McMaster, L.R.; 1979: Satellite studies of the stratospheric aerosol, *Bull. Am. Met. Soc.*, **9**, 1038-1046.
2. Russell, P.B.; Swissler, T.J.; McCormick, M.P.; Chu, W.P.; Livingston, J.M.; and Pepin, T.J.; 1981: Satellite and correlation measurements of the stratospheric aerosol: I. A flexible optical model for data conversion. *J. Atmos. Sci.*, (1980) (in press).
3. Rosen, J.; and Hofmann, D.: Dustsonde Measurements Following the Mount St. Helens Eruption, Tenth International Laser Radar Conference, (Silver Spring, Maryland) Oct. 6-9, 1980. (Conference Abstracts, pp. 155-158.)

TABLE I. ESTIMATED STRATOSPHERIC AEROSOL MASS FOR THE NORTHERN HEMISPHERE

Date	Stratospheric Loading, tonnes
Pre-Mount St. Helens Background (1978-1979)	3.0×10^5
May 1980	0.55×10^5 (loading increase)
August 1980	2.9×10^5 (loading increase)

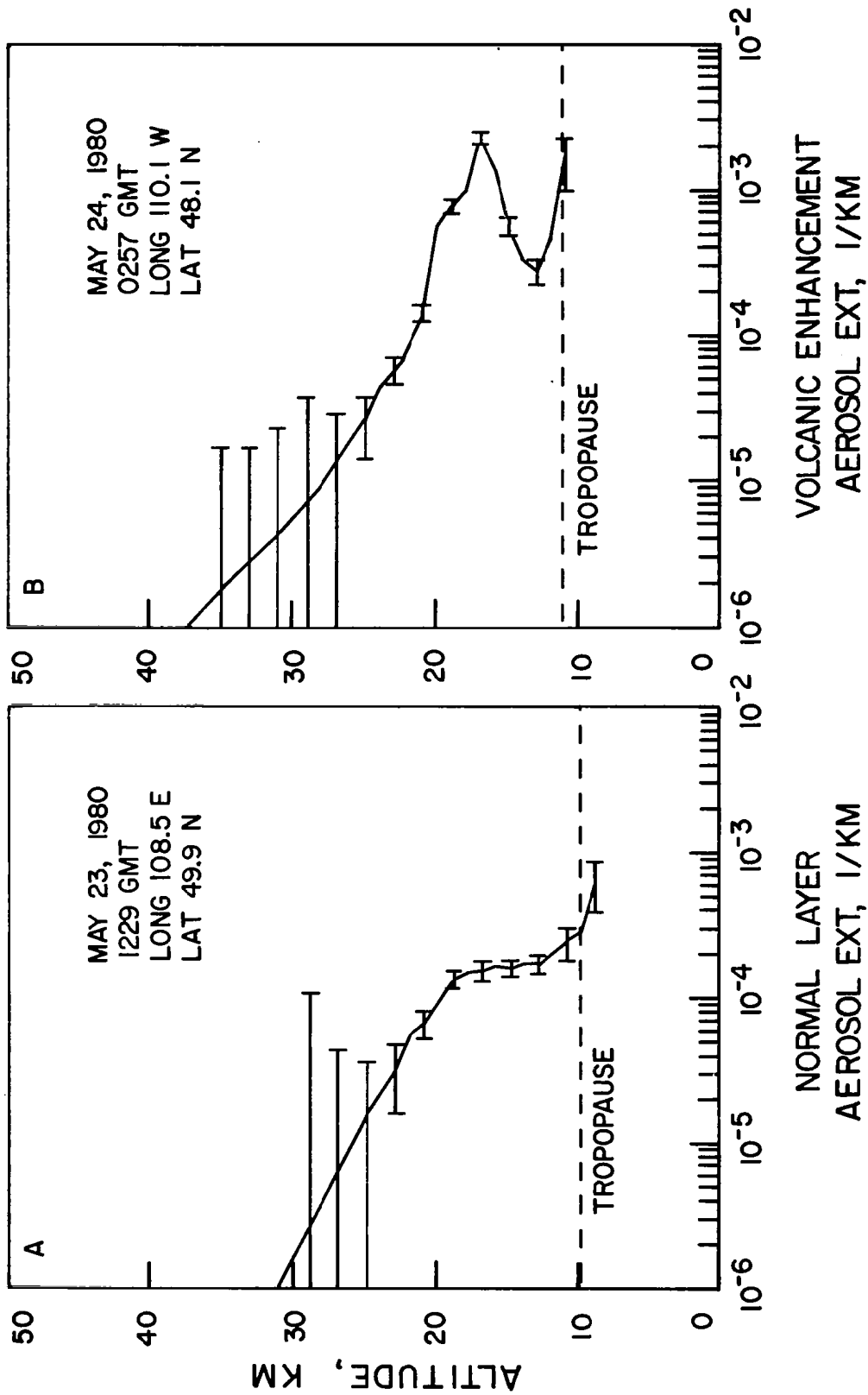


Figure 1. Stratospheric aerosol extinction profiles obtained by SAGE at a wavelength of 1 μm . (a) Normal profile unaffected by volcanic effluents. (b) Profile showing an enhancement caused by Mount St. Helens.

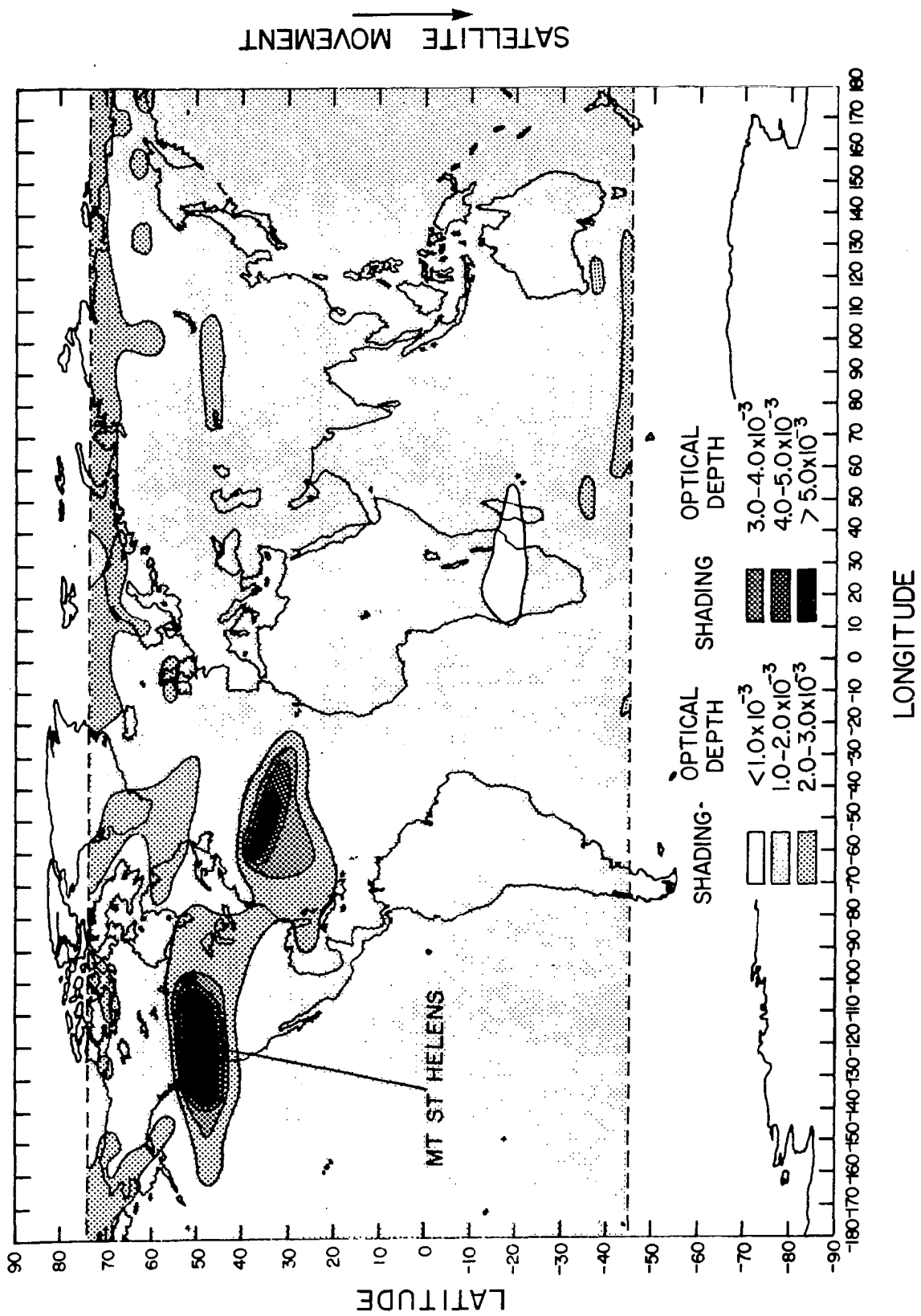


Figure 2. SAGE map of the stratospheric aerosol distribution shortly after the May 18 eruption. SAGE observations are confined to the regions between the dashed lines. The differential motion of material at separate altitudes is apparent.

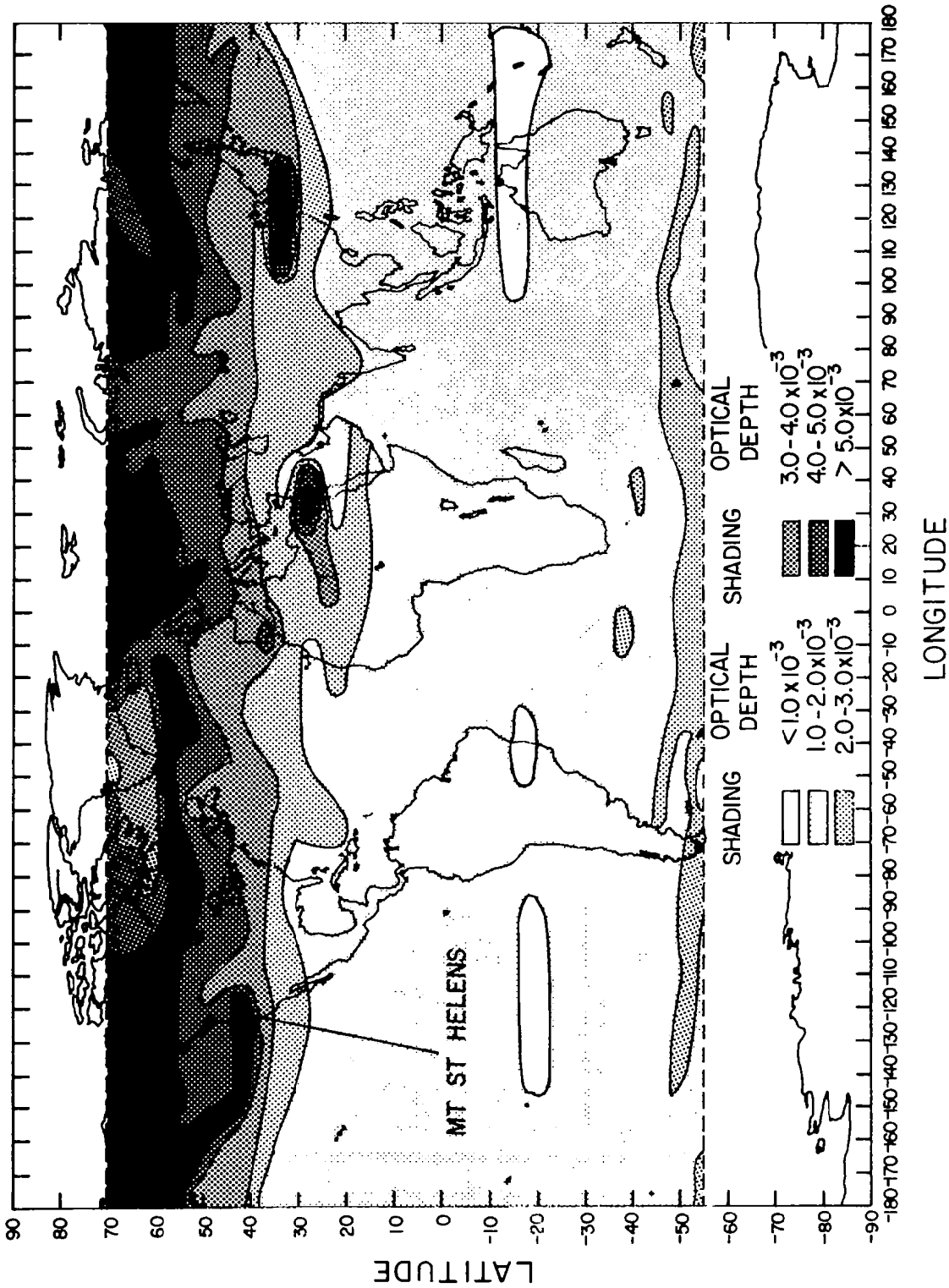


Figure 3. SAGE map of the stratospheric optical depth, July 21-August 26, 1980. Note that the material is still heavily concentrated towards the north.



MEASUREMENTS OF STRATOSPHERIC AEROSOL OVER MAUNA LOA, HAWAII, AND BOULDER, COLORADO

John J. Deluigi, Bernard G. Mendonca, and Kirby J. Hanson
National Oceanic and Atmospheric Administration, Boulder, Colorado

The direct solar radiation transmission record at Mauna Loa, dating from 1958 to the present, has revealed with remarkable precision the presence of stratospheric aerosol from volcanic activity (1). This record can be used to quantify the intensity of the stratospheric volcanic aerosol perturbation following a significant eruption in reference to the Agung event in 1963. The Mount St. Helens' stratospheric cloud was first detected by lidar at 18 km over Mauna Loa on 17 July. The atmospheric transmission was seen to decrease slightly after that time, but only a few tenths of 1 percent. Although it is still fairly early to draw a definite conclusion on the ultimate magnitude of the Mount St. Helens stratospheric aerosol from the Mauna Loa results, it can be stated that the stratospheric aerosol optical depth presently observed is comparable with that observed from Fuego which erupted in 1974. At Boulder, Colorado, the atmospheric debris from Mount St. Helens was observed by lidar on a number of occasions. Also, observations of the diffuse, total and direct transmission of solar radiation were made on June 3 and 4. The latter set of observations is useful for deriving information on the scattering properties of the volcanic cloud. The lidar and solar radiation data are presented and some of their special features are discussed.

I. DEPLETION OF SOLAR RADIATION BY THE MOUNT ST. HELENS' DUST CLOUD

On the 3rd of June 1980, the dust cloud from Mount St. Helens' eruption of 18th May was present again over Boulder, Colorado, after the cloud had circled the globe for the first time. On the following day, little of the stratospheric cloud remained according to lidar observations made on the evenings of the 3rd and 4th of June. Pyranometer and pyrheliometer measurements were obtained on both days and the ratio of the change in total to change in direct $\Delta T/\Delta I$ radiation was calculated. This value represents the rate at which the stratospheric aerosol prevents solar radiation from reaching the surface. The stratospheric aerosol will attenuate direct solar radiation in its downward propagation to the surface, but much of the attenuated radiation will show up as an increase in the downward diffuse-sky radiation because of scattering by the dust.

The following table gives the change of total to direct radiation (where the direct is normal to the horizontal) for a few solar zenith angles. Note that a zenith angle of 60° is the area-weighted mean solar zenith angle for the sunlit side of the Earth's atmosphere. Thus, if a stratospheric aerosol were spread around the entire globe, the mean effect would be similar to the effect seen at a solar zenith angle of 60° .

Solar zenith angle, deg., $\Delta T/\Delta I$	
61.6	0.256
59.7	0.239
57.8	0.227

Another interpretation is that of ΔT alone; eleven percent of the solar radiation did not reach the surface on the 3rd as compared with the 4th.

For a comparison with Agung, it is noted that $\Delta D/\Delta I = 0.2$ for 1963, 0.25 for 1964, and 0.30 for 1965 (2). These results imply that the Agung particles may have been slightly larger than the particles from Mount St.

Helens because larger particles scatter in the forward direction more efficiently. On the other hand, uncertainties in the measurements at Aspendale may be responsible for at least part of the difference.

II. REMOTE SENSING OPTICAL ABSORPTION BY THE MOUNT ST. HELENS' CLOUD

The diffuse-sky radiation is controlled by scattering and absorption from molecules and dust. Outside any significant molecular absorption bands, molecular scattering remains invariant, and the diffuse-sky radiation then depends on the presence of dust and its optical nature. The two optical characteristics of dust that determine the magnitude of any variation to the diffuse-sky radiation are phase function and absorption. The ratio of diffusely transmitted to directly transmitted solar (2) radiation contains information on the phase function and absorption by dust.

Information on the phase function, which is related to particle size, can be derived from spectral extinction characteristics of aerosols. The relationship between spectral extinction and the Junge power law for size distribution is given by the two expressions:

$$\frac{dN}{d \log r} \propto r^{-\nu^*}$$

and

$$\Delta t_d(\lambda) \propto \lambda^{-\gamma}$$

where

$$\nu^* = \gamma + 2$$

N = Number concentration

r = Particle radius

r = Particle radius

Δt_d = Change in optical depth from 3rd to 4th of June

and

ν and γ are simple powers.

Figure 1 shows a plot of spectral extinction observations Δt_d for June 3-4. The line fit yields a γ of 0.47.

Spectral measurements of diffuse and direct radiation were obtained at Boulder, Colorado, on the 3rd and 4th of June. On the 3rd of June the Mount St. Helens' dust cloud was much more intense than on the 4th, and this condition permitted us to take the rate of change of diffuse to direct ($\Delta D/\Delta I$) for analysis. This measurement diminishes considerably the strong dependence of the diffuse radiation on surface reflectivity and tropospheric aerosol, both of which remained nearly constant from one day to the next. Figure 2 shows an analysis of $\Delta D/\Delta I$ for refractive index. The continuous curves are theoretical calculations of $\Delta D/\Delta I$ against wavelength and $\nu^* = 2.5$. The observed $\Delta D/\Delta I$ are shown as dots representing the average and spread of five nearby points. The solution absorption term of the complex refractive index n_r ranges from nearly 0 to 0.002. The results indicate that the dust cloud is only weakly absorbing solar radiation.

It is worthwhile to note that a similar analysis (2) was done with solar radiation data (4) taken shortly after eruption of Agung in 1963 at Aspendale, Australia. The result of this analysis indicated that the dust from Agung also did not absorb strongly.

III. LIDAR OBSERVATIONS OF THE MOUNT ST. HELENS' DUST CLOUD AT BOULDER, COLORADO

A substantial number of lidar observations of the Mount St. Helens' cloud were obtained at Boulder from mid-May until mid-July. In figures 3 and 4 observations taken on the 20th and 21st of May are shown.

By 0915 MST on the 19th, the thickest part of the volcanic cloud had passed over Boulder, Colorado. During the morning, a thin layer of dust fell on the surface. The maximum optical depth observed was 1.6, but cirrus clouds may have contributed to this high value. A few other measurements were grouped around an optical depth of 1.2.

By evening, dust clouds still existed. Two lidar soundings are shown to illustrate the considerable vertical structure that prevailed in the dust cloud that lagged behind the major cloud, which by this time had already traveled several hundred miles beyond Boulder. Note that the times of the two soundings are a few hours apart, but by this time the lower layer observed at 2112 had disappeared by 0057 MST on the 20th. On the other hand, not much change was seen in the lidar signals at the higher levels.

Observations made until July revealed the occasional presence of dust layers near the tropopause on different occasions. A layer near 19 km became a rather persistently observed feature during the later period of measurement.

IV. MAUNA LOA TRANSMISSION—VARIATIONS AFTER MOUNT ST. HELENS

A lower than normal atmospheric transmission decrease was observed at Mauna Loa after the Mount St. Helens' eruption. Measurements of the direct component of solar radiation during clear-sky periods at Mauna Loa have been made since 1958. From this data set secular decreases in atmospheric transmission have been determined after explosive volcanic eruptions (1). These decreases in atmospheric transmission have been interpreted as an indicator of the global spread of volcanic debris in the high troposphere and low stratosphere. Residence and recovery times have been deduced from these measurements as well. Research on what possible climatic effects may result from such atmospheric loading is continuing.

The most recent decreases in atmospheric transmission observed at Mauna Loa occurred after the eruptions of DeFuego (1974), Soufriere and Sierra Negra (1979), and Mount St. Helens in 1980. The perturbation in atmospheric transmission for Agung (1963) was the largest measured at Mauna Loa and resulted in a 2 percent decrease in transmission from the pre-Agung or undisturbed period (1958-1962) at Mauna Loa. The decreases in atmospheric transmission after DeFuego were 0.75 percent and 0.57 percent after Soufriere and 0.55 percent after Sierra Negra, and 0.58 percent after Mount St. Helens. Because of the closeness between the eruptions of Soufriere, Sierra Negra, and Mount St. Helens, it is difficult to distinguish between the effects of each event since it is assumed that some residue of the earlier episodes are superimposed on the succeeding ones as they are measured in the late spring and early summer transmission values at Mauna Loa.

It is important to note that the transmission values at Mauna Loa have not returned to the pre-Agung values nor to the high values measured in 1976 and 1977 when a shift in the planetary circulation in the mid-latitudes during winter resulted in extremely clear skies at Mauna Loa.

Figures 5 and 6 show plots of atmospheric transmission at Mauna Loa for the most recent period; figure 5 shows monthly averages for 1978 to 1980, and figure 6 shows a 6-month smoothing of transmission for the entire period 1958 to 1980.

REFERENCES

1. Mendonca, B.G., Hanson, K.J., and DeLuisi, J.J., (1978): Volcanically related secular trends in atmospheric transmission at Mauna Loa Observatory Hawaii. Science, 202, pp. 513-515.
2. Herman, B.M., Browning, R.S., and DeLuisi, J.J., (1975): Determination of the effective imaginary term of the complex refractive index of atmospheric dust by remote sensing: The diffuse-direct radiation method. J. Atmos. Sci., 32, 918-925.
3. DeLuisi, J.J., and Herman, B.M. (1977): Estimation of solar radiation absorption by volcanic stratospheric aerosols from Agung using surface-based observations. Jour. Geophys. Res., 82, 3477-3480.
4. Dyer, A.J., and Hicks, B.B., (1965): Stratospheric transport of volcanic dust inferred from solar radiation measurements. Nature, 208, 131-133.

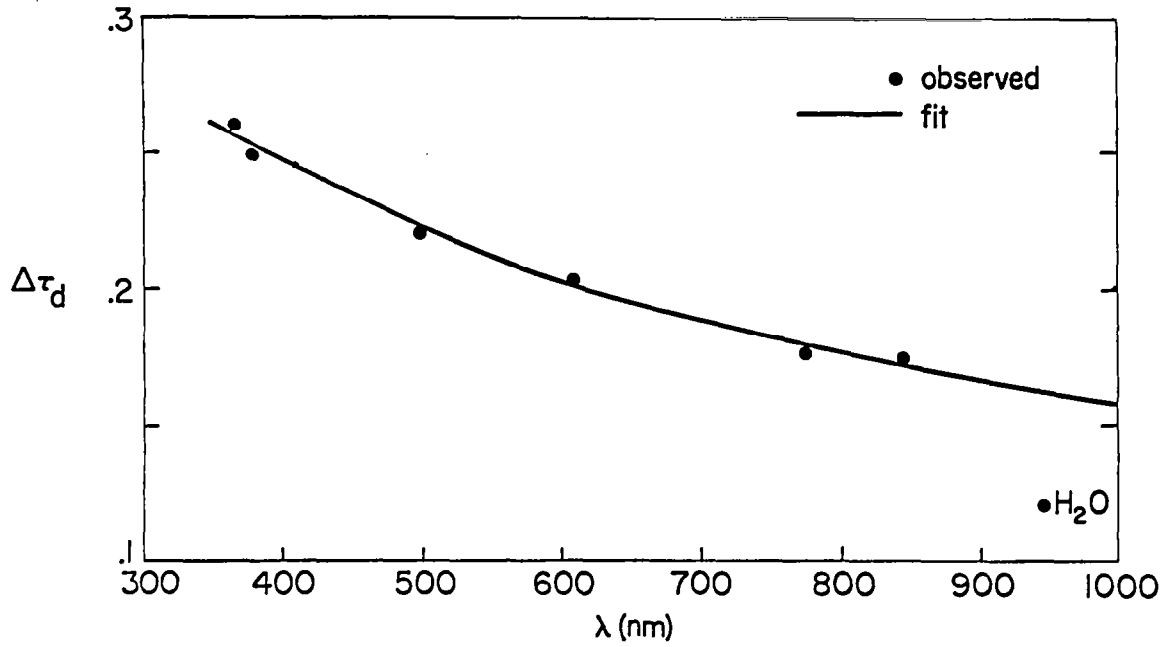


Figure 1. Spectral extinction of the Mount St. Helens' stratospheric cloud after it circled the globe, 3 June 1980, Boulder, Colorado.

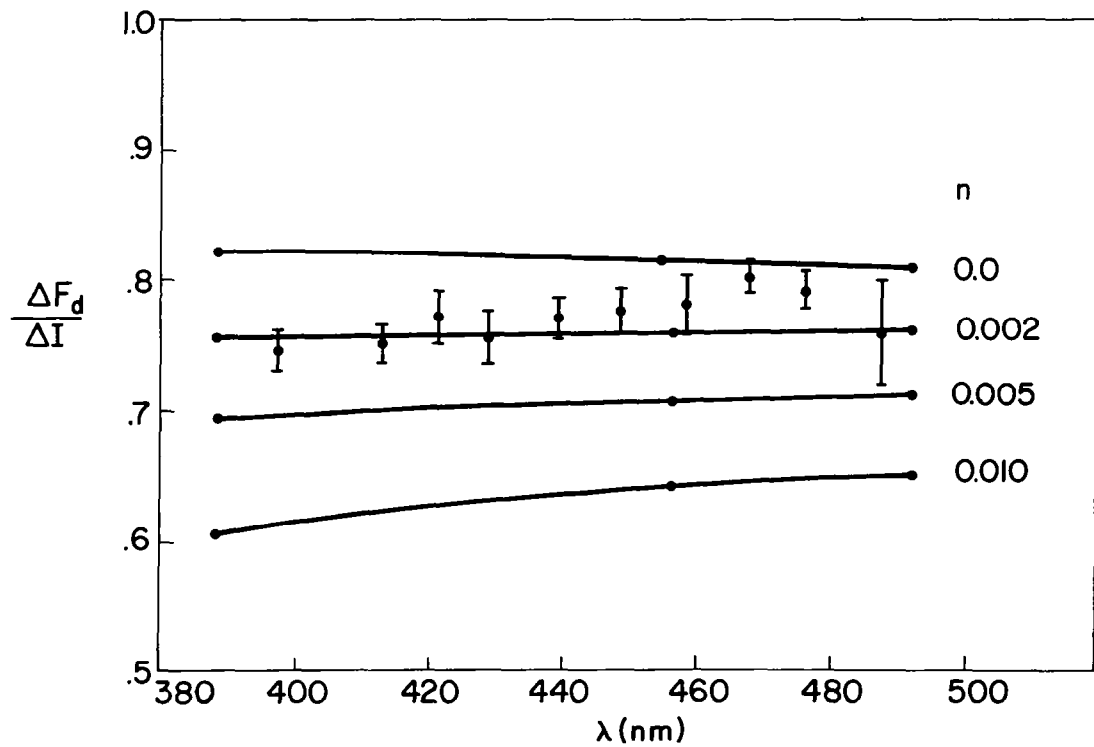


Figure 2. Imaginary term of the complex refractive index, shown as dots, of the Mount St. Helens' stratospheric cloud after it circled the globe, 3 June 1980, Boulder, Colorado.

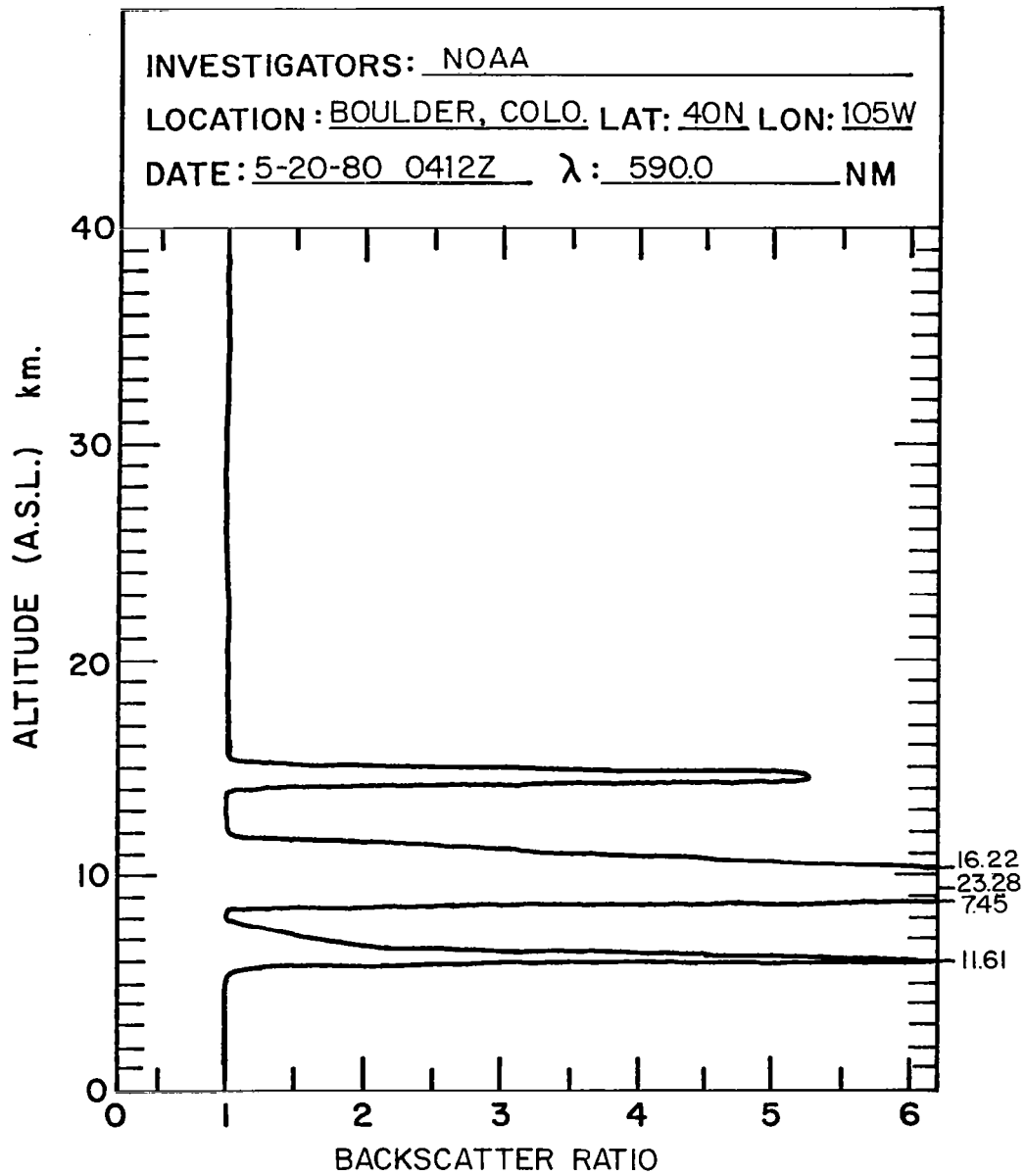


Figure 3. Lidar profile of the Mount St. Helens' cloud during passage over Boulder, Colorado, about one day after the 18 May 80 eruption. Profiles are in terms of the backscatter ratio: total backscatter to Rayleigh backscatter.

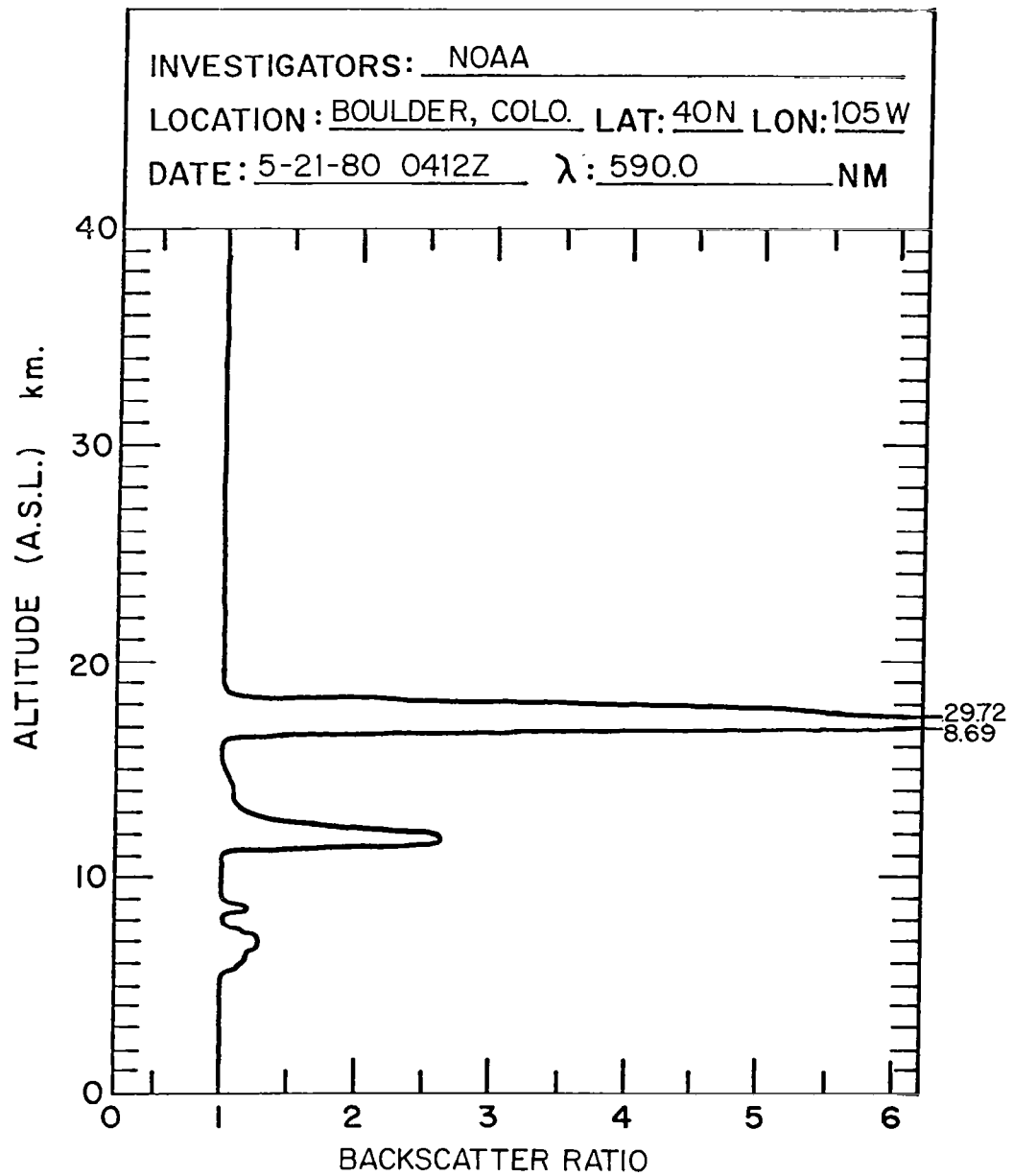


Figure 4. Lidar profile of the Mount St. Helens' cloud during passage over Boulder, Colorado, about one day after the 18 May 80 eruption. Profiles are in terms of backscatter ratio: total backscatter to Rayleigh backscatter.

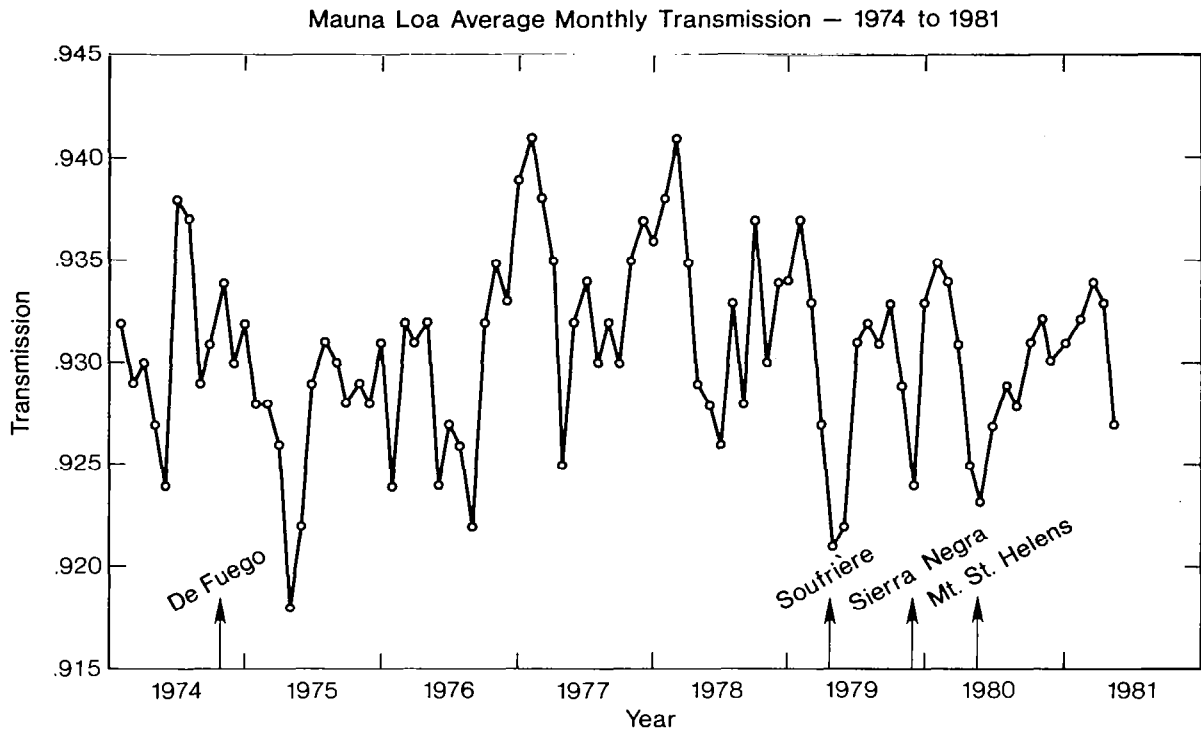


Figure 5. Plot of atmospheric transmission at Mauna Loa for monthly averages 1978-1980.

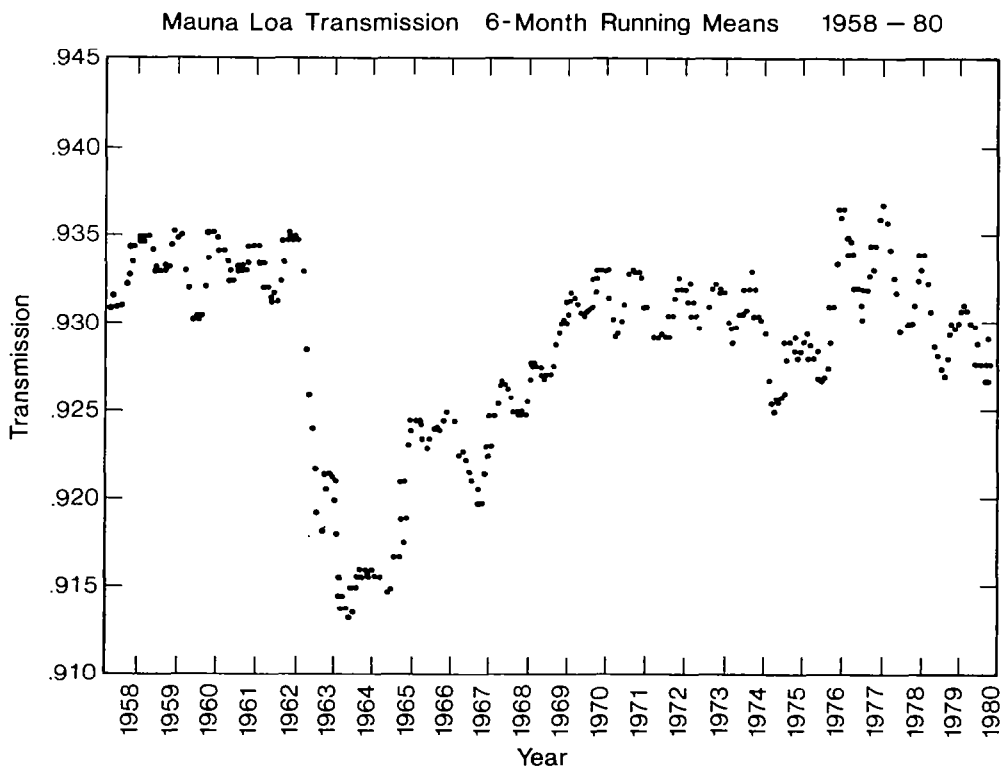


Figure 6. Historical transmission record for Mauna Loa using a 6-month running average smoother.



GROUND-BASED AND AIRBORNE MEASUREMENTS OF THE MOUNT ST. HELENS STRATOSPHERIC EFFLUENTS

M. P. McCormick, NASA-Langley Research Center, Hampton, VA

Shortly after the 18 May eruption, a series of airborne lidar flights were made over the Eastern United States. During the same period, ground-based systems were activated throughout the world. This paper will put together, into a consistent set, the available worldwide lidar data. These data show the dispersion of material at different altitudes during the early global circuits. The material in the lower stratosphere and upper troposphere was very patchy in horizontal extent with backscattering ratio values over the east coast of the United States greater than 100 at the ruby wavelength of $0.6943 \mu\text{m}$. Two wavelength ratios and depolarization values for the material in the lower stratosphere (12 to 18 km) appear to have returned to the pre-18 May values within a month after the eruption, and this indicated a rapid conversion to spherical shapes and normal indices of refraction. The material above 20 km moved slowly westward while most of the ejecta moved eastward at various speeds and directions which varied considerably with altitude. The westward material was detected first by the Japanese lidar system and then subsequently by the European and American ground-based systems. It circuted the globe in about 60 days. An airborne lidar flight in early September across the continental United States showed the layers to have homogenized considerably one broad layer between about 14 and 21 km peaking at 18 to 19 km and another more intermittent thin layer between 21 and 22 km. The ruby peak backscattering ratio of the broad layer was between 1.3 and 1.5. These data will also be compared with the SAGE data and the long-term pre- and post-Fuego lidar data that have been compiled at NASA-Langley Research Center (LaRC).

I. INTRODUCTION

The 18 May 1980 eruption of Mount St. Helens sent material into the stratosphere where it was then carried rapidly around the globe in the upper-air zonal winds. The lower material (14-to 20-km altitude) was carried rapidly eastward across the United States and the Atlantic Ocean to Europe and was observed by a succession of lidar stations and airborne lidar flights within these regions. The upper material (20 to 23 km) moved slowly westward and was observed by lidar over Japan and then later over Europe and the United States as it completed its global circuit. This paper describes the data obtained during airborne lidar flights over the United States and interprets the data obtained in terms of the movements of the aerosol. The data are also used to determine the mass of material injected into the stratosphere.

The various measurements have all been made by using either ruby ($\lambda = 0.6943 \mu\text{m}$) or neodymium-YAG ($\lambda = 1.0 \mu\text{m}$) laser systems. In addition to the standard measurement of scattered-signal amplitude some measurements of signal polarization are also available. These measurements show a change with time of the nature of the stratospheric material.

II. LIDAR MEASUREMENTS

Lidar measurements are made by observing the atmospheric backscatter from molecules and particles as a laser pulse propagates through the atmosphere. The intensity of this range-resolved laser backscatter is dependent upon the molecular air density and particle concentration as well as the particle refractive index, shape, and size distribution. The most commonly used measure of particle concentration is the lidar backscatter ratio calculated by ratioing the total lidar backscatter (molecular plus aerosol) to the molecular

backscatter only (ref. 1). Typical mid-latitude vertical profiles of the backscatter ratio taken by using a ruby lidar system prior to the St. Helens eruption showed a peak value of about 1.1 at a height of 18 to 23 km. Because of the differences in scattering characteristics at $1.06\ \mu\text{m}$, the values for Nd:YAG lidar systems were somewhat greater, with peak values of about 1.3.

Lidar data have been obtained by the Langley Research Center (LaRC) by using two different systems. One is a large ground-based system located at LaRC ($37^\circ\ \text{N}$, $76^\circ\ \text{W}$) and generally operated at the ruby wavelength only. The other is airborne and operates at either the ruby or NdYAG wavelength. A typical profile obtained before the eruption, using the LaRC ground-based system, is shown in figure 1(a). It may be noted that the peak-scattering ratio does not exceed 1.1. In contrast, the profile in figure 1(b), taken shortly after the eruption of 18 May, shows strong scattering layers at heights of 14.0 and 17.6 km.

III. LIDAR DATA OBTAINED AFTER 18 MAY 1980

Following the eruption of 18 May 1980, several flights were made by the LaRC airborne system over the Eastern United States with the objective of interpreting and observing layers of volcanically injected stratospheric material (see fig. 2). In the first of these flights, on 21 May, peak backscatter ratios as high as 107 at $1.06\ \mu\text{m}$ were recorded south of Lake Erie at an altitude of 13.6 km. On this evening, the layer was about 1-km thick with its leading edge spread from north central Pennsylvania southwest to southern Indiana. Other flights were taken on the evenings of 22, 26, and 27 May. The aircraft flight paths for 21 and 22 May were chosen according to predictions of the air mass motions at the altitude of the volcanic layers. The 26 and 27 May flights were chosen to underfly and ground truth a satellite system making stratospheric aerosol measurements (see ref. 2). All these flights showed similar layering of high-density material at altitudes between 12 and 14 km. Finding material at these altitudes during this time is consistent with air mass trajectory analysis (see ref. 3).

Material at slightly higher altitudes of 14 to 16 km was found to have moved on a more southerly trajectory than the 12- to 14-km material. Backscatter data were obtained on the evening of 27 May, which showed 14- to 16 km-material near the coast of South Carolina, in accordance with predictions. Two-color lidar data showed values for the relative backscatter ratios at $1.06\ \mu\text{m}$ and $0.6943\ \mu\text{m}$ to be lower than normal for the stratospheric aerosol. The values obtained suggest that these initial low stratospheric clouds were probably composed of silicate-type particles. This interpretation is supported by depolarization measurements of LaRC which showed anomalous values during this period. Both the two-color lidar ratios and the depolarization values returned to pre-18 May values after about 1 month.

Data from the LaRC ground-based system show that although layers below 20 km were detected very soon after the 18 May eruption, layers above this height were not seen until the first week in July. This result is consistent with the eastward movement of the material below 20 km and the westward movement of the material above this height, which arrived back over LaRC on 7 July, after traveling around the globe. This interpretation is supported by movements at other northern hemisphere lidar stations which are presented in figure 3. The material above 20 km, primarily at two distinct altitudes, 21.5 km and 23 km, was caught above the wind reversal over Mount St. Helens and moved in a westward direction. The upper layer moved at a faster average speed (about 8 m/sec compared with 6 m/sec for the lower layer). The dots in figure 3 are for the upper layer and the asterisks are the slightly lower layer. The shaded area represents wind speeds reasonable for these altitudes during this time of year. It is bounded by values given by Newell and others (ref. 4) for 20 km at $40^\circ\ \text{N}$ and 23 km at $30^\circ\ \text{N}$. As this material moved west from Mount St. Helens, the first lidar station to detect its arrival was at Nagoya, Japan ($35^\circ\ \text{N}$, $137^\circ\ \text{E}$,) (ref. 5). It was then detected at L'aquila, Italy ($42^\circ\ \text{N}$, $23^\circ\ \text{E}$) (ref. 6), then Garmisch-Partenkirchen, Germany ($48^\circ\ \text{N}$, $11^\circ\ \text{E}$) (ref. 7), Haute Provence, France ($44^\circ\ \text{N}$, $6^\circ\ \text{E}$) (ref. 8), Slough, England ($51^\circ\ \text{N}$, $1^\circ\ \text{W}$) (ref. 9), LaRC ($37^\circ\ \text{N}$, $76^\circ\ \text{W}$), Urbana, Illinois ($42^\circ\ \text{N}$, $23^\circ\ \text{E}$) (ref. 10), Madison, Wisconsin ($43^\circ\ \text{N}$, $89^\circ\ \text{W}$) (ref. 11), and finally, Boulder, Colorado ($40^\circ\ \text{N}$, $105^\circ\ \text{W}$) (ref. 12). All these data are seen to generally agree with predicted average wind profiles and are consistent with each other.

Data from the airborne lidar mission in September across the United States and ground-based data taken at LaRC suggest that the volcanic layers had become much more homogenized. Typically, the stratospheric material at this time was spread from just above the tropopause through 22 km with a peak backscatter ratio of 1.35 at about 18 km. The higher altitude material was present at this time but sporadic. Whenever detected, the two upper layers were merged into one.

IV. MASS LOADING

The backscatter values have been used to provide an estimate of the increase in aerosol mass loading produced by Mount St. Helens. By September, the observed lidar backscattering is thought to be primarily due to sulfuric acid/water particles. This belief assumes that all the gases have converted into sulfuric acid droplets and the solid particles that have not gravitated into the troposphere represent a small fraction of the total stratospheric aerosol mass. Based on this assumption, optical model conversion procedures as described in Russell et al. (ref. 13) were utilized to derive from the lidar profile data the vertical distribution of aerosol mass concentration. By comparing this with data obtained prior to the eruption, the increase produced by Mount St. Helens has been estimated. The value obtained is approximately 5×10^9 tonnes. This value may be compared with a pre-volcanic total for the whole globe of approximately the same value. The eruption has thus produced a doubling in the stratospheric mass loading. This loading is smaller than that of other recent eruptions. Mount Agung in 1963 is believed to have injected about 3×10^7 tonnes of material into the stratosphere and Mt. Fuego in 1974 about 5×10^6 tonnes (ref. 14). Calculations by Hansen et al. (ref. 15) with a one-dimensional radiative-convective model showed that tropospheric temperatures cooled by about 0.4°C because of the new material from Mount Agung. His calculations showed that at an altitude of 20 km the stratosphere warmed by 4° to 8°C . If Agung is compared with Mount St. Helens which added a factor of about 100 less, then one would not expect any significant temperature change to occur.

V. ACKNOWLEDGMENTS

The author wishes to thank Mr. William H. Fuller, Jr., and his group at LaRC for providing the experimental lidar data and Mrs. Mary Osborn, Dr. G. S. Kent, and Dr. T. J. Swissler for their help in its analysis. The author also wishes to thank the various worldwide researchers at the stations listed in figure 3 who so graciously provided data prior to their own publication of these data.

REFERENCES

1. McCormick, M. P., Swissler, T. J., Chu, W. P., and Fuller, W. H. Jr., Post-volcanic stratospheric aerosol decay as measured by lidar. *J. Atmos. Sci.*, Vol. 35, 1978, pp. 1296-1303.
2. McCormick, M. P., Hamill, P., Pepin, T. J., Chu, W. P., Swissler, T. J., and McMaster, L. R., Satellite studies of the stratospheric aerosol. *Bull. Am. Met. Soc.*, Vol. 9, 1979, pp. 1038-1046.
3. Danielsen, E., Trajectories of the Mount St. Helens eruption plumes. *Science*, Vol. 211, 1981, pp. 819-821.
4. Newell, R. E., Kidson, J. W., Vincent, D. G., and Boer, G. J., *The General Circulation of the Tropical Atmosphere, I.*, Massachusetts Inst. Tech. Press, Cambridge, MA.
5. Iwasaka, Y., and Hayashida, S., Lidar measurements of dust-cloud particles loaded into the stratosphere by the volcanic eruption of St. Helens. Tenth International Laser Radar Conference Abstracts, Oct. 6-9 (Silver Springs, Maryland), 1980, pp. 142-143.
6. D'Altorio A., and Viscount G., Lidar detection of volcanic aerosols in the atmosphere following the Mount St. Helens eruption. *Geophys. Res. Lett.*, Vol. 8, 1981, pp. 63-65.
7. Reiter, R., Jager, H., Carnuth, W., and Funk, W., Lidar observations of the Mount St. Helens eruption clouds over Mid-Europe, May to July 1980. *Geophys. Res. Lett.*, Vol. 7, 1980, pp. 1099-1101.
8. Houchedorne, A., Lefrere, J., Megie, G., and Chamin, M. L., Lidar observations of stratospheric aerosol layers over France after the Mount St. Helens Eruption. Tenth International Laser Radar Conference Abstracts, Oct. 6-9 (Silver Spring, Maryland), 1980, p. 146.
9. Thomas, L., Chaloner, C. P., and Bhattacharyya, S. K., Laser-radar measurements in southern England of aerosols from Mount St. Helens. *Nature*, Vol. 289, 1981, p.473.

10. Gardner, C. S., Sechrist, C. L.F., Jr., and Shelton, J. D., Lidar observations of the Mount St. Helens dust layers over Urbana, Illinois. Tenth International Laser Radar Conference Abstracts, Oct. 6-9 (Silver Springs, Maryland), 1980, pp.140-141.
11. Eloranta, E. W., Lidar observations of stratospheric dust over Madison, Wisconsin, after the Mount St. Helens eruption. Tenth International Laser Radar Conference Abstracts, Oct. 6-9 (Silver Springs, Maryland) 1980, pp. 144-145.
12. Deluisi, J., Derr, V., Fegley, R., McNice, T., Lidar observations of atmospheric debris from the Mount St. Helens eruption at Boulder and Mauna Loa. Tenth International Laser Radar Conference Abstracts, Oct. 6-9 (Silver Springs, Maryland), 1980, p. 147.
13. Russell, P. B., Swissler, T. J., McCormick, M. P., Chu, W. U., Livingston, J. M., and Pepin, T. J., Satellite and correlative measurement of the stratospheric aerosol: I. A flexible optical model for data conversion. J. Atmos. Sci., June 1981.
14. Cadle, R. D., Fernald, F. G., and Frush, C. L., Combined use of lidar and numerical diffusion models to estimate the quantity and dispersion of volcanic eruption clouds in the stratosphere Volcan Fuego, 1974, and Augustine, 1976. J. Geophys. Res., Vol. 82, 1977, pp. 1783-1786.
15. Hansen, J. E., Wang, W. C., and Lacis, A. A., Mount Agung eruption provided a test of a global climatic perturbation, Science, Vol. 199, 1978, pp. 1065-1068.

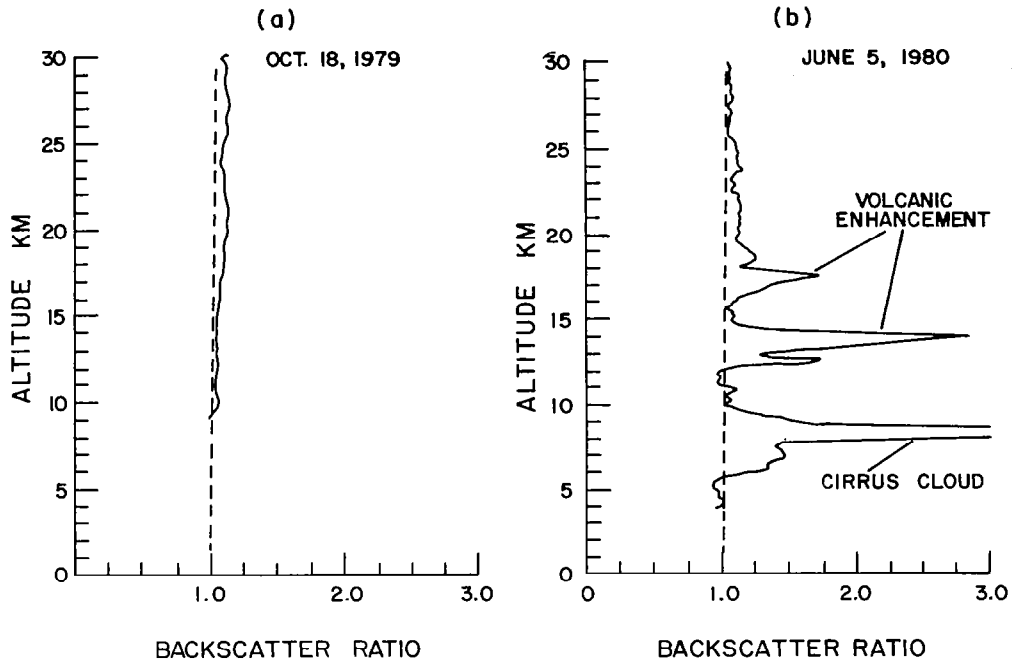


Figure 1. (a) A typical lidar profile obtained at LaRC before the Mount St. Helens eruption. (b) Lidar profile obtained after the eruption, showing strong scattering layers.

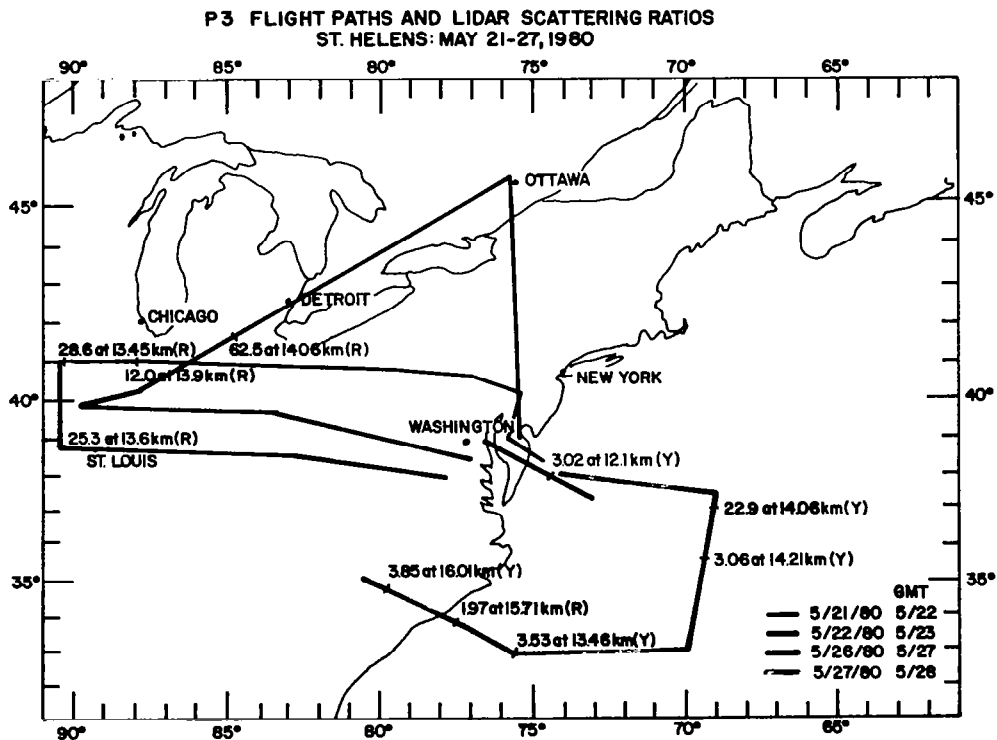
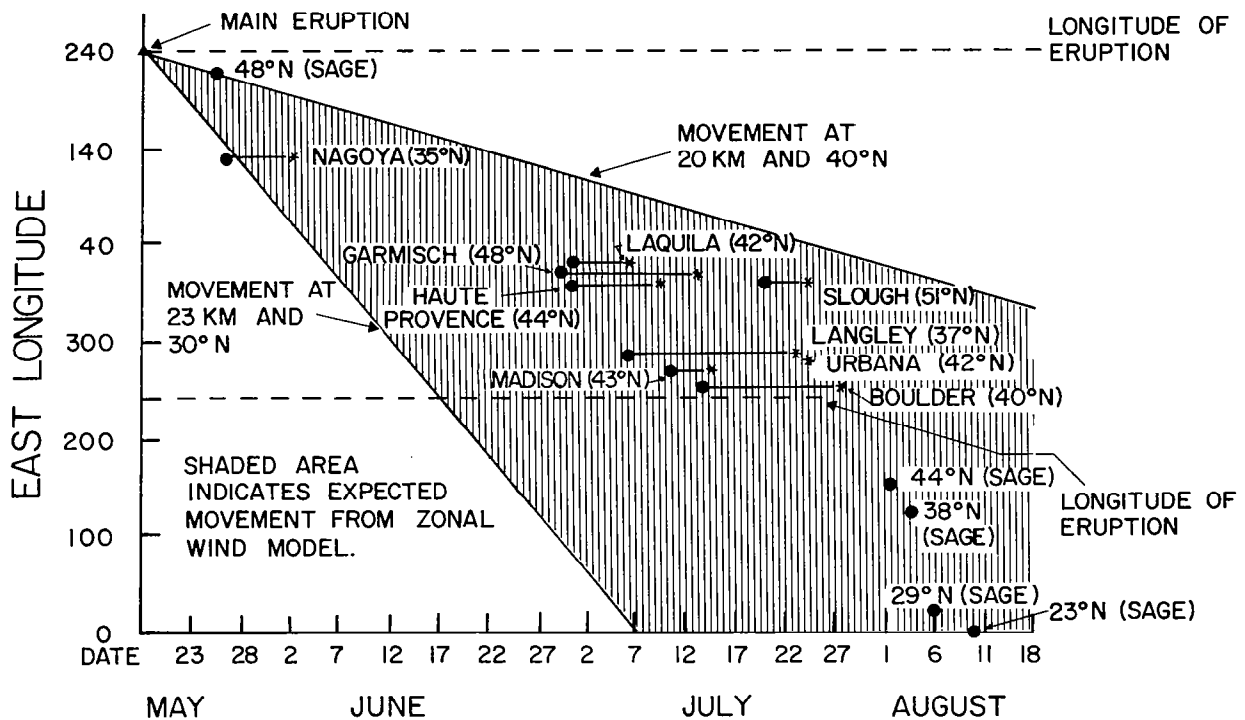


Figure 2. Map showing flights made by the LaRC airborne lidar system. The heights and magnitudes of the peak backscatter ratios are shown alongside the flight paths.



SAGE AND LIDAR OBSERVATIONS OF SCATTERING LAYERS ABOVE 20KM

Figure 3. Times of arrival of aerosol layers above 20 km as observed by various lidar stations around the globe.

- * Layer at 20 → 22 km
- Layer at 22 → 24 km

The cross-hatched area represents the average expected range of stratospheric air movements. Also shown are the dates and longitudes of satellite observations of the aerosol layers.

DISTRIBUTION OF MOUNT ST. HELENS DUST INFERRED FROM SATELLITES AND METEOROLOGICAL DATA

James D. Laver
Climate Analysis Center, Washington, DC

Visible and infrared pictures from two Geostationary Operational Environmental Satellite (GOES) Systems satellites, in circular orbits at about 19,000 nautical miles, are available continuously at approximately 30 minute intervals. Still pictures and film loops from this system vividly depict the events associated with the May 18, 1980 eruption of Mount St. Helens. The initial explosion, shock wave, and visible horizontal dust distribution during the following week are readily apparent. Meteorological wind and height fields permit the inference of the vertical distribution of volcanic dust as well as explain the atmospheric behavior which caused the visible and nonvisible dust distribution.

I. INTRODUCTION

The effects of the Mount St. Helens eruption, which forced ash up to approximately 70 mb (18.6 km above sea level) and across the U.S., on May 18 1980, can readily be seen by using both meteorological data and Geostationary Operational Environmental Satellite (GOES) System pictures. Prevailing westerly winds at most levels spread ash across the northern half of the United States where radiosonde wind data are plentiful and the National Meteorological Center (NMC) analyses are well defined. A minimum of cloudiness over the western half of the U.S., during the first several days after the eruption, permitted an unprecedented observation of volcanic ash movement by visible GOES pictures. Volcanic ash, caught in a weak upper-air circulation, lingered over the east coast of the United States for possibly 10 days after the eruption, although at maximum wind levels ash crossed the United States in about 3 days.

This paper presents some of the products available at NMC and the National Environmental Satellite Service (NESS) and some qualitative interpretations of each. These products depict the meteorological situation and afford a visible look at the atmosphere during the May 18, 1980 eruption and the following week. Distribution of Mount St. Helens dust is inferred from the NMC and NESS products with reference to the important work done at the National Oceanic and Atmospheric Administration's (NOAA) Air Resources Laboratories (ARL) in Silver Spring, MD. Film loops, using visible GOES pictures at approximately one-half hour intervals, depict visible dust movement at certain levels during the 4 days immediately following the eruption.

II. BACKGROUND ON NMC DATA AND PRODUCTS

Radiosonde temperature and wind data, in the form of vertical profiles, are available on a bidaily (00Z and 12Z) basis from well over 100 stations in the U.S., Canada, and Mexico. Figure 1 shows selected levels of information from a radiosonde report in western Idaho, which was downstream from the volcano, when considering the upper tropospheric wind pattern. Note that the leading edge of volcanic dust would have been in the jet stream at 10 to 11 km. The tropopause is at or just above this level of maximum wind. Full radiosonde reports contain data at the 15 mandatory levels, the surface, the tropopause, and significant winds and temperatures (deviation from linear) in between these levels. Other types of data, such as satellite profiles (no winds), satellite cloud track winds, aircraft reports, etc., are important to the NMC analysis systems. The right hand side of figure 1 indicates the range over which NMC performs analyses and some of the data inputs to these analyses. Various analysis and forecast schemes are run at 6-and 12-hour intervals,

which could be useful in studying trajectories and dispersions in events such as Mount St. Helens. The meteorological analysis figures in this paper are taken from either of two Cressman (successive iteration) analysis techniques used at NMC (1,2).

Through the NMC computer system these data and analyses are available on a real-time basis on disk and selected graphics products. Eventually, these products are put on tape and/or microfilm and become available at the National Climate Center (NCC) in Asheville, NC, the National Center for Atmospheric Research (NCAR) in Colorado, and various other government and private installations across the United States. NMC's Climate Analysis Center (CAC) has been running a global analysis package for the mid and upper stratosphere (to 55 km) which will soon become part of the general archive set of analyses.

III. THE METEOROLOGICAL SITUATION AND DUST TRAJECTORIES

In the lowest 3 km of the troposphere, on May 18, 1980, a high pressure ridge drove a clockwise circulation centered over eastern Idaho and western Wyoming. This system steered the initial low-level volcanic ash from west to east. (See figs. 2 and 3—NMC 15Z Surface Analysis and 12Z 850 mb Analysis for May 18, 1980.) Surface dust observations occurred over southern Canada and into North Dakota 48 hours after the eruption. (See figure 4.)

In the midtroposphere the broad upper-air ridge over the Western United States pushed ash southeastward toward a trough in the Midwest. Note the changing 500 mb (5.7 km) flow pattern at successive 2-day intervals on May 18, May 20, and May 22. (See figs. 5-7.) Ash progress, as calculated by the NOAA's ARL in a memo dated May 29, 1980, is also shown in figures 6 and 7 (3). A similar pattern at 300 mb (9.4 km), but with stronger wind speeds and a slightly deeper trough, took the dust on a southward trajectory toward Texas and then northeastward off the New England coast in less than 3 days.

A closed low (counterclockwise circulation) formed near the mid-Mississippi Valley at all levels up through 18 km by May 21. Visible GOES satellite pictures during May 21 to 24 show that apparently some dust, most likely in the 10-to 14 km-range, got caught up in this closed low circulation as the system drifted slowly eastward and dissipated over the Atlantic states. At these same levels a large amount of dust was also carried directly off the Northeast United States coast much earlier as shown in figure 8 (4). Figure 9 (4) continues the 12-km trajectory around the globe until it reaches the Northwestern United States on May 31, 2 weeks after the first eruption.

Wind speeds decreased upward from 12 km through 18 km in the lower stratosphere during the May 18-31 period. At 100 mb (16 km), figure 10 (3) shows that it would have taken more than 5 days for the dust at that level to cross the United States. At 70 mb (18.6 km) the circulation was so light that dust at this level probably traveled southeastward over Colorado by May 23 and then reversed toward Washington again. Dust at these stratospheric levels was not visible on satellite pictures. Figure 11 shows the 70 mb (18.6 km) field on May 23 as a trough off the northwestern coast that was digging into the westerly wind pattern and reversing the dust flow eventually back toward the northwest.

IV. VISIBLE SATELLITE PICTURE INTERPRETATION

Numerous GOES pictures were monitored by several NOAA groups, immediately following the Mount St. Helens eruption, to satisfy requests from various experimenters, researchers and others interested in the effects of the eruption. The difficulty and expense of reproducing these photographs precludes their inclusion as figures in this text. Reference copies of selected still pictures and film loops can be viewed at CAC, NMC or obtained from NESS.

A GOES picture taken at 1646 GMT, approximately 75 minutes after the May 18, 1980, eruption of Mount St. Helens, shows ash spreading more than 90 km east of the volcano site. At 1845 GMT, on the same day, a second eruption occurred, and a 2015 GMT satellite photograph indicates a new mushroom shaped cloud which probably shows this second eruption. The 2345 GMT picture clearly shows that the leading edge of volcanic dust spreads into western Montana at 9 to 12 km by nightfall on May 18, 1980.

By the evening of May 19, horizontal dispersion had significantly increased. High cloudiness obscured some of the dust at and below about 700 mb (3 km) over Montana and southern Canada. The dust between 500 mb and 200 mb (5 to 12 km) had dispersed across Wyoming and Colorado with its leading edge covering the Texas panhandle. Coincidentally, ash at 100 mb through 70 mb (16 to 18 km) remained over Idaho and Washington. In the vertical the maximum concentration of volcanic ash, approximately 32 hours after the first Sunday morning eruption, lay in an upward-spiraling clockwise path skewed southeastward at jet stream levels over the Central Plains. Vertically changing wind direction had greatly dispersed the visible dust and obviously the invisible dust was dispersed to an even greater extent.

During May 20-21 visible GOES pictures clearly show the upper-tropospheric ash shift from a southeast trajectory to a northeast one implying rotation about a large upper-air trough. (See figs. 6 and 8.) Satellite photographs coincide extremely well with the positions calculated by the ARL. Development of an upper-tropospheric closed low over the mid-Mississippi Valley brought some obscuring cloudiness to the Southeastern United States. Volcanic ash is clearly drawn back over the Central Plains States (especially Oklahoma and Kansas) by May 22, and strong winds also stretch a line of maximum dust concentration just south of the Great Lakes across New England and over the Mid-Atlantic. (See figure 9.) Meanwhile, the lower-tropospheric ash had crossed southern Canada and appears to show a line of maximum visible concentration merging upward with the higher level ash over northern New England.

From May 23 to May 28 the closed low aloft dissipated slowly, but there is evidence that thin layers of dust may have lingered near the Mid-Atlantic States for up to 10 days after the initial eruption. At the same level (12 km), dust caught in the jet stream very possibly had travelled three-quarters of the way around the globe across China and over the western Pacific Ocean.

V. CONCLUDING REMARKS

Satellite film loops, which combine the GOES still photographs at approximately one-half hour intervals, yield an informative time continuity of dust trajectory and dispersion. Although qualitative in nature and difficult to interpret in the vertical atmospheric sense, still pictures and film loops fill an important gap when combined with meteorological data and the multitude of ground-based and other airborne measurements.

Much more could be said about the volcanic dust distribution at higher levels (up to 23 km) and over longer periods of time. Derivations of complex vertical and horizontal dispersions and the explanation of thin layers of relatively higher concentrations of observed volcanic ash are beyond the scope of this discussion. The intent here is to expose some of the products which are available for continued research into the effects of the Mount St. Helens eruption.

REFERENCES

1. Cressman, G.: An Operational Objective Analysis System, Monthly Weather Review, Vol. 87, No. 19, Oct. 1959.
2. Finger, F. G., Woolf, H. M., Anderson, C. E.: A Method for Objective Analysis of Stratospheric Constant-Pressure Charts. Monthly Weather Review, Vol. 93, No. 10, Oct. 1976.
3. Air Resources Laboratories: Memo for the Record, May 29, 1980.
4. Draxler, R. R.: Observing and Forecasting the Path of Volcanic Emissions after an Eruption. Presented at the Tenth International Laser Radar Conference, (Silver Spring, Maryland), Oct. 6-9, 1980.

TABLE I. ANALYSIS OF FILTER SAMPLES FOR ⁷Be AND SOLUBLE ANIONS

Flight number (a)	Date (1980)	Sampling time, min	Flight altitude, km	Tropopause, km	ΔH , mbar	Latitude range, °N	Longitude range, °W	Beryllium 7, pCi/10 ⁵ scm	Sulfate $\mu\text{g}/\text{m}^3$	Nitrate, $\mu\text{g}/\text{m}^3$	Chloride $\mu\text{g}/\text{m}^3$	Filter (b)
108	6-4	90	11.3	12.1	- 28	39.8-41.5	81.1-89.6	≤ 150	0.100 ± 0.01	0.350 ± 0.01	--	--
109	6-5	50	13.1	12.8	8	42.7-46.4	82.4-84.3	3080 ± 190	1.86	0.200	≤ 0.02	--
110	6-10	62	13.7	10.2	111	41.7-46.4	82.4-84.3	7315 ± 505	0.170	0.310	--	--
111	6-11	55	12.5	10.9	50	42.5-44.0	85.3-87.5	4722 ± 390	0.421	0.258	--	--
112	6-16	45	12.5	11.2	39	41.5-43.6	75.5-81.3	6180 ± 420	0.700	0.390	--	--
112L	6-16	45	11.3	11.2	6	41.5-45.0	73.5-80.2	4215 ± 260	0.510	0.280	--	--
113	6-17	45	13.1	10.8	92	41.5-44.8	73.5-81.3	5665 ± 600	0.730	0.341	--	--
113L	6-17	45	10.7	10.8	16	41.9-45.0	75.5-80.3	497 ± 210	0.320	0.270	--	--
114	6-18	35	13.7	11.2	70	39.8-41.5	83.0-89.6	3390 ± 360	0.381	0.276	--	--
114L	6-18	45	11.9	11.2	21	39.8-40.7	83.4-89.6	4300 ± 310	0.674	0.390	--	--
115	6-19	80	13.1	10.7	75	41.2-46.4	82.1-84.3	4008 ± 230	0.368	0.158	--	--
115L	6-19	80	13.1	10.7	75	41.2-46.4	82.1-84.3	4583 ± 265	0.353	0.073	--	B
116	6-29	50	11.9	10.4	36	42.2-46.2	84.3-91.0	4173 ± 400	0.630	0.459	--	--
117	6-30	45	12.5	12.3	7	41.8-45.9	83.1-90.5	3211 ± 255	0.649	0.268	--	--
118L	7-7	45	12.5	12.3	64	41.7-43.2	73.8-81.2	2610 ± 245	0.415	0.130	--	--
118	7-7	75	11.0	11.0	64	73.8-43.2	73.8-81.2	3140 ± 270	0.406	0.466	--	B-G
119	7-28	30	12.5	12.3	6	42.6-44.7	81.1	1720 ± 310	0.256	0.498	≤ 0.02	B-G
120	7-25	60	13.1	15.9	- 57	36.9-38.3	74.0-81.8	1335 ± 250	0.108	0.168	≤ 0.02	B-G
121	7-25	60	13.1	15.9	- 57	36.9-38.3	74.0-81.8	1470 ± 225	0.137	0.177	≤ 0.02	B-G
122	7-30	50	13.7	13.1	16	42.7-43.2	83.5-86.2	2960 ± 260	0.225	0.189	--	B-G
122L	7-30	50	13.7	13.1	16	42.7-43.2	83.5-86.2	3320 ± 400	0.274	0.198	≤ 0.02	B-G
123	8-1	65	12.5	11.8	20	42.7-46.8	84.6-92.2	3340 ± 420	0.256	0.326	--	B-G
124	8-4	35	12.5	13.2	- 19	43.0-44.0	83.7-86.5	496 ± 125	0.108	0.204	--	B-G
125	8-6	75	12.5	12.5	1	42.4-46.0	84.1-92.2	1330 ± 135	0.100	0.177	--	B-G
126	8-6	30	12.5	12.0	1	43.3-45.2	87.5-84.3	≤ 780	0.117	0.066	--	B-G
127	8-8	30	13.1	14.0	- 22	46.2-48.1	87.2-89.3	≤ 1160	0.138	0.144	--	B-G
127L	8-8	20	13.1	13.0	- 8	46.2-43.2	87.2-84.3	≤ 1030	0.128	0.055	--	B-G

^aL—Left pod; all others, right pod.^bFilters OPC-1478 impregnated with dibutyltin diethylphthalate except as noted. B denotes 0.1% Na₂CO₃; G denotes glycerine.^cTime interpolated.

MANDATORY RADIOSONDE LEVELS AND PARTIAL SOUNDING FROM A SOUTHWEST IDAHO STATION FOR 12Z MAY 18, 1980				NMC DATA AND ANALYSIS AVAILABILITY AT MANDATORY PRESSURE LEVELS				
PRESSURE MB	HEIGHT KM	HEIGHT KFT	WIND DEG/KNTS PLOT	AVAILABLE DATA	AVAILABLE GRID ANALYSIS	PRESSURE MB		
0.4	55	170	(360 =NORTH)	SATellite AND SOME ROCKET		0.4		
1	47	154				1		
2	42	138				2		
5	35	115				5		
10	30	98		RADIOSONDE AND SATELLITE	HEIGHT AND TEMPERATURE	10		
20						--		
30						30		
50	21	66	020/05			AIRCRAFT	U AND V WIND COMPONENTS	50
70	18	60	290/10					70
100	16	53	270/15			CLOUD TRACK WINDS		100
150								150
200	12	39	320/50					200
250	11	34	330/65					250
300	9.4	30	320/50				300	
400					400			
500	5.6	18	240/15		500			
700	3.1	10	CALM		700			
850	1.5	5	200/05		850			
1000					1000			
SURFACE						SURFACE		

Figure 1. Selected levels of information from a radiosonde report in western Idaho, May 18, 1980.

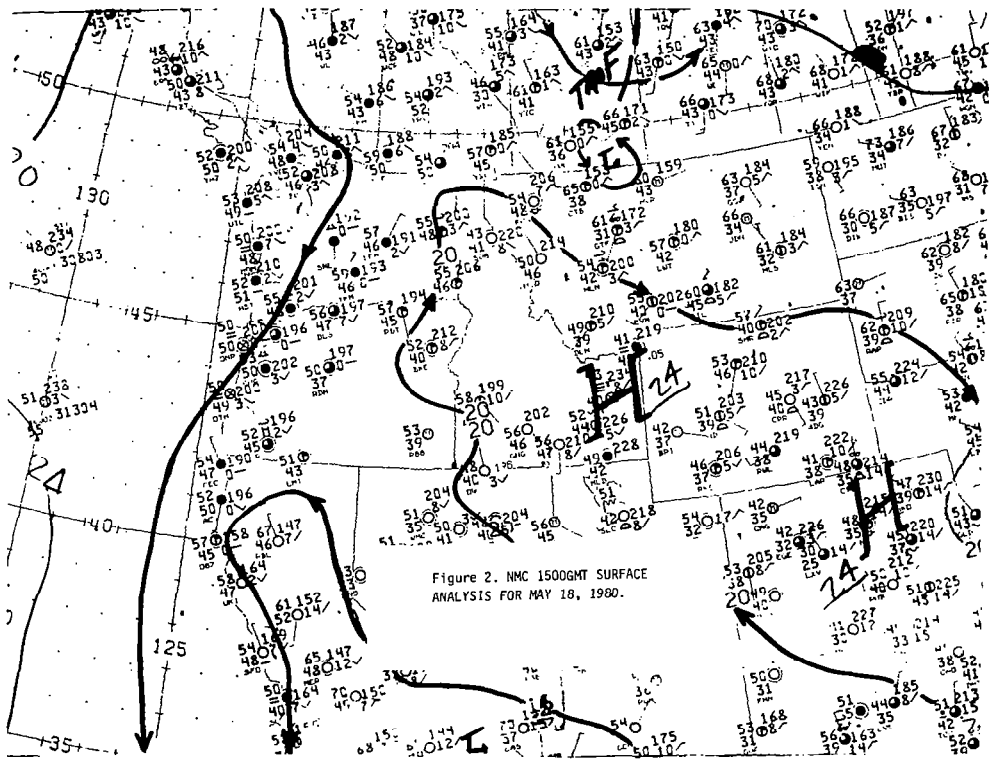


Figure 2. NMC 1500 GMT surface analysis for May 18, 1980.

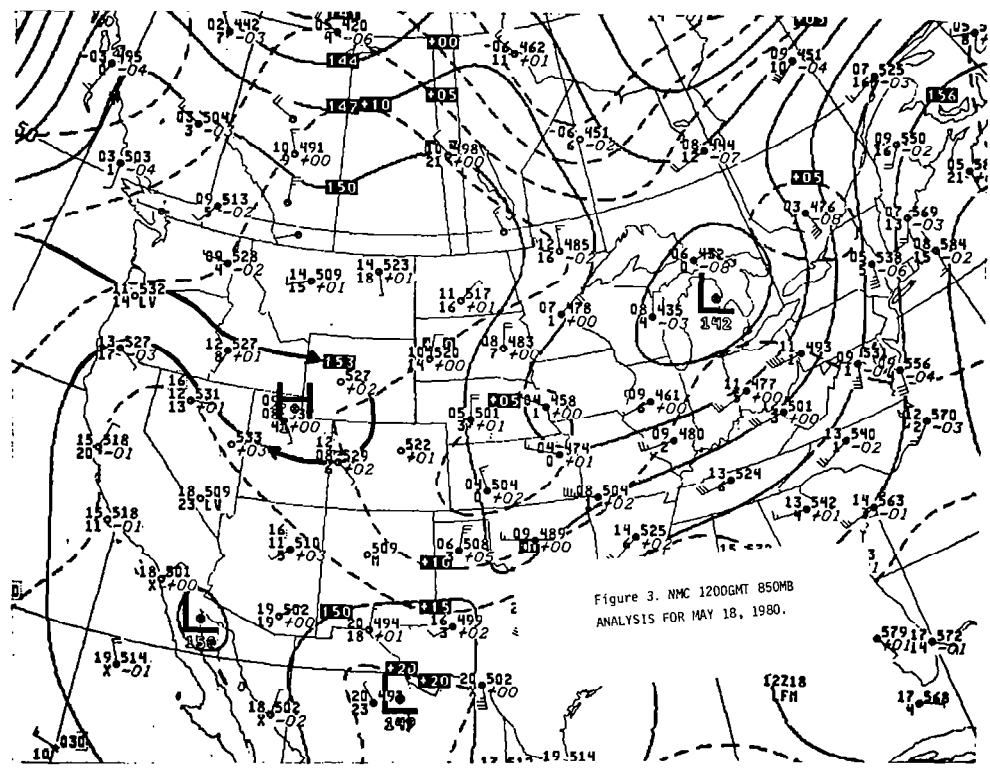


Figure 3. NMC 1200 GMT 850 mb analysis for May 18, 1980.

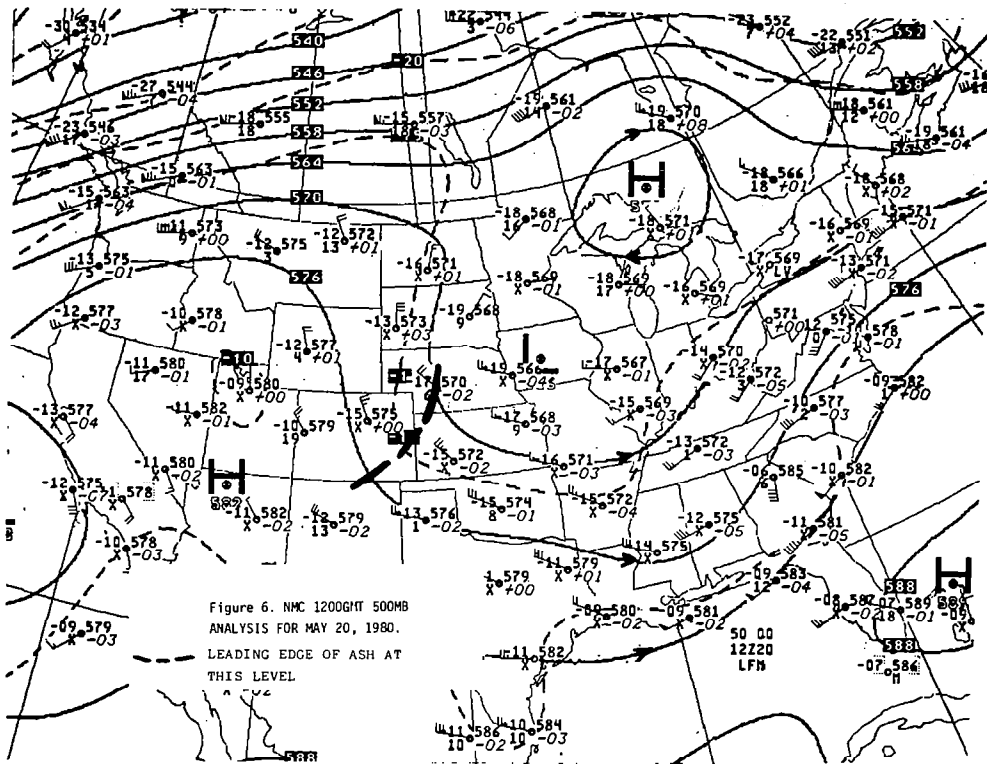


Figure 6. NMC 1200 GMT 500 mb analysis for May 20, 1980. Leading edge of ash at this level.

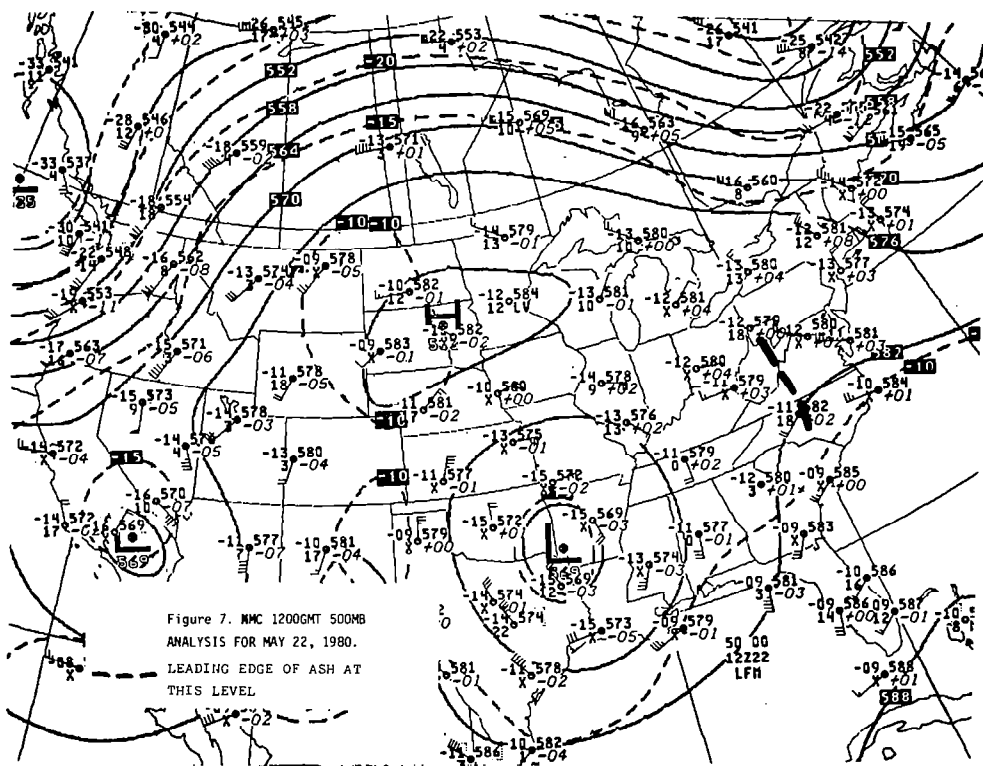


Figure 7. NMC 1200 GMT 500 mb analysis for May 22, 1980. Leading edge of ash at this level.

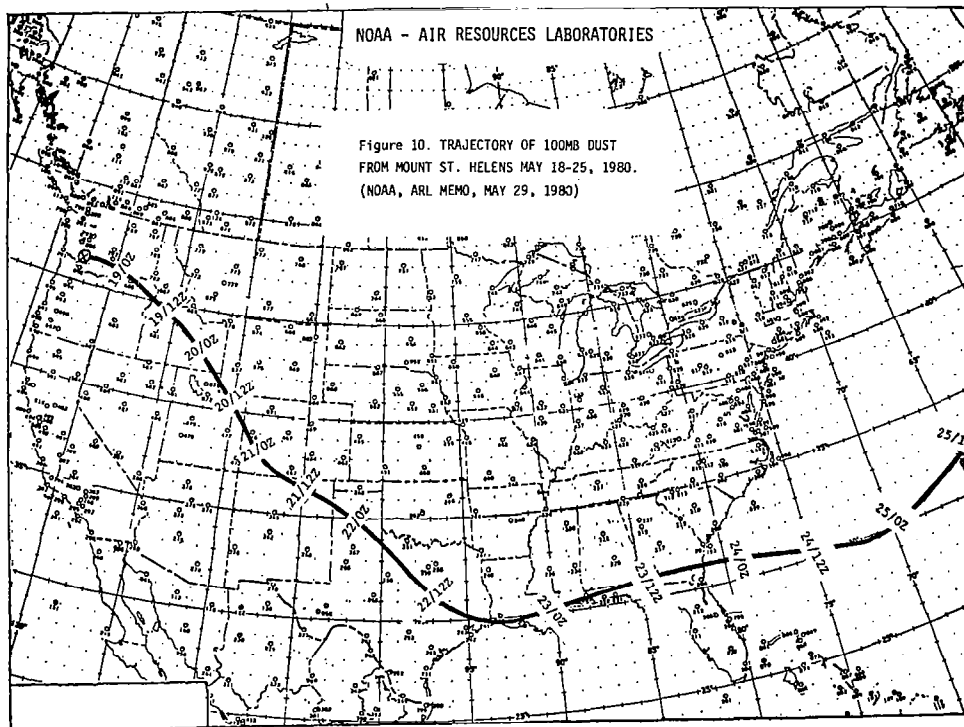


Figure 10. Trajectory of 100 mb dust from Mount St. Helens, May 18-25, 1980 (3).

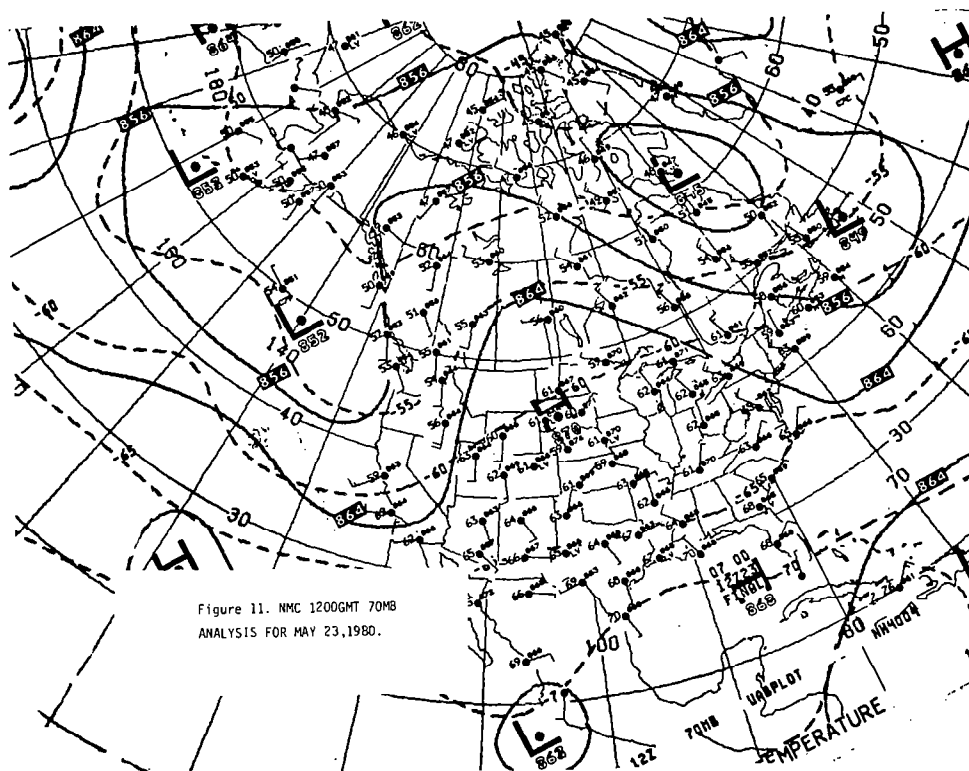


Figure 11. NMC 1200 GMT 70 mb analysis for May 23, 1980.

MOUNT ST. HELENS PLUME DISPERSION BASED ON TRAJECTORY ANALYSES

Edwin F. Danielsen
NASA-Ames Research Center, Moffett Field, California

The major eruption of Mount St. Helens on 18 May 1980, had sufficient energy to traverse the troposphere (9 km above the mountain top) and to penetrate an additional 10 km into the stratosphere. This plume, initially quasi-vertical, rapidly acquired the horizontal momentum of the environmental winds and suffered differential rotation due to a positive speed shear in the troposphere and a negative shear in the stratosphere. Advected rapidly eastward by the undulating jet stream, the lower stratospheric portion of the plume circled the globe at an average speed of $\sim 25 \text{ m s}^{-1}$, reentering North America over California in early June. During the same period, the uppermost portion slowly looped over the northwestern United States and then moved westward over the northern Pacific Ocean. Thus, plume dispersion was initiated by the vertical shears of the horizontal winds which converted a nearly vertical plume to a thin, quasi-horizontal, quasi-zonal lamina. Horizontal shears then dispersed the lamina meridionally while small-scale, wave turbulent motions spread it slowly vertically.

I. INTRODUCTION

The awesome power of the 18 May eruption is evident in figure 1. When viewed from the west side of Mount St. Helens, from an aircraft flying at about 3.05 km (10,000 ft.), the eruption cloud resembles a free jet expanding as it rises through the troposphere. Shear vorticity generated at the boundaries between the vertical velocities of the jet and horizontal velocities of the environment is rapidly converted to curvature vorticity, to rolling motions that entrain the environmental air, while giving the cloud its cauliflower-shaped surface. The entrainment of the environmental air and the associated mixing reduces the vertical velocity of the ascending plume, increases its horizontal velocity, and causes the plume to tilt downwind in the troposphere. This tilt is not evident in figure 1 because the photograph is taken downwind.

II. DISCUSSION

When viewed from above, from the TIROS (NOAA-6) satellite, 1 hour and 22 minutes after the eruption began, the cloud resembles the anvil of a gigantic thunderstorm. The original photograph, obtained from the National Environmental Satellite Service at Redwood City, California, had no state boundaries and, therefore, no explicit length scale. The boundaries shown here were determined by identifying portions of the major rivers, reservoirs, and lakes in Washington and Oregon, whose surfaces are bright due to reflected sunlight (see fig. 2).

Looking down on the eruption cloud the effects of entrainment can be seen in the expansion of the anvil and its elongation and movement to the east. The widest part north-south is about 130 km, but the east-west part is about 180 km. Its leading edge merges with cirrus clouds and the mean speed of this leading edge for the 82 minute interval is approximately 35 to 36 m s^{-1} . As will be shown, these conditions are compatible with those of the environment at the tropopause, and they imply that the leading edge is about 12 km above mean sea level. There is evidence, also, in the varying grey tones and the length of the shadow cast from the western edge of the cloud that the anvil has a vertical structure. Based on the horizontal position and height of the satellite and the angles to the sun, one can compute heights (correcting for parallax errors) varying from 18 to 24 km, depending upon one's interpretation of the effective limits of the shadow.



Either limit implies a significant stratospheric penetration, the cloud top decreasing in height from a position close to the volcano to the leading edge which is approaching the bend in the Columbia River. The fact that the eruption cloud penetrated cirrus clouds makes it difficult to distinguish its attenuated leading edge, but there is little doubt that the plume is now sheared in the direction of the winds and that the plume dispersion is beginning.

Eleven hours and six minutes after the eruption, the third photograph (enhanced infrared) from the same satellite (fig. 3) shows the eruption cloud as an elongated curving plume and reveals the large-scale flow in which it is embedded. The leading edge has passed the ridge over northern Idaho and is moving southeastward into Montana, eastern Idaho, and into eastern Utah and Wyoming. According to the enhancement curve, the coldest temperatures—from -50°C to -56°C (the darkest inner grey)—are over southeastern Washington, extending into Idaho. The light grey surrounding it implies temperatures from -44°C to -50°C and the black area is another 6°C warmer. Note the evidence for several eruption surges in the effective temperature pattern of the plume. The highest surge according to radar measurements was at 2330 UT, and was just before the major eruption ceased.

These effective radiation temperatures can be compared with those obtained at the nearest upwind radiosonde station, Salem, Oregon, about 3 hours prior to eruption (fig. 4). The temperatures decrease to a minimum of -63.5°C at 195 mb or 11.9 km. Above a shallow inversion the lower stratosphere is almost isothermal at -57°C to 50 mb or approximately ~ 20 km. Thus, the coldest portion of the plume, as depicted by the infrared satellite photographs, is comparable with the observed temperatures in the lower stratosphere.

On the right side of figure 4 the west wind velocity profile (a positive value is a wind from the west) shows the sharply defined jet, referred to earlier, at the tropopause or 12 km. Note that the speed is reduced to one-half of the maximum within 2 km above the jet and approximately 3 km below the jet. It follows that the leading edge of the eruption plume will be drawn out into a thin layer or lamina, which will be increasingly difficult to detect by either visible or infrared photography. Note also that the observed cirrus cloud layer is confirmed in the left side of the figure by the small difference between the temperature and the dew-point temperature. The latter is unreliably measured at very cold temperatures and is not plotted here for temperatures colder than -45°C . But, in this case, the cirrus probably extends to the tropopause level as suggested in figure 2.

The south wind velocity profile at Salem (not plotted here) increases to a maximum of 10 m s^{-1} at about 6 km, then decreases with increasing height, becomes near zero at 14 km, and remains negative at less than 5 m s^{-1} in the middle stratosphere. Thus, the plume is advected northward and eastward in the troposphere, eastward in the upper troposphere and lower stratosphere, and slowly southward and eastward in the lower middle stratosphere. However, the dominant transport is toward the east as is the major tilt of the plume.

Figure 5 shows that the stratospheric portion of the plume would be converted to a thin, inclined layer by the strong windspeed shear. This cross section and the flight paths above it were prepared for the U2 flight on the 19th of May. The latitudes are expressed in thousands of feet for the convenience of the pilot. The plume was intercepted over northeastern Oregon where it appeared brownish in color. As the pilot descended the color changed to white or near white. At slightly below 43,000 ft or 13 km, over Wyoming, the plane broke out beneath the plume.

The apparent ascent of the leading edge of the plume, from 12 to 13 km, is not due to rising air or ascending velocities in the leading edge of the plume. Quite the contrary, the air is descending after it passes the ridge and moves southeastward over Wyoming. As shown in figure 6, the air in the upper troposphere, from 300 to 200 mb, turns southward over eastern Utah and western Colorado before the higher level air moves into Wyoming. Note that the black trajectory arrow in figure 6 starts at the 200 mb, 12 km level, and then descends to about 260 mb or 10.1 km over the panhandle of Texas. This trajectory represents an isentropic trajectory, which follows the three-dimensional flow, rather than an isobaric trajectory. After the leading edge of the plume passes the trough over Oklahoma and Arkansas, it accelerates in speed, moves toward the Atlantic coast and passes over New York City.

The rapid dispersion of the plume due to the large velocity shears in the stratosphere is delineated in figure 6. Moving at slower speeds, the 100-mb flow requires two more days to reach the Texas panhandle. Then it continues to spread southward, especially along the faster moving right flank, and crosses the northern and central Florida coast. Between the 20th and 21st of May, at 70 mb, ~ 18.5 km, and at 50 mb, ~ 20.5 km, the trajectories loop anticyclonically as the high pressure area over Oregon damps and is replaced by a weak pressure trough. At these levels the plume then moves northward into Montana and Washington.

Direct confirmation of this northward transport in the stratosphere was obtained from the second flight of the U2 on the 22nd of May. The pilot observed the thin debris layer and penetrated it at ~ 20 km (66,000 ft) over the Idaho panhandle. He also observed that the layer extended into Washington and appeared to be moving westward. The trajectories indicate northwest flow on the 23rd and 24th of May, with the 50-mb trajectory extending off the Pacific coast and then over the northern Pacific Ocean.

This westward transport by the stratospheric easterlies reflects the influence of the summer anticyclone at the 50-mb level. Fluctuations in the weak pressure patterns at 70 mb produce complex trajectories, one branch turning eastward over northwestern Canada and another branch turning southward to return toward the volcano and the northwestern United States.

Estimates of the global trajectories at 200 mb (continuous lines) and at 50 mb (broken lines) are illustrated in figure 8. At 200 mb the plume moves rapidly eastward following the undulating path of the polar jet. Crossing the west coast over California on the 3rd of June, the mean west wind speed was ~ 25 m s⁻¹. Although this mean trajectory oscillates from 35° to 60°N, the dispersion normal to the jet is probably suppressed by the convergence which maintains the jet against lateral diffusion. Consequently, at the level of maximum winds the main dispersion is most probably in the zonal direction.

The slower transport by the summer stratospheric easterlies at 50 mb has been reconstructed here through 27 June, the time limit of consecutive charts available to me. Because of the slow wind speeds and the weak and varying pressure patterns, these trajectories are presented only as reasonable estimates. Certainly, the zonal transport is slow and the meridional dispersion is enhanced by the anticyclonic loops and diffluent patterns.

Figures 9 and 10 are the final two included to illustrate the large differences in the trajectories and plume dispersion between successive eruptions. During the early portions of the second eruption, 24 May, the trajectories at 200 and 300 mb turned cyclonically over western Oregon, California, Nevada, Utah, and Wyoming. Later, with the passage of a shear line, the trajectories turned anticyclonically over British Columbia and the Hudson Bay. At 70 mb, the diffluent patterns imply both cyclonic and anticyclonic flows, one branch moving towards the Hawaiian Islands.

After the 12 June eruption, the lower stratospheric flow turned cyclonically and then moved rapidly eastward across the northern United States as the western cyclone rapidly damped. The arrow extending from southeastern Wyoming to western Montana traces the motion of a thin layer at 70 mb detected by a balloon ascent at Laramie, Wyoming. My best estimate of the origin of this layer is shown in figure 7. The branch of the 70 mb flow that returned close to the volcano and then turned anticyclonically across Montana and eastern Wyoming, that is, the trajectory in figure 10, completes the large anticyclonic loop. The extreme complexity of the flow at this level is related to the transient conditions in the transition from lower stratospheric westerlies to the upper level easterlies.

ACKNOWLEDGMENTS

The author gratefully acknowledges the excellent cooperation of the NOAA personnel in the Analysis and Information Branch of the Climate Analysis Center, Washington, D.C., and the National Weather Service and Satellite Service Offices at Redwood City, California.

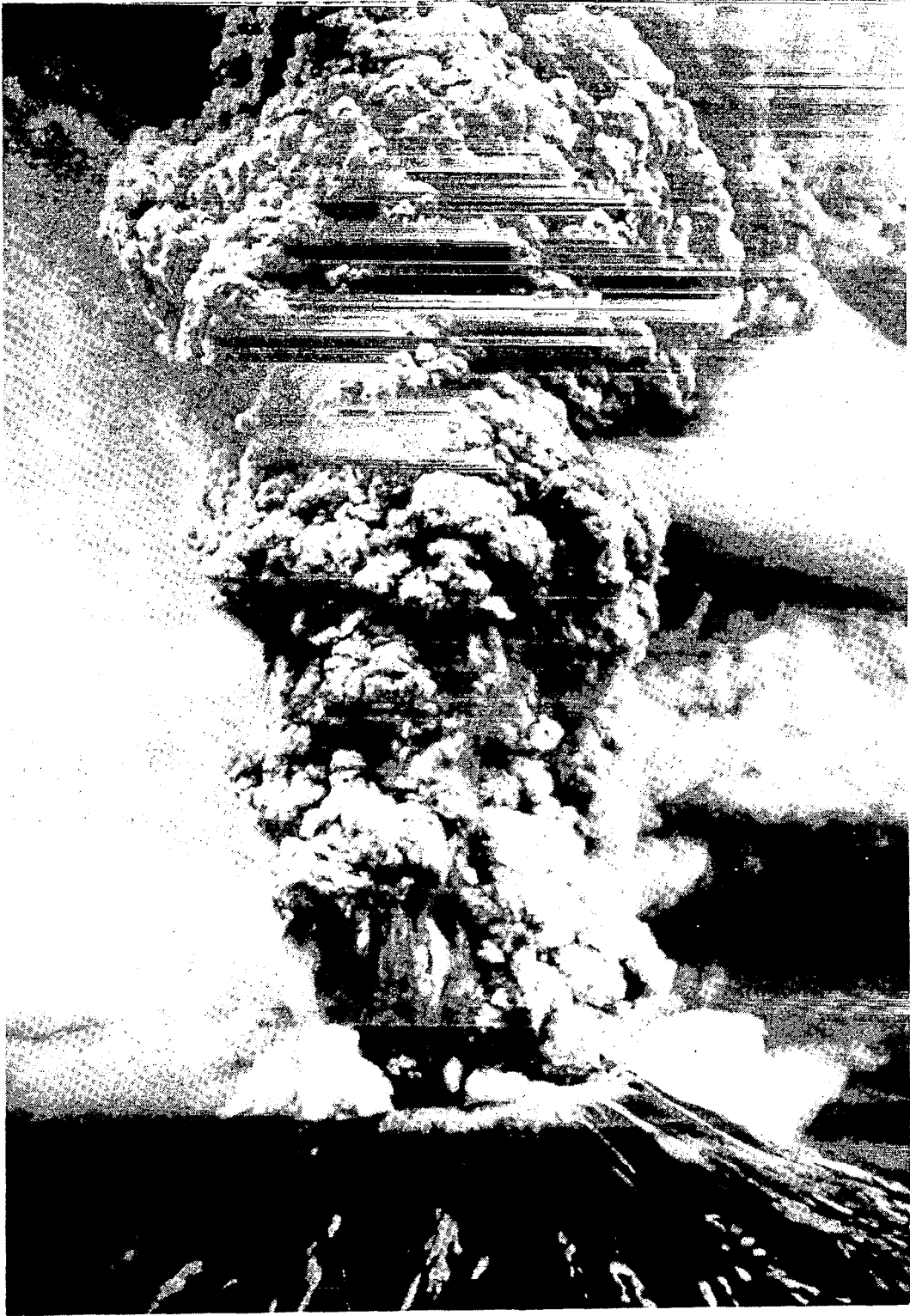


Figure 1. 18 May 1980 eruption of Mount St. Helens viewed from the west-southwest.

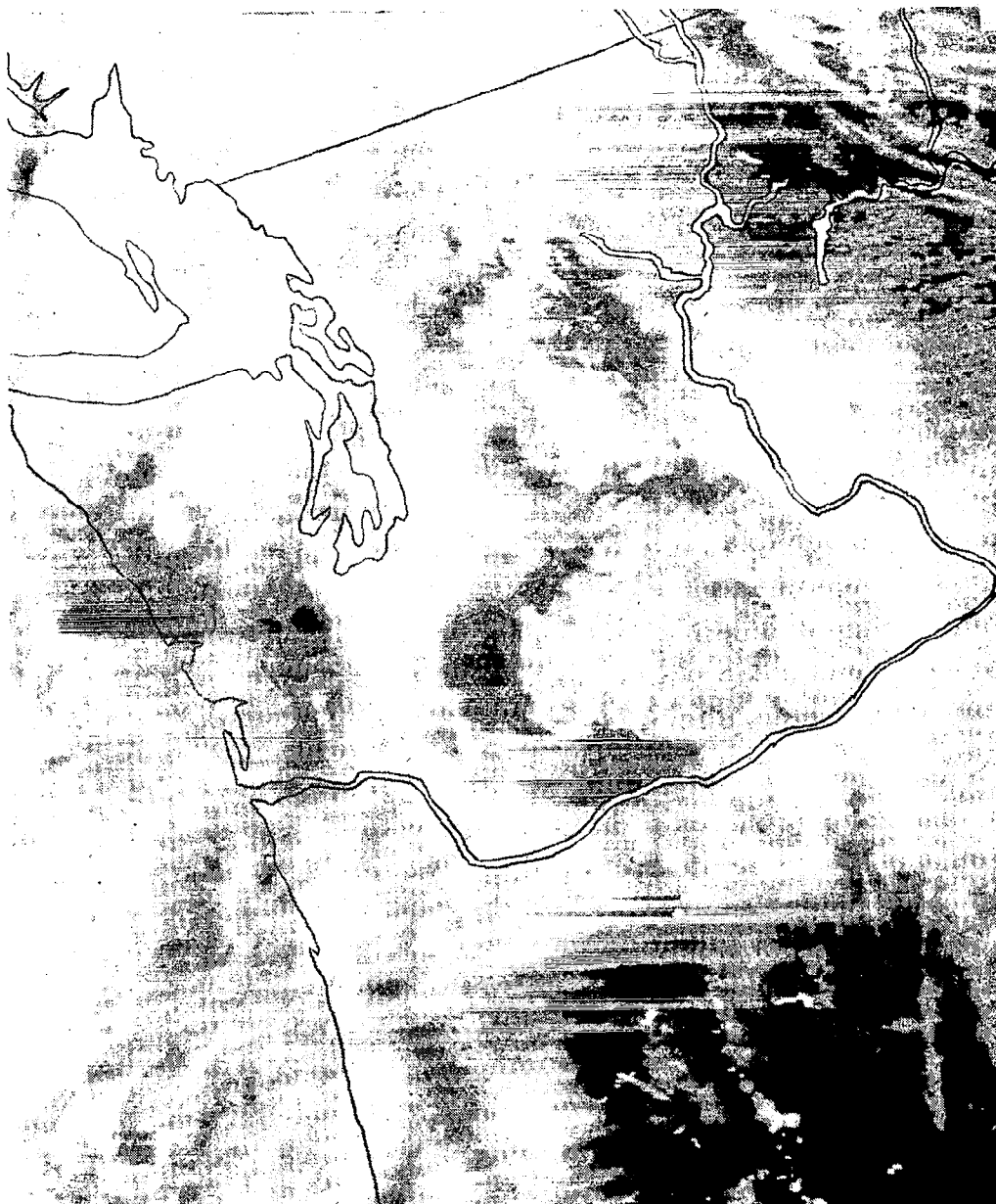


Figure 2. Photograph in visible light from the TIROS-NOAA 6 satellite taken at 1654 UT, 18 May 1980.

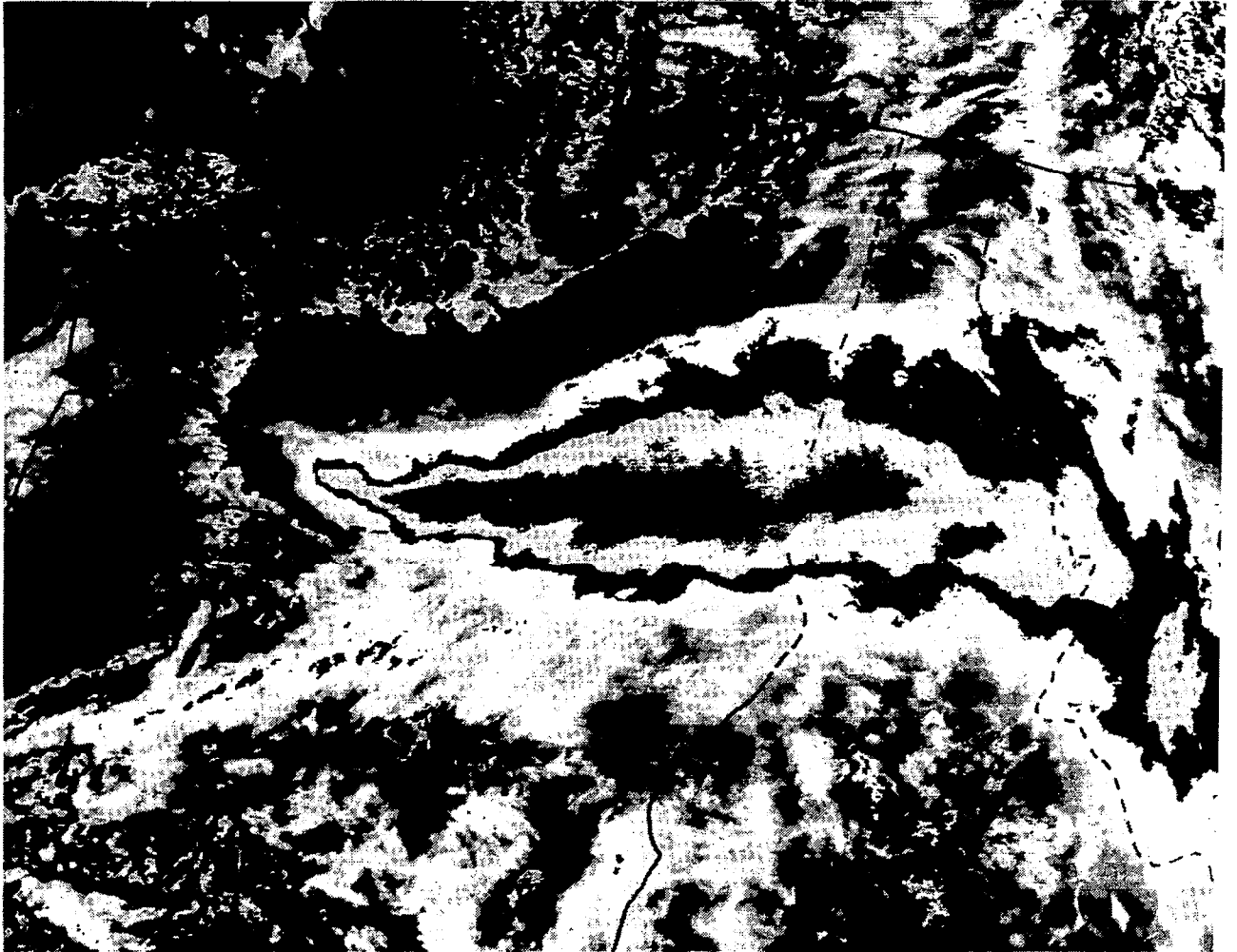


Figure 3. Enhanced infrared photograph from the TIROS satellite taken at 0238 UT, 18 May 1980.

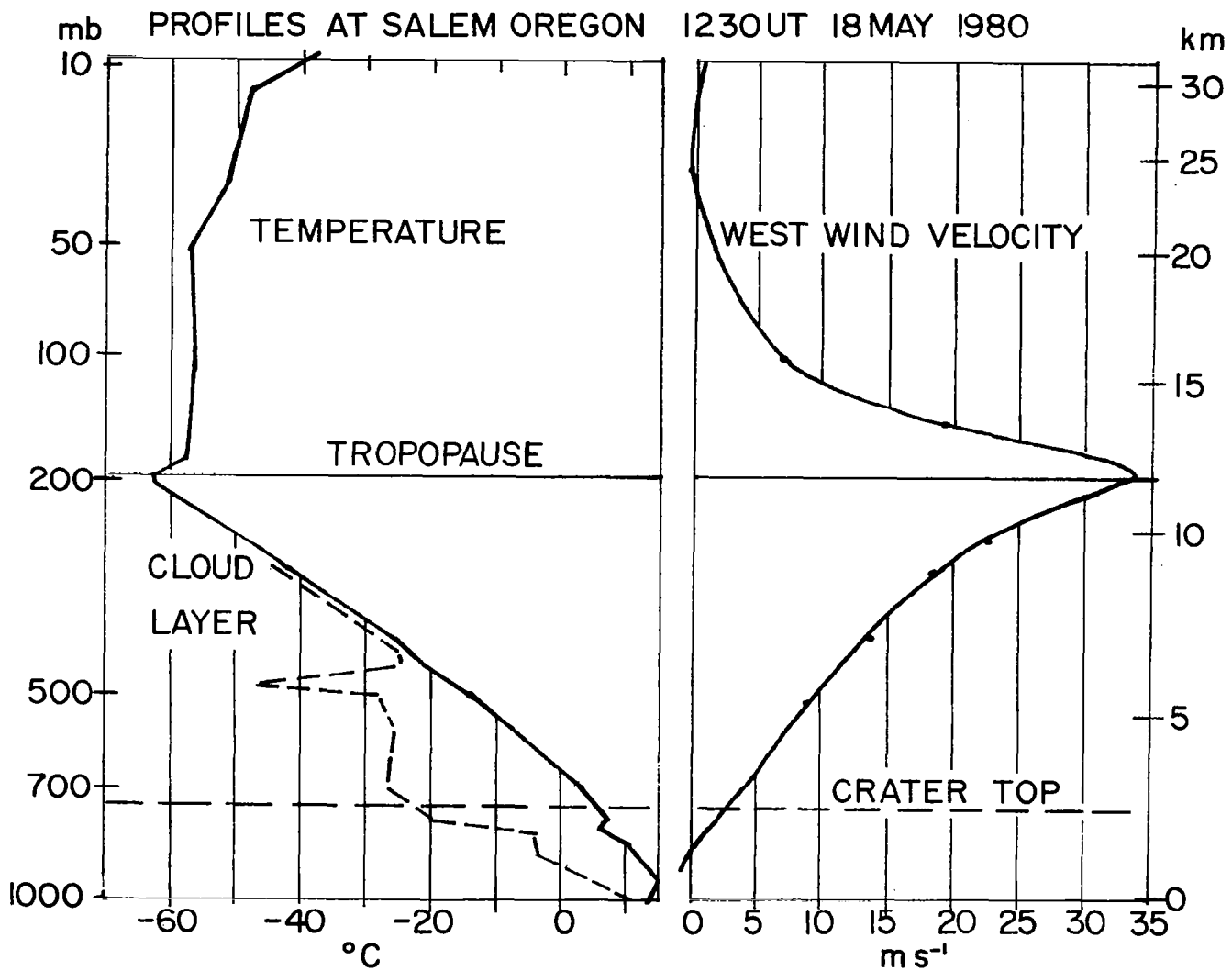


Figure 4. Temperature and west wind profiles from Salem, Oregon, 1230 UT, 18 May 1980.

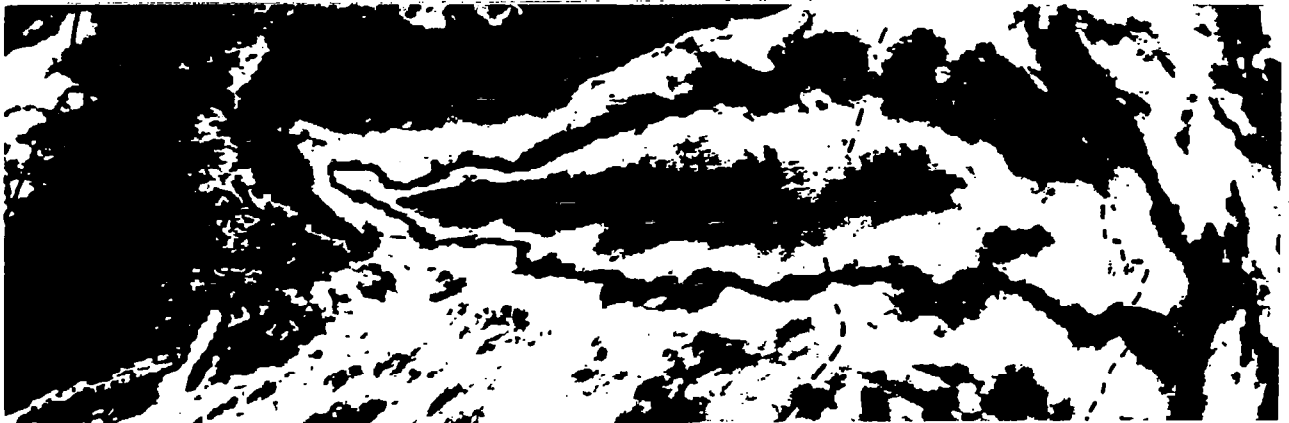
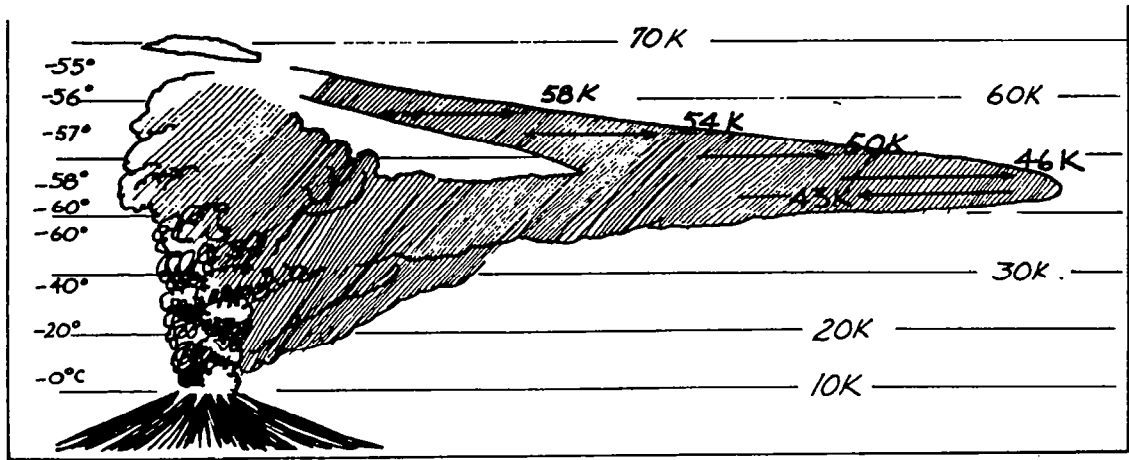


Figure 5. Schematic cross section of plume direction caused by wind shears and predicted flight paths for U2 aircraft on 19 May 1980. Heights are expressed in thousands of feet for convenience of pilot.

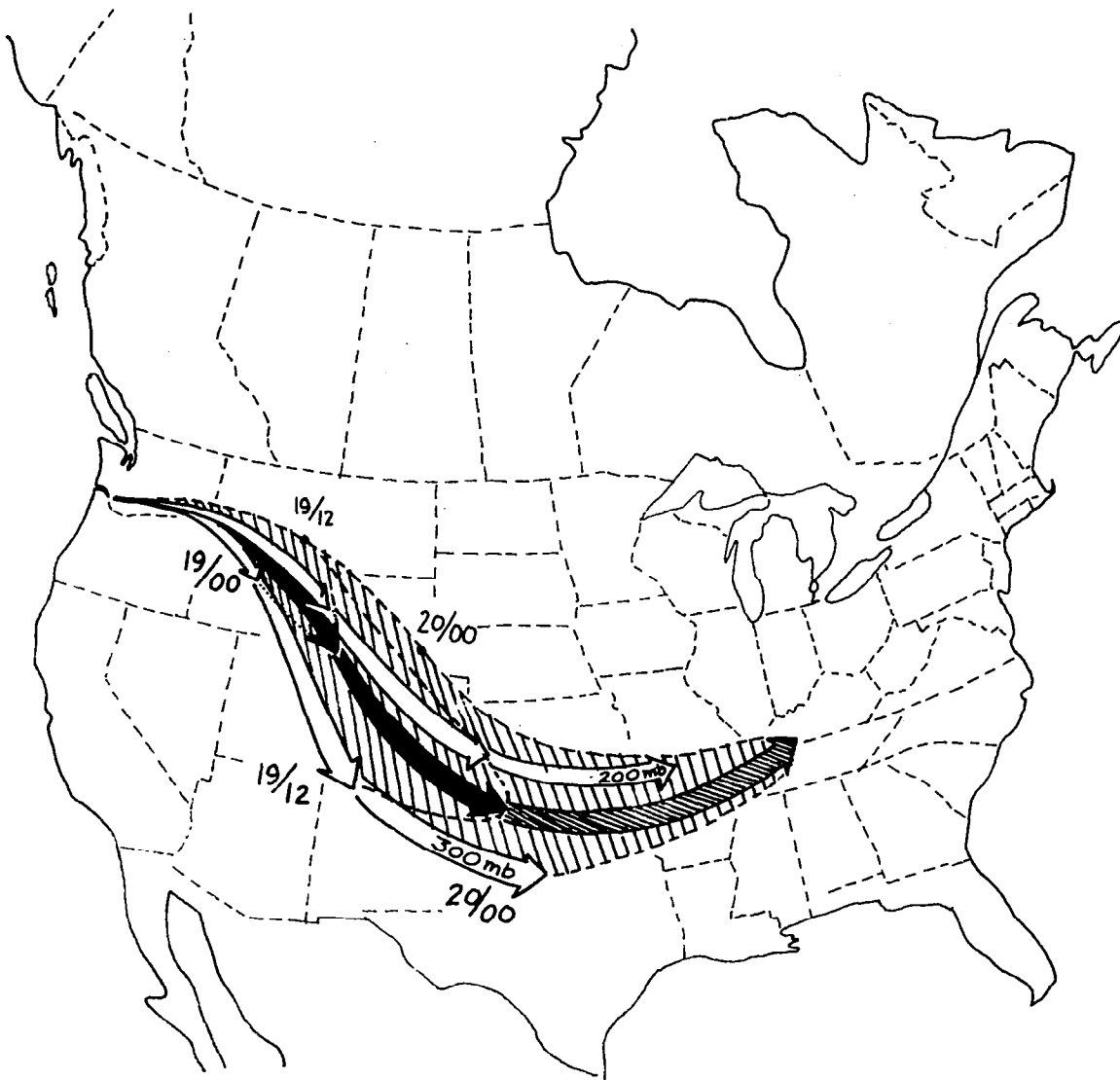


Figure 6. Trajectories of 18 May 1980 eruption for the 300 and 200 mb levels and black arrow depicting the path of the isentropic trajectory starting at 200 mb. Days and hours, in Universal Time, are appended.

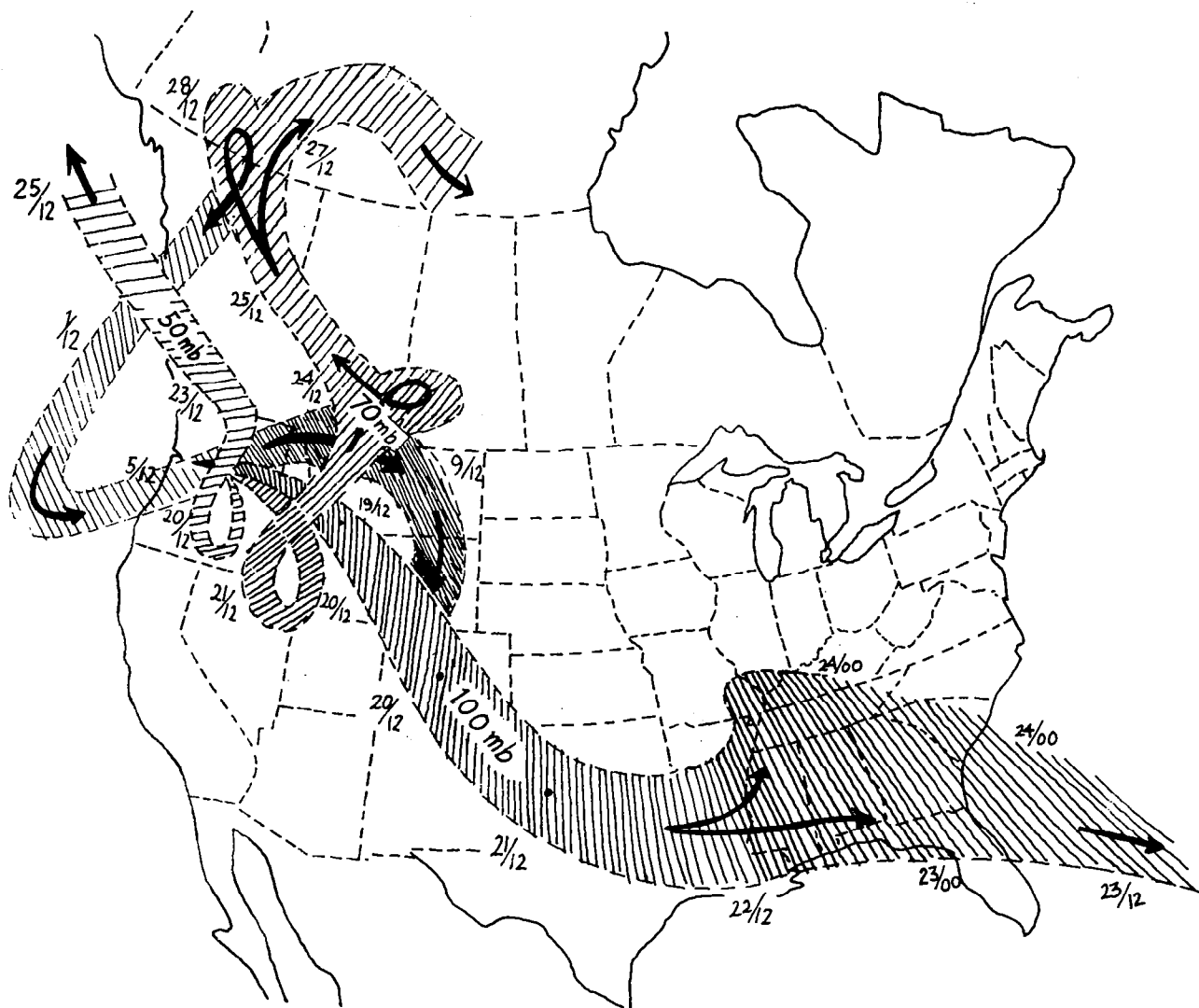


Figure 7. Trajectories of 18 May 1980 eruption for the 100-, 70- and 50- mb levels.

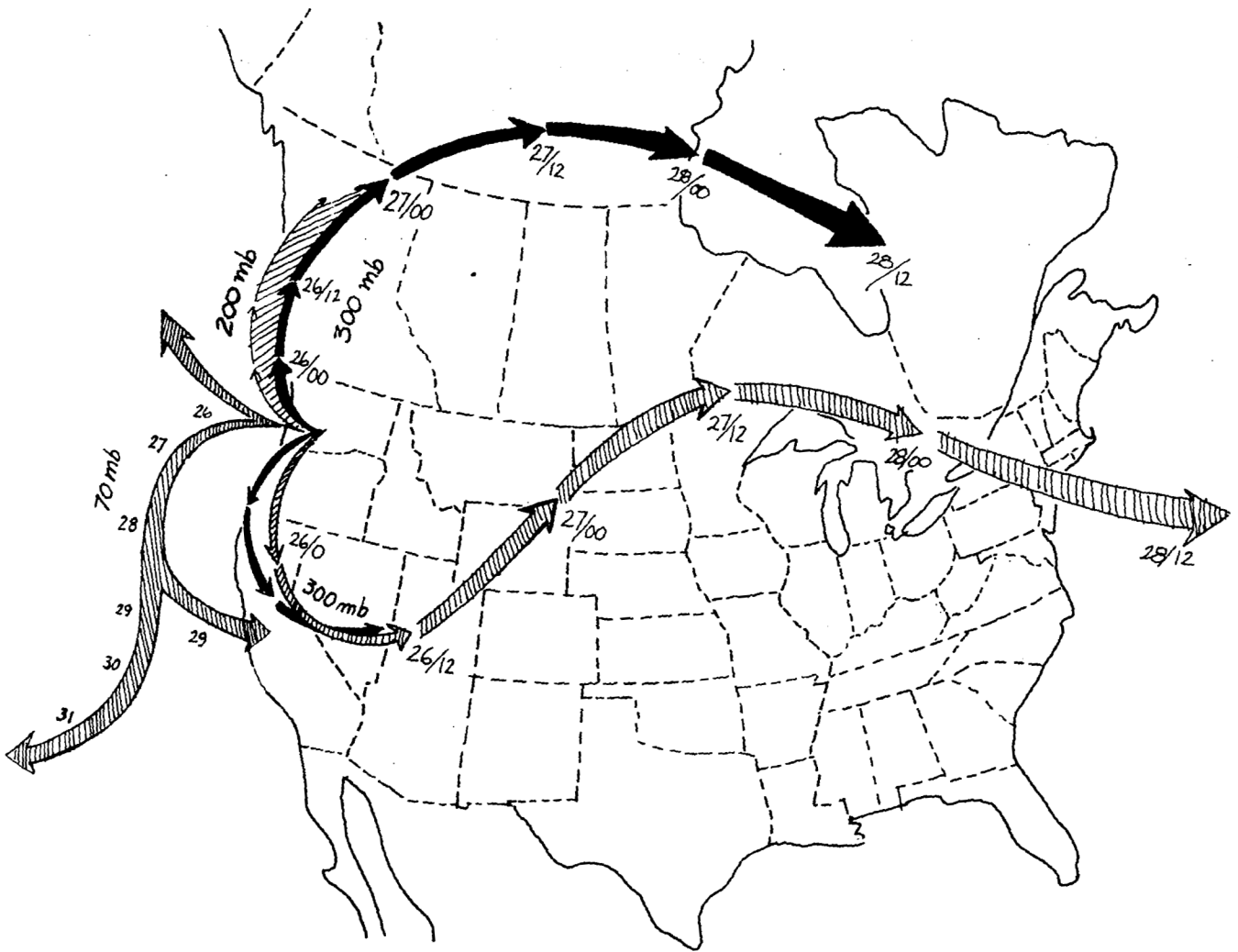


Figure 9. Trajectories from 25 May 1980 eruption.

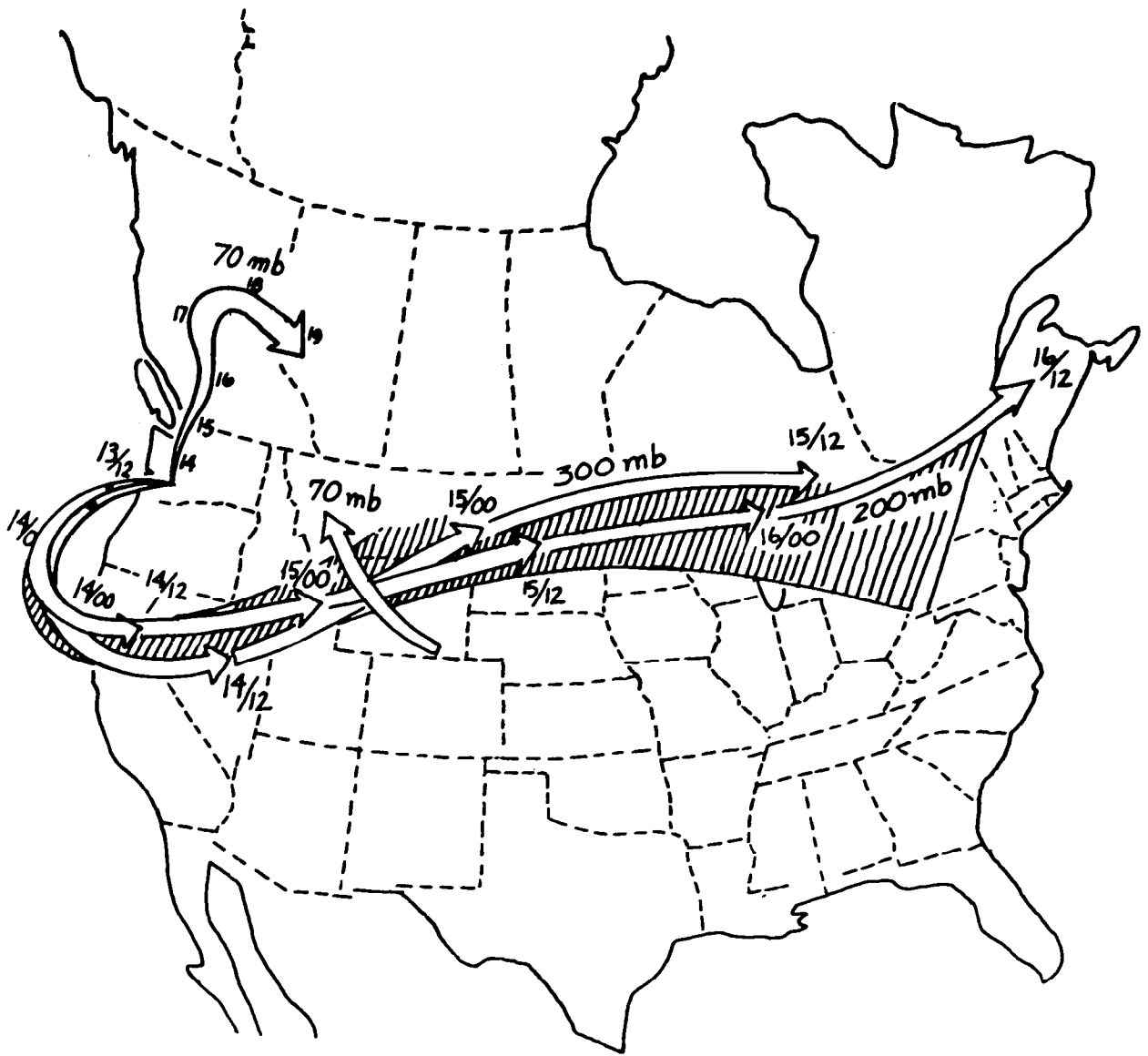


Figure 10. Trajectories from 12 June 1980 eruption.

A COMPARISON OF CONSTITUENTS OF MOUNT ST. HELENS ERUPTION CLOUDS WITH THOSE OF SOME OTHER VOLCANOS

Richard D. Cadle¹ and Leroy Heidt
The National Center for Atmospheric Research,² Boulder, Colorado

Gases from Mount St. Helens were collected from the eruption clouds using an airplane during the period April 2 to April 8, 1980, and were analyzed for CO₂, H₂, CH₄, and COS. The results were of similar magnitude to those obtained from magmatic eruptions in Central America. Thus, although the eruptions were evidently largely phreatic, magmatic gases may have played a larger role in these early small eruptions than has generally been believed.

Electron micrographs of ash particles collected from the Mount St. Helens eruption clouds showed that the particles were for the most part much larger than those from the Central American eruptions.

I. INTRODUCTION

During the spring of 1980 Mount St. Helens erupted in several stages. The first, phreatic, stage began as a long series of small eruptions on March 28 following several days of earthquakes. Toward the end of April these eruptions waned but a bulge on the north face of the mountain rapidly grew and the second phase was a tremendous magmatic explosion that occurred on May 18, 1980. This explosion has been followed by dome growth and additional large eruptions every few weeks throughout the summer and fall.

During the week April 3 to April 10, samples of the eruption clouds were collected by using a Queen Air aircraft. An assortment of collection devices was placed on the aircraft for a number of university and government organizations. Samples were collected for analysis by the National Center for Atmospheric Research (NCAR) with evacuated canisters and with a single stage impactor. The purpose of this article is to compare the results obtained for the samples taken from Mount St. Helens by NCAR with some results obtained by NCAR for magma eruptions at explosive (Guatemalan) and Hawaiian volcanos, and thereby draw some conclusions concerning the phreatic stage of the Mount St. Helens eruptions.

II. VOLCANIC CONDITIONS

The three volcanos studied in Guatemala are all strato-volcanos. Pacaya was fuming intensively in both 1978 and 1980. Vulcan Fuego, which usually erupts basalt, in 1978 was undergoing a number of small volcanic eruptions per day interspersed with periods of fuming for 1 or 2 days. Both types of eruption clouds were sampled. A lava flow was issuing from a breach in the summit crater. Santiaguito, which is a dacite dome on the side of Santa Maria volcano, was erupting ash-rich clouds several times a day from the Caliente crater both in 1978 and 1980, and in 1980 a "blocky" flow was issuing from the same crater. Vulcan Fuego was merely fuming in 1980.

The fumes from two volcanic regions were sampled in Hawaii. One was the crevasse which had formed across the floor of Mokuaweoweo caldera of Mauna Loa, and the other was the "Sulphur Bank" of Kilauea near the Volcano House. The Sulphur Bank is a solfataric area which has been active since it was first observed by missionaries in about 1825.

¹Present address - 4415 Chippewa Dr., Boulder, CO.

²The National Center for Atmospheric Research is sponsored by the National Science Foundation.

Mount St. Helens was erupting one or more times a day during the sampling period. A typical eruption during this time began with explosive steam emissions followed within a minute or so by nearly black ash-laden clouds. Some of these clouds rose thousands of feet into the air, whereas others poured down the side of the mountain. The coarse ash fell rapidly from the clouds and blackened the slopes of the mountain. The eruptions were less frequent than those in Guatemala; thus, only a few samples could be obtained.

III. COLLECTION AND ANALYSIS

The methods of gas sampling and gas chromatographic analysis have been described by Heidt (1) and by Rose et al. (2). The samples were taken through probes on top of the aircraft and flights were made through, across, or along the eruption clouds.

Samples of particles were collected from the eruption clouds with a single stage impactor on Parlodian-covered electron microscope grids (3) and examined by transmission and scanning electron microscopy and by energy dispersive X-ray analysis (EDXRA).

IV. RESULTS AND DISCUSSION

The results of the gas analysis are shown in table I as values or ranges of values. Perhaps the most interesting feature of these is the similarity in the magnitude of the values for the phreatic eruptions of Mount St. Helens and those for the magmatic eruptions of Fuego and Santiaguito. Subjectively, the eruption clouds penetrated by the aircraft contained similar quantities of ash. One might have expected much lower concentrations of volcanic gases in the Mount St. Helens eruption clouds than in the others, and these results suggest that magmatic gases may have played a greater role in the phreatic eruptions than had generally been believed.

It is of interest to note that according to a NASA-DOT Bulletin (4), several measurements of the sulfur-containing gases by Univ. of Washington scientists both before and after the May 18 eruption showed that the sulfur-containing gases were largely H_2S , whereas in Central America SO_2 was the main sulfur-containing gas.

The concentrations of volcanic gases in the samples collected in Hawaii were much larger than those obtained elsewhere because the former were collected directly from fumaroles. The samples collected in Hawaii had much larger ratios of CO_2 to the other gases than did any of the other samples. The origin of methane found in volcanic gases has been controversial. Stoiber et al. (5) believed that such organic compounds were produced by the heating of fossil soil or sedimentary layers by the magma. Methane was emitted by all of the volcanos of the present study, including those in Hawaii where contamination by methane from a nonmagmatic source is highly unlikely. Therefore, the methane was almost certainly of magmatic origin.

The particles collected in Central America by impaction in 1978 are described by Cadle et al. (6) and by Rose et al. (7). Those collected in 1980 were similar, except from Fuego. The particles in the Fuego eruption clouds were mainly ash in 1978, but in 1980 there were mainly sulfur-rich droplets, probably impure sulfuric acid, in the Fuego fume.

Ash particles collected from the Mount St. Helens eruption clouds during the early phreatic stages were much larger than those collected from the clouds from the Central American volcanos. The former particles often tore through the Parlodian films on the electron microscope grids and were collected mainly on the wires. In addition, many small sulfur-rich droplets were collected that were probably impure sulfuric acid (see figure 1). The large Mount St. Helens ash particles probably consisted of material torn from the conduit.

In addition, a few particles were found among the Mount St. Helens ash particles which were salts or ash particles encrusted with salts such as chlorides or sulfates or elemental sulfur. A possible source of these particles was old decomposition of material in the mountain by hydrothermal action. Similar particles were found in the fume from Pacaya and the eruption clouds of Santiaguito.

REFERENCES

1. Heidt, L. E.: Whole Air Collection and Analysis. Atmos. Technol., vol. 3, National Center for Atmospheric Research publication, 1978, pp. 3-7.
2. Rose, W. I., Jr., Cadle, R. D., Heidt, L. E., Friedman, I., Lazrus, A. L., and Huebert, B. J.: Gas and Hydrogen Isotope Analysis of Volcanic Eruption Clouds in Guatemala Sampled by Aircraft. J. Volcanol. Geotherm. Res., vol. 7, 1980, pp. 1-10.
3. Cadle, R. D.: The Measurement of Airborne Particles. Wiley-Interscience, 1975, pp. 110-111.
4. NASA-DOT Upper Atmospheric Program Bulletin No. 80-3, Washington, D.C., 1980.
5. Stoiber, R. E., Leggett, D. C., Jenkins, T. F., Murrmann, R. P., and Rose, W. I., Jr.: Organic Compounds in Volcanic Gas From Santiaguito Volcano, Guatemala. Geol. Soc. Am. Bull., vol. 82, 1971, pp. 2299-2302.
6. Cadle, R. D., Lazrus, A. L., Huebert, B. J., Heidt, L. E., Rose, W. I., Jr., Woods, D. C., Chuan, R. L., Stoiber, R. E., Smith, D. B., and Zielinski, R. A.: Atmospheric Implications of Studies of Central American Volcanic Eruption Clouds. J. Geophys. Res., vol. 84, 1979, pp. 6961-6968.
7. Rose, W. I., Jr., Chuan, R. L., Cadle, R. D., and Woods, D. C.: Small Particles in Volcanic Eruption Clouds. Am. J. Sci., vol. 280, 1980, pp. 671-696.

TABLE I. VALUES OR RANGE OF VALUES FOR FOUR CONSTITUENTS OF ERUPTION CLOUDS FROM MOUNT ST. HELENS, GUATEMALAN VOLCANOS, AND HAWAIIAN VOLCANOS.

Volcano	Value in ppmv ^a			Value in ppbv ^a
	CO ₂	H ₂	CH ₄	COS
Pacaya (1978)	16	nd ^b	0.3	0.27
Pacaya (1980)	< 3	nd	nd	0.03-0.087
Fuego (1978)	9-27	nd-9.6	nd-0.1	0.26-9.4
Fuego (1980)	< 3-3	— ^c	nd-0.27	—
Santiaguito (1978)	17	0.31	nd	0.015
Santiaguito (1980)	< 3-7	nd-0.8	nd-0.3	—
Mauna Loa (1979)	557-2.1x10 ⁴	0.8-20	0.8-2.9	0.09-51
Kilauea (1979) (Sulphur Bank)	1.7x10 ⁴ -1.5x10 ⁵	0.9-1.2	nd-0.45	4.1-10
Mount St. Helens (April 1980)	< 3-19	0.12-0.23	nd-0.59	nd-0.22

^aNet, after background concentrations subtracted.

^bDenotes not detected.

^cIndicates that the analysis was not performed.



Figure 1. Transmission electron micrograph of particles collected on April 7, 1980, from Mount St. Helens eruption cloud. Distance across the micrograph is 6 μm .

SIMULATION STUDIES OF THE PHYSICAL AND CHEMICAL PROCESSES OCCURRING IN THE STRATOSPHERIC CLOUDS OF THE MOUNT ST. HELENS ERUPTIONS OF MAY AND JUNE 1980¹

R. P. Turco

R & D Associates, Marina del Rey, California

O. B. Toon, R. C. Whitten, and R. G. Keesee
NASA Ames Research Center, Moffett Field, California

P. Hamill

Systems and Applied Sciences Corp., Palo Alto, California

The physical and chemical properties of the stratospheric Mount St. Helens eruption clouds of May 18, May 25, and June 13, 1980, are investigated. The large and diverse set of observational data collected in the high-altitude clouds is organized and analyzed for trends which reveal the processes at work. The data are used to guide and constrain detailed model simulations of the volcanic eruptions. For this purpose, a comprehensive one-dimensional model of stratospheric sulfate aerosols, sulfur precursor gases, and volcanic ash and dust particles is utilized. The model accounts for homogeneous and heterogeneous chemistry in the clouds, aerosol nucleation and growth, and cloud expansion. Computational results are given for the time histories of the gaseous species concentrations, sulfate aerosol size dispersions, and ash burdens in the eruption clouds. The long-term buildup of stratospheric aerosols in the Northern Hemisphere and the persistent effects of injected chlorine and water vapor on ozone are discussed. It is concluded that SO₂, water vapor, and ash are the most important substances injected by the volcano into the stratosphere, with respect to both the widespread effects on composition and the impact on climate. Despite the seemingly large magnitude of the Mount St. Helens eruption, it is found that the volcano probably had little influence on the climate (< 0.05 K global surface cooling) or on stratospheric ozone (< 0.2 percent maximum hemispherical reduction).

I. INTRODUCTION

At 8:32 a.m. local time on May 18, 1980, the long-dormant Mount St. Helens volcano (46.2°N, 122.2°W), which had been threatening for weeks, began to erupt in earnest. The initial May 18 explosion blasted away the top (914.4 m) of the mountain and lofted debris 23 km into the atmosphere. Towering eruptions followed on May 25 and June 13. All three of the major explosions injected large quantities of material into the stratosphere. Teams of scientists immediately began the largest observational study of a volcanic eruption ever undertaken. In situ measurements in the eruption clouds were made from balloons and a variety of aircraft platforms. Satellites and lidar probes monitored the movement and dispersion of the clouds. The gaseous emissions and ashfall around the volcano were sampled and analyzed for quantity and composition.

The data acquired during the extended period of Mount St. Helens activity are used here to constrain detailed model simulations of the eruption clouds. By utilizing a sophisticated model, the consistency of the data is tested, and interpretations of the data—in terms of the fundamental physics and chemistry occurring in eruption clouds—are sought. The one-dimensional aerosol and chemistry model employed for this purpose is described in a series of reports [1-5].

¹This research was partially supported under NASA Contract NAS2-9881.

This paper is organized as follows. In Section II the Mount St. Helens data relevant to the present work are summarized. The model of aerosols and gases used to make volcano simulations is discussed in Section III. Calculations for the Mount St. Helens eruption clouds are discussed in Section IV, and conclusions are given in Section V.

For convenience, it is stipulated that all particle sizes discussed in this paper refer to particle radius, unless otherwise stated.

II. THE MOUNT ST. HELENS DATA BASE

Table 1 indicates the important species emitted by volcanoes, describes their possible roles in the atmosphere, and gives an intercomparison of the relative abundances of each species in ambient air, in the gas near the Mount St. Helens volcano (fumarolic), and in the stratospheric eruption plume of Mount St. Helens. Note, in particular, that water vapor is greatly enhanced over ambient values in the Mount St. Helens eruption clouds. This has important consequences for the SO_2 oxidation rate in the volcanic clouds.

According to table 1, SO_2 was the dominant sulfur-bearing gas found in the stratospheric clouds (6). On the other hand, Rasmussen et al. [7] have suggested that OCS and CS_2 adsorbed on ash might constitute the main sulfur emission of volcanoes which affects the stratosphere. This suggestion appears to contradict the direct measurements of small OCS and CS_2 concentrations in the stratospheric clouds, unless OCS and CS_2 can be desorbed from the ash and oxidized to SO_2 in times less than 1 day (see below). In the presence of sufficient water vapor, hydrometeors would form on ash grains and these could (1) accelerate the "rainout" removal of the ash before sulfur desorption could occur, and (2) hydrolyze the OCS and CS_2 into sulfates condensed on the ash. There is also direct evidence from gas emission measurements conducted on the clouds around Mount St. Helens that little CS_2 and OCS were present [8]. Cadle et al. [9] found this to be true at other volcanoes as well.

Another important feature of the data in table 1 is the behavior of the S/Cl ratio. The observations indicate that chlorine is fractionated from the volcanic emissions before they stabilize in the stratosphere. The stratospheric values of S/Cl of 1 to 100 in table 1 indicate that, on the average, 90 percent or more of the chlorine is depleted from the rising plume. Lazrus et al. [10], who detected the same effect in other sizable eruptions, attribute the fractionation to "rainout" of the very soluble HCl vapor during the early development of the eruption plume. One implication of a low S/Cl ratio is that volcanic chlorine may not have a significant impact on stratospheric ozone, as had been previously suggested [11,12]. This point is elaborated later.

Mount St. Helens represents the first time in the history of volcanology that extensive measurements were made in the high-altitude clouds of a major volcanic eruption. Much of the stratospheric data are summarized in table 2 (13-18). In utilizing the data, substantial uncertainties must be recognized. According to most accounts, the clouds were highly inhomogeneous. The clouds, moreover, were generally sampled only once or twice. The experiments themselves were intrinsically difficult but, fortunately, were numerous and diverse enough that overlap between some of the observations allows a degree of cross calibration. Owing to the variety of conditions under which observations were made, the absolute concentrations of many of the species varied widely from sample to sample. Although each individual cloud could be simulated, the data set for any single cloud (as specified in table 1 by eruption number and cloud height relative to the tropopause) is very much smaller than the total data set. In addition, the general behavior and evolution of the clouds is of more interest than individual case studies.

With these considerations, it is logical to reduce the data to ratios of species concentrations; for example, $\text{SO}_4^-/\text{SO}_2$. The ratios, it is believed, should exhibit a more regular behavior from cloud to cloud, as the ratios pertain to the composition of the injected gas and are relatively independent of the effects of cloud dilution. The authors also chose to normalize the ratios measured in the volcanic clouds to the ratios observed in ambient air. Thus, it will be apparent when an air mass is highly disturbed. Of course, the absolute variations in the abundances of gases and particles must also be considered in making judgements about the properties of the clouds. The ambient concentrations of stratospheric gases and particles adopted for comparisons were obtained from standard references (e.g., ref. 6); for the sulfur-bearing constituents, current values predicted by models are in reasonable accord with observational data (e.g., refs. 2-4).

Figures 1 to 3 give, respectively, the ratios of SO_4^- to SO_2 and of H_2O and OCS to total oxidized sulfur (i.e., $\text{O}_x\text{S} \equiv \text{SO}_4^- + \text{SO}_2$) in the Mount St. Helens clouds. The ratios in figures 1 to 3 correspond to a specific subset of the data in table 2. Only the ratios of constituents which were measured simultaneously from the same platform are plotted. Most of these measurements, in addition, were taken with instruments that "integrate" over long distances through the clouds, e.g., filter collectors and cryogenic traps. The use of such measurements further mitigates the interpretive problems caused by inhomogeneities in the cloud. Accordingly, these precautions—use of ratios of simultaneous data averaged over long distances—should reveal most clearly the general temporal trends in the composition of the Mount St. Helens clouds.

At first glance, the $\text{SO}_4^-/\text{SO}_2$ data in figure 1 appear to vary randomly over a wide range of values. However, when the average trend is considered, the data show a surprising behavior. The ratio appears to increase dramatically during the first 3 days after the eruption and then remains relatively constant. Notice that one data point taken 27 days after the May 18 eruption, and which has been associated with that eruption, is inconsistent with this interpretation. If that data had actually been obtained in the June 13 eruption cloud, 1 day old, they would fit the pattern of the other data. During the June 14 U-2 flight, in fact, there was some confusion as to the origin and locations of the clouds. Nevertheless, it is also possible that this was simply a different type of cloud than the others, contained much less ash and water, and had undergone much slower SO_2 -to- SO_4^- conversion.

The ratio of water vapor to O_xS (total oxidized sulfur) in figure 2 exhibits values much smaller than the ambient value. Thus, most of the plumes appear to be quite enriched in sulfur over water compared with ambient stratospheric air. Both water and sulfur are subject to rapid heterogeneous removal processes (e.g., condensation and rainout) and, indeed, are probably closely related. Thus, one might expect to see a correlation between the H_2O and O_xS variations, as suggested in figure 2. The ratio of OCS to O_xS (fig. 3) shows a rapidly increasing ratio the first few days and a fairly constant ratio thereafter. The trend is reasonable on physical grounds inasmuch as OCS is a (relatively) stable gaseous chemical compound in the clouds, whereas O_xS is subject to rapid heterogeneous removal in the early cloud.

The chloride (Cl^-) data in table 2 are interesting because they indicate that very little acidic chlorine vapor (HCl) or particulate chloride was found in the Mount St. Helens eruption clouds. The data of Inn et al. [15], showing up to 10 ppbv (parts per billion by volume) of chloride, are highly uncertain due to complications in the laboratory analysis for chloride. The data of Gandrud and Lazrus [14] are more reliable, and are in agreement with other volcano studies which imply low levels of stratospheric chloride [10].

The nitrate (NO_3^-) data of Inn et al. [15] are very erratic. Gandrud and Lazrus [14] reported no significant enhancements in gaseous NO_3^- concentrations in the Mount St. Helens clouds. Nitrogen oxides (the precursors of nitrate ions) are not usually emitted in large quantities by volcanoes [19,20]. Moyers [8] detected slight enhancements in NO above background amounts in the volcanic clouds near the St. Helens mountain (50-100 pptv, compared with 20 to 30 pptv in ambient ash). Hobbs et al. [21,22] found NO concentrations generally at or below background levels, with only occasional enhancements. There are at least two possible sources of odd-nitrogen (NO_x) gases for the stratospheric clouds. First, nitrosyl and ammonia compounds contained in the (nonmagmatic) soil incorporated into the plume could decompose into gaseous NO_x when the soil is heated. No attempt has been made to quantify this source.

Lightning accompanying violent volcanic eruptions can also generate NO_x (and CO as well). Cobb [23] measured up to eleven discharges per minute during the May 18th Mount St. Helens eruption. A total of 164 bolts was detected during a 2-hour period. The intensity of the strokes was not determined, but Cobb noted that they appeared to be much weaker than typical thunderstorm lightning (based on recorded electric field strengths). Most of the lightning appeared to strike the mountain top, and thus much of the lightning-generated NO_x could be swept up in the rising plume. The total quantity of NO_x created by the lightning may be crudely estimated by assuming 300 strokes 1 km in length each having an energy density of 10^4 joule/m (thunderstorm lightning has an energy density in the range of 10^4 to 10^5 joule/m). The NO_x production per joule of energy is taken as 10^{17} molecules/joule [24,25]. These assumptions imply $\approx 3 \times 10^{26}$ NO_x molecules produced during the May 18th eruption, or about 10 kg NO . This amount of NO , although quite uncertain, is very small and could be neglected (unless the NO_x is highly localized).

The CO production by lightning is probably three orders of magnitude smaller than the NO production [26]. Nonetheless, Inn et al. [15] detected CO concentrations as high as 2 to 4 ppmv on one occasion.

Volcanoes do not usually emit such large quantities of CO. In such amounts, the CO could interfere in the OH reaction sequence and affect the rate of SO₂ oxidation. Most of the measurements show much smaller, and therefore inconsequential, CO concentrations.

In accordance with these arguments, the uncertain injections of CO and NO_x into the stratosphere by the volcano are neglected. As noted, the consequences of small amounts of injected CO and NO_x are unimportant in any case.

Measurements of the volcanic ash lofted by the Mount St. Helens eruptions reveal some interesting features. Apparently, large dry angular ash and shattered mineral particles up to 30 μm in size (possibly with a light coating of ice) were observed on May 19 below 18 km [27,28]. The ash burden was as high as 620 μg/m³ [29]. However, on May 22nd the ash between 18 and 20 km had a quite different character. The particles were, for the most part, smaller than 3 μm and many were flooded with sulfuric acid solution [27,28]. The ash mass, moreover, was ≤10 μg/m³ [29,30] Rosen and Hofmann [31] noted a similar change in the clouds over Wyoming where initially large, involatile particles quickly (within several weeks) were replaced by predominantly volatile aerosols.

The ash injected into the stratosphere by a rising volcanic plume—as a result of either the explosion or resulting thermal buoyancy—is expected to be fractionated with height. The large particles are raised less effectively than small particles by a vertical airstream, because of the stronger influence of gravitational sedimentation on the former. Once deposited at high altitude, the large particles fall faster and are therefore removed more rapidly than the small particles. If most of the initial weight of the ash is held by a few large particles, the ash mass of the cloud will diminish rapidly with time. The mass would also tend to decrease faster at higher altitudes because particle fall-speeds increase with height.

Two ash size distributions, which are derived from the observational data, are adopted here as initial conditions for model calculations. One, measured by Farlow et al. [28] in the stratospheric clouds of Mount St. Helens several days after the May 18th eruption, is represented by a log-normal distribution with a mode size $\bar{r} \approx 0.5 \mu\text{m}$ and mode width $\sigma \approx 0.5$. The log-normal distribution is used to simulate the fine dust in the clouds. The second size distribution selected was measured by Barrett et al. [32] in an ash cloud about 56 km downwind from Mount St. Helens volcano. The size distribution is dominated by large particles, and has been extrapolated for our purposes to a radius of 32 μm. The distribution is roughly indicated in figure 4 for radii > 3 μm by the curve depicting the volcanic cloud 1 day after injection. The Barrett et al. size distribution is presumed to simulate the coarse ash observed in the early eruption clouds. An average density of about 1.7 g/cm³ is assumed for all the ash particles and reflects their irregular shapes and fluffy texture (e.g., refs. 17 and 33).

The measured size characteristics of the sulfate aerosols formed in the wake of the volcano are discussed in Section IV.

III. A MODEL FOR STUDYING VOLCANIC CLOUD EVOLUTION

A comprehensive physiochemical model of volcanic eruption clouds was developed for this study. The cloud model is based on the one-dimensional stratospheric aerosol model of Turco et al. [1] and Toon et al. [2]. That model treats the sulfur vapor chemistry and microphysics of a highly dispersed sulfate aerosol at altitudes from 0 to 58 km. A complete description of the basic simulation can be found elsewhere [1-5]. Several extensions and improvements to the model were made to facilitate the volcano study. The particle size range was extended to encompass the range from 10 Å to 32 μm. Dry volcanic particles are treated as a separate aerosol, whereas the ash component of the sulfuric acid aerosols is calculated by using the multicomponent analysis technique of Turco et al. [3]. Ash is incorporated into the acid aerosols as “cores” through nucleation and coagulation processes. Particle nucleation mechanisms are handled by using the formalism described by Hamill et al. [5].

Three additional important effects are taken into account in the volcano simulations: cloud expansion, heterogeneous chemistry, and chemical coupling between OH, SO₂, and H₂O. In the present work, the expanding volcanic clouds are assumed to have a uniform spatial composition. As a cloud grows, ambient air

is mixed in and the original cloud material is diluted. The rate of horizontal expansion of the cloud is specified through a simple empirical relation which is based on observations of the growth rates of clouds of different sizes in the lower stratosphere [34]:

$$A = \frac{\pi}{2} K(t_0 + t) \quad (1)$$

In equation (1), A is the horizontal area of the cloud (cm^2), K is the horizontal "diffusion" coefficient (cm^2/s), and t is the expansion time(s) measured from the "initial" time, t_0 . By use of equation (1), the effect of expansion on the concentration of an active or inert gaseous or particulate species in the cloud can be expressed as an additional rate term in the species continuity equation in one dimension. That is, at each height,

$$\left(\frac{dn}{dt} \right)_{\text{expansion}} = - \left(\frac{n - n_0}{t + t_0} \right) \quad (2)$$

where n is the concentration (cm^{-3}) in the cloud and n_0 is the concentration in ambient air. The expansion term [equation (2)] is dropped once the cloud area [equation (1)] fills a hemisphere. In the present calculations, the same dispersion rate is applied to all the cloud levels in a given simulation.

In addition to horizontal dispersion, the volcanic clouds are subject to strong wind shears, causing injected material at different altitudes to be blown in different directions [35]. In the one-dimensional model, only individual cloud layers ≥ 2 km in thickness are treated. Alternatively, it is possible to analyze the entire vertical eruption column simultaneously. The latter approach is most economical because it allows the study of all of the cloud layers at once. It is also scientifically sound, the basic limitations of a one-dimensional simulation being considered. In the long term, of course, horizontal dispersion causes the cloud layers to overlap, and a one-dimensional approximation of the problem is more appropriate. In the short term, separate cloud layers can interact only through particle sedimentation; vertical diffusion in the lower stratosphere has a long characteristic time, ≈ 1 month/km. Thus, individual clouds will mature more or less independently. Particles larger than ≈ 1 mm are eventually separated from the cloud layers by sedimentation. However, the mass of these large particles typically decreases with height through the eruption plume. Hence, contamination of the lower cloud levels by particles from the upper cloud levels should not be a dominant factor in the present simulations, particularly when the uppermost cloud layers are considered.

The large quantities of dust in the Mount St. Helens eruption plumes caused the volcanic clouds to warm significantly (J. B. Pollack and T. Ackerman, calculations in progress, 1981). This created instabilities which enhanced vertical mixing in the cloud layers. However, the overall effect on vertical dispersion of the clouds was probably small and is neglected here.

Heterogeneous chemistry cannot be treated in detail in the present model. Heterogeneous reaction mechanisms are complex and depend greatly on aerosol composition. Mineralogical and elemental analysis of Mount St. Helens ash collected on the ground downwind from the volcano revealed a silicate matrix impregnated with numerous metallic compounds that could participate in aqueous chemical reactions or act as surface catalysts [33,36,37]. Samples of ash also produced basic solutions in water; thus, an ability to buffer sulfate formation is indicated [33]. Accordingly, two general heterogeneous reaction mechanisms for the oxidation of SO_2 are considered. One is assumed to involve the ash. The rate of SO_2 oxidation is made proportional to the surface area of the ash available for reactions per cm^3 of air (conservatively assuming spherical ash particles). The second mechanism involves solution reactions. The SO_2 oxidation rate in this case is taken to be proportional to the aerosol solution volume per cm^3 of air. For each mechanism, a maximum initial conversion rate is specified in the clouds (e.g., 10 percent/hr). The reaction rate per unit surface area or volume at each altitude is then normalized either to the maximum initial ash surface area at any level within the clouds or to the maximum initial sulfate volume (with SO_2 expressed as an equivalent mass of SO_2). Subsequently, each rate is calculated in proportion to the instantaneous ash surface area or acid volume of the aerosols at each point in the clouds. Of course, the initial conversion rates are treated as variable parameters in the calculations. By estimating the kinetically limited rates of reaction with the aerosols, it was ascertained that, for the given magnitude of the injections, the selected maximum reaction rates implied reaction efficiencies per collision < 1 .

Ash surfaces may become poisoned and ineffective for oxidizing SO₂. Poisoning was accounted for by reducing the surface reaction rate by a factor

$$e^{-\gamma(1-f)} \quad (3)$$

where γ is an adjustable number, and f is the ash volume fraction of an aerosol droplet. Thus, f describes the relative size of the ash "cores" in the sulfuric acid aerosols. Fresh ash particles have $f = 1$, whereas ash grains flooded with acid have $f \ll 1$. The value of f is a function of particle size, altitude, and time, as predicted by the model. Because the surface reaction rate is proportional to the ash surface area, another factor of $f^{2/3}$ enters into the rate expression. The present treatment of heterogeneous chemistry, although quite crude, should serve to place some limitations on the effects of such reactions.

The interactive chemistry in the OH/H₂O/SO₂ system is analyzed by using a semiempirical photochemical relation which links the concentrations of these constituents,

$$P_o[\text{OH}] + P_1[\text{H}_2\text{O}] - k_1[\text{OH}][\text{SO}_2] - k_o[\text{OH}]^2 = 0 \quad (4)$$

where square brackets indicate concentrations (cm⁻³). The terms P_o and P_1 represent the odd-hydrogen sources due to methane and water vapor decomposition, respectively, calculated by using data from a detailed ozone photochemistry model (see below), and k_1 is the rate coefficient for the reaction of OH with SO₂. By using ambient profiles for OH, H₂O, and SO₂, and predetermined values for P_o , P_1 , and k_1 , the "effective" odd-hydrogen recombination coefficient k_o is initialized by inverting equation (4). At subsequent a time, [OH] is calculated from equation (4) using the time dependent H₂O and SO₂ concentrations from the aerosol model and the initialized chemical parameters P_o , P_1 , k_o , and k_1 . The SO₂ concentration is calculated interactively in the aerosol model. H₂O, however, is treated as a tracer in the cloud. According to equation (2), H₂O evolves as

$$[\text{H}_2\text{O}]_t = [\text{H}_2\text{O}]_a + ([\text{H}_2\text{O}]_o - [\text{H}_2\text{O}]_a) \left(\frac{t_o}{t + t_o} \right) \quad (5)$$

where subscripts "a" and "o" refer to the "ambient" and "initial" values, respectively. As OH evolves, it is assumed that the concentrations of HO₂ and CH₃O₂—which have a secondary role in sulfur photochemistry—change in proportion to OH.

The OH concentrations predicted by equation (4) were compared with those computed by using a fully interactive one-dimensional photochemical model involving stratospheric oxygen-hydrogen-nitrogen-chlorine-sulfur-carbon species. The resultant OH variations agreed within 30 percent. OH chemistry is closely tied with all the reaction cycles identified in the stratosphere. Hence, a full calculation for OH would involve literally dozens of species and more than a hundred reactions. All this chemistry is incidental to aerosol formation and would tax computer capabilities. Accordingly, the full OH chemistry was not included in the model for this work.

The photochemical model mentioned above is also employed to study the effects of the Mount St. Helens emissions on stratospheric trace gas composition. The specific intent here is to explore the impact of the gaseous effluents on the ozone abundance of the stratosphere. The structure of the photochemical model is described by Turco and Whitten [38,39]. A complete and modern chemical kinetics scheme is utilized [40]. Sulfur chemistry is also included, but aerosols are not. In simulation studies, the species H₂O, SO₂, OCS, CH₃Cl, and HCl are assumed to be injected by the volcano at the heights and in the amounts observed. The early (< 1 yr) effect of horizontal dispersion on the species concentrations is computed by using equation (2).

Three distinct types of simulations of the Mount St. Helens eruption clouds were made for this study. A description of each type of simulation, and the initialization parameters employed, is given in table 3. Some of the initial conditions were obtained from table 2. The other initial conditions are explained in Section IV. The three basic types of calculations deal with short-term aerosol evolution, long-term aerosol evolution, and long-term ozone effects. In each case, volcanic material was injected over the height range ≈ 14 to 22 km to simulate the massive May 18 stratospheric eruption plume. For the long-term runs, the different

cloud layers eventually merge and the widespread effects depend upon the total injection. For the short-term runs, the different cloud layers do not interact strongly, owing to weak vertical mixing in the lower stratosphere. Thus, the computational approach selected for the short-term simulations allows us to study several different cloud layers at once, as noted earlier.

The aerosol and chemistry models used for calculations have some additional limitations and uncertainties not brought out in the previous discussion. For example, the radiation fields are held fixed, independent of the volcanic clouds. Obviously, this would be a questionable approximation during the first day after the eruption. However, for 1 or 2 days following each eruption the clouds were optically thin, and the radiation that influences photochemistry would not have been severely altered. The model also oversimplifies the cloud dispersion process and ignores advection and other large-scale meteorological transport and removal mechanisms. As far as the basic uncertainties associated with the aerosol model physics and chemistry are concerned, these are reviewed by Turco et al. [1] and Toon et al. [2] and references cited therein.

The computational uncertainties pertaining to one-dimensional ozone photochemistry models are amply surveyed in reference 6.

IV. VOLCANIC SIMULATION RESULTS AND DISCUSSION

The different types of volcano simulation are discussed in the order indicated in table 3. For all the calculations which include cloud expansion effects, the simulation is started at 1 day after the eruption when the clouds had presumably stabilized. The only exception is the long-term volcanic cloud simulation, in which case the injected material is initially spread over the Northern Hemisphere.

A. Short-Term Volcanic Clouds

To calculate the first 30 days of cloud history, cloud horizontal spreading parameters were chosen that roughly duplicate the observed expansion rate of the May 18 Mount St. Helens eruption clouds [35,41,42]. One day after the eruption, the main cloud at ≈ 14 km had an area $\approx 10^6$ km². By using equation (1), this condition translates into an average horizontal diffusion coefficient $\approx 10^{11}$ cm²/s the first day. A broad base of data for the lower stratosphere indicates that this value is close to the upper limit observed for the growth of passive clouds [34]. The effective diffusion coefficient normally increases from $\approx 10^8$ cm²/s after several minutes to $\approx 10^{11}$ cm²/s after several days. It might be expected, however, that the violent mode of injection and the extended period of eruption caused the initial volcanic clouds to spread laterally at a much faster average rate. Therefore, we have adopted a constant horizontal diffusion coefficient of 10^{11} cm²/s for calculations on all time scales. The cloud expansion model just described applies to all the short-term simulations reported here, although other expansion rates were tested in the course of this work.

For the short-term calculations, a maximum (initial) heterogeneous SO₂ oxidation rate of 15 percent/hr in the clouds was selected. This is probably an upper limit judging from contemporary reviews of the possible reaction mechanisms [43,44]. A surface reaction process was chosen over a solution process because of the high acidity of the aqueous aerosols, which acts to inhibit SO₂ oxidation in solution. However, Martin and Damschen [45] recently discovered that SO₂ oxidation by dissolved H₂O₂ can occur rapidly at very low pH. Other combinations of surface and solution reaction rates were tested in the course of preliminary model computations; these tests led to the choice of heterogeneous rate parameters given in table 3.

In figure 1 the short-term model simulations are plotted against the data. The calculation which includes the heterogeneous reaction mechanism appears to match most of the data from several eruptions. Without heterogeneous reactions, none of the data are matched. However, the initial conditions might be varied from those in table 3 to obtain better agreement. No cases were run with large initial SO₄⁻ concentrations. None of the May 19 stratospheric data, nor any of the data collected around the volcano, suggest initial concentrations of SO₄⁻, exceeding those of SO₂ in the ejected material. Hence, it is felt that models without heterogeneous chemistry violate either the data, or reasonable initial conditions, for most of the ash clouds.

The results in figure 1 imply that heterogeneous chemistry is important in the early clouds. One data point taken in the May 25 cloud, however, shows a much larger SO₄⁻/SO₂ ratio than is simulated by the model. In table 2, it appears that the SO₂ concentration is unusually low in this cloud (≈ 11 pptv) compared with ambient concentrations (≈ 30 to 50 pptv).

An induction period before the onset of SO_2 to SO_4 conversion is apparent in the cloud of figure 1 (and figs. 5 and 6 as well, see below). The data suggest that much less SO_4^- was formed during the first day after each eruption than during the second day. The induction period might be due to a lack of oxidants in the early cloud and/or a lack of a reaction medium. For example, ice probably condensed on the active dust grain surfaces in the humid and rising plumes, blocking surface reactions. When SO_2 is very concentrated (< 1 day), ambient oxidants such as O_3 and H_2O_2 that are mixed into the cloud cannot effectively deplete the SO_2 abundance. As the cloud thins and the SO_2 concentration approaches the oxidant concentration, depletion by oxidation can become apparent. The early cloud is also optically thick; thus, radiation is shielded from the core of the cloud, which might further retard photochemical oxidation.

Without heterogeneous chemistry acting in the cloud, and by ignoring possible significant direct injections of SO_4^- by the volcano, the calculated $\text{SO}_4^-/\text{SO}_2$ ratio behaves as shown in figure 1. Basically, the SO_4^- concentration in the cloud is determined by the ambient SO_4^- concentration in the air which dilutes the cloud plus the small amount of SO_4^- produced by homogeneous photochemical SO_2 oxidation. The slow increase in the ratio seen in figure 1 is due principally to SO_2 dilution, not SO_2 oxidation, in the cloud.

Comparison of the calculations and data in figure 1 indicates that a 15 percent/hr maximum SO_2 to SO_4^- conversion rate can explain both the low (early) $\text{SO}_4^-/\text{SO}_2$ ratios and high (late) $\text{SO}_4^-/\text{SO}_2$ ratios. If heterogeneous chemistry did not occur, then two distinct types of initial eruption clouds would be envisioned: those rich in SO_2 and those rich in SO_4^- . However, according to the results shown in figure 1, an SO_2 -rich cloud would not explain the low $\text{SO}_4^-/\text{SO}_2$ ratio at day 27 unless some combination of the following effects also applies: (i) the cloud dilution rate is significantly slower than that adopted in the model, (ii) the initial SO_2 concentrations in some regions of the eruption plume are much larger than the maximum values observed in other regions (i.e., SO_2 concentrations ≥ 200 ppbv would be called for after 1 day), and (iii) the homogeneous chemical conversion rate of SO_2 into SO_4^- in the cloud is smaller than the simulated rate. On the other hand, the results for OCS and H_2O suggest that the adapted dilution rate is roughly correct (see figs. 2 and 3). As previously mentioned, the data at day 27 in figure 1 may actually be associated with the June 13 eruption, and be at 1 per day. The other points are taken up again in the following paragraphs.

The high $\text{SO}_4^-/\text{SO}_2$ ratios, likewise, could be explained by direct massive sulfate injections in these clouds. However, this would be an exceptional circumstance in volcanology. The low-altitude clouds (< 18 km) of the May 18 eruption were mainly gaseous sulfur in the early stages, as evidenced by direct sampling [14,15]. Farlow et al. [27], Chuan et al. [30], and Rosen and Hofmann [31] also determined that the initial particles were nonvolatile; this condition suggests a rock or glass material with little sulfate (e.g., H_2SO_4) present. The high-altitude clouds (> 18 km) of the May 18 eruption were not sampled for several days; at that time high concentrations of sulfate were found [14]. Rosen and Hofmann [31] also found mainly volatile (sulfate) aerosols in these layers after several weeks. Nonetheless, it seems highly unlikely that sulfates (most likely in a condensed state) would be preferentially lofted above 18 km during the May 18 eruption.

Model calculations were made for lower heterogeneous reaction rates on ash (e.g., 10 percent/hr initially), and with solution (volume) reactions in addition to the surface reactions at various rates. The total initial rate of SO_2 oxidation was always limited to 15 percent/hr. The best results were obtained for the 15 percent ash surface reaction rate including poisoning, but with no solution reactions. Solution reactions alone resulted in a slower overall rate of total sulfur oxidation and removal because, initially, the dry ash did not catalyze SO_2 conversion into condensed SO_4^- , whereas the large ash grains fell out of the stratosphere before they could collect much sulfate. One might conjecture that the ash grains accelerated SO_2 conversion to SO_4^- in the presence of background ozone by providing mineral surfaces that catalyzed the reaction and/or by buffering the acidic solution as it accumulated on the ash [33,36,37].

Certain solution reactions, particularly the reaction of H_2O_2 with SO_2 , can occur in acidic solutions [45]. The source of H_2O_2 in the volcanic plume would be ambient stratospheric air mixed into the clouds at concentrations ≤ 1 ppbv; H_2O_2 is not generated from the water vapor injected with the volcanic clouds because the hydrogen radical precursors of H_2O_2 formation are effectively scavenged by injected SO_2 . Moreover, because the ratio of H_2O_2 to O_3 in background stratospheric air is very small ($\approx 10^{-4}$), it can be demonstrated that H_2O_2 cannot be a dominant volcanic cloud oxidizing agent.

In figure 2 the calculated $\text{H}_2\text{O}/\text{O}_2\text{S}$ ratios are shown. Chemistry has a secondary effect on the ratio, in that SO_2 to SO_4^- conversion produces condensed sulfur which is removed on particles by sedimentation more

efficiently than gaseous sulfur, whereas water vapor is removed principally by diffusion (after 1 day). Inasmuch as the water content of the aerosols is comparable with the sulfur content, the aerosols do not represent a significant sink for H₂O. Even so, the slow increase in the predicted H₂O/O_xS ratio with time in figure 2 is due primarily to dilution of sulfur relative to water as ambient air (which has much more H₂O relative to O_xS than the volcanic emissions) mixes into the clouds.

The H₂O injection is assumed to be 1000 times as large (by number of molecules) as the SO₂ injection in the present simulations. This H₂O injection not only leads to reasonable agreement with the ratio data, but also yields time-dependent H₂O concentrations in accord with the data of Murcray et al. [16] (see table 2). Water vapor emissions are expected to be large in phreatic volcanic explosions such as occurred at Mount St. Helens on May 18. The initial (1 day) H₂O concentrations given in table 3 are below ice saturation levels at typical midlatitude stratospheric temperatures. Extrapolation to the initial eruption plume yields H₂O concentrations which strongly suggest that the water injection is limited by a cold-trap condensation process.

Figure 3 shows data and model calculations for the ratio OCS/O_xS. Heterogeneous chemistry has only a small effect on this ratio. The model reproduces reasonably well the temporal behavior of the ratio. As with water vapor, the volcanic clouds are depleted in OCS relative to O_xS compared with ambient air. Thus, the ratio increases as ambient air is mixed into the clouds.

The time dependence of the absolute concentrations of cloud constituents can provide additional analytical information concerning cloud processes. To this end, specific clouds (altitudes) from the May 18 eruption are considered for which several data points spread over a substantial time interval are available. The data for SO₂, SO₄⁻, and ash concentrations are reproduced in figures 5 to 7, respectively.

The measured SO₂ concentrations in the May 18 eruption clouds (at two different altitude levels) are compared with model calculations in figure 5. The model simulation of the lowest-lying "tropopause" cloud fits very closely the in situ data of Inn et al. [15] and Meixner et al. [18]. Calculations made without heterogeneous chemistry, and without any chemistry at all, do not fit the data. In these latter two cases, the overall fit could be slightly improved by adjusting the initial SO₂ concentrations and cloud dispersion rates (within reasonable bounds) by assuming that the observed values were atypical for the clouds.

A comparison of these two cases also reveals that the gas-phase chemical reactions can deplete SO₂ significantly during the first month. The homogeneous chemistry is accelerated by the high water vapor concentrations in the cloud. The model calculations for the high-altitude clouds which include heterogeneous chemistry are also in accord with the data. However, in this case the limited data could be roughly fitted by the model without surface chemistry if it is assumed that the initial SO₂ concentrations in the clouds 1 day after the eruption were quite low (≈ 1 ppbv). This result would seem to contradict the appearance several weeks later of dense aerosol layers of volatile particles with radii $> 0.1 \mu\text{m}$ [31,46]. As in figure 1, the data points at 27 days in figure 2 appear to be unusual, unless they are associated with the June 13 eruption.

The volcanic clouds with active heterogeneous chemistry are depleted of SO₂ after several weeks (figure 6). The SO₂ concentrations can actually drop below background levels, because of the continuing enhanced concentrations of water vapor and OH in the clouds. These results imply that the major long-term effects of a volcanic eruption are caused by the small aerosols formed during the first month, which are subsequently dispersed around the globe. The quantity of SO₂ gas which survives the early cloud chemistry and spreads over the hemisphere depends sensitively on the initial rates of heterogeneous chemical reactions and their duration, and the water vapor content of the clouds. The amount of SO₂ surviving may also depend on the magnitude of the injection; the larger the eruption, the more likely that SO₂ will persist in the early clouds. For example, higher initial concentrations of SO₂ and fixed oxidant levels would inhibit SO₂ loss in the clouds.

The Mount St. Helens eruption was apparently a small eruption compared, for example, with Agung in 1963. Following Agung, the aerosol mass in the stratosphere remote from the volcano did not peak for several months. The time delays due to SO₂ to SO₄⁻ conversion and cloud dispersion created this apparent aerosol behavior at distant sites. The present calculations suggest that, for some of the Mount St. Helens

clouds, the aerosols may have been formed in ≈ 1 month but took several months to disperse over the Northern Hemisphere. In the next section alternative long-term calculations in which SO_2 is spread “instantaneously” over the hemisphere and aerosol enhancements are caused by homogeneous chemical oxidation of SO_2 are discussed.

The sulfate mass in the high-altitude (> 18 km) clouds is shown in figure 6. The trend in the sulfate data is much less obvious than the trend in the SO_2 data. Nonetheless, the model calculation with heterogeneous chemistry roughly matches the data. A fast rise in SO_4^- is predicted due to reactions on ash grains. Some of the sulfate is promptly removed on the large ash particles. The SO_4^- formed on small ash grains is subsequently diluted by cloud expansion. Sulfate is also continuously generated in the cloud by homogeneous SO_2 oxidation, which helps to maintain the SO_4^- concentration at an elevated level for a longer period of time (fig. 6).

If both fast surface chemistry and substantial sulfate injection by the volcano are neglected, the model prediction in figure 6 falls far short of the measurements. If direct injections of sulfates are proposed, they would have to yield sulfate abundances $\approx 10 \mu\text{g}/\text{m}^3$ after ≈ 3 days. Moreover, initial $\text{SO}_4^-/\text{SO}_2$ ratios > 10 would be required according to table 2 and figure 6. These conditions are generally inconsistent with other measurements of the emissions taken near the volcano [22].

The time-varying burden of volcanic ash in the eruption clouds is shown in figure 7. The selection of a bimodal ash size dispersion (one mode $< 3 \mu\text{m}$, one 3 to $32 \mu\text{m}$, with 5 percent of the mass in the small mode) provides a reasonable match with the time-dependent mass measurements. Note that only ≈ 0.1 $10\text{-}\mu\text{m}$ particles/ cm^3 are needed to carry the requisite mass. The results for the 18 to 20 km clouds appear to imply either slightly smaller initial ash masses at these heights, or less mass in the smaller (longer-lived) size mode. The measurement by Chuan et al. [30] 1 month after the May 18 eruption provides only an upper limit for the ash mass; at that time, much less than $1 \mu\text{g}$ ash/ m^3 -air was observed. Model simulations including a larger fraction of small, buoyant ash particles exhibit sizable overestimates of the long-term ash burden. By allowing for uncertainties, it appears that not more than ≈ 10 percent of the mass of the volcanic ash initially reaching the stratosphere was likely to be in the form of particles $< 3 \mu\text{m}$ in size. Chemistry has only a small impact on the ash burden. The sulfate mass accumulating on ash particles can accelerate ash as well as sulfate removal by sedimentation, although the effect on the ash is small because the sulfate mass is less than the ash mass (except perhaps for very tiny ash grains).

The simulated development of the aerosols in the main cloud of the May 18 Mount St. Helens eruption is depicted in figure 4. Three size modes are prominent in the model calculation. The smallest mode (mode 1, $\approx 0.04 \mu\text{m}$) corresponds to the background aerosol, which is maintained in nearly a constant state as ambient particles are mixed into the cloud. During the evolution of the cloud, the small aerosols grow substantially as H_2SO_4 vapor builds up in the cloud. The mode-1 radius nearly doubles after several days but returns toward ambient over the next month. The mode-1 aerosols are predominantly sulfuric acid, with an admixture of tropospheric Aitken material.

The second aerosol mode (mode 2, $\approx 0.4 \mu\text{m}$) is composed of the fine ash injected by the volcano. These particles decrease steadily in number. During the first week, they also grow in size by accumulating sulfates (mainly H_2SO_4). The ash “core” volume fractions (that is, the fraction of the total particle volume occupied by the ash), which are given in figure 4, indicate that the mode-2 particles are ≤ 30 percent ash after 8 days. After a month, the mode-2 particles dominate the cloud mass (although their numbers are fairly small). These particles contribute to the long-term optical and climate effects which will be discussed shortly.

The largest particle size mode (mode 3, from $3 \mu\text{m}$ to $32 \mu\text{m}$) consists of coarse ash (pyroclasts and glass). Although it is not obvious from the figure, the mode-3 particles initially dominate the mass of the aerosols. Most of the large ash grains fall out of the stratosphere within a week, however, and thus remove the bulk of the injected ash mass.

Chuan et al. [30; also private communication] measured an aerosol mass mode at $0.02 \mu\text{m}$ on July 24, 40 hours after the July 22 eruption, $0.12 \mu\text{m}$ on May 27, 58 hours after the May 25 eruption, and $0.210 \mu\text{m}$ on May 22, 100 hours after the May 18 eruption. (Because of the intake configuration of their instrument on the U-2 aircraft, no particles larger than a few microns were sampled.) The aerosols collected were essentially “pure” sulfuric acid. Chuan et al. interpreted the data in terms of a single aerosol mode which continuously grew in size following injection. The model prediction of figure 4 shows that the mode-1 (ambient)

acid aerosols grow during the first few days, as suggested by the Chuan et al. data. Most of the mass in the model calculation resides in the larger ash modes 2 and 3, whereas Chuan et al. reported a large mass mode ($\approx 1 \mu\text{m}$) on just two occasions (in the high-altitude volcanic cloud samples taken on June 17 and July 24). However, by considering that the Chuan et al. U-2 samples probably excluded the larger ash particles, the correspondence between their observations and the model calculations of the aerosol mode structure is generally satisfactory.

Farlow et al. [27,28] measured ash grain size distributions. In the early clouds they reported a few large particles ($> 1 \mu\text{m}$), whereas in the later clouds they found moderate-sized particles (≈ 0.1 to $1.0 \mu\text{m}$). Because the $0.5\text{-}\mu\text{m}$ ash size mode of Farlow et al. was used to initialize the present calculations, the simulation results agree with their observations fairly well.

Theoretical calculations were made by including homogeneous and ion nucleation. Although such calculations are exceedingly complex and difficult to carry out accurately, it was thought that even rough estimates of nucleation rates in the clouds would be useful. Accordingly, the approximate treatment of nucleation developed by Hamill et al. [5] was employed.

The sulfuric acid supersaturations in some of the clouds are very large at early times ($S \gg 10^6$), and many new particles are generated by homogeneous nucleation. Total particle concentrations $\approx 10^5/\text{cm}^3$ are calculated by the second day at 14 km and 20 km. Most of the particles are smaller than $0.01 \mu\text{m}$. For example, the particle size distributions above $0.06 \mu\text{m}$ in figure 4 are only slightly affected by homogeneous nucleation. However, a nucleation size mode (mode 0) is prominent below $0.06 \mu\text{m}$. This mode, of course, contains sulfuric acid/water solution and no ash.

The supersaturation in some of the cloud layers remains high for several weeks, mainly because of the large initial water vapor injections which are assumed. The supersaturations steadily return to prevolcanic values ($\approx 10^3$ to 10^5) as the injected water vapor dissipates. Ion nucleation is always kinetically limited in the clouds [5]. Homogeneous nucleation is strongly limited by several factors, including unfavorable thermodynamic conditions in the lower stratosphere and H_2SO_4 vapor concentrations that do not build up significantly in the clouds. The latter effect is a consequence of the preponderance of H_2SO_4 formation on ash particles and in droplets where it is permanently sequestered, the slow rate of homogeneous SO_2 oxidation in the cloud, and the large increase in the aerosol surface area upon which H_2SO_4 vapor can collect.

Most of the particles formed by homogeneous nucleation eventually coagulate with the numerous droplets and ash particles already present in the clouds. None of the pure acid nuclei grow spontaneously to large sizes ($\geq 0.1 \mu\text{m}$) in the model, again because of the slow homogeneous SO_2 oxidation rate. However, as mentioned earlier, solution reactions may have occurred which caused some of the small acid aerosols to swell into large droplets. Nevertheless, the present results appear to be consistent with the fact that most of the large acid particles detected in the early clouds of the May 18 eruption contained ash material (although one isolated layer of very pure, large acid aerosols was seen by Farlow et al. [28], and Hofmann and Rosen [46] also reported layers of volatile aerosols over Wyoming, although the composition was not determined). Ash can also be scavenged by originally pure acid aerosols, although this possibility is less likely than aerosol nucleation and growth on ash particles. Thus, although the simulated aerosol concentrations increase dramatically with the onset of homogeneous nucleation, natural processes (coagulation, dispersion) limit the concentrations in the clouds a few weeks old to $\leq 100/\text{cm}^3$.

Homogeneous nucleation does not greatly affect the SO_2 to SO_4^- conversion rate, because the sulfate has to be generated before nucleation can occur. At late times (> 1 month) the supersaturation actually fell slightly below background values, because the enhanced particle surface area reduces H_2SO_4 vapor concentrations, which are only slowly replenished by homogeneous photochemistry.

One month after the May 18 eruption, Rosen and Hofmann [31] reported unusually high condensation nuclei (cn) concentrations ($\approx 500/\text{cm}^3$ with radii $> 0.01 \mu\text{m}$) in the remnant stratospheric clouds at altitudes from 13 to 15 km and 18 to 20 km. Background cn concentrations are typically ≈ 1 to $10/\text{cm}^3$. At about the same time, Rodgers et al. [47] found cloud condensation nuclei (ccn) concentrations of 100 to $200/\text{cm}^3$ in aged volcanic plumes at ≈ 19 km. By comparison with the observations, after 1 month the model predicts $\approx 100/\text{cm}^3 > 0.01 \mu\text{m}$ and $\approx 250/\text{cm}^3 > 0.005 \mu\text{m}$ at 14 km, and $\approx 50/\text{cm}^3 > 0.01 \mu\text{m}$ and $\approx 60/\text{cm}^3 > 0.005 \mu\text{m}$ at 20 km. Accordingly, the observed enhancements in small stratospheric aerosols may have been due to nucleation in the early clouds, as calculated here.

In the model simulation, the concentration of particles with radii greater than $0.15\ \mu\text{m}$ ($n_{0.15}$) decreases from an initial value $\approx 20/\text{cm}^3$ to about $1/\text{cm}^3$ after 30 days, both with and without homogeneous nucleation. The data of Rosen and Hofmann [31] show values about 10 times larger than the model predictions in some of the cloud layers, but values reasonably close to the model in other layers. Importantly, the Rosen and Hofmann data are not spatially or temporally averaged to a great degree, as is the bulk of the data employed in the present analysis. Their data do provide an indication of significant cloud heterogeneity, however.

The calculated aerosol size ratio (i.e., $n_{0.15}/n_{0.25}$) increases steadily with time from an initial value of about 1.0 to a value of about 2.0 in 30 days. The Rosen and Hofmann [31] data show a similar trend, but with much larger ratios (≈ 10) in some of the later clouds. This result indicates that the calculated size distribution in figure 4 has fewer particles $\geq 0.1\ \mu\text{m}$ and/or more particles $\geq 0.25\ \mu\text{m}$ than were observed in certain eruption clouds. On the other hand, the model prediction is in general agreement with the detailed size distribution measurements of Chuan et al. [30] and Farlow et al. [27,28]. The concentration of particles larger than $0.1\ \mu\text{m}$ has a strong bearing on the optical properties of the aerosols. A substantial uncertainty is therefore implied by the disagreements between some of the data and the model simulations.

The findings of the short-term simulations of the Mount St. Helens stratospheric eruption cloud can be summarized as follows. A comparison of model calculations with observational data suggests that heterogeneous chemistry proceeded rapidly during the early stages of cloud development (< 3 days). However, the existing measurements are inconclusive, and alternative—although less compelling—explanations of the data are possible. The volcanic particle size distribution may have consisted of (at least) four modes. Mode 0, below $0.01\ \mu\text{m}$, contained homogeneously nucleated particles. Mode 1, between ≈ 0.01 and $0.1\ \mu\text{m}$, was comprised essentially of ambient aerosols which mixed into the cloud, and which grew in size. Modes 2 and 3 consisted of volcanic ash particles, often mantled in acid. The large ash grains (mode 3, above $\approx 3\ \mu\text{m}$) promptly fell out of the stratosphere (< 1 week). The mode-2 particles, between ≈ 0.1 and $3.0\ \mu\text{m}$, were mostly acid within a few days of each eruption, and persisted for several weeks. After a month, an enhanced “ambient” aerosol layer was apparent, which was maintained by slow homogeneous oxidation of injected SO_2 into vapors that could plate out onto pre-existing cloud particles.

B. Long-Term Volcanic Clouds

For the long-term Mount St. Helens aerosol simulations, specific quantities of sulfur gases, water vapor, and fine ash are injected simultaneously throughout the stratosphere over the Northern Hemisphere (table 3). The initial conditions for these simulations are based on the gas and ash measurements taken in the major eruption clouds in the stratosphere on May 19 (e.g., table 2). The initial injection masses are derived by using measured concentrations and estimated plume volumes [35]. The mass inventories are, hence, only rough approximations. Injection heights of 14 and 20 km are chosen to represent the low altitude “tropopause” cloud and the high altitude cloud(s), respectively. The early dispersive cloud processes and heterogeneous chemistry are ignored. The possible cumulative effects of the secondary eruptions of May 25 and June 13 are also neglected, as these were much smaller events. Because of differences in the mode of injection and the physical processes treated, the long-term aerosol calculations cannot be compared directly with the short-term calculations for the same time intervals. Calculations coupling the early and late time regimes are best carried out by using multidimensional models.

Previously, a preliminary calculation was made of the impact of the 1963 Mount Agung eruption on the global stratospheric aerosol [48]. A very rapid increase in aerosol size and mass following Mount Agung was found, with substantial effects on the radiation balance of Earth. The simulated Mount St. Helens sulfur injections are much smaller than those of Mount Agung; consequently, the related aerosol effects are expected to be smaller.

The calculated variations in the optical depth of the stratospheric aerosols at 550 nm caused by the Mount St. Helens eruptions of May and June are summarized in figure 8. The opacity is computed by assuming the optical constants and Mie scattering coefficients of pure sulfuric acid droplets. In accord with published estimates of the physical extent of the clouds and SO_2 concentrations in the clouds [15], a total SO_2 injection of 10^6 tonnes (1 tonne = 10^6 g)—half at 14 km and half at 20 km—is chosen. In one simulation, a massive amount of water vapor (10^9 tonnes) is also injected to evaluate its effect on chemical time constants. A case

with a larger sulfur injection (10^7 tonnes of SO_2) is included in order to contrast a “minor” eruption with a “major” one. About 10^6 tonnes of fine ash is initially included in each calculation. (See table 3 for details.)

The perturbation optical depth ($\Delta\tau$) due to the volcano is the difference between the total optical depth of figure 8 and the optical depth obtained from an ambient aerosol simulation [2], which is about 3×10^{-3} . The ash immediately contributes an optical depth of 3×10^{-3} to the total opacity. The ash opacity diminishes by one-half in about 1 month; however, with an SO_2 injection of 10^6 tonnes, the aerosol opacity roughly triples in 4 months ($\Delta\tau \approx 7 \times 10^{-3}$), then decreases over the next 1 to 2 years and returns to ambient values.

With the larger SO_2 injection, the oxidation time is lengthened to about 6 months. This condition is expected because at high SO_2 concentrations the rate of the key oxidation reaction



is limited by the rate of formation of odd hydrogen ($\text{OH} + \text{HO}_2$) [49]. Thus, in equation (4), the maximum rate of homogeneous SO_4^- production is limited to $P_1[\text{H}_2\text{O}]$ molecules/ $\text{cm}^3\text{-s}$. As the amount of SO_2 increases, therefore, the fractional rate of SO_2 oxidation decreases. It follows that H_2O injection can accelerate SO_2 oxidation, other factors remaining equal. This effect is demonstrated by the $\text{SO}_2/\text{H}_2\text{O}$ injection curve in figure 8, where the peak optical depth occurs after only 2 to 3 months. The H_2O acceleration assumes, among other things, that the radiation and ozone fields are not significantly perturbed. Note that an H_2O injection of 10^9 tonnes is roughly equivalent to doubling the stratospheric water vapor content. For the Mount St. Helens clouds beyond a week or so, $\Delta\tau \leq 10^{-2}$ implies little effect on the average radiation intensities reaching the ground. Calculations to be discussed shortly reveal, in addition, that ozone is not greatly affected by the Mount St. Helens injections.

A ten-fold increase in the SO_2 injection yields a four- to five-fold increase in $\Delta\tau$ from $\approx 7 \times 10^{-3}$ to $\approx 3 \times 10^{-2}$. The lower “optical” efficiency of a large SO_2 injection is explained by a reduced SO_2 to SO_4^- conversion rate (creating a time lag during which sulfur may be removed from the stratosphere), and by the fact that the particle optical cross section varies as $\approx r^2$ while the particle mass varies as $\approx r^3$ and the particle removal rate as $\approx r^{4.5}$ (where r is the particle radius). Thus, a large mass injection leads to larger particles that may be optically less efficient per unit mass than slightly smaller particles; these larger particles also remain in the stratosphere a shorter time.

The SO_2 injection of 10^6 tonnes causes the particles at 20 km to grow from $\approx 0.08 \mu\text{m}$ to $\approx 0.16 \mu\text{m}$. A ten-fold increase in the SO_2 injection leads to particle growth from $\approx 0.08 \mu\text{m}$ to $\approx 0.32 \mu\text{m}$. In both cases, the SO_2 injection at 14 km has a much smaller effect than the injection at 20 km, because the injected gases and perturbed aerosols at 14 km have a shorter residence time in the stratosphere.

The injection of 10^7 tonnes of SO_2 into the stratosphere yields an optical depth which is only ≈ 20 percent of that observed after the Mount Agung eruption. This result suggests that Agung may have injected $\approx 10^8$ tonnes of SO_2 into the stratosphere, or perhaps less SO_2 but at higher altitudes. This injection figure is more than 100 times the yearly sulfur input to the background aerosols.

Toon [50] discusses the possible climatic impact of the Mount St. Helens eruptions. He points out that optical measurements of the clouds made prior to their spreading over the entire hemisphere yielded a perturbation optical depth $\Delta\tau \approx 3 \times 10^{-2}$. This is roughly consistent with the present estimates, if the clouds are confined to roughly one-third of the Northern Hemisphere during the first 3 months. Toon [50] concluded that the Mount St. Helens eruption had little effect on climate. By utilizing previous radiation transport calculations carried out by Pollack et al. [51] and the optical depths predicted here, a maximum surface temperature decrease during 1980/81 < 0.05 K is forecast for the Northern Hemisphere.

C. Long-Term Ozone Perturbations

Previous theoretical studies of the effects of volcanic eruptions on stratospheric ozone were hampered by a lack of critical data. Volcanic emissions that can affect ozone concentrations include chlorine gases, water vapor, and nitrogen oxides. Stolarski and Butler [11] attempted to estimate the amount of chlorine injected above the tropopause by a large volcanic eruption and had considerable trouble arriving at a reliable number. They also neglected the water vapor injection, which clearly may be important [52]. Fortunately,

the St. Helens cloud measurements of Inn et al. [15], Gandrud and Lazrus [14], and Murcray et al. [16] provide a fairly complete data set upon which detailed ozone calculations can be based. A key observation was the depletion of HCl relative to SO₂ in the clouds. The major chlorine-carrying compound detected by Inn et al. [15] is methyl chloride. This interesting finding is reflected in the Mount St. Helens injection inventories listed in table 3. The Cl injection is about 10⁴ to 10⁵ tonnes, compared with about 10⁶ to 10⁷ tonnes of SO₂ and 10⁸ to 10⁹ tonnes of H₂O. NO_x injections are neglected, as discussed earlier. Effects of the clouds on radiation are also ignored. The ozone abundance is calculated in an expanding cloud with a complete photochemical reaction scheme without aerosols. Vertical mixing is accounted for. Horizontal expansion is halted when the cloud fills a hemisphere.

The computed stratospheric ozone column concentration decreases with time to a minimum of about 0.2 percent below ambient values after 1 year. The ozone steadily recovers to background values in about 2 years. The effect of the volcano is minor because the magnitude of the chlorine injection is small compared with the yearly budget of stratospheric chlorine ($\approx 10^6$ tonnes Cl/yr), and the photochemical response time of ozone in the lower stratosphere is comparable with, or greater than, the dispersion time of the cloud. That is, the chlorine injections could only lead to substantial ozone changes if maintained in a localized cloud. The argument applied to the chlorine injection can also be applied to the water vapor injection of Mount St. Helens. Thus, although a large quantity of water was deposited in the stratosphere, the global-scale H₂O perturbation was relatively small. Finally, the volcanic injections which lie close to the tropopause have a short stratospheric lifetime, and little impact on ozone.

The OH concentrations in the volcanic clouds vary in accordance with the injected quantities of SO₂ and H₂O. The simple empirical OH [equation (4)] was checked against the detailed OH calculations of the ozone model and the accuracy of equation (4) was ascertained. OH is a critical stratospheric species which participates in many other photochemical reaction cycles. Hence, any attempt to model the chemistry of volcanic eruption clouds must take into account the H₂O and SO₂ influence on OH abundances.

V. CONCLUSIONS

Based on detailed physicochemical simulations of the Mount St. Helens eruption clouds of May 18, May 25, and June 13, 1980, provisional conclusions about the nature of the stratospheric plumes have been reached.

1. Heterogeneous chemical conversion of SO₂ into sulfate may have contributed to the early development of the Mount St. Helens eruption clouds. The SO₂ and SO₄⁻ data collected in the clouds provide circumstantial evidence for an initial SO₂ oxidation rate (involving ash particles) of 15 percent/hr. Rapid poisoning and removal of the ash may have terminated the reaction. Some measurements suggest that large quantities of SO₄⁻ (relative to SO₂) were injected directly into the stratosphere; this hypothesis is less plausible based on the preponderance of observations made in the clouds and near the volcano, including data from previous volcano studies.

2. Stratospheric water vapor injection by the volcano was important in several respects: it created a medium in which aqueous sulfur reactions could occur, it generated excess OH radicals which affected the SO₂ oxidation rate via homogeneous chemistry, it established the conditions under which homogeneous nucleation could proceed freely, and it participated in the chemical cycles that control stratospheric ozone.

3. The volcanic ash lofted into the stratosphere by the Mount St. Helens eruption consisted of numerous small particles (< 3 μm) containing < 10 percent of the mass, and a relatively few large particles (> 3 μm) holding the rest of the mass. The large ash promptly fell out of the stratosphere (≈ 1 month), leaving acid aerosols, some with ash cores, as the dominant long-term volcanic particles. Even so, most of the fine volcanic ash particles were removed from the stratosphere by sedimentation and diffusion after ≈ 3 months.

4. The size dispersion of the volcanic particles may have exhibited at least four modes. The smallest mode (< 0.01 μm) consisted of aerosols formed by homogeneous nucleation. A size mode from about 0.01 to 0.1 μm was dominated by ambient aerosols continuously mixed into the cloud. Two additional size modes related to the volcanic ash injection were mentioned in conclusion 3.

5. The Mount St. Helens eruption could have produced roughly a three-fold aerosol enhancement over the Northern Hemisphere in the fall and winter of 1980. The maximum volcanic turbidity (optical depth) at 550 nm averaged over the hemisphere was estimated as $\approx 7 \times 10^{-3}$ 4 months after the major eruption of May 18. Accounting for incomplete hemispheric dispersion of the aerosol during this time span, the increase in optical depth observed at mid-latitudes could have been as large as 2 to 3×10^{-2} . This turbidity increase is about one-half of that attending the Fuego eruption in 1974, and one-tenth of that in the Northern Hemisphere following the Agung eruption of 1963. Accordingly, the climatic impact of Mount St. Helens may be crudely forecast as a Northern Hemisphere surface cooling ≤ 0.05 K for about 1 year, which is negligible.

6. The effects of the Mount St. Helens emissions on stratospheric ozone are very small. A maximum ozone depletion ≤ 0.2 percent is predicted for early 1981. The chlorine injected above the tropopause by the eruption was only 1 to 10 percent of the sulfur injection. Rainout of soluble chlorine in the eruption plume is thought to explain the chlorine fractionation [10]. If Mount St. Helens is typical, volcanoes are only a small source of stratospheric chlorine. Overall volcanic production of CO and NO_x is found to be negligible.

The reported model simulations demonstrate the usefulness of detailed theoretical calculations in organizing and interpreting the wide variety of data which can be collected in volcanic eruption clouds by modern instruments. A model can blend the diversity of information pertaining to cloud heights and sizes, gaseous constituent concentrations, and ash and droplet masses and size dispersions, and can provide a unified picture of the chemistry and physics occurring in the clouds. However, full utilization of the model requires a consistent data set to guide the simulations. In the present case, the data base is incomplete in several respects (e.g., lack of simultaneous measurements of the time variations of SO₂ and SO₄⁻ concentrations in individual cloud layers, together with aerosol droplet and ash size distributions), and final scientific conclusions cannot be reached. Nonetheless, a variety of helpful inferences are drawn by systematic analysis of the Mount St. Helens data and by comparison of data with particle/gas simulations.

What is needed in future experimental work on high-altitude volcanic eruption clouds is a time series of measurements of the particles and gases (including oxidants such as ozone) in specific clouds. The measurements should begin within 1 day of the eruption and continue periodically for several weeks to 1 month afterwards. Obviously, such a program would be extremely difficult to undertake, involving the isolation and accurate tracking of particular clouds, the complex logistics of intercepting target clouds, and the technical problems associated with precise sampling of gases and aerosols in the clouds. Eruption clouds in the upper troposphere are more accessible, but are subject to strong meteorological influences and are short-lived. Moreover, it is unlikely that the emission inventories of tropospheric clouds can be applied directly to the stratospheric clouds. Yet practically all the important long-term, widespread impacts of volcanic eruptions are dependent on the stratospheric clouds. Due to the fact that these latter clouds lie well above the flight ceilings of most aircraft, have high velocities, and are difficult to track, extraordinary means will have to be devised to retrieve the valuable scientific information which they hold.

ACKNOWLEDGMENT

The authors thank the many researchers who participated in the NASA Ames U-2 flights into the Mount St. Helens eruption clouds for the early use of their data and continuing advice and insights into results which made this work possible. We particularly acknowledge discussions with E. C. Y. Inn and N. H. Farlow of NASA Ames, A. L. Lazrus of NCAR, and J. M. Rosen of the University of Wyoming.

REFERENCES

1. Turco, R. P., Hamill, P., Toon, O. B., Whitten, R. C., and Kiang, C. S. (1979): A one-dimensional model describing aerosol formation and evolution in the stratosphere: I. Physical processes and mathematical analogs, *J. Atmos. Sci.*, vol. 36, pp. 699-717.
2. Toon, O. B., Turco, R. P., Hamill, P., Kiang, C. S., and Whitten, R. C. (1979): A one-dimensional model describing aerosol formation and evolution in the stratosphere: II. Sensitivity studies and comparison with observations, *J. Atmos. Sci.*, vol. 36, pp. 718-736.
3. Turco, R. P., Toon, O. B., Hamill, P., and Whitten, R. C. (1981): Effects of meteoric debris on stratospheric aerosols and gases, *J. Geophys. Res.*, vol. 86, pp. 1113-1128.
4. Turco, R. P., Whitten, R. C., Toon, O. B., Inn, E. C. Y., and Hamill, P. (1981): Stratospheric hydroxyl radical concentrations: New limitations suggested by observations of gaseous and particulate sulfur, *J. Geophys. Res.*, vol. 86, pp. 1129-1139.
5. Hamill, P., Turco, R. P., Toon, O. B., Kiang, C. S., and Whitten, R. C. (1981): On the formation of sulfate aerosol particles in the stratosphere, *J. Aerosol Sci.*, (in press).
6. Hudson, R. D., and Reed, E. I., Eds. (1978): *The Stratosphere: Present and Future*, NASA RP-1049
7. Rasmussen, R. A., Dalluge, R. W., Penkett, S. A., and Jones, B. (1982): Carbonyl sulphide and carbon di-sulphur from the eruption of Mount St. Helens, *Science*, 215, 665-667.
8. Moyers, J. (1980): Results of the September 22, 1980 RAVE study of the Mount St. Helens plume, paper presented at the NASA Symposium on Mount St. Helens Eruption: Its Atmospheric Effects and Potential Climatic Impact (Washington, D.C.), Nov. 18-19, 1980. (Paper not included in this compilation.)
9. Cadle, R. D., Lazrus, A. L., Huebert, B. J., Heidt, L. E., Rose, W. I., Jr., Woods, D. C., Chuan, R. L., Stoiber, R. E., Smith, D. B., and Zielinski, R. A. (1979): Atmospheric implications of studies of Central American volcanic eruption clouds, *J. Geophys. Res.*, vol. 84, pp. 6961-6968.
10. Lazrus, A. L., Cadle, R. D., Gandrud, B. W., Greenberg, J. P., Huebert, B. J., and Rose, W. I., Jr. (1979): Sulfur and halogen chemistry of the stratosphere and of volcanic eruption plumes, *J. Geophys. Res.*, vol. 84, pp. 7869-7875.
11. Stolarski, R. S., and Butler, D. M. (1978): Possible effects of volcanic eruptions on stratospheric minor constituent chemistry, *Pure & Appl. Geophys.*, vol. 117, pp. 4009-4017.
12. Johnston, D. A. (1980): Volcanic contribution of chlorine to the stratosphere more significant to ozone than previously estimated, *Science*, vol. 209, pp. 491-493.
13. Evans, W. F. J., Asbridge, I. A., Kerr, J. B., Mateer, C. L., and Olafson, R. A. (1981): The effects of SO₂ on Dobson and Brewer total ozone measurements, preprint, Atmos. Env. Service (Ontario, Canada).
14. Gandrud, B. W., and Lazrus, A. L. (1981): Filter measurements of stratospheric sulfate and chloride in the eruption plume of Mount St. Helens, *Science*, vol. 211, pp. 826-827.
15. Inn, E. C. Y., Vedder, J. F., Condon, E. P., and O'Hara, D. (1981): Gaseous constituents in the plume from eruptions of Mount St. Helens, *Science*, vol. 211, pp. 821-823.
16. Murcray, D. G., Murcray, F. J., Barker, D. B., and Mastenbrook, H. J. (1981): Changes in stratospheric water vapor associated with the Mount St. Helens eruption, *Science*, vol. 211, pp. 823-824.
17. Sedlacek, W. A., Heiken, G. H., Mroz, E. J., Gladney, E. S., Perrin, D. R., Leifer, R., Fisenne, R., Hinchliffe, L., and Chuan, R. (1980): Physical and chemical characteristics of Mount St. Helens airborne debris, *Atmospheric Effects and Potential Climatic Impact of the 1980 Eruptions of Mount St. Helens*, NASA CP-2240, 1982. (Paper no. 8 of this compilation.)
18. Meixner, F. X., Georgii, H. W., Ockelmann, G., Jager, H., and Reiter, R. (1981): The arrival of the Mount St. Helens eruption cloud over Europe, *Geophys. Res. Lett.*, vol. 8, pp. 163-166.
19. Heald, E. F., Naughton, J. J., and Barnes, I. L., Jr. (1963): The chemistry of volcanic gases, *J. Geophys. Res.*, vol. 68, pp. 545-557.
20. Stith, J. L., Hobbs, P. V., and Radne, L. F. (1978): Airborne particle and gas measurements in the emission from six volcanoes, *J. Geophys. Res.*, vol. 83, pp. 4009-4017.
21. Hobbs, P. V., Radke, L. F., Hegg, D. A., Elgroth, M. W., and Tuell, J. P. (1980): Comparisons between airborne measurements of the volcanic emissions from Mount St. Augustine 1976 and Mount St. Helens 1980, *Trans. Am. Geophys. Union*, vol. 61, p. 1153.

22. Hobbs, P. V., Radke, L. F., Elgroth, M. W., and Hegg, D. A. (1981): Airborne studies of the emissions from the volcanic eruptions of Mount St. Helens, Science, vol. 211, pp. 816-818.
23. Cobb, W. E. (1980): Electric fields and lightning in the Mount St. Helens volcanic cloud, Trans. Am. Geophys. Union, vol. 61, p. 978.
24. Chameides, W. L. (1979): Effect of variable energy input on nitrogen fixation in instantaneous linear discharges, Nature, vol. 277, pp. 123-125.
25. Hill, R. D., Rinker, R. G., and Wilson, H. D. (1980): Atmospheric nitrogen fixation by lightning, J. Atmos. Sci., vol. 37, pp. 179-192.
26. Levine, J. S., Hughes, R. E., Chameides, W. L., and Howell, W. E. (1979): N₂O and CO production by electric discharge: Atmospheric implications, Geophys. Res. Lett., vol. 6, pp. 557-559.
27. Farlow, N. H., Snetsinger, K. G., Oberbeck, V. R., Ferry, G. V., Polkowski, G., and Hayes, D. M. (1980): Time variations of aerosols in the stratosphere following Mount St. Helens eruptions, paper presented at Mount St. Helens Symposium (Washington, D. C.), Nov. 18-19, 1980.
28. Farlow, N. H., Oberbeck, V. R., Snetsinger, K. G., Ferry, G. V., Polkowski, G., and Hayes, D. M. (1981): Size distributions and mineralogy of ash particles in the stratosphere from eruptions of Mount St. Helens, Science, vol. 211, pp. 832-834.
29. Vossler, T., Anderson, D. L., Aras, N. K., Phelan, J. M., and Zoller, W. H. (1981): Trace element composition of the Mount St. Helens plume: Stratospheric samples from the 18 May eruption, Science, vol. 211, pp. 827-830.
30. Chuan, R. L., Woods, D. C., and McCormick, M. P. (1981): Characterization of aerosols from eruptions of Mount St. Helens, Science, vol. 211, pp. 830-832.
31. Rosen, J. M., and Hofmann, D. J. (1980): Dustsonde measurements following the Mount St. Helens eruption, Abstracts of the Tenth International Laser Radar Conference (Silver Spring, Md.), Oct. 6-9, 1980, AMS, pp. 155-156.
32. Barrett, E. W., Pueschel, R. F., and Wellman, D. L. (1980): Temporal variations of physical and optical properties of Mount St. Helens volcanic aerosol size distribution, Abstracts of the Tenth International Laser Radar Conference (Silver Spring, Md.), Oct. 6-9, 1980, AMS, pp. 153-154.
33. Fruchter, J. S., et al. (1980): Mount St. Helens ash from the 18 May 1980 eruption: Chemical, physical, mineralogical, and biological properties, Science, vol. 209, pp. 1116-1125.
34. Bauer, E. (1974): Dispersion of tracers in the atmosphere and ocean: Survey and comparison of experimental data, J. Geophys. Res., vol. 79, pp. 789-795.
35. Danielsen, E. F. (1981): Trajectories of the Mount St. Helens eruption plume, Science, vol. 211, pp. 819-821.
36. Hooper, P. R., Herrick, I. W., Laskowski, E. R., and Knowles, C. R. (1980): Composition of the Mount St. Helens ashfall in the Moscow-Pullman area on 18 May 1980, Science, vol. 209, pp. 1125-1126.
37. Taylor, H. E., and Lichte, F. E. (1980): Chemical composition of Mount St. Helens volcanic ash, Geophys. Res. Lett., vol. 7, pp. 949-952.
38. Turco, R. P., and Whitten, R. C. (1977): The NASA Ames Research Center One- and Two-Dimensional Stratospheric Models, Part I: The One-Dimensional Model, NASA TP-1002, 29 pp.
39. Turco, R. P., and Whitten, R. C. (1978): A note on the diurnal averaging of aeronomical models, J. Atmos. Terr. Phys., vol. 40, pp. 13-20.
40. DeMore, W. B., Stief, L. J., Kaufman, F., Golden, D. M., Hampson, R. F., Jr., Kurylo, M. J., Margitan, J. J., Molina, M. J., and Watson, R. T. (1979): Chemical Kinetic and Photochemical Data for Use in Stratospheric Modeling, JPL Publication 79-27, 124 pp.
41. Draxler, R. R. (1980): Observing and forecasting the path of volcanic emissions after an eruption, Abstracts of the Tenth International Laser Radar Conference (Silver Spring, Md.), Oct. 6-9, 1980, AMS, pp. 136-137.
42. McCormick, M. P., Fuller, W. H., Jr., Hunt, W. H., and Swissler, T. J. (1980): Lidar measurements of ash clouds from the Mount St. Helens volcanic eruption, Abstracts of the Tenth International Laser Radar Conference (Silver Spring, Md.), Oct. 6-9, 1980, AMS, pp. 138-139.
43. Moller, D. (1980): Kinetic model of atmospheric SO₂ oxidation based on published data, Atm. Env., vol. 14, pp. 1067-1076.

44. Peterson, T. W., and Seinfeld, J. H. (1979): Heterogeneous condensation and chemical reaction in droplets—Application to the heterogeneous atmospheric oxidation of SO₂, Advances in Environmental Science and Technology (J. N. Pitts, R. L. Metcalf, and D. Grosjean, eds.), vol. 10, pp. 125-180.
45. Martin, L. R., and Damschen, D. E. (1980): Aqueous oxidation of sulfur dioxide by hydrogen peroxide at low pH, preprint, Aerospace Corp., El Segundo, CA.
46. Hofmann, D. J., and Rosen, J. M. (1981): Balloon-borne observations of stratospheric aerosol and condensation nuclei during the year following the Mount St. Helens eruption. U. of Wyoming Report AP-63, 79 pp.
47. Rodgers, C. F., Hudson, J. G., and Kocmond, W. C. (1981): Measurements of cloud condensation nuclei in the stratosphere around the plume of Mount St. Helens, Science, vol. 211, pp. 824-825.
48. Turco, R. P., Toon, O. B., Whitten, R. C., Hamill, P., and Kiang, C. S. (1977): Properties of the stratospheric aerosol layer studies with a one-dimensional computer model, Proceedings Fourth Joint Conf. Sensing Environmental Pollutants, Am. Chem. Soc., pp. 683-688.
49. Cadle, R. D. (1980): Some effects of the emissions of explosive volcanoes on the stratosphere, J. Geophys. Res., vol. 85, pp. 4495-4498.
50. Toon, O. B. (1980): Volcanoes and climate, paper prepared for NASA workshop on the potential climate effects of Mount St. Helens (Washington, D.C.), Nov. 20-21, 1980.
51. Pollack, J. B., Toon, O. B., Sagan, C., Summers, A., Baldwin, B., and Van Camp, W. (1976): Volcanic explosions and climatic change: a theoretical assessment, J. Geophys. Res., vol. 81, pp. 1071-1083.
52. Bauer, E. (1979): A catalog of perturbing influences on stratospheric ozone, 1955-1975, J. Geophys. Res., vol. 84, pp. 6929-6940.

TABLE 1. COMPOSITION OF THE EMISSIONS OF MOUNT ST. HELENS

Emitted Species	Principal Roles	Relative Abundances		
		Ambient Air (1)	Fumarolic (2)	Stratospheric Plume (3)
H ₂ O	Cloud formation, initiate HO _x chemistry, washout of SO ₄ ⁻ , Cl ⁻ and NO ₃ ⁻	3-5 x 10 ⁻⁶	~ 10 ⁻²	~ 10 ⁻⁴
SO ₂	} Precursors of sulfate aerosols Consume OH radicals	~ 5 x 10 ⁻¹¹	} ~ 10 ⁻⁵	~ 10 ⁻⁷
H ₂ S		≤ 10 ⁻⁹		≤ 10 ⁻⁹
OCS		1-5 x 10 ⁻¹⁰		~ 10 ⁻⁹
CS ₂		≤ 10 ⁻¹²		≤ 10 ⁻¹⁰
HCl	} Ozone catalysis	~ 10 ⁻¹⁰	} ~ 10 ⁻⁵	≤ 10 ⁻⁹
CH ₃ Cl		~ 10 ⁻¹⁰		~ 10 ⁻⁹
CH ₃ Br		~ 10 ⁻¹¹		—
S/Cl (4)		~ 0.1 - 1.0	~ 1.0	1.0 - 100.0
CO ₂	Infrared transmission	3.6 x 10 ⁻⁴	~ 3.6 x 10 ⁻⁴	3.6 x 10 ⁻⁴
CO	Tracer of OH	~ 10 ⁻⁸	?	~ 10 ⁻⁷
NH ₃	Aerosol reactions	≤ 10 ⁻¹⁰		—
N ₂ O	Precursor of NO _x	~ 10 ⁻⁷	?	~ 10 ⁻⁷
NO _x	Active in ozone cycles	≤ 10 ⁻⁸		~ 10 ⁻⁸

1. Air in the lower stratosphere. The source of information is Hudson and Reed (1979).
2. Clouds near the volcano. Data sources are given in the text.
3. See the text for a discussion of the stratospheric data.
4. Molar ratio, for gases plus particles.

TABLE 2. GASEOUS AND CONDENSED SPECIES¹ IN THE STRATOSPHERIC MOUNT ST. HELENS CLOUDS

Date/Height/ Eruption (mo-d/km/⊕)	Lat/Long/UT (°N/°W/hour)	SO ₄ [*] (ppbv)	SO ₂ (ppbv)	H ₂ O (ppmv)	CH ₃ Cl (ppbv)	Cl ⁻ (ppbv)	OCS (ppbv)	NO ₃ ⁻ (ppbv)
5-18 ①								
5-19/13.1/1		3.9 (g)				0.40 (solid) (g)		
14.0	44.4/108.6/16:06	2.7 (g)	> 111. ± 24. (174. ± 17.) (i)		2.9 ± 0.4 (i)	~ 10. (i) ² 0.27 (solid) (g) 2.0 (gas)	0.87 ± 0.11 (i)	6.2 ± 0.6 (i)
15.2	45.2/111.0/15:39	1.1 (g)	> 10.4 ± 1.0 (42.0 ± 4.0) (i)		2.0 ± 0.3 (i)	0.20 (solid) (g) 0.28 (gas)	0.47 ± 0.04 (i)	222. ± 22. (i) ³
16.5	45.8/114.0/15:08		> 1.8 ± 0.4 (i)		0.3 ± 0.04 (i)		0.067 ± 0.009 (i)	
17.7		4.1 (g)				1.6 (solid) (g)		
5-20/15.2/1	39/100/	8.0 (s)						
5-20/>12/1	44/79/22:		~ 200. (e) ⁴					
5-21/>12/1	44/79/18:		~ 100. (e) ⁴					
5-22/18.3/1	~ 38/107/	0.2-11.0 (s)						
5-22/18.6-20.1/1	46:1/113.3/18:38	6.4 (g)	0.091 ± 0.011 (i)	24.-60. (m)	1.3 ± 0.2 (i)	0.06 (solid) (g)	0.38 ± 0.11 (i)	
20.1-20.7	47.0/113.5/19:38	79.0 (g)	0.082 ± 0.037 (i)	30.-160. ⁵	5.0 ± 1.2 (i)	0.07 (solid) (g)	1.2 ± 0.36 (i)	
20.1	46.3/114.0/20:09	25.0 (g)	> 4.2 ± 0.55 (i)	4.5-38. (m)	3.2 ± 0.4 (i)	0.30 (solid) (g)	0.91 ± 0.36 (i)	
20.7	47.3/112.6/19:38	0.93 (g)	0.083 ± 0.011 (i)	3.8-7.5 (m)	0.2 ± 0.02 (i)	0.016 (solid) (g) 0.42 (gas)	0.022 ± 0.004 (i)	
5-25 ②								
5-26/10-13/1	58/-3/12:		0.40 ± 0.10 (x)					
5-27/15.2/2	52.3/129.0/1:41	8.4 (g)	0.017 ± 0.004 (i)		0.4 ± 0.05 (i)		0.28 ± 0.037 (i)	
16.8/2	51.0/127.6/2:07		0.011 ± 0.004 (i)	~ 7.0 (m)	0.7 ± 0.09 (i)	0.48 (solid) (g) 0.90 (gas)	0.19 ± 0.025 (i)	
18.3/2 ⁶	48.5/125.4/2:35	(2.7 ± 0.27) (i) ⁷	0.26 ± 0.033 (i)		0.21 ± 0.03 (i)	~ 4.7 (i) ²	0.044 ± 0.066 (i)	6.1 ± 0.6 (i)
/2	46.4/124./2:56		0.067 ± 0.020 (i)		0.35 ± 0.05 (i)		0.28 ± 0.037 (i)	
6-13 ③								
6-14/12.8/3		0.27 (g)				0.07 (gas) <0.1 (solid) (g)		
13.1/3	48.4/112.1/21:17		0.13 ± 0.023 (i)	2.3-7.8 (m)			0.073 ± 0.009 (i)	
13.7/3	47.5/112.0/21:44	0.12 (g)	0.072 ± 0.012 (i)	↑ patchy		0.15 (gas) (g)	0.33 ± 0.057 (i)	
14.6/3	45.6/114.6/22:12	0.063 (g)	0.054 ± 0.01 (i)	↓ 2.3-7.8 (m)	0.3 ± 0.04 (i)	0.13 (gas) (g)	0.049 ± 0.008 (i)	
18.9/1	45.8/113.1/20:39	0.42 (g)	> 2.26 ± 0.29 (i) (5.7 ± 0.6)			~ 9.0 (i) ² 0.60 (solid) (g) 0.30 (gas)	0.20 ± 0.026 (i)	48. ± 5.0 (i) ³
6-17/18.3/1	40.0/104.6/19:42	2.3 (g)	0.027 ± 0.004 (i)	3.0-4.0 (m)		<0.1 (solid) (g)	0.24 ± 0.031 (i)	
18.9/1	40.2/104.7/20:11	1.8 (g)	0.046 ± 0.006 (i)	↑ briefly ~ 9.0	0.38 ± 0.05 (i)	<0.1 (solid) (g)	0.23 ± 0.030 (i)	
18.9/1	42.5/107.4/21:12	0.60 (g)	0.039 ± 0.007 (i)	↓	0.30 ± 0.05 (i)	<0.1 (solid) (g)	0.10 ± 0.018 (i)	
18.9/1	42.4/114.3/22:04	(4.0 ± 0.6) (i) ⁷	0.038 ± 0.007 (i)	3.0-4.0 (m)	0.54 ± 0.10 (i)	~ 6.7 (i) ²	0.25 ± 0.044 (i)	< 3.5 ± 0.5 (i)

References: e = Evans et al. (1981); g = Gandrud and Lazrus (1981); i = Inn et al. (1981); m = Murcray et al. (1981); s = Sedlacek et al. (1980); x = Meixner et al. (1981).

¹Inn et al. (1981) detected no H₂S in the stratosphere, some CS₂: ~ 2.8 ± 1.4 pptv on 5-19/15.2 and < 55.0 pptv on 5-19/14.0, and CO: 0.27 and 0.12 ppmv on 5-19/12.2 and 15.2 km respectively, ~ 2.2-4.3 ppmv on 5-22/18.8 and 0.16-0.36 on 5-28/15.2. N₂O, CO₂, CF₂Cl₂ and CFC₃ were unperturbed.

²The Inn et al. (1981) total Cl⁻ (gas plus particle) is based on 1% of the observed Cl⁻ signal (see Inn et al. for an explanation).

³Gandrud and Lazrus (1981) found no significant enhancements of NO₃.

⁴Evans et al. (1981) measured the SO₂ column concentration. The SO₂ has been spread over 5 km altitude.

⁵Determined cryogenically by Inn and coworkers (private communication).

⁶These samples may have been collected outside the plume.

⁷Where no independent sulfate measurements are available, the SO₄⁻ values of Inn et al. (1981) are shown; these correspond to the total sulfur in the cryogenic trap that produced sulfate in aqueous solution.

TABLE 3. MOUNT ST. HELENS SIMULATIONS AND INITIAL CONDITIONS

Simulation	Constituents	Computational Factors	Initial Conditions	14 km	16 km	18 km	20 km	22 km		
Short-term Volcanic Cloud, Heterogeneous Chemistry	Sulfate Aerosols, Ash Particles, Sulfur Vapors (SO ₂ , OCS, CS ₂), OH and H ₂ O	1 day ≤ time ≤ 1 month t ₀ = 1 day A ₀ = 10 ⁶ km ² Injection, 14-22 km	ΔSO ₂ (ppbv)	174.0	20.0	2.0	100.0	0		
			ΔOCS (ppbv)	1.0	0	0	0	0		
			ΔAsh (μg/m ³)	620.0	300.0	260.0	500.0	0		
			ΔH ₂ O = 1000 ΔSO ₂ (by number); ΔCS ₂ = 0 Ash Size Distribution: Farlow et al. (1981) 0.1-3 μm; Barrett et al. (1980) 3-32 μm; 5% of the mass in the small size mode. Heterogeneous Chemistry: Surface, 15%/hr maximum; Volume, 0%/hr; γ = 1							
Short-term Volcanic Cloud, No Hetero- geneous Chemistry	Sulfate Aerosols, Ash Particles, Sulfur Vapors (SO ₂ , OCS, CS ₂), OH and H ₂ O	1 day ≤ time ≤ 1 month t ₀ = 1 day A ₀ = 10 ⁶ km ² Injection, 14-22 km	ΔSO ₂ (ppbv)	200.0	40.0	20.0	20.0	0		
			ΔOCS (ppbv)	1.0	0	0	0	0		
			ΔAsh (μg/m ³)	600.0	300.0	150.0	75.0	0		
			ΔH ₂ O = 1000 ΔSO ₂ (by number); ΔCS ₂ = 0 Ash Size Distribution: Farlow et al. (1981) 0.1-3 μm; Barrett et al. (1980) 3-32 μm; 5% of the mass in the small size mode.							
Long-term Volcanic Cloud	Sulfate Aerosols, Ash Particles, Sulfur Vapors (SO ₂ , OCS, CS ₂), OH and H ₂ O	0 ≤ time ≤ 5 years Uniform Hemispherical Spreading Injection, 14-22 km	ΔSO ₂ (10 ⁶ tonnes over N.H.)	0.5	0	0	0.5	0		
			ΔAsh (10 ⁶ tonnes over N.H.)	0.5	0	0	0.4	0		
			ΔH ₂ O = 1000 ΔSO ₂ (by mass); ΔOCS = ΔCS ₂ = 0 Ash Size Distribution: Farlow et al. (1981) log-normal, 0.5 μm mode size. No Heterogeneous Chemistry.							
			ΔSO ₂ (ppbv)							
Long-term Photochemical Ozone Trends	Ozone, Chlorine Gases (CH ₃ Cl, HCl), Water Vapor, Sulfur Vapors (SO ₂ , OCS), Trace Composition (O _x -HO _x -NO _x - Cl _x)	1 day ≤ time ≤ 10 years t ₀ = 1 day A ₀ = 10 ⁷ km ² A _{max} = Hemisphere Injection, 14-22 km	ΔSO ₂ (ppbv)	174.0	20.0	2.0	100.0	40.0		
			ΔH ₂ O (ppmv)	174.0	20.0	2.0	100.0	40.0		
			ΔHCl (ppbv)	1.0	1.0	1.0	1.0	1.0		
			ΔCH ₃ Cl (ppbv)	3.0	2.0	2.0	5.0	3.0		
ΔOCS = 0										

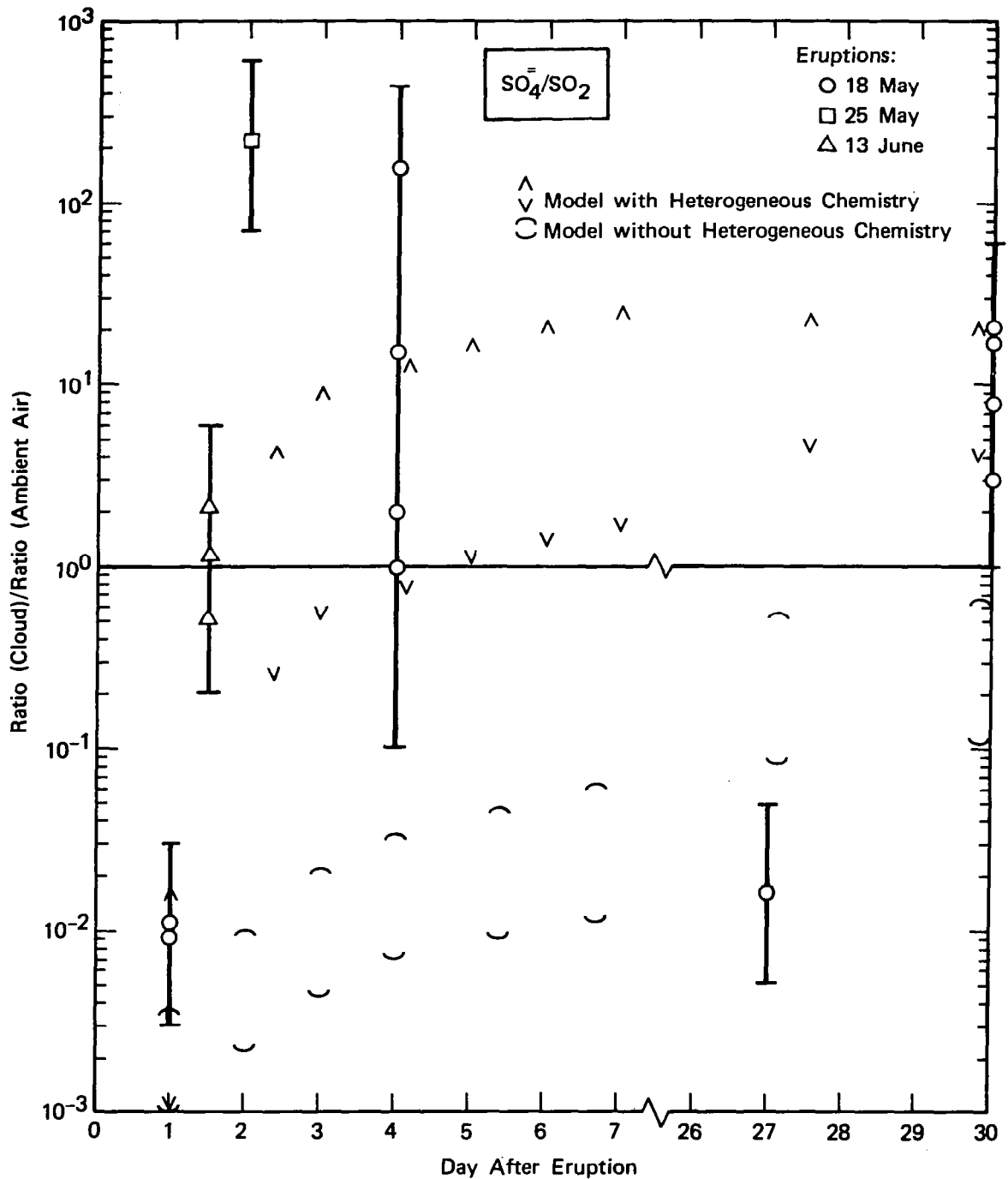


Figure 1. The concentration ratio of $\text{SO}_4^{2-}:\text{SO}_2$ in the Mount St. Helens eruption clouds. The ratio is taken relative to the ambient ratio. (Thus, the ratio of the ratios is given.) Symbols define the eruption of origin for each data point. The data are plotted as a function of the number of days after the eruption of origin. (Notice the compression of the time scale between days 7 and 26.) Data taken at different heights on the same day are plotted as individual symbols in a vertical cluster. The range of the ratios in each cluster, including an arbitrary factor of 3 uncertainty, is indicated by a solid vertical bar. Model calculations of the ratios for the height interval 14 to 22 km are delimited by open pairs of symbols. (See the text for a description of the model simulations.)

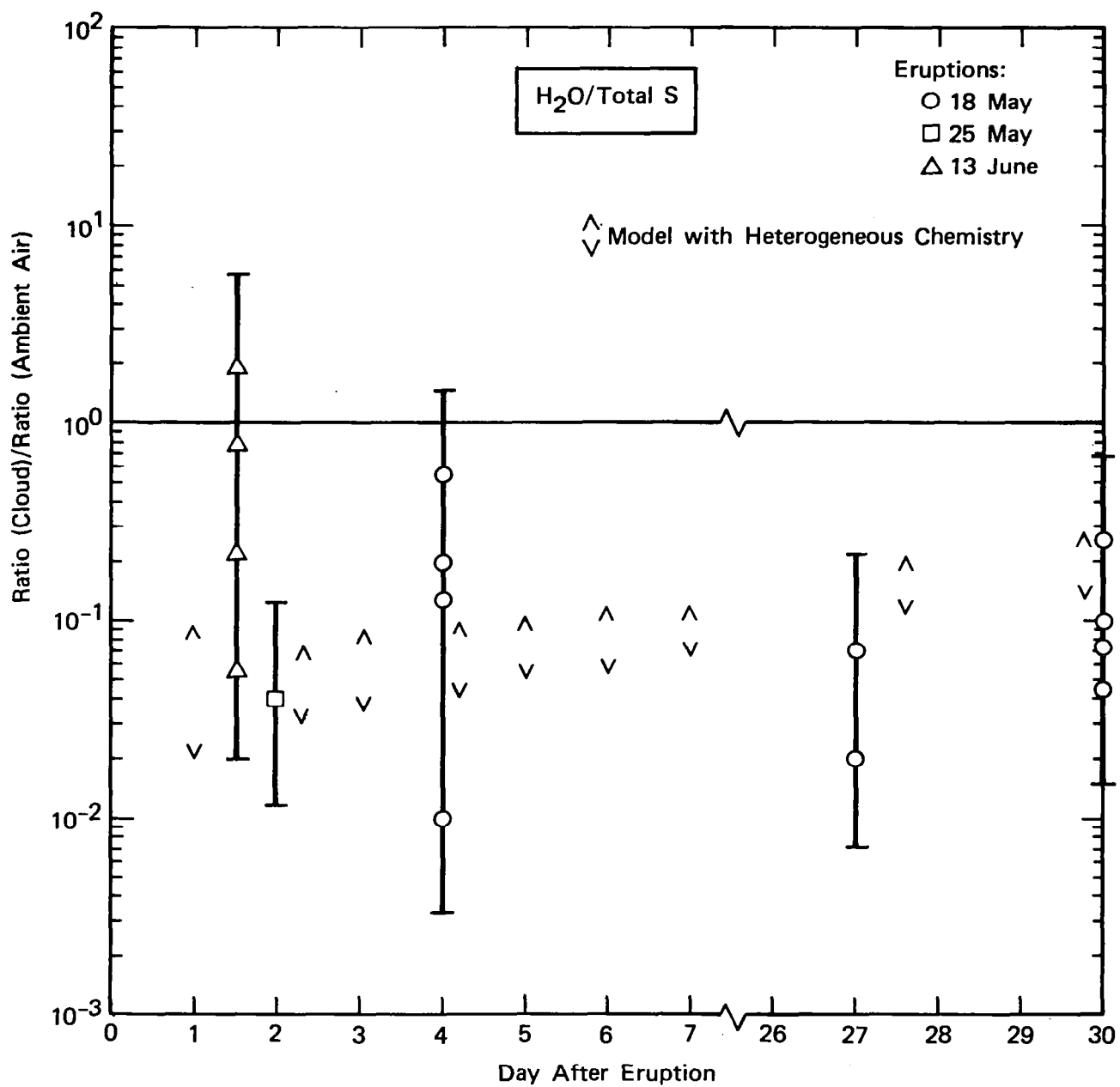


Figure 2. The concentration ratio of H₂O to total sulfur. See figure 1 for an explanation of the symbols.

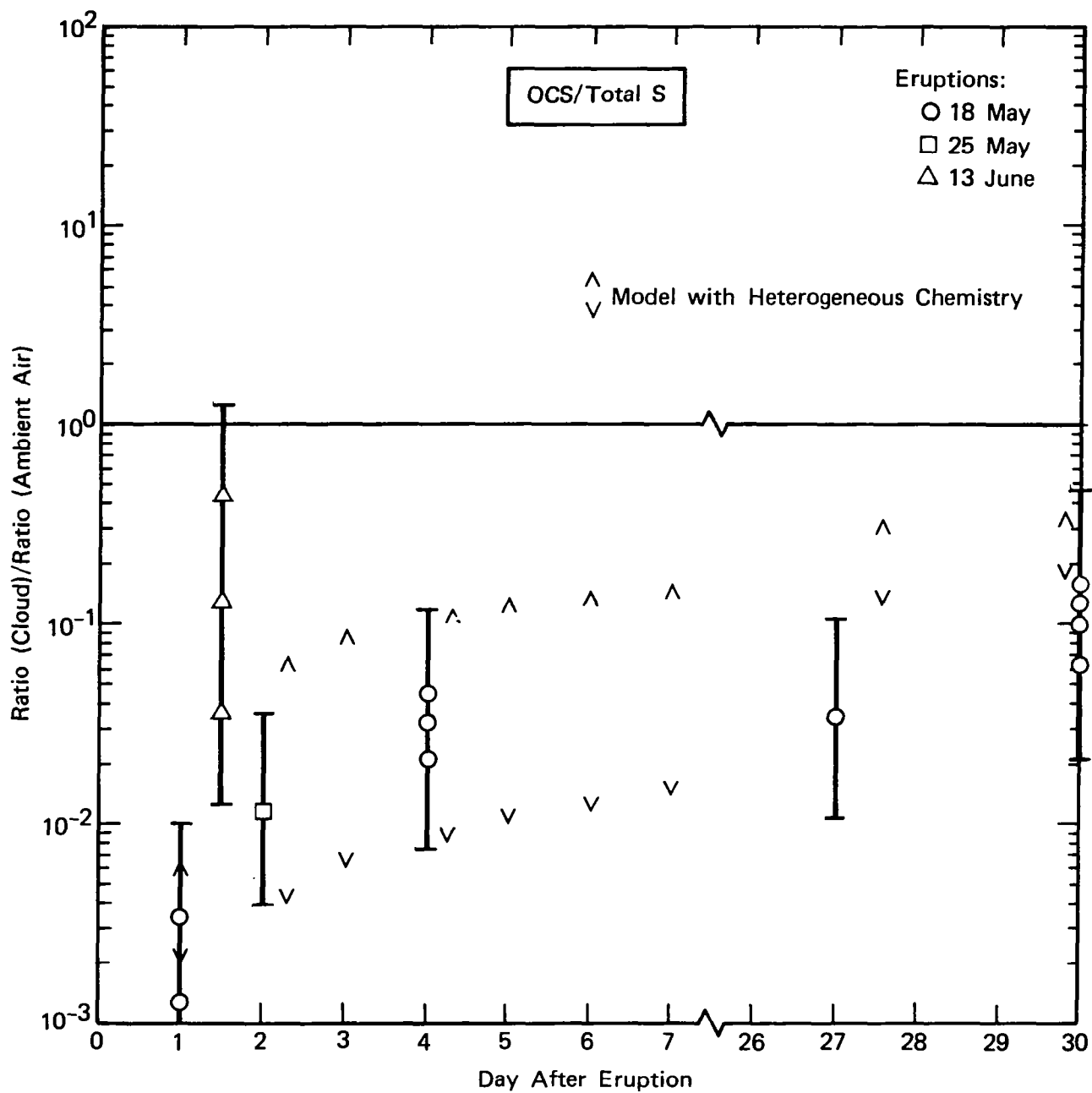


Figure 3. The concentration ratio of OCS to total sulfur. See figure 1 for an explanation of the symbols.

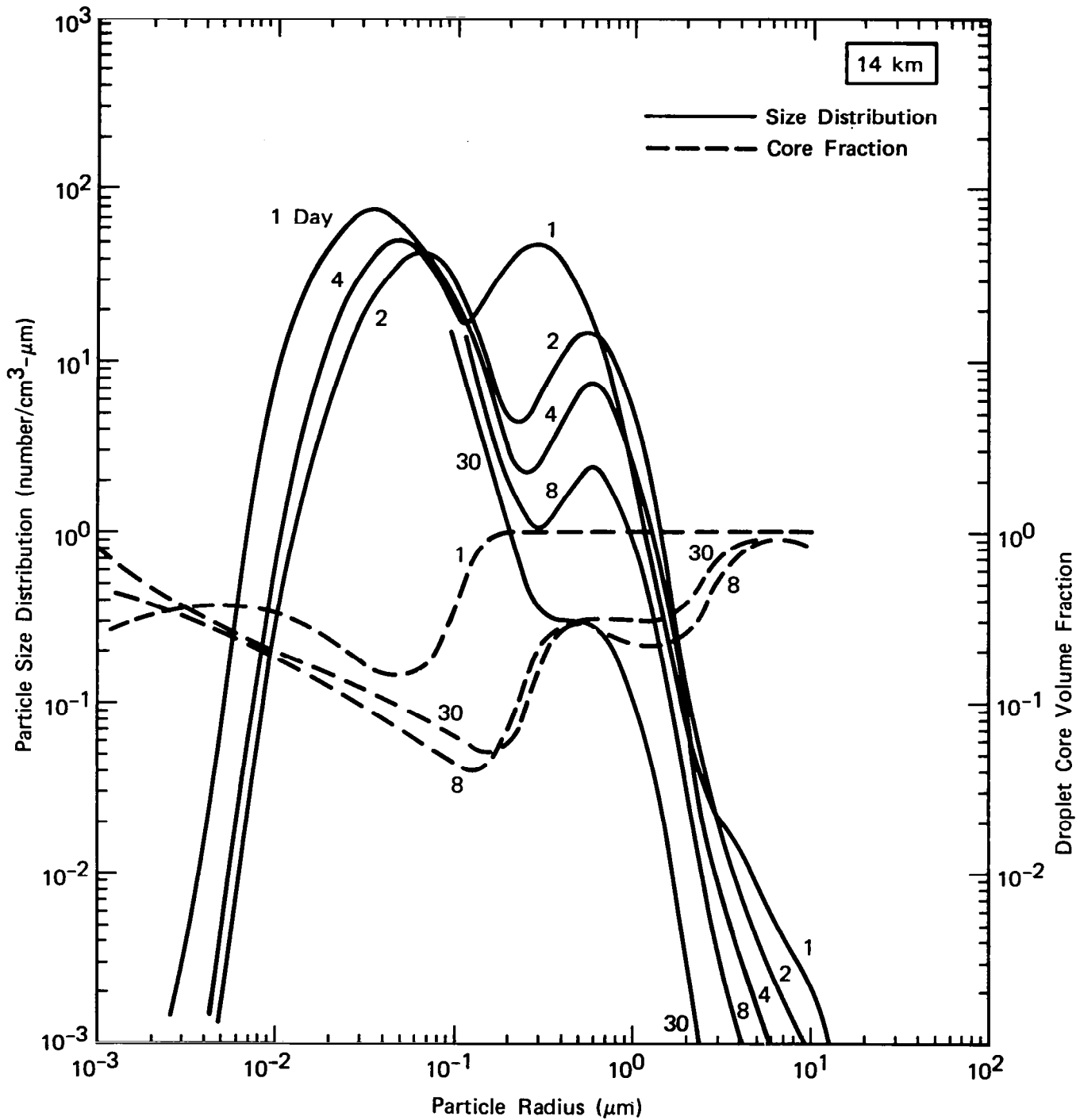


Figure 4. Predicted size distributions of volcanic cloud aerosols at 14 km after the May 18 Mount St. Helens eruption. The size distributions after 1, 2, 4, 8, and 30 days are shown. Also illustrated are the aerosol droplet “core” volume fractions after 1, 8, and 30 days. The calculations include heterogeneous sulfur chemistry, but not homogeneous sulfuric acid nucleation. Note that, at 1 day, 95 percent of the aerosol mass resides above 3 μm radius.

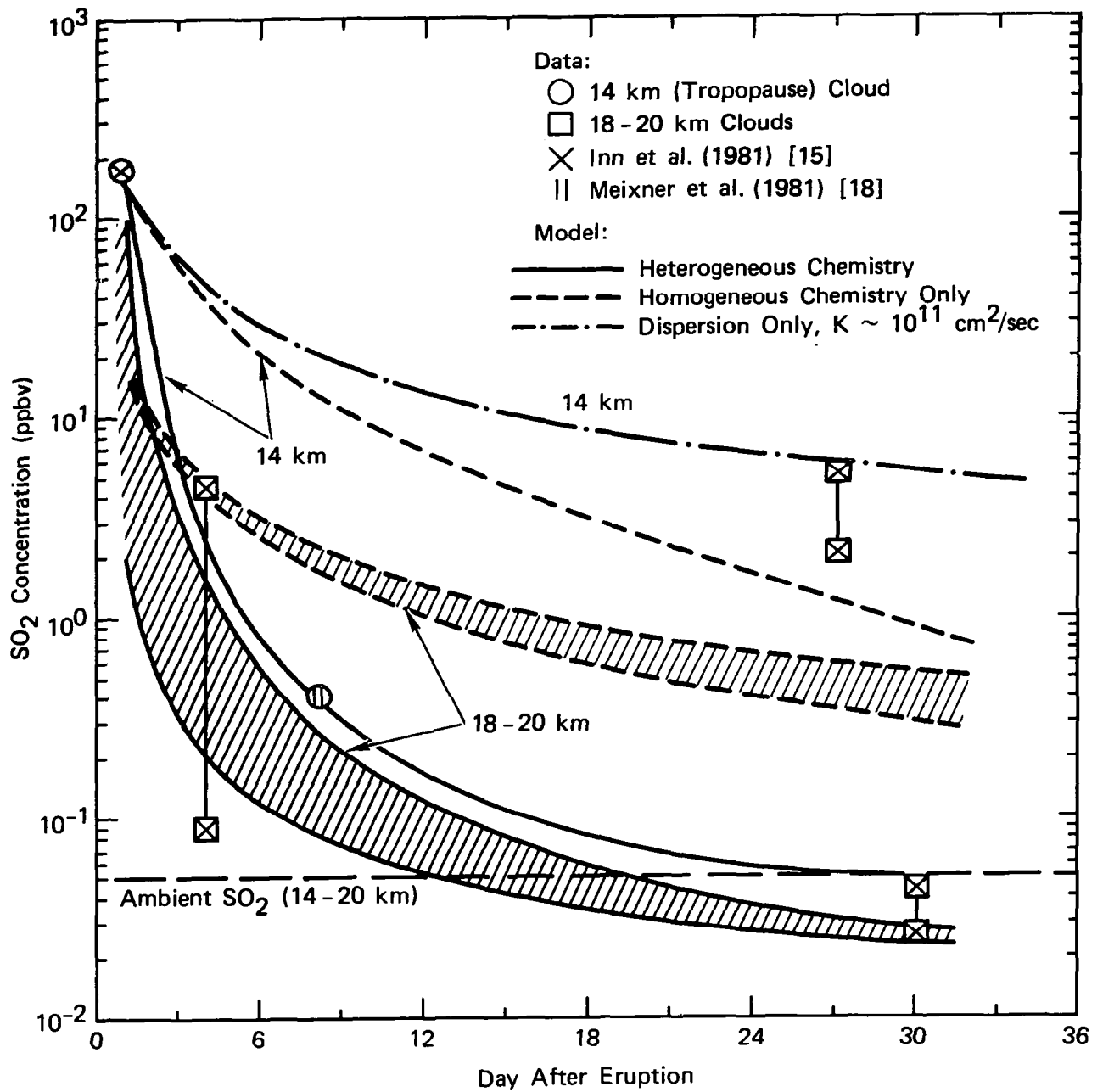


Figure 5. SO₂ concentrations following the May 18, 1980 eruption of Mount St. Helens. Shown are measurements taken in the low-lying tropopause cloud (≈ 14 km) and in the upper-level clouds between 18 and 20 km. All data correspond to the May 18 eruption. Several model calculations are compared. (See the text.) The hatched area defines the range of the predicted values for the height interval indicated. Typical ambient SO₂ concentrations in the lower stratosphere are also indicated.

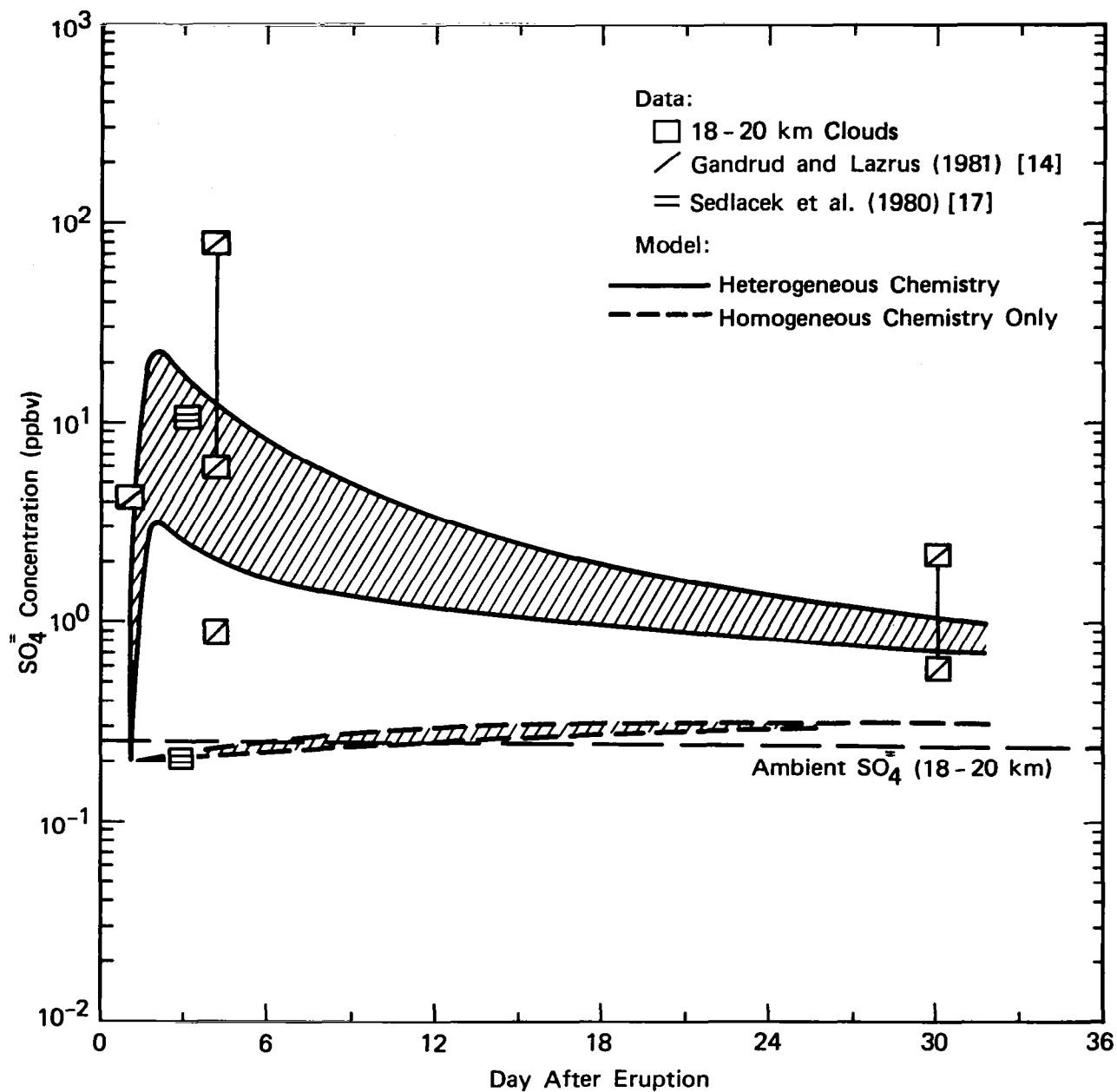


Figure 6. SO_4^- concentrations following the May 18, 1980 eruption of Mount St. Helens. Shown are measurements taken in the clouds between 18 and 20 km. Model calculations are contrasted with the observation. (See the text). The hatched area defines the range of predicted values for the height interval indicated.

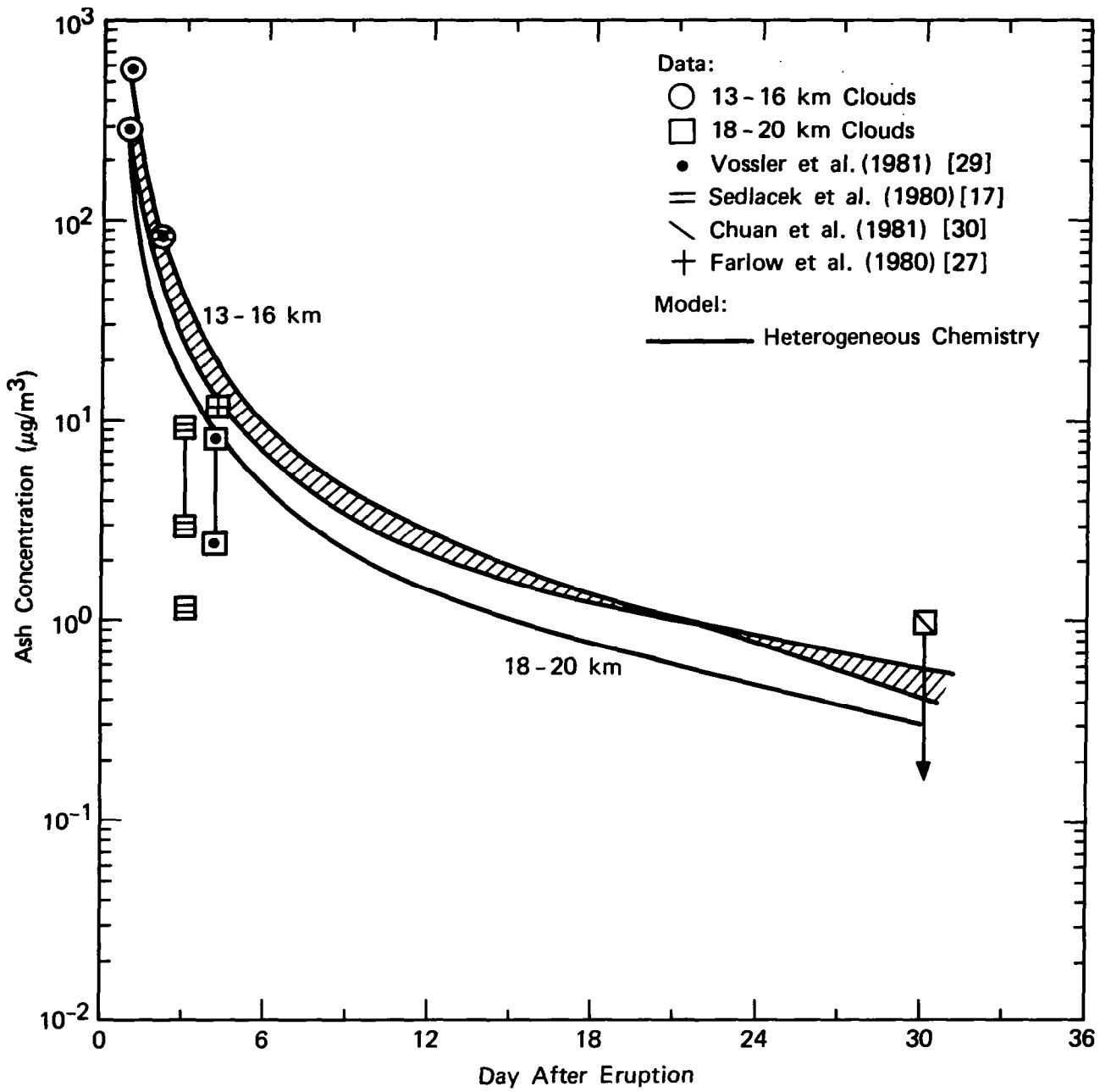


Figure 7. Ash concentrations following the May 18, 1980 eruption of Mount St. Helens. Given are measurements collected in two cloud layers (13-16 km and 18-20 km). Model calculations are compared. (See the text.)

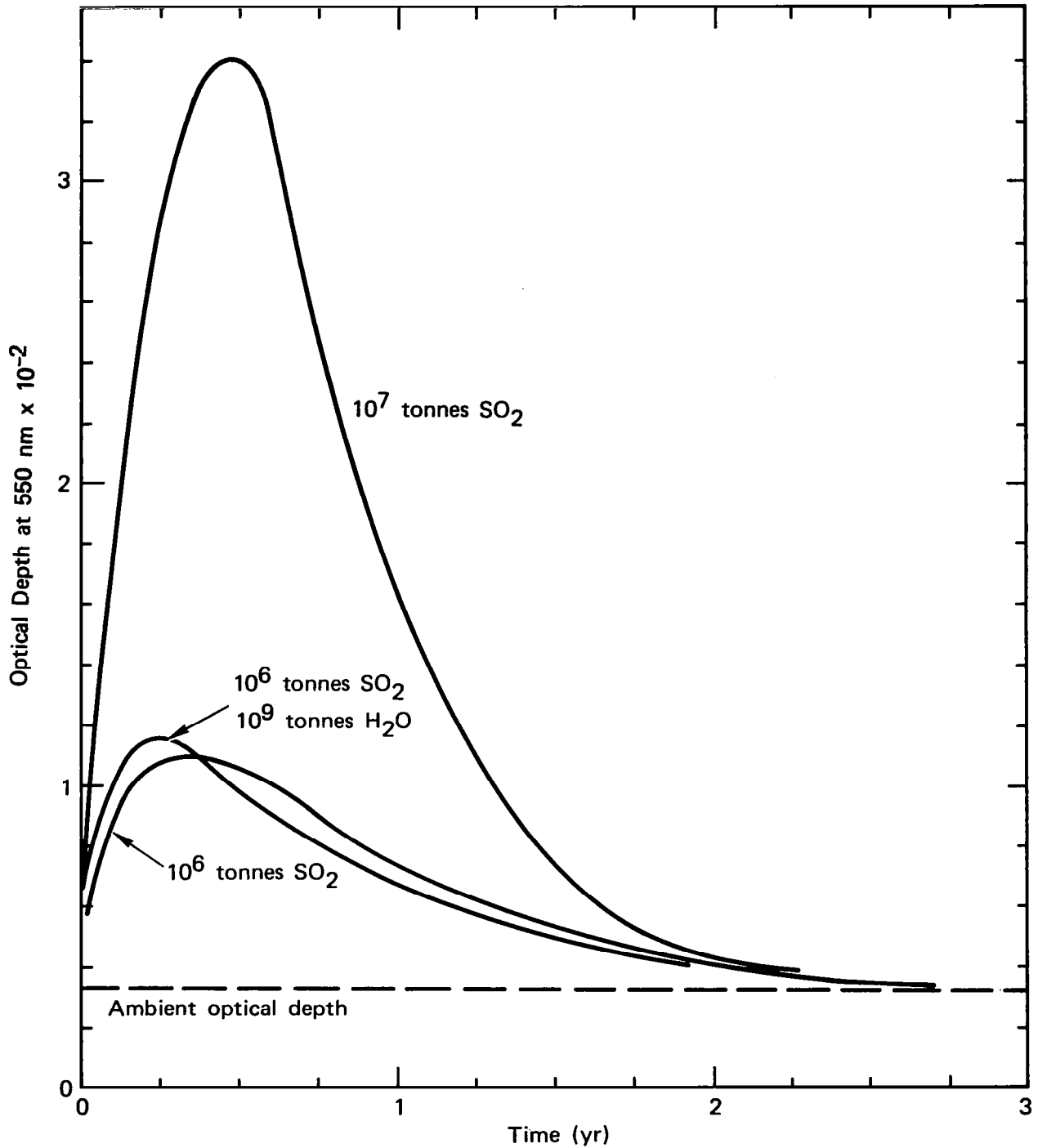


Figure 8. Long-term variations in the stratospheric aerosol layer optical depth (at 550 nm) averaged over the Northern Hemisphere caused by a volcanic eruption of the magnitude of Mount St. Helens (in terms of the total SO₂ injection) and by an eruption 10 times that magnitude. Fine ash injection (< 3 μm) is also accounted for. (See text.)

THE CLIMATIC EFFECT OF EXPLOSIVE VOLCANIC ACTIVITY: ANALYSIS OF THE HISTORICAL DATA

R. A. Bryson and B. M. Goodman

Center for Climatic Research, Institute for Environmental Studies, University of Wisconsin, Madison

By using the most complete available records of direct beam radiation and volcanic eruptions, an historical analysis of the role of the latter in modulating the former was made. A very simple fallout and dispersion model was applied to the historical chronology of explosive eruptions. The resulting time series explains about 77 percent of the radiation variance, as well as suggests that tropical and subpolar eruptions are more important than mid-latitude eruptions in their impact on the stratospheric aerosol optical depth.

The simpler climatic models indicate that past hemispheric temperature can be simulated very well with volcanic and CO₂ inputs and suggest that climate forecasting will also require volcano forecasting. There is some evidence that this is possible some years in advance.

I. THE STUDY

In the discussion that follows, an attempt will be made to present data pertinent to a question posed by Benjamin Franklin in 1789 (1): whether explosive volcanic activity has a widespread effect on climate. The initial question will be whether the many volcanic eruptions of the past century, varying in intensity and frequency, have had a significant impact on the transparency of the atmosphere and hence on the intensity of solar radiation reaching the earth's surface. The data will show that most of the variance in observed Northern Hemisphere beam radiation intensity can be reasonably related to hemispheric volcanic activity levels. The role of the volcanically modulated radiation in determining the hemispheric mean temperature will then be explored both empirically and with the use of a hemispheric "heat budget" model with many feedback loops. Finally, having shown that the course of hemispheric temperature over the past century can be simulated very well with variable atmospheric transparency due to volcanic aerosol variation and carbon dioxide variation, the predictability of volcanic activity levels will be considered.

II. THE HISTORICAL VOLCANISM DATA BASE

In this study the fairly complete listing of observed eruptions compiled by Hirschboeck (2) will be used. There are other such listings, such as that of Lamb (3), but the Hirschboeck listing was chosen for two reasons: it contains a factor of ten more observed eruptions (ca. 6000 as opposed to ca. 600), and the Lamb chronology is somewhat circular in that the intensity of an eruption is assessed on the basis of its perceived climatic effect. This paper will attempt an assessment of the latter.

All such chronologies are weak data sets. Although it is unlikely that few important Northern Hemisphere eruptions went totally unobserved in the last century, intensities are mostly subjective. Even when the height of the plume was recorded, it was usually an estimate, although some were very carefully made. Such potentially valuable calibration data as those of Hammer et al. (4) on the acidity of ice layers in Greenland are not yet sufficiently elucidated to provide a reliable estimate of volcanic intensity. For example, an enormous input of sulfuric acid aerosol is attributed to the eruption of Laki in Iceland in 1783, but whether it was all due to Laki or some to the other nine eruptions elsewhere that year is not established.

III. THE VOLCANIC AEROSOL VEIL

Given a series of crudely classified volcanic events, with only a few located more precisely in time than just the year of eruption, a number of processes that intervene between the throat of the volcano and the high atmosphere aerosol veil that might influence the climate must be located.¹ There seem to be two significant types of ejecta: fine rock particles and gases. The most significant gas is probably sulfur dioxide, which immediately starts a process of conversion to sulfuric acid. Since sulfuric acid is hygroscopic, the eventual product is submicron droplets of 75 percent aqueous solution of sulfuric acid (5). These and other gas-to-particle conversion products added to the submicron rock fragments make up the volcanic aerosol veil, after lateral diffusion (6).

The formation and removal rates of the rock particles and acid droplets are different, and the amount resident in the aerosol veil depends on both production rate and fallout rate. By using a gas-to-particle conversion time constant of 115 days and a mean residence time of 400 days (average or consensus value from the literature), the curves shown in figure 1 can be constructed. Since the ash is "formed" essentially instantly, only the fallout rate is significant (fig. 2). The annual sulfuric acid component of submicron particles seems to be approximately twice the annual ash component (7). By using this 2:1 weighting, figure 3 is derived from figures 1 and 2 and is normalized so that the total amount of material from a single eruption is set equal to unity.

By assuming for the moment that all "great" or explosive eruptions are equal, the curve of figure 3 can be applied to the eruption history dates and produces a synthetic volcanic dust veil history if it is further assumed that diffusion throughout the hemispheric stratosphere occurs within the year. This is shown for three latitude bands in figures 4 to 6. The three bands used were: subpolar, 50°-90°N; mid-latitude, 20°-50°N; and equatorial, 10°S-20°N. In order to combine these three synthetic series into a hemispheric measure, each series must first be calibrated in absolute units, since the effectiveness of the eruptions may vary with latitude for both geological and atmospheric reasons. This calibration is accomplished by regressing the three synthetic series against the observed equivalent optical depth time series.

IV. THE OBSERVED VARIATION OF BEAM RADIATION

The wavelength-integrated normal incidence beam radiation intensity has been recorded at a number of places in the hemisphere since 1883, but not continuously at one place. Since beam radiation is measured only during cloudless times, it provides a measure of either variations in the solar "constant" (if the effect of variations in atmospheric transparency is removed first) or variations in atmospheric transparency (if the solar "constant" is constant). The variations of the beam radiation since 1883 of about 6 percent are much too large to be entirely due to variations of the solar constant (8,9). For the present discussions it is assumed that beam radiation arriving at the earth's surface is only a function of optical depth of the atmosphere. Each observation is adjusted for beam path length, time of year, altitude, and radiation scale. By averaging the optical depths after area weighting for the station latitude, an approximate history of atmospheric optical depth since 1883 can be constructed. Removing the total extinction due to the fixed gases and average water vapor yields the equivalent² aerosol optical depth time series plotted in figure 7 (solid line). The dashed line in figure 7 is discussed later.

¹In the discussion that follows only explosive volcanoes are considered, those types which are unlikely to make significant inputs directly into the stratosphere being ignored.

²"Equivalent" here means the optical depth variation that gives the same observed radiation intensity variation assuming no variation in the input at the top of the atmosphere.

V. CALCULATIONS OF THE VOLCANIC AEROSOL VEIL TIME SERIES

When the aerosol optical depth time series is regressed against the three synthetic volcanic aerosol series, the regression coefficients give the relative intensity of an average "large" explosive eruption in each of the three latitude bands (Table I). It appears that:

- (1) Subpolar volcanoes (such as Katmai) are more effective at modifying the aerosol optical depth than are mid-latitude and equatorial volcanoes, by a factor of two
- (2) Approximately 77 percent of the variance of optical depth can be attributed to variation of volcanic numbers and locations; this is significant at the 0.001 level
- (3) There is a background aerosol optical depth of about 0.03

Weighting the three synthetic series with the regression coefficients and adding them together yields figure 8. The combined effect of all three latitude bands is also shown as the dashed line in figure 7.

VI. CLIMATIC EFFECT OF THE VOLCANIC AEROSOL VEIL

By considering both the modulation of incoming radiation by the volcanic aerosol veil and the modulation of terrestrial back radiation by increasing carbon dioxide, it is possible to assess the climatic impact of eruptions either empirically or with a physical model.

Prior to World War I, there were very few beam radiation stations and the record has a great deal of noise. By using, therefore, the post-1920 equivalent aerosol optical depth, of which 77 percent of the variance appears due to volcanic eruptions, it is possible to regress against the "observed" Northern Hemisphere temperature record according to Borzenkova et al. (10) (fig. 9). The correlation coefficient of 0.91 is about as high as might be expected because of uncertainty in the hemispheric temperature record. The residuals from this regression should contain the CO₂ effect. Surprisingly, neither the exponential nor the linear trend, which were each fit simultaneously to the temperatures, showed any detectable CO₂ warming and contributed nothing to the explained variance.

Instead of regressions, a hemispheric heat budget model designed to take as inputs the observed or calculated mean annual optical depth and CO₂ concentration may be used. The model for this purpose is an updated version of the Bryson and Dittberner model (11). This updated version includes water vapor content and infrared water vapor emissivity parameterized as functions of the surface temperature (12), along with an albedo-temperature feedback loop. This coupled to an oceanic mixed layer, the temperature of which varies with the mean air temperature. It has a linear parameterization for the mean latent heat plus sensible heat flux from the surface, and uses a CO₂ emissivity formulation which gives the same sensitivity of temperature to CO₂ content as Manabe and Wetherald (13) when the feedback loops are made comparable. It includes the infrared emissivity of tropospheric aerosols. The water vapor-CO₂ emissivity overlap is also parameterized as a function of CO₂ content and surface temperature. Although the feedback loops are highly parameterized, the whole model is not empirically tuned.

By using as inputs to this three-layer model a small exponential increase of lower tropospheric aerosol (7), the variation of CO₂ as given by Keeling et al. (14), and the synthetic stratospheric volcanic aerosol loading derived above, the simulations of Northern Hemisphere mean surface temperature since the 1880s given in figure 10 are obtained. The fit of the modeled temperature to the actual temperature according to Borzenkova (10) is about as good as the likely fit of Borzenkova's time series to the truth: $r^2 = 0.65$. Running the model with the appropriate inputs for the Southern Hemisphere suggests that its mean annual surface temperature has been rising over the last 40 years (7). This is in accord with the estimates of Damon and Kunen (15).

Despite the crudeness of the volcanic eruption record and the poverty of beam radiation data (especially before 1920), it appears from these results that a considerable fraction of the interannual variation of hemispheric radiation could be attributed to variations of volcanic activity. It is clear that the "natural" variations of hemispheric temperature in the last century (fig. 8 of ref. 16) are natural in the sense that volcanism is natural, and not in the sense of an inherent randomness.

The methodology described above also provides a simple, tested method for assessing the hemispheric temperature impact of events such as the eruption of Mount St. Helens, provided that the assessment is made in the proper relation to other contemporary volcanism, such as the high-latitude eruption of Hekla.

VII. VOLCANIC ACTIVITY AND CLIMATE PREDICTION

It seems clear to the authors that the results presented here indicate that if climate is to be predicted, the future state of the aerosol optical depth as well as the CO₂ concentration must also be predicted. It is not enough to have every refined general circulation model with all feedback loops identified and correctly interlinked. The extrinsic inputs that modulate the behavior of the climate system must also be specified.

The prediction of individual volcanic events is known to be very difficult, and the prediction of the intensity of individual events even more so. This is especially true with lead times of months to years. Is there any hope then of predicting the volcanic aerosol veil? The authors believe there might be.

Without discussing the entire body of data and analysis that has been developed in connection with this question, in figure 11 a strong suggestion of general volcanic level predictability is presented. Figure 11 is one of a group of variance spectra produced for each tectonic region with adequate data. The record for the Mediterranean region is well observed and long. The spectrum is surprisingly simple. There is some trend to the time series as indicated by variance at the lowest frequencies. There is a low background level that may be noise, and three distinct spectral lines of significant variance (17).

The significant lines in figure 11 may be aliases of response to higher frequency forcing functions, since the Nyquist frequency on this spectrum is 0.5 y⁻¹. If so, there are two candidate mechanisms. The period at about 6 years corresponds to the alias of the Chandler pole tide in the earth's crust, and the other two spikes are possible aliases of lunar-solar crustal tides. These tides are all predictable.

The 2.37-year period in volcanic activity is particularly interesting in that it is exactly the same period as the maximum variance of equatorial high-level zonal wind components, the so-called quasi-biennial oscillation (18). It is unlikely that high-level wind reversals drive volcanism, but it is reasonable that stratospheric aerosol veils with quasi-periodic variation might excite a quasi-periodic stratospheric phenomenon.

It is clear that much more research must be done.

REFERENCES

1. Franklin, B.: Meteorological Imaginations and Conjectures. Memoirs of the Literary and Philosophical Society of Manchester, vol. 2, 1789, pp. 373-377.
2. Hirschboeck, K.: A New Worldwide Chronology of Volcanic Eruptions. Palaeo, Palaeo, Palaeo, vol. 29, 1980, pp. 223-241.
3. Lamb, H. H.: Volcanic Dust in the Atmosphere; With a Chronology and Assessment of its Meteorological Significance. Philosophical Transactions of the Royal Society of London, Ser. A, vol. 266, 1970, pp. 425-533.
4. Hammer, C. U., Clausen, H. B., and Dansgaard, W.: Greenland Ice Sheet Evidence of Post-Glacial Volcanism and Its Climatic Impact. Nature, vol. 288, 1980, pp. 230-235.
5. Lazrus, A. L., Cadle, R. D., Gandrud, B. W., Greenberg, J. P., Huebert, B. J., and Rose, W. I., Jr.: Sulfur and Halogen Chemistry of the Stratosphere and of Volcanic Eruption Plumes. Journal of Geophysical Res., vol. 84, 1979, pp. 7869-7875.
6. Goodman, B. M.: Modeling Mean Annual Stratospheric Aerosol Loading in the Northern Hemisphere Due to Large Volcanic Activity. Proceedings of the 5th Annual Climate Diagnostic Workshop (Seattle, Washington) 1980.
7. Dittberner, G. J.: Climatic Change: Volcanoes, Man-Made Pollution, and Carbon Dioxide. IEEE Transactions on Geosci. Electr., vol. GE-16(1), 1978, pp. 50-61.
8. Hoyt, D. V.: The Smithsonian Astrophysical Observatory Solar Constant Program. Review of Geophysics and Space Physics, vol. 17, 1979, pp. 427-458.
9. Bryson, R. A., and Goodman, B. M.: Volcanic Activity and Climatic Change. Science, vol. 27, 1980, pp. 1041-1044.

10. Borzenkova, I. I., Vinnikov, K. Ya, Spirina, L. P., and Stekhnvsky, D. I.: Change in the Air Temperature of the Northern Hemisphere for the period 1881-1975. Office of International Fisheries, National Marine Fisheries Service, NOAA (Washington, D.C.) 1976. (English translation of *Meteorologiya i Gidrologiya* , vol. 7, pp. 27-35).
11. Bryson, R. A., and Dittberner, G. J.: A Non-Equilibrium Model of Hemispheric Mean Surface Temperature. *Atmos. Sci.*, vol. 33, 1976, pp. 2094-2106.
12. Redmond, K.: An Emissivity Parameterization Suitable for Climate Modeling. *Monthly Weather Review*, vol. 108, 1980, pp. 663-675.
13. Manabe, S., and Wetherald, R. T.: The Effects of Doubling the CO₂ Concentration on the Climate of a General Circulation Model. *Atmos. Sci.*, vol. 32, 1975, pp. 3-15.
14. Keeling, C. D., Bacastow, R. B., Bainbridge, A. E., Ekdahl, C. A., Jr., Guenther, P. R., and Waterman, L. S.: Atmospheric Carbon Dioxide Variations at Mauna Loa Observatory, Hawaii. *Tellus*, vol. 28, 1976, pp. 538-551.
15. Damon, P. E., and Kunen, S. M.: Global Cooling. *Science*, vol. 193, 1976, pp. 447- 453.
16. Mitchell, J. Murray, Jr.: Anthropogenic Impact on Climate. *Prospects for Man: Climatic Change*, Miller, J. R., ed., York University, Toronto, 1978.
17. Roscoe, R. J.: A Statistical Assessment of the Effects of Selected Earth Tides on Regional Volcanic Activity. M.S. Thesis, Department of Geography, Univ. of Wisconsin, Madison, 1979.
18. Brier, G. W.: The Quasi-Biennial Oscillation and Feedback Processes in the Atmosphere-Ocean-Earth System. *Monthly Weather Review*, vol. 106, 1978, pp. 938- 946.

TABLE I. MULTIPLE REGRESSION COEFFICIENTS. (The multiple regression coefficients represent the average annual contribution by a single eruption to the mean annual aerosol optical depth.)

MODEL I—REGRESSION OVER THE ENTIRE PERIOD 1883-1976	
SUBPOLAR	0.030 ± 0.004
MIDDLE LATITUDE	0.014 ± 0.004
EQUATORIAL	0.016 ± 0.003
CONSTANT	0.031 ± 0.002
R = +0.876.	
R ² = 0.767 (SIGNIFICANT AT THE 0.0010 LEVEL)	
SE = ±0.016	

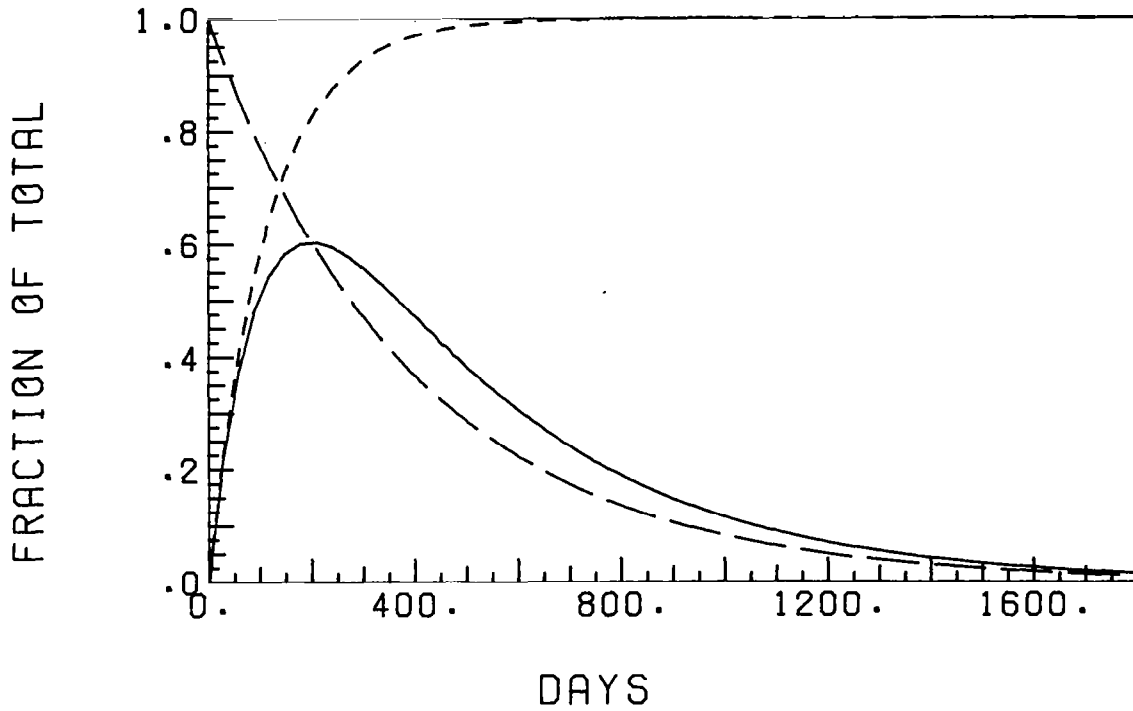


Figure 1. Fraction of total suspended H_2SO_4 aerosol as a function of time, normalized to unit area. The short dashed line is the gas-to-particle production, the long dashed line is the gravitational fallout, and the solid line is the convolution of the two.

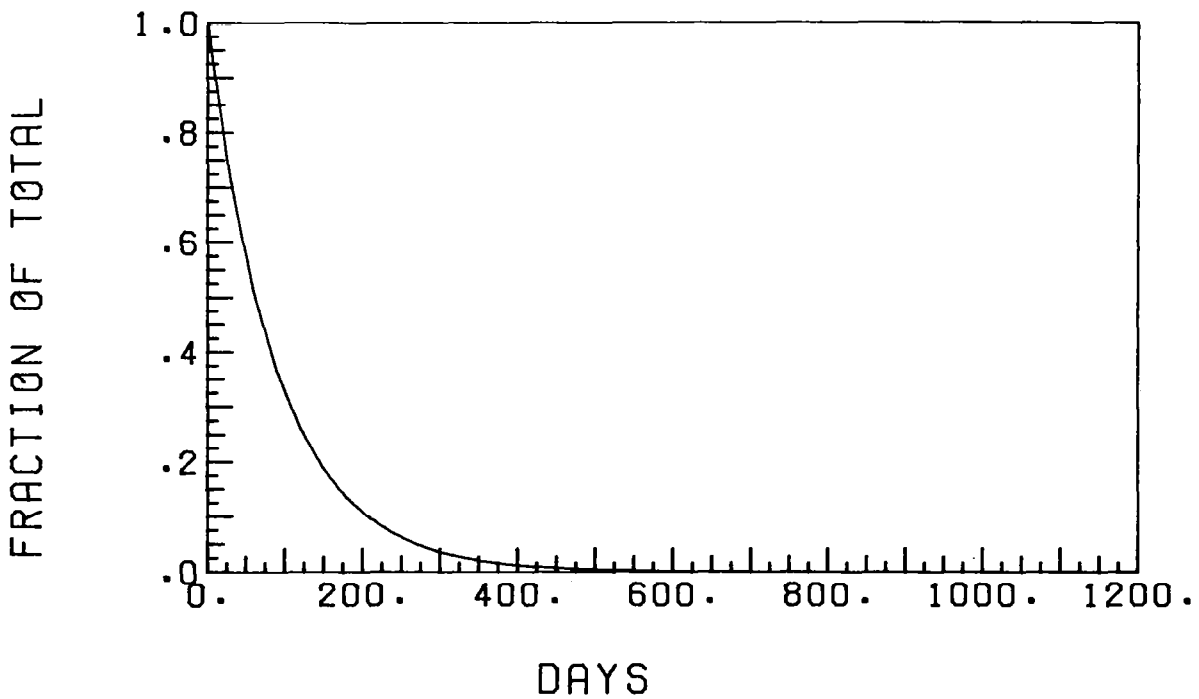


Figure 2. Fraction of total suspended ash particles as a function of time, normalized to unit area.

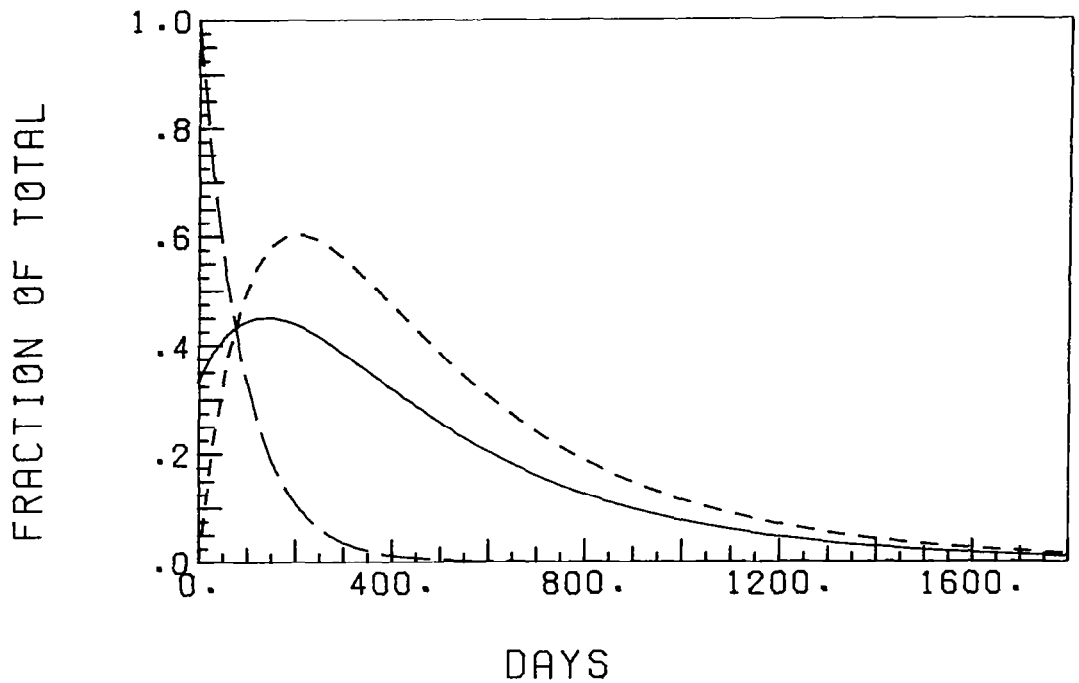


Figure 3. Fraction of total suspended ash and H_2SO_4 aerosol. The short dashed line is the H_2SO_4 time profile, the long dashed line is the ash time profile, and the solid line is the 2:1 weighting combination of H_2SO_4 : ash, normalized to unit area.

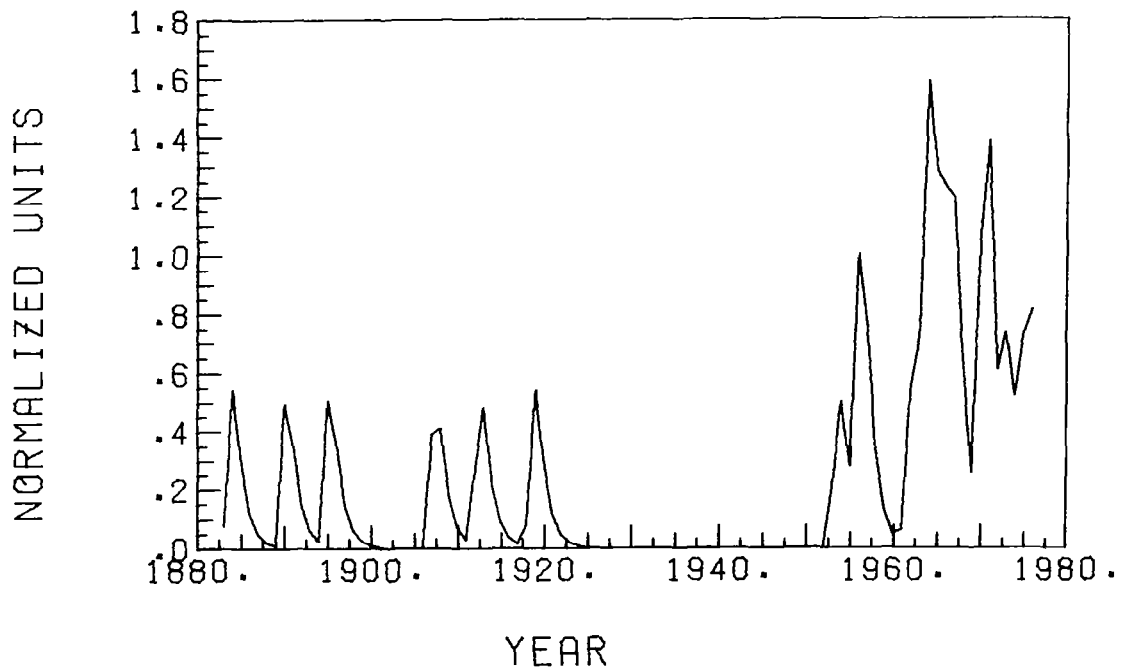


Figure 4. Combined H_2SO_4 and ash aerosol loading contributed by “large” subpolar eruptions.

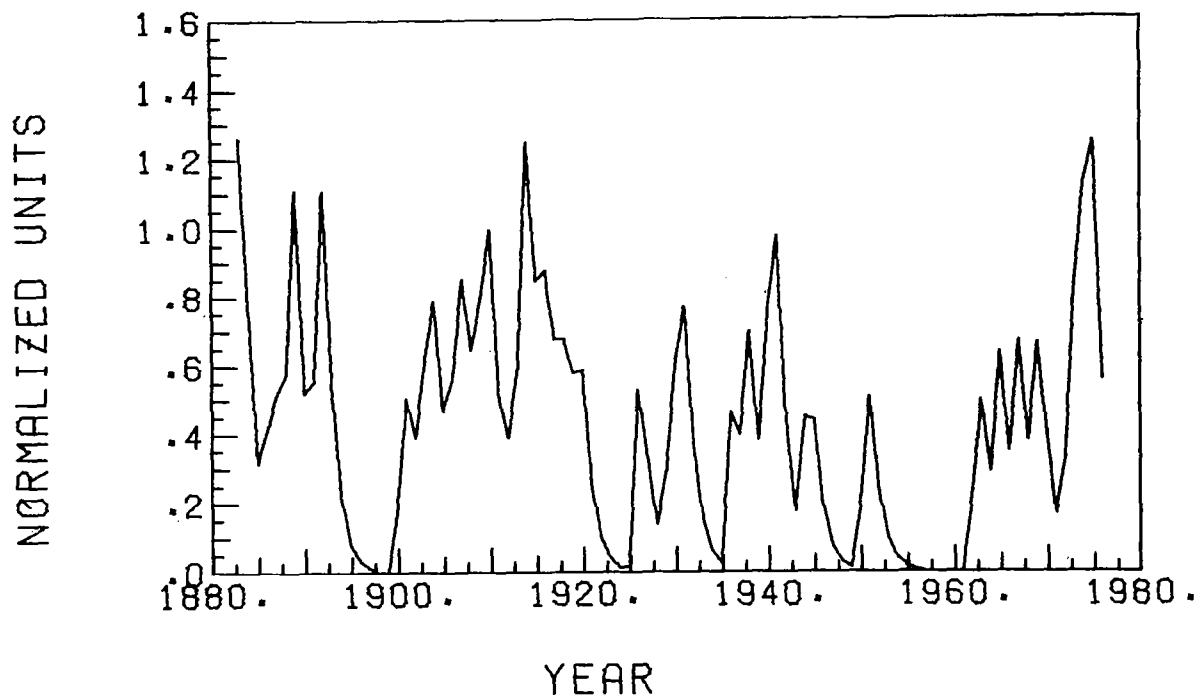


Figure 5. Combined H_2SO_4 and ash aerosol loading contributed by "large" middle latitude eruptions.

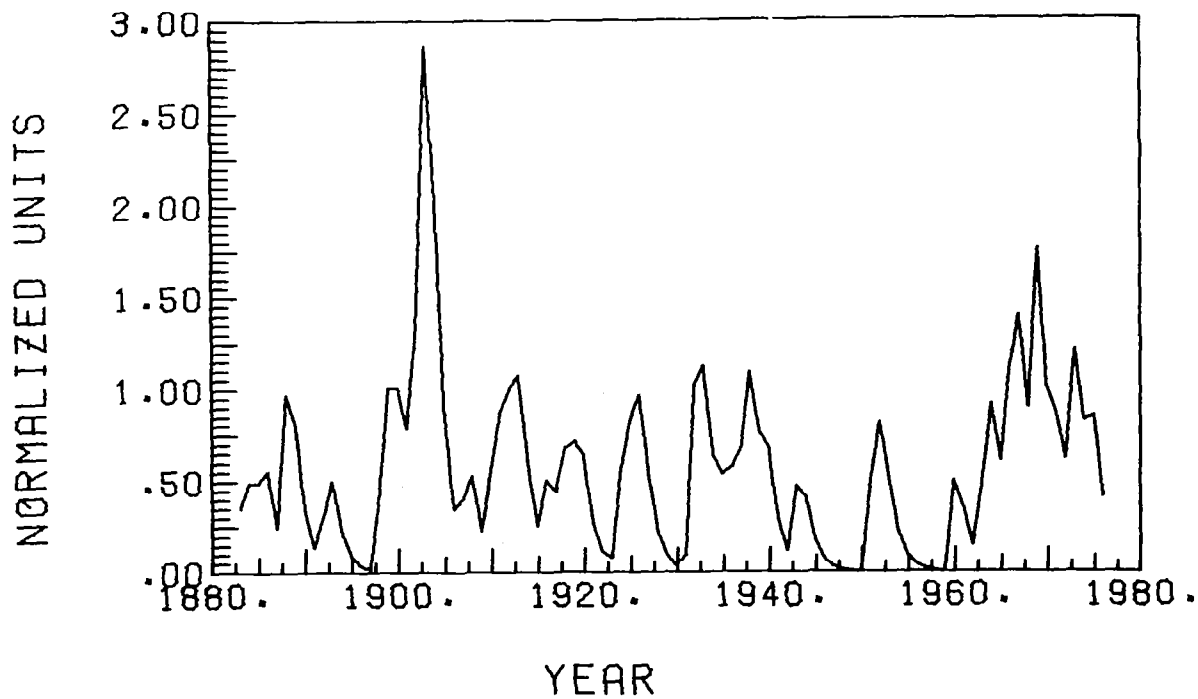


Figure 6. Combined H_2SO_4 and ash aerosol loading contributed by "large" equatorial eruptions.

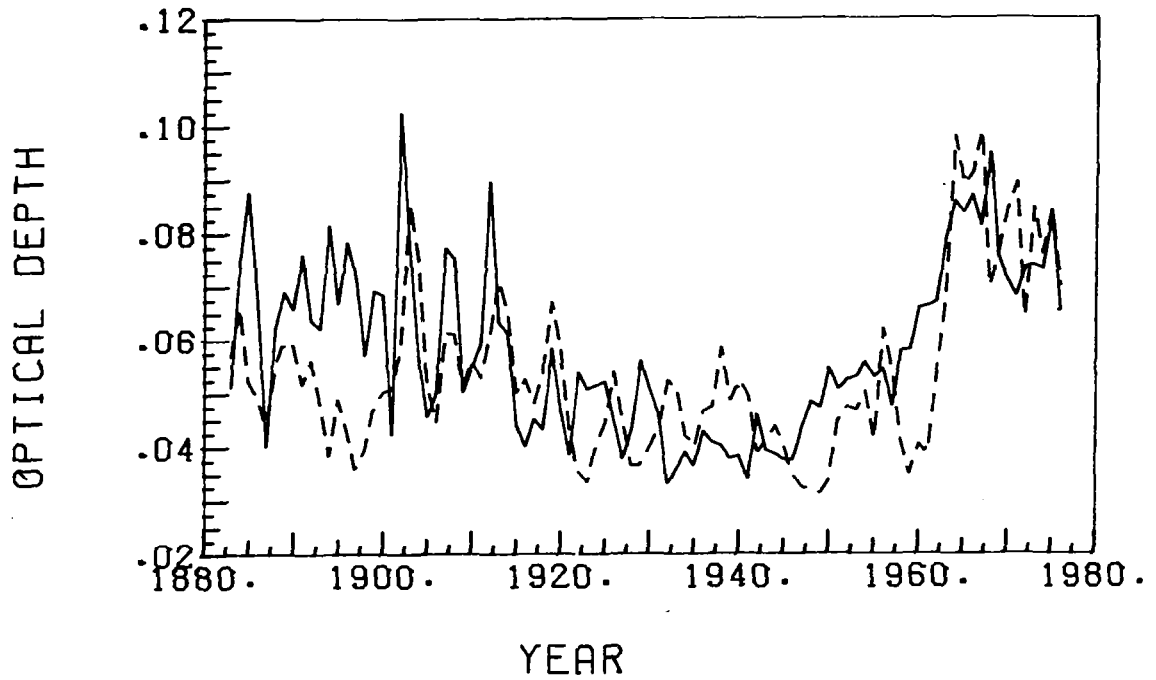


Figure 7. The regression model for aerosol optical depth compared with observations. The dashed line is the regression model result and the solid line is the observed time series.

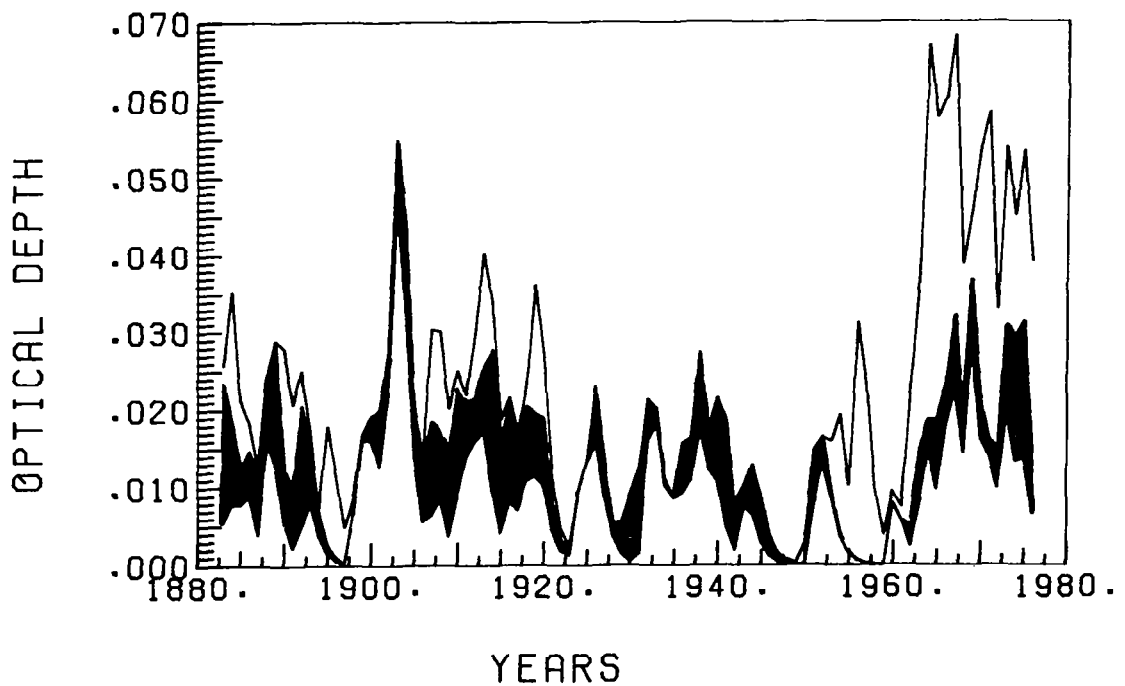


Figure 8. Volcanic contribution to aerosol optical depth by the three latitude bands. The lower clear area represents contributions by the equatorial band eruptions, the solid area, by the middle latitude band eruptions, and the upper clear area, by the subpolar band eruptions.

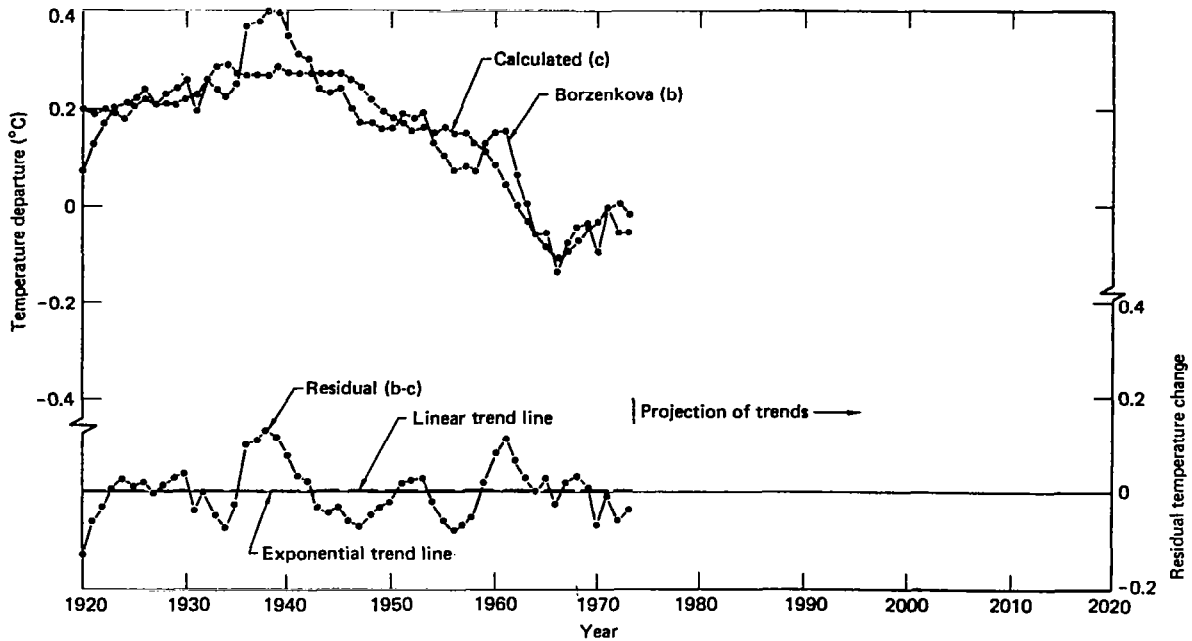


Figure 9. Empirical determination of the CO₂ effect on Northern Hemisphere mean surface temperature. The top curves are the Borzenkova (10) “observed” Northern Hemisphere surface temperature and the estimated value obtained by regression of the mean annual aerosol optical depth against the observed temperature. The bottom curves are the residual from this regression fitted to both linear and exponential curves.

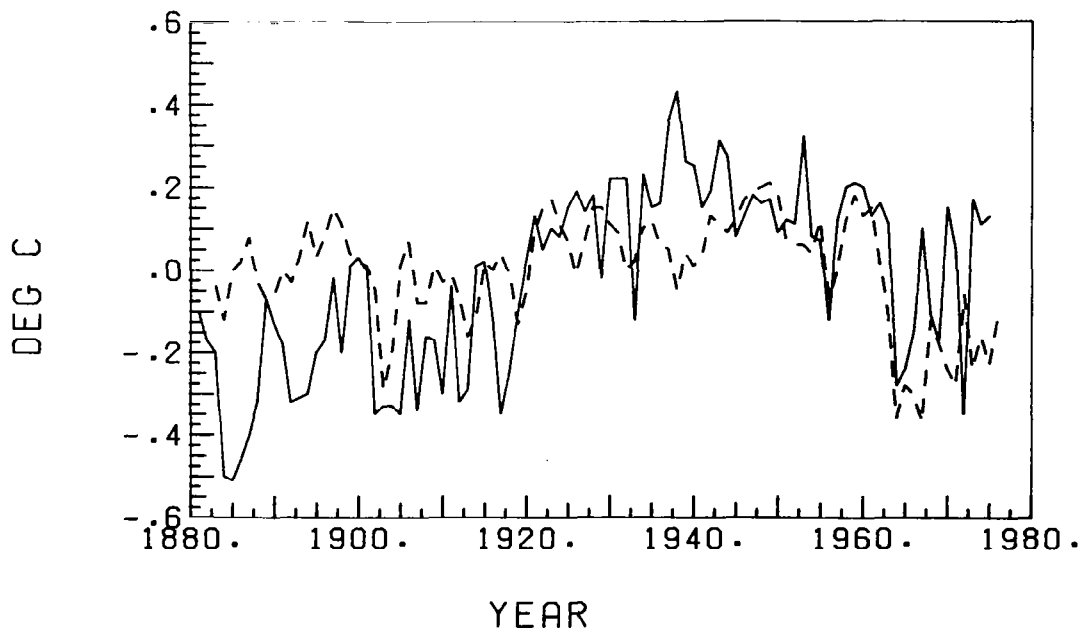


Figure 10. The hemispheric climate model using the regression model for aerosol optical depth compared with the Borzenkova (10) “observed” Northern Hemisphere surface temperature. The dashed line is the climate model result and the solid line is the observed value.

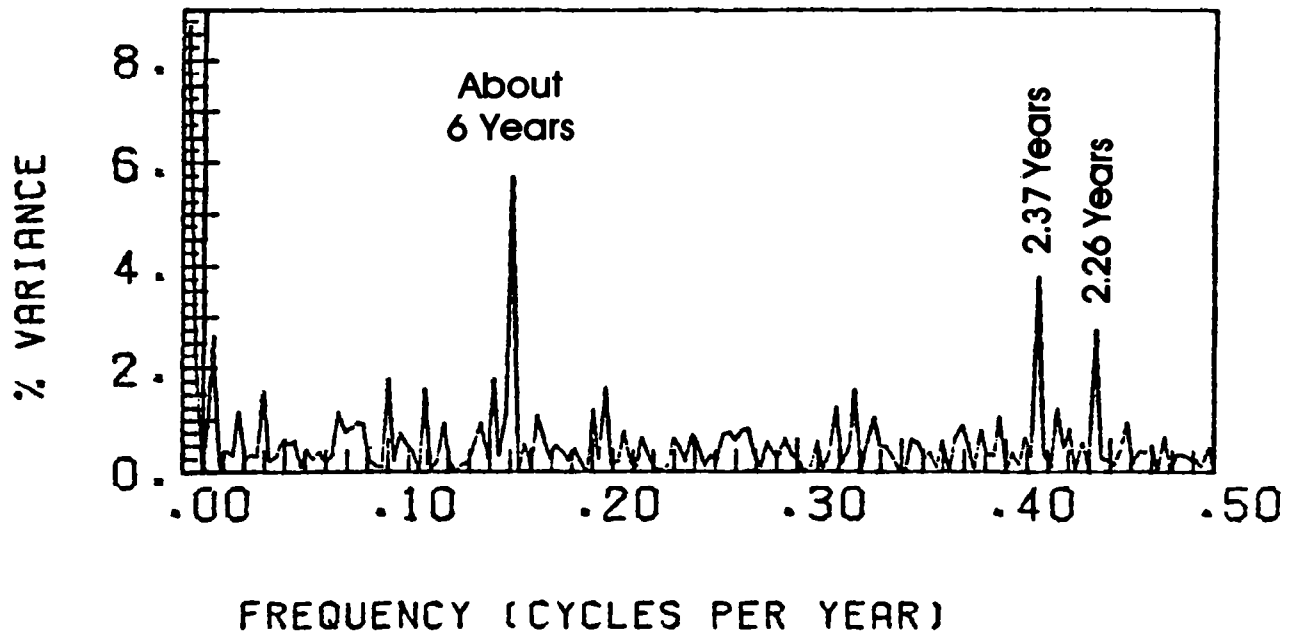


Figure 11. Variance spectrum of the yearly total number of volcanic eruptions in the Mediterranean region from 1631 to 1960.

PROBLEMS IN THE CLIMATOLOGY OF THE 1980 MOUNT ST. HELENS ERUPTIONS

Howard J. Critchfield

Western Washington University, Office of the State Climatologist, Bellingham, WA

Relations between climate and the volcanic activity of Mount St. Helens during 1980 are complex and, in certain respects, reciprocal. They suggest a variety of questions for physical, regional, and applied climatology. Atmospheric conditions affected the eruptive events and the dispersion of ash and gases, which in turn have influenced regional weather (especially solar radiation and visibility) in the short term and have potential implications for macroclimates over a longer period. Mesoscale destruction of snow fields and vegetation, a revised mountain profile, and ash deposits have altered the surface heat and water budgets. Impacts on hemispheric climate are more difficult to isolate from the effects of factors such as other transient aerosols or the role of an active sun; they are contingent on the amount of mass transport into the stratosphere. An accompanying result of the major volcanic episodes has been the disruption of normal climatological observations in the areas directly affected by explosions and ashfall. Environmental and economic consequences of the eruptions have generated a wide range of studies that require climatic data and information. Examples include applications in construction, water resource management, reforestation, wildlife restoration, tourism, insurance, pollution abatement, and health.

I. INTRODUCTION

The potential climatic impact of the 1980 Mount St. Helens eruptions is understandably a matter of public concern as well as a focus of interest among earth scientists. Perhaps no other volcano has attracted so much attention in such a short period. The relations between climate and volcanic activity are complex, and, in certain respects, they are reciprocal. They raise a variety of questions in physical, regional, and applied climatology. The succession of eruptions at different intensities under varying atmospheric conditions affords an exceptional opportunity for theoretical models. Classified in terms of cause and effect, the climatological problems fall into two groups: (a) effects of climate and weather on eruptive events and subsequent dispersion of ash and gases, and (b) influences of eruptions on climate and climatology. The following brief review does not attempt to assign relative importance to these categories or the individual effects.

II. EFFECTS OF CLIMATE AND WEATHER ON ERUPTIONS

One of the credible hypotheses of climatic change invokes volcanic ash as a cause. A reverse chain of processes has been discussed by Rampino, Self, and Fairbridge, who suggest that climatic fluctuations induced by solar variability or other nonvolcanic factors may have resulted in redistribution of continental ice sheets and ocean water and could lead to crustal stresses and volcanism (1). Thus, rather than initiating past glacial periods, volcanic explosions may have been triggered by climatic events. If the hypothesis is valid, it is also general and cannot explain fully the eruption of a single volcano such as Mount St. Helens at a particular time. Atmospheric tides and circulation could augment other causes of crustal stress and trigger an eruption. The eruptions of Mount St. Helens have begun at various phases in the diurnal cycle of atmospheric tides, which has its maximum at solar noon over western Washington. Superimposition of circulation patterns on the atmospheric tides does not yield an evident correlation between barometric pressure and eruptive events, although the possible connection merits further investigation. Whereas atmospheric forces may have been negligible as causes of actual eruptions, they may be traceable to common origins in the climate system.

Whether atmospheric conditions were part of the cause of the eruption, it is clear that they affected associated phenomena, especially the variable paths of the aerosol. In their 1978 monograph which predicted an eruption of Mount St. Helens, "perhaps even before the end of the century," Crandell and Mullineaux included an inverse wind rose indicating a maximum probability of wind directions toward the east or northeast at altitudes of 3000 to 16000 meters in the vicinity of the volcano (2). (See figure 1.) The fall of ash ejected by Mount St. Helens on 18 May 1980 followed this path across Washington State towards northern Idaho and Montana with remarkable congruity. The pattern of ashfall also conformed closely to the modal wind direction at upper levels, as shown by a preliminary map of ash depth prepared by Rigby. (See figure 2.) The force of the explosion and strength of upper winds produced a lofting of airborne ash and maximum deposition in eastern Washington. Gusty surface winds accentuated drifting in some areas and led to exaggerated estimates of ash depth.

It is not feasible here to analyze the synoptic weather in detail for each eruptive phase, but selected cases illustrate contrasting patterns. On Sunday, 25 May, 1 week after the initial explosion, a less violent eruption again propelled ash to high levels, but the ensuing fallout was greater over southwestern Washington in response to easterly and southeasterly winds aloft. Centralia-Chehalis, Kelso-Longview, and Vancouver in Washington and metropolitan Portland in Oregon were major areas experiencing ashfall and reduced visibility. Light ashfall also was detected well to the north in the Puget Sound region. However, the general weather system over Washington on 25 May produced widespread rain which helped to contain surface ash from that day's eruption and ameliorated the residual ash nuisance over much of the eastern part of the state. Ash from an eruption on 7 August again traveled northeastward, and reached beyond Spokane, Washington. Winds during a more recent phase (16-18 October) carried ash first southward toward Portland and then eastward and southeastward along the Washington-Oregon border zone toward Idaho. Throughout the series of eruptions, ash that penetrated to the stratosphere has moved generally eastward across the United States. The bulk of ashfall from the troposphere has settled toward the east-northeast, but single events confirm that even a 1 percent chance of anomalous flow can become a reality.

Humidity, cloudiness, precipitation, and vertical stability were other possible factors in the dispersal of ash and gases. An incidental atmospheric effect was pressure-wave refraction in the wake of the 18 May explosion. Informal preliminary surveys indicate that maximum surface audibility, apart from the vicinity of the mountain, was at a distance of approximately 200 km. Muffled explosive sounds were heard as far north as Vancouver, British Columbia, and eastward into northern Idaho. Shock waves registered on barographs throughout the state and even as far away as Washington, D.C. (3). (See figure 3.) An examination of concurrent atmospheric density patterns could provide data for the climatology of pressure waves and acoustics.

III. MESOSCALE EFFECTS ON WEATHER AND CLIMATE

Atmospheric heating was minimal during early eruptive phases (4), but it obviously was intense in the 18 May explosion. Perturbations initiated by the blast and the ensuing pressure waves probably affected cloudiness in the region and may have modified circulation slightly on a larger scale. Lightning was observed in the turbulent ash cloud above the volcano, and the Yakima National Weather Service Office (135 km to the northeast) reported frequent thunder during a more than 6-hour period as hot ash and gases drifted overhead.

Areas under the ash plume experienced a rapid diminution of solar radiation and decreasing visibility as ash sifted to the ground. Blowing ash continued to reduce visibility during later periods of drying winds. To the extent that weather accumulates to become climate, these ephemeral conditions are of climatic significance. Of greater importance are the mesoscale changes in the surface heat and water budgets owing to destruction of snow fields, fresh water systems, and vegetative cover. The resulting alterations of evapotranspiration and albedo will affect soil moisture and temperature as well as the boundary-layer climate for

many years. Where deep ash layers insulated the snowpack on adjacent slopes, they retarded melting well beyond the normal seasonal runoff.¹ Thinner ash deposits also changed the surface albedo, but except in the immediate zone of violent destruction alpine snowfall or vegetative growth offset the effect within a few weeks. The albedo of ash re-exposed by the late summer wheat harvest in the Big Bend and Palouse farmlands was again modified by the fallout from stubble burning.

A catastrophic change that will modify local topoclimates is the revised profile of Mount St. Helens, which suddenly became a truncated cone on 18 May. A reduction in height by about 400 meters has decreased the potential alpine snow cover and the barrier effect on winds. The long-term result will be felt in the immediate lee of the mountain, unless further volcanic activity restores the cone.

IV. MACROSCALE EFFECTS

The impact of the eruption on subsequent weather over areas remote from Mount St. Helens is more conjectural. The principal theoretical mechanisms entail changes in the radiation balance and stimulation of cloud formation by ash particles and gases as the aerosol moved eastward in the upper troposphere and the stratosphere (5-8). It is unlikely that these or other conceivable models based on Mount St. Helens' prior activity can explain the drought which began in early May on the Canadian Prairies and northern Great Plains, the tornadoes of the 12th and 13th in Missouri and Michigan, or the heavy rains from the 13th to 17th along the U.S. Gulf Coast (9). It is equally doubtful that the 18 May eruption contributed to the cool, wet spring in Britain and the wine districts of western Europe, although no plausible cause and effect relation should be dismissed without careful examination.

Impacts of volcanic ash and gases on future hemispheric climate are contingent on the amount of mass transport into the stratosphere, and they are difficult to isolate from the effects of other factors. Since transient gases and particulates are known to have a longer residence time in the stratosphere than in the troposphere, it is assumed that any resulting abnormalities in the radiation balance, ice nuclei efficiency, or photochemical processes (10-11) will have a protracted influence on weather and climate. If the connecting link is a gross adjustment in the general circulation, the related fluctuations of climate can be expected to appear as diverse regional trends (12). The consensus appears to be that global effects will be slight, but, in any case, they are complicated by other aerosols and gases, an active sun, or causes yet to be discovered in the climate system.

V. CLIMATIC RECORDS

An accompanying result of the major volcanic episodes was a disruption of normal surface weather records. Although destruction of observation sites, temporary or permanent abandonment of others, and the deposition of ash in rain gages are not directly climate related, they are of significance to climatology. A standpipe storage gage formerly maintained by the U.S. Forest Service about 3 kilometers northeast of the crater was destroyed along with a large tract of forest on 18 May (13). Observations at other stations in the federal-state fire danger network were curtailed for various periods. The Plains of Abraham snow course, which had been the site of snow survey measurements on the north side of the mountain in the Cowlitz River drainage since 1944, was obliterated by the main blast; it has been reestablished at approximately the same location (14). The temperature record at a hydroelectric station on the Lewis River 10 km east of Cougar was interrupted by the involuntary absence of permanent personnel for the remainder of the month, although precipitation observations were maintained by daily visits.² A substation at Kid Valley, within the "Red Zone" of prohibited entry, has been closed permanently. Rain gages throughout the ashfall zone collected various amounts of ash. The NWS gage at Yakima recorded the equivalent of 10.4 millimeters of rain over a 9-hour period. (See figure 4.)

¹Robert T. Davis, Snow Survey Supervisor, Soil Conservation Service, Spokane, Washington, personal communication.

²Earl Pickering, NWS Substation Specialist, Seattle, Washington, personal communication.

An incidental problem arises from the lack of a synoptic code number and symbol for volcanic ash. Surface analysis charts for a period during which ash was prevalent do not distinguish ash from dust or smoke as an obstruction to visibility, nor do they distinguish ash from other causes of an obscured sky. Several standard record forms likewise permit ambiguous coding that can persist long after information in a remarks column has been digested by card punches or computers. In view of the near certainty that there will be future pyroclastic eruptions somewhere in the world, it may be advisable to review the notation system for records destined to enter climatic archives.

From the climatological point of view, a fortunate result of the Mount St. Helens eruptions has been the establishment of a relatively dense event-actuated precipitation and river gage network in the vicinity of the mountain under the auspices of the National Weather Service and the U.S. Geological Survey.³ The Soil Conservation Service and cooperating agencies have increased the number of SNOTEL installations for monitoring temperature, precipitation, and snowmelt water equivalent in the drainage basins around the mountain. In addition, the U.S. Forest Service is augmenting its fire, weather, and avalanche monitoring sites in the Gifford Pinchot National Forest with automatic equipment. Data from these enhanced networks will be of great value for modeling boundary-layer changes and in applied studies. Although remote sensing via satellite can monitor surface conditions with increasing resolution, it might be prudent to assess the potential scientific benefits of similar networks farther north in the Cascade Range, where Mount Baker has been emitting plumes during recent years.

VI. APPLICATIONS

Environmental and economic consequences of the eruptions have generated a wide range of studies that employ climatic data and information. Examples based mainly on requests to the Office of the Washington State Climatologist since the first eruptive phase on 27 March 1980 illustrate the variety of applications.

Initial public reactions focused on earthquakes, flooding, and ashfall. Climate was not the primary concern, but the media was quick to add climatic changes to the list of possible effects. The scientific community and emergency services were generally alert to the need for careful monitoring and prediction of ash and gas dispersal (14-16). Accordingly, upper level mean wind data were much in demand for scheduling aerial reconnaissance and projecting ashfall paths. The tempo accelerated after 18 May as representatives of the press, radio, and TV began requesting probability forecasts of ash paths, the effect on immediate weather, and future implications for severe winters, drought, flood, food shortages, and the next ice age. Individual perception of climatic processes often raced ahead of scientific knowledge.

Following the direct destruction by the explosion, mudslides, and flooding, the need for climatic data applications soon became apparent in engineering design and construction. Plans for dredging operations in the Cowlitz and Columbia Rivers had to take into account the increased potential for soil erosion and flooding in relation to probable rainfall intensity and frequency. Insurance companies required supporting evidence for claims and adjustments and for review of premium rates. Planning for timber salvage, reforestation, and wildlife restoration also depended on climatic information. Studies in the agricultural sector have dealt with the effects of ash on soil climate and crop phenology, often at the microscale. Procedures instituted by manufacturers to protect equipment and personnel were based in part on climatic uncertainties.

Federal, state, and local health-related services face immediate and continuing decisions; even such an apparently trivial matter as allocation of dust masks entailed climatic probabilities. Pollution monitoring took on new dimensions in the areas affected by ash. Mingling of volcanic ash with smoke from a coal-fired power plant at Centralia, Washington, presented a unique problem. Urban authorities had to choose the best leeward site for storage of ash trucked from streets or estimate the relative chance that rains would flush or clog storm sewers.

³Michael K. Holzinger, NWSFO, Seattle, Washington, personal communication.

Agencies concerned with recreation and tourism sought assurance that future ashfalls would follow predictable patterns, whereas organizers of conventions and sporting events hastened to change venues or cancel programs. The manager of a professional football team considered the advisability of moving a summer training camp from Cheney, Washington, (near the median path of the 18 May ashfall) to an alternate location. It is unclear whether the potential traffic hazard, the cool wet spring of 1980, or the price of gasoline was the leading cause of a decline in out-of-state visitors.

VII. CONCLUDING REMARKS

A comprehensive climatology of the Mount St. Helens eruptions can increase the understanding of climate dynamics and their impact on environment and society, but to date it offers more problems than solutions. Consequently, refined models of the interactions between climate and volcanic activity at all scales of space and time are needed. It is essential, however, that singular events, hypothetical causes, and regional effects are treated in the perspective of the entire climate system, insofar as the inadequate knowledge permits. The question implied by the title of this symposium continues to merit our attention: What atmospheric effects and climatic impacts can be assigned specifically to Mount St. Helens—1980?

REFERENCES

1. Rampino, M. R., Self, S., and Fairbridge, Rhodes W.: Can Rapid Climatic Change Cause Volcanic Eruptions? *Science*, Vol. 206, 1979, pp. 826-829.
2. Crandell, D. R., and Mullineaux, D. R.: Potential Hazards from Future Eruptions of Mount St. Helens Volcano, Washington, U.S. Geological Survey Bulletin 1383-C (Washington), Government Printing Office, 1978, p. 21.
3. Hoecker, W.: Pressure Waves from Eruption Recorded in Washington D.C. Weatherwise, Vol. 33, No. 3, 1980, p. 121.
4. St. Lawrence, W., Qamar, A., Moore, J., and Kendrick, G.: A Comparison of Thermal Observations of Mount St. Helens Before and During the First Week of the Initial 1980 Eruption, *Science*, Vol. 209, 1980, pp. 1526-27.
5. Bray, J. R.: Volcanic Eruptions During the Past 500 Years, in Climate Change and Variability, A. D. Pittock, L. A. Frakes, D. Janssen, J. A. Peterson, and J. W. Zillman, eds., Cambridge Press, 1978, pp. 256-262.
6. Bryson, R. A., and Goodman, B. M.: Volcanic Activity and Climatic Changes, *Science*, Vol. 207, 1980, pp. 1041-1044.
7. Toon, O. B., and Pollack, J. B.: Atmospheric Aerosols and Climate, American Scientist, Vol. 68, 1980, pp. 268-278.
8. Wexler, H.: Volcanoes and World Climate, Scientific American, Vol. 186, No. 4, 1952, pp. 74-80.
9. Impact Assessment of Major Climatic and Other Natural Events. Center for Environmental Assessment Services, NOAA, May 1980, p. 2.
10. Schneider, S. H., and Kellogg, W. W.: The Chemical Basis For Climate Change, in Chemistry of the Lower Atmosphere, S.I. Rasool, ed., Plenum Press, 1973, pp. 203-249.
11. Johnston, D. A.: Volcanic Contributions of Chlorine to the Stratosphere More Significant to Ozone Than Previously Estimated, *Science*, Vol. 209, 1980, pp. 923-924.
12. Balling, R. C., Jr.: Regional Patterns Associated with Climatic Change, National Weather Digest, Vol. 5, No. 2, 1980, pp. 13-16.
13. The Cooperative Observer, Western Region, Summer 1980, p. 12.
14. Stoiber, R. E., Williams, S. N., and Malinconico, L. L.: Mount St. Helens, Washington, 1980 Volcanic Eruption Magmatic Gas Component During the First 16 Days, *Science*, Vol. 208, 1980, pp. 1258-1159.
15. Fruchter, J. S. et al.: Mount St. Helens Ash From the 18 May 1980 Eruption: Chemical, Physical, Mineralogical, and Biological Properties, *Science*, Vol. 209, 1980, pp. 1116-1125.
16. Hooper, P. R., Herrick, I. W., Laskowski, E. R., and Knowles, C. R.: Compositions of the Mount St. Helens Ashfall in the Moscow-Pullman Area on 18 May 1980, *Science*, Vol. 209, 1980, pp. 1125-1126.

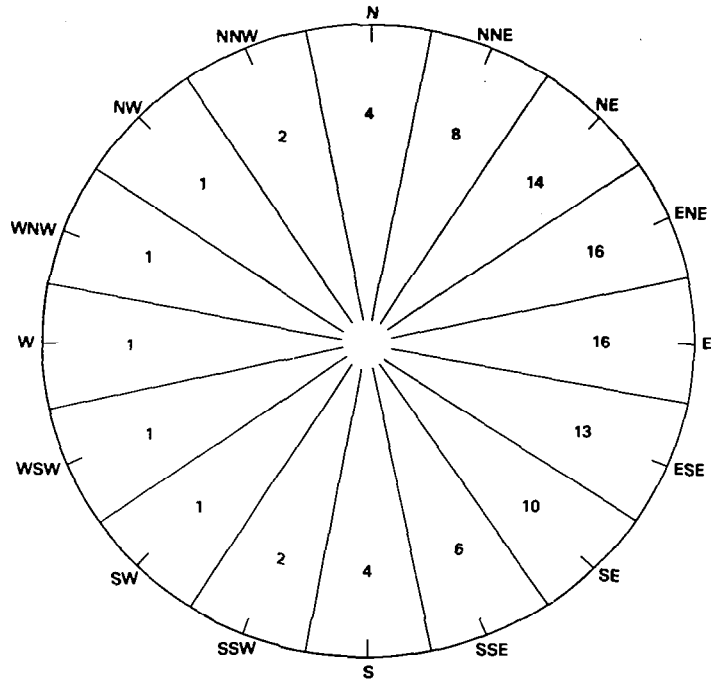


Figure 1. Percentage probability of upper-level wind directions away from Mount St. Helens, based on composite of mean winds at 3000 to 16000 meters. (From reference 2.)

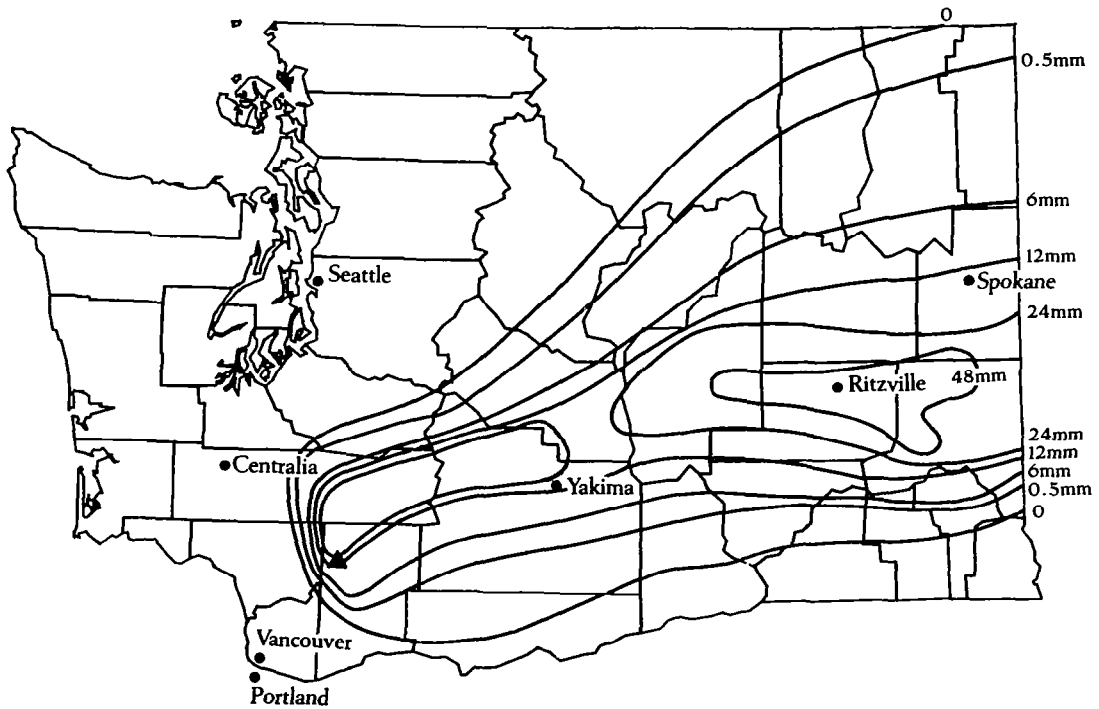


Figure 2. Distribution of ash depth (mm) in Washington State following the 18 May 1980 Mount St. Helens eruption. (Adapted from a map by James G. Rigby, Washington State Department of Natural Resources.)

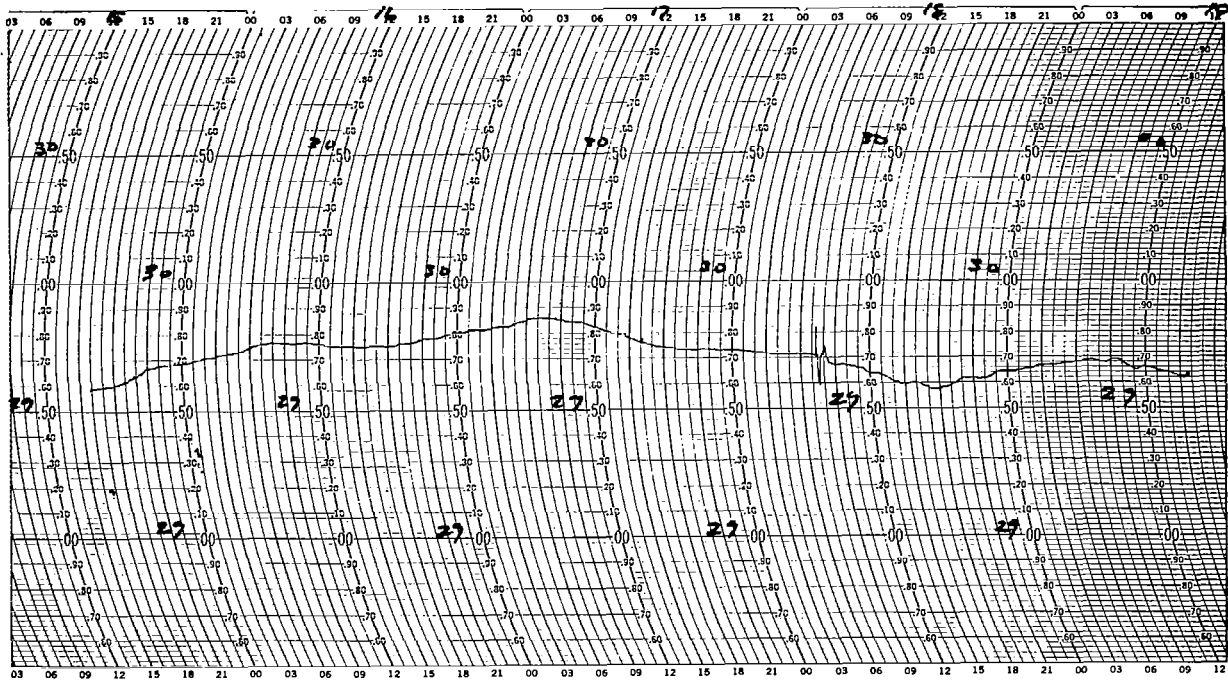


Figure 3. Pressure wave from Mount St. Helens explosion registered on barograph at Toledo, Washington, 18 May 1980. (Courtesy National Climatic Center.)

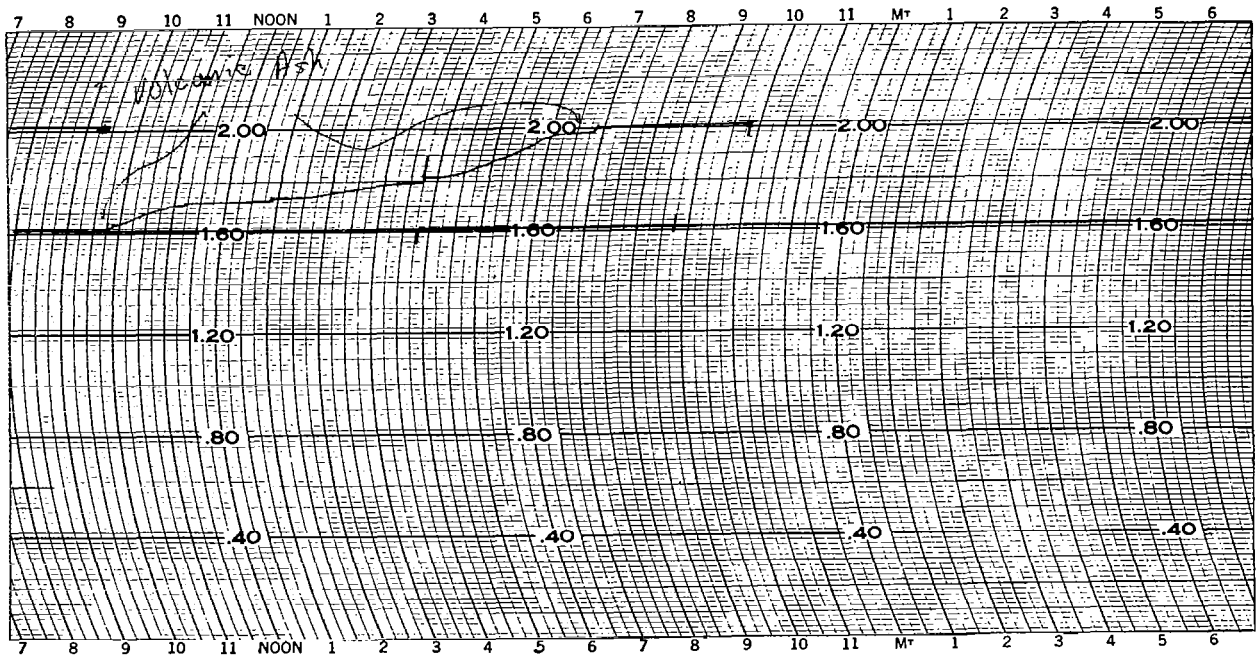


Figure 4. Ashfall recorded by rain gage at Yakima, Washington, 18 May 1980. (Courtesy National Climatic Center.)



THE MECHANISMS OF FINE PARTICLE GENERATION AND ELECTRIFICATION DURING MOUNT ST. HELENS VOLCANIC ERUPTION

Roger J. Cheng

Atmospheric Sciences Research Center, State University of New York at Albany

Microscopical investigation of volcanic ash collected from ground stations during Mount St. Helens eruptions reveal a distinctive bimodal size distribution with high concentrations of particle ranges at (1) 200-100 μm and (2) 20-0.1 μm . Close examination of individual particles shows that most larger ones are solidified magma particles of porous pumice with numerous gas bubbles in the interior and the smaller ones are all glassy fragments without any detectable gas bubbles. Very few of the fragments are below 0.1 μm and no evidence could be found to indicate that the small particles are formed by the condensation process. Elemental analysis demonstrates that the fine fragments all have a composition similar to that of the larger pumice particles. Laboratory experiments suggest that the formation of the fine fragments is by bursting of glassy bubbles from a partially solidified surface of a crystallizing molten magma particle. The production of gas bubbles is due to the release of absorbed gases in molten magma particles when solubility decreases during phase transition. Diffusion cloud chamber experiments strongly indicate that sub-micron volcanic fragments are highly hygroscopic and extremely active as cloud condensation nuclei. Ice crystals also are evidently formed on those fragments in a supercooled (-20°C) cloud chamber.

It has been reported that charge generation from ocean volcanic eruptions is due to contact of molten lava with sea water. This seems to be insufficient to explain the observed rapid and intense lightning activities over Mount St. Helens eruptions. Therefore, a hypothesis is presented here that highly electrically charged fine solid fragments are ejected by bursting of gas bubbles from the surface of a crystallizing molten magma particle. The charge-separation process by thermal electric effect is taking place within this crystallizing particle, and their polarities are determined by a temperature gradient between the colder surface of the solid glassy bubbles and the interior of the particle with a much higher temperature. After bursting, positively charged fine fragments are ejected and carried by convection to the top of a volcanic plume and negatively charged and heavier solidified plume particles gradually fall by gravity to the base of the plume and eventually reach the ground.

It is suggested that the fragmentation of volcanic ash and its accompanying electrification may play an important role in the generation of electric fields which may become strong enough to initiate lightning during a volcanic eruption and also to have a definite impact on climatological effects in the atmosphere.

I. DISCUSSION

Microscopical investigation of volcanic ash collected from ground stations during Mount St. Helens eruption on May 18, 1980 reveals a distinctive bimodal size distribution (fig. 1) with high concentration of particle ranges at 200 to 100 μm and 20 to 0.1 μm . Particle size data reported by Fruchter et al. (1) shows similar bimodal distributions and suggests that there are at least two different types of materials, possibly old material blown out of the volcano by eruption and fresh magmatic material.

Close examination of individual particles shows that most larger ones are solidified magma particles of porous pumice with numerous gas bubbles at their interior (fig. 2a,b) and that the smaller ones are fragments of angular glassy shards and plates with arcuate and forked forms. Ninety percent of these particles by count are less than 30 μm , and more than fifty percent are less than 3 μm (respirable size) (fig. 3a,b). Very few of the fragments are below 0.1 μm and no evidence could be found that indicated that the small particles are formed by the condensation process. Elemental analysis demonstrates that the fine

fragments have a composition similar to that of the larger pumice particles with major composition (by weight) of Si (> 70%), Al (15%), Ca (5%), Fe (4%), and some trace elements of S, K, Ti, Mn, P, etc.

The result of laboratory experiments, by injection of air bubbles into a small portion of molten ash, strongly suggest that the formation of the fine fragments is by bursting of glassy bubbles from a partially solidified surface of a crystallizing molten magma particle. The production of the gas bubbles is due to the release of absorbed gases in the molten magma particle when the solubility of the gases decreases during a phase transition.

Meteorological properties of volcanic ash examined in the laboratory diffusion cloud chamber experiments (2) strongly indicate that sub-micron volcanic fragments are highly hygroscopic and extremely active as cloud condensation nuclei. (See fig. 4.) Ice crystals also evidently formed on those fragments in a supercooled (-20°C) cloud (3).

High electric field and lightning activities during Mount St. Helens eruption are reported (4-7). Lightning bolts, some as long as 2 miles (4), and balls of lightning at elevations from the ground level into the ash cloud over Yakima, Washington (140 km east northeast of the volcano) (5) are also observed. Electric field measurements from NOAA aircraft by Cobb (7) show that as high as 20,000 V m⁻¹ are observed and both the horizontal and vertical field measurements indicated a positively charged volcanic cloud. One hundred and sixty-four lightning discharges are recorded. The more predominant discharges indicate the lowering of positive charge to the ground and many discharges of the opposite polarity suggest the existence of something other than a monopole charge structure in the volcanic cloud.

The possible mechanisms for the generation of electric field and lightning discharges during volcanic eruption have been suggested to be (1) collision of particles (6,8), (2) chemical reactions (9), and (3) induction of charged particles in ash clouds. Blanchard's experiment (10, 11) confirmed that charge generation from ocean volcanic eruption [Surtsey, 1964 (12)] is due to contact of molten lava with saline water. This result does not seem to be applicable as an explanation of the observed rapid and intense lightning activities over the land volcanic eruption at Mount St. Helens.

Based on previous laboratory studies of the fragmentation and electrification of water droplets during phase transition (13,14), similar technique is used to determine the polarity of the ejected fragments during the laboratory experiment. The preliminary results indicate that more than 70 percent of the fine fragments ejected by bursting of glassy bubbles are positively charged.

At present, an hypothesis is therefore presented here that highly electrically charged fine solid fragments are ejected by bursting of gas bubbles from the surface of a crystallizing molten magma particle. The charge separation process by the thermal electric effect is taking place within this crystallizing particle, and the polarity is determined by the temperature gradient between the colder surface of the solid glassy bubbles and the interior of the particle with a much higher temperature. After bursting, positively charged fine fragments are ejected and carried by convection to the top of a volcanic plume and negatively charged and heavier solidified plume particles gradually fall by gravity to the base of the plume, and eventually reach the ground.

II. CONCLUDING REMARKS

It is suggested that the fragmentation of volcanic ash and its accompanying electrification may play an important role in the generation of electric fields which may become strong enough to initiate lightning during volcanic eruption, and also have definite impact on climatological effects in the atmosphere.

REFERENCES

1. Fruchter, J. S., et al.: Mount St. Helens Ash from 18 May Eruption: Chemical, Physical, Mineralogical, and Biological Properties. *Science*, vol. 209, no. 4461, 1980, pp. 1116-1125.
2. Jiusto, J. E.: Cloud Condensation Nucleus Counters. *Atmospheric Technology-NCAR*, Nov. 8, 1976, pp. 43-49.
3. Schaefer, V. J., and Cheng, R. J.: The Effect of the Nucleus on Ice Crystal Structure. *Proceedings of International Conference on Cloud Physics*, Toronto, 1968, pp. 255-259.

4. E O S Trans., vol. 61, no. 23, 1980, p. 481.
5. E O S Trans., vol. 61, no. 36, 1980, p. 611.
6. Hobbs, P. V., Radke, L. F., Eltgroth, M. W., and Hegg, D. A.: Airborne Studies of the Emissions from the Volcanic Eruption of Mount St. Helens. Science, vol. 211, 1981, pp. 816-818.
7. Cobb, W. F.: Electric Fields and Lightning in the Mount St. Helens Volcanic Cloud. Paper presented at AGU, Fall Meeting (San Francisco, California), 1980.
8. MacDonald, G. A.: Volcanoes. Prentice-Hall, 1972.
9. Hatakeyama, H.: On the Disturbance of the Atmospheric Electric Field Caused by the Smoke Cloud of the Volcano Asama-yama. Meteorol. Geophys. (Tokyo, Japan) vol. 8, Nov. 4, 1958, pp. 302-316.
10. Blanchard, D. C.: Charge Separation From Saline Drops on Hot Surfaces. Nature, vol. 201, no. 4925, 1964, pp. 1164-1166.
11. Bjornsson, S., Blanchard, D. C., et al.: Charge Generation Due to Contact of Saline Water With Molten Lava. J. Geophys. Res., vol. 72, no. 4, 1967, pp. 1311-1323.
12. Anderson, R., Bjornsson, S., Blanchard, D. C., et al.: Electricity in Volcanic Clouds. Science, vol. 148, no. 3674, 1965, pp. 1179-1189.
13. Cheng, R. J.: Water Drop Freezing—Ejection of Microdroplets. Science, vol. 170, no. 3965, 1970, pp. 1395-1396.
14. Cheng, R. J.: Ice Pellet Melting-Ejection of Microdroplets. AMS Conference on Cloud Physics and Atmospheric Electricity (Issaquah, Washington), 1978, pp. 35-38.



Figure 1. This photomicrograph shows a bimodal size distribution of volcanic ash with larger particles of 200 to 100 μm and fine fragments of 20 to 0.1 μm .

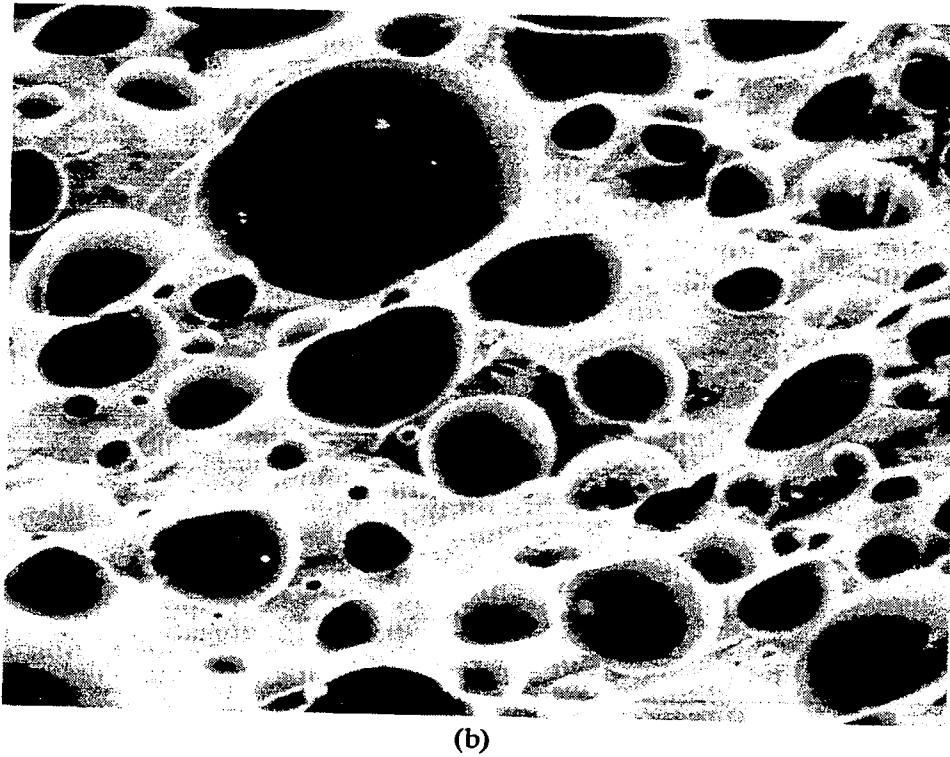
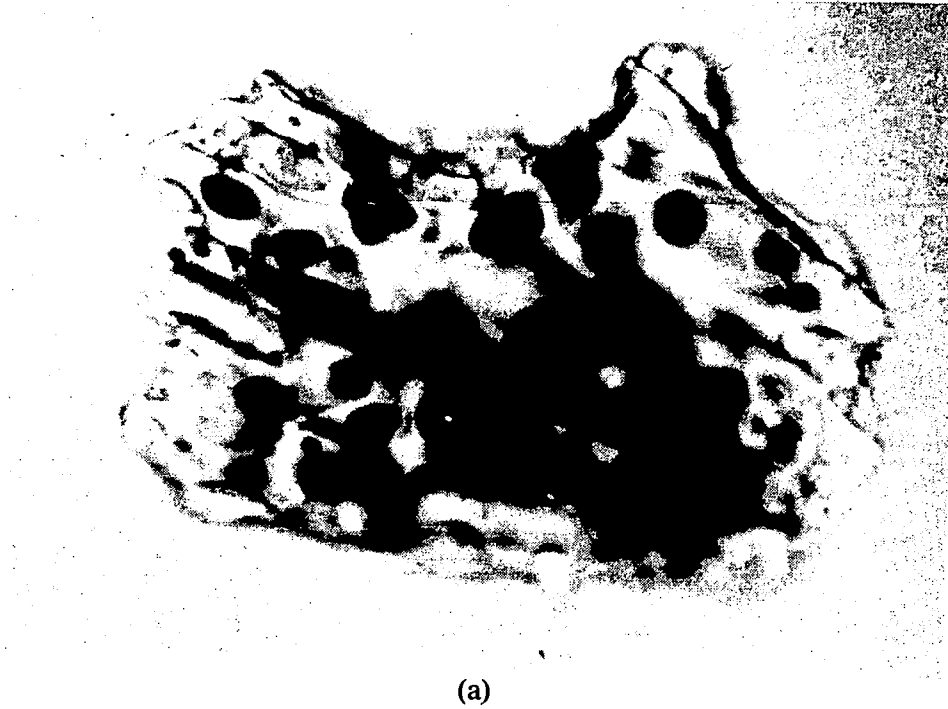


Figure 2. Pumice particles. (a) Photomicrograph of a porous pumice particle with numerous gas bubbles of 20 to 40 μm at its interior. (b) SEM micrograph of cross-section of a pumice particle.



(a)



(b)

Figure 3. TEM micrographs of 2- μm volcanic ash of angular glassy shard and plates with numerous sub-micron particles attached to its surface.

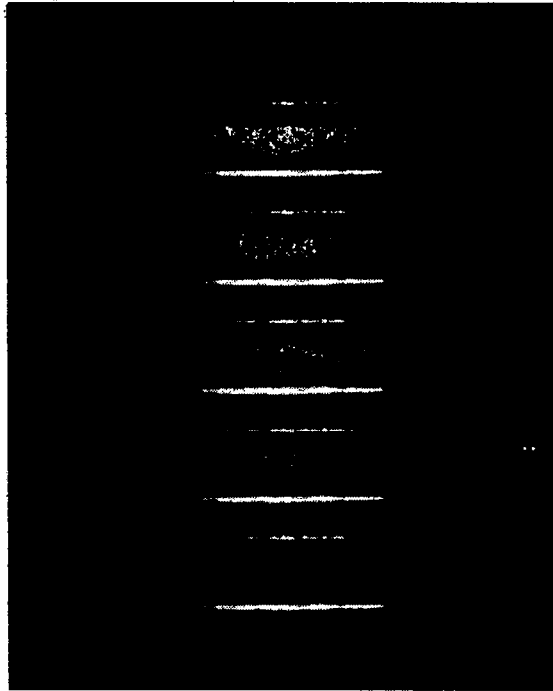


Figure 4. Photograph of condensed water droplets formed in a diffusion cloud chamber from fine volcanic ash at supersaturations of 2%, 1%, 0.5%, 0.2%, and 0%.

MEASUREMENTS OF SO₂ IN THE MOUNT ST. HELENS DEBRIS

J.B. Kerr, W. F. J. Evans, and C. L. Mateer
Atmospheric Environment Service, 4905 Dufferin Street Downsview, Ontario, Canada

Routine measurements of ozone and SO₂ are made with the Dobson and Brewer spectrophotometers at the Atmospheric Environment Service in Downsview Ontario. On May 20 and 21, 1980, large values of column SO₂ were observed with both spectrophotometers at the time of passage of the Mount St. Helens debris. Enhanced SO₂ values were first observed at 1800Z on May 20. The maximum column amount of SO₂ measured was 0.06 cm at 2200Z. On May 21, SO₂ values slowly decreased from 0.03 cm at 1100Z to 0.01 cm at 2000Z. Typical SO₂ amounts due to pollution at the Downsview site are approximately 0.003 to 0.005 cm. At the same time of maximum SO₂ enhancement, both Dobson and Brewer spectrophotometers measured a 0.040 cm decrease of total ozone. It is not clear whether the decrease of total ozone was caused by the volcanic cloud or natural ozone variability. Air mass trajectories indicate that the altitude of the debris cloud, which passed over Downsview at the time, was between 10 km and 12 km.

I. INTRODUCTION

Several spectrophotometric and filter instruments make use of the strong ozone absorption spectrum at wavelengths shorter than 340 nm to measure stratospheric ozone. The Dobson ozone spectrophotometer has monitored stratospheric ozone on a routine basis for nearly 50 years in the world ozone network. More recently, the Brewer ozone spectrophotometer has been developed to replace or supplement the Dobson instrument in the network (1).

Sulfur dioxide also has strongly banded absorption features in the spectral region used for ozone measurements (Fig 1). Evans et al. show that SO₂ causes interference with the Dobson total ozone measurements and they outline a method by which SO₂ is measured and used to correct the ozone measurements (2). Kerr et al. describe the method by which ozone and SO₂ are measured with the Brewer ozone spectrophotometer (3).

Routine ozone and SO₂ measurements are made with the Dobson and Brewer spectrophotometers at the Atmospheric Environment Service in Downsview, Ontario. On May 20 and 21, 1980, enhanced values of SO₂ were observed which were several times larger than SO₂ values normally observed in heavy pollution situations. The enhanced SO₂ values coincided with the passage of the debris cloud from the Mount St. Helens eruption of May 18, 1980. Measurements of SO₂ during the passage of the volcanic debris are reported. The total amount of SO₂ injection is estimated by using the column amount of SO₂ measured in the debris cloud and satellite images to determine the extent of the cloud.

II. RESULTS

The daily average values for the column amount of SO₂ over Downsview for the period from September 1979 to June 1980 are shown in figure 2. Typical SO₂ amounts due to pollution are approximately 0.004 cm and heavy pollution situations rarely cause the daily average to exceed 0.010 cm. On May 20 and May 21, the daily average for SO₂ was greater than 0.030 cm.

Measurements of SO₂ with both the Brewer and Dobson instruments for the period from May 20 to May 23 are shown in Figure 3. The column amount of SO₂ started to increase at about 1800Z on May 20 and peaked at 0.065 cm at 2300Z. On May 21, the SO₂ values remained between 0.030 and 0.040 cm for most of the day and slowly dropped after 2000Z. Normal SO₂ values were observed on May 22 and May 23.

Figure 4 shows the total ozone measurements between May 20 and May 23. On May 20, total ozone dropped from 270 Dobson Unit to 230 DU as the volcanic cloud passed. On May 21, the ozone slowly increased during the day from about 250 DU to 265 DU. Total ozone values on May 22 and May 23 are significantly lower than they were before the onset of the volcanic cloud. The apparent ozone decrease during the volcanic event could be due to one of two effects. First, the presence of the volcanic debris could photochemically destroy the ozone. Second, the injection of ozone free air from the lower troposphere during the eruption would cause a dilution of stratospheric ozone.

The volcanic cloud was identified on the GOES satellite images for the period from May 19 to May 23. There is good agreement with the presence of the satellite feature over the Downsview area and the enhanced SO₂ values. Analysis of the upper air wind maps suggests that the leading edge of the cloud was at the height of the jet stream or 10 km. Debris passing over Downsview later in time was most likely at a higher altitude. The altitude of the cloud over Downsview on May 21 is estimated to be between 13 and 15 km.

Using the satellite data, the area of the volcanic cloud at the time it passed over Toronto was estimated to be approximately 5×10^5 km². The average column amount of SO₂ measured within the cloud during the pass over Toronto was 0.040 cm. These figures suggest a total volume of 2×10^8 m³ of SO₂ within the cloud or 0.6×10^6 tonnes of SO₂.

REFERENCES

1. Brewer, A. W., A replacement for the Dobson spectrophotometer? Pure and Applied Geophysics, Vol. 106-108, pp. 919-927, 1973.
2. Evans, W. F. J., Asbridge, I. A., Kerr, J. B., Mateer, C. L. and Olafson, R. A., The Effects of SO₂ on Dobson and Brewer total ozone measurements. Proceedings of the International Ozone Symposium, Boulder, Aug., 1980.
3. Kerr, J. B., McElroy, C. T., and Olafson, R. A., Measurements of Ozone With the Brewer Ozone Spectrophotometer. Proceedings of the International Ozone Symposium, Boulder, Aug., 1980.

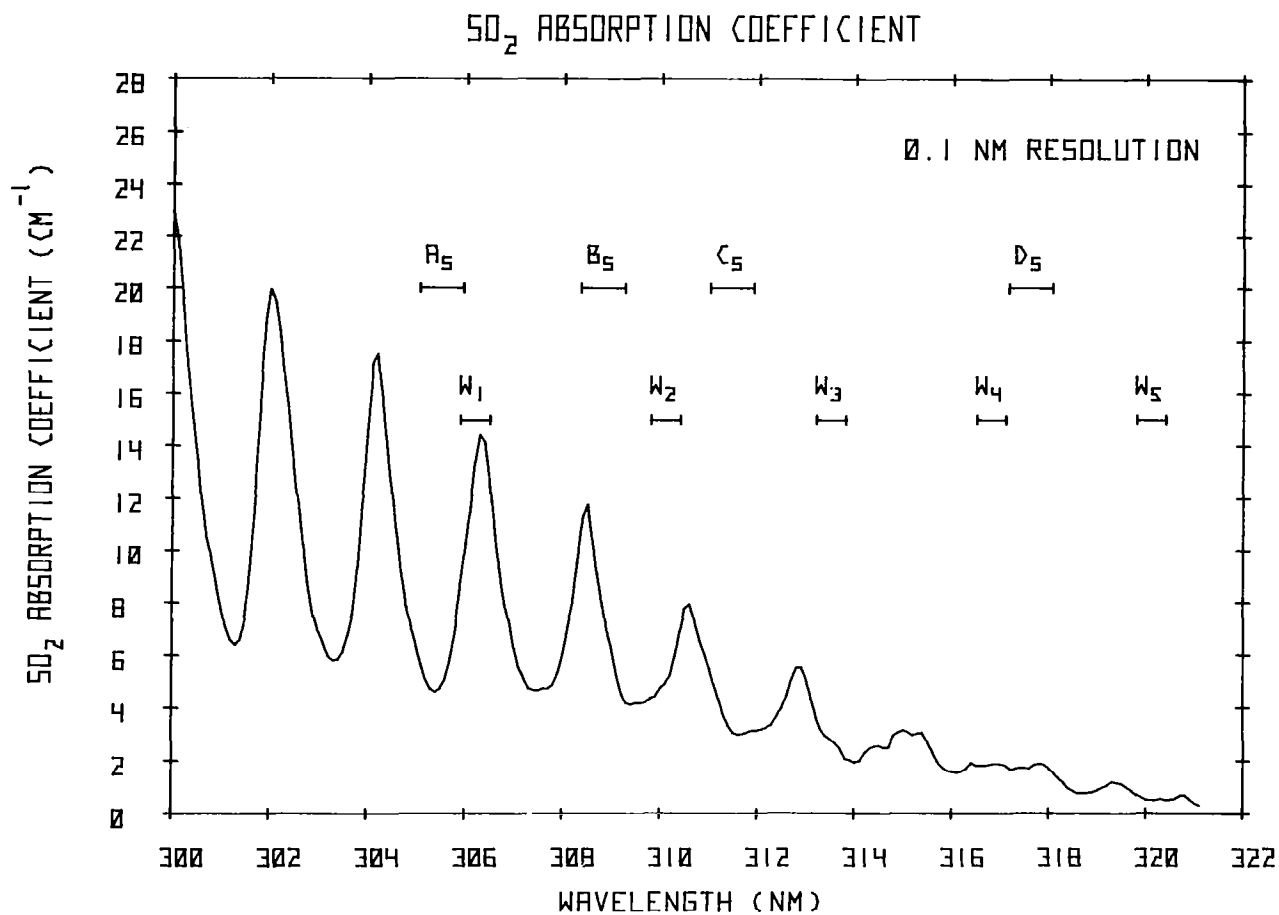


Figure 1. The absorption spectrum of SO₂. Wavelengths for the Dobson and Brewer ozone spectrophotometers are indicated. Wavelength B, for the Dobson instrument and wavelength W₁ for the Brewer instrument are on SO₂ absorption peaks. A detailed description of the method by which SO₂ is measured is described by Evans et al. for the Dobson instrument and by Kerr et al. for the Brewer instrument (2,3).

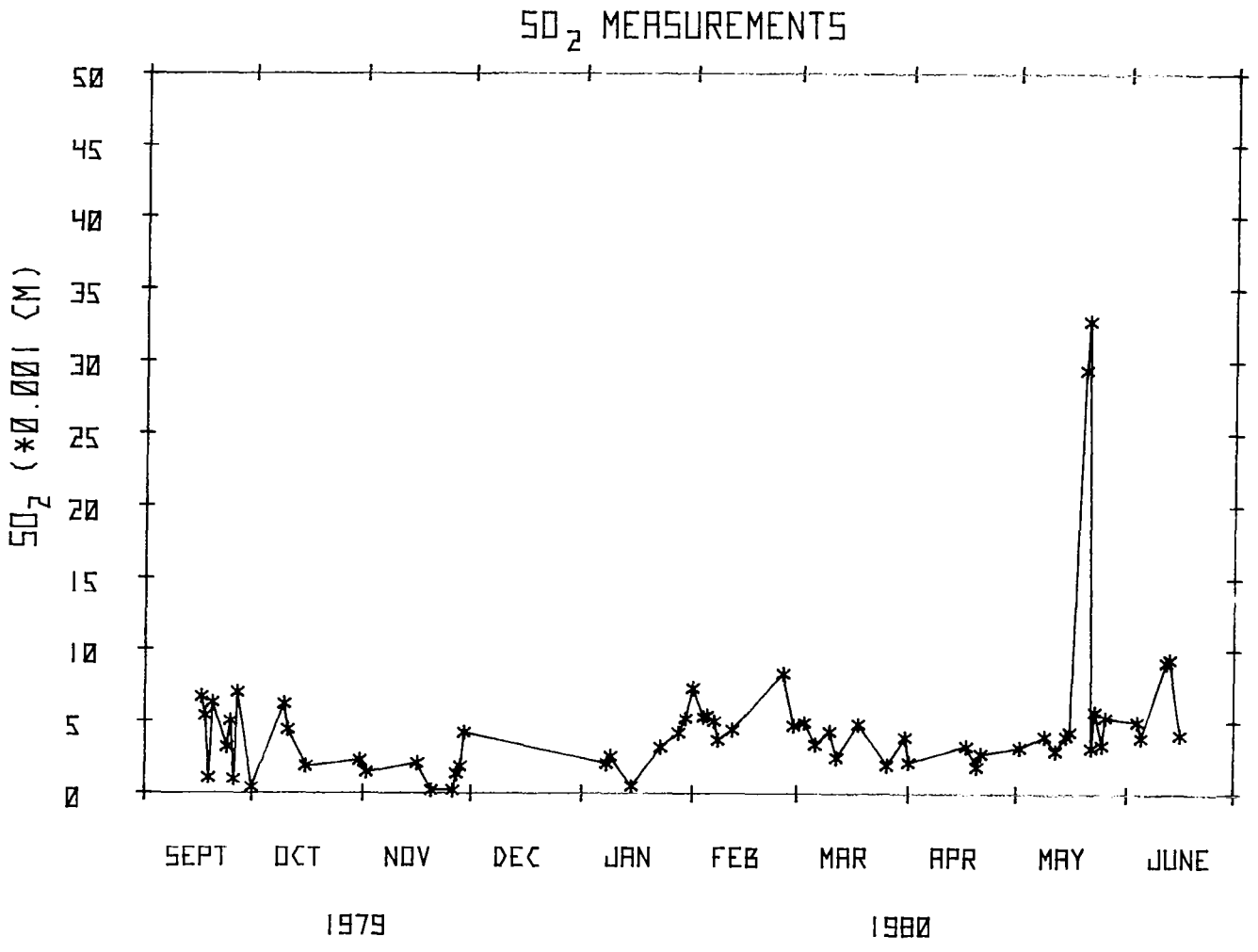


Figure 2. Time record for daily averages of SO₂ measurements made at Toronto between September 1979 and June 1980. Heavy local pollution situations in Toronto rarely cause the daily average to exceed 0.010 cm. The average values for May 20 and May 21 are larger than 0.030 cm.

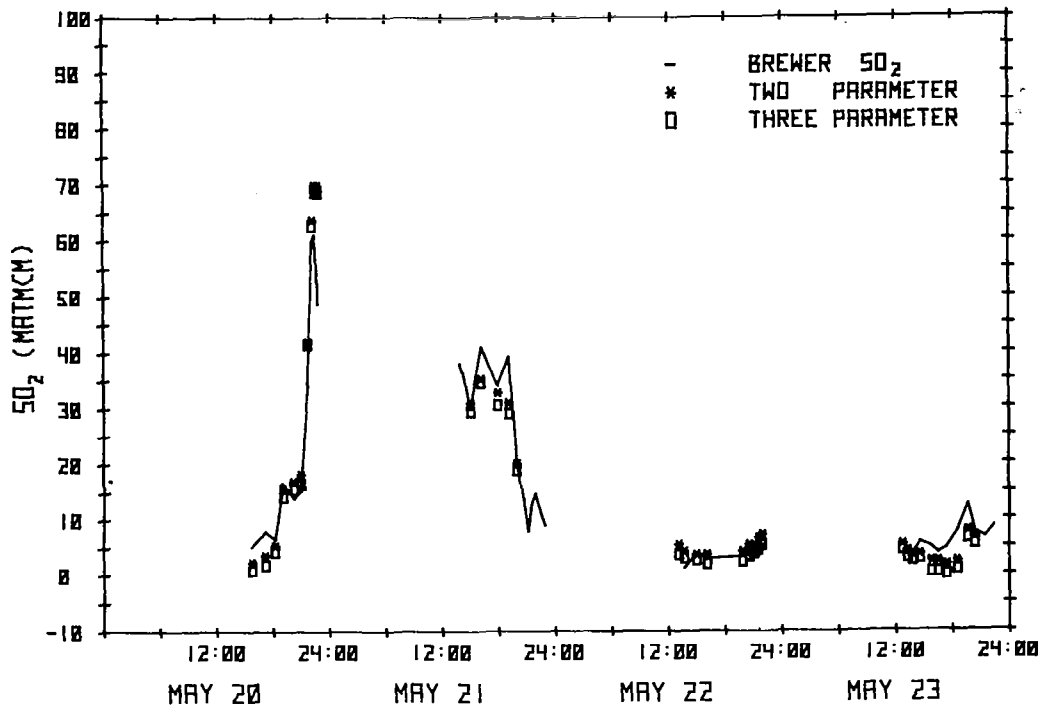


Figure 3. Brewer and Dobson SO₂ measurements at Toronto between May 20 and May 23. Both instruments measured significant amounts of SO₂ on May 20 and May 21. Measurements made on May 22 and May 23 are typical for Toronto.

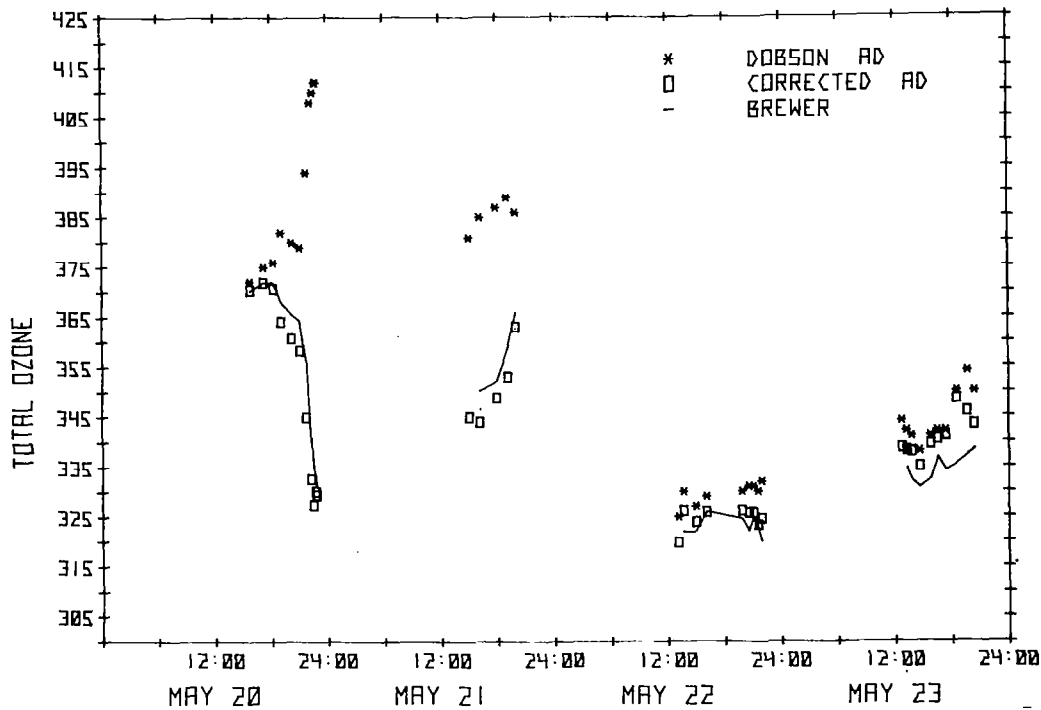


Figure 4. Brewer and Dobson ozone measurements at Toronto between May 20 and May 23. Both instruments indicated a drop of about 0.040 cm on May 20 at the peak of the SO₂ event. It is not clear whether the ozone decrease was due to the volcanic debris or whether it was due to natural variations.

ASH LOADING AND INSOLATION AT HANFORD, WASHINGTON, DURING AND AFTER THE ERUPTION OF MOUNT ST. HELENS¹

N. S. Laulainen
Battelle Pacific Northwest Laboratory, Richland, WA

The effects of volcanic ash suspended in the atmosphere on the incident solar radiation was monitored at the Hanford Meteorological Station (HMS) subsequent to the major eruption of Mount St. Helens on May 18, 1980. Passage of the ash plume over Hanford resulted in a very dramatic decrease of solar radiation intensity to zero. A reduction in visibility to less than 1 km was observed, as great quantities of ash fell out of the plume onto the ground. Ash loading in the atmosphere remained very high for several days following the eruption, primarily as a result of resuspension from the surface. Visibilities remained low (2 to 8 km) during this period. Estimates of atmospheric turbidity were made from the ratio of diffuse-to-direct solar radiation; these turbidities were used to estimate extinction along a horizontal path, a quantity which can be related to visibility. Comparisons of observed and estimated visibilities were very good, in spite of the rather coarse approximations used in the estimates. Atmospheric clarity and visibility improved to near pre-eruption conditions following a period of rain showers. The diffuse-to-direct ratio of solar radiation provided a useful index for estimating volcanic ash loading of the atmosphere.

I. INTRODUCTION

Major volcanic eruptions, although infrequent in time, have injected considerable quantities of dust and ash into the atmosphere. Volcanic ash penetrating into the stratosphere may remain suspended for several years. Such dust layers have the potential to alter climate by redistribution of solar radiation reaching the earth's surface. The eruption of Mount St. Helens on May 18, 1980, with its associated massive ash plume which spread across the United States, was of sufficient magnitude to be seriously studied for possible climate and weather modification. The eruption has been documented better than any other in historical times by means of satellite images, atmospheric and surface dust collections for analysis of chemical and optical properties, and, in certain locations, solar radiation measurements.

Pacific Northwest Laboratory (PNL) has a continuing program of monitoring insolation and atmospheric turbidity in addition to other meteorological parameters at the Hanford Meteorological Station (HMS). Insolation and turbidity measurements are carried out routinely at the Rattlesnake Mountain Observatory (RMO). These measurement programs have been used for insolation assessment for solar energy applications and for research into the optical properties of atmospheric hazes and clouds and their effects on the redistribution of solar radiation received at the earth's surface.

This paper describes observations of insolation before and after the May 18, 1980 eruption of Mount St. Helens. The results inferred from the insolation records during the time period May 16-31, 1980, are based on an empirical relationship between the ratio of diffuse-to-direct solar radiation and atmospheric turbidity (aerosol optical depth) at 550 nm wavelength. This relationship was derived from insolation and turbidity measurements obtained from an intensive experiment conducted during September and October 1979 (1). Turbidities derived from the diffuse-to-direct ratio are used to estimate visibilities, which are then compared with observed visibilities.

¹Work Supported by the U.S. Department of Energy under Contract DE-ACO6-76RLO-1830.

II. OBSERVATIONAL DATA

King and Herman (2,3) have defined the ratio of diffuse-to-direct solar radiation flux as

$$\phi = \mu_0 F^- / (G - F^-) \quad (1)$$

where

G = Measured global solar radiation flux

F^- = measured downward component of diffuse solar radiation flux

μ_0 = $\cos Z$

Z = solar zenith angle.

They have further shown that ϕ is sensitive to turbidity (aerosol optical depth), ground albedo, and the light absorption index of atmospheric particles.

An empirical relationship between the diffuse-to-direct ratio ϕ as defined by equation (1) and atmospheric turbidity (aerosol optical depth) τ at a wavelength of 550 nm was derived from insolation and turbidity measurements made during September/October 1979 at HMS and RMO (3). Instrumentation consisted of Eppley precision spectral pyranometers (used for calibration) and Lambda silicon cell pyranometers, each equipped with a motorized shadow band which occluded the direct solar beam every 5 minutes (4). Operating in this manner, the silicon cell pyranometers provided direct values for the global solar radiation G and the downward component of diffuse solar radiation F^- . Since both G and F^- were measured with the same instrument and since G and F^- also occur only in a ratio, no absolute values of solar radiation were required. Multi-wavelength sunphotometers were used to determine atmospheric turbidities. The results of the 1979 study are shown in figure 1 for a variety of solar zenith angles and turbidities.

Two curves are shown in figure 1. The dashed curve represents a least squares fit to a limited set of data points ($\tau < 0.22$) and the solid curve is a least squares fit to all data, including a dust storm event on October 8, 1979 (not shown). The correlation coefficients of the fits are better than 0.97 and indicate an excellent correlation between ϕ and τ . For the purposes of this study, the relationship derived from all the data is used, namely

$$\phi = 0.52\tau + 0.014 \quad (2)$$

From measurements of ϕ during cloud-free sky conditions, estimates of τ may be obtained from equation (2).

Use of equation (2) as a turbidity estimator implicitly assumes that the aerosol size distributions during the present study period were similar to those from which equation (2) was derived (2). For low turbidity conditions (e.g., $\tau < 0.1$), turbidity measurements at HMS since 1974 indicate that size distributions of atmospheric haze are indeed very similar. High turbidity conditions (e.g., $\tau > 0.4$) have occurred usually during dust storm events, where aerosol size distributions are dominated by coarse particles typically larger than 1 μm . Comparison of particle size distributions measured at Hanford during dust storms and suspended volcanic ash after the May 18 eruption indicated that the latter distributions had a larger fraction of mass in the 0.5 to 1 μm size range. The influence of this size difference on the relationship between ϕ and τ given by equation (2) is not known at this time, but other evidence indicates that the slope would not change by more than 20 to 30 percent.

Examples of the insolation records during the time period of May 16 to 31, 1980, are shown in figures 2 to 6 for May 16, 18, 19, 20, and 31, respectively. Except for May 16 and 31, which were clear, cloud interference (e.g., cirrus, altocumulus or fair weather cumulus) presented a severe problem in evaluating the diffuse-to-direct ratios. Only those portions of the charts where cloud effects were thought to be minimized were used in obtaining ϕ . In some cases, the NOAA weather satellite images were useful in selecting appropriate portions. Cloud effects would tend to increase ϕ and hence to overestimate the turbidity.

The record for May 16 (figure 2), 2 days prior to the eruption, is typical of clear, low haze conditions. Figure 3 shows the progression of solar radiation on May 18. Scattered to broken cirrus was reported over HMS prior to the arrival of the ash plume. A dramatic increase in diffuse radiation is seen after ≈ 0830 PST, approximately 1 hour after the eruption. Shortly after 0900 PST, total insolation began to decrease and sharply decreased around 0930 PST. By 1000 PST, insolation was essentially zero and remained zero for the remainder of the day. Ash fall began around 1100 PST. Prior to ash fallout visibilities were in excess of 24

km but rapidly deteriorated to ≈ 2 km after 1100 PST. A surface accumulation of 2.5 mm of ash was recorded at HMS. Satellite (GOES-West) images of the volcanic plume approximately 2 hours and 7.5 hours after eruption are shown in figures 7 and 8, respectively. In these images, the eastward motion and lateral spread of the plume is clearly evident.

On May 19 visibility continued to be very low (≈ 2 km) for most of the day because of the fine volcanic ash still suspended in the atmosphere. Although surface observations of cloud cover were difficult to make during this period, a satellite image 24 hours after eruption clearly showed cirrus bands over most of eastern Washington (figure 9). Diffuse-to-direct ratios were quite large (figure 4), very probably as a result of the cirrus. Mass loadings of suspended ash on the southern boundary of the Hanford Site were found to range between 150 to 600 $\mu\text{g}/\text{m}^3$.

Visibilities improved only very slowly during the next 4 or 5 days. After May 27, conditions dramatically improved as a result of a substantial precipitation (≈ 2 cm). Mass loading decreased by a factor of 100 to near normal values of 1 to 6 $\mu\text{g}/\text{m}^3$. By May 31, visibilities and diffuse-to-direct insolation values had also returned to near normal values (figure 6).

III. RESULTS AND DISCUSSION

The results of the diffuse-to-direct ratio determinations and turbidities at 550 nm estimated from these ratios (equation (2) being assumed valid for suspended volcanic ash) are shown in table I. In many cases, as pointed out earlier, the ϕ values are probably over estimated as a result of cirrus or other cloud contamination. Table I also shows a comparison of visibilities derived from the diffuse-to-direct ratio through the turbidity.

The chain of reasoning leading to an estimate of visibility from ϕ proceeds in the following manner. Visibility depends upon extinction along a horizontal path whereas turbidity depends upon extinction integrated along a path through the vertical. If it is assumed that the aerosol particles are well mixed up to some height H with a negligible amount above H, then the mean extinction coefficient in the mixed layer is

$$b_{ext} = \tau/H \quad (3)$$

where τ is derived from equation (1). The Koschmeider formula (5) relates the visual range to the effective atmospheric extinction coefficient along the line of sight by

$$V = K/b_{ext} \quad (4)$$

The constant K, which is related to the liminal contrast, has been frequently set at a value of 3.9 although other values between 1.7 and 4 have been suggested. (See for example, ref. 6 for a discussion.) For this study, a value of 3 is arbitrarily used. By combining equations (3) and (4), the expression

$$V = 3H/\tau \quad (5)$$

is easily found. From aircraft sounding conducted during June 1980, a value of H between 1 and 2 km was frequently observed, in this work H = 1 km was adopted to a first approximation.

It is seen in table I that the comparison between the visual range (visibility) derived from equation (5) is generally much better than might be expected when the number of approximations used in proceeding from the measurement of ϕ to the estimate of V is considered. Only on May 18 and 19 were the estimated visibilities poor in comparison with the observations. On May 18 the plume was overhead with very little ash between it and the surface. Therefore, vertical extinction could not be easily related to horizontal extinction. When the ash was falling, the insolation was zero; consequently, no estimate for ϕ could be made. On both May 18 and 19, cirrus clouds were probably present in sufficient quantity to invalidate the use of equation (2).

A number of problems with the ash fallout continue to occur. Ash from subsequent eruptions (for example, the July 22 eruption) and ash resuspended from the surface will continue to produce significant atmospheric ash loadings, especially in those areas where ash fall was the greatest. Continued observations of insolation and turbidity will be required to document any significant changes in atmospheric transparency as a result of the Mount St. Helens eruption.

Ash loading events continued to occur during the summer and fall of 1980 as a result of subsequent eruptions and resuspension from the surface, especially in those areas where ash fall was the greatest. An example of one such occurrence is illustrated in figure 10. In this example the variation of the diffuse-to-direct ratio as a function of the cosine of the solar zenith angle over a period of several days based on insolation measurements taken at Hanford, coinciding with an eruption of Mount St. Helens on July 22, 1980, is shown. Turbidity measurements were also carried out during this period. Volcanic ash from this eruption dispersed in eastern Washington during the night of July 22 and during the day of July 23, assisted by drainage winds at night and solar heating during the day. The relationship shown in figure 1, developed for all data taken in September/October 1979, is repeated in figure 11, along with individual points from the observations made during the measurement period July 21 to 28, 1980. The good agreement between the new measurements and the solid curve show that this relationship is also reasonable for suspended volcanic ash.

Inspection of the curves in figure 10 reveals several interesting observations. The curves for the diffuse-to-direct ratio of figure 10 during the morning of July 21 and during the morning and afternoon of July 27 are typical of cloud-free, low-haze conditions. Near mid-day on July 23, however, diffuse radiation increased dramatically as blowing ash obscured visibility. Similar high haze conditions persisted during the day on July 24 and 25, also a gradual improvement occurring during the afternoon on July 26. Similar behavior for ash loading and diffuse radiation increases from ash resuspension on windy days with directions out of the northerly sector during dry periods have also been observed in the insolation data but have not yet been analyzed. The rather frequent occurrence of volcanic ash related events during the summer of 1980 emphasizes the need for continued observations of insolation, turbidity, and airborne ash concentrations to document any significant changes in atmospheric transparency as a result of Mount St. Helens eruptions. The Hanford Site is uniquely situated, since it is generally downwind of the volcano, to monitor these ash-related changes.

IV. CONCLUDING REMARKS

The insolation and turbidity monitoring program at Hanford Meteorological Station has provided a method of estimating ash loading in the atmosphere after the May 18 eruption of Mount St. Helens. Comparisons of visibilities derived from the diffuse-to-direct insolation ratio with those observed at Hanford Meteorological Station were generally good, in spite of the rather coarse approximations and assumptions which were made.

Additional work relating insolation and turbidity at Hanford over more varied conditions than those encountered during the 1979 study, from which the correlation of the ratio of diffuse-to-direct solar radiation and atmospheric turbidity was derived, is required. Documentation of subsequent eruptions of Mount St. Helens resulting in ash fallout over Hanford and/or resuspension of ash already present will continue. Hopefully, these studies may provide insights into understanding radiative effects of volcanic aerosol and therefore the effects of volcanic aerosol on climate modification.

REFERENCES

1. Michalsky, J. J.; Laulainen, N. S.; Stokes, G. M.; and Kleckner, E. W.: Differential Turbidity in an Arid Environment. Abstract Design of Workshop on Atmospheric Aerosols—Their Formation, Optical Properties and Effects, Institute for Atmospheric Optics and Remote Sensing, (Baltimore, Maryland), November 6-8, 1979, p.23.
2. King, M. D.: Determination of Ground Albedo and the Index of Absorption of Atmospheric Particulates by Remote Sensing. Part 2, Application. *J. Atmos. Sci.*, vol. 36, 1979, pp. 1072-83.
3. King, M. D.; and Herman, B. M.: Determination of Ground Albedo and the Index of Absorption of Atmospheric Particles by Remote Sensing, Part 1, Theory. *J. Atmos. Sci.*, vol. 36, 1979, pp. 163-173.
4. Wesely, M. L.: Measurement of Atmospheric Turbidity in an Arc Downwind of St. Louis. Radiological and Environmental Research Division Annual Report—Atmospheric Physics, ANL-75-60, Part IV, Argonne National Laboratory (Argonne, Il), 1975, pp. 22-30.
5. Middleton, W. E. K.: Vision Through the Atmosphere. University of Toronto Press, 1952, p. 250.
6. Griffing, G. W.: Relationships Between the Prevailing Visibility, Nephelometer Scattering Coefficient and Sunphotometer Turbidity Coefficient. Atmos. Environ. vol. 14, 1980, pp. 577-584.

TABLE I. Measured Diffuse-to-Direct Solar Radiation Ratio, Turbidity at 550 nm and Estimated/Observed Visibilities at Hanford Meteorological Station for Various Days Before and After the Mount St. Helens Eruption of 18 May 1980. [$\tau' = 1.92 \phi - 0.027$; $V^* = 3 H/\tau$, $H \approx 1$ km.]

Date	ϕ	τ' (550)	$V^*(\text{km})$	$V_o(\text{km})$	Comment
16 May 80 a	0.063	0.10	30	24+	Clear sky, light haze
p	0.071	0.11	27	24+	
17 May 80 a	0.11	0.19	16	24+	CS (1.0)
p	0.095	0.16	19	24+	Scattered Ci (0.1)
18 May 80 8	0.24	0.44	6.9		Scattered Ci (0.3)
9	0.59	1.11	2.7		Broken Ci (0.6)
10	3.2	6.1	0.5		CS, Volcanic Plume (1.0)
19 May 80 a	3.2	6.2	0.5	2.7	Ci (1.0?), very dusty, hazy
20 May 80 a	0.49	0.92	3.3	3.6	Ci, (0.8) Continued hazy
21 May 80 a	0.28	0.51	5.9	7.5	Scattered AC (0.4)
22 May 80 9	0.46	0.88	3.4	2.7	Broken Cu (0.6)
10	0.29	0.53	5.6	6.4	Scattered Cu (0.2)
11/12	0.23	0.42	7.2	16	Scattered Cu (0.4)
23 May 80 a	0.14	0.24	12.4	24+	Ci, AC (0.8)
28 May 80 a	0.185	0.33	9.1	24+	Scattered Ci, AC, Cu. (0.4)
30 May 80 p	0.15	0.26	11.5	24+	Scattered Ci, AC, CU (0.5)
31 May 80 a	0.067	0.10	29	24+	Clear sky, light haze
p	0.082	0.13	23	24+	Scattered Ci (0.5)

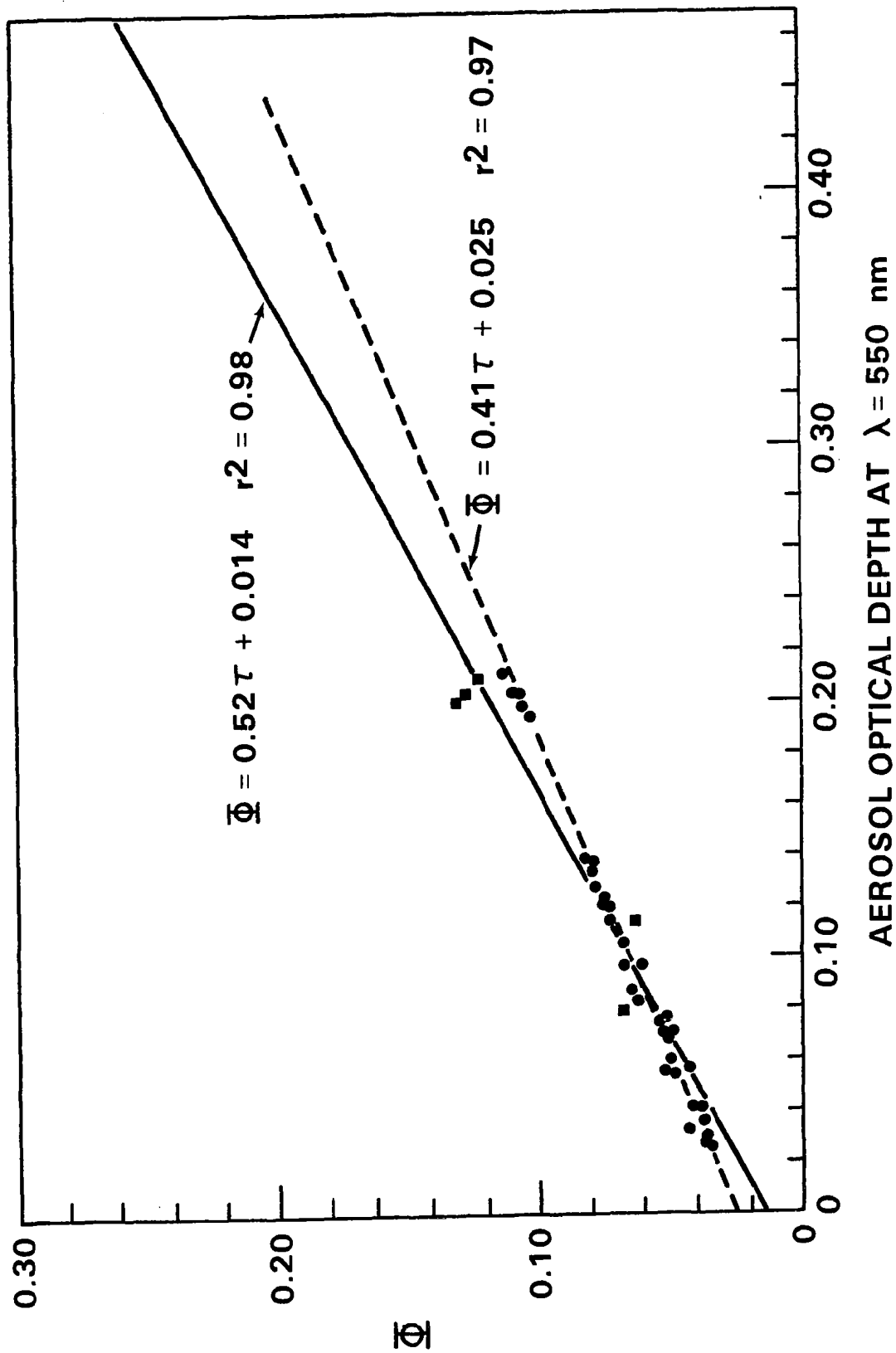


Figure 1. Least squares fit of the diffuse-to-direct ratio ϕ against measured aerosol optical depth τ at $\lambda = 550 \text{ nm}$. Solid curve represents the fit for all data, and the dashed curve excludes data points ($\tau > 0.6$) from a dust storm event.

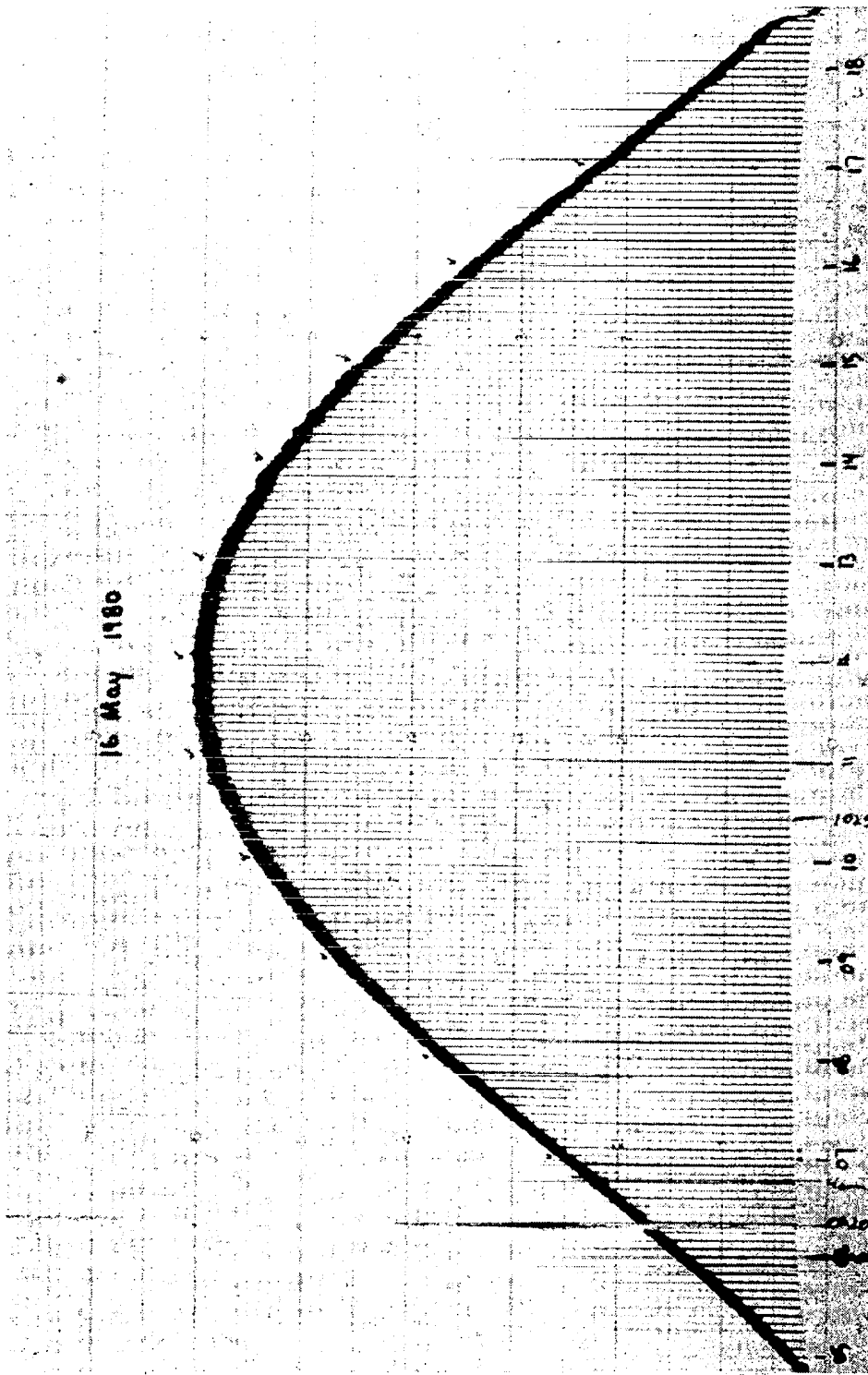


Figure 2. Global and diffuse solar radiation records for Friday, May 16, 1980, for clear, cloud-free skies.

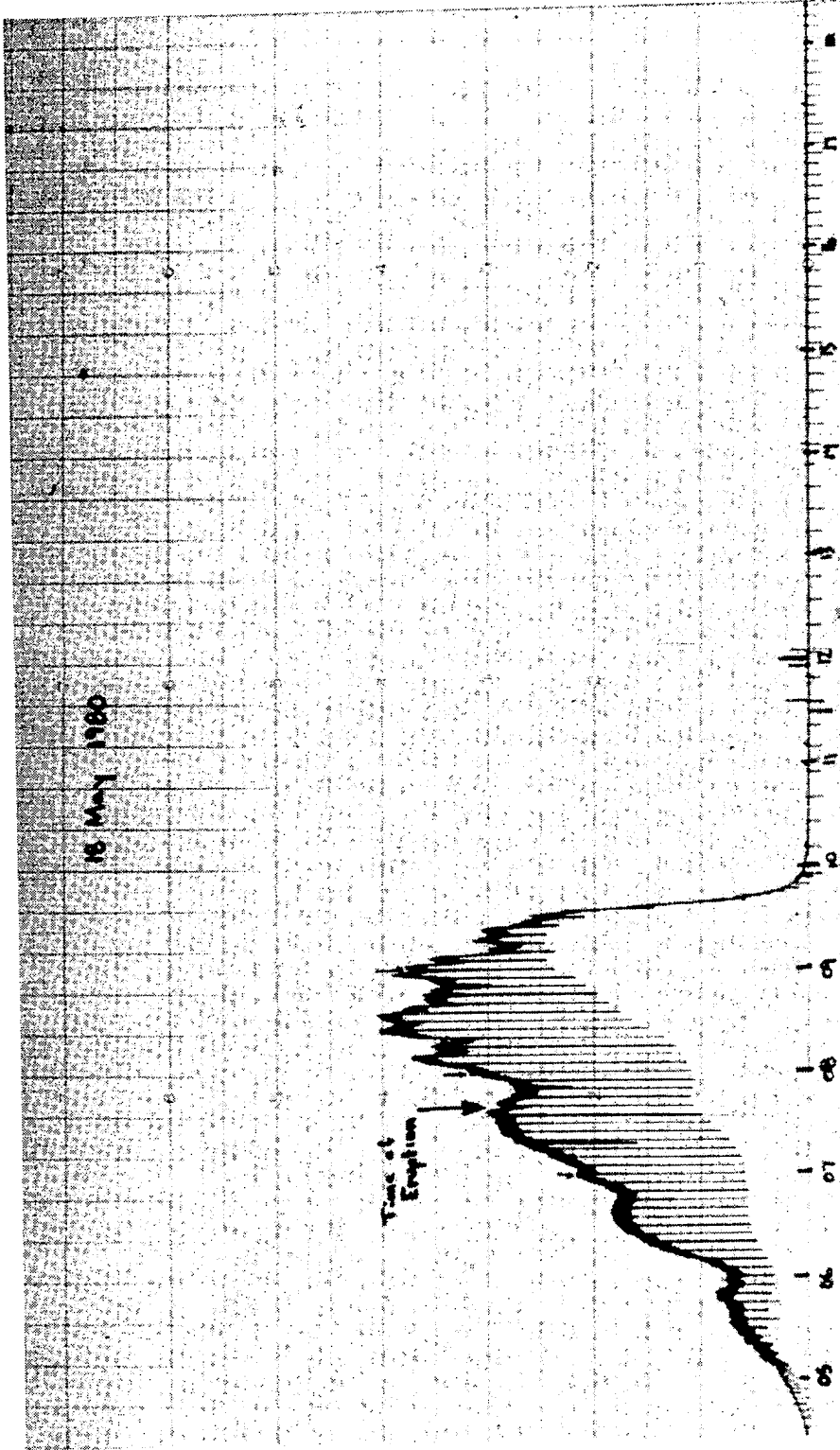


Figure 3. Insolation record for Sunday, May 18, 1980, showing early morning cirro-stratus clouds and the abrupt decrease of insolation to zero after 0930 PST.

19 May 1980

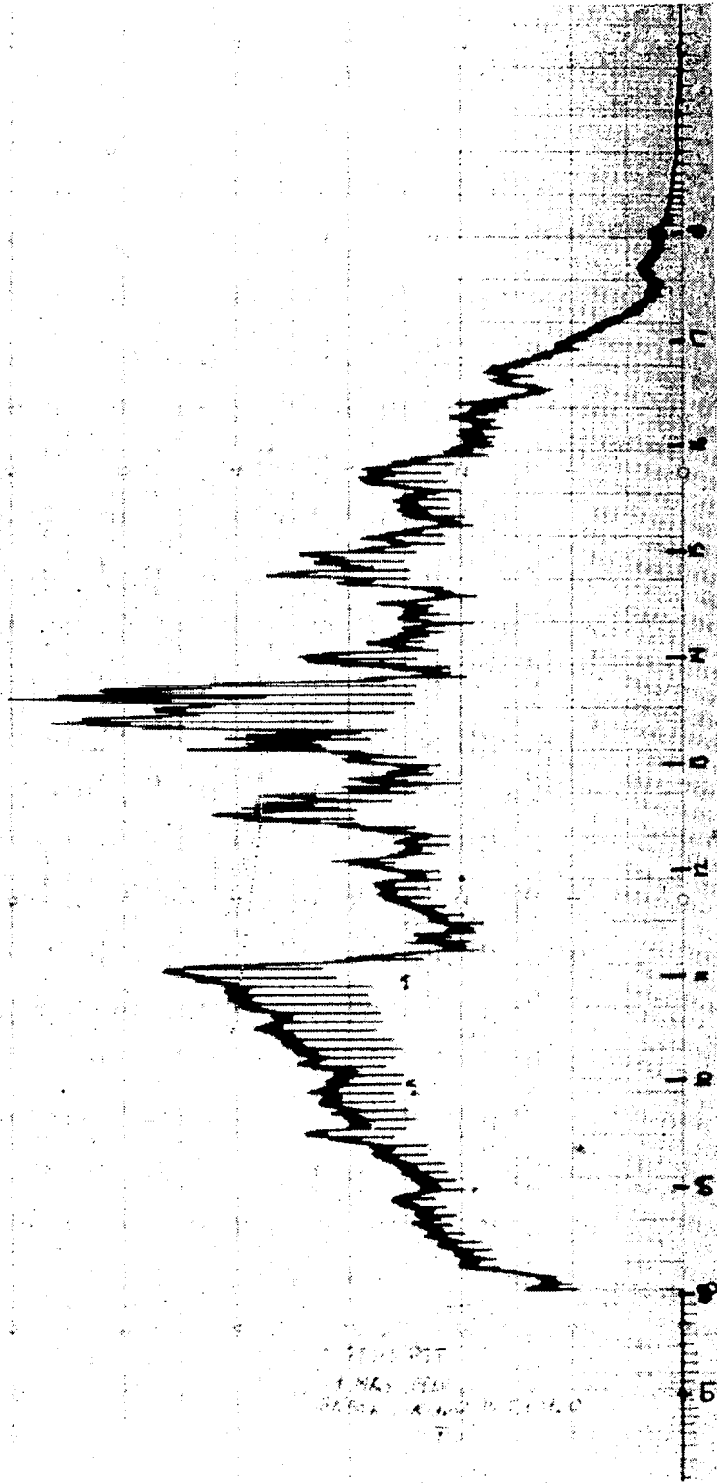


Figure 4. Insolation record for Monday, May 19, 1980 showing not only cloudiness but also highly turbid air resulting in a large diffuse component.

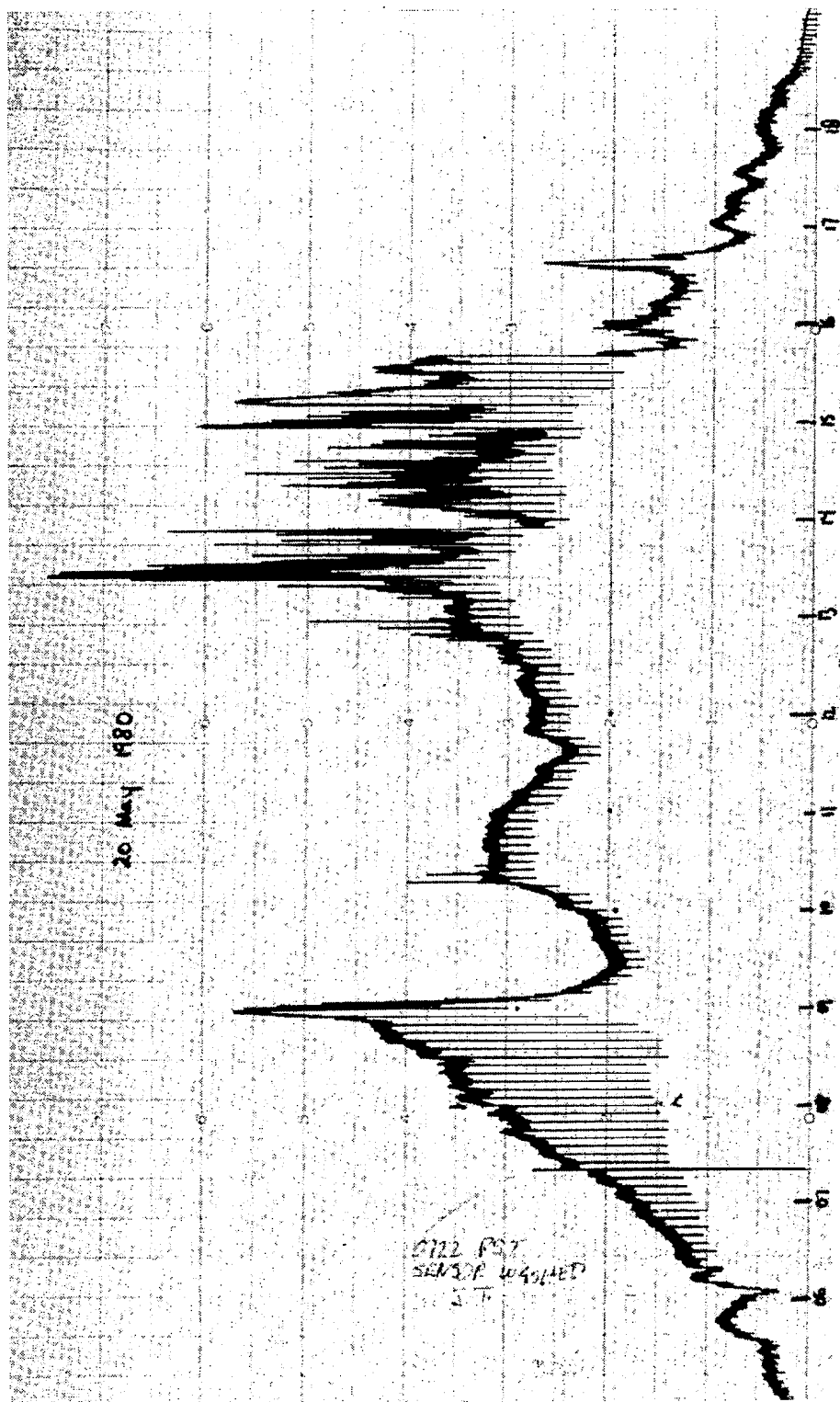


Figure 5. Insolation record for Tuesday, May 20, 1980, showing a continued large diffuse component.

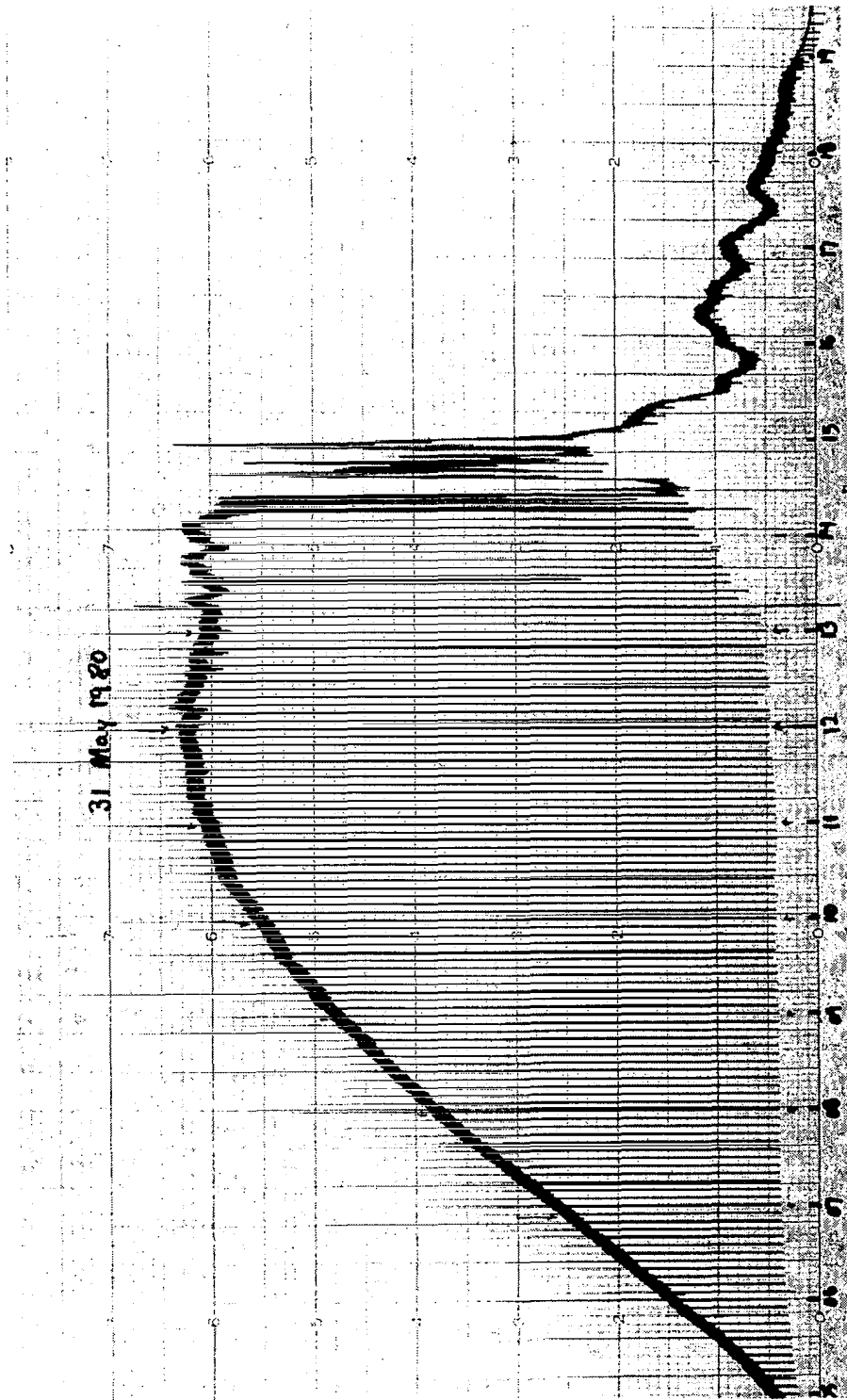


Figure 6. Insolation record for Saturday, May 31, 1980, showing diffuse component at nearly normal values.

1745 18MY80 35A-2 01231 26072 KB7



MAY 18, 1980 GOES-MET
05 A.M. PDT

Figure 7. GOES-West satellite image showing that the volcanic plume, approximately 2 hours after the eruption of Mount St. Helens, has spread out over central and eastern Washington.

2315 18MY80 35A-2 01214 26062 KER



May 18, 1980
4:15 P.M. PDT
ERUPTION + 7 Hrs 35 MIN

Figure 8. GOES-West satellite image showing the volcanic plume spreading into Western Montana approximately 7.5 hours after eruption.

1545 19MY80 35A-2 01223 26082 KB7



Figure 9. GOES-West satellite image showing the volcanic plume approximately 24 hours after eruption over Montana, Wyoming, and Eastern Colorado.

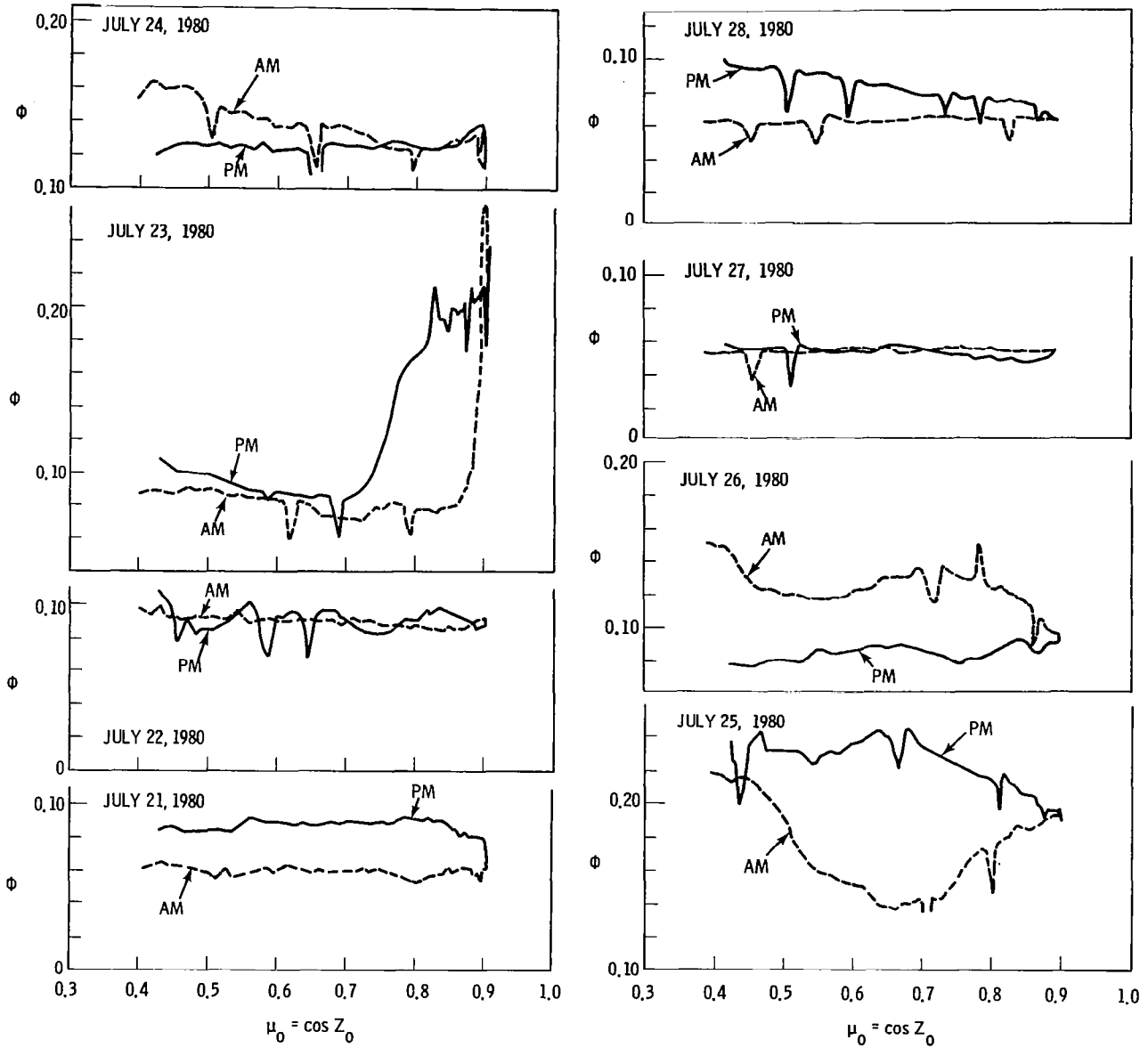


Figure 10. Diffuse-to-direct ratio of insolation as a function of time ($\cos Z_0$) over the time interval 21 July to 28 July, 1980. Incursion of Mount St. Helens volcanic ash over the Hanford Site is readily seen near mid-day on 23 July.

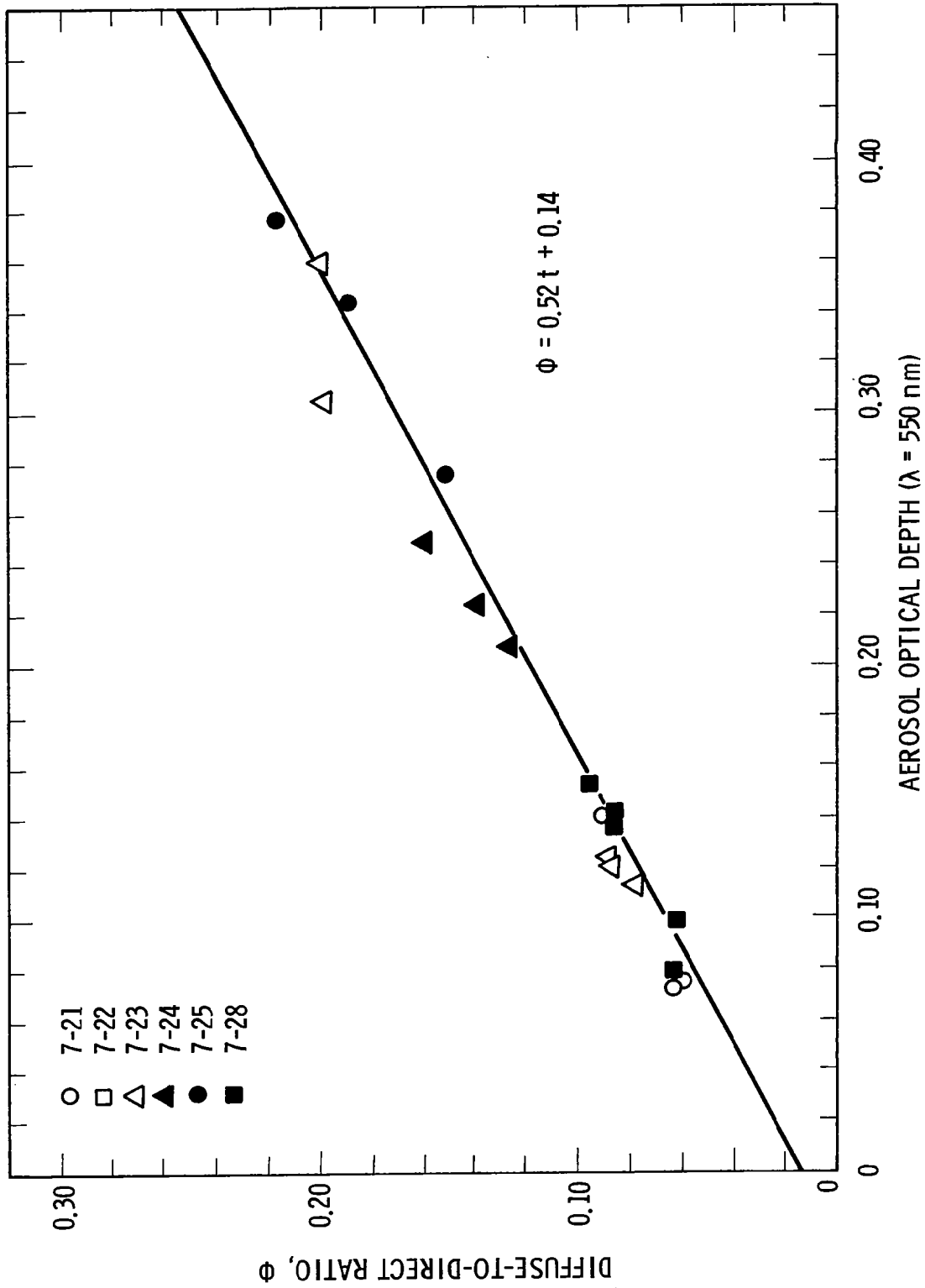


Figure 11. Comparison of the relationship between the diffuse-to-direct ratio and aerosol optical depth of figure 1 and observations obtained during the period July 21 to July 28, 1980.

MOUNT ST. HELENS DUST VEIL OBSERVED AT BOULDER, COLORADO, BY OPTICAL TECHNIQUES

Gordon Lerfald
NOAA, Environmental Research Laboratories, Boulder, Colorado

Following the May 18, 1980, eruption of Mount St. Helens, photometric and photographic observations were taken at Boulder, Colorado, to record the optical effects of volcanic dust atmospherically transported to this area. The instruments used included a narrow-beamwidth solar photometer which recorded solar irradiance in eight narrow-bandwidth channels in the wavelength range 0.3 to 1.1 μm , a solar aureole photometer, and two time-lapse camera systems.

The eight-channel solar photometer data have been analyzed to obtain the wavelength dependence of optical thickness. At the longer wavelengths, on May 20, 1980, the optical thickness was as much as nine times that expected from a "clean atmosphere" model. During the first several days following the eruption, the dust veil sometimes exhibited sufficient spatial structure that its motion can be seen on the time-lapse films.

The results of analysis to date are presented and the plans for additional analysis are outlined.

I. OBSERVING TECHNIQUES

The equipment used to make measurements on the optical characteristics of the dust veil consisted of an eight-channel solar photometer, a solar aureole photometer, and two time-lapse camera systems (1,2). The equipment was operated during every day but one, from May 19 to June 2, 1980, at which time it was necessary to discontinue measurements to prepare for a scheduled field program. The photometric data were recorded on digital magnetic tape and the photographic data on super-8 color movie film. Figure 1 shows a photograph of the instruments mounted on a solar tracker.

II. DATA ANALYSIS METHODS

A. Eight-Channel Solar Photometer

Each channel of the eight-channel solar photometer is sampled once per second and the data points are recorded on digital magnetic tape. Analysis is performed off-line by using computer programs which allow considerable flexibility in the output format.

The usual set of computer-graphic outputs produced routinely to guide the analysis and give a good overall picture of the data set include the following:

(1) Langley plots [\log_{10} (Irradiance) against relative air mass] for each wavelength for each morning and afternoon period, that is, 2 plots per day for each wavelength. Figure 2 shows Langley plots for three wavelengths traced onto a single graph.

(2) Time-series plots of \log_{10} (Irradiance) for each wavelength for each morning and afternoon period, that is, two plots per day for each wavelength. Figure 3 shows a time-series plot for the wavelength of 0.875 μm , where the morning and afternoon portions are traced onto a single graph.

(3) Plots of vertical optical thickness against wavelength for the eight measured wavelengths [optical thickness against $\log(\lambda)$] using 5-minute averages at half-hour intervals.

The Langley extrapolation technique is used to determine the "zero air mass" irradiance as reference in computing total optical thickness. It is necessary to be highly selective in order to choose optimum periods for applying the Langley method. Cloud-free conditions are essential to the method, and time-lapse sky photography is a very useful means of detecting the presence of cloud types such as thin cirrus, thin altostratus, and condensation-level hazes, all of which can result in subtle shifts on the Langley plots. Most other cloud types (e.g., cumulus) give obvious evidence of themselves on Langley plots and time-series plots by virtue of their rapid and often large changes in optical thickness.

Another requirement for accurate determination of the "zero air mass" irradiance by the Langley extrapolation method is that the aerosol loading does not change significantly during the time period used for the determination. Comparison of the Langley plots for times before and after local solar noon is helpful in choosing days characterized by stable levels of aerosol loading. (If aerosol loading remains constant, the plots will be identical.) Usually, there is some advantage in using data from days having the smallest aerosol optical thicknesses but only if stability criteria are also met. In the case of wavelength bands which include strong gaseous absorption lines, the Langley extrapolation must be done by using a curved, rather than a straight, line fit. This effect is due to the saturation in strong absorption lines of water vapor in the $0.94\ \mu\text{m}$ absorption band and of ozone in its ultraviolet absorption bands. Paltridge and Platt summarize experimental and theoretical results on ozone and water vapor absorption as a function of the amount of gas in the sun-instrument path (3).

The initial analysis procedure is to produce the Langley plots and time-series plots, and to use these, along with the time-lapse films, to select the best time periods to apply the Langley extrapolation technique. Once the zero air mass reference irradiance values are established, the plots of optical thickness against wavelengths can be produced. Figure 4 shows an example of the computer-produced plots of the latter, note that the wavelength identifications have been added. The $0.941\text{-}\mu\text{m}$ band includes water vapor absorption and the $0.314\text{-}\mu\text{m}$ and $0.596\text{-}\mu\text{m}$ bands include some ozone absorption. These bands may therefore be somewhat less useful for study of particle size distributions than the other five channels.

The thermal stability of the photometer is better than 2 percent for the temperature range 0°C to 40°C . Based on Langley extrapolations applied to numerous data sets, the uncertainty in the optical thickness values ranges from ± 0.01 at the longest wavelengths to ± 0.05 at the shortest wavelengths.

B. Solar Aureole Photometer

The aureole photometer data have not yet been analyzed. The instrument scans to 8° above and below the sun's center. The data (angular scattering functions in the near-forward direction) are influenced most strongly by the larger particles in the size distribution, and it is hoped that the analysis will permit inferences about the large-particle tail of the dust veil size distribution.

C. Time-Lapse Cameras

Two time-lapse camera systems are used; an all-sky camera, which exposes 2 frames per minute and an aureole camera, with a 30° field view which exposes 4 frames per minute. The films are normally viewed in the usual movie mode and are very useful in observing general atmospheric conditions, the type, motion, and geometry of clouds, and atmospheric optical phenomena, such as halos, color changes, etc. Although qualitative, they are very useful in the selection of time periods most suitable for analysis and sometimes help explain the results obtained from the quantitative data.

III. SELECTED PRELIMINARY RESULTS

A. Aerosol Loading by Langley Plot Slope Method

The usual expression for optical thickness of a beam of solar radiation penetrating the atmosphere is

$$I = I_0 e^{-\tau M} \quad (1)$$

where I is the observed irradiance, I_0 the original beam irradiance before entering the atmosphere, τ is the vertical (zenithal) atmospheric optical thickness, and M is the relative air mass. If this equation is rearranged to the form

$$\tau = \frac{\ln I_0/I}{M} \quad (2)$$

the slope of the line on a Langley plot is proportional to the zenithal optical thickness. The accuracy of this method for estimating the aerosol loading is subject to the effects of temporal changes in the aerosol conditions during the considerable time it takes to make the measurement. Nevertheless, it was obvious there were systematic changes in slope on the Langley plots for several days following the May 18 eruption, and the slopes were determined during suitable data periods. The results are shown for three wavelengths in figure 5. Several days did not have suitable data because of clouds.

The ratio between the extinctions on the days having large dust concentration (e.g., May 20 and 21) and relatively clean conditions (e.g., May 25) is much larger for the longest wavelength. This is because under "clean" atmosphere conditions the extinction due to Rayleigh scatter relative to aerosol extinction is considerably larger at shorter wavelengths than it is at longer wavelengths. Figure 5 indicates that on May 20 and May 21 the turbidity at $\lambda = 0.875 \mu\text{m}$ was approximately five times greater than that expected on a normal clear day. The rate of decrease between May 21 and May 25 appears to be more rapid for the longer wavelengths. This result may be indicative of the fallout of larger particles during that time period. However, it is also possible that local aerosols in the Denver area could have affected the $0.333\text{-}\mu\text{m}$ and $0.501\text{-}\mu\text{m}$ extinctions.

B. Aerosol Loading by Direct Determination of Optical Thickness

The only advantage of the Langley slope method of determining optical thickness is that it can be applied without knowledge of the photometer calibration. If in Equation (2) the "zero air mass" irradiance I_0 is known, the optical thickness can be determined whenever accurate measurement of photometer irradiance I is available. This direct method of obtaining optical thickness has the distinct advantage that it can be applied without regard for the temporal stability of the absorbing layers.

The data were screened to select periods free from clouds or equipment problems, and plots of optical thickness against wavelength were produced (for example, figure 4). From these plots minima, maxima, and mean optical thicknesses were derived for selected wavelengths for each day for which suitable data were available. These measured optical thicknesses and their ratio to the Air Force "clean atmosphere" optical thicknesses (4) were computed and are plotted in figure 6 for $\lambda = 0.875 \mu\text{m}$. The considerable range between daily maxima and minima is indicative of the spatial structure of the dust veil, particularly during the first days following its arrival above Colorado. The decrease in dust loading, at least through May 23, appears to be very systematic. There appears to be a significant increase again on May 30 and June 2, which are, respectively, 12 and 15 days after the primary eruption of May 18.

IV. CONCLUDING REMARKS

The dust veil from Mount St. Helens resulted in significant atmospheric effects over Colorado, with up to roughly 10 times the normal turbidity at wavelengths near $1 \mu\text{m}$. There is some indication the size distribution changed with time, the larger sizes falling out in a few days. There was considerable spatial structure to the dust veil, especially during the first days following the eruption. Unusual sunset color effects were recorded on time-lapse films on May 21 and May 23.

It is planned that additional analyses will be performed. In particular, the solar aureole photometer data may permit examination of changes in the large-particle tail of the dust particle size distribution (radii greater than $1\ \mu\text{m}$). The wavelength-dependence of extinction measured by the 8-channel solar-photometer can potentially yield information on the size distribution of particles with radii of $1\ \mu\text{m}$ or less. Thus, combined analyses of data from these two photometers should allow estimations of the size distribution of the volcanic dust over a large size range.

REFERENCES

1. Lerfald, G. M.: A Solar Aureole Photometer for Use in Measuring Size Distributions of Particles in the Atmosphere, NOAA Tech. Memo., ERL WPL-36. 1977.
2. Lerfald, G.; and Ericson, H.: Time-Lapse Sky Photography Using Low-Cost Camera Systems NOAA Tech. Memo., ERL WPL-43, 1979.
3. Paltridge, G. W.; and Platt, C. M. R.: Solar Radiation Within the Atmosphere. Ch. 5 of Radiative Processes in Meteorology and Climatology, Elsevier Scientific Publishing Co., 1976.
4. Elterman, L.; and Toolin, R. B.: Atmospheric Optics. Ch. 7 of Air Force Handbook of Geophysics and Space Environments, Shea L. Valley, ed., McGraw Hill, 1965.

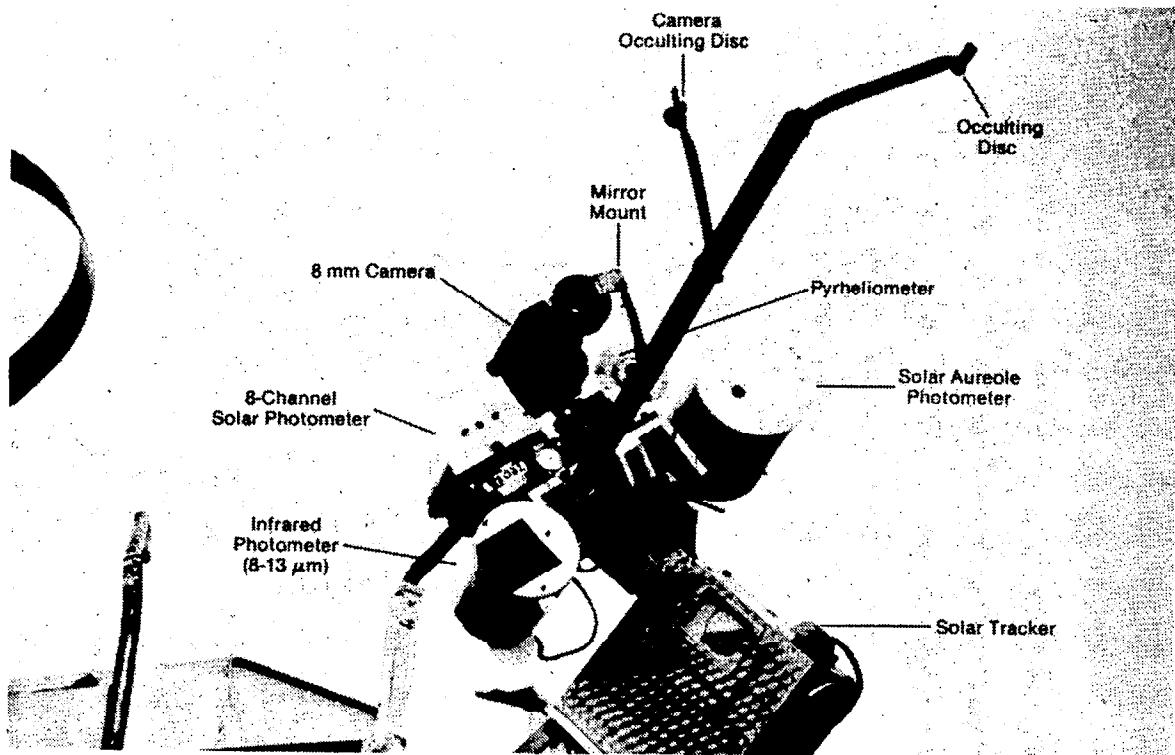


Figure 1. Photograph of instruments mounted on the solar tracker. The 8-channel solar photometer, the solar aureole photometer, and the aureole time-lapse camera (labeled 8-mm camera) were used in this experiment.

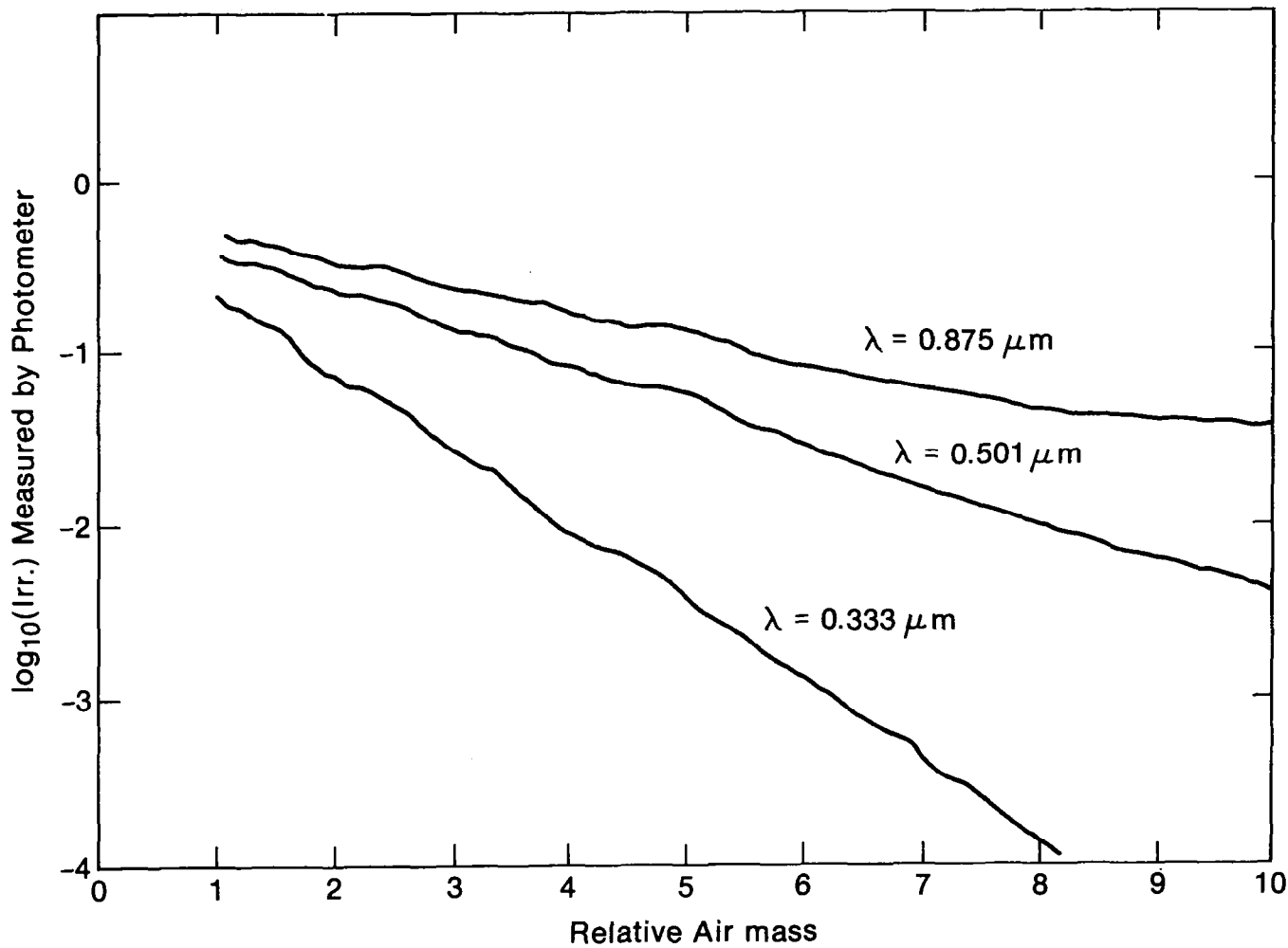


Figure 2. Langley plots for three wavelengths recorded during the afternoon of May 21, 1980. These plots have been traced from three separate computer-produced graphs.

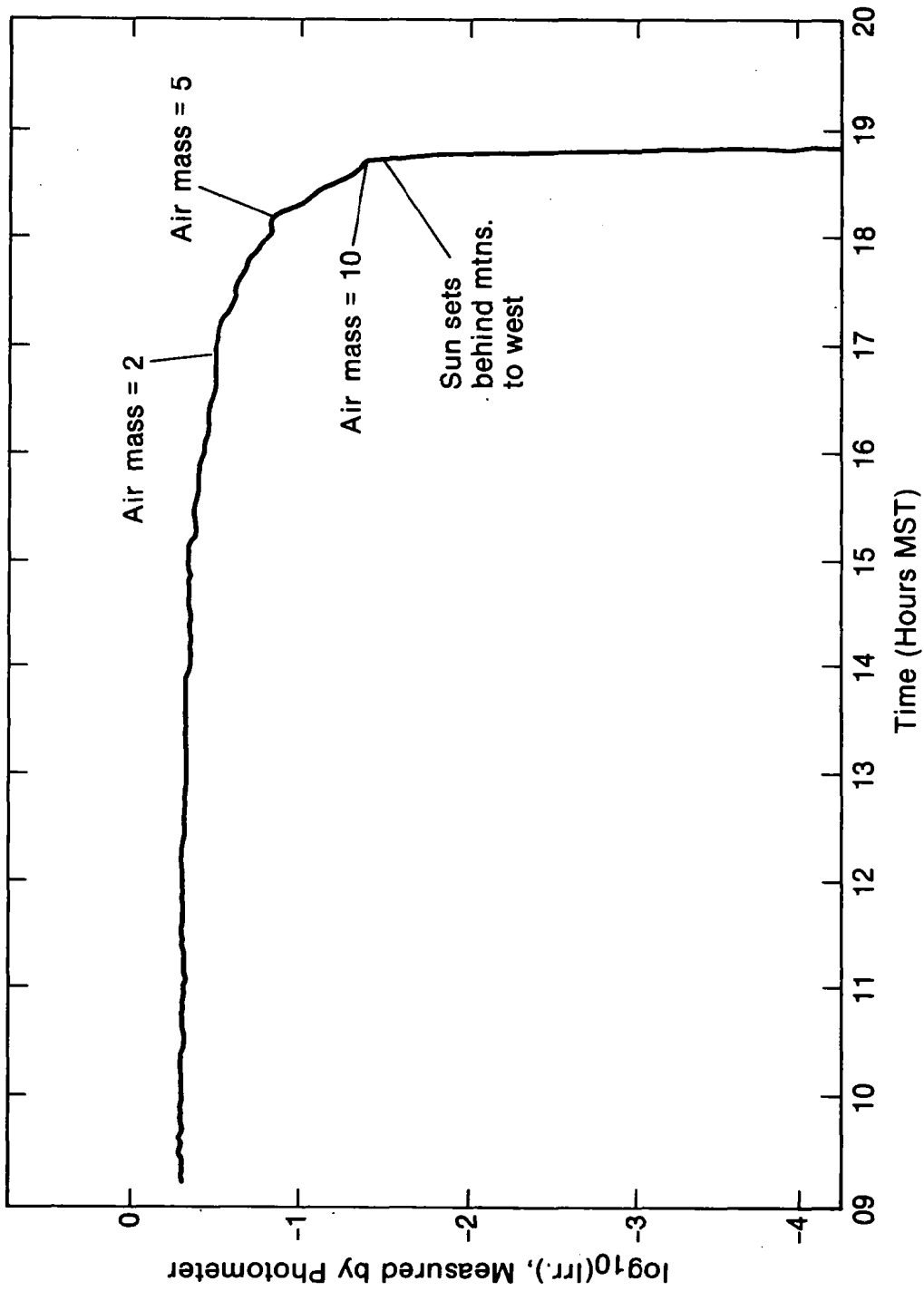


Figure 3. Time-series plot of the $\log_{10}(\text{Irradiance})$ values measured by the $0.875 \mu\text{m}$ channel of the 8-channel photometer during May 21, 1980. (Traced from computer plots for a.m. and p.m. periods.)

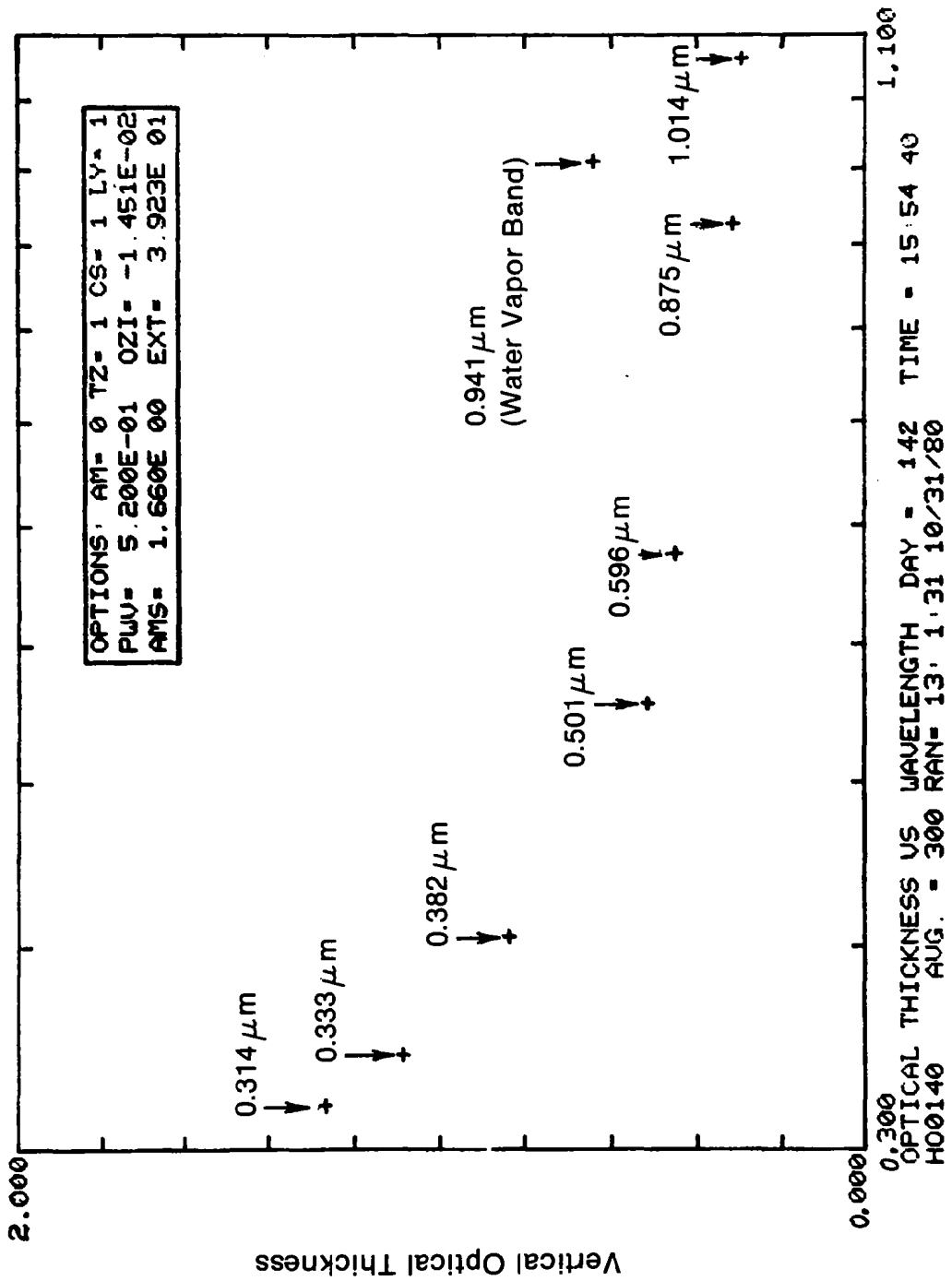


Figure 4. Computer-produced plot of vertical optical thicknesses measured by 8-channel solar photometer at 15:54 MDT on May 21, 1980 (note that wavelength identifications have been added).

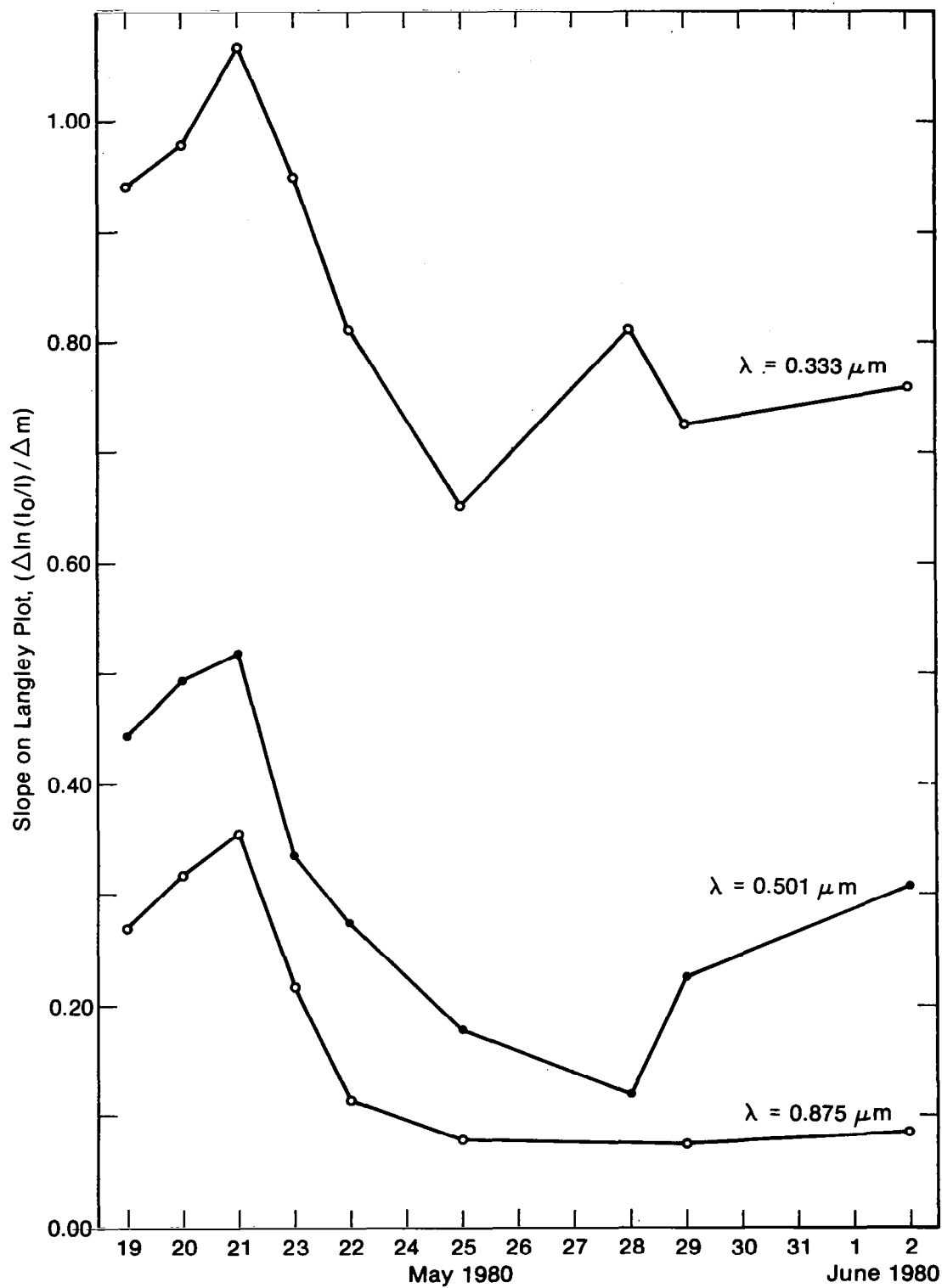


Figure 5. Values of the slope from Langley plots for three wavelengths measured on days with suitable data following the May 18 eruption of Mount St. Helens.

Daily Ranges of Optical Thickness at Boulder, Colorado,
 May 19-June 2, 1980

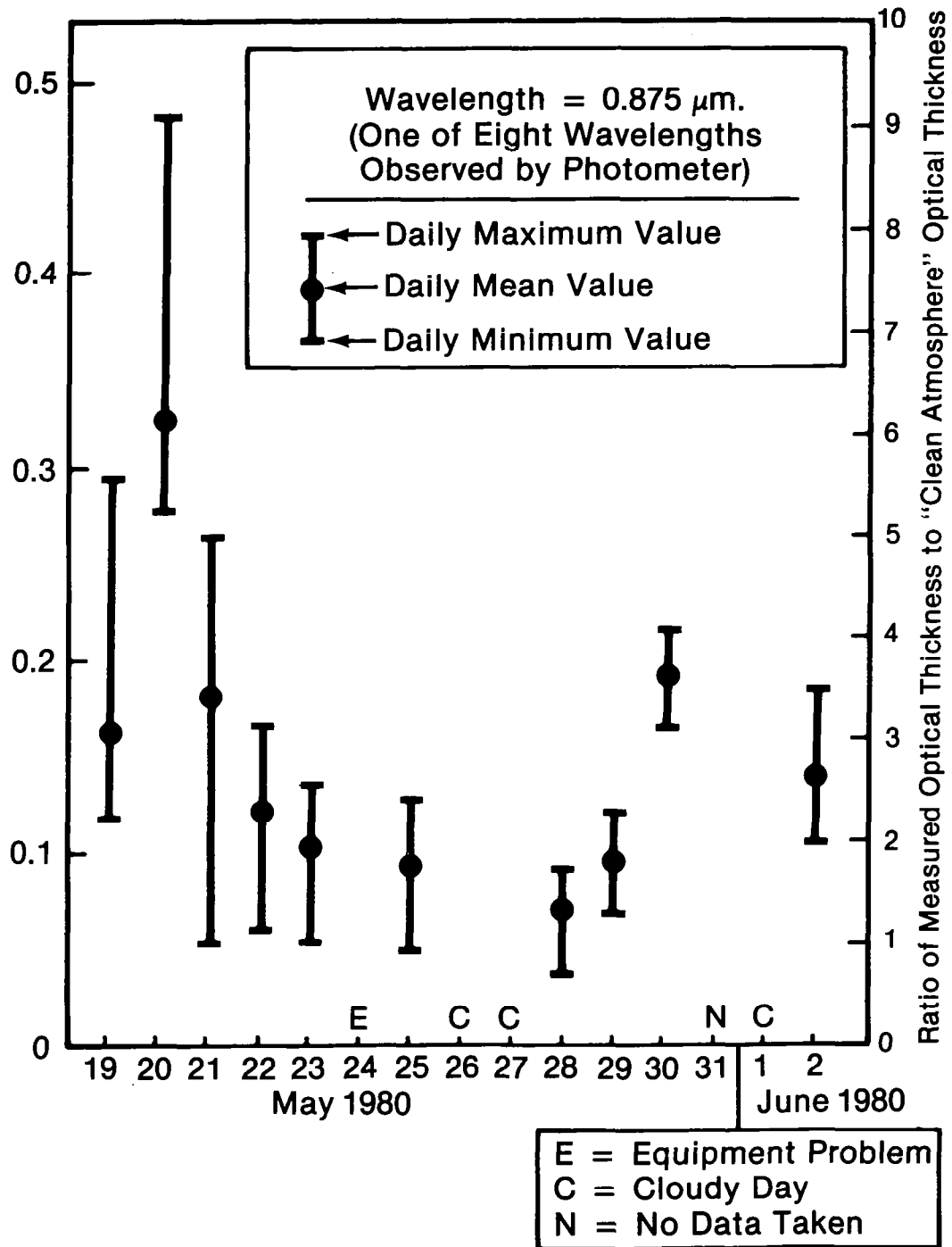


Figure 6. The optical thicknesses (daily maxima, minima, and means) determined by solar photometry at the wavelength 0.875 μm are normalized to the vertical and plotted (left-hand scale). The scale at the right shows the ratio of measured optical thickness to the Air Force "clean atmosphere model" optical thickness (4). Similar measurements were made at seven other wavelengths in the range 0.3 to 1.02 μm .

AIRCRAFT SAMPLING OF THE SULFATE LAYER NEAR THE TROPOPAUSE FOLLOWING THE ERUPTION OF MOUNT ST. HELENS

Erwin A. Lezberg, Dumas A. Otterson, William K. Roberts, and Leonidas C. Papathakos
National Aeronautics and Space Administration, Lewis Research Center, Cleveland, Ohio

Twenty filter sampling flights of the NASA Lewis F-106 aircraft were conducted in the Great Lakes region between June 4 and August 8, 1980, following the major eruption of Mount St. Helens, Washington on May 18. The IPC-1478 filters were exposed over an altitude range spanning the local tropopause. These were analyzed for ^7Be as a stratospheric tracer. Quarter sections were analyzed for sulfate and nitrate by ion-chromatography and selected samples were analyzed for chloride by selective ion electrode. A search for trace elements was made by X-ray fluorescence analysis. A filter sample taken above the tropopause on June 5 indicated a sulfate level of 50 times the baseline measurements, which is consistent with the trajectory predictions of the leading edge of the cloud on its second transit of the Earth. Subsequent measurements over a period of 2 months showed an initial drop-off and formation of a persistent layer of sulfate above the tropopause with a concentration of 10 to 18 times previously measured background levels. Concentrations of nitrate above the tropopause exhibited considerable variability and showed some enhancement (2 to 10 times) compared with previously measured concentration levels. The source of the nitrate may also be volcanic as evidenced by its temporal relationship to the sulfate concentration changes. Based on the null results of X-ray fluorescence measurements, there is no evidence of ash particle concentrations greater than $3.4 \mu\text{g}/\text{m}^3$ persisting in the layer above the tropopause after the second transit of the cloud.

I. INTRODUCTION

The recent eruptions of Mount St. Helens, Washington (May 18 to August 8, 1980) presented a unique opportunity to study the changes in the stratospheric aerosol induced by an impulsive injection of gases and ash particles into the lower stratosphere and the characteristic time periods for transport of aerosol constituents horizontally and vertically in the stratosphere and from the stratosphere to the troposphere.

It has long been speculated that the major source of the sulfuric acid aerosol layer is the injection of sulfur gases into the stratosphere by explosive volcanoes. The increase and subsequent decline in aerosol levels following the recent eruption of Fuego in October, 1974 (1-3) and changes after the eruption of Agung in 1963 reinforced the viewpoint that the observed changes in the layer are due to large injections of sulfur dioxide by explosive volcanoes. There remain a number of unanswered questions as to the source, magnitude, and composition of the sulfur gases as well as the sequence of chemical reactions responsible for the conversion of these gases to sulfuric acid aerosol. The availability of various direct sampling and remote sensing instruments after the eruption of Mount St. Helens enabled a number of independent investigators to assess a large body of ground-based and aircraft measurements. These measurements should provide answers to some of these questions.

Our sampling program involved direct filter sampling with the F-106 aircraft based at NASA Lewis and began on June 4, 17 days after the first major eruption, and continued for 2 months. The instrumentation and techniques were from an earlier sampling program of the upper troposphere and lower stratosphere (5).

In this paper, we present the results of chemical analysis of the filters for sulfate, nitrate, and chloride ions and X-ray fluorescence analysis of the ash content in these filters for elements with atomic numbers ≥ 25 . Beryllium 7 activity is used to identify stratospheric samples. The measurements of the sulfate layer above the tropopause are compared with the previous measurements which had been taken from 1976 to 1978. The temporal changes during this sampling period are described.

II. METHODS

Aircraft sampling of aerosol particles and gases were conducted at altitudes of 10.7 to 13.7 km. Flights were generally over the Great Lakes area between June 4 and August 8, 1980. Timing and flight routing were guided when possible by predictions of the volcanic cloud trajectories at the 200 mbar level obtained from NOAA ARL.¹ Tropopause heights were obtained from an average of local soundings at locations bracketing the flight route, when available, and were taken except as noted at the nearest reporting time without interpolation.

Air samplers were installed in wing pods, which are mounted on one or both wings, depending on the prior commitment of the aircraft to another experiment in which case, only one of the filter sampling pods was available and the sampling altitude was restricted to a constant 12.5 km. Sampling times varied from 20 to 90 minutes. The sampler consisted of an external sampling probe isolated with a remotely operated cap when not sampling, ducting, a single-filter insertion mechanism, a metering venturi, and an exhaust isolation valve. Samples were collected on 7.6-cm-diameter IPC-1478 filter paper. Details of the sampling procedures and subsequent preparation and analysis of the filters by ion-chromatography are described by Lezberg et al. and Humenick et al. (5,6). Whatman-41 filters were flown on the left pod samplers on the first two flights, but because of their much higher resistance, negligible flow was indicated across the metering venturi. Analysis of these samples showed only small amounts of sulfate and nitrate collected. The filter samples were initially analyzed for radioactive ⁷Be concentration by using a Ge (Li) detector and multichannel pulse height analyser. Beryllium 7 is produced by cosmic-ray bombardment of stratospheric nitrogen and oxygen (7), and its concentration can be used as a natural tracer of stratospheric air (8,9).

Quarter sections of the filters were subsequently analyzed for soluble ions by ion chromatography. Chloride and fluoride could not be determined from ion-chromatographic analysis of the carbonate-bicarbonate eluant from the filter samples because interfering ions overlapped the chloride and fluoride elution peaks. The interferences are believed to be due to hydrolysis products of the dibutoxyethylphthalate (DBEP), an ester to coat the cellulose fiber material to improve its particle trapping efficiency. Later in the sampling program, IPC filter material, which had not been treated with DBEP, was washed and impregnated with about 0.1 percent Na₂CO₃ solution and glycerine (~ 2 mg of Na₂CO₃ + 0.2 ml glycerine/filter). The base impregnated IPC-1478 filters absorbed SO₂ quantitatively in the laboratory and appeared at the sulfate peak during the ion-chromatographic analysis. Interferences with chloride and fluoride persisted, however, apparently from slight hydrolysis of the glycerine in the chromatograph ion-exchange column. The glycerine was used to ensure better absorption of the SO₂. Sulfur dioxide is absorbed more efficiently from water-saturated air than from dry air. Several of the samples were subsequently analysed for chloride by selective ion electrode, but no chloride was detected above the level of the blanks.

A search for trace elements with atomic numbers above 25 was performed on about half of the filters by X-ray fluorescence analysis. The minimum total filter burden sensitivity over $25 \leq z \leq 42$ and > 70 is 2.3 μg .

III. RESULTS AND DISCUSSION

The results of the filter analysis are summarized, by flight, in Table I. The ⁷Be analysis results shown in figure 1 are in good agreement with the pressure difference of the flight altitude from the reported tropopause. A linear regression of the data yielded a correlation coefficient of 0.75. Errors bars are shown for ⁷Be counting statistics and for the uncertainty in the tropopause height (range over the nearest reporting stations and differences between 12-hour reporting times, time span if available). Dutkiewicz and Husain from an analysis of filter samples exposed in the earlier sampling program indicate a minimum limiting value of 2330 pCi/10³ scm for stratospheric air and a tropospheric average of 520 pCi/10³ scm for upper tropospheric samples (10). Presumably, intermediate values represent mixed stratospheric and tropospheric samples.

¹Drexler, personal communication, 1980.

The first sample, taken on June 4th, was clearly a tropospheric sample. Flight routing was based on the volcanic cloud trajectory calculations performed by NOAA ARL starting with the eruption of Mount St. Helens on May 18, and corresponded to the predicted passage of the leading edge of the 200 mb cloud trajectory through the Great Lakes region on its second pass around the Earth.² Sulfate and nitrate concentration of the sample was moderately high compared with previous upper tropospheric measurements (5).

The sample taken on June 5 at 13.1 km was stratospheric and indicates the highest sulfate concentration of the flight series ($1.9 \mu\text{g}/\text{m}^3$), about 50 times the previously measured average stratospheric levels. Nitrate concentrations again were only moderately higher than the stratospheric baseline. Beginning with flight 115 on June 19, some comparisons were made between Na_2CO_3 impregnated filters and the conventional IPC-1478 material exposed at the same time from paired filter samplers. Since the hydrolysis products of the DBEP interfered with the identification of chloride, fluoride, and nitrate, an attempt was made to remove the DBEP from the first filter group used (flight 115 and laboratory experiments) before impregnating the filters with a 0.1 percent Na_2CO_3 solution. Later sampling flights employed IPC-1478 material that had not been treated with DBEP. Carbonate impregnated filters were evaluated in the laboratory for absorption of SO_2 . Results indicated nearly quantitative absorption, but some loss of collection efficiency with dry gas. The sulfur dioxide appeared at the sulfate peak elution time so it was apparently oxidized to sulfate on the filter.

Results shown in Table I for chloride are only reported for selected samples, which were analyzed by a selective ion electrode since slight hydrolysis of the glycerine in the ion exchange column of the chromatograph also interfered with chlorine and fluoride peaks. No significant chloride was found above the contamination level of the blanks ($\leq 10 \mu\text{g}/\text{filter}$).

In three flights with paired samples (115, 118, and 122) using the carbonate-impregnated filters and the DBEP-treated IPC filters, sulfate was slightly lower but within the uncertainty of residual sulfate on the carbonate impregnated blanks, there was no significant collection of SO_2 . However, no conclusion can be drawn from these results about SO_2 levels at time periods closer to the May 18 eruption.

X-ray fluorescence analysis of two ash samples (one from the Mount Ranier area and the other from the Seattle area) revealed that the elemental composition for samples consisting of dust $< 2 \mu\text{m}$ in diameter as compared with bulk samples was roughly the same. The major constituents for $z \geq 25$ were Fe and Sr. By assuming that any dust collected on the filters would have this same elemental distribution, a minimum detectable burden of 0.76 mg on a 7.6-cm-diameter filter can be calculated. Only on the June 4th IPC filter was a significant difference found between filter blanks and exposed filters for this tropospheric sample at about 5.6x background. This would correspond to a maximum ash burden of $13 \mu\text{g}/\text{m}^3$. Since no Sr was detected in the sample and since other elements (Cr, Ni, Mn, Cu) were found above background which were not present in Mount St. Helens ash, it is probable that contamination of the sample is responsible for the higher Fe content of the June 4th sample. Hence, the maximum dust burden of any of the filters is assumed to be below the minimum detectable (0.76 mg or nominally $3.4 \mu\text{g}/\text{m}^3$). This conclusion, of course, relies on submicrometer dust having the same elemental composition as bulk dust.

The time sequence of stratospheric samples is shown in figure 2, where sulfate and nitrate concentrations are plotted against flight data after the May 18 eruption. Subsequent eruptions are indicated by the arrows below the abscissa and the NOAA ARL prediction of the leading edge of the cloud for the 200 mb level by the leaders above the abscissa. The prediction of the second transit for May 18 eruption, however, has a low confidence level. Identification of a sample as stratospheric was based on the ^7Be activity being greater than $2300 \text{ pCi}/10^3 \text{ scm}$. Some interesting observations are apparent from the plot. Although the nitrate concentration measured does not show a peak corresponding to a very high sulfate concentration measured on June 5, subsequent maxima and minima in the nitrate concentration correlate quite well with the sulfate concentrations. Based on a cloud transit time of 13 days from the 200 mb ARL trajectory predictions, the subsequent peaks are separated by 12 or 13 days, possibly corresponding to third and fourth transits of the original cloud. The correspondence of the sulfate and nitrate temporal change also suggests that the nitrate may be volcanic in origin. Subsequent eruptions of Mount St. Helens may have obscured the temporal changes but no indication of significantly increased levels was found on samples (either stratospheric or tropospheric) taken following the predicted leading-edge passage for the other eruptions.

²R. Drexler, Personal Communication, 1980.

Concentrations of sulfate are shown in figure 3 plotted against the pressure increment from the local tropopause. The data appear to indicate a layer with a step increase at the tropopause. With the exception of the flagged point corresponding to the June 5 sample, the sulfate concentrations peak at 0.4 to 0.7 $\mu\text{g}/\text{m}^3$.

The layer appears to persist at these levels for an interval of 80 mb above the tropopause. Because of the seasonal rise in tropopause levels later in the sampling program and the altitude limitation of the aircraft, it was not possible to verify the persistence of the peak beyond June. The sulfate concentration levels found in the previous measurements are indicated by the shaded bars below and above the tropopause and represent averages $\pm 1\sigma$. The newly formed sulfate layer represents a 10- to 18-fold increase over these baseline measurements.

Concentrations of nitrate are shown in figure 4. Although, the nitrate concentrations are significantly higher than baseline measurements by 2σ to 10σ the variability is very high, and there does not appear to be a well-defined layer. The comparison of nitrate collected on base impregnated filters with conventional filters is confusing (Table I). Samples from flight 122 indicate approximately equal collection, but the other two comparative flights (115 and 118) show large and opposite differences between the two samples. The impregnated filter used on flight 115 was a first attempt, did not contain glycerine, and may not have been uniformly impregnated with the carbonate solution and thus result in a low collection efficiency. This explanation, however, would need to assume also that the base impregnated filters without DBEP were less efficient for collecting particulate nitrate and that particulate nitrate represents a large fraction of the total nitrate, a result consistent with Lazrus and Gandrud (11). Samples from both flights appeared to be stratospheric and thus implied low water vapor content; both collected equivalent amounts of sulfate, presumably sulfuric acid aerosol. A slower reaction of dry nitric acid with the sodium carbonate impregnated filter than its absorption rate on the DBEP-treated cellulose could account for a lower collection efficiency during flight 115. A more far reaching speculation is based on the tentative identification of nitrosyl sulfate (NOHSO_4) and NOHS_2O_7 in stratospheric aerosol (12). If these compounds are a significant fraction of the aerosol, the moisture content of the filters could influence their degree of hydrolysis and result in a loss of nitric oxide from the collected sample.

IV. CONCLUDING REMARKS

After the major eruption of Mount St. Helens on May 18, 1980, a series of aircraft filter sampling flights was initiated on June 4, these flights corresponded to the volcanic cloud trajectory predictions of the second transit around the Earth at the 200-mb level. A filter sample taken on June 5 above the tropopause indicated a sulfate level of 50 times the baseline measurements. This result is consistent with the trajectory predictions of the cloud passage. Later measurements over a period of 2 months showed an initial drop-off and formation of a persistent layer of sulfate above the tropopause with a concentration of 10 to 18 times previously measured background levels. Concentrations of nitrate above the tropopause exhibited considerable variability and showed some enhancement of the layer (2 to 10 time) compared with previously measured concentration levels but not to the extent shown by the sulfate concentrations. The source of the nitrate may also be volcanic as evidenced by the temporal relationship with the sulfate concentration changes. There did not appear to be a correlation between nitrate and ^7Be activities, which would have been indicative of increased downward transport from the stratospheric due to meteorological changes (e.g., tropopause folding events), but any conclusions should be based on a detailed analysis of the sampling results.

Based on the null results of the X-ray fluorescence measurements, there is no evidence of ash particle concentrations greater than $3.4 \mu\text{g}/\text{m}^3$ persisting in the layer above the tropopause after the second cloud transit.

REFERENCES

1. Cadle, R. D.; Fernald, F. G.; and Frush, C. L.: Combined Use of Lidar and Numerical Diffusion Models to Estimate the Quantity and Dispersion of Volcanic Eruption Clouds in the Stratosphere: Vulcan Fuego, 1974 and Augustine, 1976, *J. Geophys. Res.*, vol. 82, no. (12), 1977 pp. 1783-1786.
2. Gras, J. L.; and Laby, J. E.: Southern Hemisphere Stratospheric Aerosol Measurements 2. Time Variations and the 1974-1975 Aerosol Events. *J. Geophys. Res.*, vol. 84, no. C1, 1979, pp. 303-307.

3. Hofmann, D. J.; Rosen, J. M.; and Kiernan, J. M.: Stratospheric Aerosol Measurements IV, Global Time Variations of Aerosol Burden and Source Considerations. J. Atmos. Sci., vol. 33, no. 9, 1976, pp. 1782-1788.
4. Cadle, R. D.; and Grams, G. W.: Stratospheric Aerosol Particles and Their Optical Properties. Rev. Geophys. Space Phys., vol. 13, no. 4, 1975, pp. 1783-1786.
5. Lezberg, E. A.; Humenik, F. M.; and Otterson, D. A.: Sulfate and Nitrate Mixing Ratios in the Vicinity of the Tropopause. Atmos. Environ., vol. 13, no. 9, 1979, pp. 1299-1304.
6. Humenik, F. M.; Lezberg, E. A.; and Otterson, D. A.: Sulfate and Nitrate Collected by Filter Sampling Near the Tropopause, NASA TP 1567, 1980.
7. Lai, D.; and Peters, B.: Cosmic Ray Produced Radioactivity on the Earth. Handbuch der Physics, S. Flugge and K. Sitte, eds., Springer Verlag, (Heidelberg), 1967, pp. 551-612.
8. Husain, L.; Coffey, P. E.; Meyers, R. E.; and Cederwall, R. T.: Ozone Transport from Stratosphere to Troposphere. Geophys. Res. Lett., vol. 4, no. 9, 1977, pp. 363-365.
9. Ludwick, J. D.; Fox, T. D.; and Wendell, L. L.: Ozone and Radionuclide Correlations in Air of Marine Trajectory at Quillayute, Washington. J. Air Pollut. Control Assoc., vol. 26, no. 6, 1976, pp. 565-569.
10. Dutkiewicz, V. A.; and Husain, L.: Determination of Stratospheric Ozone at Ground Level Using ⁷Be/Ozone Ratios. Geophys Res. Lett., vol. 6, no. 3, 1979, pp. 171-174.
11. Lazrus, A. L.; and Gandrud, B. W.: Distribution of Stratospheric Nitric Acid Vapor. J. Atmos. Sci., vol 31, no. 4, 1974, pp. 1102-1108.
12. Farlow, N. H.; Snetsinger, K. G.; Hayes, D. M.; Lem, H. Y.; and Tooper, B. M.: Nitrogen-Sulfur Compounds in Stratospheric Aerosols. J. Geophys. Res., vol. 83, no. C12, 1978, pp. 6207-6211.

TABLE I. ANALYSIS OF FILTER SAMPLES FOR ⁷Be AND SOLUBLE ANIONS

Flight number (a)	Date (1980)	Sampling time, min	Flight altitude, km	Tropopause, km	ΔH , mbar	Latitude range, °N	Longitude range, °W	Beryllium 7, pCi/10 ³ scm	Sulfate, $\mu\text{g}/\text{m}^3$	Nitrate, Mg/m^3	Chloride, Mg/m^3	Filter (b)
108	6-4	90	11.3	12.1	- 28	39.8-41.5	81.1-89.6	≤ 150	0.100 ± 0.01	0.350 ± 0.01	--	--
109	6-5	50	13.1	12.8	8	42.7-46.4	82.4-84.3	3080 \pm 190	1.86	0.200	≤ 0.02	--
110	6-10	62	13.7	10.2	111	41.7-46.4	82.4-84.3	7315 \pm 505	0.170	0.310	--	--
111	6-11	55	12.5	10.9	50	42.5-44.0	85.3-87.5	4722 \pm 390	0.421	0.258	--	--
112	6-16	45	12.5	11.2	39	41.5-43.6	75.5-81.3	6180 \pm 420	0.700	0.390	--	--
112L	6-16	45	11.3	11.2	6	41.5-45.0	73.5-80.2	4215 \pm 260	0.510	0.280	--	--
113	6-17	45	13.1	10.8	92	41.5-44.8	73.5-81.3	5665 \pm 600	0.730	0.341	--	--
113L	6-17	45	10.7	10.8	16	41.9-45.0	75.5-80.3	497 \pm 210	0.320	0.270	--	--
114	6-18	35	13.7	11.2	70	39.8-41.5	83.0-89.6	3390 \pm 360	0.381	0.276	--	--
114L	6-18	45	11.9	11.2	21	39.8-40.7	83.4-89.6	4300 \pm 310	0.674	0.390	--	--
115	6-19	80	13.1	10.7	75	41.2-46.4	82.1-84.3	4008 \pm 230	0.368	0.158	--	B
115L	6-19	80	13.1	10.7	75	41.2-46.4	82.1-84.3	4583 \pm 265	0.353	0.073	--	B
116	6-29	50	11.9	10.4	36	42.2-46.2	84.3-91.0	4173 \pm 400	0.630	0.459	--	--
117	6-30	45	12.5	12.3	7	41.8-45.9	83.1-90.5	3211 \pm 255	0.649	0.268	--	--
118L	7-7	45	12.5	12.3	64	41.7-43.2	73.8-81.2	2610 \pm 245	0.415	0.130	--	--
118	7-7	75	11.0	11.0	64	73.8-43.2	73.8-81.2	3140 \pm 270	0.406	0.466	--	B-G
119	7-28	30	12.5	12.3	6	42.6-44.7	81.1	1720 \pm 310	0.256	0.498	≤ 0.02	B-G
120	7-25	60	13.1	15.9	- 57	36.9-38.3	74.0-81.8	1335 \pm 250	0.108	0.168	≤ 0.02	B-G
121	7-25	60	13.1	15.9	- 57	36.9-38.3	74.0-81.8	1470 \pm 225	0.137	0.177	≤ 0.02	B-G
122	7-30	50	13.7	13.1	16	42.7-43.2	83.5-86.2	2960 \pm 260	0.225	0.189	--	B-G
122L	7-30	50	13.7	13.1	16	42.7-43.2	83.5-86.2	3320 \pm 400	0.274	0.198	≤ 0.02	B-G
123	8-1	65	12.5	11.8	20	42.7-46.8	84.6-92.2	3340 \pm 420	0.256	0.326	--	B-G
124	8-4	35	12.5	13.2	- 19	43.0-44.0	83.7-86.5	496 \pm 125	0.108	0.204	--	B-G
125	8-6	75	12.5	12.5	1	42.4-46.0	84.1-92.2	1330 \pm 135	0.100	0.177	--	B-G
126	8-6	30	12.5	12.0	1	43.3-45.2	87.5-84.3	≤ 780	0.117	0.066	--	B-G
127	8-8	30	13.1	14.0	- 22	46.2-48.1	87.2-89.3	≤ 1160	0.138	0.144	--	B-G
127L	8-8	20	13.1	13.0	- 8	46.2-43.2	87.2-84.3	≤ 1030	0.128	0.055	--	B-G

^aL - Left pod; all others, right pod.^bFilters OPC-1478 impregnated with dibutylxyethylphthalate except as noted. B denotes 0.1% Na₂CO₃; G denotes glycerine.^cTime interpolated.

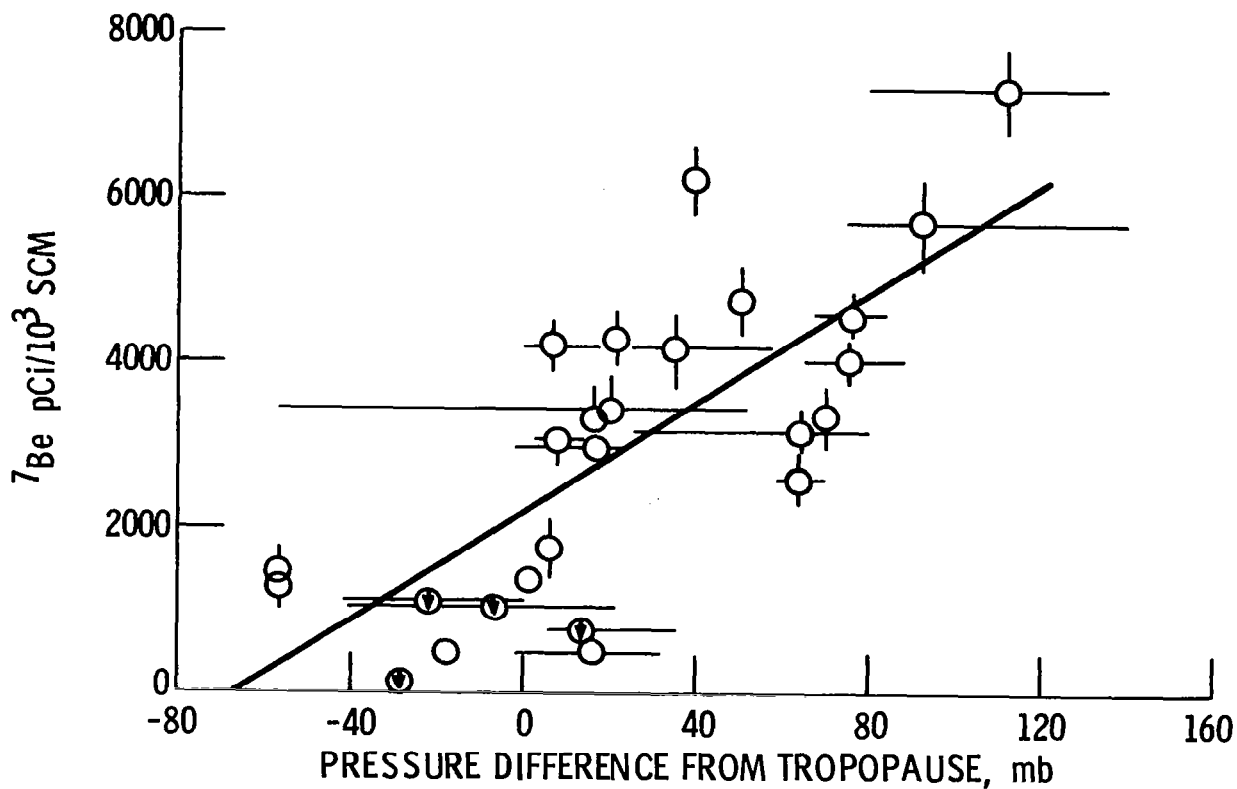


Figure 1. Correlation of ${}^7\text{Be}$ activity with pressure increment from tropopause. Correlation coefficient = 0.75.

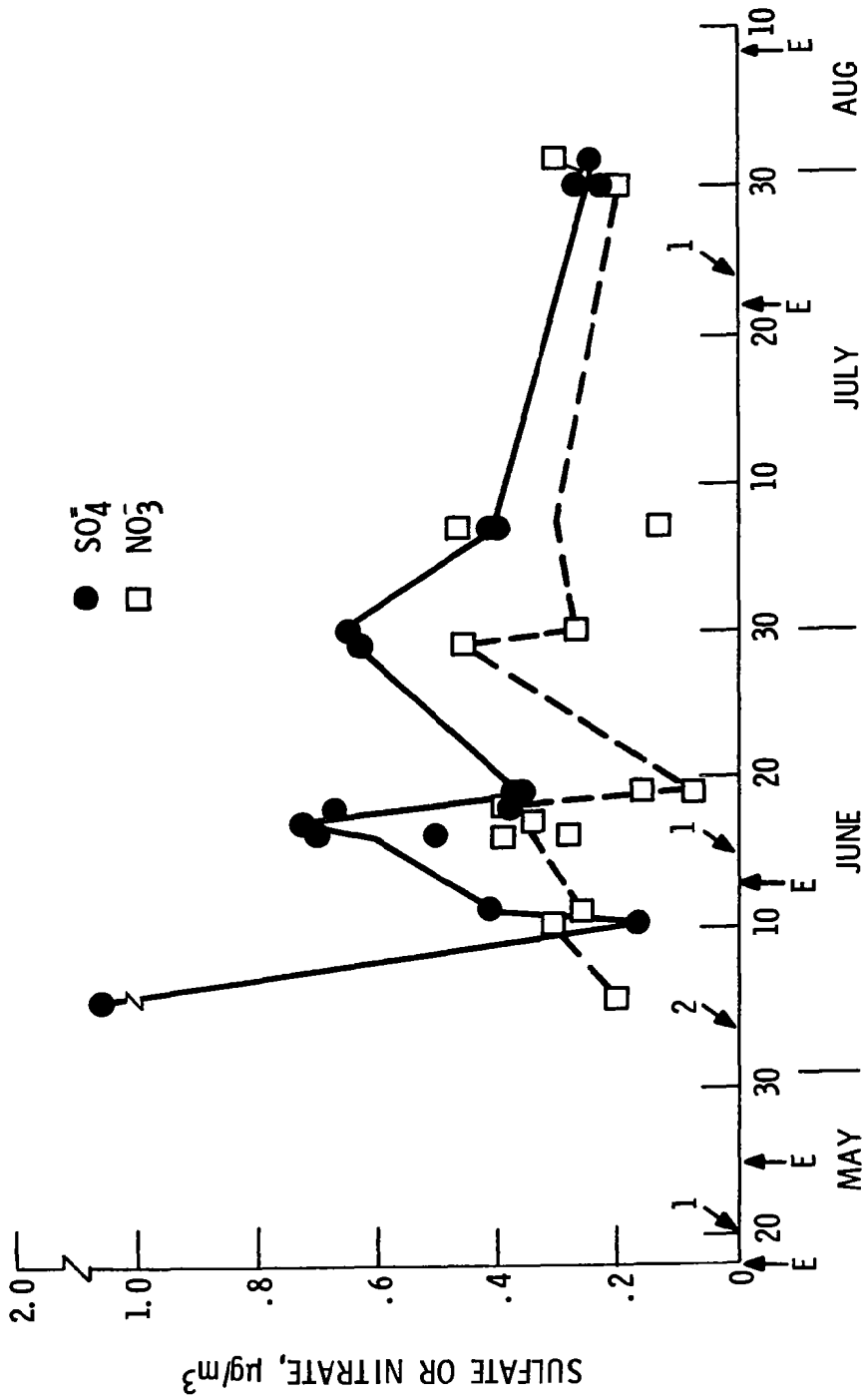


Figure 2. Temporal changes in sulfate and nitrate above the tropopause following the eruption of Mount St. Helens. E indicates major eruption; 1, 2 indicate the predicted arrival of the leading edge of the eruption cloud in the Great Lakes area for the first or second pass.

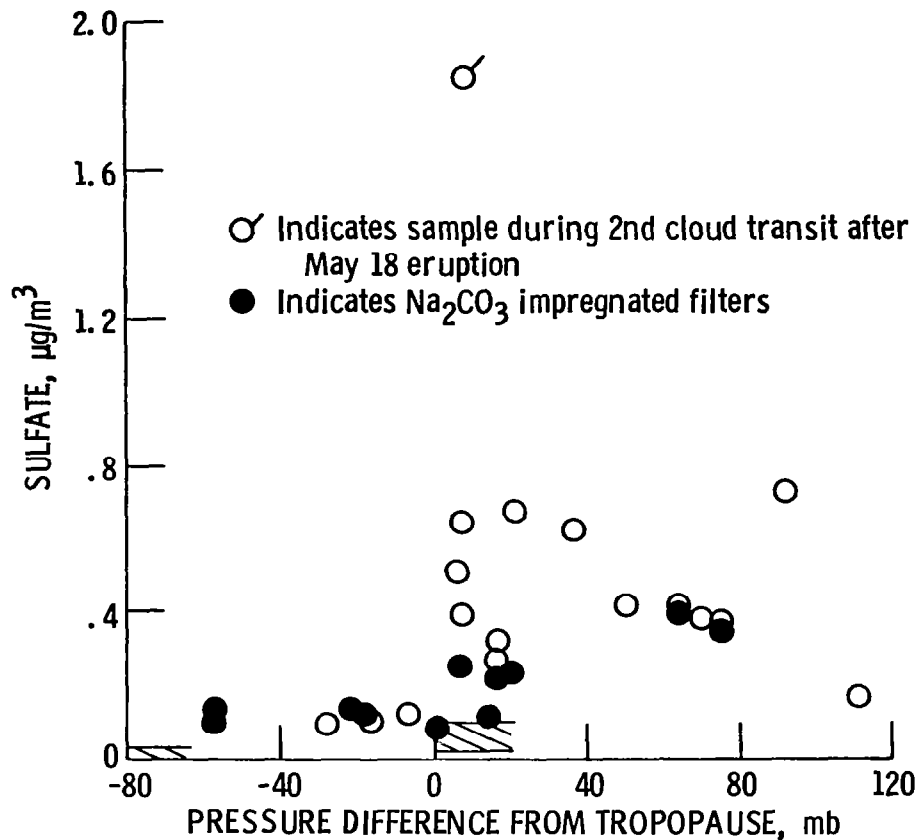


Figure 3. Sulfate concentrations near the tropopause following the eruption of Mount St. Helens.

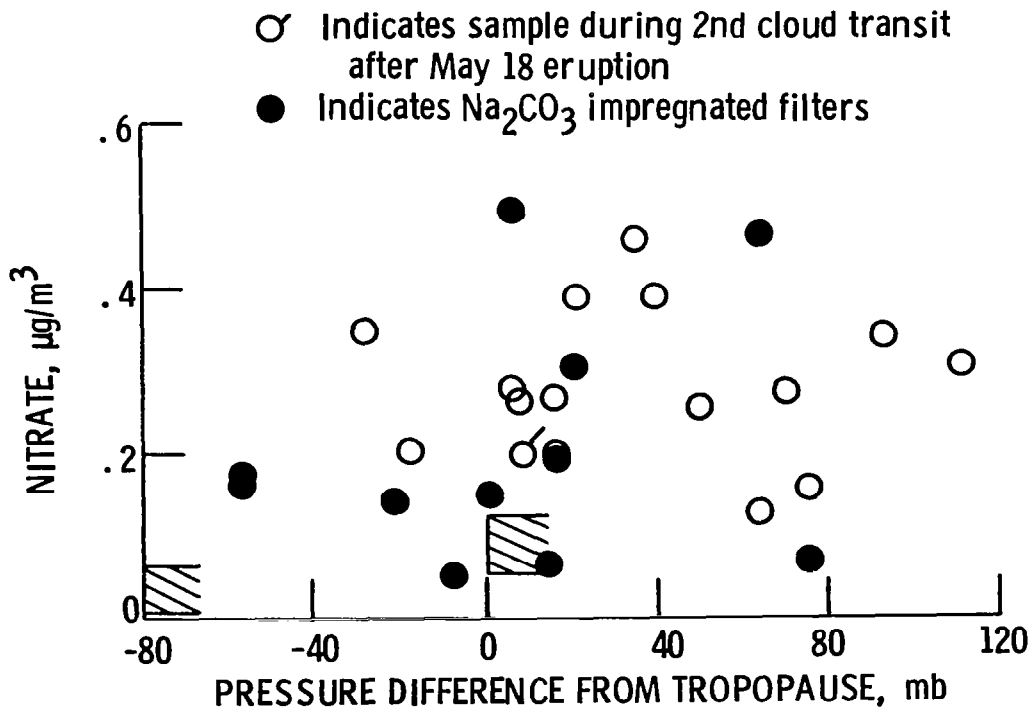


Figure 4. Nitrate concentration near the tropopause following the eruption of Mount St. Helens.

AN INCURSION OF DUST IN THE SOUTHWESTERN UNITED STATES FROM APRIL 1980 ERUPTIONS OF MOUNT ST. HELENS

L. A. Mathews, G. R. Roquemore, P. St. Amand,
Earth & Planetary Sciences Division, Research Department

J. P. Gibson
Naval Oceanography Command Detachment, Naval Weapons Center, China Lake, CA

An intrusion of volcanic dust occurred over the northern Mojave Desert in April 1980, a month before the explosive eruption of 18 May 1980. Visibility was reduced to 15 to 30 miles (24 to 48 km) during meteorological conditions that should have yielded a visibility in excess of 100 miles (160 km). This intrusion was documented by particle size distributions, scanning electron microscope analysis of Nuclepore filter samples, insolation measurements, observations by Navy and NASA aircraft, and meteorological data. No further incidents have been observed to date because of a lack of simultaneous volcanic activity with the particular wind patterns that existed in April. These wind patterns usually occur for 2 or 3 days at a time several times a year, from autumn to spring. Therefore, under certain meteorological conditions, the desert of the southwestern United States (southern California and Arizona) could be significantly affected by volcanic ash from an eruption of Mount St. Helens.

I. INTRODUCTION

The U.S. Navy and U.S. Air Force have missile testing ranges throughout the desert area. The testing depends on high visibility for precise photographic and optic works. Presently, with increasing pollution sources around these range complexes, high visibility days usually occur when air flows aloft from the Pacific Northwest. On 13 April 1980, air came from the Pacific Northwest but the visibility was low. Fine ash from the 13 April eruptions of Mount St. Helens was transported by upper level winds to the Mojave Desert area and beyond. This paper discusses the effects of the ash on local visibility and insolation.

II. SYNOPSIS OF THE EVENT

Eighteen steam and ash eruptions ranging in duration from a few minutes to 45 minutes were observed between 0515 to 1830 PST on 13 April (1). At the 500-mb level (~ 5.5 km MSL) and above, the northerly flow aloft was adequate to transport ash-laden air from above the volcano to the northern Mojave Desert within a period of 20 hours. The ash was ejected in bulk to at least 5.5 km MSL during one of the eruptions, or perhaps fine ash particles were convectively elevated by intense heat release during a series of pyroclastic flows, by mesoscale processes, or by a combination of the above. Multiple columns of fine dust being carried aloft during a pyroclastic flow was recorded photographically on 13 April by John Keller of KOIN-TV, Portland, Oregon.¹ On page 27 of the booklet entitled "Mt. St. Helens: The Volcano Explodes" (2), Photograph No. 28 by Keller shows a thick, glaciated cloud directly above what appears to be a pyroclastic flow. The temperature at the 500-mb level was about -16°C and cloud chamber tests of Cheng² show that the particles evidently are active ice nuclei at -20°C thus, it is possible the fine particles may have caused the glaciation above the 500-mb level.

¹John Keller, KOIN-TV, 4 November 1980, personal communication.

²Published in this Symposium.

Flow aloft (for example, see fig. 1 at the 500-mb level) caught these fine ash particles, swept them down the eastern scarp of the Cascade Range and Sierra Nevada, and brought milky white haze to the skies of the northern Mojave Desert by the afternoon of 14 April. On that day, the haze layer was found at elevations ranging from 15,000 to 25,000 ft. (4.6 to 7.6 km) by both U.S. Navy and NASA aircraft.³ The air beneath the layer was exceptionally clear, but by evening the dust settled to the surface as a high pressure cell moved into, and stagnated, over the Arizona and southern California area.

Visibility at the Naval Weapons Center, China Lake, California (located about 1200 km SSE of Mount St. Helens) decreased from over 160 km to between 24 and 48 km, a condition that persisted until 18 April when the high pressure area began to break down. During this period (13 to 18 April), winds at the surface were insignificant throughout the local area, including the Owens Valley, thus, the possibility of windblown dust was precluded. Normally, for the meteorological conditions that existed, the initial days of the period (e.g. 13 to 15 April) should have yielded visibilities in excess of 160 km with visibility then degrading slightly toward the end of the period (17 to 18 April).

The Mojave Desert was not the only area affected by the dust. On 15 April, a Navy pilot reported descending into a haze at about 23,000 to 26,000 feet (7 to 8 km) and coming out beneath the haze into clear air at about 15,000 feet (4.5 km) over Yuma, Arizona. Visibility within the haze was estimated to be about 3 to 5 miles (5 to 8 km). Surface visibility at Yuma was 45 miles (72 km) on 15 April but was reduced to 15 miles (24 km) the next day. Another Navy pilot reported the top of the dust to be higher than 30,000 feet (9 km) over Tucson, Arizona on 15 April. One of the authors flew to Montana and back during this episode. Haze, presumably from the ash, was present over the entire route at altitudes in excess of 10,000 feet (3 km) MSL, whereas below, the air was relatively clear.

No further incidents in southeastern California have been observed to date presumably because of a lack of simultaneous volcanic activity with the particular wind patterns that existed in April. These wind patterns usually occur several times between October and May and last for 2 or 3 days.

III. SURFACE MEASUREMENTS

During the incident (14 to 18 April), there were no clouds in the sky. Solar radiation on a horizontal surface, measured by a pyrhelimeter, showed a 2.5 percent decrease during the incident when compared with the data for other cloudless days. For comparison, dust storms with visibilities ranging from 5 to 25 km cause a reduction in solar radiation ranging from 10 to 6 percent.

During the episode, size distributions of the dust particles were measured at China Lake by using a TSI Model 3000 Electrical Aerosol Analyzer (EAA) and a Royco Instruments Inc., Model PC200 Optical Particle Counter (OPC). The EAA counts particles having diameters between 0.0075 and 0.6 μm , the OPC counts particles having diameters from 0.3 to 10 μm . Normalized particle volume distributions are shown in fig. 2 for data taken during 15 April at China Lake and for NASA data (3) taken on 7 April in an eruption plume. The China Lake data were normalized by the total volume of particles under 10 μm and the NASA data were normalized for under 12 μm . The particle distribution measurements of NASA were made with a quartz-crystal microbalance cascade impactor. These NASA data show that most of the particle mass in the plume was for particle diameters greater than 12.5 μm . The data taken in the plume of the volcano yield a steep slope on the volume distribution plot for particle diameters greater than 5 μm , and the data taken at China Lake show a decrease in slope above 5 μm . Data taken during the morning of 15 April at China Lake have higher concentrations in the 0.2 to 1 μm range than those data for the late afternoon of 15 April. The

³Collaborated with Environmental Engineering Office, Naval Weapons Center and NASA pilot at Edwards Air Force Base, 15 April 1980.

curve shown in the plot is the average of these data. Both the China Lake and NASA data have 0.2 to 0.3 μm . Although the total concentrations in the haze at China Lake and in the plume differ by over a factor of 500, the plots have similar shape for fine particles during the eruptions of 7 April and 13 April.

Dust particles were collected on two Nuclepore filters in series having 8 and 0.4 μm pore diameters. This is similar to the method of Spurny et al. (4) for asbestos fractionation. The air was drawn through the filters at 7 liters/min from 1000 PST, 16 April to 0900 PST, 17 April. The filters were located 20 feet above the ground. The particles were fairly well separated on the filter substrate and allowed single particle analysis by the SEM. Some of these particles are shown in figures 3 and 4.

Figure 3 presents photographs of scanning electron microscope (SEM) images of the dust particles. Figure 3(a) shows a smooth conchoidal surface typical of glassy materials. Figure 3(b) shows a glass shard with a suggestion of a vesicular surface texture. This particle, also, shows broken edges possibly caused by abrasion between other particles during early stages of the eruption. Figure 3(c) is a vesicular, needle-shaped shard also typical of glassy materials. The holes seen in figures 3(a), 3(b) and 3(c) in the surface of a Nuclepore filter are 8 μm in diameter. Figure 4 is also a SEM image of these dust particles. Here, besides a knife-edged glass shard and other fragments, are unidentified spherical particles. The holes, seen in fig. 4 in the surface of a Nuclepore filter, are 0.4 μm in diameter. The spherical particles are responsible for the secondary maximum in particle size distribution at about 0.2 μm (fig. 2).

Elemental analysis showed that the particles with jagged surfaces or sharp edges usually had silicon to iron ratios of about 9 and aluminum to iron ratios of 4. Lesser amounts of calcium, potassium, and nickel were found in these particles. The particles are considered to be fragmented rock from the eruptions.

IV. CONCLUDING REMARKS

The measurements and observations indicate that an intrusion of volcanic dust occurred over southeastern California, western Arizona, and possibly northern Sonora, in mid-April 1980.

Frequent eruptions (of ash reaching above 5 km MSL) from Mount St. Helens as well as from other Pacific Northwest volcanoes could have a significant effect on visibility, and possibly the climate, of the California and Arizona deserts. Days having exceptionally high visibility in the deserts usually depend on northerly flow aloft of pristine air. This air descends into an approaching high pressure area that eventually centers over the desert. However, visibility, on those days when high pressure builds and lingers, would be degraded if this air were to become contaminated with fine ash particles as it passed over the Pacific Northwest.

REFERENCES

1. Anon.: Volcanic and Seismic Activity at Mount St. Helens, U.S. Geological Survey, Report 0900, April 14, 1980.
2. Palmer, L. and KOIN-TV Newsroom 6 of Portland, Oregon: "Mt. St. Helens: The Volcano Explodes," SINO Publishing Co., 1980, p. 27.
3. Chuan, R., Woods, D. C., and McCormick, M. P.: Characterization of aerosols from Mount St. Helens eruptions, *Science*, 1981.
4. Spurny, K., and Lodge, J. P.: Analytical methods for determination of aerosols by means of membrane ultrafilters: XII Filtration mechanisms of pore filters studied by means of electron microscopy. *Coll. Czechoslov. Chem. Comm.*, Vol. 33, 1968, pp. 3931-3943.

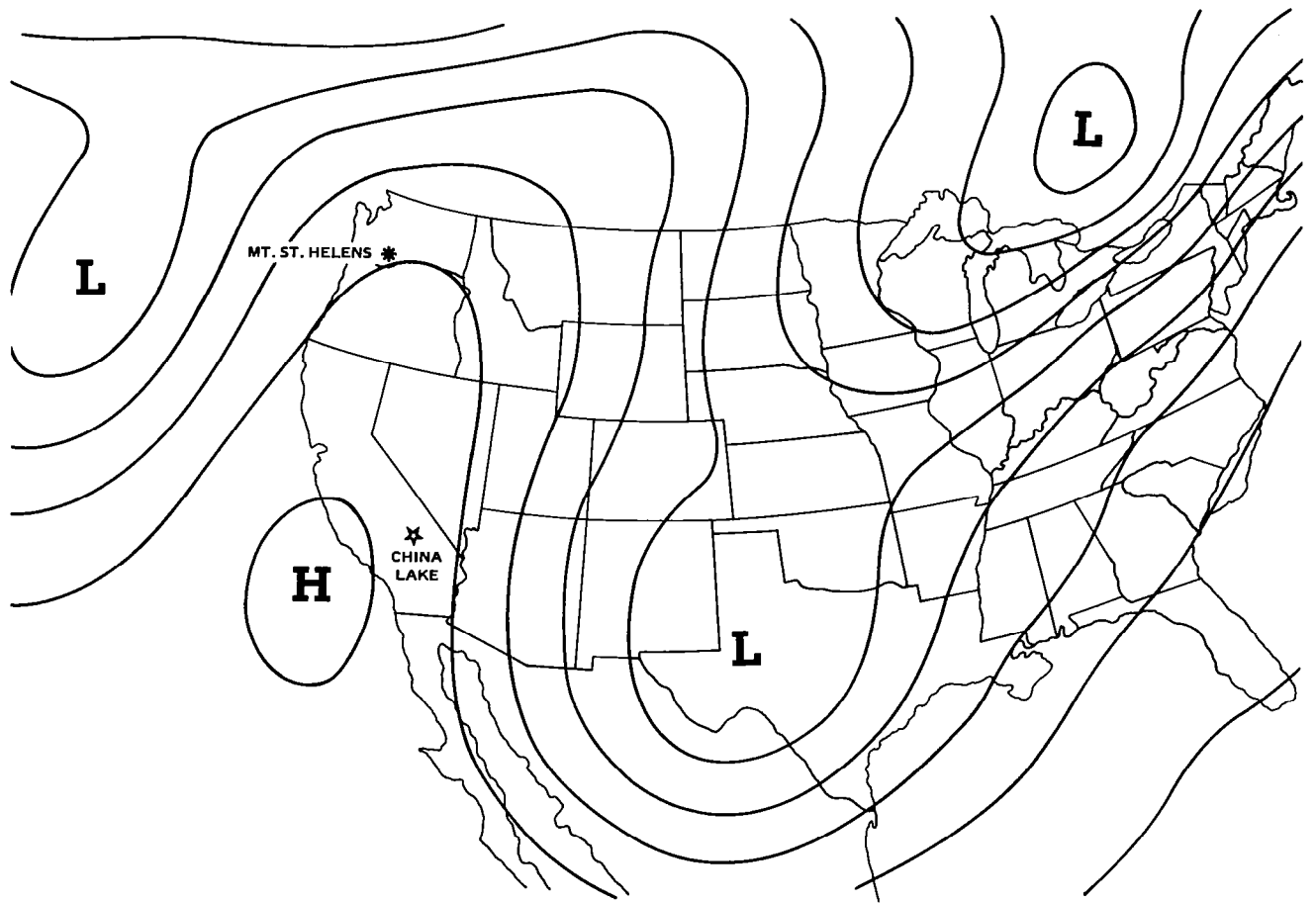


FIGURE 1. Isobars at 500 mb on 13 April 1980.

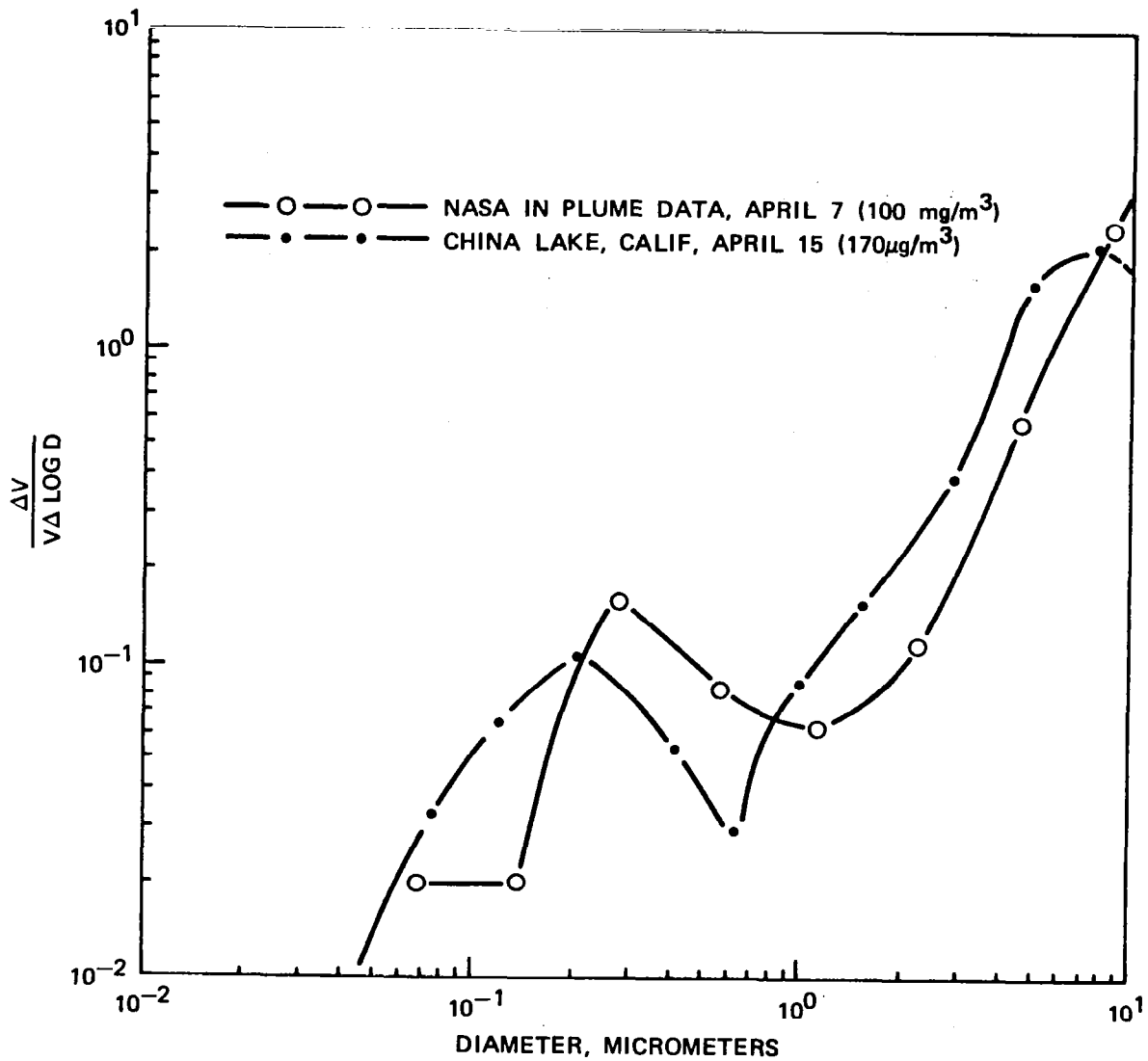


FIGURE 2. Normalized particle size distributions. The China Lake data were taken on 15 April; a result of transport of ash ejected on 13 April, and the NASA data were taken by an aircraft flying through ash plumes on 7 April.

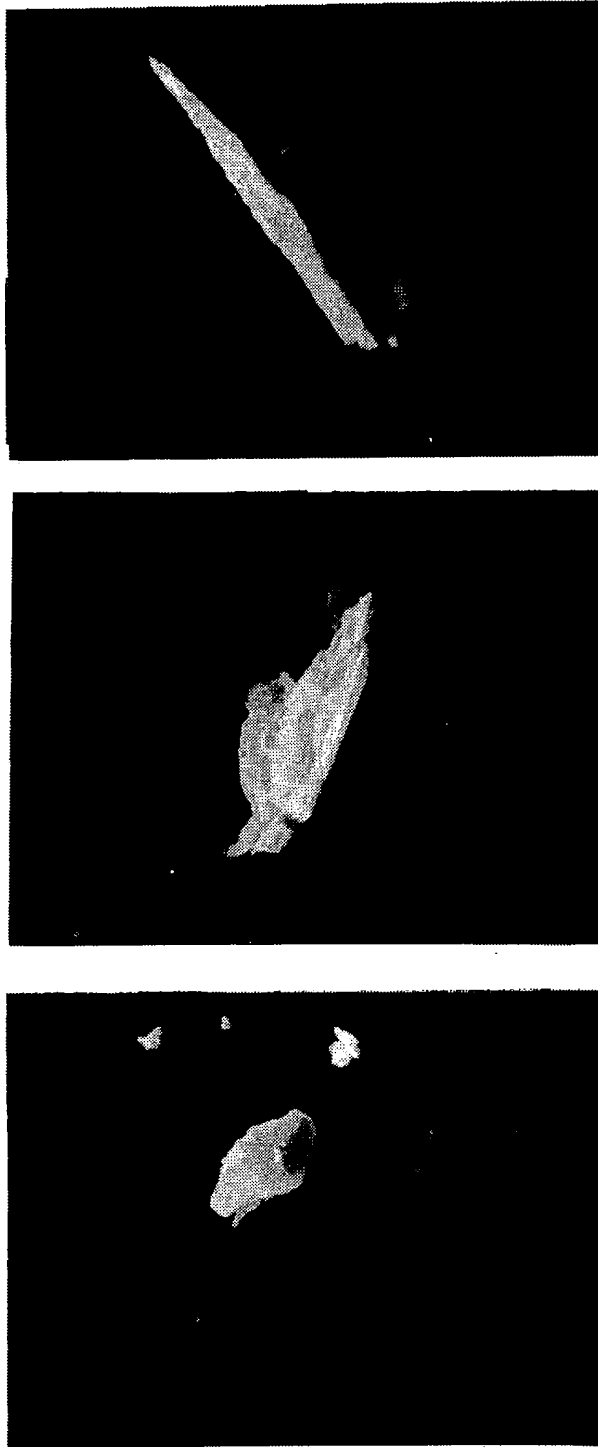


FIGURE 3. Photographs of SEM images of dust particles captured on a Nuclepore filter. The holes in the surface of the filter are 8 micrometers in diameter.



FIGURE 4. Photograph of SEM images of dust particles captured on a Nuclepore filter. The holes in the surface of the filter are 0.4 micrometers in diameter.

MOUNT ST. HELENS RELATED AEROSOL PROPERTIES FROM SOLAR EXTINCTION MEASUREMENTS¹

J. J. Michalsky, E. W. Kleckner, and G. M. Stokes
Battelle Pacific Northwest Laboratories, Space Sciences Section, Richland, WA

A network of solar radiometers, operated on the North American Continent for an average of 2 years before the first major eruption of Mount St. Helens, Washington, continues to collect direct solar data through the eruptive phase of this volcano. The radiometers collect spectral data through 12 interference filters spanning the sensitivity of the photodiode used as detector. The data are collected every 5 minutes in seven filters and every 15 minutes in five additional filters. A variant of the classical Langley method has been used to measure the optical depth of the aerosols as a function of wavelength. The eight-station network spans a latitude range from 35°N to 61°N and a longitude range from 74°E to 120°E. The network, which is the nearest station, is located some 180 kilometers east of the volcano, well within range of noticeable effects during much of the minor as well as major activity. The wavelength dependence of the aerosol-optical depth before and after the 22 July 1980 major eruption, which was well characterized because of favorable meteorological conditions, will be discussed.

I. PURPOSE

The long range goal of this research is to quantify, as a function of time, the optical extinction due to the introduction of aerosols and aerosol-precursors into the troposphere and stratosphere during the major eruptive phase of Mount St. Helens, Washington. This report concentrated on the 2-week period centered on the major eruption of 22 July 1980.

II. TECHNIQUE OF INVESTIGATION

Direct solar radiation was measured with the mobile automatic-scanning photometer (1). Two 45° altazimuth-mounted mirrors transfer radiation from any look direction in a hemisphere to a 6-inch refracting telescope. Interference filters define 12 passbands through which direct and circumsolar radiation are measured within a 1.5° field of view. From sunrise to sunset, sampling is every 5 minutes in seven filters and every 15 minutes in five additional filters.

By plotting the natural logarithm of the measured flux against airmass (approximately the secant of the zenith angle), one obtains a straight line the slope of which is equal to the total optical depth. This result follows from the equation in figure 1, namely,

$$\ln F(\lambda) = \ln F_0(\lambda) - \tau(\lambda)m \quad (1)$$

¹This work was sponsored primarily by the Office of Basic Energy Sciences and in part by the Office of Health and Environmental Research and the Office of Conservation and Solar Energy, all within the U.S. Department of Energy.

The total optical depth is due to Rayleigh scattering, ozone absorption, and aerosol extinction (absorption and scattering). Molecular absorption bands are avoided because of their nonlinear dependence on air mass. Subtracting Rayleigh and ozone attenuation and plotting the optical depth due to aerosols against wavelength for each filter yields a plot similar to that in figure 2.

Junge (2) noted that optically important ($> 0.1 \mu\text{m}$) aerosols often have a size distribution of the form

$$\frac{dN(r)}{dr} = CR^{-\nu-1} \quad (2)$$

where $N(r)$ is the number of particles with radii between r and $r + dr$ and C and ν are constants. Further, he showed that under certain assumptions about the upper and lower limits of the size distribution, namely these limits can be neglected, the attenuation due to Mie aerosols depended on wavelength λ according to

$$\tau = \beta \lambda^{-\nu+2} = \beta \lambda^{-\alpha} \quad (3)$$

where β characterizes the total loading and α is a function of the mean particle size. If the particles are very small, $\alpha \approx 4$; that is, Rayleigh scattering occurs. If the particles are large compared with the wavelength, then $\alpha \approx 0$; that is, neutral attenuation occurs. For hazes that normally occur over landmasses, $\alpha \approx 1.3$. Taking the natural logarithm of both sides of this equation yields

$$\ln \tau = \ln \beta - \alpha \ln \lambda \quad (4)$$

By plotting $\ln \tau$ against $\ln \lambda$, the numerical value of α can be obtained from the slope of the resulting straight line. Traditionally, the optical depth is evaluated at some standard wavelength ($0.5 \mu\text{m}$) and in terms of the decadic turbidity, that is,

$$B = \log_{10} e \tau(0.5 \mu\text{m}) \quad (5)$$

III. OBSERVATIONS AND RESULTS

The event around 22 July 1980 was chosen because of the preponderance of clear and partially clear days before and after this event. Figure 3(a) is a plot of the decadic turbidity coefficient B against day number. Figure 3(b) is a plot of the wavelength exponent α against day number (day 204 is 22 July). By referring to figure 2, a derivation has been made for each such plot of the correlation coefficient R , that is, a measure of the linearity of the relationship, in other words, an evaluation of the appropriateness of the Junge distribution. Figure 3 includes only turbidity and wavelength coefficients from Junge-distributed aerosols. Because of diurnal variations associated with various uses of the land surrounding the Battelle Observatory site, the data plotted are from the same time period each day.

Figure 3(a) indicates rather low, but not unreasonable, turbidity before the eruption followed by a sharp increase immediately following the eruption. The turbidity rose even higher 2 and 3 days after the eruption before dropping to more normal background values. In figure 3(b) the exponent α was slightly below normal and indicated rather large particles on the low-turbidity days preceding the eruption. This result is, perhaps, indicative of large resident stratospheric aerosols from the three previous stratospheric injections due to eruptions. On the day following the eruption, α assumed a very low value and indicated a preponderance of large particles. Then on days 2, 3 and 4 following the eruption α climbed to values larger than normal for hazes over landmasses; that is, the particles were very small. The tentative interpretation of this change is that the dust from the volcano clearly dominated on the day following the eruption, but after that time, small sulfate aerosols, formed from the precursor gases SO_2 and H_2S , assumed a dominant role in the extinction. This latter interpretation is consistent with the large release of these gases by Mount St. Helens, but may not be consistent with the conversion of these to optically important aerosols in the time it takes for the winds to carry these gases over the observatory site.

IV. CONCLUDING REMARKS

The optical extinction due to aerosols above Battelle Observatory around the time of the 22 July eruption of Mount St. Helens has been reported. The mean size of these aerosols has also been identified.

Although the present results are of considerable interest in their own right, the more significant question, that of climatological consequences of extinction resulting from aerosols introduced into the stratosphere, is the one we would most like to address.

Figure 4 is a map of the mobile automatic-scanning photometer sites on the North American continent. On the average, 2 years of data preceding the eruption of Mount St. Helens were obtained at each site giving us some notion of turbidity in nonvolcanic times and of the seasonal turbidity. Now an assessment of the difference in the mean turbidity on a continental scale following the eruptive phase of this volcano and, perhaps, the tracking of it until the stratosphere returns to pre-18 May 1980 conditions, would be desirable.

REFERENCES

1. Kleckner, E. W., Michalsky, J. J., Smith, L. L., Schmelzer, J. R., Severtsen, R. H., and Berndt, J. L.: A Multipurpose Computer-Controlled Scanning Photometer. *Appl. Optics*, 1981.
2. Junge, Christian E.: *Air Chemistry and Radioactivity*. Academic Press, 1963, p. 382.

DIRECT BEAM MEASUREMENTS

- BOUGUER-LANGLEY METHOD

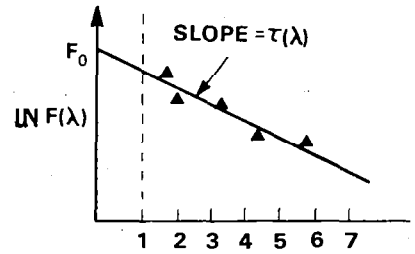
$$F(\lambda) = F_0(\lambda) \text{EXP} \{-\tau(\lambda)m\}$$

$F(\lambda)$ NARROWBAND TERRESTRIAL SOLAR FLUX

$F_0(\lambda)$ NARROWBAND EXTRATERRESTRIAL SOLAR FLUX

$\tau(\lambda)$ OPTICAL DEPTH

m AIR MASS



$$\begin{aligned} \tau(\lambda) = & \tau_R(\lambda) \text{ RAYLEIGH} \\ & + \tau_A(\lambda) \text{ AEROSOL} \\ & + \tau_{O_3}(\lambda) \text{ OZONE} \\ & + \tau_{MOL}(\lambda) \text{ MOLECULAR} \end{aligned}$$

Figure 1. The Bouguer-Langley method of extracting aerosol optical depth.

TYPICAL WAVELENGTH DEPENDENCE OF τ FOR JUNGE DISTRIBUTION

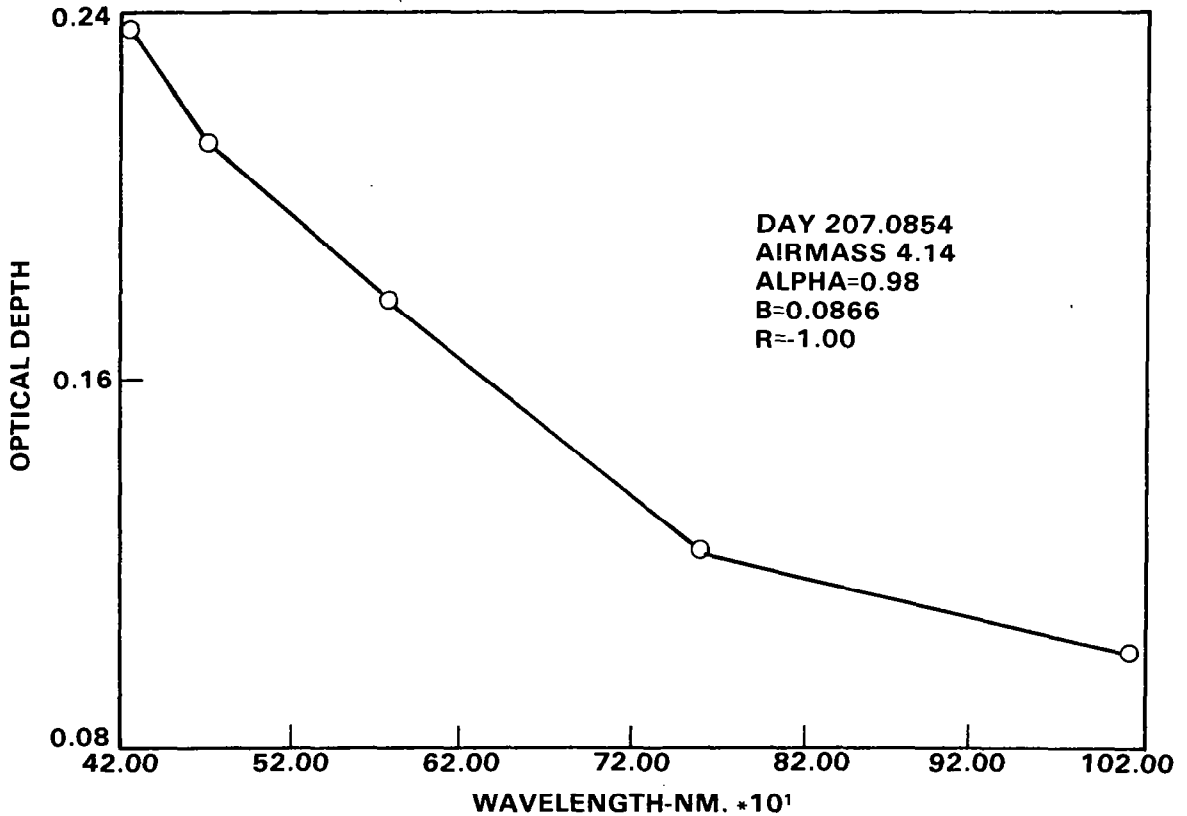
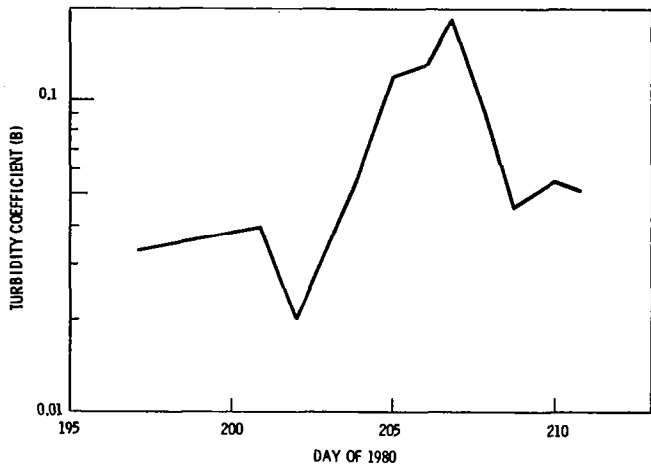
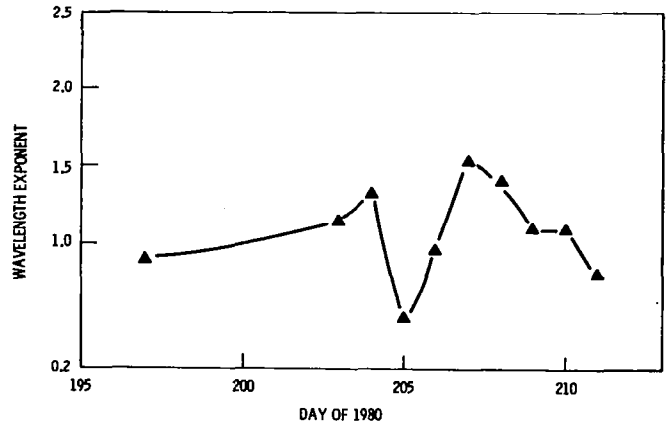


Figure 2. Typical plot of aerosol optical depth against wavelength.



(a)



(b)

Figure 3. Decadic turbidity coefficient and wavelength exponent as a function of day of 1980. (a) Decadic turbidity coefficient. (b) Wavelength exponent.

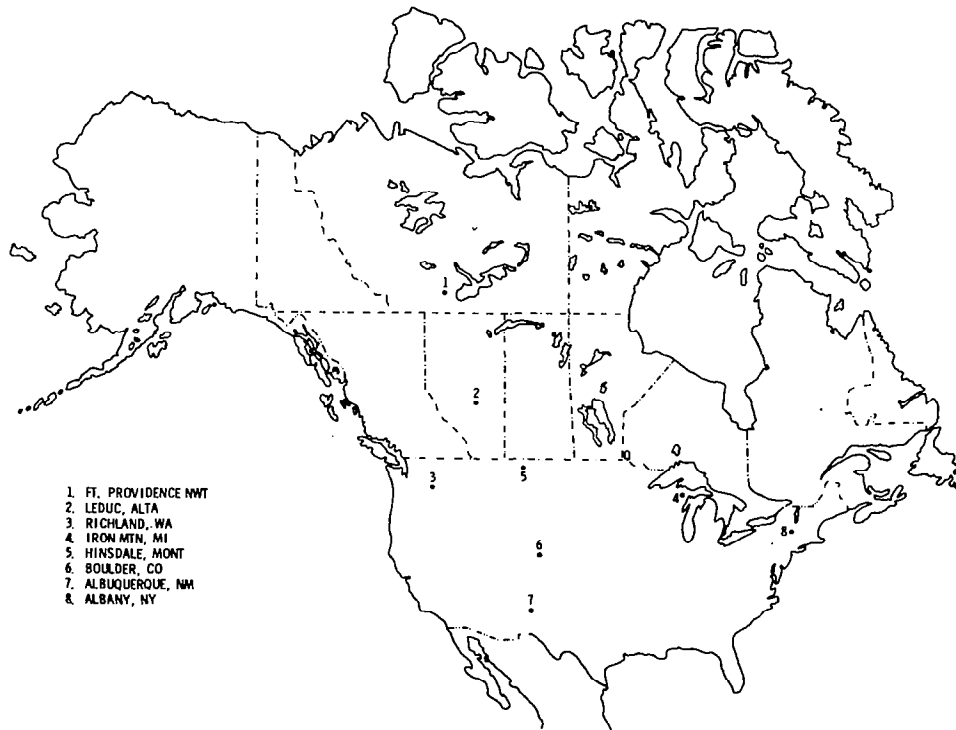


Figure 4. Mobile automatic-scanning photometer network preceding 18 May 1980.

DEPOSITION AND DOSE FROM THE MAY 18, 1980 ERUPTION OF MOUNT ST. HELENS¹

Kendall R. Peterson
Lawrence Livermore National Laboratory

The downwind deposition and radiation doses have been calculated for the tropospheric part of the ash cloud from the May 18, 1980 eruption of Mount St. Helens, by using a large-cloud diffusion model. At that time the naturally occurring radionuclides of radium and thorium, whose radon daughters normally seep very slowly from the rocks and soil, were violently released to the atmosphere.

The largest dose to an individual from these nuclides is small (in the microrem range), but the population dose to those affected by the radioactivity in the ash is about 100 person-rem. This population dose from Mount St. Helens is much greater than the annual person-rem routinely released by a typical large nuclear power plant. It is estimated that subsequent eruptions of Mount St. Helens have doubled or tripled the person-rem calculated from the initial large eruption; this total population dose is about the same as the lower-bound estimate of the population dose from the 1979 accident at the Three Mile Island nuclear power plant.

The long-range global ash deposition of the May 18 eruption has been estimated through 1984, by use of a global deposition model. The maximum deposition is nearly 1000 kg/km² and occurs in the spring of 1981 over middle latitudes of the Northern Hemisphere.

I. INTRODUCTION

The May 18, 1980 explosive eruption of Mount St. Helens produced an ash cloud that extended vertically to about 18 km and was propagated around the world. Heavy ashfall extended about 1000 km downwind and caused problems with transportation, crop damage, and clean-up. Initially, the ash was thought to produce lung damage because of the high silica content; however, recent preliminary results indicate that the physical composition of the ash is nontoxic (1).

Since the Earth's crust was formed, uranium and thorium minor constituents of the crustal material have decayed and produced a number of daughter radionuclides. These daughter products emit ionizing radiation that causes a natural background dose averaging about 100 mrem over the United States. The purpose of this paper is to estimate the additional doses to the people within the contiguous United States from the May 18 eruption. A comparison is made with the dose caused by the 1979 Three Mile Island nuclear power plant accident. Estimates of the global deposition of Mount St. Helens' ash are also given.

II. RADIATION DOSE TO U.S. POPULATION

The May 18, 1980 eruption of Mount St. Helens ejected some 1.1 km³ of ash into the atmosphere (2). The resultant plume reached well into the lower stratosphere, up to 18 km. This material, as does all soil, contained uranium and thorium and their daughters formed during radioactive decay. Figures 1(a) and 1(b) show the decay chains of these nuclides. The nuclides with double lines are those that are most important of all the daughters from the standpoint of dose. In between the boxes for each nuclide are indications of the type of decay (α or β) and the half-life in seconds (s), minutes (m), days (d), or years (y). Alpha particles travel a much shorter distance than beta particles before producing a disintegration. Alpha particles are

¹Work performed under the auspices of the U.S. Department of Energy by the Lawrence Livermore National Laboratory under Contract W-7405-Eng-48.

only potentially hazardous to man through inhalation or ingestion. Beta particles are only potentially hazardous through skin absorption as well as the pathways for alpha particles; however, normal clothing will stop most beta particles.

Calculations of doses to man from the uranium-226 and thorium-228 released by the May 18 eruption have been made by using a large-cloud diffusion code called 2BPUFF (3). This model moves a cloud of pollutants in Lagrangian coordinates along the cloud trajectory. The pollutant assumes the shape of a vertically oriented right-circular cylinder with a Gaussian distribution in both the horizontal and vertical. Input parameters include time-variable ground and cloud center altitudes above sea level, surface and cloud center vertical-diffusion coefficients, horizontal atmospheric dissipation rates, and bases and tops of mixing layers. Previous post-facto calculations using 2BPUFF for nuclear cratering tests and foreign atmospheric nuclear testing have verified within a factor of three with measurements. Draxler's 500- to 200-mbar trajectory (4) has been used with 2BPUFF. These pressure levels correspond to heights from about 6 to 12 km above sea level. Most of the ash below 6 km deposited within a few hundred kilometers; this portion has been ignored in the calculation. The following information was used in determining the source terms for the two more important radionuclides:

- (1). The volume of airborne ash = 1.1 km^3 (2).
- (2). The respirable fraction of the ash ($\leq 5 \mu\text{m}$ particles) was assumed to be 0.29 by weight.²
- (3). The density of the ash was assumed to be the same as that of typical soil, or about 2500 kg/m^3 .
- (4). Half of the airborne ash was assumed to be injected into the troposphere between 6 and 11 km. The latter height is the tropopause height as measured near the eruption time at Salem, Oregon.
- (5). The quantity of radium-226 at the time of eruption is assumed as 0.40 pCi/g . This value is based on downwind ash measurements made by Koranda (6) and Fruchter et al. (1).
- (6). The quantity of thorium-228 is 0.27 pCi/g , based on Koranda's measurements (6).

From these data, the source terms are determined to be $1.6 \times 10^{14} \text{ pCi}$ of radium-226 and $1.1 \times 10^{14} \text{ pCi}$ of thorium-228.

The 2BPUFF code gives as part of its output the surface concentration in pCi/m^3 , deposition in pCi/m^2 , and doses in rem by various pathways. For this report the inhalation pathway was considered first. Figure 2 shows dose contours (in microrem) to individuals for the combined dose from the radium-226 and thorium-228 released on May 18. The exposure has been integrated by the 2BPUFF code during the passage of the upper tropospheric ash cloud. The dashed line in figure 2 is the cloud center trajectory.

The largest dose, within 10 km of Mount St. Helens, is less than 20 rem. This dose, as are the dose contours in figure 2, is to an individual by inhalation. Ingestion pathways, including milk, meat, and above-surface crops, were also considered. The radioactive ash deposits on grass blades and leaves and is consumed by cattle or adheres to crops consumed by people. If the inhalation isopleths in figure 2 are multiplied by 40, they represent isopleths for all the ingestion pathways.

The doses to an individual, shown in figure 2, are small. Ingestion doses are 40 times larger, but still small. An average person in the United States receives about 0.1 rem/year or about $1 \mu\text{rem}/6 \text{ min.}$ from natural soil and cosmic ray sources. However, many health physicists believe that any radiation dose above the amount received naturally can cause life shortening to some segments of the population due to cancer or other radiation-related causes. Since we are concerned with cell changes involving a portion of the population, it is necessary to leave the concept of dose to an individual, and focus on population dose, usually expressed in person-rem. During the past decade person-rem doses compared with life-shortening relationships have been developed and accepted by those concerned with routine and accidental dose estimates and

²R. Landingham, Personal Communication, Oct. 1980.

their effects from nuclear power reactors. Given the total population dose over an area, risk assessment techniques can predict what fraction of the population involved might contract cancer. Admittedly, as the individual doses to the population exposed decrease to low values, the error bars of such estimates increase since such risk assessment methods are based on animal exposures at moderate radiation levels.

The dose contours presented in figure 2 have been combined with population data obtained from the Bureau of the Census reports (6,7). Integration of the product of dose and population over the swath of the ash plume across the United States gives a total of 2.5 person-rem. A similar integration for the ingestion pathways gives an additional 91 person-rem. Note that the dose from the heavy ashfall over the downwind portions of Washington, Idaho, and Montana has not been included. This fallout consisted of mostly larger, non-respirable particles. However, some of these particles would be reduced to respirable particles through abrasion caused mainly by vehicular traffic; resuspension of such particles due to wind will allow a small but long-term dose to the lungs. The larger particles will decay eventually to radon gas which is readily inhaled.

The population dose from Mount St. Helens has been compared with the population dose due to the 1979 accidental release at the Three Mile Island nuclear power plant (TMI), located south of Harrisburg, Pennsylvania. The radioactive noble gases krypton-88 and xenon-133 were released, along with very small amounts of radioiodine (8). The product of (a) the quantity of nuclide released and (b) the factor that converts air concentrations to dose shows that xenon-133, with a half-life of 5.25 days, is by far the most significant nuclide accidentally released at TMI. The only significant pathway for xenon-133 is immersion within the plume of gas; dose from inhalation is negligible and there are no food pathways. Population dose estimates range from 275 to 2800 person-rem (8,9). Subsequent eruptions of the volcano have placed significant quantities of additional ash into the troposphere and have increased the U.S. person-rem by at least a factor of two or three. In addition, the nearby ashfall over Washington, Idaho, and Montana, not calculated in this study, exposed the population to daughters of radium and thorium radionuclides, primarily radon gas and its immediate daughter products. The total population dose estimate from Mount St. Helens is about the same as the lower-bound estimate from the TMI accident.

III. GLOBAL DEPOSITION OF ASH

A global deposition model, named GDEP, based on strontium-90 deposition from atmospheric nuclear testing was prepared by the author (10). Since strontium-90 has a half-life of 28 y, GDEP may be used with minor modifications to estimate the global deposition of the small-particle Mount St. Helens ash that was injected into the stratosphere on May 18. The GDEP model places sources into one or more of six stratospheric compartments from which it eventually is deposited within 20° latitude bands each 3 month season for up to 6 years. The source term for the stratospheric ash less than 5 μm was assumed to be the same as the upper tropospheric ash source term used in the 2BPUFF model. The output from GDEP, shown in figure 3, gives the deposition in kilograms per square kilometer for the 30°N to 50°N latitude band through the spring of 1984. Doses from the ash were not calculated since the dose to an individual would be very small and the population dose is unlikely to be valid for global deposition of ash over 6 years. Figure 3 shows that the maximum ash deposition occurs in the spring (March to May) of 1981 and amounts to nearly 1000 kg/km². This represents an average ash depth around the latitude band of about 0.4 μm .

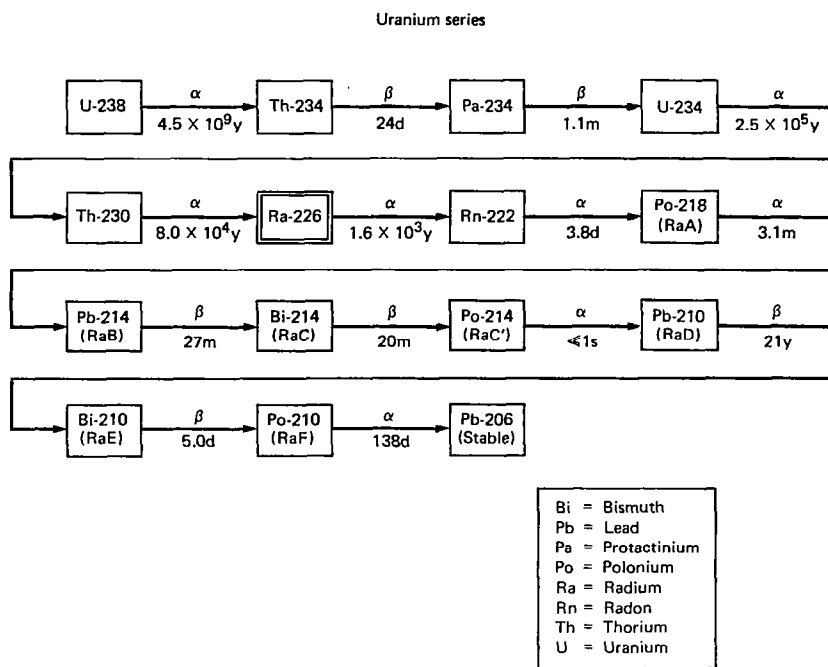
Validation of the GDEP model against global deposition from atmospheric nuclear tests not used in preparing the model indicates agreement within 10 percent out to 4 years if the output is summed to obtain total global deposition on an annual basis. Figure 4 presents such data for the ash injected into the stratosphere by the May 18 eruption of Mount St. Helens. The ordinate is in 10¹¹ x kg of ash. The sum of the 6 years of deposition data amounts to 4.1 x 10¹¹ kg. At the end of 6 years, over 95 percent of the stratospheric ash has deposited on the surface.

IV. CONCLUDING REMARKS

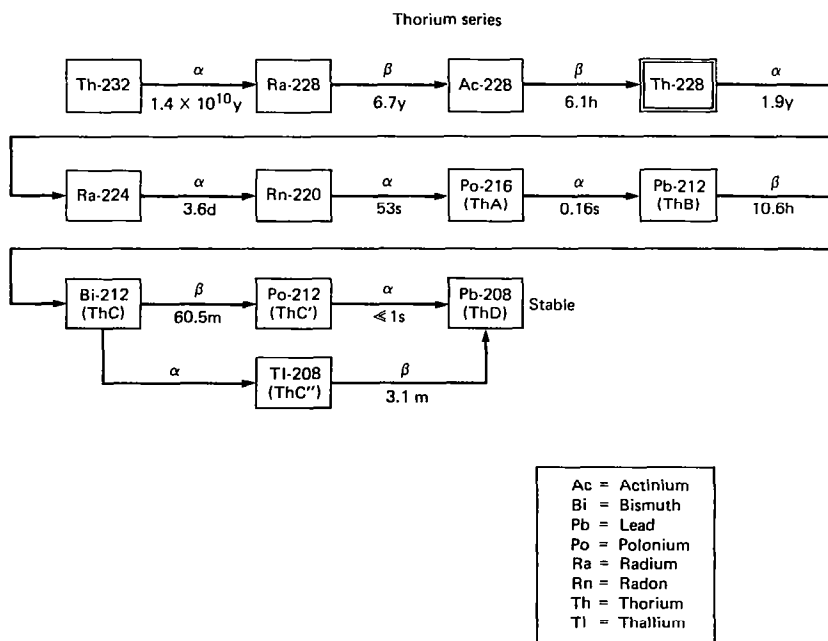
It has been shown, by using conservative assumptions, that the May 18 Mount St. Helens eruption released radioactive radium and thorium isotopes into the troposphere that gave a total of about 100 person-rem. If the person-rem from the heavy ashfall in the Pacific Northwest together with subsequent eruptions of Mount St. Helens are added to the person-rem calculated in this report, the total is about the same as the lower-bound estimate of the population dose from the 1979 accidental release at the Three Mile Island nuclear power plant. The global deposition of small-particle stratospheric ash released May 18 will reach a maximum deposition of about 1000 kg/km² between March to May, 1981 over middle latitudes of the Northern Hemisphere. Over 95 percent of the stratospheric ash had deposited 6 years after the eruption.

REFERENCES

1. Fruchter, J.S. et al.: Mount St. Helens Ash from the 18 May 1980 Eruption: Chemical, Physical, Mineralogical, and Biological Properties. *Science*, Vol. 209, (Sept. 5, 1980), pp. 1116-1125.
2. Waitt, R.: Geophysical Events, Volcanic Activity. *EOS*, Vol. 61, No. 35, (Aug. 26, 1980), pp. 597.
3. Crawford, T.: A Computer Program for Calculating the Atmospheric Dispersion of Large Clouds. Lawrence Livermore National Laboratory Report UCRL-50179, Nov. 1966.
4. Draxler, R.: Observing and Forecasting the Path of Volcanic Emissions After an Eruption. Air Resources Laboratory, NOAA, Sept. 1980. Presented at the Tenth International Laser Radar Conference, Silver Spring, Maryland, Oct. 6-9, 1980.
5. Koranda, J.: Analyses of Mt. St. Helens Ash. *Energy and Technology Review*, Lawrence Livermore National Laboratory, Sept. 1980.
6. Bureau of the Census: *Statistical Abstract of the United States*, U.S. Dept. of Commerce, Washington, DC, 1979.
7. Bureau of the Census: *Illustrative Projections of State Populations by Age, Race, and Sex: 1975 to 2000*, Washington, DC, 1979.
9. Knox, J.B.; Dickerson, M.H.; Greenly, G.D.; Gudiksen, P.G.; and Sullivan, T.J.: Utilization of the Atmospheric Release Advisory Capability (ARAC) Services During and After the Three Mile Island Accident, Report UCRL-52959, Lawrence Livermore National Laboratory, July 1980.
10. Auzier, J.; Berger, C.D.; Eisenhower, C.M.; Gesell, T.F.; Jones, A.R.; and Masterson, M.E.: Report of the Task Group on Health Physics and Dosimetry. Report of The President's Commission on Three Mile Island, Washington, DC, Oct. 1979.
11. Peterson, K.: An Empirical Model for Estimating World-Wide Deposition. From Atmospheric Nuclear Detonations. *Health Physics*, Vol. 18, 1970, pp. 357-378.



(a)



(b)

Figure 1. Decay chains of uranium-238 and thorium-232. The type of particle emitted and the radioactive half-life are shown between the boxes. The most important radionuclide from the standpoint of dose is depicted by the double lines.

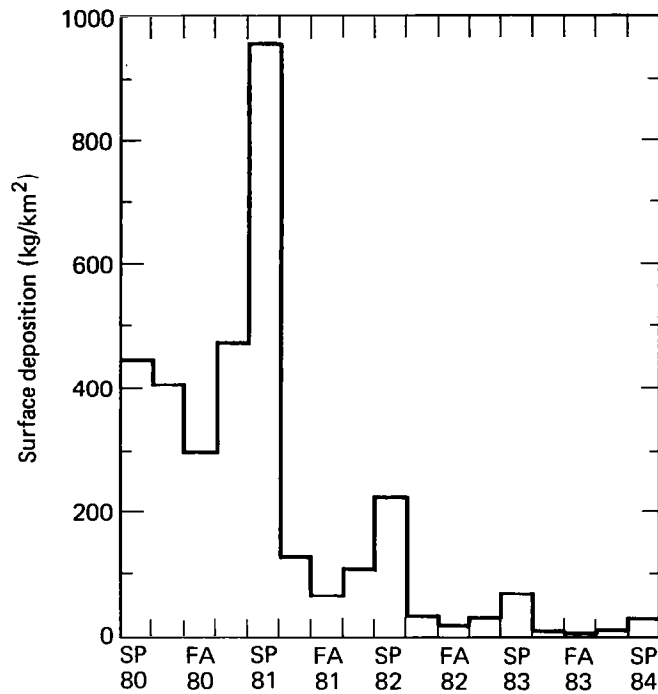


Figure 3. Average deposition between 30°N and 50°N, in kg/m², of stratospheric portion of the ash cloud produced by the May 18, 1980 eruption of Mount St. Helens. Deposition is shown by 3-month seasons, where, for example, spring of 1981 represents the months of March through May.

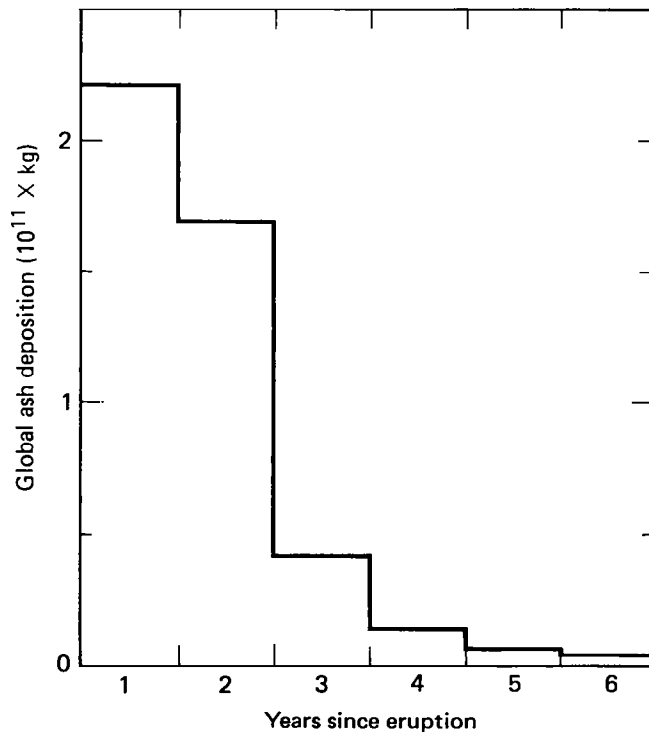


Figure 4. Global deposition of the stratospheric portion of the May 18, 1980 volcanic ash cloud, in 10¹¹ kg, shown by years, beginning with the spring of 1980.

AMBIENT AIRBORNE SOLIDS CONCENTRATIONS INCLUDING VOLCANIC ASH AT HANFORD, WASHINGTON, SAMPLING SITES SUBSEQUENT TO THE MOUNT ST. HELENS ERUPTION¹

G.A. Schmel
Pacific Northwest Laboratory, Richland, Washington

Airborne solids concentrations were measured on a near daily basis at two Hanford, Washington sites after the eruption of Mount St. Helens on May 18, 1980. These sites are about 211 km east of Mount St. Helens. Collected airborne solids included resuspended volcanic ash plus normal ambient solids. Average airborne solids concentrations were greater at the Hanford meteorological station sampling site which is 24 km northwest of the Horn Rapids dam sampling site. These increased concentrations reflect the sampling site proximity to greater ash fallout depths. Both sites are in low-ash fallout areas although the Hanford meteorological station site is closer to the greater ash fallout areas. Airborne solids concentrations were decreased by rain, but airborne solids concentrations rapidly increased as surfaces dried. Airborne concentrations tended to become nearly the same at both sampling sites only for July 12 and 13, the last days for the current report period.

I. INTRODUCTION

A major eruption of Mount St. Helens, Washington, occurred on May 18, 1980. The resulting airborne plume of volcanic ash (pulverized rock) was transported by easterly winds. Particle dry deposition from this plume resulted in downwind ash fallout of varying depths. The maximum fallout centerline was north of the geographic area shown in Fig. 1. The Hanford area, northwest of Richland, Washington, was within the edge of the fallout plume. Within the Hanford area were airborne particulate sampling sites used in prior wind resuspension experiments. These sampling sites were reactivated to collect airborne volcanic ash. To investigate some local airborne effects of the eruption, airborne solids concentrations and airborne particle size distributions were measured at two sites in the Hanford area between May 19 and July 13. Measured concentrations included collected solids contributions from both airborne volcanic ash still airborne from the eruption and resuspended volcanic ash and surface solids. As shown in Fig. 1, the Horn Rapids sampling site is near the southwestern boundary of the Hanford area, and the meteorological station sampling site is 24 km northwest of the Horn Rapids dam site. Both sites received relatively low ash deposits which were about 1 to 2 mm and 3 to 4 mm in depth, respectively.

The sampling sites were selected because of equipment and electric power availability from prior investigations and because both sites were distant from urban activity. Thus, concentrations were to be measured from area sources rather than from local surface disturbances. This investigation set out to determine a time history of airborne volcanic ash concentrations immediately after the eruption (starting the following day, May 19) at two sampling sites. In addition to recording airborne solid concentrations, any changes in airborne volcanic ash concentrations with time were of potential use for application to wind-resuspension investigations of surface-contaminated areas. In other investigations, wind resuspension is investigated with controlled inert-tracer sources or tracers of opportunity from larger surface-contaminated areas. Volcanic fallout ash was a tracer of opportunity for investigating wind resuspension from a near "infinite" surface source area of freshly deposited solids.

¹Work supported by the U.S. Department of Energy under Contract DE-ACO6-76RLO 1830

II. SAMPLING EQUIPMENT

Airborne solids concentrations were measured by using filters for the collection of solids on an average daily basis (or several days) by (a) sampling continuously for all wind directions and speeds at the Horn Rapids and meteorological station sampling sites and (b) sampling only during 220° to 290° wind directions at the meteorological station sampling site. Winds from the south are from 180° while winds from the west are from 270°. To determine the mass of solids collected, filters were equilibrated with low-humidity laboratory air both prior to and after sample collections. Solid weights were determined after equilibration.

Airborne particulates were classified while airborne into two or more size fractions with three different types of sampling equipment:

(1). A cyclone preseparator² with a 5.5- μm 50-percent cut-off diameter, followed by a 20- x 25-cm glass-fiber filter. The 5.5- μm diameter collection is termed "respirable" in this paper even though a 3.5- μm diameter is often considered more accurate in describing the respirable diameter range. During sampling, the cyclone-preseparator cylindrical sampler inlet was continuously oriented into the wind with a tail fin. The air-sampling flow rate was 1.1 m³/min at a sampling height of 1.4 m. Except during rain, sampling was continuous for times of about 24 hours. After sampling weighing, airborne solids concentrations were calculated separately from the filter collection and the total of filter-plus-cyclone-separator collections.

(2). A 20- x 25-cm filter sampler (shown in Fig. 2). The sampler inlet was oriented toward a direction of 225°. In this sampler, airborne particles either settled in the sampler inlet (1.9- x 25 cm cross section) or were collected on the backup filter. Although the relative efficiency of particle collection on the inlet compared with that of the filter has not been completely investigated as a function of particle diameter, aerodynamic considerations indicate that essentially all respirable particles collect on the filter (1). The relative collection site for nonrespirable particles within the sampler is a more complex function of particle diameter. However, for nonrespirable particles, gravity settling, and hence, particle collection, are expected to be relatively more important in the inlet. The air-sampling flow rate was 1.1 m³/min at a sampler inlet height of 1.4 m. Airborne solids concentrations were calculated from only the filter collection.

(3). A laser optical particle counter.³ This optical counter sizes airborne particles electronically and accumulates number counts in diameter increments as small as 0.07 μm . Airborne particles were sampled at 0.9 m above ground during selected time periods between May 22 and May 30 at a site near the Hanford meteorological station. Measurements were for 30-minute time increments. Results are reported as the volume distribution:

$$\frac{\Delta V}{\Delta \ln D} = \frac{\pi D^4 \Delta N}{6 \Delta D}$$

which has units of m³/cm³. The particle volume is V, the diameter is D, and the number of particles per unit volume is N.

III. AIRBORNE SOLIDS CONCENTRATIONS

Airborne solids concentrations in $\mu\text{g}/\text{m}^3$ are shown in Fig. 3 along with selected meteorological data recorded at the Hanford meteorological station. The meteorological data are shown below the figure, and a mixed time scale is indicated. The horizontal bar through each data point illustrates the airborne solids sampling time—the day of starting airborne solids sampling to the day of ending samplings. Filter changes were usually made in the morning. In contrast to the airborne solids collection time periods, meteorological

²Model 230CP Cyclone preseparator, Sierra Instrument Co., Carmel Valley, CA.

³Active Scattering Aerosol Spectrometer, Particle Measuring Systems, Inc., Boulder, CO.

data are routinely summarized for a time period between midnight to midnight. Thus, in cross-comparing airborne solids concentrations to meteorological data, there is about a one-half-day shift in time scale.

A. Horn Rapids Site Results

Two cyclone filter samplers were used at the Horn Rapids sampling site to investigate airborne solids concentrations and sampling reproducibility. The two samplers were 2 m apart. Average concentrations for these two samplers are shown by both open- and solid-data symbols in Fig. 3. Each datum point is plotted at the average concentration calculated from these two samplers. The limits of the vertical bar through each datum point are solids concentrations determined from each sampler. If limits are not shown, the limits are within the datum symbol. At this site, sampling began on May 19, the day after the eruption. During the initial sampling day, the daily average concentration for respirable particles, i.e., 5.5- μm diameters, was 1430 $\mu\text{g}/\text{m}^3$; the total, including the cyclone-preseparator collection, was 2610 $\mu\text{g}/\text{m}^3$. The respirable content of the airborne solids was 55 percent.

Subsequently the daily average airborne solids concentrations decreased. Between May 20 and May 27, concentrations were between 150 and 600 $\mu\text{g}/\text{m}^3$ and were still high compared with normal (prior to eruption) concentrations. Thus, the measured concentrations are attributable to volcanic ash. Starting from May 25 and May 27, airborne solids samples were to be collected for 2 days rather than 1 day. (Rain fell on May 26.) The actual airborne solids concentrations during these two days, May 25 and May 26, were probably greater than the average plotted in Fig. 3. Conversely, the mass loading on May 26 to May 27 was probably less than the average plotted in Fig. 3. These uncertainties arise since sampling was for 2 days and since the samplers were automatically deactivated during rain on both days to prevent increased filter resistance or complete blockage of airflow through the filter.

There were three rain periods including four successive days from May 25 to May 28 which could have affected the wind resuspendability of volcanic ash, 0.11 in., 0.79 in., and 0.01 in., and a trace, respectively on these 4 days. From a comparison of rain accumulation each day and airborne solids concentrations, an estimate can be made of the rain accumulation which can remove airborne particulates and prevent wind resuspension of surface solids by wetting ground surfaces. Decreased airborne solids concentrations were evident on May 27 and May 28 when the concentrations decreased two orders of magnitude at both sampling sites and on June 12 and June 13 when the concentrations decreased one order of magnitude at the meteorological station sampling site. Subsequently, airborne solids concentrations increased as ground surfaces dried and resuspension occurred.

Although resuspension and, hence, airborne solids concentrations are a function of both surface and meteorological parameters, an estimate is made for the amount of rain required to significantly reduce resuspension. There were only three significant rain periods recorded:

- (a). 0.79 in. on May 26
- (b). 0.22 and 0.35 in. (0.57 in. total) on June 12 and 13
- (c). 0.19 in. on June 20.

Significant (that is, an order of magnitude) reductions in airborne solids concentrations occurred only during the first two rain periods (0.79 and 0.57 in.) and not during the last period (0.19 in.). Thus, a tentative conclusion is that from 0.2 to 0.6 in. of rain may be required to significantly reduce airborne solids concentrations arising from wide-area resuspension sources. However, the duration of reductions may be short, for example, a day.

Average airborne solids concentrations showed daily fluctuations throughout the time period investigated. After a May 29 rain until July 9, concentrations from about 10 to 100 $\mu\text{g}/\text{m}^3$ might be typical of airborne solids concentrations prior to the eruption. However, on July 10 and July 11 the average airborne solids concentration was 384 $\mu\text{g}/\text{m}^3$. It is hypothesized that the increased concentration was caused by the volcanic ash resuspension.

B. Hanford Meteorological Station Site Results

Airborne solids concentrations at the Hanford meteorological station were investigated by (a) sampling continuously, and (b) sampling only as a function of the wind direction to investigate the direction from which resuspended particulates were transported. Concentrations were investigated principally by sampling continuously with the fixed-orientation sampler shown in Fig. 2. These data are shown by the triangle data symbols in Fig. 3. In comparison with Fig. 2, Fig. 3 samples collected continuously, some particulate samples were collected in a cyclone-filter sampler which was automatically operated only during 220° and 290° wind directions. These wind-direction-collected samples were collected from May 23 to June 7 and are represented by the inverted triangle data symbols in Fig. 3.

In this investigation, the largest airborne solids concentrations were measured at the Hanford Meteorological station sampling site. These concentrations are shown by the upper curve in Fig. 3. These larger concentrations reflect resuspension from the nonuniform distribution of volcanic ash fallout. The meteorological station sampling site is in a region of greater volcanic ash fallout (3- to 4-mm depth) than the Horn Rapids dam sampling site (1- to 2-mm depth) and is closer to the more northern areas which received fallout (over 5-cm depth) from the eruption-airborne-plume centerline.

Although airborne solids concentrations were greater for continuous sampling at the meteorological station sampling site, concentrations were much less when only the 200° to 290° wind directions were sampled. In fact, for 7 of the 9 days between May 28 and June 6, concentrations measured for the 220° to 290° wind directions were even less than concentrations measured at the Horn Rapids sampling site.

To quantify the relative airborne solids concentrations at each site, further concentration ratios are shown in Fig. 4. The upper concentration ratio curve is the concentration ratio for continuous sampling:

$$\frac{(\text{Hanford meteorological station})}{(\text{Horn Rapids Dam Site})} = \frac{(\text{HMS continuous sampling})}{(\text{HRD continuous sampling})}$$

The average concentration ratio was about 4 until July 10. Subsequently, the ratio varies around unity. To quantify the relative concentrations as a function of wind direction at the meteorological station sampling site, the lower concentration ratio curve in Fig. 4 represents the ratio:

$$\frac{(\text{HMS directional sampling during } 220^\circ \text{ to } 290^\circ \text{ winds})}{(\text{HMS continuous sampling})}$$

This ratio ranged from 0.06 to 0.04.

To explain the relative differences in concentrations for continuous and wind-direction sampling, it is felt that most of the collected particles were transported on winds coming from the north which contained volcanic ash resuspended from areas of greater ash depth. These northern winds were sampled during continuous sampling, but air transported from the north was sampled less when sampled only toward the 220° to 290° wind direction sector. This wind direction explanation thus suggests that airborne solids concentrations would increase with increasing northerly sampling locations and hence towards areas of greater ash fallout. However, it is uncertain how or if one should extrapolate the concentration data in Fig. 3 to geographic areas of other ash depth.

IV. AIRBORNE-VOLUME DISTRIBUTION RANGES

Airborne-volume distributions calculated from the optical counter operated near the Hanford meteorological station are shown in Fig. 5 as a function of particle diameter. The ranges of optical counter results during May 22 to May 30, 1980, are shown by the cross-hatched area. Also shown are ranges determined at Hanford in 1975 during dust storms and on clear days (2). Note the smaller diameter range investigated for volcanic ash as compared with the 1975 dust data. This diameter decrease was caused in part by a change in instrument calibration. The ranges for the volcanic ash overlay the 1975 data. Thus, during measurement times, the maximum airborne volcanic ash concentrations for the particle diameters investigated were similar to dust concentrations during the most severe dust storms measured in 1975 by

Sehmel (2). However, a significant difference between volcanic ash and dust storm data occurs for particle diameters between 0.3 and 0.5 μm . For this diameter range, the maximum ash concentration was about four times greater than reported for dust storms.

V. CONCLUDING REMARKS

Airborne solids concentrations of volcanic ash increased from a sampling site in the Hanford area to another site 24 km northwest. This second site was closer to the maximum ash fallout area. At both sampling sites, a rain of 0.79 in. on May 26 decreased airborne solids concentrations two orders of magnitude. Subsequently, airborne solids concentrations increased as surfaces dried and resuspension occurred. Changes in airborne solids concentrations after subsequent rains were interpreted to indicate that 0.2 to 0.6 in. of rain may be required to significantly reduce, at least for a day, airborne solids concentrations from area-wide resuspension sources. Even after the initial rain, airborne solids concentrations have remained relatively high at the meteorological station sampling site. Airborne solids concentration data are still being obtained at both sampling sites in order to investigate the long-term airborne effects of this surface resuspension source.

REFERENCES

1. Sehmel, G.A., "Isokinetic Air Sampler." In. Pacific Northwest Laboratory Annual Report for 1977 to the DOE Assistant Secretary for the Environment, Atmosphere Sciences, PNL-2500-3, Pacific Northwest Laboratory, (Richland, WA), 1978, pp.1.32-1.34.
2. Sehmel, G.A., "The Influence of Soil Insertion on Atmospheric Particle Size Distributions." In. Pacific Northwest Laboratory Annual Report for 1975, Atmospheric Sciences, BNWL-2000-3, Pacific Northwest Laboratory (Richland, WA), 1976. pp. 99-102.

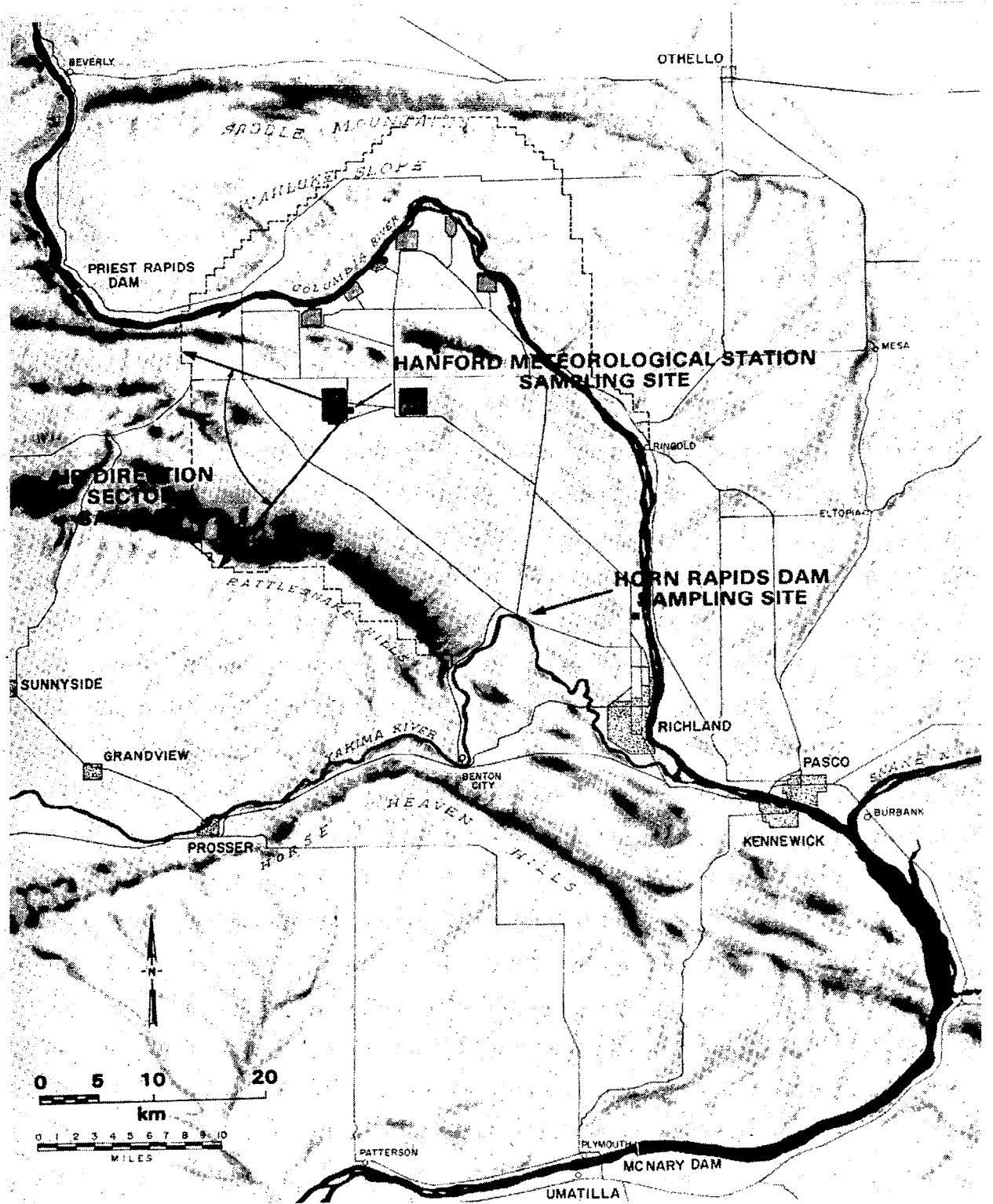


FIGURE 1. Sampling site locations (the air direction sectors sampled at Hanford Meteorological Station were 220° to 290° and all directions).

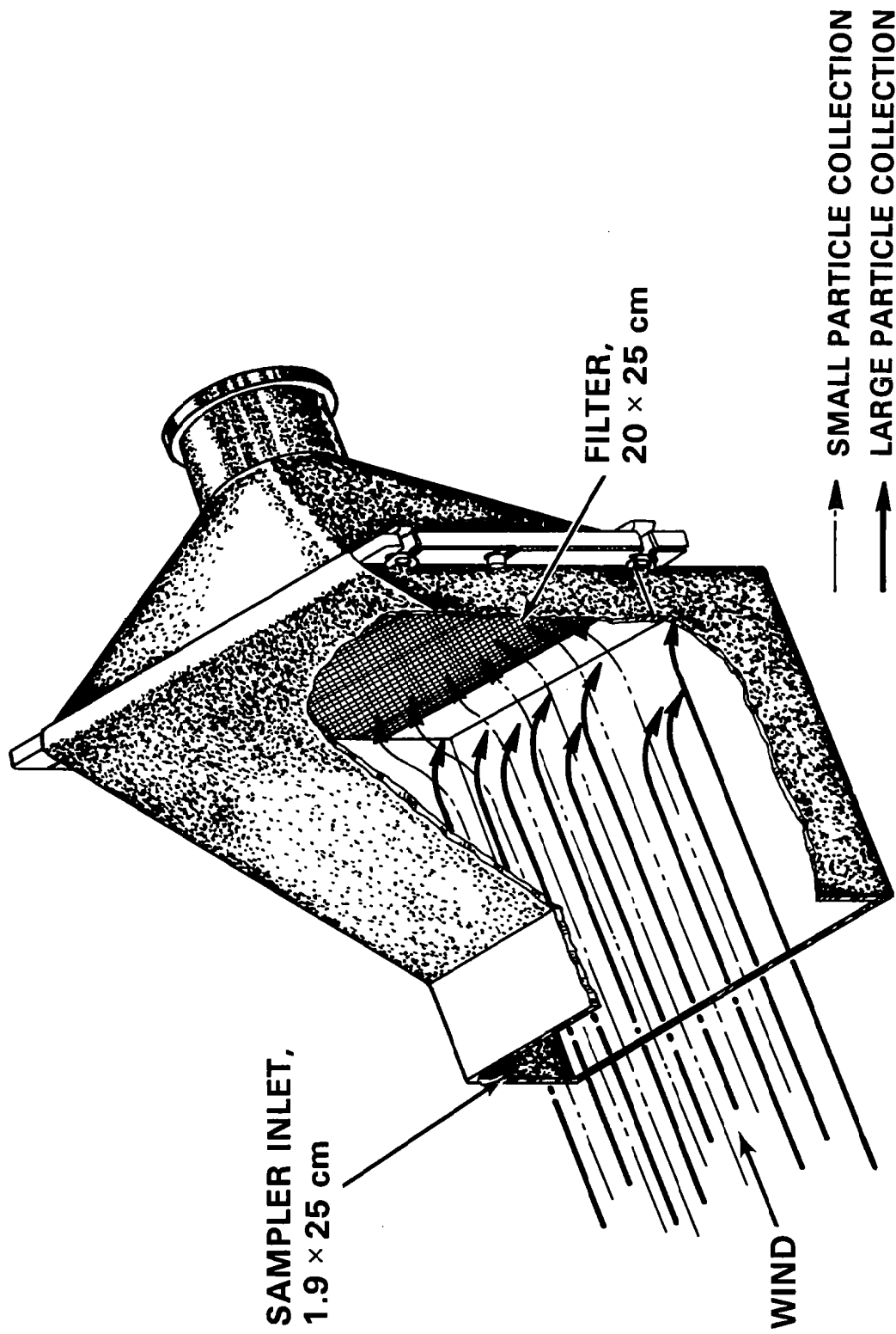


FIGURE 2. Airborne particulate sampler.

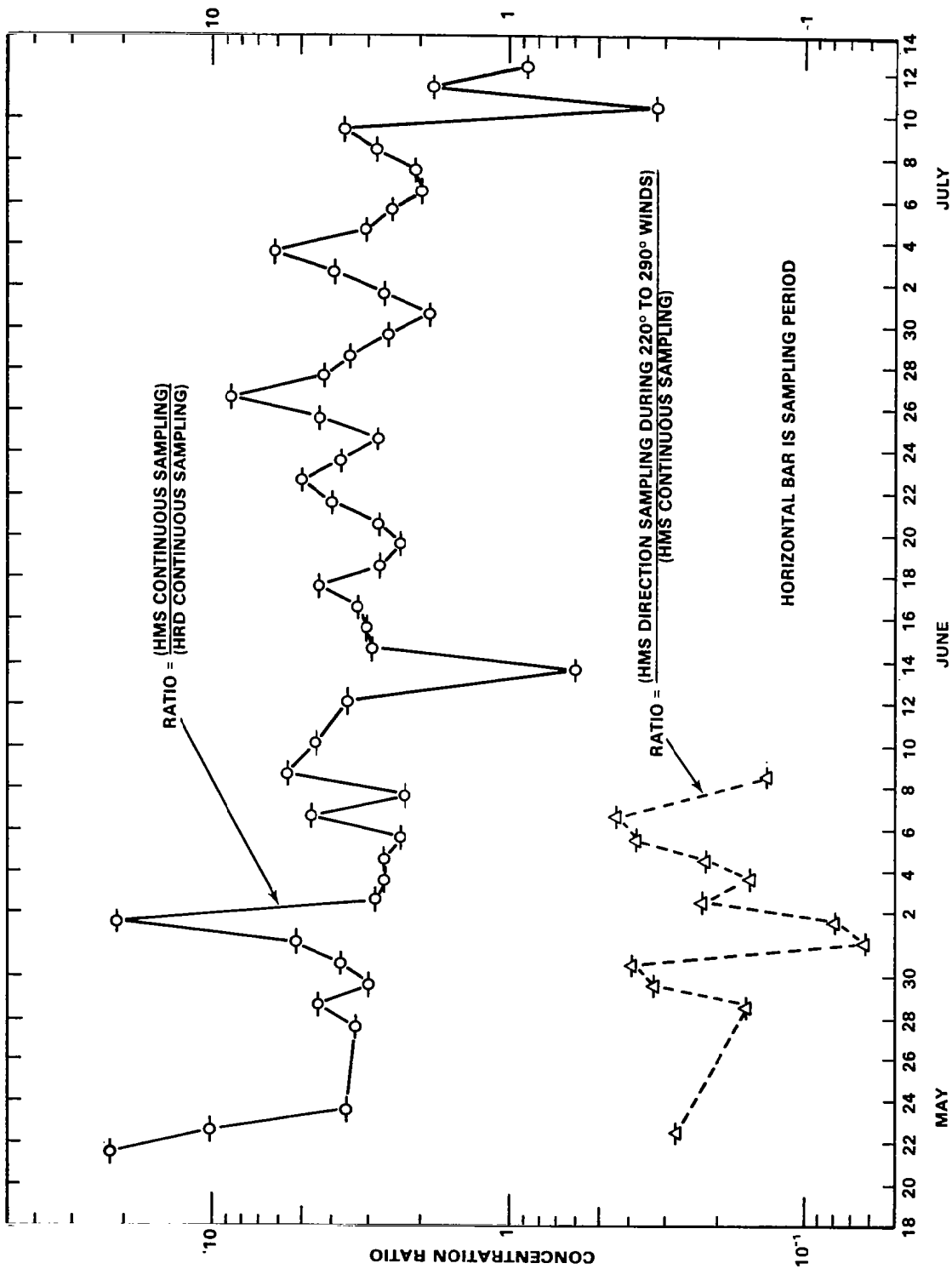


FIGURE 4. Ratios of average airborne solids concentrations at Hanford near the Hanford Meteorological Station (HMS) and the Horn Rapids Dam (HRD).

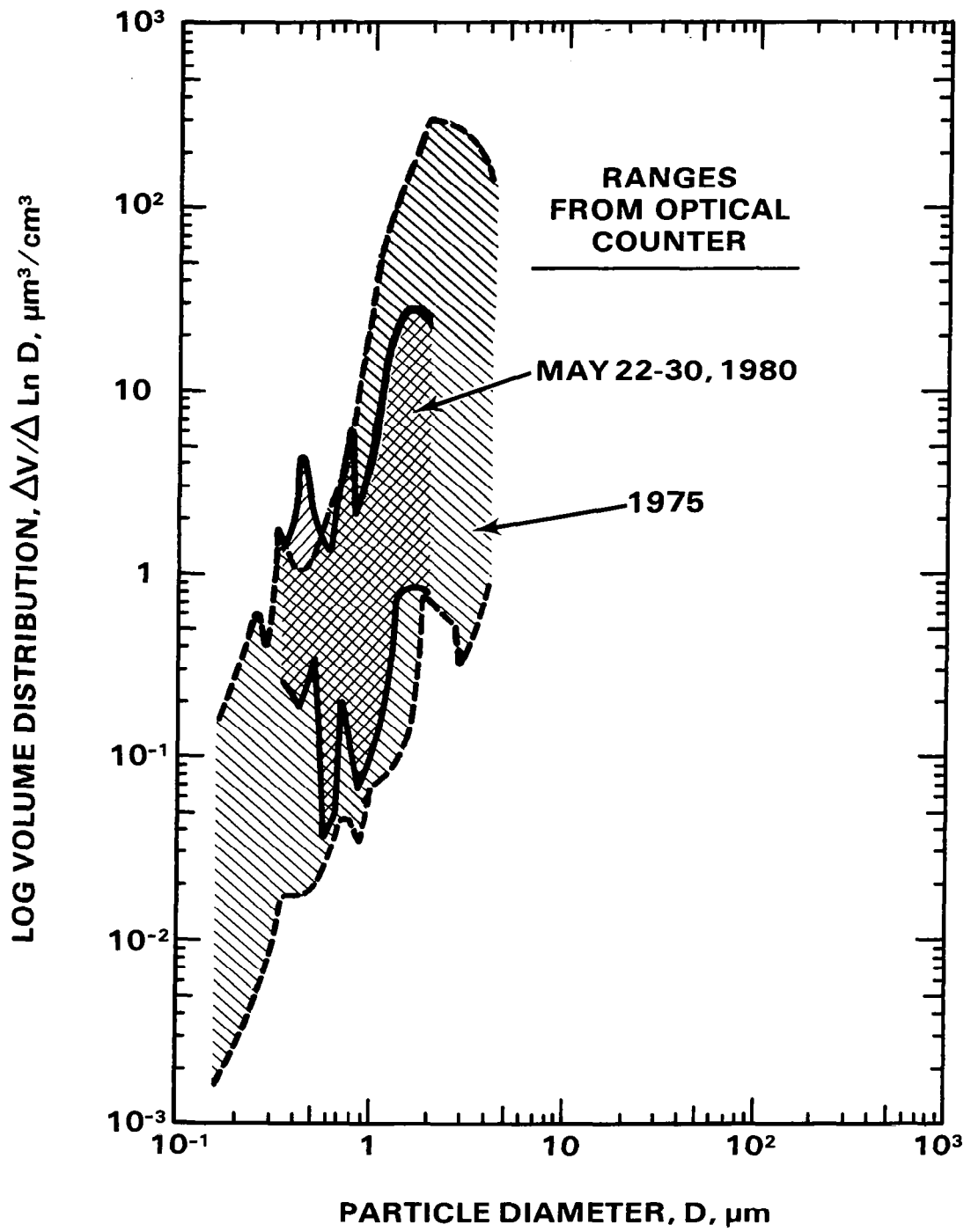


FIGURE 5. Ambient airborne particle volume distributions.

THE FORMULATION OF LAMB'S DUST VEIL INDEX¹

P. M. Kelly and C. B. Sear²

Climatic Research Unit, University of East Anglia, Norwich NR4 7TJ, United Kingdom

I. INTRODUCTION

The key work of Lamb (1970) on the possible influence of volcanic aerosols and dust particles on climate has been drawn upon or cited in numerous studies during the last 10 years. In addition to a thorough review of the subject, Lamb presented a catalog of the major explosive volcanic eruptions since 1500 AD and formulated the Dust Veil Index (DVI). The DVI is an attempt to quantify the impact on the earth's energy balance of changes in atmospheric composition due to explosive volcanic eruptions. The DVI for a particular eruption quantifies the climatic impact of the dust and aerosol injection from the eruption integrated over the years following the event. For any particular eruption, Lamb's assessment of the DVI is based on a range of different types of historical information.

Many researchers have used the DVI and in a number of cases have attributed an unwarranted degree of certainty to the Index, the many caveats given by Lamb (1970) in the original publication being ignored.

In this paper the formulation of the DVI is described in detail. Unless otherwise stated, all references are to Lamb (1970). A distinction is made between the catalog of volcanic activity (Appendix I, pp. 500-525) which includes much information besides the DVI, and the tabulation of the northern hemisphere DVI apportioned over the years (Appendix II, pp. 526-527). DVI data have been updated to 1975 (Lamb, 1977). Note that for any particular eruption, the catalog gives three DVI values: global, southern hemisphere, and northern hemisphere. Unless it is stated otherwise, the global DVI given in the catalog is considered. The other two DVIs relate to the impact on the hemispheres considered separately and their estimation involves an additional factor apportioning the dust veil between the hemispheres on the basis of the latitude of injection.

II. THE FORMULATION OF THE DVI

The formulation of the DVI was based on a review of observational, empirical, and theoretical studies of the possible impact on climate of volcanic "dust veils," in the general sense of particulate matter and primary and secondary aerosols. The formulation was, in essence, a summary of the state of knowledge in the 1960s concerning links between volcanic eruptions and climate. Both climate and radiation information were used explicitly in the assessment of the climatic significance of certain historical eruptions. The justification for using climate data in estimating DVI values was given by Lamb in the review of prior research which precedes the formulation of the DVI. As Lamb notes (p. 476), the use of climate data in the formulation of the DVI leads inevitably to the possibility of circular argument if the DVI is correlated with climate data.

There are five main estimation methods for the DVI. The final values given by Lamb are averages, sometimes subjectively corrected, of the estimates produced by as many of these methods as the available data permitted. The five methods were intercalibrated to give a DVI of 1000 for the eruption of Krakatoa in

¹Paper submitted after the meeting.

²The authors were partially supported by U.S. Office of Naval Research Grant N00014-77-G-0074 during the preparation of this article. C. B. Sear holds a N.E.R.C. Research Studentship.

1883. Although the tabulation of the DVI does not contain details of which estimation methods were used to produce a particular Index value, in most cases the catalog does. The reliability of any DVI value depends, inter alia, on the method(s) used in its estimation. The details of the derivation must therefore be considered in any analysis employing the DVI.

The formulation and estimation of the DVI took place over a number of years. The five methods are discussed in historical order.

A. Method A: "Free" Estimates

An initial catalog of volcanic eruptions was based on previous compilations by the Royal Society (1888), Sapper (1917, 1927), Shaw (1936), and Humphreys (1940). These compilations are secondary historical sources whose reliability needs to be assessed accordingly (see, for example, Bell and Ogilvie, 1978; Ingram et al., 1978). Additional information was obtained from other sources. Data for the present century were also obtained from Gutenberg and Richter (1954), Bulletin Volcanologique (1924-1960), and Bulletin of Volcanic Eruptions (1961 onwards). Recently the Event Cards distributed by the Smithsonian Institute's Center for Short-Lived Phenomena (Cambridge, Massachusetts) have been used (Lamb, 1977).

The initial catalog contained information on the date, duration, and location of major volcanic eruptions, any available estimates of the dust produced (for example, Sapper's ratings of the lava and tephra magnitude), and documentary observations of optical effects due to the dust veils. It did not include the climate and radiation data associated with particular eruptions which were given by Lamb in the final (that is, published) catalog.

The information in the initial catalog, with the exception of Sapper's ratings, was used to make "free" (that is, subjective) estimates of DVI values. Particular attention was paid to the visual observations of optical effects from which the composition of each veil could be derived, and to information concerning each veil's extent and duration. These estimates were remade after 6 months by using the same data and were reviewed after a year. In cases where it was not possible to use other estimation methods, these free estimates were given in brackets in the published catalog.

The next three estimation methods used by Lamb used ancillary data not included in the initial catalog. Three formulae were devised to systematize the estimation of the DVI after the initial free estimates had been made. These formulae include parameters related to the quantity of material injected into the stratosphere, the geographical (latitudinal) extent of the veil, and the duration of the veil. Two parameters occur in all three formulae and are discussed first. These parameters, weighting factors dependent on veil extent and duration, were determined by consideration of the differing cumulative impact on global climate of veils of different extent and duration. It is these weighting factors which made the DVI a measure of the cumulative impact on climate of any dust veil, rather than simply a measure of the dust loading of the stratosphere.

The geographical extent of the veil, E_{max} , for any eruption is dependent on the latitude of the particular volcano. E_{max} is:

- 1.0 for an eruption between 20°N and 20°S
- 0.7 for an eruption between 20° and 35°
- 0.5 for an eruption between 35° and 40°-42°
- 0.3 for an eruption in higher latitudes.

These values of E_{max} are based on "rule of thumb" estimates of the difference in global climate impact of eruptions in different latitude zones, and not simply on the differing areal extent of the resulting veils. The determination of the characteristic spread of dust into a veil was based on observational evidence from historic eruptions and on tracer studies undertaken by the U.K. Meteorological Office, for example, of material from nuclear bomb tests. E_{max} is listed in the catalog for each eruption, except in cases where an eruption was assumed to have occurred solely on the basis of reports of a veil (that is, there was no first-hand evidence of an eruption of a particular volcano).

The quantity t_{mo} is an estimate of veil duration in months. Whether or not an eruption penetrated the stratosphere is estimated subjectively on the basis of descriptions of the violence of the eruption and reports

of a veil. The value of t_{mo} was generally estimated from (a) documentary observations of the veil and/or (b) the duration of radiation and/or (c) temperature departures associated by Lamb with a particular eruption. In the last two cases, t_{mo} was the time taken for the temperature or radiation values to return to pre-eruption levels. A single estimate of t_{mo} is given in the catalog, when available, and is based on any or all of these data. In most cases, it is clear from the catalog which type(s) of data were used in estimating t_{mo} .

A scaling factor (the numerical constant in the following formulae) was included in each formula to give the eruption of Krakatoa in 1883 a DVI of 1000.

The final parameter for the formulae is a measure of the amount of "dust" injected. Three methods were used to estimate this parameter and they are considered separately in the following sections.

B. Method B: Radiation Data

In the first formula, radiation data were used to assess the magnitude of the injection:

$$DVI = 0.97 R_{max} E_{max} t_{mo}$$

R_{max} is the greatest percentage of depletion of direct radiation following the eruption, as registered by monthly averages in middle latitudes of the hemisphere concerned. The greatest depletion may not occur until a couple of years after the eruption. Lamb assumed that the total radiation loss approximated to a fixed fraction of the direct radiation loss and that middle latitude estimates sufficed to represent the hemisphere, although the latitude of injection did need to be considered.

Radiation data were used for the period 1883 onward, mostly for the northern hemisphere alone. A suffix "1" against the DVI for a particular eruption in the catalog denotes the use of this formula in estimating the value for that eruption.

C. Method C: Temperature Data

In the second formula, surface air temperature data were used to estimate the injection:

$$DVI = 52.5 T_{Dmax} E_{max} t_{mo}$$

T_{Dmax} stands for the estimated lowering of average temperature in degrees Celsius over the middle latitude zone of the hemisphere affected in the year most affected following an eruption. In order to reduce the climate dependence inherent in this formulation of the DVI, the short-term temperature departure from the longer-term trend is used. Lamb argues that although the DVI estimated in this way cannot safely be used in short-term temperature correlation studies, any longer-term dependence on climate inherent in the formulation is thereby reduced.

The temperature data used were limited in geographical coverage and quality, particularly prior to 1900. No data were available prior to 1750 and few estimates were derived by use of this equation for 20th century eruptions. In certain cases, estimates of the DVI given in the catalog have been based on this method alone, and on no other evidence. A suffix "2" in the catalog indicates a DVI value has been derived by using this equation.

D. Method D: Volume Ejected

In the final formula, estimates of the volume of material ejected were used:

$$DVI = 4.4 qE_{max} t_{mo}$$

where q is the estimated value in cubic kilometers of solid matter dispersed as dust in the atmosphere. The only estimates used were those derived from the measured dust deposit about the volcano. Lamb considers this equation to be the least reliable of the three equations and suggests that its main value may lie in providing an estimate of q after the DVI has been estimated by other methods. A suffix "3" in the catalog indicates that this equation has been used.

E. Method E: Sapper's Ratings

For many of the earlier eruptions, no data were available other than Sapper's rating of the lava and tephra magnitude of the eruption. Lamb calculated an average DVI value for each of Sapper's tephra ratings for eruptions for which independent data were available. With a correction for eruption latitude and sometimes an additional subjective correction, he then used these average values for eruptions for which Sapper's ratings alone were available. Lamb notes that the comparison of his independent DVI estimates with those based on Sapper's rating suggested that Sapper changed his standards about 1900. Sapper's ratings were therefore not used for the period 1900 to 1914. These estimates appear in the catalog with the suffix "av" or "adj" (the latter indicates some adjustments to the DVI estimated from Sapper's rating).

III. SUMMARY

The methods used to derive the DVI estimate for any particular eruption can generally be determined from the catalog. Eruptions prior to 1750 were assessed solely on the basis of methods A (free estimates), D (volume ejected), or E (Sapper's ratings). Method C (temperature data) was used for some eruptions during the period 1750 to date, and method B (radiation data) was used for certain events during the period 1883 to date. In determining a final value of the DVI, preference was given to methods B and C (averaged if both were available), checked and possibly modified by consideration of methods A and D. If no other data were available, method E was used. In some cases, it was not possible to distinguish veils from eruptions occurring in rapid succession and a cumulative DVI for the series of eruptions is given (in italics in the catalog).

Clearly, the DVI estimated by any of these methods is subject to considerable error. Lamb compared estimates arising from all five methods and, also by considering the nature of the evidence, concluded that rounded values obtained by averaging estimates from methods B and C should be reliable in the case of well-defined and observed eruptions and dust veils, at least to the extent of indicating order of magnitude.

So far, the derivation of the global DVI values has been discussed. The DVI for any eruption is given for the globe, for the northern hemisphere, and for the southern hemisphere in the catalog. The global DVI for each eruption was estimated first, then the hemispheric DVIs were calculated by using a second weighting factor dependent on the latitude of the eruption (E_{max} was the first). In apportioning the global DVI between hemispheres, for eruptions within about 15° latitude of the equator, the DVI was equally divided between the hemispheres. For eruptions between 15° and 20° latitude, the DVI was split two thirds to the hemisphere of injection, one third to the other hemisphere. For eruptions poleward of 20° latitude, the DVI was attributed solely to the hemisphere of injection. Because of this apportioning, the hemispheric DVIs are not as dependent on the latitude of injection as the global DVI.

Two sets of northern hemisphere DVI values are given in the tabulation. One set includes a few estimates based on temperature data alone (method C), that is, no other evidence of an eruption or veil was available. The other set does not contain any such estimates. For the tabulation, the DVI values were linearly apportioned over the years following the eruption to simulate the decay of the dust veil: first year, 40%; second year, 30%; third year, 20%; fourth year, 10%. For example, Krakatoa, an equatorial eruption with a global and hemispheric DVI of 1000 in the catalog, contributed an index of 400 in 1883, 300 in 1884, 200 in 1885, and 100 in 1886, to the tabulation. Note that the initial annual value is 400, not 1000; the DVI in the catalog is a measure of the impact of the eruption integrated over time. All events are considered to have occurred at the beginning of the year of eruption.

Chance and Kelly (1979) have discussed the effects of the 4-year decay model on the variance spectrum of the DVI. It introduces an apparent periodicity at wavelengths of 7 to 8 years. In a few cases where there was evidence of a veil of longer duration, the dust was linearly decayed over a longer period. In other cases of continuing, although usually small, eruptions the DVI was evenly distributed over the appropriate period of years.

The accuracy of the cumulative values of the DVI given in the tabulation is obviously dependent inter alia on the identification of all major explosive eruptions (or veils). Following Sapper (1917), Lamb considered the catalog of the occurrence of major eruptions to be relatively complete for the northern hemisphere since

1780 (although in many cases the information available was insufficient to derive a reliable DVI), but not complete until recent times for the southern hemisphere. For the 17th century onward, Lamb considered that most of the larger northern hemisphere eruptions ($DVI \geq 100$) were known, except perhaps for the equatorial zone. At times, however, the paucity of detail necessitated the estimation of the DVI as less than, or not less than, a certain value.

IV. CONCLUSIONS

Many investigators have placed far more faith in the reliability of the DVI than Lamb intended, particularly when using the tabulation of the DVI. To quote Lamb (p. 472):

Even when the reckoning of the dust veil index has been systematized by the use of these routine formulae, there is still a good deal of unavoidable estimation involved . . . It must simply be recognized that this is about as far as one can go towards objectivity in the assessment of past eruptions. The method seems at least reliable as an indicator of order of magnitude.

The use of the three formulae (methods B, C, and D) in the formulation of the DVI may, however, lend an air of reliability and objectivity to the Index which appears unwarranted on consideration of the evidence upon which the formulation is based.

There is still a definite need for a long-term history of volcanic activity related to potential climatic impact for assessment of the conclusions of studies using numerical models and recent observational data. Furthermore, information and knowledge are now available which would aid a revision of the DVI. Additional volcanological data have been recently compiled for historical eruptions. These data have been included in two new catalogs (Hirshboeck, 1979-1980; Newhall and Self, 1982). They contain details of eruptions unknown to Lamb, and new, more reliable data on eruptions included in Lamb's catalog. There is now greater knowledge of the mechanisms involved in the development of a "dust veil" (particularly secondary aerosol formation) and the mechanisms by which the energy balance is affected (for example, the importance of sulfate aerosols). Hammer, Clausen and Dansgaard (1980) have shown that acidity profiles from ice cores may provide a long-term record of sulfate aerosols from volcanic eruptions.

Before such a revision is attempted, users of the DVI are advised to:

1. Only use DVI values to indicate order of magnitude
2. Not use any DVI value without reference to the method(s) used in its estimation, that is, gauge each value's reliability
3. Beware of circular argument if DVI values based on climate data have to be used

ACKNOWLEDGMENT

We thank Professor Hubert Lamb for providing unpublished information concerning the formulation of the DVI. The authors were partially supported by U.S. Office of Naval Research Grant N00014-77-G-0074 during the preparation of this article. C. B. Sear holds a N.E.R.C. Research Studentship.

REFERENCES

- Bell, W. T., and A. E. J. Ogilvie, 1978: Weather compilations as a source of data for the reconstruction of European climate during the Medieval period. *Climatic Change*, 1(4), 331-348.
- Bulletin of Volcanic Eruptions, 1961: I.U.G.G. (International Association of Volcanology and Volcanological Society of Japan), Tokyo.
- Bulletin Volcanologique, 1924-1960: I.G.G.I. (Association Internationale de Volcanologie), Brussels.
- Chance, A., and P. M. Kelly, 1979: An apparent periodicity in an index of volcanic activity. *Nature (London)*, 280, 671-672.
- Gutenberg, B., and C. F. Richter, 1954: Seismicity of the Earth. Princeton Univ. Press.
- Hammer, C. U., H. B. Clausen, and W. Dansgaard, 1980: Greenland ice sheet evidence of post-glacial volcanism and its climatic impact. *Nature (London)*, 288, 230-235.

- Hirshboeck, K. K., 1979-1980: A new worldwide chronology of volcanic eruptions. Palaeogeography, Palaeoclimatology, Palaeoecology, 29, 223-241.
- Humphreys, W. J., 1940: The Physics of the Air. McGraw-Hill (New York and London).
- Ingram, M. J., D. J. Underhill, and T. M. L. Wigley, 1978: Historical climatology. Nature (London), 276, 329-334.
- Lamb, H. H., 1970: Volcanic dust in the atmosphere, with a chronology and assessment of meteorological significance. Phil. Trans. Roy. Soc. (London), A 266(1178), 425-533.
- Lamb, H. H., 1977: Supplementary volcanic dust veil index assessments. Climate Monitor, 6(2), 57-67.
- Newhall, C. G., and S. Self, 1982: The volcanic explosivity index (VEI): An estimate of explosive magnitude of volcanic eruptions. J. Geol. Res., 87, 1231-1238.
- Royal Society, 1888: The Eruption of Krakatoa and Subsequent Phenomena. (Report of the Krakatoa Committee of the Royal Society, G. J. Symons, editor.) Harrison and Tribner (London).
- Sapper, K., 1917: Beitrage zur Geographic der tatigen Vulkane. Z. Vulk. (Berlin), 3, 65-197.
- Sapper, K., 1927: Vulkankunde. Engelhorn Verlag (Stuttgart).
- Shaw, N., 1936: Manual of Meteorology, Vol. II: Comparative Meteorology. Cambridge Univ. Press.

FORWARD SCATTERING AND BACKSCATTERING OF SOLAR RADIATION BY THE STRATOSPHERIC LIMB AFTER MOUNT ST. HELENS ERUPTION¹

M. Ackerman and C. Lippens

Institut d'Aeronomie Spatiale de Belgique, 3, Avenue Circulaire, B 1180 Brussels, Belgium

Stratospheric limb-radiance profiles versus altitude of closest approach of the line of sight to the Earth's surface have been measured before and after the Mount St. Helens eruptions by means of photographs taken from a Sun-oriented balloon gondola floating above 35-km altitude over France. Preliminary data have been reported (Ackerman et al., 1980) for flights in October 1979 and in May and June 1980. The radiance integrated along the line of sight as in-situ radiance (R^*) can be derived taking into account absorption by ozone and air. The onion-peeling inversion method has been used to derive the vertical-radiance (R^*) profiles shown in figures 1 and 2 for June 5 and October 15, respectively. The values of R^* have been determined in the solar azimuth, at respective solar elevation angles equal to 6° and 6.7° , and 180° from the solar azimuth at solar elevation angles respectively equal to 12° and 11.8° . The solar elevation angles have been chosen larger for the backscattering observation than for the forward-scattering observation in order to deal with as similar illumination conditions as possible despite the Earth's sphericity.

In the first approximation only direct-solar illumination of the stratosphere is considered. The scattering angles, θ , for one altitude are indicated. The backscattering radiances are represented by the dotted curves while the forward-scattering radiances are represented versus altitude by the dashed curves. The backscattering signal shows little structure versus altitude. Since it is mainly due to Rayleigh scattering, its subtraction from the forward signal leads to the solid curves representing the forward scattering almost solely due to the aerosols.

Eventually, figure 3 shows versus altitude the ratio between aerosol forward scattering in blue light (Wratten filter nr. 47) and in red light (Wratten filter nr. 25) deduced from simultaneously taken photographs in the previously described solar illumination conditions.

Several conclusions can be drawn from these preliminary data. On June 5, a large enhancement of forward aerosol scattering is observed below 16 kilometers showing a layered structure of the volcanic aerosol. The horizontal homogeneity is doubtful from the observations themselves so that backscattering and forward scattering can hardly be correlated even if the latter one shows an effect due to the volcano. On the other hand, on October 15, the volcanic aerosol below 18 km shows a great horizontal homogeneity. A comparison between back and forward signal indicates an increase of the forward to backscattering aerosol ratio with decreasing altitude indicating a change of optical properties of the aerosol with altitude. An aerosol peak appears at 23.5 km with horizontally inhomogeneous extensions up to 27 km. The color ratio shown in figure 3 indicates also a variation of optical properties versus altitude. Minima of the ratio are observed at 17 and at 23 km where layers have been frequently observed in red light in the background aerosol on the occasions of previous flights.

The aerosol enhancement on June 5 peaking at 15.5 km appears to have modified the limb radiance at higher altitudes. This represents an observational support to theories emphasizing the effect of aerosol layers on atmospheric-optical measurements relying on scattering of radiation such as ozone measurements performed by means of the "umkehr" and of the B.U.V. methods (DeLuisi, 1979, and DeLuisi et al., 1979).

Ramanathan and coworkers (1969) have already suggested that the "second umkehr effect" is due to aerosol scattering which is typically variable, present at all altitudes up to 35 km as observed by us and even at 50 km as observed by Giovane et al. (1976).

¹Paper submitted after the meeting.

REFERENCES

- Ackerman, M.; Lippens, C.; and Lechevallier, M. (1980), Volcanic material from Mount St. Helens in the stratosphere over Europe, Nature, **287**, 614-615.
- DeLuisi, J. J. (1979), Umkehr vertical ozone profile errors caused by the presence of stratospheric aerosols, J. Geophys. Res., **84**, 1766-1770.
- DeLuisi, J. J.; Mateer, C. L.; and Heath, D. F. (1979), Comparison of seasonal variations of upper stratospheric ozone concentrations revealed by Umkehr and Nimbys 4BUV observations, J. Geophys. Res., **84**, 3728-3732.
- Giovane, F.; Schuerman, D. W.; and Greenberg, J. M. (1976), J. Geophys. Res., **81**, 5383-5388.
- Ramanathan, K. R.; Angreji, P. D.; and Shah, G. M. (1969), The second umkehr observed in zenith sky twilight and its interpretation, Ann. Geophys., **25**, 243-248.
- Reiter, R.; Jäger, J.; Carmith, W.; and Funk, W. (1980), Lidar observations of the Mount St. Helens eruption clouds over Mid-Europe, May to July 1980, Geophys. Res. Lett., **7**, 1099-1101.

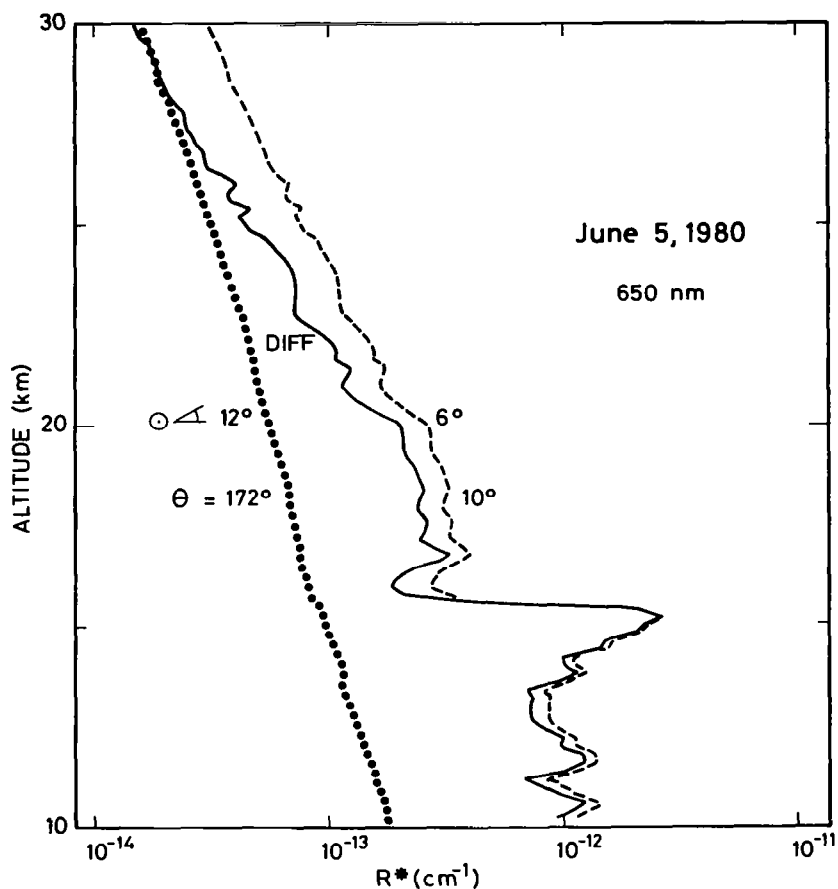


Figure 1. June 5, 1980, radiance per unit slant path and in units of solar radiance at the altitude of closest approach to the earth surface versus altitude. The observation conditions have been described by Ackerman et al. (1980). Solar elevation angles ($\odot \sphericalangle$) are indicated as well as scattering angle, θ , for the direct-solar radiation. The dashed curve shows the near forward scattering, the dotted curve represents the near back-scattering and the solid curve corresponds to the difference between the two which means radiance almost solely due to the injection of volcanic material. The back signal is slightly increased at that altitude but no correlations with the forward signal are possible since the inspection of the photographs shows horizontal inhomogeneities in the layer.

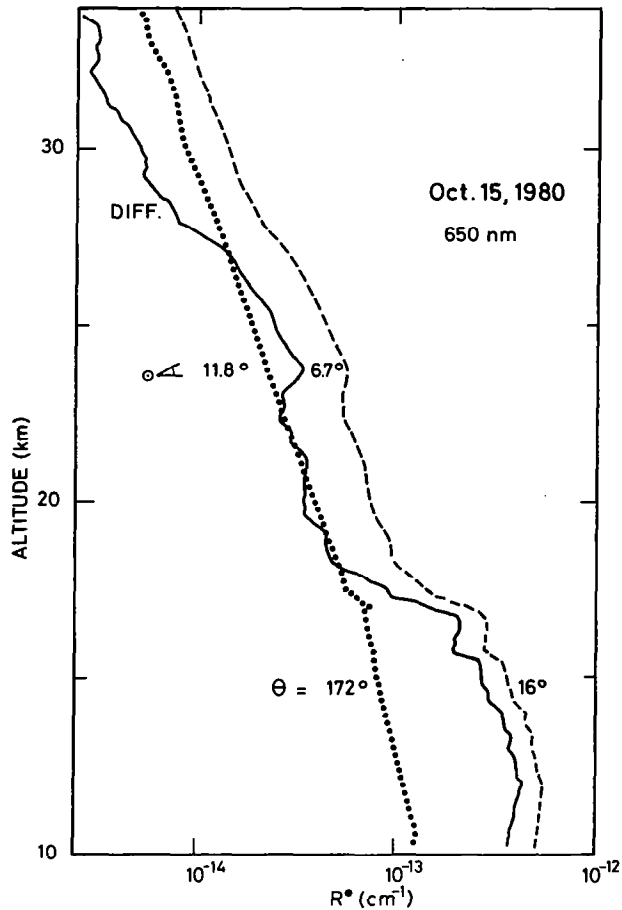


Figure 2. Identical as figure 1 but for October 15, 1980. After five months the injected material has spread horizontally so that layers not observed at 24-km altitude before the end of June over Europe (Reiter et al., 1980) are now visible over large horizontal extent. Some of it seems to extend up to 27-km altitude. A backscattering abrupt enhancement is observed below 17 km which in terms of lidar backscattering ratio would amount to $R = 1.15$. It should be noticed that the back signal at 30-km altitude almost exclusively due to Rayleigh scattering is in this case a factor of two lower than on June 5. In this latter case the 15.5-km strong aerosol layer leads to a large increase of atmospheric radiance at all altitudes above it.

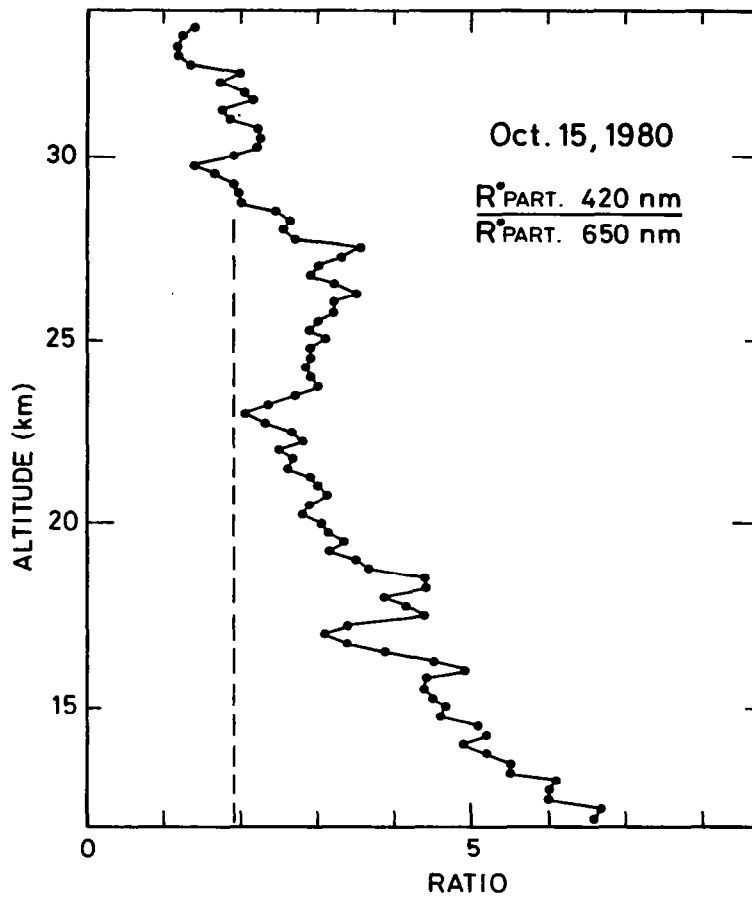


Figure 3. Ratio of in-situ radiance, R^* , in blue light to radiance in red light. The radiance increase corresponding to decreasing wavelength is not the same at all altitudes showing a variation of the aerosol optical properties with altitude.

1. Report No. NASA CP-2240		2. Government Accession No.		3. Recipient's Catalog No.	
4. Title and Subtitle ATMOSPHERIC EFFECTS AND POTENTIAL CLIMATIC IMPACT OF THE 1980 ERUPTIONS OF MOUNT ST. HELENS				5. Report Date Oct. 1982	
				6. Performing Organization Code 665-40-40-10	
7. Author(s) Adarsh Deepak, editor				8. Performing Organization Report No. L-15488	
9. Performing Organization Name and Address NASA Langley Research Center Hampton, VA 23665				10. Work Unit No.	
				11. Contract or Grant No.	
12. Sponsoring Agency Name and Address National Aeronautics and Space Administration Washington, DC 20546				13. Type of Report and Period Covered Conference Publication	
				14. Sponsoring Agency Code	
15. Supplementary Notes Adarsh Deepak: Institute for Atmospheric Optics and Remote Sensing, Hampton, Virginia					
16. Abstract <p>A symposium was organized to provide a forum at which a multidisciplinary group of scientists engaged in measurements and studies of the 1980 Mount St. Helens volcanic eruptions could exchange information. The symposium was held in Washington, DC, on 18-19 November 1980, just six months after the most violent eruptions of Mount St. Helens on 18 May 1980. The papers presented were primarily invited and were divided into six sessions: (1) Nature and Impact of Volcanic Eruptions, (2) In Situ Measurements of Effluents, (3) Remote Sensing Measurements, (4) Transport and Dispersion of Volcanic Effluents, (5) Chemistry of Volcanic Effluents, and (6) Weather and Potential Climate Impact. In all, 28 invited and contributed papers are contained in this publication. Most of the data were unpublished at the time of the symposium, and researchers all freely shared their results. The hallmark of the meeting was this multidisciplinary exchange among geologists, atmospheric scientists, volcanologists, and experimentalists in these fields. Following this two-day open symposium of presented papers was a two-day workshop where smaller groups summarized what was known about the Mount St. Helens eruptions and their atmospheric effects and potential climatic impact. The workshop proceedings were published as NASA SP-458.</p>					
17. Key Words (Suggested by Author(s)) Volcanic eruptions Mount St. Helens Volcanic effluents Remote sensing Climatic impact of volcanoes			18. Distribution Statement Unclassified—Unlimited Subject Category 46		
19. Security Classif. (of this report) Unclassified		20. Security Classif. (of this page) Unclassified		21. No. of Pages 314	22. Price A14

National Aeronautics and
Space Administration

Washington, D.C.
20546

Official Business

Penalty for Private Use, \$300

SPECIAL FOURTH CLASS MAIL
BOOK

Postage and Fees Paid
National Aeronautics and
Space Administration
NASA-451



7 1 10, E, 820910 S00903DS
DEPT OF THE AIR FORCE
AF WEAPONS LABORATORY
ATTN: TECHNICAL LIBRARY (SUL)
KIRTLAND AFB NA 37117

NASA

POSTMASTER: If Undeliverable (Section 158
Postal Manual) Do Not Return
